Solid Fuels and Heavy Hydrocarbon Liquids

Solid Fuels and Heavy Hydrocarbon Liquids

Thermal Characterization and Analysis

Second Edition

Rafael Kandiyoti
Imperial College London, London, United Kingdom

Alan Herod
Imperial College London, London, United Kingdom

Keith Bartle
University of Leeds, Leeds, United Kingdom

Trevor Morgan
Hawaii Natural Energy Institute, Honolulu, HI, United States

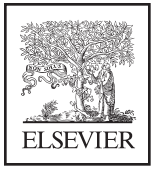

elsevier.com

Elsevier
Radarweg 29, PO Box 211, 1000 AE Amsterdam, Netherlands
The Boulevard, Langford Lane, Kidlington, Oxford OX5 1GB, United Kingdom
50 Hampshire Street, 5th Floor, Cambridge, MA 02139, United States

Notices
Knowledge and best practice in this field are constantly changing. As new research and experience broaden our understanding, changes in research methods, professional practices, or medical treatment may become necessary.

Practitioners and researchers must always rely on their own experience and knowledge in evaluating and using any information, methods, compounds, or experiments described herein. In using such information or methods they should be mindful of their own safety and the safety of others, including parties for whom they have a professional responsibility.

To the fullest extent of the law, neither the Publisher nor the authors, contributors, or editors, assume any liability for any injury and/or damage to persons or property as a matter of products liability, negligence or otherwise, or from any use or operation of any methods, products, instructions, or ideas contained in the material herein.

British Library Cataloguing-in-Publication Data
A catalogue record for this book is available from the British Library

Library of Congress Cataloging-in-Publication Data
A catalog record for this book is available from the Library of Congress

ISBN: 978-0-08-100784-6

Publisher: Candice Janco
Acquisition Editor: Amy Shapiro
Editorial Project Manager: Tasha Frank
Production Project Manager: Vijayaraj Purushothaman
Designer: Greg Harris

Typeset by MPS Limited, Chennai, India

Preface to the first edition

A little fortuitously, this book on coal, biomass and heavy hydrocarbons is approaching publication during a period of high and unstable oil and gas prices and amidst mounting uncertainty over future supplies. The underlying trend facing energy markets is one of steady, relentless rise in demand and little spare or excess capacity. The realization that the giant economies of Asia are dependent on increasing energy supplies, no less than much of the already industrialized world, cannot be denied. The USA alone expects its energy requirements to double by 2050. Many of the older industrialized countries also face a baffling set of options regarding the replacement of obsolescent electricity-generating capacity.

Within this framework, how governments, industry and individuals should respond to conflicting personal, economic and environmental requirements remains to be debated. Economic growth and improved living standards require security of supply and freedom from terror attacks. However, we also desire a cleaner planet and fear the possible threat of climate change. Our objectives are at odds with each other. Much recent planning has focused on short-term solutions. Longer-term expectations have been placed on expensive and dangerous hydrogen on the one hand and technically as well as economically unrealistic CO_2 sequestration on the other. The world, the industrialized nations and the UK are all in need of reviewing feasible options that are publicly acceptable. This is a complex task that can no more be left to the market to resolve, than could be resolved by excluding it.

Overall, however, the picture we face is one of a gradually degrading environment and of a diminishing resource base. Many of the alterations suffered by the planet are of an irreversible nature. An unknown but no doubt large proportion of the readily extractable oil has already been used up. The present rush to gas can indeed delay the end of plentiful hydrocarbon supplies but cannot avoid it. All combustion processes generate greenhouse gases as well as pollutants, such as toxic trace elements and sulphur oxides. Spillages from oil tankers and pipelines, coal mining and cleaning operations pollute the environment and are causing largely irreparable damage on grand scale.

Unfortunately, the ‘renewables’ options do not appear as attractive, close up, as they do on first mention. The use of biomass as fuel can only assist in providing marginal amounts of energy; its large-scale use would compete directly with food production. Other renewable energy options, including wind power, suffer from high capital costs and affect the environment adversely. The inherent instabilities of wind-generated power impose a ceiling of a mere several percent contribution to the grid. In the coming decade, these difficulties will probably require bringing back the nuclear energy option.

Perhaps we have now collectively learned to care about decommissioning costs and those of nuclear waste storage. It would in any case be interesting to compare these costs with those of CO_2 sequestration. We will also need to live with and account for the dangers of ploughshares being turned into swords, since nuclear reactors can be used to manufacture fissile material for nuclear weapons.

Against this background of uncertain supply, a major long-term share for coal in power generation appears inevitable. Countries as diverse as the USA, China and India are all committed to increasing their use of coal-fired power generation, despite pollution from its mining, cleaning, transport and utilization and indeed despite its associated CO_2 emissions. As noted in all comparisons with oil and gas, the distribution of coals across the continents is more evenly spread. Furthermore, current and future coal use is not restricted to combustion. In albeit smaller tonnages, coal has maintained its position as a source of carbon in steel making and as raw material for high-value carbon products. Furthermore, current high oil and gas prices have significantly changed the established cost calculations. The economic prospects of coal gasification, already under consideration as an efficient and less polluting alternative, and that of coal liquefaction for transport fuels, will be re-examined if oil and gas prices appear to stabilise at their current high levels.

The first stage in the processing of coal nearly always involves thermolytic reactions and one main purpose of this book is to summarise and assess the current state of knowledge about the thermochemical reactions of coals. These synoptic accounts have relied mainly on results of experimental work carried out in our laboratories at Imperial College London and the University of Leeds over the past two and a half decades. The work has been put in the context of the extensive literature on the thermochemical reactions of coals.

Several major strands run through the present manuscript. The first is the focus on the design and operation of experimental thermochemical reactors. The emphasis has been on isolating effects due to reactor design on the measured fundamental properties of solid fuels. In simple terms, this amounts to requiring the decoupling of experimental method from the properties being measured, as in any field of scientific endeavour. The clearer methodology emerging from this work has enabled the identification of similarities and differences between thermal breakdown in pyrolysis and liquefaction. The other major strand in the book has emerged from attention paid to changing product characteristics during reactor-related developments. New analytical procedures have been developed and applied to the characterization of liquid products from coal and biomass pyrolysis, coal liquefaction and petroleum-derived heavy hydrocarbons.

Large molecular mass materials have been detected in coal-derived liquids, in soot, in petroleum asphaltenes and vacuum residues, in solvent extracts of amber and wood, as well as in ‘craft’ products such as Stockholm tar, used as a caulk and preservative in the ‘Mary Rose’, famous flagship of Henry VIII. We will describe chromatographic and mass spectrometric methods developed for detecting and characterizing large molecular mass materials that have hitherto received relatively little attention. The increasing arrival of heavier crudes in oil refineries makes these developments more necessary than in the past. Controversies surround aspects of the characterization of

large molecular mass materials and new insights made possible by the use of novel mass spectrometric techniques will be presented.

Little of the work described in these pages would have been possible without the untiring work of our students and associates at Imperial College and the University of Leeds. The authors take pleasure in acknowledging how much they have learned from them all, too many to name here, but whose names will appear as co-authors of many publications cited in this manuscript. We would like to thank them for their efforts and for many lasting friendships.

The authors would also like to thank the many sponsors of the work presented in these pages. Our special thanks go to the British Coal Utilisation Research Association, the Engineering and Physical Sciences Research Council, the UK Department of Trade and Industry, the Ministry of Science and Technology (China), SASOL of South Africa, CORUS and the European Community. We would like to remember the Coal Research Establishment (British Coal), which supported our laboratories with care and constancy over the years. The effective closure of British Coal by the conservative governments of the early 1990s caused much pain in the country but allowed us to recruit AAH, who would like to thank them for giving him this opportunity. A special word of thanks must also go to all our friends and collaborators, spread over all five continents, to whom we humbly present the results of our work, with the hope that this book may help them in theirs.

Last but certainly not least, we would like to express our gratitude to our wives, Christine Bartle, Barbara Herod and Denise Kandiyoti, for their patience and support during the writing of this book and for putting up with us over the years.

R. Kandiyoti and A. Herod
London

Keith Bartle
Leeds, United Kingdom

Preface to the second edition

In the aftermath of the 'United Nations Conference on Climate Change' in Paris (November–December, 2015), some 177 countries have, to date, signed the 'Paris Agreement'. Among other decisions, the Conference agreed 'on the need for global emissions to peak as soon as possible'. Meanwhile, global yearly fossil fuel consumption has increased by nearly 4000 MTOE (million ton oil equivalent) in the last two decades, while total yearly renewable energy production stands at a little over 300 MTOE. Clearly, much work is needed to develop more efficient and cost-effective methods for delivering renewable energies. Meanwhile, the expanding use of fossil fuels suggests there must be no letup in the attempt to devise ways to utilise fossil fuels more efficiently and in environmentally more sensitive ways.

This book outlines developments in the fundamental study of the thermochemical processing of lignocellulosic biomass and coals. This second edition picks up where the first edition left off in outlining new and important experimental tools and new results. The description of work on lignocellulosic biomass has been expanded to cover such vital topics as the synergistic effects between biomass components as well as the unity of reactor design for experiments on coals and biomass. New developments in experimenting with mixed streams of high-pressure steam and hydrogen have been described. The reaction stages of injectant coals into blast furnace tuyeres and raceways have been simulated at bench scale. Reactor design considerations in liquefaction have been used to help outline the sequential stages of thermal breakdown during the pyrolysis, gasification, and liquefaction of solid fuels. As ever, there is much that rides on the analytical characterization of the liquid products from these reactions. The several avenues of progress reported include the improved and more accurate use of laser-desorption mass-spectrometry as well as putting solution state ^{13}C-NMR into service for correlating the structural features and molecular masses of coal-, biomass- and petroleum-derived heavy hydrocarbons. Finally, much of the text has been rewritten to make it an easier read.

Once again, the authors would like to thank our former students and colleagues, spread over all the continents, for their collaboration and support. The hundreds of citations of their work in the text tells a story all its own.

Finally, the authors would like to reiterate our gratitude to our wives, Christine Bartle, Barbara Herod and Denise Kandiyoti, and there must also be an honourable mention for Kiriku, a beautiful calico cat who lives in Hawaii.

R. Kandiyoti and A. Herod
Imperial College London, London, United Kingdom
K. Bartle
University of Leeds, Leeds, United Kingdom
T. Morgan
Hawaii Natural Energy Institute, Honolulu, Hawaii, United States

Fossil fuels and renewables

1

Chapter Outline

1.1 Introduction: the state of energy utilisation in brief

The first 15 years of the new millennium have seen a six-fold increase in renewable energy generation. It seems to be an encouraging trend. Unfortunately, this development is dwarfed by the surge in fossil fuel consumption during the same period. In two decades, crude oil utilisation increased by nearly 32%, natural gas by 63%, and coal consumption, by a striking 78%. In terms of absolute numbers, the *total* renewable energy consumption of 316 MTOE (million ton oil equivalent) in 2014 stands a little forlorn when compared with the *increase* in two decades of nearly 4000 MTOE in the yearly consumption of fossil fuels (BP Statistical Review of World Energy, multiple years).

These developments present a dual challenge for the environmentally-conscious fuel scientist. There is a clear need to continue developing more efficient and cost-effective methods for delivering renewable energies. Meanwhile, the expanding use of fossil fuels suggests there must be no letup in attempting to devise ways of utilising fossil fuels more efficiently and in environmentally more sensitive ways.

This book focuses on progress in two specific areas of research concerning the thermochemical processing of coal and lignocellulosic biomass. The first is the development of experimental methods for exploring the mechanics of thermal the breakdown of lignocellulosic biomass and coal. We then turn to the development of methods for the analytical characterization of heavy hydrocarbon liquids, produced by the thermochemical reactions of solid fuels. Similarities of approach will enable extending the scope of this analytical work to cover the characterization of petroleum-derived heavy fractions.

The structure of the work presented below aims to explore the unifying strands between sample characterization, reactor design, and product analysis. This conceptual integration is relevant to the study of the thermochemical reactions of solid fuels in a very practical sense. Put simply, most products formed during thermal breakdown are themselves reactive. Interactions between reacting solids, tar precursors, and reactive volatiles directly affect eventual product distributions. In addition to reactor and

Solid Fuels and Heavy Hydrocarbon Liquids. DOI: http://dx.doi.org/10.1016/B978-0-08-100784-6.00001-1

sample configuration, reactor design parameters such as heating rates, carrier gas flow rates, reactant, and product-residence times and the design of quench zones, all affect the outcome of the experiment. The designer's task is, first, to identify the effect of each parameter on the outcome of the experiment and, then, to enable the measurement of the response to changes in specific reaction parameters in isolation. Just as in any other field of scientific measurement, we will aim to decouple the results of a measurement from the design of the particular experiment. We will see in Chapter 3, Pyrolysis of solid fuels: experimental design and applications, Chapter 4, High-pressure reactor design: pyrolysis, hydropyrolysis, and gasification, Chapter 5, Liquefaction: thermal breakdown in the liquid phase, Chapter 6, Elements of thermal breakdown: heating rate effects and retrogressive reactions, how attempts to distinguish between these two vital elements will lead us to a clearer picture of thermal breakdown than has been hitherto achieved. We will also present examples of bench-scale experimental work that have proved able to assist in the design and operation of pilot and plant scale equipment.

The second major strand running through this book is the development of analytical techniques for characterising liquid products released during the thermochemical reactions of solid fuels. In this type of analytical work, two distinct issues loom large. The first is the complex nature of the product mixtures, with individual chemical components only appearing in low concentrations. The second problem relates to the high molecular masses of many of the product fractions. Many of these materials do not allow analysis by the more powerful conventional methods available to the analytical chemist, such as gas chromatography coupled with mass spectroscopy, because much of the sample is too involatile to pass through the chromatographic column. The final section of this book is devoted to describing efforts to extend the ranges of some of these powerful techniques, and to the development of alternative methods for studying these larger molecular mass materials. The latter techniques range from size exclusion chromatography (SEC) and laser desorption mass spectrometry (LD-MS), to novel applications of solution state ^{13}C-nuclear magnetic resonance spectroscopy (NMR). In addition to coal- and biomass-derived products, we will show how many of these techniques may be applied to the structural characterization of heavier petroleum-derived fractions.

1.2 Lignocellulosic biomass as an alternative source of energy

In Chapter 9, In closing: the current state and new perspectives, we will attempt to calculate the amounts of arable land that would be required to raise crops for energy production. It turns out that the effort to deliver even several percent of the earth's energy requirement would lead to quite unrealistic levels of competition with food production. The parameters governing energy production from agricultural, forestry and municipal solid waste are more favourable, although several caveats are worth keeping in mind.

Compared to coal, most biomass and wastes have lower mass and energy densities. Keeping transport costs low requires working within relatively small catchment areas, which works against the economies of size. The operations of the 240 MW boiler facility in *Pietarsaari* (Finland) have been hampered by the limited availability and the seasonal character of forestry waste, which was planned to provide up to 50% of the fuel. Instead, the plant has been constrained to burn far more coal than had been originally intended. The operations of this important installation have been described, among others, by Kokko and Nylund (2005).

Moreover, the successful operation of biomass waste processing for energy production requires the convergence of several techno-economic parameters. One clear advantage of working with wastes is the 'gate fee' credit that plants receive from relevant local authorities in return for disposing of the waste. In general, process economics is enhanced by extending the role of such installations to the provision of district heating.

At present, most waste biomass processing for energy takes place in incinerators. Gasification of the waste prior to combustion provides improved cycle efficiencies. Moreover, gasifier design is generally more amenable to the installation of equipment for controlling harmful emissions. At the time of writing, however, relatively few gasifiers seem commercially available for operation on a turn-key basis. Clearly, the wider requirement is for research on plant design and development. The next few chapters will survey aspects of the thermochemical processing of lignocellulosic biomass investigated at the bench scale level, for assisting in the design and operation of larger scale plant.

1.3 Coal: a fuel for producing energy and a carbon source for making steel

There is still much that we do not know about the combustible sedimentary rock that has fuelled so much of the early industrial age. For instance, our understanding of the gelification process that transforms ancient plant debris into the vitrinite component of coals is surprisingly imprecise. Similarly, our grasp of how the solid coal matrix is held together is limited. However, mankind could not have been expected to wait until scientists had completed their studies. In the second half of the 18th century, coal was needed for burning as a source of heat and for raising steam. Early on, it was also widely used as source of carbon to reduce ore and make iron and steel.

The ancients appear to have known about the properties of coal but there is not much evidence that they made extensive use of it. Perhaps they found the smell offensive. There appear to have been banning orders against the use of coal for domestic heating and cooking as far back as the reign of Edward I (1272–1301), with the noxious fumes deemed unacceptable by the Parliament of the day (Elliott, 1981). Freese (2003) has described the impact of coal, both in terms of wealth production during the Industrial Revolution, and in terms of its impact on human health and environment pollution.

Until the relatively late use of coal in a big way, wood and charcoal had served as the fuels of choice since time immemorial. Even the gun foundries of Henry VIII were mainly fired with charcoal from the south of England, causing much deforestation. It is no accident that Sweden, with its vast supply of timber, became the next great manufacturer of guns and steel. However, as metal working techniques improved, new inventions and new technologies demanded more concentrated forms of energy. Coal was denser and gave more heat per unit weight and per unit volume. It was therefore cheaper to transport. It rapidly replaced both waterpower and wood and charcoal and contributed to the expansion of industry, mainly in northern Europe and North America. The widespread use of coal also brought massive environmental pollution. As late as the mid-1920s, air pollution in Manchester was being blamed for the failed salad crops of the working classes, whose window boxes did not receive enough sunlight because of thick smog (Report, 1924).

Meanwhile, steam engines were being improved to power trains and ships. They shrank distances and made faraway places more accessible. By the time oil was discovered in Pennsylvania in the late 1850s, coal had been king for nearly a century, occupying centre stage in an industrialising world, not just as a fuel but also as a prime source of chemicals. Advances in the chemistry of aromatic compounds were driven by, and were leading to, the production of high-value synthetic dyes, pharmaceuticals, militarily important trinitrotoluene (TNT) and a whole raft of products for everyday use. Mostly, the source of these chemicals was coal tar, but the 19th century also saw the use of ‘illumination gas’, produced by pyrolyzing coal, first for palaces and elegant households, then for city streets and finally for the common home. In any case, coal tar and gas were the sought-after products of ‘coal carbonisation’, well into the 20th century.

In the competition for markets between petroleum products and coal, the development of the internal combustion engine toward the end of the 19th century could probably be taken as a turning point. Up to that time, petroleum was being refined mostly to produce liquid fuels for lighting and heating. It did not greatly impinge on technologies geared to the use of coal. Nevertheless, even before the advent of motor cars and oil-fired marine engines, the extraction, transport and refining of petroleum had grown to become a large and lucrative businesses. However, the penetration of petroleum and its products was restricted by the geography of availability. After the United States, crude oil extraction started in a big way, first in Mexico and then in Venezuela. In Asia, Shell struck oil in Sumatra in the 1880s, whilst Baku and hapless Grozny emerged as the early sources of petroleum in the Russian Empire. By 1914, production volumes in Burma, Iran, and India had not caught up with the volumes coming from the Americas. Only Russia could claim a comparable share of world production whilst Europe, the industrial continent, had no oil to speak of. Coal, on the other hand, could be mined on all continents and, at the time, in much greater quantities than oil.

World War I changed all that. By the 1920s, the industrialized world, both in and out of uniform, had become addicted to the use of the internal combustion engine, for transport, for flying machines, and, not least, for fighting machines: the tank and the armoured car. By then, oil companies were shifting massive quantities of crude oil

from one end of the globe to the other, and the relegation of coal to second place was nearly completed. In the lead up to, and indeed in the aftermath of World War II, coal carbonisation could simply not produce the quantities of chemical feedstocks required to satisfy demand. Always hungry for cheap, abundant raw materials, the industrialized world turned to, and eventually became entirely dependent on, petroleum-derived fuels and chemicals and eventually on natural gas.

When it comes to considering the post–World War II rush to gas, however, a feeling of déjà vu seems inevitable. In fact, the urban environment had been familiar with the use of gas for domestic illumination, heating, and cooking for nearly two centuries. The city of Baltimore, Maryland was the first conurbation to enjoy the use of gas for lighting in residences, streets and businesses (1816). Soon, gas plants were being constructed by small groups of local entrepreneurs in increasing numbers of towns and cities. They mainly used standard gas works kits built in New York City and shipped west by all means available. In the latter half of the 19th and early part of the 20th century, gas works spread to towns and cities the world over. It has been estimated that in the United States alone, some 52,000 local gas plants were built over the period in most towns of 10,000 or more residents (Hatheway, http://hatheway.net/01_history.htm).

Usually fuelled with coal, these gas plants were almost invariably heavily polluting installations. Some of the by-products of these processes, such as tars and effluent gases containing aromatic compounds are today considered as highly toxic. But, that is not why they eventually disappeared. In the United States, the Federal Government had invested heavily during World War II to construct oil pipelines connecting the Texas oil fields to the Eastern Seaboard. At the end of the war, these lines were bought by the natural gas industry and converted for gas transmission. Coupled with discoveries of large gas fields in Texas and Louisiana, it spelled the end for manufactured gas. In Western and Northern Europe, a similar trend was repeated, with the tapping of North Sea gas and the arrival of piped gas from North Africa and the Soviet Union. The switch to natural gas was mostly completed in the late 1960s and early 1970s.

1.4 Fossil fuels: some general trends

Coal utilisation is rightly perceived as a source of pollution. In the industrialized world, whenever possible, it is replaced by either petroleum-derived fuels or natural gas, nuclear power or renewable energy. However, during the past several decades, newly emerging industrial powers have, in their turn, relied on coal to power their development. China's vision involves stabilizing yearly coal consumption at about 4 billion tons by the year 2030.

The rush to coal by industrializing countries has always come at heavy costs in terms of environmental pollution and damage to human health. However, there is still a hard backbone of coal consumption in already industrialized countries that is unlikely to disappear quickly. In the United States, the 1990s saw a 10% upward drift in consumption, which stabilized toward the end of the decade at a little over 1 billion

tons pa (US DoE, 2002), mainly for use in power generation. In the second decade of the new millennium, however, with cheap shale gas from 'fracking' swamping the market, North American coal has given way to natural gas, only to resurface as cheap coal imports into European power plants.

The other large consumer of quality coals is the metallurgical coke industry. The latter is a notoriously dirty and costly process, but blast-furnace technology is still today the conventional route for making iron and steel, and iron-makers consume large quantities of coke.

Many observers have suggested that petroleum will probably run out in the next 30 years or so. In fact, doomsday scenarios about depletion have been common in the oil industry since the end of the 19th century. There is no evidence that we will run out soon; however, there is plenty of evidence showing that oil exploration is increasingly turning to more difficult terrains, from the Alaska 'North Slope' to the Sakhalin offshore and the permafrost of Yakutsk in North Eastern Siberia. During the surge in crude prices, producers also moved toward processing progressively heavier crudes and exploiting increasingly unorthodox sources of hydrocarbons that were more expensive to process. These include the large reserves of tar sands and bitumens in the Americas; they would not be expected to do well in the current low price environment.

The surge in natural gas production and the expanding worldwide trade in piped gas and LNG have been reviewed elsewhere (Kandiyoti, 2012, 2015). At the time of writing, producers appear stranded between rapidly increasing supplies and stagnating demand, leading to depressed prices, much as in the crude oil industry.

We may also note in passing that the apparently unstoppable rise in fossil fuel utilisation has been taking place alongside raging debates about climate change, CO_2 capture, and sequestration as well as the amazing notion of using hydrogen as a primary fuel. These two tracks seem to be running in parallel to one another, with seemingly no working mechanism to provide a link between them.

1.5 Outline: what's in this book?

Coal characterization is a narrowly specialized art. Most industrial consumers of coal have developed methods relevant to their particular technological needs. Coke-makers determine the swelling and agglomeration properties of coals and coal blends. Vitrinite reflectance measurements and scanning electron microscopy of polished test samples are also used in helping to compose feedstock blends. Operators of coal-fired power stations have entirely different perspectives. Flame stability, char reactivity, slagging and fouling are some of their main concerns. Pf-grade coal injection and combustion is also relevant to blast furnace operations, where 'injectant' coals are used to generate part of the heat required in the blast furnace; this helps to reduce the direct combustion of some of their expensive coke. A number of standard – and several novel – tests give good estimates of volatile release and char reactivity to help select feedstocks. Meanwhile, the chemistry of slagging and fouling of coal ash is a science and an art on its own, where high temperature viscometry, x-ray diffraction,

infrared spectroscopy and scanning electron microscopy serve as some of the primary tools.

The much-invoked hike in oil prices of the 1970s stimulated an enormous volume of research. The drive to uncover chemical routes to liquid fuels from coal reawakened interest in some of the processes left over from World War II and others developed since 1945. The new needs were addressed by quantum leaps in analytical sophistication. Every new technique was enthusiastically turned to examining 'the structure of coal' and its products. Every analytical technique offered a distinct perspective. None was able to tell the whole story, not unlike so many blind men examining the proverbial elephant.

In fact, the examination of coal structure is a static concept. Somewhat less frequently, available tools have been deployed to study *processes* taking place during the thermal and other transformations of coals. Throughout this book, we will attempt to shift the focus of the discourse a little toward thermal transformations and to enquire whether the course of these transformations may tell us something more of the nature and structure of coals and of biomass. Risking the reuse of the well-worn metaphor, we will attempt to improve our knowledge by disturbing the elephant and observing how it runs. It is bound to be a bumpy ride.

Two omissions: Relatively little attention has been paid in this book to two important aspects of fuel science. First, combustion-related aspects have been left to one side in order to concentrate on aspects more directly relevant to fuel characterization and thermal breakdown. The other major omission concerns the kinetic modelling of processes involved in pyrolysis, gasification and liquefaction. It seems clear that such models come into their own when an existing knowledge base about the processes involved is relatively sound. One such model has been developed for coal liquefaction (see chapter: Liquefaction: thermal breakdown in the liquid phase). It distinguishes between dissolution and mass transfer related processes taking place at low temperatures from processes involving covalent bond scission, leading to the dissolution of much of the coal mass at higher temperatures. The two stages present significantly different energies of activation. The model also takes account of mass loss *during heatup* to the peak experimental temperature. The assumptions underlying the model were based on observations from a (then) novel 'flowing-solvent' reactor, developed in-house and described in the same chapter.

In Chapter 2, Solid fuels: origins and characterization, we present a brief review of the origins of solid fuels and methods for their characterization. Much of what we know about this subject is generally available in the literature. We will also briefly visit several recent reviews on the structures of lignocellulosic biomass. The brief overview on the origins of fossil fuels presented in Chapter 2, Solid fuels: origins and characterization, might assist the general reader. We will briefly trace the evolution of coal and oil formation and discuss the links between coals and kerogen macerals through terrestrial and marine organic debris.

Chapter 3, Pyrolysis of solid fuels: experimental design and applications, Chapter 4, High-pressure reactor design: pyrolysis, hydropyrolysis and gasification, Chapter 5, Liquefaction: thermal breakdown in the liquid phase, Chapter 6, Elements of thermal breakdown: heating rate effects and retrogressive reactions, will focus on

experimental reactors, developed for determining the thermochemical behaviour of solid fuels. As in any other area of study, the quality of data from these experiments depends largely on experiment design. One major strand running through this book will be a critique of laboratory-based techniques, developed for characterising the thermochemical reactions of solid fuels and how these designs relate to the actual process conditions they are meant to simulate. The second major strand running through these chapters will be a focus on the pathways of thermal breakdown. We will examine elementary processes common to pyrolysis and liquefaction and contrast outcomes of experiments, with close attention paid to the influence of reactor design.

Chapter 4, High-pressure reactor design: pyrolysis, hydropyrolysis and gasification, will focus on high-pressure pyrolysis, hydropyrolysis and hydrogasification experiments, as well as gasification-reactivity determinations in CO_2, steam-air and steam-oxygen environments. The reactors described in this chapter have been used to generate data in support of the design and operation of several types of pilot plants. Some examples will be presented as case studies.

Most bench-scale liquefaction experiments are performed in batch reactors, where extracts released from the sample remain within the reaction zone until the termination of the experiment. Opportunities thus exist for products and reactants to mingle and react freely. It is often difficult to deduce the sequence of reactions of the original sample from the reaction mixture that is eventually recovered. Chapter 5, Liquefaction: thermal breakdown in the liquid phase, will describe the configuration of, and results from, a liquefaction reactor conceived for decoupling the outcome of a coal liquefaction experiment from the design of the apparatus. Information gleaned from comparing results from this 'flowing-solvent' reactor and a conventional batch reactor was found useful in reviewing the successive stages of the thermal breakdown process.

Chapter 6, Elements of thermal breakdown: heating rate effects and retrogressive reactions, will present an attempt to unify observations made on the thermal breakdown mechanisms of coal by juxtaposing results from pyrolysis and liquefaction experiments. The data was reviewed with the aid of results from earlier experiments using electron-spin-resonance spectroscopy. Reference will be made to the way reaction conditions during thermal breakdown affect the course of subsequent coking, gasification and combustion-related processes.

Chapter 7, Analytical techniques for low mass materials: method development, and Chapter 8, Analytical techniques for high-mass materials: method development, will focus on aspects relating to the analytical characterization of liquid products derived from the reactions of coal and biomass materials and the fractionation of petroleum-derived liquids. In Chapter 7, Analytical techniques for low mass materials: method development, we review established techniques as well as recent method developments intended for investigating the relatively smaller molecular mass materials in the mass range below about 500 u.

Not all fossil fuel and biomass-derived materials evaporate (even) under vacuum or, for that matter, pass through a chromatographic column at elevated temperatures. There are no exact methods for determining the molecular mass distributions or for identifying the structural features of these larger molecular mass materials.

We are no longer able to talk of *analysing* samples, but focus on *characterising* them. Chapter 8, Analytical techniques for high-mass materials: method development, will present a discussion of methods developed for assessing the molecular mass distributions of coal-, biomass- and petroleum-derived liquids and methods available for their structural characterization. These include size exclusion chromatography (SEC) and several mass spectrometric methods where ionisation is thought to occur before analyte molecules desorb/evaporate from the sample matrix. Fractionation methods and results from bulk characterization techniques such as NMR and FT-IR spectroscopy will be described. The work is relevant to situations ranging from the modelling of volatile combustion rates in pf-combustors, to the evaluation and upgrading of heavy tars and petroleum residues.

We will attempt to pull together these diverse strands in a short concluding Chapter 9, In closing: the current state and new perspectives. Where possible, we will place matters in the context of work performed and ideas developed in the wider scientific community. Inevitably, however, we will rely heavily on work done in laboratories at Imperial College and at the University of Leeds. This is because the conceptual framework of this book reflects the ideas that have guided our own experiments, spanning over three decades of research.

References

BP Statistical Review of World Energy (1993; 2000; 2005; 2014; 2015) <http://www.bp.com/en/global/corporate/energy-economics/statistical-review-of-world-energy.html>.

Elliott, M.A. (Ed.), 1981. Chemistry of Coal Utilization, 2nd Supplementary Volume. John Wiley & Sons, NY.

Freese, B., 2003. Coal, A Human History. Perseus Publishing, Cambridge, MA.

Hatheway, A.W., (2008) History and chronology of manufactured gas, FMGP. <http://hatheway.net/01_history.htm>. (Accessed on 21 July 2016).

IEA (2005) Energy Statistics of OECD Countries 2002-2003, OECD/IEA, Paris. IP Information Service (1987), Institute of Petroleum, 61 New Cavendish Street, London W1M 8AR, UK.

Kandiyoti, R., 2012. Pipelines: Oil Flows and Crude Politics. IB Tauris, London.

Kandiyoti, R., 2015. Powering Europe: Russia, Ukraine, and the Energy Squeeze. Palgrave Macmillan Palgrave Pivot, New York, NY.

Kokko, A., Nylund, M. (2005) 18th International Conference on Fluidized Bed Combustion, May 22-25, 2005, Toronto, ON; FBC2005-78035.

Report, 1924. Report of the Smoke Abatement Conference November 4-6, 1924. Town Hall, Manchester 147.

US DoE (2002) International Energy Annual 2002. <http://www.eia.doe.gov/emeu/iea/table14.html>.

Solid fuels: origins and characterization

2

Chapter Outline

This chapter presents a brief introduction to the origins and compositions of lignocellulosic biomass materials and coals. The aim is to provide a preliminary framework for subsequent chapters focusing on the thermochemical reactions of biomass and coals. The basic outline provided below has been supplemented with references to some of the wide selection of available reviews.

2.1 The structure and composition of lignocellulosic biomass – in brief

The structures and compositions of the vast array of available biomass materials and biomass characterization methods have been reviewed in considerable detail (e.g., see Mettler et al., 2012; Vassilev et al., 2010, 2012). Of the many types of biomass materials, the discussion in this book will focus on the thermochemical reactions of wood and woody biomass as well as agricultural and forestry wastes. Reference will also be made to the thermal processing of tropical and semitropical feedstocks (Cui et al., 2012).

Lignocellulosic biomass materials are made up mainly of cellulose, hemi-celluloses and lignins in variable proportions, together with relatively small amounts of organic extractables and inorganic 'mineral matter'. Vassilev et al. (2012) have classified large numbers of samples according to the relative abundance of cellulose, hemi-celluloses and lignins. The average cellulose content in their selection of samples was about 40%, with 35% hemi-celluloses and 25% lignin, although relative abundances varied widely between particular samples. Prominent among the outliers was wood

Solid Fuels and Heavy Hydrocarbon Liquids. DOI: http://dx.doi.org/10.1016/B978-0-08-100784-6.00002-3

bark with nearly 45% lignin, while many familiar wood varieties presented lignin contents in the 22–26% range.

In the next several chapters, we aim to explore the fundamentals of thermal breakdown in both biomass and coals. Biomass generally contains less carbon, mostly in the 45–55% range, somewhat higher hydrogen contents (5.8–6.2%) and are characterised by far high higher oxygen contents, generally in the 35–45% range (Vassilev et al., 2010). Typical nitrogen contents are usually below 0.5%. Sulphur contents are also generally low, of the order of 0.1%. The far higher oxygen contents of lignocellulosic biomass make these materials more reactive than coals. The onset of thermal breakdown in biomass generally takes place at about 100–120°C below the characteristic temperatures for most coals. Furthermore, pyrolytic tars/oils largely reflect the compositions of the original substrates, and biomass tars/oils turn out to be more highly oxygenated, far more reactive and unstable during storage. The greater reactivity of biomass materials and their primary pyrolysis products requires particular attention to reactor design, in order to distinguish between the thermal response of the samples and reactor related effects (Morgan and Kandiyoti, 2014).

Despite significant differences between the structures, compositions and thermal behaviour of coals and biomass, their responses to thermochemical reaction parameters reveal remarkably similar trends. Both tar/oil and total volatile yields are observed to increase with increasing heating rate, leaving less char residue, compared to slow heating. Similarly, many coals and some biomass samples have been observed to soften and display plastic behaviour when heated at high heating rates, suggesting analogous, if not similar, pathways regarding the mechanics of coal and biomass pyrolysis. Technologies proposed for commercialising the fast pyrolysis of biomass (Mohan et al., 2006; Brownsort, 2009; IEA, 2014, 2015) and the related operations involved in drying and grinding have been reviewed (e.g., see Klass, 1998).

2.2 Precursors and formation of coals

In sifting through published works on the formation of coals and their macerals, first mention would go to *Stach's Textbook of Coal Petrology* (Stach et al., 1982) and two Supplementary Volumes of *The Chemistry of Coal Utilisation* (Lowry, 1963; Elliott, 1981). *Coal* by van Krevelen (1993) provided a review of available methods at the time, for examining the composition of coals. The work of Given (1984) and of Speight (1994) are well worth revisiting for background information on coals.

The origin of coals: Most coals consist of derivatives of lignin, cellulose, hemicelluloses, tannins and seeds from plants, transformed by changes of temperature and pressure in the earth's crust over long periods (see also Chapter 2 in Francis, 1961; Mukhopadhyay, 1994). Coal may also be considered as a sedimentary rock, formed, in the main, from plant debris, which was biotically converted to peat and then subjected to metamorphic geological changes during burial. The widely accepted view is that typical Northern Hemisphere coals were formed from peats deposited in swamps and marshes, under predominantly anaerobic and at least partly reducing conditions. After deposition, the plant material was covered by sediment or more plant-derived

matter. Some aquatic cover is thought to have been necessary to preserve organic deposits from destruction by oxidation and aerobic bacterial action. With subsidence leading to compaction, the pressures on the deposits increase and temperatures rise with increasing depths of burial. The burial conditions of peat (temperature, pressure and time period under different conditions) have a marked influence on the degree of metamorphic change, which we call coalification. The severity of these conditions determines the so-called 'rank' (see Section 2.3.4) of the resulting coal.

Peat→lignite, or brown coal→subbituminous coal→bituminous coal→anthracite

Broadly, changes in elemental composition as a function of coalification follow the pattern shown in Table 2.1. The trends are dominated by oxygen loss and increasing aromatisation during maturation and eventual coalification.

The transformation of larger deposits of terrestrial plants gives rise to humic coals. Sapropels are coals formed from algae, fungal spores, pollen and marine biota in shallow marine and lake environments; they differ from humic coals particularly in their higher content of hydrogen. A detailed discussion of plant remains as fossils in coals has been given by Francis (1961). Such coals sometimes contain fossilised but well-preserved botanical remains including leaves, woody structures and pollen (Given, 1988). The type of original plant precursors govern the maceral composition of coals (see Section 2.3) and the degree of change leads to the observed variation in coal rank (see Section 2.3.4). The progression in the degree of coalification, termed the 'rank' of a coal, correlates well with increasing organic carbon contents and with the ability of the vitrinite component to reflect light under the microscope. The proportion of oxygen (as high as 40–45% in live plant material) is reduced with maturation. Following the 'bituminisation' stage, the proportion of aromatic carbon and the degree of cross-linking in bituminous coals increase with rank, thus eventually reversing the depolymerisation process associated with the maturation of biomass. Hydrogen contents show less pronounced but definite downward trends in middle rank coals, usually above 85–86% elemental carbon content.

Table 2.1 Elemental composition of coals[a]

Coal rank	Carbon	Hydrogen	Oxygen
	% w/w. dry ash free		
Peat	58	6	35
Lignite	71	5	23
Subbituminous	75	5	16
Bituminous			
High-volatile	81	6	10
Low-volatile	88	4	4
Anthracite	94	3	2

Source: Data taken from Kershaw, J.R., 1989. In: Kershaw, J.R. (Ed.), Spectroscopic Analysis of Coal Liquids. p. 1. Elsevier, Amsterdam. (Kershaw, 1989).
[a]Representative values, excluding nitrogen and sulphur content, which show little rank dependence.

2.3 Coal macerals and petrography

2.3.1 Coal macerals

'Macerals' are the organic components of coals, defined in terms of their morphologies, as observed by optical microscopy. Broadly, these morphological features correspond to the structures of original plant material deposited in peat bogs. With maturation, the properties of the different biomasses tend to converge toward nearly similar values. Each principal maceral group (vitrinites, liptinites and inertinites) includes arrays of macerals classified in subgroups. The level of possible detail is comparable with the variety and state of fossilised plant material in the original deposit (Stach et al., 1982; van Krevelen, 1993). Table 2.2 presents a list of the more frequently occurring maceral types, alongside their plant precursors. Density-gradient centrifugation has allowed good separations of the main maceral groups, as well as individual maceral types including cutinites, resinites, sporinites, fusinites and semifusinites (Crelling and Bensley, 1995).

Table 2.2 Classification of coal macerals

Material group	Maceral	Precursor
Vitrinite[a]	Telnite	Cell walls
(humite in brown coals)	Collinite	Wood, bark and cortical tissue
	Vitrodetrinite	Vitrinite fragments
Liptinite (Formerly exinite)	Alginite	Algal remains
	Cutinite	Cuticle
	Resinite	Resins, oils, fats and waxes
	Sporinite	Spores, pollen
	Suberinite	Walls of cork tissue
	Bituminite	Altered algal and humic materials
	Exsudatinite	Secondary 'resinite'
	Fluorinite	Fluorescing secondary 'resinite'
	Liptodetrinite	Fragments of other 'liptinite'
Inertinite	Fusinite	Well-preserved 'carbonised' woody tissue
	Semifusinite	Cellular 'carbonised' woody tissue
	Macrinite	Unspecified detrital matter (10–100 μm)
	Micrinite	Unspecified detrital matter (<10 μm)
	Sclerotinite	Fungal tissue and spores
	Inertodetrinite	Fragments less than one cell

Source: Reproduced from Hutton, A.C., 1995. Composition, geochemistry and conversion of oil shales. In: Snape, C.E. (Ed.) NATO ASI Series C, vol. 455. Kluwer, Dordrecht, p. 125 (Hutton, 1995). Copyright 1995 Kluwer Academic Publishers, with permission of Springer.

[a]Macerals originating from the Gondwanaland supercontinent are classified differently.

In general, vitrinites show evidence of woody and possibly also of root tissue as starting material. In Northern Hemisphere coals, vitrinites usually represent a large proportion of the coal mass (between ~60% and 90%). When heated, the vitrinite component softens ('melts'). Good coking coals also swell to impart the desired agglomerating properties to the overall mass. Liptinites usually make up less than 20% of the coal mass. They contain the more aliphatic fossilised components, chiefly sporinites (spores and pollen), cutinites (cuticles, waxes), resinites (fossil resins) and the highly paraffinic alginites (Stach et al., 1982; van Krevelen, 1993). Liptinites also contain relatively higher proportions of elemental-H (up to ~8%, dmmf) and, compared to other macerals, release the largest proportions of volatile matter during pyrolysis. Most liptinites readily melt on heating but do not normally swell.

Inertinites are so-named because, mostly, they do not soften or swell during coking, although there are many exceptions. They usually contain higher proportions of elemental-C and lower proportions of elemental-H compared to vitrinites and liptinites. Inertinites usually make up less than 20% of the coal mass in many Northern Hemisphere coals. A little surprisingly, some good coking coals (e.g., Cortonwood Silkstone, UK) contain nearly 40% inertinites. Within this maceral group, fusinites and semifusinites also show fossilised woody structure, but contain less hydrogen and more carbon than vitrinites (e.g., cf. Parks, 1963). Densities also increase from liptinites through vitrinites to inertinites, from about 1.15 to about 1.45. Although individual macerals may be separated from ground coals by hand picking, less laborious procedures make use of the difference in the densities of the maceral groups: liptinite, 1.20–1.25; vitrinite, 1.30–1.35 and inertinite 1.40–1.45. Float-sink methods employ liquids, with densities in the range 1.2–1.5 g mL^{-1}, which may be organic solvents or aqueous salt solutions. Centrifugation is used to make the separation more rapid, and continuous centrifugation methods have been developed.

A considerable advance was the development of a density-gradient maceral separation method by Dyrkacz and Horwitz (1982). For samples of higher rank, say, above ~87% C, microscopic and other physical differences diminish and distinct macerals become more difficult to detect and separations more difficult to achieve. The reader will find a wealth of information relating to the formation, morphology and geochemistry of coal macerals in the classic *Stach's Textbook* (Stach et al., 1982) and in Given (1984).

2.3.2 Coal petrography

Coal petrography is the study of the organic constituents of sedimentary rocks, originally, by optical microscopy of thin sections (transmitted light) or of polished blocks (reflected light) (Unsworth et al., 1991). Coal macerals have different colours and fluorescence intensities and can be identified under the microscope. Fluorescence microscopy is used to complement the more traditional approaches, since all three major maceral groups may be recognised by this technique. Vitrinites show up as light grey or grey and fluoresce weakly, while liptinites show up as dark grey and fluoresce

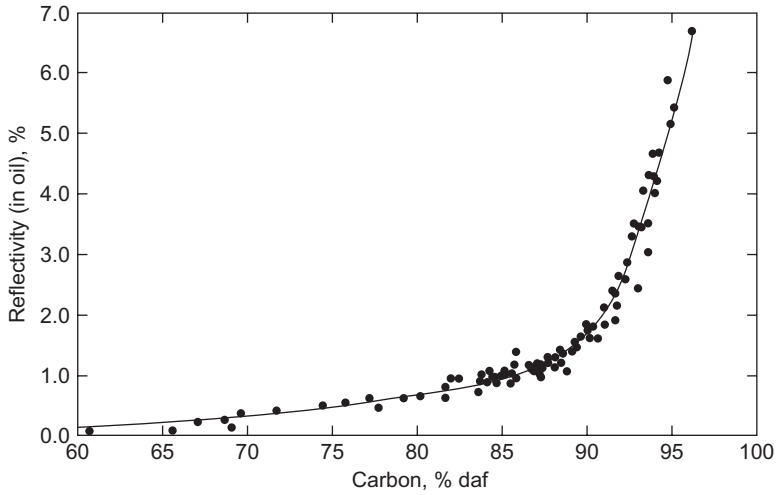

Figure 2.1 Dependence of vitrinite reflectance on coal rank (percent carbon).
Source: Reprinted from Berkowitz, N.N., 1997. Fossil Hydrocarbons: Chemistry and Technology. Academic Press, San Diego (Berkowitz, 1997). Copyright 1997, with permission from Elsevier.

more intensely. They also reflect light less intensely than vitrinites. Inertinites show up as light grey or white; they reflect light more strongly than vitrinites but fluoresce less intensely than other macerals. The reflectance of individual coal macerals also increases with coal rank and there is a close relation between vitrinite reflectance and the carbon content of the parent coals (Fig. 2.1).

A petrographic examination of a coal would normally involve first the optical microscopy of a polished surface with reflected white light to allow identification of vitrinite and inertinite group macerals, and by fluorescence to identify the liptinite group. This is usually followed by the measurement of the vitrinite reflectance, as the accepted indicator of coal rank. Automated procedures are available for determining the volumetric abundance of the macerals (Hutton, 1995).

2.3.3 Characteristics of coal macerals

Conveniently, the microscopically identifiable morphological features of macerals correlate reasonably well with trends in measured chemical properties (e.g., elemental composition; aliphatic/aromatic content) and observed pyrolytic behaviour. For macerals of comparable maturity, infrared and NMR spectroscopy show a progression in aromatic carbon content ('aromaticity'), from low values for liptinites (~0.4) to higher values for vitrinites and highest for inertinites (up to ~0.9).

The maceral distribution in a coal is heterogeneous, with individual domains varying from 1 µm to 1 mm (Fig. 2.1). Maceral compositions are reflected in their morphologies and behaviour during thermochemical reactions (Given and Dyrkacz,

1988). For any given rank of coal, the elemental composition of maceral groups would be expected to change as follows:

Carbon content:	inertinite > liptinite ≈ vitrinite
Hydrogen content:	liptinite > vitrinite > inertinite
Oxygen content:	vitrinite > inertinite > liptinite
Sulphur content:	liptinite > vitrinite > inertinite

H/C ratios increase in the order inertinite < vitrinite < liptinite. The f_a value (aromaticity) follows the reverse sequence to H/C ratios, increasing from liptinites to vitrinites and to inertinites (Botto, 1987). Information concerning values of f_a within a maceral group is scarcer, but among liptinites, resinites and alginites have much lower aromaticity than sporinites. Within the inertinite group, fusinite has a higher f_a value than micrinite. While maceral aromaticity remains the most commonly reported structural parameter, further NMR peak discrimination suggests (Kasueschke et al., 1989) that the fraction of nonprotonated aromatic carbon increases in the order liptinite < vitrinite < inertinite, and the fraction of protonated aromatic carbon remains approximately constant. Aliphatic CH and CH_2 carbon decrease in the order liptinite > vitrinite > inertinite, but CH_3 in aliphatic structures is unchanged between macerals. FT-IR data for maceral concentrates from French coals have been interpreted (Unsworth et al., 1991) to make detailed assessments of the relative importance of a wide variety of structural elements in the three maceral groups. Consistent with trends in H/C ratio and aromaticity for the principal maceral groups, volatile matter release during pyrolysis normally decreases in the sequence liptinite > vitrinite > inertinite.

Southern Hemisphere coals are believed to originate from the Gondwanaland supercontinent and to have been deposited in subarctic conditions, whereas many of the Northern Hemisphere Carboniferous coals are thought to have been deposited in warmer climates, during ages when the deposition sites were nearer the equator (Stach et al., 1982; van Krevelen, 1993). The petrographic compositions of Gondwana coals vary more widely than Carboniferous coals of the Northern Hemisphere. Vitrinite contents rarely exceed 80% and occurrences of less than 50% have been observed. Contents of liptinite group macerals are seldom greater than several percent, whilst inertinite concentrations can be unusually high. By contrast, Northern Hemisphere carboniferous coals usually contain more than 70% vitrinites, and less than 20% of inertinites; 5–10% liptinites are not unusual.

The concentrations of semifusinites in Gondwana coals have been found to change in parallel with two other inertinite group macerals (macrinite and inertodetrinite). This suggests a different route for their formation than forest fires, as has been proposed for the fusinites and semifusinites of Northern Hemisphere coals. Instead, the high inertinite contents of Gondwana coals have been explained in terms of relatively dry conditions during coalification, with greater extents of peat oxidation. These semifusinites are thought to have formed via the alteration of vitrinites by bacterial and fungal action under mildly oxidising conditions, rather than charring during vigorous oxidation (van Krevelen, 1993). Some of these ‘semifusinites’ are reported to be more reactive during coking and liquefaction, compared with macerals of similar

morphology (i.e., semifusinites) in Northern Hemisphere coals. We will present data on the thermochemical reactions of Southern Hemisphere coals and their maceral concentrates in Section 3.7.

2.3.4 Coal rank

Coalification of precursors is brought about by the influence of pressure, temperature and time during burial. The rank of a coal indicates its degree of maturity, i.e., the extent to which metamorphic transformations have taken place. Increasing depth of burial and volcanic or folding disturbances within the strata bring about increasing temperature and pressure leading to accelerated maturation of the deposits, and to increasing rank.

A number of classification systems for the determination of coal rank were originally devised on the basis of technologically important parameters: volatile matter (or 'fixed carbon') content, calorific value and behaviour during pyrolysis (coke type, swelling or agglomeration properties). The National Coal Board (United Kingdom) classification system specifies numerical codes for coal rank. Its usefulness is restricted, however, by its applicability to UK Carboniferous period coals only. Other, more widely applicable, coal rank classification systems are the ASTM (USA) and the United Nations/European Economic Community (UN/ECE) systems, both based on volatile matter and calorific value. The latter system also specifies numerical codes. A corresponding system, which extends the UN/ECE system, has also been proposed for Southern Hemisphere coals.

Some of these properties could be determined from the elemental composition, but this, and the other properties above are averages, depending not only on coal rank, but also on maceral composition. It is necessary, therefore, to determine rank from a single rank-related property that is measured for a simple maceral group in the coal. Optical reflectance is related to the coal carbon content, and hence to the coal aromaticity (see Section 2.4). The percent random reflectance (R_o) of the vitrinite domains in a polished coal sample, determined by an automated procedure is, therefore, a suitable estimate of coal rank. A petrographic system based on vitrinite reflectance appropriate to vitrinite rich coals is shown in Table 2.3, along with the equivalent classes in the ASTM and international (UN/ECE) systems.

2.3.5 Variation of coal properties with rank

Many of the coal chemical properties change with rank. The trend of diminishing oxygen contents with increasing maturity is clear from Table 2.1. Another trend, which has an important bearing on the variation of coal reactivity with rank is the increase in aromaticity ($f_a=C_{ar}/C$), which is the fraction of the total carbon in aromatic rings (Miknis, 1995). Quantitative NMR of carbonaceous solids is made difficult by the low abundance (1.1%) of the magnetic ^{13}C isotope, and the consequent necessity of transferring magnetisation from the abundant ^{1}H nucleus. Values of f_a determined in this way clearly increase with rank (Fig. 2.2) but there is considerable scatter in

Table 2.3 A petrographic system for describing coal rank[a]

Coal class	Percent vitrinite reflectance	Percent carbon content of vitrinite[b]	Equivalent classes	
			ASTM	UNIECE
Lignite	≤0.40	<75	Lignite A Lignite B	12–15
Subbituminous	0.41–0.50	75–80	Subbituminous A, B, C	10–11
Low-rank bituminous	0.51–1.00	80–85	High-volatile Bituminous A, B, C	6–9
Medium-rank bituminous	1.01–1.50	85–89	Medium-rank Bituminous	4–5
High-rank bituminous	1.51–2.00	89–91	Low-volatile Bituminous	3
Semianthracite	2.01–2.50	91–93	Semianthracite	2
Anthracite	>2.50	>93	Anthracite	0–1

[a]Data taken from Unsworth, I.E., Barrett, D.J., Roberts, P.T., 1991. Coal Quality and Combustion Performance, Elsevier, Amsterdam (Unsworth et al. 1991).
[b]Approximate. Dry mineral matter free basis.

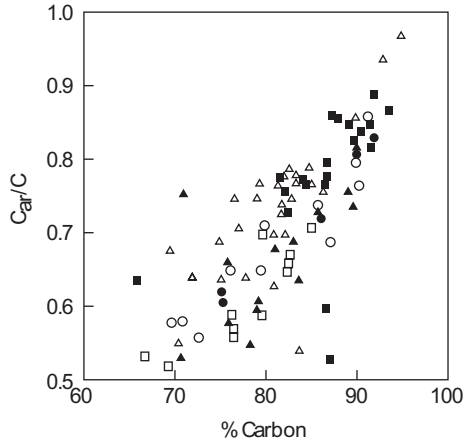

Figure 2.2 Variation of aromatic carbon with coal rank (percent carbon). (○) Furimsky and Ripmeester (1983); (●) Sfihi et al., (1986); (△) Gerstein et al. (1982); (▲) Russel et al. (1983); (□) Dereppe et al. (1983); (■) Pugmire et al. (1983)
Source: Reprinted from Sfihi, H., Quinton, M.F., Legard, M.F., Pregermain, S., Carson, D., Chiche, P. (1986) Fuel, 65, 1006 (Sfihi et al., 1986). Copyright 1986, with permission from Elsevier.

the data. The reliability of f_a values determined by NMR has been the subject of a 'debate in print' (Snape et al., 1989). It was concluded that measured aromaticity may be underestimating the aromatic content by up to 15%. The best 'recipe' for reliable f_a values was to work at low spinning speeds and with single pulse excitation (Love et al., 1993). Radical quenching with SmI_2, e.g., was also found useful.

Carbon functionality in coals can also be determined by Fourier-transform infra-red (FT-IR) spectroscopy (Fredericks, 1989), although spectral deconvolution methods are generally necessary. Absorptions attributed to aromatic C–H bending are particularly useful as indicators of changes in aromatic substitution patterns with rank. FT-IR has also been used to estimate CH_2 in long aliphatic chains, and heteroatom functionality such as hydroxyl, ether and carbonyl groups.

2.4 The chemical composition of coals

The problem of structure has been approached by analysing high yield extracts of coals. Thus statistical structural analysis of coal-extract asphaltenes suggests the presence of linked small (1–4 ring) aromatic clusters in asphaltenes, with a variety of alkyl substituents (Bartle, 1988). The actual presence of linked 2–4 ring aromatic structures has been confirmed by electrochemical analysis (Tytko et al., 1987). However, cross-linked macromolecular material comprises the major organic constituent of most coals, and has been investigated as such by a wide variety of methods, including oxidation, pyrolytic methods coupled GC and GC-MS analysis of products. Both NMR and IR spectroscopy show the presence of small alkyl and naphthenic groups, in agreement with ruthenium VIII oxidation (Tse and Stock, 1983). Products of oxidation by sodium dichromate (Hayatsu et al., 1975) are 1–4 ring aromatic and heteroaromatic carboxylic acids, in agreement with findings from NMR. A comparison of products from different coals suggests greater contributions from larger ring systems with increasing coal rank, consistent with solid-state NMR-derived aromaticities (Section 2.3.5) and with findings from Py-GC-MS. It is significant that these are just the aromatic clusters both identified directly in low-MM fractions of coal extracts and also indicated by statistical structural analysis and electrochemical analysis by differential-pulse voltammetry as being linked together in higher-MM fractions. It may be concluded that the predominant organic matter present in coal comprises molecules of varying MM, but with similar basic structural types: alkyl and naphthenic-substituted small aromatic clusters. In these analyses, much of the larger molecular mass material remains undetected, however.

Many aspects of the reactivity of coals in thermal processes are thought to arise from the presence of hydroaromatic structures in the coal. As long ago as 1963, Ladner and Stacey (1963) inferred from broad-line ^1H NMR spectra the presence of hydroaromatics in liptinites and vitrinites; however, their direct determination by modern ^{13}C NMR has proved difficult, although changes in NMR-determined average structural parameters of pyrolysis chars have been cited (Fletcher et al., 1990) as evidence of the presence of hydroaromatics in the original coals. The results of hydrogen-transfer reactions with 9-fluorenone (Choi and Stock, 1984), e.g., also show

that such structures are responsible, at least in part, for the differing reactivities of coal macerals: liptinite (especially sporinite and cutinite) > vitrinite > inertinite.

The heteroatom-containing functional groups in coal play a vital role in its structure and reactions. Oxygen, mainly present as phenolic hydroxyl and, especially in low-rank coals as carboxyl groups has been extensively characterised by wet chemistry and by IR spectroscopy. Ether groups, especially in furan rings in benzofuran and dibenzofuran structures, are significant contributors to oxidation products, and are also present in pyrolysis and liquefaction products. Nitrogen is present in (mainly pyridine and its benzologues) bases, which may be extracted by acids, but secondary, pyrrole, nitrogen is also present as shown by the indoles and carbazoles identified in pyrolysis products. X-ray photoelectron spectroscopy (XPS) allows ready and quantitative differentiation of pyridine and pyrrole nitrogen in solid coals and a clear rank dependence is evident in their relative concentrations (Wallace et al., 1989).

A variety of techniques has been used to speciate sulphur in coal – vital information given the importance of this element in emissions and processing chemistry (Markuszewski and Wheelock, 1990; IEA Coal Research, 1989). As well as pyrite, coal also contains sulphate and elemental sulphur – probably oxidation products of pyrite – but significant amounts of organic sulphur (Snape et al., 1995). The latter has been studied by XPS and by X-ray absorption near-edge spectroscopy (XANES); both techniques suggest that coals contain both aromatic bonded (e.g., in thiophenes and aryl sulphides) and aliphatic sulphides. Benzo-, dibenzo- and naphthothiophenes are prominent in coal oxidation and pyrolysis products. Chemical analysis methods have also been applied to coals to determine sulphur functionality, in particular temperature-programed reduction (Mitchell et al., 1994) and oxidation. These studies confirm that thiophene rings in 1–3 ring structures predominate, but that aliphatic sulphides are significantly present, especially in low-rank coals.

References

Bartle, K.D., 1988. New trends in coal science In: Yurum, Y. (Ed.), NATO ASI Series C, vol. 244. Kluwer, Dordrecht, pp. 169.

Berkowitz, N., 1997. Fossil Hydrocarbons: Chemistry and Technology. Academic Press, San Diego.

Botto, R.E., 1987. Energy Fuels 1, 173.

Brownsort, P.A., 2009. UKBRC Working Paper 5. <www.biochar.org.uk>.

Choi, C.-Y., Stock, L.M., 1984. Chemistry and characterization of coal macerals.. In: Winans, R.E., Crelling, J.C. (Eds.), ACS Symposium Series No. 252. American Chemical Society, Washington, D.C, pp. 157.

Crelling, J.C., Bensley, D.F., 1995. In: Pajares, J.A., Tascon, J.M.D. (Eds.), Coal Science. Elsevier, Amsterdam, pp. 235.

Cui, H., Morgan, T., Petrik, T., Turn, S., 2012. Analysis of Integrated Tropical Biorefineries, cooperative agreement No. DE-FC26-06NT42847. US Department of Energy & Hawaii Distributed Energy Resource Technologies for Energy Security.

Dereppe, J.M., Bodou, J.P., Moreaux, C., Durand, B., 1983. Fuel 62, 575.

Dyrkacz, G.R., Horwitz, P., 1982. Fuel 61, 3.

Elliott, M.M. (Ed.), 1981. Chemistry of Coal Utilization Second Supplementary Volume. John Wiley, NY.

Fletcher, T.H., Solum, M.S., Grant, D.M., Critchfield, S., Pugmire, R.J., 1990. Proceedings of the 23rd International Symposium on Combustion, p. 1231. The Combustion Institute, Pittsburgh PA.
Francis, W., 1961. Coal, Its Formation and Composition, second ed. Edward Arnold, London.
Fredericks, P.M., 1989.. In: Kershaw, J.R. (Ed.), Spectroscopic Analysis of Coal Liquids. Elsevier, Amsterdam, pp. 129.
Furimsky, E., Ripmeester, J., 1983. Fuel Processing Technology 7, 191.
Gerstein, B.C., Murphy, P.D., Ryan, L.M. (1982) 'Coal Structure', (Ed. R. A. May), p. 87.
Given, P.H., 1984. In: Gorbaty, M.L. Larsen, J.W. Wender, I. (Eds.), Coal Science, vol. III. Academic Press, NY.
Given, P.H., 1988. New trends in coal science In: Yurum, Y. (Ed.), NATO ASI Series C, vol. 244. Kluwer, Dordrecht, pp. 1.
Given, P.H., Dyrkacz, G.R., 1988. New trends in coal science In: Yurum, Y. (Ed.), NATO ASI Series C, vol. 244. Kluwer, Dordrecht, pp. 53.
Hayatsu, R., Scott, R.G., Moore, L.P., Studier, M.H., 1975. Nature 261, 77.
Hutton, A.C., 1995. Composition, geochemistry and conversion of oil shales In: Snape, C.E. (Ed.), NATO ASI Series C, vol. 455. Kluwer, Dordrecht, pp. 125.
IEA Bioenergy Task Force 34 (2014) – Pyrolysis; Issue 35 July 2014.
IEA Bioenergy Task Force 34 (2015) – Pyrolysis; Issue 36 January 2015.
IEA Coal Research, 1989. The problems of sulfur Reviews in Coal Science. Butterworths, London.
Kasueschke, I., Riepe, W., Gerhards, R., 1989. Erdoel, Kohle, Erdgas, Petrochemie 42, 209.
Kershaw, J.R., 1989.. In: Kershaw, J.R. (Ed.), Spectroscopic Analysis of Coal Liquids. Elsevier, Amsterdam, pp. 1.
Klass, D.L., 1998. Biomass for Renewable Energy, Fuels and Chemicals. Academic Press, San Diego CA.
Ladner, W.R., Stacey, A.E., 1963. Fuel 42, 75.
Love, G.D., Law, R.V., Snape, C.E., 1993. Energy Fuels 7, 639.
Lowry, H.H. (Ed.), 1963. Chemistry of Coal Utilization Supplementary Volume. Wiley, NY.
Markuszewski, R. Wheelock, T.D. (Eds.), 1990. 'Processing and Utilisation of High Sulfur Coals III' Coal Science and Technology Series, vol. 16. Elsevier, Amsterdam.
Mettler, M.S., Vlachos, D.G., Dauenhauer, P., 2012. J. Energy Environ. Sci. 5, 7797.
Miknis, F.P., 1995. Composition, geochemistry and conversion of oil shales In: Snape, C.E. (Ed.), NATO ASI Series C, vol. 455. Kluwer, Dordrecht, pp. 69.
Mitchell, S.C., Snape, C.E., Garcia, R., Ismail, K., Bartle, K.D., 1994. Fuel 73, 1159.
Mohan, D., Pittman Jr., C.U., Steele, P.H., 2006. Energy Fuels 20, 84.
Morgan, T.J., Kandiyoti, R., 2014. Chem. Rev. 114, 1547.
Mukhopadhyay, P.K., 1994. Vitrinite reflectance as maturity parameter; Chapter 1 in Vitrinite reflectance as a maturity parameter. In: Mukhopadhyay, P.K., Dow, W.G. (Eds.), ACS Symposium Series. American Chemical Society, pp. 570.
Parks, B.C., 1963. In: Lowry, H.H. (Ed.), Chemistry of Coal Utilization Supplementary Volume. Wiley, NY, pp. 4.
Pugmire, R.J., Woolfenden, W.R., Mayne, C.L., Karas, J., Grant, D.M. (1983) Prept. ACS Div. Fuel Chem., Seattle, Washington, 28 (l), 103.
Russel, N.J., Wilson, M.A., Pugmire, R.J., Grant, D.M., 1983. Fuel 62, 601.
Sfihi, H., Quinton, M.F., Legard, M.F., Pregermain, S., Carson, D., Chiche, P., 1986. Fuel 65, 1006.
Snape, C.E., Axelson, D.E., Botto, R.E., Delpeuch, J.J., Tekely, P., Gerstein, B.C., et al., 1989. Fuel 68, 547.

Snape, C.E., Ismail, K., Mitchell, S.C., Bartle, K.D., 1995. Composition, geochemistry and conversion of oil shales In: Snape, C.E. (Ed.), NATO ASI Series C, vol. 455. Kluwer, Dordrecht, pp. 125.
Speight, J.G., 1994. The Chemistry and Technology of Coal, second ed. Marcel Dekker, New York.
Stach, E., Mackowsky, M.T., Teichmüller, M., Taylor, G.H., Chandra, D., Teichmüller, R., 1982. Stach's Textbook of Coal Petrology. Gebrüder Borntraeger, Berlin, Stuttgart.
Tse, K.T., Stock, L.M., 1983. Fuel 62, 974.
Tytko, A., Bartle, K.D., Taylor, N., Amaechina, I.O., Pomfret, A., 1987. Fuel 66, 1060.
Unsworth, I.E., Barrett, D.J., Roberts, P.T., 1991. Coal Quality and Combustion Performance. Elsevier, Amsterdam.
van Krevelen, D.W., 1993. Coal, third ed. Elsevier, Amsterdam, New York.
Vassilev, S.V., Baxter, D., Andersen, L.K., Vassilev, C.G., 2010. Fuel 89, 913.
Vassilev, S.V., Baxter, D., Andersen, L.K., Vassilev, C.G., Morgan, T.J., 2012. Fuel 94, 1.
Wallace, S., Bartle, K.D., Perry, D.L., 1989. Fuel 68, 1450.

Pyrolysis of solid fuels: experimental design and applications

3

Chapter Outline

Solid Fuels and Heavy Hydrocarbon Liquids. DOI: http://dx.doi.org/10.1016/B978-0-08-100784-6.00003-5

This is the first of several chapters describing the development of experimental methods for exploring the thermochemical behaviour of coals and lignocellulosic biomass.

For a wide variety of solid fuels, the early stages of thermal breakdown set in motion broadly similar physical and chemical processes. Most of the primary products formed after the onset of thermal breakdown are themselves reactive. In addition to the usual reaction parameters, the intensity and extent of subsequent secondary reactions depend on the initial sample shape and size, as well as the design of the reactor. This is a defining common feature of all pyrolytic processes and directly affects final product distributions. Secondary reactions often make it difficult to distinguish between the fundamental thermochemical behaviour of the fuel and effects due to sample configuration and reactor design. Thus the basic approach to designing thermochemical reactors differs significantly from conventional chemical reaction engineering.

The key challenge in developing thermal characterization methods, therefore, is to formulate experimental methods that discriminate between the thermal response of the fuel and effects arising from reactor design and sample configuration. To this end, it is essential to maintain close control of reaction parameters affecting the pyrolyzing sample as well as factors affecting the composition of evolving 'volatile' products. These constraints typically require the use of small amounts of sample, usually in the form of small particles – usually as small as can be handled. In this context, bench-scale tests can be rapid and relatively inexpensive. With careful design, it is often possible to isolate and quantify the effect of individual reaction parameters, while keeping other conditions unchanged. Again, with careful design, bench-scale experiments can be helpful in accurately mimicking operating conditions in selected locations of pilot or plant scale equipment. We will show later on in this and the next chapter that such experiments may be useful in the design and development of larger scale process equipment, as well as assist in trouble-shooting to support the operation of pilot and process plant.

The experimental reactors described in these chapters have originally been developed either for characterising the thermochemical behaviour of coals, or of lignocellulosic biomass. However, there are compelling reasons for considering research on the fundamental aspects of biomass and coal pyrolysis under the same heading. Most coals and biomass materials respond to increases in temperature in remarkably similar ways. Differences between experimental approaches are often marginal and the reaction conditions quite similar. Furthermore, it is possible to begin explaining reported observations from biomass pyrolysis in terms of what we already know from coal pyrolysis, and vice versa. For example, we may begin to explain the reported incipient

fluid behaviour in rapidly heated wood particles, in terms of what we already know about the plastic behaviour of coals during pyrolysis (see chapter: Elements of thermal breakdown: heating rate effects and retrogressive reactions).

In the next several chapters, we will explore several aspects of the thermal characterization of coal and biomass. We will address the problems inherent in designing pyrolysis experiments and survey how the configurations of specific bench-scale pyrolysis reactors affect the results of experiments. We will attempt the conceptual integration of sample characterization and reactor design in evaluating product distributions from pyrolysis experiments and explore how reactor design affects tar/oil recovery. Several types of bench-scale reactors will be compared, to identify differences in biomass behaviour depending on reaction conditions. The final section will describe two case studies, where bench-scale experiments were used to develop a better understanding of the behaviour of solid fuels in larger scale plant operation.

3.1 Introduction: designing pyrolysis experiments

Consider first the simple homogeneous gas phase reaction sequence, A→B→C. In this example, the product composition at the end of the experiment depends, among other factors, on several parameters related to reactor design and operation. Short-to-medium residence times (after which the reaction is quenched) are likely to favour larger concentrations of the intermediate compound 'B'. Longer reaction times would favour greater concentrations of the product, 'C'. If the energies of activation of the two reactions were significantly different, furthermore, temperature changes during the reaction would alter the relative rates of the two reactions, possibly quite substantially. What concerns us most in this simple example is that, as in most pyrolysis reactions, the eventual product distribution depends primarily on the relative reactivity of the intermediate product.

When considering the pyrolysis of complex solids such as wood or coal, many parallel sets of sequential reactions must be visualised. Primary reactions produce reactive solids and volatiles, the latter partly in the form of tar/oil aerosols. Many primary products of pyrolysis are reactive. These components may be expected to react with each other at widely differing rates. Secondary reactions would produce new reactive intermediates and possibly some stable (final) products. In the case of such complex reaction schemes, terminal product distributions depend critically on spatial temperature–pressure distributions, as well as the time, temperature and pressure histories of the reacting species. Amounts of tars/oils and other volatiles recovered during a pyrolysis experiment are sensitive to the rate of heating, the patterns of flow, the design of the reaction zone and to the configuration (particle shape, size and stacking – if any) of the sample.

In practice, the variety of designs on offer for coal/biomass pyrolysis experiments is testimony that generally accepted schemes, which offer unambiguous results reflecting the properties of the sample alone, have proved elusive. The underlying complication in most cases turns out to be the reactivity of intermediate products.

In particular, when coal or biomass particles are stacked together in the form of a fixed-bed, the outcome of the experiment is affected by reactions between evolving volatiles and heated solid particles. Evolving tar/oil vapours are likely to deposit on pyrolyzing solid surfaces, repolymerize to a char, or partially crack to release lighter volatiles.

Carefully designed early experiments by Griffiths and Mainhood (1967) have shown that coal tar molecules or aerosols move through heated fixed beds of coal/char particles in the manner of molecules moving through a chromatographic column. They sequentially adsorb onto, and desorb from, successive heated particles. If temperatures are sufficiently high, the volatiles react with bed solids, producing more char, lighter tar vapours and more gas. In fixed-bed reactor experiments, observed volatile releases from a coal sample can differ by as much as 6–8%, depending on the extent of solids-volatiles contact (Gonenc et al., 1990). Compared to coals and lignites, greater differences in volatiles release may be observed during the pyrolysis of wood and cellulose. The analysis of the problem is complicated by the wide differences in reactivity between tars of different origin, primarily determined by the chemical makeup of the original fuels. Compared to lignite or bituminous coal tars, the more oxygenated pyrolysis tars/oil vapours that evolve from the pyrolysis of, say, pure cellulose or wood samples are thermally more sensitive, and crack to give gaseous products at lower temperatures (Stiles and Kandiyoti, 1989).

In what follows, we will focus on methods which aim to characterise the underlying behaviour of the pyrolyzing material itself, with as little interference from effects due to sample or reactor configuration as possible. More formally stated, determining the fundamental pyrolytic behaviour of a solid fuel requires the strict decoupling of the observations, from effects due to the design of the particular experiment and of the shape and dimensions of the sample. This is simply another way of stating the standard scientific requirement that the result of a measurement should be entirely independent of the method of measurement. However, pyrolysis is a difficult art. Often, we will have to make do with results that are as independent as possible from the method of measurement. Nevertheless, the importance of striving to minimise the effect of sample and reactor configuration on the results of pyrolysis experiments cannot be overstated.

One practical consequence of these rather rigid rules is the need to assess the behaviour of sample particles – as much as possible – in isolation from one another. It is important to subdivide the sample particles as finely as practicable, since intra-particle reactions of tar/oil precursors affect the amount of tar/oil and other volatiles released from individual particles. As will be discussed in detail below, wire-mesh reactors (e.g., Howard, 1981; Gonenc et al., 1990; Cai et al., 1998), entrained-flow (‘drop-tube’) reactors (e.g., Hindmarsh et al., 1995), and fluidised bed pyrolyzers (Tyler, 1979, 1980; Stiles and Kandiyoti, 1989; Morgan et al., 2015a) approach these stringent criteria more closely than other types of reactors, commonly used for pyrolysis experiments.

Within this framework, the ease of time-temperature programing and relatively good repeatability of thermogravimetric (TG) balances offers a tempting combination of instrumental characteristics for pyrolysis experiments. However, these instruments fail to conform to several of the requirements introduced in the present discussion.

The sample holder in a TG balance is usually a small pan on which sample particles are stacked. Clearly, the particles are not isolated from one another. When this assembly is heated, contact between evolving volatiles and the pyrolyzing sample particles cannot be avoided. Due to secondary reactions of the volatiles, the product distribution, in part, reflects the size of the pile and the manner of stacking of the particles. Moreover, in most TG balances, the carrier gas flows around (i.e., outside) the heating device ('furnace') within which the sample pan is suspended. Ordinarily the 'furnace' has the shape of a hollow cylinder with an open top. This configuration does not allow forcing a flow of gas through the sample bed, in order to sweep evolving volatiles out of the heated zone.

In effect, what is being determined during such an experiment in a TG balance is the pyrolytic behaviour of the particular pile of sample particles, heated externally and in the absence of forced convection for carrying volatiles away from the reaction zone. The shape and dimensions of the 'small pile' of particles are also likely to differ between experiments, and between TG balances (pan size, sample size, depth of pile). How measured values or deduced parameters can be generalised to the fundamental behaviour of the fuel then becomes a matter of conjecture (Kandiyoti, 2002). In particular, kinetic parameters calculated from the differentiation of such data would be open to criticism.

Analogous difficulties arise concerning the validity of results from instruments, such as TG-FT-ir and TG-MS. Such tandem-configuration instruments seem attractive in principle. In addition to problems inherent in the use of TG balances, however, transmitting tar/oil vapours over any distance without loss of content and modification of volatile composition seems supremely difficult to achieve.

Another limitation of TG balances concerns the ranges of available heating rates. Often TG systems are nominally rated for work at up to about 100°C min^{-1}. However, furnaces of TG balances are delicate components and do not usually last long, if operated repeatedly at rates much faster than 30–40°C min^{-1}. Clearly, heating rate ranges relevant to the pyrolysis of solid fuels during pf combustion or fluidised-bed gasification are far higher. They *begin* at around 1000°C s^{-1}. There is therefore a gap between the capabilities of TG balances and the ranges of heating rates required for studying aspects of more common industrial applications. Moreover, heating a small pile of solid fuel in a TG balance rapidly would give rise to additional difficulties. Outer particles of the pile might indeed experience the applied heating rate. However, the penetration of the temperature front through a pile of particles would be governed by the thermal conductivity of the fuel particles themselves as well as the structure of the pile. In Chapter 4, High-pressure reactor design: pyrolysis, hydropyrolysis and gasification, we will revisit the mass transfer limitations involved in the diffusion of reactive gas molecules to fuel particle surfaces in TG balances for performing combustion and gasification experiments (Jess and Andresen, 2010).

The past contribution of TG balances to our understanding of the pyrolytic behaviour of solid fuels has been pathbreaking. TG systems were even used to demonstrate the effect of changes in heating rate on pyrolysis product distributions, although admittedly this was done over a lower and rather limited range of heating rates (Howard, 1963). It is clear, however, that the course of pyrolytic reactions is altered

by the sample and furnace configuration as well as the presence of the TG-balance pan itself. It is still possible to put these delicate instruments to some legitimate and important uses, including the determination of 'relative combustion reactivities' of chars (e.g., cf. Cai and Kandiyoti, 1995) and boiling point distributions of heavy hydrocarbon mixtures (Zhang et al., 1996). In this chapter, we will also discuss the use of TG balances to compare pyrolysis weight loss profiles and pinpoint the onset of weight loss of biomass components, during the initial stages of thermal breakdown. Where the objective is to determine product distributions and rates of sample weight loss, however, the use of TG balances cannot, in our opinion, be considered an acceptable procedure.

Similar shortcomings are also often encountered in the design of micro-pyrolyzers, widely used as sample input devices for gas chromatographs. The wide variety of sample holders available precludes a detailed review. However, little attention appears to have been paid, in the design of devices encountered by the present authors, to minimise contact between reacting solids and evolving volatiles.

In this context, it is as well to mention that it makes sense to design pyrolysis experiments with due regard to the purpose of the measurement. If, for example, the technological requirement is to understand the behaviour of large lumps of coal, as in chain grate industrial boilers or coke ovens, it might well be reasonable to conduct experiments with rather large lumps of coal.

A brief word must also be said about standard volatile matter determinations, undertaken as part of 'proximate' analyses. The tests prescribed by agencies such as ASTM, British Standards Institute and others do not differ greatly. Briefly, the procedure involves placing about one or several grams of powdered solid fuel in a crucible covered with a lid, and placing the crucible in a furnace pre-heated to 900 ± 5°C for about 7 min. The weight loss determined during this experiment is recorded as the 'volatile matter' content of the sample. This procedure unabashedly suffers from many of the secondary reactions described above, in relation to pyrolysis in fixed beds. The presence of the lid adds to complications of volatile escape.

Gibbins et al. (1990) compared crucible test results with total volatile yields, determined in an atmospheric pressure wire-mesh pyrolysis reactor (described below). ASTM proximate analysis volatile matter ('VM') determinations for the Argonne Premium Coal Samples (Vorres, 1990) were found to be between 6% and 15% lower than values observed in the wire-mesh reactor. In these tests, the wire-mesh reactor was operated at 5000°C s^{-1}, and the samples covered a carbon-content range from 73% to 90%. When the wire-mesh reactor was operated at a heating rate thought to match that of the crucible test (16°C s^{-1}), the 'VM' test results were still low by about 7–10%.

However, the crucible test is simple to use under variable and possibly difficult field conditions. Using these tests, results that are internally consistent to within perhaps 1–2% may be obtained without recourse to complicated equipment and extensive operator training. More important, the crucible test is well established, practically the world over, with databases accumulated over decades. Power station operators consider its results meaningful, particularly when comparing different feedstocks. The proximate analysis 'VM' test is therefore likely to retain its pre-eminence in power plant and other traditional industrial applications for the foreseeable future.

Procedures designed to adapt TG balances for proximate analysis also exist (e.g., cf. Gaur and Reed, 1998). Differences with the crucible-based method are small and the test is rapid and useful, so long as the limitations of the determination are well understood.

Before closing the discussion on TG balances and volatile matter determinations, it seems useful to briefly explore the significance of the commonly agreed finding that TG balance–based determinations and crucible tests for 'VM' values give results that are close, usually within ±1%. Recalling the comparison of wire-mesh reactor experiments by Gibbins et al. (1990) with crucible test results provides some indication of errors inherent in TG balance based volatile matter determinations.

The next few sections will focus on coal pyrolysis followed by Section 3.7 on the pyrolysis of coal macerals, kerogens and Southern Hemisphere coals. Sections 3.8 and 3.9 will describe lignocellulosic biomass pyrolysis experiments and explore links with the pyrolysis of coals and lignites. Finally, Section 3.10 will review two applications of bench scale pyrolysis experiments to larger scale plant design and operation.

3.2 Product distributions from pyrolysis experiments: general trends

We next review basic trends observed in coal and biomass pyrolysis. We will then describe the development of several types of pyrolysis reactors and compare results obtained using common sets of samples.

3.2.1 Effect of temperature on product distributions

When a sample of low-to-middle rank bituminous coal is heated at several degrees per minute in an inert atmosphere, initially, water vapour, hydrogen and small amounts of hydrogen sulphide are released together with some light hydrocarbon gases. Depending on the degree of coalification of the sample, covalent bond scission reactions begin somewhere between 310°C for low rank coals and 350°C for more mature bituminous coal samples (Fowler et al., 1989). At this point, greater volumes of hydrocarbons and other gases begin to evolve. Sample weight loss is observed to increase more rapidly between 350°C and 400°C. This is when tar precursors begin to crack within the solid matrix and some of the lighter products begin to evaporate. When applying slow heating rates (say, 5–10°C s^{-1} or less), tar evolution often continues until about 525–550°C (e.g., see Taupitz, 1977), where the tar yield curve begins to level off. Above 700–800°C, the solid residue consists mainly of char, which continues to expel small and diminishing amounts of CH_4, CO and hydrogen, up to perhaps 1800°C (Kobayashi et al., 1977).

In contrast to low and middle rank coals, lignocellulosic biomass usually contains far more oxygen (between 35% and 45%). Such materials are thermally more labile than coals. Woody biomass begins to decompose at lower temperatures (~250–300°C) than geologically more mature samples, such as lignites and coals (e.g., see Shafizadeh,

1968). Most volatile evolution is usually completed by about 400–450°C. Depending on experimental design, the proportion of char yield from a particular sample may range from the near extinction of solid residue, to 28–30% of the original sample mass. Flash-heating finely divided (~100 μm or less) wood particles in inert or in reactive atmospheres – i.e., during gasification – may leave practically no char behind above 600–700°C. Larger particles of the same woody material may give higher char yields, between 10% and 30% of the original sample mass, depending on the heating rate and on whether tar vapours are swept away or allowed to linger in situ (Zaror et al., 1985; Fraga-Araujo et al., 1991; Pindoria et al., 1998a,b). We will return to these experiments in Sections 3.8 and 3.9.

3.2.2 Effect of heating rate on product distributions

When solid fuels are heated rapidly, the sequence of pyrolytic events observed during the successive stages of slow pyrolysis outlined above is overtaken by the rapid rise in temperature. In other words, the temperature rises before the events expected at particular temperatures are allowed to run to completion. At rates above 100–200°C s^{-1}, therefore, the sequence of pyrolytic events is shifted up the temperature scale and telescoped into a shorter time interval. For example, when coal samples are heated slowly, say at ~1°C s^{-1}, tar release reaches completion between 550°C and 600°C, whereas during heating at 1000°C s^{-1}, the temperature interval where tar yields level-off, is pushed up to between 600°C and 700°C (e.g., see Fig. 3.3).

Greater heating rates are generally observed to boost volatile (tar plus gas) yields by as much as 6–8%, depending on the nature of the coal sample (e.g., see Gibbins-Matham and Kandiyoti, 1988). Data presented below show that product distributions from many lignocellulosic biomass materials are even more sensitive to the heating rate. In coal pyrolysis, the increase in volatiles often tends to match the accompanying increase in tar yields. This is explained in terms of the greater survival of tars during faster heating. The rapid buildup of internal pressure in volatile filled bubbles is thought to force the faster ejection of tar precursors, thereby reducing the probability of retrogressive repolymerisation reactions (Gray, 1988). This mechanism is consistent with tars from fast-pyrolysis experiments showing broader ranges of molecular masses (Li et al., 1993a,b).

In Chapter 6, Elements of thermal breakdown: heating rate effects and retrogressive reactions, we will review evidence suggesting that locally available (i.e., sample derived) hydrogen may be incorporated into the pyrolyzing mass more effectively during rapid heating. It is thought that hydrogen released – or 'donated' – within the sample mass during early stages of the pyrolysis process serves to quench and stabilise some of the more reactive free radicals associated with tar precursors. With an increasing heating rate, pyrolytic events triggered during progressively shorter time intervals facilitate the overlapping of hydrogen release and covalent bond scission in a manner likely to assist the partial blocking of repolymerisation reactions, thereby favouring more tar survival. The resulting enhanced plasticity observed in coals, lignites, and biomass related samples will be reviewed in Chapter 6, Elements of thermal

breakdown: heating rate effects and retrogressive reactions. Cenosphere formation as a result of enhanced plasticity has been observed during pf combustion and plasma heating, where the latter process is thought to reach several thousand degrees at very high heating rates (Anderson et al., 1968; Anthony and Howard, 1976).

Relationship between heating rate and reactor design: The combined effect of the heating rate and the reactor shape on the 'temperature versus tar yield' curve may be quite complicated. When coal sample particles are introduced into an already heated fluidised-bed reactor, particle heating rates would be high, forcing the release of correspondingly high proportions of volatiles and tar/oil vapours. However, when the temperature is above, say, 600°C, the fluidised-bed configuration allows sufficient residence time for extensive secondary reactions to take place before tar vapours can sequentially exit from the fluidised bed itself and the reactor freeboard.

When experiments are performed at a succession of increasing temperatures in a fluidised-bed reactor, tar/oil yields initially increase. However, with increasing temperature, some charring may occur in the bed and tars/oils begin to crack in the bed and the reactor freeboard. When the increase in tar production is matched by tar cracking reactions, the tar-yield versus temperature curve goes through a maximum and declines with further increases in temperature (Fig. 3.6b). For bituminous coals, the tar-yield maximum has been observed between 550°C and 600°C. For thermally more sensitive materials such as cellulose, silver birch wood or banagrass, the analogous tar-yield maximum is observed at lower temperatures, between 400°C and 450°C (Stiles and Kandiyoti, 1989; Morgan et al., 2015a).

In fixed-bed reactors, the temperature-tar yield relationship again depends on a combination of factors. In this type of reactor, tars released by coal particles may be altered by contact with other coal particles, through cracking and char forming reactions. Due to their thermal inertia, fixed-bed reactors cannot be heated at rates much faster than about 10°C s^{-1} (O'Brien, 1986; also see below). When the coal column inside the fixed-bed reactor is high (~30–40 cm), evolving tars would encounter progressively rising temperatures on their way towards the exit of the reactor. The effect would lead to tar repolymerisation and cracking reactions. Tar loss was evident in the work of Hiteshue and coworkers, when using the higher range of peak experimental temperatures (Hiteshue et al., 1957, 1960, 1962a,b). However, when the reactor is reasonably short, tars that survive secondary reactions in the shorter span of the fixed-bed can exit from the reactor, *before* the intended peak temperature of the experiment is reached. In other words, since the heating rate is relatively low, some tar vapours can exit the reactor without experiencing temperatures very much higher than those at which they were released from their parent coal particles. In short reactors with relatively shallow sample beds (e.g., ~4 mm) the overall effect is of tar yields *from the reactor* initially rising with temperature, then flattening out between 500°C and 600°C. This is because tar production stops at these temperatures and tar vapours leave the *short* reactor more quickly, irrespective of the final, possibly much higher temperature that the reactor might reach (see Fig. 3.6a). Comparing data from common sets of samples, peak tar yields reached in fixed beds are usually lower than yields that can be attained in wire-mesh or fluidised-bed reactors.

3.2.3 The effect of pressure on product distributions

When pyrolysis experiments are performed at reduced pressures ('vacuum'), volatile and tar release tend to increase compared to operation at atmospheric pressure. Somewhat counter-intuitively, the increase in tar yields due to operation under reduced pressures is often a little larger than the corresponding increase in total volatiles. Depending on the nature of the sample, the incremental increase in tar yield could be as much as 5% (Table 3.8). These observations suggest that reduced external pressure allows tar precursors to exit from parent coal particles more rapidly. The effect seems analogous to fast heating, where the rapid build-up of internal pressure tends to force tar precursors from parent coal particles more rapidly. The data suggest that when the initial external pressure is reduced from atmospheric to about 1×10^{-9} bar (initial pressure), intraparticle tar loss through recondensation (repolymerisation) reactions of some tar precursors is measurably reduced. Conversely, as the pressure is raised toward atmospheric pressure, some tar precursor material is lost through repolymerisation processes giving off gas and char and perhaps some lighter tar as well.

Experiments conducted at reduced pressures thus highlight the level of intraparticle reactions and loss of tar product (and of tar precursors) taking place, when operating at atmospheric and higher pressures. Increasing the external pressure thus acts against internal forces, which tend to drive volatiles out of coal particles. Higher external pressures tend to slow down (1) the flow and diffusion of volatiles towards external particle surfaces, and (2) the diffusion from external particle surfaces to the surrounding bulk gas.

When the external pressure of inert gas is raised above atmospheric pressure, volatile and tar yields initially tend to diminish rapidly, up to about 5 bars. With increasing pressure, this trend slows down and appears to level off above 40 bars. Compared with atmospheric pressure results, the overall decline in total volatiles may be as much as ~10–12%. The effect was first reported and explained by Howard and coworkers (cf. Howard, 1981), in terms of the partial suppression of volatile release by the physical effect of increasing external pressure.

3.2.4 Effect of particle size

Volatile yields tend to diminish with increasing particle size, again providing indications of the extent of intraparticle volatile loss during pyrolysis. However, the effect is difficult to evaluate quantitatively at higher heating rates, since the propagation of the temperature front toward the centre of a large particle is limited by the thermal conductivity of the intervening sample mass (Suuberg, 1977). High rates of heating imposed at the boundary would not be 'seen' by the mass of sample inside large particles. Instead, the temperature front would advance at a rate modulated by the thermal conductivity of the mass of sample. The effect of particle size is discussed further in Section 3.3.5.

3.3 Designing bench-scale pyrolysis reactors: wire-mesh reactors

The discussion in Section 3.1 sets us a nearly impossible task. The ideal pyrolysis reactor is required to heat all sample particles uniformly, at a precisely defined rate. Evolving volatiles must not contact any heated surfaces after being released from individually reacting, infinitesimally small particles. These volatiles must then be instantaneously quenched and quantitatively recovered. By imposing our own exacting conditions, we appear to have stumbled on requirements that are difficult to work into the design of a real experiment.

Historically, numerous reactor configurations have been devised for determining the pyrolytic behaviour of solid fuels. A useful review of pre-1963 literature on coal pyrolysis (Howard, 1963) describes 'laboratory assay methods' for estimating coking properties, alongside experiments for examining the thermal reactions and behaviour of coals.

The 'short-path vacuum still' developed by the same author and his team is an early attempt to apply uniform heating to sample particles and to suppress the secondary reactions of evolving volatiles (Sun et al., 1958). The use of relatively low pressures (~10^{-6} bar) tended to reduce sample plasticity and was deemed to help remove volatiles. 'Concentric square-bottomed grooves' were machined into an aluminium plate and only half-filled with coal particles, before applying electrical heating. The grooves were intended to reduce heat transfer problems, correctly identified as being 'accentuated in vacuum systems'. The apparatus had a top temperature of 550°C. It was equipped with a water-cooled plate, which was placed directly above the sample holder to condense tars evolving from pyrolyzing sample particles. Interestingly, heating rates did not receive much attention: 'Approximately 90 min was required to reach the desired operating temperature…' With plenty of hindsight, the stacking of particles in this device may be considered a little too dense and the escape path for the volatiles a little ill-defined. Nonetheless, many of the concepts used in the construction of this apparatus are essential to the design of pyrolysis reactors intended to resolve problems associated with sample geometry, heat transfer limitations and volatile removal. The work was based on the recognition of uniform heating as a critical factor and that rapid cooling of tars might help reduce secondary reactions. Not unlike so many others who followed in their tracks, these experimenters could not help being drawn to the black arts of molecular mass estimation and speculations about the structural aspects of coal pyrolysis tars. We will review current work on the characterization of pyrolysis tars/oils in Chapter 7, Analytical techniques for low mass materials: method development and Chapter 8, Analytical techniques for high mass materials: method development.

We next describe several types of bench-scale reactors, frequently used in characterising the pyrolytic behaviour of solid fuels. These include fixed and fluidised-bed reactors, entrained-flow ('drop-tube') reactors and a versatile wire-mesh ('heated-grid') reactor, which will be described in detail. Results will be compared between experimental systems using common sets of coal samples. When matched against our

'wish list' of idealised pyrolysis parameters, each reactor type turns out to suffer from inherent shortcomings, which limit the ranges of conditions where useful experiments may be carried out. The ways in which some of these designs may be adapted for high-pressure operation will be described in Chapter 4, High-pressure reactor design: pyrolysis, hydropyrolysis and gasification.

3.3.1 Wire-mesh reactors

The basic design concept is straightforward and is intended to minimise the effect of sample and reactor geometry on the outcome of the experiments. Milligram quantities of sample particles are placed between two layers of folded wire-mesh. This assembly is weighed and stretched between two electrodes. Fine wire thermocouples are attached. A controlled current is then passed through the wire-mesh, which serves as a resistance heater. After the sample has been exposed to a pre-programed time-temperature profile, the weight change of the (wire-mesh plus pyrolyzed sample) assembly is determined. Depending on the purpose of the experiment, volatiles and/or tars may be recovered and characterised. This reactor configuration allows experiments to be carried out using wide ranges of heating rates between 1°C s^{-1} and 20,000°C s^{-1}, temperatures up to 2000°C and pressures up to 160 bars.

Despite their manifest advantages, wire-mesh reactors should not be considered as instruments of first resort. Considerable investment is required in electronic hardware and software design, in purchasing sensitive balances and in substantial operator training. Another major drawback is the small (milligram) sizes of the tar, char and gas samples generated during individual experiments. By contrast, a fixed-bed pyrolysis reactor is quickly built and amounts of products generated are greater, although results are never easy to interpret and the range of possible heating rates is limited. As will be discussed, fluidised-bed and entrained-flow ('drop-tube') reactors provide partial solutions to some of these problems, while introducing several difficulties of their own. We begin by outlining the major stages in the evolution of the wire-mesh reactor; it has proved to be a remarkably versatile instrument.

3.3.2 Evolution of the wire-mesh ('heated-grid') reactor

The basic design: The first rig of its kind encountered in the literature was constructed by Loison and Chauvin (1964), working at the French coal research organisation, CERCHAR. The original paper explains that, initially, the authors built a vertical furnace pyrolyzer, what in our day would have been called a 'drop-tube' reactor. However, the design does not seem to have found favour with these researchers, because they found it difficult to recover all the chars. That is a problem that has persisted and continues to worry entrained-flow ('drop-tube') reactor operators of our day.

The authors then go on to describe their original wire-mesh reactor. A coal–water paste was pressed onto a single layer of metallic mesh, held between two electrodes. It appears sample particles were held within the 'holes' of the mesh. One of the electrodes was spring-loaded, to take up the thermal expansion of the mesh during heatup.

This feature prevents the buckling that would have occurred due to thermal expansion, had the mesh, instead, been held between two rigid electrodes. Heating was achieved by passing a single electrical pulse from a variable voltage transformer: '…a thyratron time switch enabled current to be passed for times varying between 10 ms and 1 s, in steps of 10 ms'. Temperatures up to 1100°C were monitored with a Pt/Pt-Rh thermocouple, placed at the centre of the sample holder. Experiments were restricted to the heatup ramp with an average heating rate of 1500°C s^{-1}.

This design was adopted by Jüntgen and van Heek (1968), who constructed and operated a wire-mesh reactor working under vacuum and connected to a mass-spectrometer. These authors reported qualitative data on the release of light volatiles during the fast pyrolysis of coal. Relatively few results appear to have been published from this well-conceived experiment.

The wire-mesh reactor configuration is best known through the work of Howard and coworkers (Howard and Anthony, 1976; Howard et al., 1975, 1976; Anthony et al., 1974, 1975; Suuberg et al., 1978a,b, 1980) and Suuberg and coworkers (Suuberg and Unger, 1981; Unger and Suuberg, 1983, 1984; Suuberg et al., 1985). Coal pyrolysis and hydropyrolysis literature up to 1979 has been exhaustively reviewed by Howard (1981). These researchers placed a coal sample of ~10–15 mg (5–10 mg in the early work by Anthony) between two layers of a folded mesh, fixed between 'heavy' rigid electrodes, to absorb the resistive heat. The early version built at the Massachusetts Institute of Technology used direct current from a battery. Heating rates available to this instrument ranged between ~270°C s^{-1} and 10,000°C s^{-1} (650–10,000°C s^{-1} in early work by Anthony). Mesh temperatures were determined using a thermocouple placed between the two layers of mesh, without touching the mesh. There are indications that a temperature lag may have existed between thermocouple and mesh due to this lack of contact. The instrument was operated over a range of pressures from ~10^{-3} to 70 bars. As in the case of Loison and Chauvin (1964), tars were collected by washing internal surfaces of the reactor chamber with solvent. In later work, these researchers characterised tars by size exclusion chromatography, using tetrahydrofuran as eluent (Fong et al., 1986a,b; Unger and Suuberg, 1984; Suuberg et al., 1985).

Another wire-mesh instrument constructed at Bergbau Forschung used a 10 kHz heating current and analogue feedback control (Arendt, 1980; Arendt and van Heek, 1981). The system operated at heating rates above 210°C s^{-1}. Pyrolysis and hydropyrolysis experiments were carried out at pressures up to 100 bars. However, the tar yield determination relied on an indirect calculation. In constructing the cell, polymeric materials were used to make the electrode holders. The thermal sensitivity (i.e., danger of melting) of these components limited experiments to about 2 s holding time at peak temperatures between 700°C and 1100°C, the top design temperature. The instruments commercially acquired from Bergbau Forschung (later renamed DMT) by the British Gas Research Station at Solihull (UK), by the Coal Research Establishment at Stoke Orchard (UK) and by ABO Academy University (Finland) suffered from similar limitations.

The amount of sample used by different laboratories has varied over the years between 5–6 mg at Imperial College (see below) and up to 35 mg in some of the experiments conducted at Bergbau Forschung. Similarly, the rectangular wire-mesh sample

holder size has varied between approximately 15 by 60 mm at Bergbau Forschung and 30 by 90 mm at Imperial College. Sample sizes and mesh dimensions used in most other laboratories have been intermediate between these extremes.

3.3.3 Expanding the heating rate range and improving tar recovery

All the early wire-mesh instruments were able to run at high heating rates. A large current pulse is all that is required to achieve a reasonably well defined time-temperature ramp, when heating at or above 200°C s^{-1}. Arranging for a steady holding period at peak temperature may require some manipulation, but the technology required to do this could still be relatively simple. However, heating the samples with reproducible and reasonably linear temperature–time ramps over the lower heating rate ranges (~1–100°C s^{-1}) required online feedback control capabilities. In the 1970s and early 1980s, electronic components such as A/D converter cards (basic in our day) to facilitate achieving low heating rates were not commercially available.

In early rapid heating experiments, Howard and coworkers observed volatile matter and tar yields significantly greater than those from slow heating experiments, performed in standard volatile matter test crucibles and in TG balances. However, they were unable to distinguish experimentally between the enhancement of tar and volatile yields due to fast heating from the effect of fine sample dispersion in the wire-mesh reactor. The enhanced yields observed in wire-mesh reactors operated at high heating rates were, thus, thought to result from fine sample dispersion rather being due to high heating rates (Howard, 1981). In the early 1980s, researchers at Bergbau Forschung attempted to close this heating rate gap. They supplemented data from fast heating experiments in a wire-mesh reactor with weight loss data from a TG balance operated at slow heating rates (Wanzl, 1988). Once again, effects due to slow heating could not be resolved from effects due to particle stacking in the TG balance. Lower heating rates in wire-mesh reactors first became available in laboratories with facilities of their own for designing and constructing data acquisition and temperature programing systems.

Expanding the heating-rate range: The first wire-mesh instruments capable of operating at slow as well as fast heating rates have been described by Hamilton (Hamilton et al., 1979; Hamilton, 1980) at CSIRO in Sydney (Australia) and by Williams and coworkers at the University of Leeds (UK) (Desypris et al., 1982). Relatively few results were published from the latter instrument, which appears to have produced data with surprisingly wide bands of scatter, substantially swamping effects due to changes in the heating rate. Hamilton's wire-mesh reactor was also used for only a short period of time. It was capable of achieving heating rates between 10^{-1}°C s^{-1} and 10,000°C s^{-1}. The purpose built power supply was innovative for its time. It provided a current interrupted for 10 ms in every hundred, to enable reading the temperature via a thermocouple. Before being abandoned, apparently for reasons unrelated to its technical performance, the system was used for preparing coal and coal maceral chars, in order to examine changes in morphology as a function of coal rank, heating rate and peak temperature. The chars were examined by scanning

electron microscopy and valuable matrices of photomicrographs were published. Overall, the work showed that increasing heating rates enhanced the plasticity of samples of all ranks. Hamilton and coworkers did not attempt volatile-release and tar-yield measurements in their very useful looking reactor.

Problems of quantitative tar recovery: Accurate measurements of tars evolved during the pyrolysis of solid fuels may be useful in several ways. They provide maximum (limiting) tar production data for process schemes seeking to maximise or minimise liquid product yields from pyrolysis and hydropyrolysis related processes. For example, in biomass gasification, the presence of tars/oils in the product gas is considered a nuisance that must be suppressed, while in pulverised fuel combustion, evolved tars carry a substantial part of the calorific value assigned to individual coal particles. The combustion performance of coals in the near burner zone of commercial scale pf burners is closely related to the evolution and ignition of tar vapours. Tar yield measurements also provide valuable information regarding mechanisms of thermal breakdown.

In the absence of forced convective currents, tar aerosols released by the sample in wire-mesh reactors have been observed to evolve and to slowly rise in the form of a small cloud. In the absence of a facility for sweeping volatiles away from the heated zone, the cloud of tar vapours slowly circulates. Often a part of the 'cloud' settles down on the mesh. This affects the measurements (Howard, 1981). Initially, tar recovery in wire-mesh reactors was achieved by a combination of filtering the gas from the chamber and washing chamber walls with a solvent such as dichloromethane, chloroform, or methanol. In Canada, Stangeby and Sears (1978, 1981a,b) developed an atmospheric pressure wire-mesh instrument with a lateral gas sweep flowing at 3 cm s^{-1} to remove volatiles away from the reaction zone. The instrument was battery powered with operation confined to relatively high heating rates, between 250°C s^{-1} and 6000°C s^{-1}. 'Heating rate was found to have little effect on total weight loss of the coal, but a dramatic effect on the actual composition of the products. High heating rates substantially increased the yield of light hydrocarbons' (Stangeby and Sears, 1981a). With the advantage of hindsight, the results suggest that radiation from the mesh at higher temperatures gave rise to the secondary cracking of tar vapours as they were swept laterally across the surface of the rapidly heated mesh.

Niksa et al. (1982a,b, 1984) used a DC 'operational power supply' equipped to deliver two independent 'cycles', a constant current during heatup, followed by adjustable constant voltage to maintain an isothermal reaction temperature. A preheated gas stream was allowed to sweep parallel to (i.e., 'across') the face of the mesh, carrying volatiles toward a set of filters. The instrument described by Niksa et al. (1982a) was designed for heating to temperatures of 1000°C, at rates up to 10,000°C s^{-1} and was equipped with a liquid nitrogen spray for quenching the system. One of the electrodes was spring-loaded to absorb the thermal expansion of the mesh. 50 µm diameter chromel-alumel thermocouple wires were spot-welded 'to the outside' of the wire-mesh sample holder. Although the spot welds would be expected to cause local temperature distortions, little temperature variation was reported from experiments conducted using two pairs of thermocouples. Avoiding interference in temperature measurement from the power circuit was achieved through the high

impedance of the storage oscilloscope and floating the oscilloscope and power supply in common.

Initial experiments were conducted between 13 Pa and 0.22 MPa (i.e., 'vacuum' to 2.2 bars) pressure, although the system was placed in a 13.5 MPa pressure vessel. Niksa et al. (1982b) reported results from variable heating rate experiments in the 100–10,000°C s^{-1} range, under reduced pressures. At 'the highest heating rate, the uncertainty involves whether or not the actual rate was 10^4 K s^{-1}'. The authors suggested that short residence times at peak temperature may not have allowed experiments to reach completion, particularly at the lower temperatures. Nevertheless, differences of 8–10% in weight loss were reported between heating at 100°C s^{-1} and 10,000°C s^{-1}; 'experiments at 100°C s^{-1} were terminated after heatup'. The instrument was subsequently used for tar yield determinations during hydropyrolysis experiments, at up to 25 bars of hydrogen pressure (Bautista et al., 1986).

Freihaut and coworkers also developed an atmospheric pressure wire-mesh instrument (Freihaut et al., 1982; Freihaut and Seery, 1983). Initial publications describe a vertical pyrolysis chamber construction. The apparatus was directly connected to an infrared cell, for analysing light volatiles. Tars were defined as material condensed on reactor cell walls, liners and the glass wool filter placed between the chamber and the infrared cell. The pyrolysis chamber appears to have been initially 'slightly pressurised' to remove volatiles from the vicinity of the wire-mesh. Heating rates ranged between 1–1000°C s^{-1}. Photomicrographs in a later publication showed that the thermocouples had been spot-welded to the mesh, creating a metal bead of about 180 μm across (Freihaut and Proscia, 1989). Positioning this mass of metal onto the mesh might be expected to distort the temperature distribution as well as create a time lag in the temperature measurement. In an entirely different context, the present author has found it perfectly possible – although not easy – to weld 25 μm wires across each other with no apparent distortion in the wire (Kandiyoti, 1969; Kandiyoti et al., 1972). Tar yields reported in the published work of Freihaut and coworkers showed evidence of substantial decline at higher temperatures. This suggests that secondary cracking of volatiles could not be avoided, probably due to the absence of a forced flow induced movement of tar vapours away from the vicinity of the heated mesh.

Installing a vertical sweep flow: Two wire-mesh reactors were constructed at Imperial College, the first for vacuum and atmospheric pressure operation and the second for high-pressure work up to 160 bars (Gibbins-Matham and Kandiyoti, 1988; Gibbins and Kandiyoti, 1989a,b). Fig. 3.1A shows the atmospheric pressure version of the reactor, equipped with an early version of the tar trap. Unlike previous designs, a brass plate with a 3 cm diameter circular hole was installed underneath the mesh. This feature served to direct the gas continuously entering the cell through a sidearm, to sweep (upward) through the horizontally placed wire-mesh sample holder, and continue upward through the offtake tube placed above the mesh. 106–152 μm sample particles (~5 mg) were evenly distributed within a smaller circle, drawn on the part of the mesh sitting above the 3 cm diameter circular hole of the brass plate. The offtake tube and tar trap placed above the mesh completed the flow path, directing the stream of pyrolysis volatiles and carrier gas out of the cell. In other words, the new arrangement provided a stream of gas flowing (upward) normal to the plane of the wire-mesh,

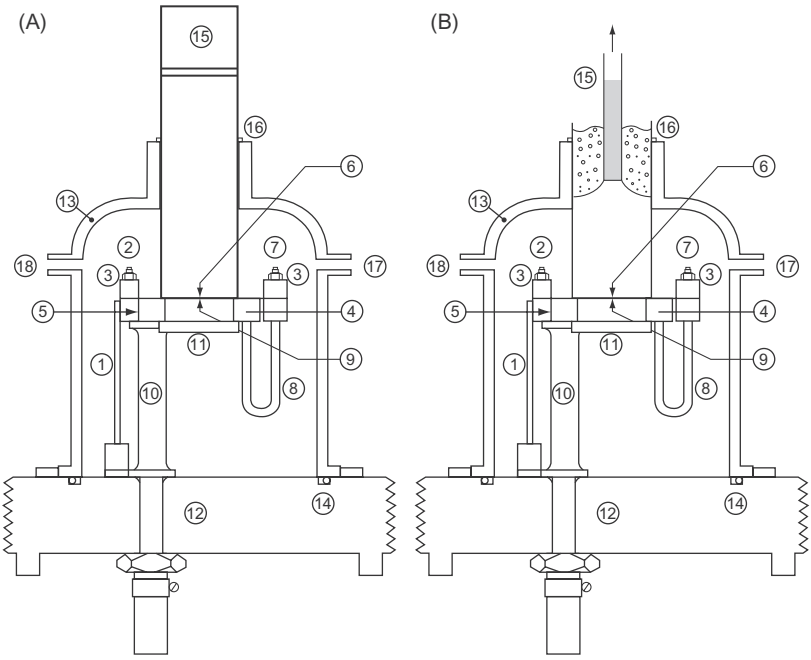

Figure 3.1 The atmospheric pressure wire-mesh reactor with the early (A) and present (B) tar trap designs. (1) Copper current carrier; (2) Live electrode; (3) Brass clamping bar; (4) Sample holder support plate; (5) Mica strip; (6) Wire-mesh sample holder; (7) Electrode; (8) Stainless steel tubes; (9) Mica layer; (10) Brass pillars; (11) Sintered pyrex Glass disk; (12) Base plate; (13) Pyrex bell; (14) O-ring seal; (15) Off-take column; (16) O-ring; (17) Carrier gas entry port; (18) Connection for vacuum pump.
Source: Reprinted from Gibbins, J.R., Kandiyoti, R., 1989b. Fuel 68, 895. Copyright 1989, with permission from Elsevier.

to sweep volatiles released by sample particles away from the reaction zone and into the cold-trap above it. The use of a stream of gas through the sample holder, directing evolved volatiles into the liquid-nitrogen cooled traps (Fig. 3.1) has enabled the determination of tar yields more reproducibly than could have been otherwise achieved.

In the Imperial College wire-mesh reactor, one of the electrodes was spring-loaded for taking up the thermal expansion of the mesh. The latter was heated by a low voltage (12–24 V) alternating current. In order to prevent overheating, the newly installed brass support plate, the two electrodes, and the tubes connecting the brass plate and the spring-loaded electrode (Item 8 in Fig. 3.1) were cooled with circulating water. This was particularly useful during slow heating experiments, when the new support plate and the electrodes were capable of absorbing large amounts of heat.

Evolution of the tar-trap design: The initial tar trap in Fig. 3.1A consisted of an off-take tube, placed vertically above the wire-mesh sample holder and sealed-off near the upper end with a porous Pyrex sinter. Liquid nitrogen poured above the sinter served to chill the flowing stream of gas. The sweep gas (He) and lighter products

(CO, H_2, etc.) exited without significant increase in reactor pressure, while heavier volatiles condensed on or near the liquid-nitrogen cooled sinter. The determination of weight uptake by the tar-traps proved to be a reliable method for quantifying tar yields. Problems emerged, however, when the quantitative recovery of the tars was required for subsequent structural characterization work. While removing the condensed tars at ambient temperature by solvent washing, some of the heavier tar components were observed to stain the initially white frit. While the amount of tar product lost in this manner was below the limit of the determination, any tar loss would have affected the subsequent structural determinations. Fig. 3.1B shows the reactor assembly, equipped with the 'Mark II' trap design that was eventually adopted for vacuum and atmospheric pressure work. Evolving volatiles were continuously swept into the central 'chimney' packed with fine strips of stainless steel wire-mesh.

In order to quantify tar deposition, the traps were dried at 50°C and weighed before and after an experiment. This modification allowed the quantitative and repeatable recovery of tars evolved during pyrolysis, provided the pressure drop across the offtake tube was kept constant, as determined during the preparation of the traps. These second-generation traps were normally made of Pyrex glass and could be operated at up to 1000°C for short periods. Quartz was used for higher temperature experiments. Tar yields from the new traps were found to be indistinguishable from results obtained with the trap in Fig. 3.1A, but the tars did not adhere to metal mesh in the same way and could be recovered quantitatively (Li et al., 1993a,b).

The wire-mesh reactor design shown in Fig. 3.1B contained a number of original features, including the horizontal support plate. This design appears to have been adopted as the generic 'wire-mesh reactor', particularly in the Asia-Pacific region, where research on the thermochemical utilisation of coal and biomass has maintained its vitality. The atmospheric pressure wire-mesh reactor of similar design constructed by Li Chun Zhu's group at Monash University (later at Curtin University, Perth) in Australia (Sathe et al., 1999) was successfully integrated into a wider research effort. Interest in the wire-mesh reactors constructed at General Electric Global Research in Shanghai appears to have waned (Zeng et al. 2008). A wire-mesh reactor was used within the framework of collaboration between Idemitsu Kosan Co., Ltd. and Kyushu University, mostly for collecting supporting data, aimed at generating kinetic constants from data collected in a TG balance (Sonoyama and Hayashi, 2011, 2013). As outlined above, contact between heated solids and evolving volatiles in stacked (albeit small) piles of particles tends to distort data from pyrolysis experiments. Such distortions are amplified when the data are differentiated for calculating kinetic constants. More recently, researchers at Huazhong University of Science & Technology (Hubei Province) and Xi'an Jiaotong University (Shaanxi Province) have also reported the construction of wire-mesh reactors of similar design (Gong et al., 2014; Pan et al., 2015).

Temperature measurement in the wire-mesh reactor: Temperature variations between different points of the sample holder tend to distort experimental results. Evenly distributing sample particles tends to even out such temperature variations. Some indication of lateral temperature variations is necessary to ensure correct

operation. The reactor shown in Fig. 3.1 was equipped with two pairs of thermocouples, to monitor lateral temperature variations in the sample holding part of the mesh. The calculated mean of readings from the two thermocouples was used as the feedback signal for on-line control. Details of the purpose built electronic instrumentation used in the mid-to-late 1980s have been described in the original publications (Gibbins, 1988; Gibbins-Matham et al., 1989).

Thermocouple wires were pressure-welded to each other and each pair pulled tight over a strand of mesh for contact. There was no need to weld the thermocouple wires to the mesh. Readings were taken every 20 ms during 3 ms interruptions in the power supply, triggered by a purpose built pulse generator (Gibbins-Matham et al., 1989). Achieving linear temperature-time ramps during fast heating could be done even with relatively simple power supplies. Fig. 3.2 shows that adequate linear temperature-time ramps could also be achieved during slow heating at 1°C s^{-1}. The wider heating-rate ranges available to the Imperial College instruments (between 0.1°C s^{-1} and 1000°C s^{-1}) combined with the improved tar yield measurement method has enabled demonstrating unambiguously that increasing heating rates have a definite effect on pyrolysis tar and total volatile yields (Gibbins-Matham and Kandiyoti, 1988). These data will be presented below.

Broadening the operating range of the wire-mesh reactor: Initially, the heating rate could be altered between 0.1°C s^{-1} and 1000°C s^{-1}, using chromel-alumel thermocouples and a sample holding mesh woven from AISI 304 stainless-steel wire (Gibbins-Matham and Kandiyoti, 1988). Cai et al. (1996) subsequently extended the heating rate range of both wire-mesh instruments up to 10,000°C s^{-1} and the temperature range to 1600°C, using Pt-Pt/Rh thermocouples and molybdenum mesh. Later work has extended the operating range of both the atmospheric

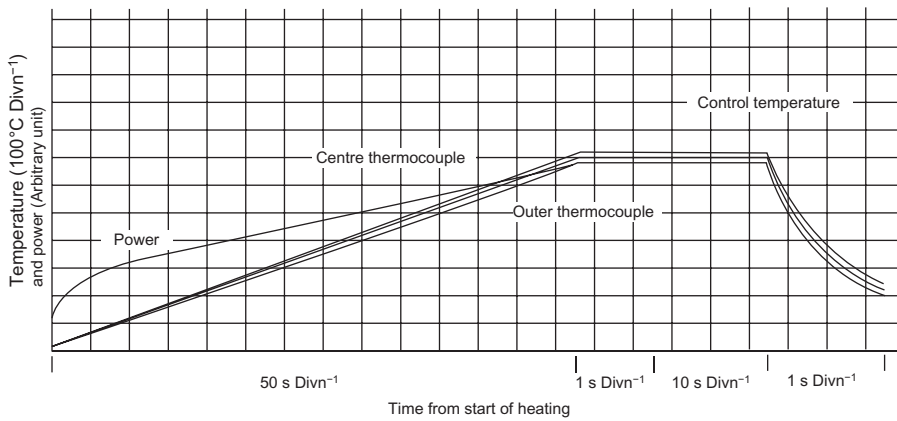

Figure 3.2 Time-temperature ramp: heating at 1°C s^{-1}. Comparison of two thermocouple outputs shows the lateral variation in temperature within the sample holding part of the mesh. The averaged output (in the middle) was used as the feedback signal for on-line control. *Source*: Reprinted from Gibbins, J.R., Kandiyoti, R., 1989b. Fuel 68, 895. Copyright 1989, with permission from Elsevier.

pressure and the high-pressure wire-mesh reactors to 2000°C, using tungsten-rhenium thermocouples ('tungsten/3% rhenium' and 'tungsten/25% rhenium'). As outlined in Chapter 4, High-pressure reactor design: pyrolysis, hydropyrolysis and gasification, the evolution of the high-pressure wire-mesh reactor has successively allowed mimicking of conditions in hydropyrolysis (850°C, 80 bars), CO_2 gasification with and without steam injection (1100°C and 30 bar) and eventually entrained flow, steam-oxygen gasification reactors (2000°C at 30 bar) (Peralta et al., 2002, 2004, 2005).

3.3.4 Coal pyrolysis in a wire-mesh reactor: product distribution trends

Effect of temperature: Fig. 3.3A presents data from the atmospheric pressure wire-mesh reactor, showing tar and total volatile yields from Linby (UK) coal, heated at 1°C s^{-1} with 30 s holding at peak temperature. The total volatile yield was observed to increase rapidly up to about 600–700°C, while the tar yield flattened out just above 500°C. At higher heating rates, tar yields levelled off at somewhat higher temperatures (Fig. 3.3B). Above about 700°C, tar yields do not usually increase significantly, but total volatile yields from coal samples tend to increase, albeit slowly, as the sample temperature is raised. Kobayashi et al. (1977) have presented evidence of minor but measurable weight loss at up to 1800°C. In most chars, there would still be a percent or two of volatiles to squeeze out by keeping the sample at these higher temperatures for longer times (Howard, 1981).

We have already signalled that fluidised-bed reactors allow tar loss through secondary reactions in the bed itself as well as in the reactor freeboard. For many middle rank coals, the tar yields measured in a fluidised-bed reactor go through a maximum near 550–600°C. Data from a fluidised-bed reactor will be presented in Section 3.5. On the other hand, above about 700–800°C, tar yields determined in wire-mesh reactors would be expected to hold stable and not to decline with increasing temperature. These is because volatiles released by coal particles are rapidly swept into a quench zone and no longer 'see' the higher temperatures that the char residue may be heated to. We do not, therefore, expect tar product to be destroyed or otherwise altered after its release from parent coal particles, always assuming careful design and operation.

Effect of heating rate: Fig. 3.3C shows that when Linby coal particles are heated at 1000°C s^{-1}, tar and total volatile yields increased by about 6%, compared to 'slow' heating at 1°C s^{-1}. When a wider array of samples was eventually tested, it became apparent that the choice of Linby coal for these initial experiments was somewhat fortuitous. The response of this coal to changes in heating rates appears somewhat greater than many other samples that were pyrolyzed. The effect is observable, however, for many low-to-middle rank coals (Li et al., 1994). As will be discussed below, the vitrinite component of coals seems more sensitive to changes in heating rates, although liptinite and inertinite group concentrates at times also show a measure of sensitivity to changes in the rate of heating. In Chapter 6, Elements of thermal breakdown: heating rate effects and retrogressive reactions, we will examine evidence

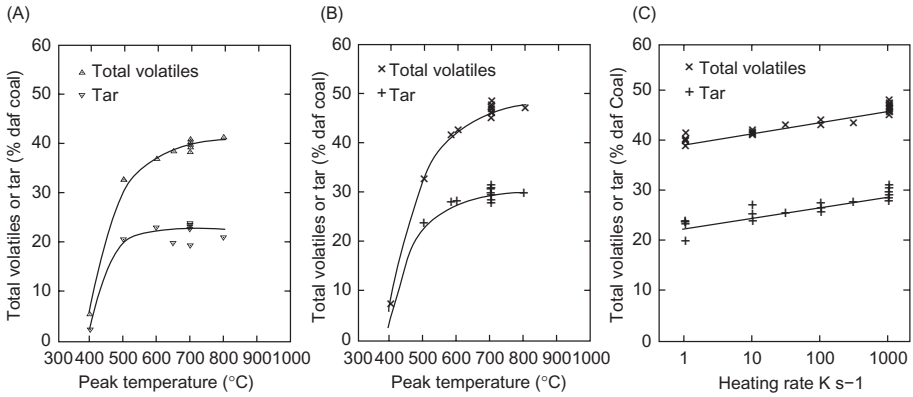

Figure 3.3 Effect of peak temperature, and heating rate on tar and total volatile yields. (A) Tar and total volatile yields at 1°C s^{-1}. (B) Tar and total volatile yields at 1000°C s^{-1}. (C) Effect of heating rate on tar and total volatile yields for a peak temperature of 700°C. Linby coal. 30 s holding at peak temperature; sweep gas, helium at 1.2 bar flowing at 0.1–0.2 m s^{-1}. Particle size range: 106–152 μm.
Source: Reprinted from Gibbins, J.R., Kandiyoti, R., 1989b. Fuel 68, 895. Copyright 1989, with permission from Elsevier.

showing that, compared to lignites or higher rank coals, low-to-middle rank coals show greater sensitivity to changes in heating rate.

Despite some experimental scatter, the data in Fig. 3.3C show that between 1°C s^{-1} and 1000°C s^{-1}, the difference between tar and total volatile yields remained approximately constant. Broadly similar behaviour has been observed for a number of other samples (Table 3.6). It thus appears that the greater volatile evolution observed at higher heating rates consists mainly of additional tar release. One likely explanation is that rapid heating enables greater tar survival, due to the faster expulsion of tars and tar precursors from parent coal particles (Gray, 1988). Slow heating allows more time for the repolymerisation of tar precursors. One further mechanism, possibly operating in parallel, is likely to have contributed to this effect. Compared to slow heating (~1–100°C s^{-1}), rapid heating has been observed to give rise to greater amounts of solvent extractable material in sample particles heated to temperatures in the 400–550°C range (Fong et al., 1986a,b; Fukuda, 2002; Fukuda et al., 2004). It seems reasonable to expect that more tar would evaporate from greater pools of liquid-like 'extractables' forming in rapidly heated coal particles.

We still need an explanation for reasons why greater amounts of extractables are actually formed in some coals during rapid heating. Likely mechanisms for the 'additional' extractable material formation will be revisited in Chapter 6, Elements of thermal breakdown: heating rate effects and retrogressive reactions.

Effect of particle size: Numerous studies have shown that both tar and volatile yields tend to diminish with increasing particle size (e.g., see Suuberg, 1977; Bennadji et al., 2014). Below, we will discuss data from coal pyrolysis experiments under 'vacuum',

showing that even for particles in the 100–150 μm size range, measurable extents of tar and volatile loss takes place through intraparticle secondary reactions.

However, tar/oil and volatile losses do not increase linearly with particle diameter. We will see below (Table 3.12) that char yields of 10–11% were recorded at 500°C, when 100–150 μm diameter particles of silver birch wood were heated slowly (at 1°C s^{-1}) in a wire-mesh reactor. When a similar sample was heated at 1000°C s^{-1} to the same temperature, the char yield was reduced to 4%.

More recently, Bennadji et al. (2014) pyrolyzed samples from three different woods ground to less than 250 μm, in a TG balance: poplar, pine sapwood, and pine heartwood. At 500°C, they reported char yields of 13.7%, 17.2% and 16%, respectively. The results appear comparable with the slow-heating (1°C s^{-1}) wire-mesh reactor result of 10–11%, if extra char formation in the TG balance is taken into account. The same authors also pyrolyzed the same woods, in the form of 2.54 and 3.81 cm diameter spheres (1- and 1.5-in., respectively), at temperatures between 375°C and 475°C. In the preheated reactors, heating rates appear to have been about 1°C s^{-1} (Figure 3 in Bennadji et al., 2014). Unfortunately, the paper only showed large particle data from two of the samples (poplar and pine sapwood) and only pine sapwood data were available for the highest temperature of about 470°C (Figure 9a in Bennadji et al., 2014). The point of all this is, char yield for the 1-in. sphere was about 21%, and only increased to 24% for the 1.5-in. sphere.

Focusing on the data from the 250 μm particles in the TG balance and the data from the highest temperature (475°C), the char yield *increment* with increasing diameter appeared to get progressively smaller. For all experiments, differences in char yields between the smaller (1-in.) and larger spheres (1.5-in., i.e., a 50% increase in diameter) were small: no larger than about 4% at 375°C, and a minimal 2–3% at 475°C (Figure 9 in Bennadji et al., 2014). Going from small to large particles, the initial sharp increase in char yield appears to nearly flatten out for much larger particle sizes. This tapering off in the increase in char yields with increasing diameter is possibly due to the increasing stability of volatiles surviving initial contact with internal surfaces. Moreover, tars formed by the breakdown of tar precursors are likely to be lighter and chemically more stable. More work on char yield versus particle diameter would be useful, in designing larger scale plant for both biomass and coal processing.

The other factor to consider is the interrelationship between particle size and heating rate. At high heating rates, the effect of particle size is difficult to evaluate. The internal transmission rate of the high temperature front is likely to be far lower than the high heating rates imposed at the particle periphery. The heating rate of the coal mass inside larger particles would be governed by the thermal conductivity of the pyrolyzing sample mass. There appears to be no straightforward way of rapidly heating large particles uniformly. We are thus unable to determine extents of intraparticle secondary reactions of larger particles directly, in isolation from heating rate effects – except when working at very low heating rates.

Effect of intraparticle reactions: For particles in the 106–152 μm size range, heated at rates faster than 1000°C s^{-1}, Cai found little change in tar yields with increasing heating rate. However, volatile release continued to increase with heating rate in relatively small increments (Cai et al., 1996).

In a parallel development, Howard and coworkers (Griffin et al., 1993; Howard et al., 1994) constructed a new wire-mesh reactor, where volatiles were drawn away from the heated-mesh by suction tubing via glass funnels, and subsequently quantified. Data were reported for atmospheric pressure pyrolysis experiments in helium, with heating rates ranging from 10°C s^{-1} to 20,000°C s^{-1}. These researchers found that tar yields remained constant above 1000°C s^{-1} for particles in the 106–125 μm diameter range. However, for 63–75 μm coal particles, they found small increases in tar yields when heating rates were raised above 1000°C s^{-1}. The result is important in underlining the interrelationships between tar yields, heating rates and particle size, touching upon the effect of intraparticle secondary reactions on tar yields. Their findings are consistent with experiments showing approximately 5% more tar yield under reduced 'vacuum' (for the same size of particle), implying that about 5% tar loss takes place through intraparticle reactions at atmospheric pressure, for particles in the 106–152 μm size range (also see Section 3.7).

As an aside, it is relatively difficult to reduce the sizes of sample particles used in wire-mesh reactors to much below the mentioned ranges (63–75 μm and 106–152 μm). Commonly used stainless meshes have 64 μm holes and molybdenum meshes available at present, about 100 μm. Clearly, sample particles must not be so small as to drop through the holes in the mesh. Smaller mesh sizes woven in stainless steel are available and may be used although smaller-weave molybdenum wire mesh does not seem to be commercially available. In any case, difficulties due to static electricity do not allow easy handling of sample particles much below 60 μm. Even in the 106–152 μm range, particles display static electricity related effects during weighing on the pan balance (Gibbins, 1988). Not widely publicised, the effect would (if ignored) tend to distort results by giving weighing errors and likely invalidate data from experiments that might have otherwise been meticulously executed. The problem is easily resolved by the use of a commercially available 'static gun'.

The size of thermocouple wires can also create problems. The common stainless steel meshes with 64 μm holes can accommodate thermocouple wires of 50 μm diameter. When smaller stainless steel mesh sizes are used, the next available standard size of thermocouple wire is 25 μm in diameter, which is quite difficult to handle on a routine basis, even by experienced operators. Moreover, the use of mesh with much smaller aperture sizes would be impractical, because of insufficient permeability for carrier gas and for the passage of evolving volatiles through the mesh. The possibility of tar cracking on the mesh has been considered and found to be negligible for the reported combinations of particle/mesh sizes (Gibbins-Matham and Kandiyoti, 1988).

3.4 Designing bench-scale fixed-bed ('hot-rod') pyrolysis reactors

In fixed-bed reactors, sample particles are stacked to the desired bed-depth. Heat usually diffuses inward from the reactor walls. As the temperature rises, released

volatiles expand, giving rise to local pressure gradients that help push volatiles out of the fixed-bed and eventually out of the reactor (e.g., cf. Berk, 1978). A steady flow of carrier gas would help maintain relatively constant volatile residence times inside the reactor. Comparable residence times would then allow comparing data from reactors of different sizes but of similar shape (Dryden and Sparham, 1963). The reactor body can be used as a resistance heater if electrodes are clamped at both ends. The original 'hot-rod' reactor configuration used in the hydropyrolysis experiments of Hiteshue et al. (1957) is completed when the reactor body is made of an alloy tube able to withstand high pressures, as well as the high reaction temperatures.

Despite inherent problems associated with secondary reactions between stacked particles and evolving volatiles, the 'hot-rod' reactor configuration has proved useful. It is relatively easy to construct and to operate. It was originally conceived at the U.S. Bureau of Mines laboratories, for examining the hydropyrolysis behaviour of coals. Several incarnations later, 'hot-rod' reactors were used at the Coal Research Establishment (British Coal, UK) for investigating the production of benzene, toluene and xylenes ('BTX'), from the hydropyrolysis of middle rank coals (Finn et al., 1980; Fynes et al., 1984).

3.4.1 Hydropyrolysis in fixed-bed ('hot-rod') reactors

In early work, Hiteshue and coworkers at the U.S. Bureau of Mines (Hiteshue et al., 1957, 1960, 1962a,b) conducted coal hydropyrolysis experiments in 'hot-rod' reactors, at pressures up to 400 bars and nearly 900°C. Sample beds of 25–40 cm height were mounted inside thick-walled stainless steel tubes. In later work, reactors with different aspect (length/diameter) ratios were tested by Graff et al. (1976) and Kershaw and Barras (1979). The version constructed and operated by Ladner and coworkers at the Coal Research Establishment (Stoke Orchard, UK) held about 10 g of coal in 75 cm long, 8 mm internal diameter reactor tubes, manufactured out of stainless steel rods (Finn et al., 1980; Fynes et al., 1984).

At Imperial College, a smaller (6 mm i.d.; 20 cm long) reactor was made, originally to produce larger amounts of tar during hydropyrolysis experiments than was possible in wire-mesh reactor experiments. Initially, between 0.5 and 1 g of sample was used, in experiments designed to examine the effects of the heating rate and carrier gas flow rates. Comparing results with the longer 'hot-rod' reactor operated at the Coal Research Establishment facilitated the observation of tar loss with increasing sample bed height (O'Brien, 1986; Bolton et al., 1987). This led to the use of much shallower (~4 mm) fixed-beds, corresponding to about 50 mg of sample (Fig. 3.4A) placed near the bottom (exit) of the reactor. The shallow bed depth helped to partially suppress secondary reactions between evolving volatiles and pyrolyzing chars (Gonenc et al., 1990). The reduced bed-height also improved axial temperature uniformity. This reactor was operated at heating rates between 10°C min^{-1} and 10°C s^{-1}. Faster heating rates were calculated to lead to unacceptably steep radial temperature gradients in the 6 mm diameter sample bed (O'Brien, 1986).

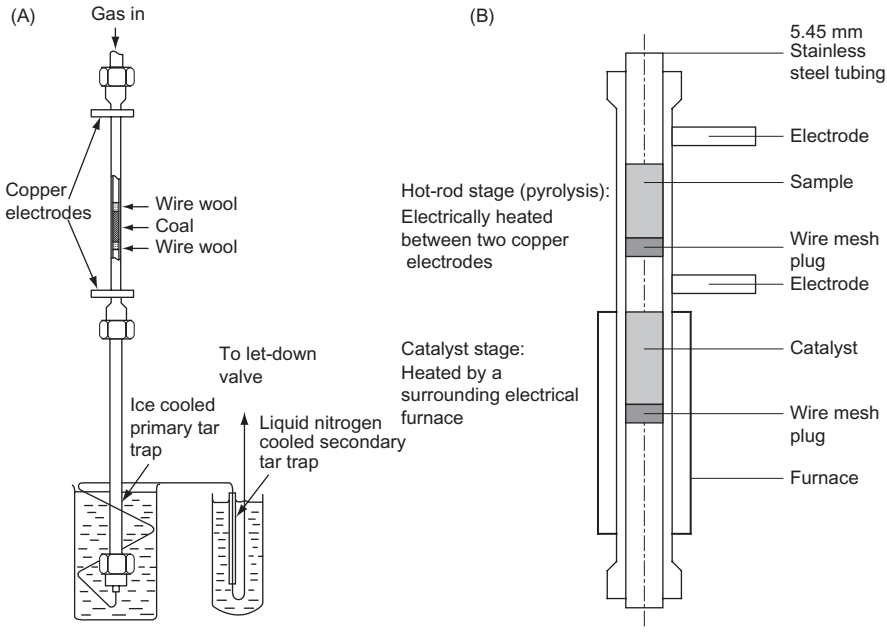

Figure 3.4 The 'hot-rod' reactor configuration. (A) The common single-bed reactor. (B) Two fixed beds in tandem; the lower bed is heated by a separate furnace and packed with catalyst for hydrotreating volatiles released by the sample pyrolyzing in the upper bed.
Source: Reprinted from: (A) Bolton, C., Snape, C.E., O'Brien, R.J., Kandiyoti, R., 1987. Fuel 66, 1413. Copyright 1987, with permission from Elsevier; (B) Pindoria, R.V., Megaritis, A., Herod, A.A., Kandiyoti, R., 1998b. Fuel 77, 1715. Copyright 1998, with permission from Elsevier.

3.4.2 Fixed-bed ('hot-rod') reactor construction

The 'hot-rod' reactor configuration allows the reactor body to act as a resistance heater as well as the pressure vessel. The design requires the vessel walls to contain the operating pressure at the temperature of the reaction. Depending on the particular experiment, 'hot-rod' reactors have been used at temperatures up to 1000°C, at elevated pressures. The original U.S. Bureau of Mines reactors consisted of small-bore, thick walled stainless steel tubes, which were discarded after one or several experiments. At British Coal, relatively long (>75 cm), 8 mm bore stainless steel reactors were made by drilling into cylindrical stainless steel rods from both ends (Finn et al., 1980; Fynes et al., 1984). Standard practice was to discard the reactor bodies after several runs. Considerable machining time went into making these reactors and their frequent renewal would have been costly.

Several high tensile strength alloys were used at Imperial College for making more durable "hot-rod" reactors, with the aim of reducing workshop time requirements. Initially, reactor tubes were made from rods of Nimonic-80 and Nimonic-105

alloys (Henry Wiggin Alloys) for use in experiments at up to 850°C and pressures up to 100 bars. These reactors could sustain repeated use. Although the design of the Imperial College reactors only required shorter (20 cm) tubes to be made, it was still necessary to drill the rods from both ends. However, Nimonic alloys require heat treatment for softening before machining and a second heat treatment stage to harden the finished reactor, after machining.

Compared to the Nimonic alloys, Incolloy 800 HT was far easier to machine and was used to make reactor bodies for CO_2 and steam gasification experiments up to 1000°C and 40 bar. Above 700°C, however, the use of rigid electrodes clamped onto the reactor body caused reactor tubes to distort due to thermal expansion. To allow for movement, power was supplied to one of the electrode clamps through woven-copper cables. Both electrode clamps were water cooled to prevent changes in resistivity (Pindoria et al., 1998a; Collot et al., 1999). Although the machining of Nimonic alloys turned out to be an extreme case, many high performance alloys are harder and more difficult to machine compared to high grade stainless steels. There is an element of compromise, therefore, between making durable reactors that are more difficult to make and shorter life reactors made from alloys that are easier to machine.

The 'hot-rod' configuration has proved versatile. In another application, trace element releases from various solid fuels were measured during the co-pyrolysis and co-gasification of coal and biomass. To prevent contamination by contact with metal walls, a larger (13.8 mm) internal diameter reactor was constructed of Incolloy 800 HT. The reactor was lined with a loose fitting quartz sleeve that housed the sample. Experiments were carried out at up to 40 bars and 1000°C (Collot et al., 1999).

Relatively few two-stage experiments using the 'hot-rod' reactor configuration have been described in the literature. Bolton et al. (1988) attached a second bed packed with hydrous titanium oxides, for catalytically cracking hydropyrolysis tars generated in the first stage. The runs were mostly carried out at 150 bars. The (upper) hydropyrolysis stage was ramped from ambient to 500°C and held constant, while the catalyst stage was pre-heated to temperatures up to 400°C and held constant throughout the experiment. The tar yield from the first stage was about 25% of the original coal mass. The authors reported the conversion of the tars into 'into colourless liquids low in heteroatoms' with about 40% boiling below 140°C.

Fig. 3.4B shows the two-stage fixed-bed reactor constructed at Imperial College for the hydropyrolysis of woody biomass followed by the hydrocracking of evolved tars/oils. The upper (shortened 'hot-rod') section was used to produce the tar/oil vapours by mild hydropyrolysis (H_2-pressure up to 40 bars). Gas flowed through the fixed-bed and swept the volatiles into the second, catalyst-packed stage, positioned below the sample and heated independently by a small furnace (Pindoria et al., 1998b). Results from this experimental setup will be outlined in Chapter 4, High-pressure reactor design: pyrolysis, hydropyrolysis and gasification. Section 3.10.2 will also present a two-stage, atmospheric pressure fixed-bed reactor design, developed for simulating the suppression of tar content in the product gas from downdraft biomass gasifiers. More recently, experiments using this reactor configuration have been carried out at Shanghai Jiaotong University (Zhang et al., 2015).

3.5 Bench scale fluidised-bed and entrained flow pyrolysis reactors

3.5.1 Bench scale fluidized-bed pyrolysis reactors

Fluidized-bed pyrolysis experiments are usually done in flash pyrolysis mode, by injecting sample particles into an already heated bed of solids. The fluidising gas sweeps evolving volatiles out of the reaction zone.

Fig. 3.5A shows an early bench-scale fluidized-bed design, developed by Tyler (1979, 1980) at CSIRO in Sydney. The reactor (~50 mm i.d.; ~350 mm high) was made of quartz. Several grams of fuel particles were dropped at a rate of about 1 g min^{-1} through the inner of two concentric tubes, into the heated bed of sand particles. The outer annular space carried cold nitrogen, to keep sample particles cool. Tyler used superficial gas velocities of about five-times minimum-fluidisation and operated the reactor at temperatures up to 900°C. At the end of an experiment, sample weight loss was determined by weighing all bed solids together and comparing with

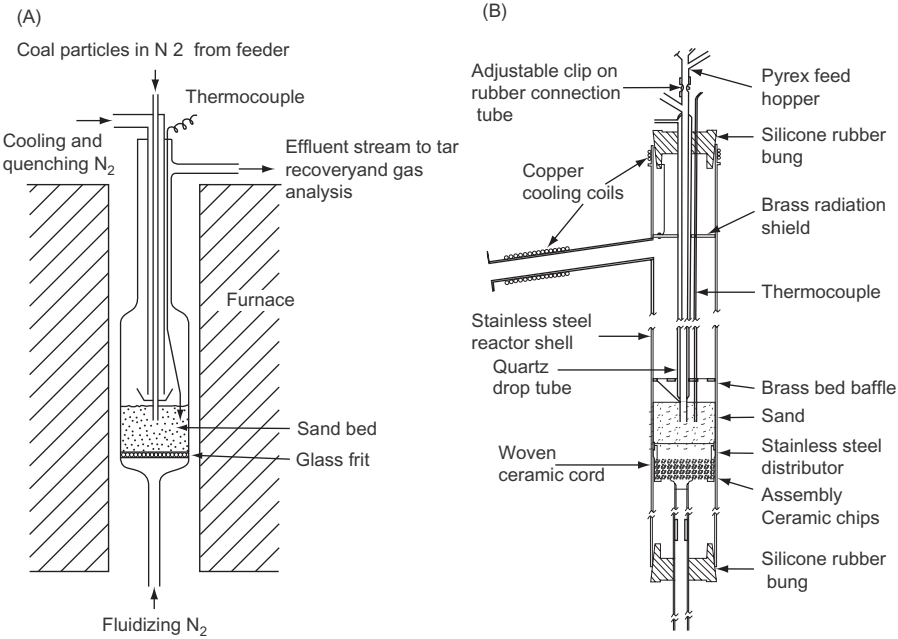

Figure 3.5 (A) Fluidised-bed pyrolyzer made of quartz (Tyler, 1979, 1980). (B) Fluidised-bed pyrolyzer with movable support plate, where volatile residence times in the freeboard may be varied without altering fluidising conditions (Stiles and Kandiyoti, 1989).
Source: Reprinted from: (A) Tyler, R.J., 1979. Fuel 58, 680; Tyler, R.J., 1980. Fuel 59, 218. Copyright 1979; with permission from Elsevier; (B) Stiles, H.N., Kandiyoti, R., 1989. Fuel 68, 275. Copyright 1989, with permission from Elsevier.

the weight of the original bed of solids and the amount of sample injected. Product tars were captured and recovered by cooling the tar traps with liquid-nitrogen.

Fig. 3.5B presents the schematic diagram of a larger (76 mm i.d.; 1000 mm high) fluidised-bed pyrolysis reactor made of stainless steel, designed and constructed at Imperial College. The design was based on Tyler's concept, with several additional features. The fluidised-bed itself was mounted on a vertically mobile support plate, enabling residence times of evolved volatiles in the reactor freeboard to be changed without altering fluidising conditions. Freeboard residence times could be changed between 0.8 and ~4 s, normally using 3–3.7 times the incipient fluidising velocity (Stiles and Kandiyoti, 1989). The variability of the freeboard height allowed collecting data for calculating kinetic constants of tar cracking reactions (Stiles, 1986).

During trial runs, it was observed that tar and char yields were distorted by solid particle carryover into the quench zone. The effect was particularly severe during operation at shorter freeboard heights and during runs with lower density substrates, such as cellulose and wood dust. A wire screen (denoted as 'brass bed baffle' in Fig. 3.5B) was placed above the fluidised-bed to block elutriation. Careful cold-trap design also pays off in this reactor configuration, to stop lighter tars from escaping from tar traps alongside light hydrocarbons.

Product trends from this reactor will be presented and compared with those from a wire-mesh reactor in Section 3.6. More recently, Morgan et al. (2015a) adopted this basic design for examining product distributions from a range of sub-tropical biomass materials. Experiments were done with samples washed with water, to remove some of the mineral matter content. As we will see below, the removal of minerals by treatment with cold water proved useful in enhancing tar/oil yields. In Morgan's design, an additional piece of wire-mesh was installed in the side-arm flange connection to catch any char that escapes past the bed screen (baffle). This feature was helpful in improving char recovery, by blowing chars out of the bed after reactor cool-down and collecting them on the screen inside the side-arm flange (Morgan et al., 2015a).

3.5.2 Bench scale entrained-flow ('drop-tube') reactors

Entrained-flow reactors (EFRs) are (usually) vertically mounted, pre-heated reactor tubes. Sample particles are injected into the heated zone in batch or continuous mode. Radiation from heated walls is estimated to heat samples rapidly ($>10^4$°C s^{-1}); pre-heating the carrier gas stream forced into the reactor may also be used to boost the heating rate. However, provision cannot be made to determine, or effectively control, particle heating rates. Co-current gas velocities may be increased to shorten residence times, although, the flow is often kept laminar to minimise particle to particle contact and particle adhesion to reactor walls. Operation in dilute particle injection mode allows monitoring the behaviour of sample particles with minimal interaction with neighbouring particles. The configuration is readily adaptable to high-pressure operation and lends itself to pyrolysis, gasification, and combustion experiments; temperatures as high as 2200°C have been attained (Kimber and Gray, 1967). EFRs have been widely used to simulate coal pyrolysis and combustion under conditions

thought to approach pulverised-fuel firing conditions (e.g., cf. Freihaut and Seary, 1981; Sun et al., 2005).

Reproducibilities of mass closure data are known to be variable, in part due to sample particle adherence to heated reactor walls. Sample weight loss in EFRs is nearly always calculated indirectly. The 'ash-tracer' method used for this purpose compares ash contents of the original sample material and of product chars. Sample weight loss (evolved volatiles) is then back calculated by assuming that ash is conserved within char particles and remains unchanged by the experiment (e.g., cf. Ballantyne et al., 2005). In Section 3.6.4, we will compare weight loss from experiments in wire-mesh reactors and EFRs using common sets of coal samples (Hindmarsh et al., 1995). Briefly, the data indicate that a distribution of particle residence times develops as particles move down the reactor, leading to differences in the levels of completion of pyrolysis reactions. As a result, the volatile release data displayed significant levels of scatter.

Researchers at Tohuku University in Japan have developed an EFR equipped with a graphite filter, 'to control the residence time of coal particles' (Tsubouchi et al. 2003, 2014). The filter serves to stop sample particles at the bottom of the reactor. The arrangement was intended to eliminate 'short' residence times, although the proposition that 'the time of 0 s means the absence of the filter' causes some difficulty, as the time of travel through the tube must be greater than 0 s. Moreover, the description of the operation requires clarification, as the papers have not explained how particles are removed from the reactor during intermediate length (40 and 120 s) residence time runs.

Another difficulty posed by the use of EFRs in pyrolysis experiments is the uncertain fate of tars/oils evolved from pyrolyzing particles during free fall or forced entrainment. Within the reaction zone, some contact of tar vapours with entrained coal particles and reactor walls may be visualised to take place over the length of the reactor. Clearly, at temperatures above 550–600 °C, 'in-flight' tar aerosol residence times longer than several hundred milliseconds in the heated zone would lead to significant extents of cracking (Stiles and Kandiyoti, 1989). Due to their greater thermal sensitivity, biomass-derived tars/oils alter more rapidly and react at lower temperatures than coal tars. Thus both the yields and the chemical structures of tars/oils from EFRs only imperfectly relate to tars/oils initially released from sample particles. Results from the quantitative evaluation and structural characterization of tars/oil produced in entrained-flow ('drop-tube') reactors are therefore affected by significant extents of thermal degradation.

On the benefit side, entrained-flow ('drop-tube') reactors do not necessarily need sophisticated instrumentation and are relatively easy to construct. Despite reservations, they have been used widely in industrial research, to collect data for modelling pulverised-fuel combustion. More recently, researchers at the National Renewable Energy Laboratory (NREL) in Golden, Colorado (USA.) have been operating several EFRs, ranging from bench-scale to pilot-scale systems, for studying the fast pyrolysis of biomass (Brown et al., 2001; Jarvis et al., 2011; Gaston et al., 2011). The reactors are reported to be equipped with on-line 'molecular beam' mass spectrometry (MD-MS) to analyse tar/oil vapours generated during pyrolysis.

The *bench-scale* EFR at NREL has been operated with residence times ranging from 0.2 to 1.0 s. Studies have also been performed at elevated pressures and global kinetics at high heating rates has been examined. The NREL 0.5 metric ton per day pilot scale EFR, described on the NREL website (NREL Website url cited in References), was constructed from a series of straight lengths, connected with u-bends. Samples may be withdrawn at each of the u-bends. Volatiles were directly admitted into the molecular beam-MS and/or quenched; char particles were recovered for characterization. The system allowed the effect of residence time to be studied by drawing sample at successive sampling-points along the length of the reactor. The shortest residence times reported for the NREL pilot scale EFR were, typically, above the 0.5 s range.

In view of inevitable tar/oil aging and cracking reactions taking place along the length of EFRs and the freeboards of fluidised bed reactors, it seems difficult to consider tar/oil samples drawn in these experiments to be primary pyrolysis products. Nevertheless, indexing tar/oil structures with increasing residence times and comparing thermal degradation seems a valid topic for research. It is also noted that the MB-MS used on the NREL reactors was stated to have a nominal range of m/z 450, although the mass ranges indicated in the data presented did not exceed m/z 220 (Jarvis et al., 2011; Gaston et al., 2011). Whether material up to m/z 450 may be considered to represent the entirety of the biomass pyrolysis tars/oils will be discussed further on in this chapter, and in Chapter 7, Analytical techniques for low mass materials: method development, and Chapter 8, Analytical techniques for high mass materials: method development, of this book.

3.6 Comparing results from several bench-scale reactors: coal pyrolysis

In this section, product trends from atmospheric pressure coal pyrolysis experiments in the fixed-bed ('hot-rod') reactor will be compared with data from the wire-mesh reactor operated in slow heating mode. Rapid-heating wire-mesh reactor data will then be compared with results from the fluidised-bed reactor, operated in 'flash' heating mode.

3.6.1 Results from wire-mesh, fluidized-bed and 'hot-rod' reactors

We have already discussed the general requirement that results from a valid measurement must be independent of the method of the measurement. In translating this principle to the design of pyrolysis experiments, however, the discussion of Section 3.3 has already indicated that we need to trim our sails a little. The aim must nonetheless be to measure product distributions in a manner that is as free as possible from effects due to reactor design and sample configuration. In this section, we will compare results from several techniques, to examine how closely data from each method reflect the fundamental behaviour of the samples. We will find that each of

the different reactor designs available for this study is suitable for generating reliable data under a particular range of reaction conditions.

Operating ranges of wire-mesh, fluidised-bed and fixed-bed reactors: Table 3.1 presents characteristic parameters of three reactors used at Imperial College for the "Three-Rig" comparison (Gonenc et al., 1990). Since the publication of the original study, improvements have been made to reduce the scatter in the data and broaden the range of available experimental conditions. The original study was conducted at atmospheric pressure, between 400–800°C, using a common sample of Linby (UK) coal (moisture, (as received): 2.1%; ash, (dry basis): 5.3%; volatile matter (dry, ash free): 40.1%. C: 81.5, H: 5.2, N: 1.8, O: 10.6% w/w (dry, ash free); S: 1.5% (dry basis); particle size range: 106–150 μm).

3.6.2 Comparing slow-heating rate data from the 'hot-rod' and wire-mesh reactors

Fig. 3.6a presents tar and total volatile yields from the 'hot-rod' reactor experiments at temperatures up to 800°C. The experiments were performed by heating 300 mg

Table 3.1 Summary of experimental parameters for the three reactor systems used at Imperial College by Gonenc et al. (1990)

	Fluidised-bed reactor	Wire-mesh reactor	Hot-rod reactor
Sample size	1–15 g	5–15 mg	50–1000 mg
Temperature range	To 900°C	To 1200°C	To 900°C
Pressure range	Atmospheric	Vacuum to 160 bar	Atmospheric 150 bar
Heating rate	Flash heating rate is function of temperature; can also operate as slow heating reactor	Very slow to 5000°C s^{-1}	Very slow to 10°C s^{-1}
Sweep gas flow rate	3–5 × minimum fluidisation	Very slow to 0.3 m s^{-1}; very slow at higher pressures	Very slow to 10 m s^{-1}
Secondary reactions	Potentially intense in the bed and freeboard; better quantified than 'hot-rod'	Minimal but non-zero	May be minimised at very high flow rate
Accuracy/Repeatability	Tar: ±2–3% Char: ±5%	Tar: ±2–3% Char: ±1–2%	Tar: ±2–3% Char: ±3–4%

Source: Reprinted from Gonenc, Z.S., Gibbins, J.R., Katheklakis, I.E., Kandiyoti, R., 1990. Fuel 69, 383. Copyright 1990, with permission from Elsevier.

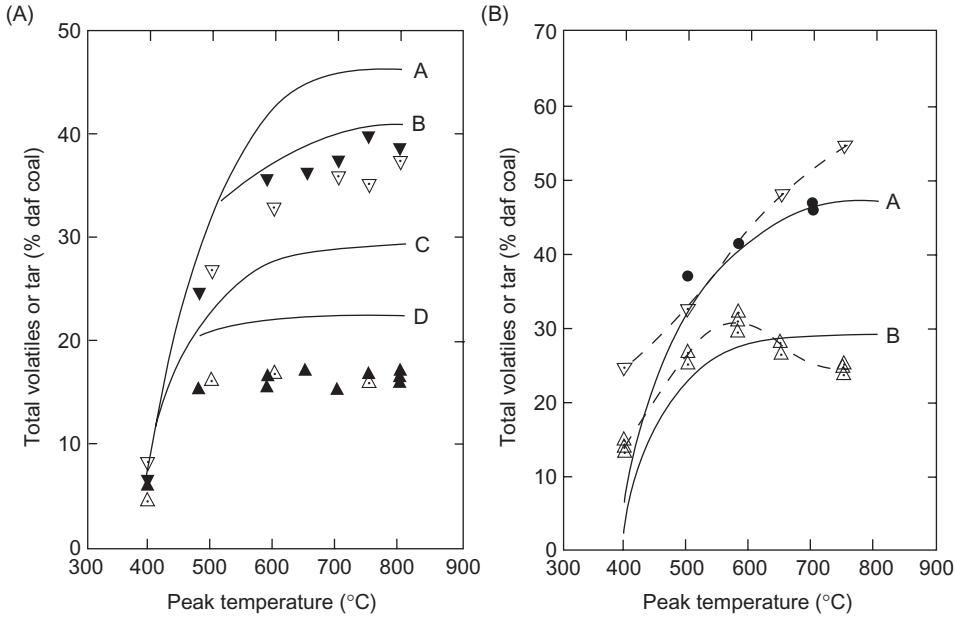

Figure 3.6 (a) Comparison of results from the wire-mesh (solid lines) and 'hot-rod' reactors. (∇,▼): Total volatile yield from the 'hot-rod' reactor with helium (∇) and H_2 (▲) as carrier gas, respectively. (Δ,▲): Tar yields from the 'hot-rod' reactor with helium (Δ) and H_2 (▲) as carrier gas, respectively. Solid lines show data from the wire-mesh reactor. (**A**) Total volatiles; 1000°C s^{-1}. (**B**) Total volatiles; 1°C s^{-1}. (C) Tar yield; 1000°C s^{-1}. (**D**) Tar yield: 1°C s^{-1}. (b) Comparison of results from the wire-mesh and fluidised-bed reactors. (∇): Total volatile yield from the fluidised-bed reactor. (Δ): Tar yield from the fluidised-bed reactor. Solid lines show data from the wire-mesh reactor (heating at 1000°C s^{-1} with 30 s holding). (**A**) Total volatiles. (**B**) Tar yield. (●): Total volatiles from wire-mesh reactor during heating at 1000°C s^{-1} with 1000 s holding at peak temperature.
Source: Reprinted from Gonenc, Z.S., Gibbins, J.R., Katheklakis, I.E., Kandiyoti, R., 1990. Fuel 69, 383. Copyright 1990, with permission from Elsevier.

of sample in helium at 5°C s^{-1}, with 200 s holding at peak temperature. These data are superposed on wire-mesh tar and total volatile yield data (shown as solid lines), from experiments performed at 1°C s^{-1} and 1000°C s^{-1}, over the temperature range. During both sets of experiments, a carrier gas superficial velocity of 0.1 m s^{-1} was used to sweep through the bed of sample.

Fig. 3.6a shows that both tar yields and total volatiles release observed in the "hot-rod" reactor (operated at 5°C s^{-1}) were measurably lower than those from the wire-mesh reactor (solid lines B and D), operated at the lower heating rate of 1°C s^{-1}. The differences between the two sets of data reflect product loss through contact between evolving volatiles and pyrolyzing solids in the fixed-bed reactor. An additional likely factor contributing to product loss was signalled by the increase in pressure drop by

Table 3.2 Comparison of the effects of bed height and sweep gas flow rate on tar yields from the 'hot-rod' reactor

	1	2	3	4
Sample size (mg)	300	300	50	50
Approximate bed depth (mm)	20	20	4	4
Superficial velocity (m s^{-1})	0.1	9.5	0.1	9.5
Approximate gas residence time in the coal bed (s)	0.2	0.002	0.03	0.0003
Tar yields (% w/w daf coal)	16.0[a]	18.0	18.6[a]	21.9[b]
Percent change in tar yield over the 'Base Case' (% w/w daf coal)	Base case	+2.0	+2.6	+5.5

Source: Reprinted from Gonenc, Z.S., Gibbins, J.R., Katheklakis, I.E., Kandiyoti, R., 1990. Fuel 69, 383. Copyright 1990, with permission from Elsevier.
[a]Average of two runs.
[b]average of three runs.

several bars across the sample bed around 500–550°C. This appears due to sample softening, which would lead to ill-defined gas flow patterns and exacerbate tar loss through vapour-solid contact within the fixed bed (Gonenc et al., 1990). The solid triangles in Fig. 3.6a represent tar and total volatile yields from operation with *hydrogen* at 1 bar in the 'hot-rod' reactor. Tar yields were unchanged while total volatile yields increased by a little more than experimental scatter. At these lower pressures, the reactivity of hydrogen appears to be relatively low.

In general, as reactor temperatures are raised above 500–550°C, any coal tar vapours lingering in the heated zone would be expected to degrade through cracking and repolymerisation reactions, the latter leading to char formation. For example, the *fluidised*-bed coal tar yield curve in Fig. 3.6b (near line B) shows just such a maximum (also see Figure 3.8, below). However, in Fig. 3.6a, tar yields from the 'hot-rod' reactor may be observed to have levelled off at about 500°C. Any decline of tar yields at higher temperatures was clearly absent, suggesting that tars released at up to about 500°C exited from the reactor before the reactor could reach much higher temperatures. This is due to the combination of sweep gas carrying tar vapours out, the short reactor tube and the (relatively) slow rate of temperature rise.

The effect of gas sweep velocity and bed depth in the 'hot-rod' reactor: We have already observed that gas–solid interactions in the fixed-bed reactor can lead to loss of tar and volatile products. Table 3.2 compares the effect of bed depth (reflecting the extent of volatiles contact with bed solids) and superficial carrier gas velocity (related to gas residence time) on tar yields.

In this configuration, it was not possible to operate with sample sizes below 50 mg, as smaller samples gave unacceptable scatter, due to recovery and weighing errors. Similarly, velocities greater than 9.5 m s^{-1} could not be attempted as the greater volumes of carrier gas could not be preheated adequately and tended to cool the sample bed. Increasing pressure drops also imposed an upper limit to the sweep gas velocities possible with the present design. Hydrogen was used as sweep gas, to minimise

increases in pressure drop across the bed, observed during the coal softening and tar evolution stages. Pressure drop fluctuations were more severe at the higher flow rates. Experiments summarised in Table 3.2 were carried out by heating at 5°C s^{-1} to 590°C.

In Table 3.2, increasing the gas velocity appears to only partially counteract tar loss through increasing bed-depth, by removing some of the tars more rapidly from the reaction zone (Gonenc et al., 1988). There is no evidence to suggest that any additional tar is removed from the pyrolyzing coal by the substantial increase in gas velocity, above and beyond what can be collected from a virtual monolayer of sample in the wire-mesh reactor using a mere 0.1 m s^{-1} gas sweep. A similar exercise involving the wire-mesh reactor showed no sensitivity to flow rate above and beyond what was needed to remove volatiles away from the reaction zone. Table 3.2 also shows that for the shorter bed and the higher flow rate, results tend toward 22%, close to the 24% tar yield expected in the wire-mesh reactor, when heating at 5°C s^{-1}.

Tar travel through a fixed bed of pyrolyzing coal: In Table 3.2, comparing data in Columns 2 and 3 with Column 1, we observe that a hundred-fold increase in the superficial gas velocity causes an increase in tar recovery comparable to reducing the bed depth by a factor of five. In an important early study, Griffiths and Mainhood (1967) passed tar vapours and model compounds through a bed of active carbon at 500°C. They reported that the 'dependence of retention time on boiling point is similar to that found in gas–liquid chromatography'. However, the active carbon acts as a cracking catalyst for the lower boiling constituents of the tar, while enhancing condensation reactions between higher boiling constituents, leading to char formation. Taken together, the evidence suggests that tar survival is less than directly related to the sweep gas velocity and more closely related to the incidence and duration of contact with heated bed solids. Table 3.2 confirms that reducing the 'chromatographic' travel time (i.e., reducing the bed depth) affects tar survival more directly than increasing the superficial velocity of the sweep gas. Axial tar transport may thus be viewed as taking place in forced convection mode, interrupted by a sequence of 'sticky', reactive collisions with pyrolyzing solids. The reexamination of data from the original 'hot-rod' reactor (Hiteshue et al., 1962a) supports this proposition. A more detailed comparison of results from the wire-mesh and 'hot-rod' reactors may be found in Gonenc et al. (1990).

3.6.3 Rapid heating: comparing data from the fluidised-bed and wire-mesh reactors

Fig. 3.6b compares tar and total volatile yields from the wire-mesh (solid lines) and fluidised-bed reactors. The latter was operated with a freeboard height corresponding to the shortest possible (0.8-s) volatiles residence time possible in this reactor. This was done to minimise tar cracking in the freeboard (Stiles and Kandiyoti, 1989). Several points have emerged from this comparison, showing up shortcomings in both designs.

First, the wire-mesh reactor gave less tar and volatiles at 400°C compared to the fluidised-bed reactor. During this set of runs, the time-temperature ramp in the wire-mesh reactor was followed by 30 s holding at peak temperature. At the relatively low

temperature of 400°C, 30 s appears to have been too short for pyrolysis reactions to run to completion. By contrast, in the fluidised-bed reactor, chars remain in the heated bed for several minutes after the furnace heating current is turned off. This is done for the solids to cool sufficiently to be removed and weighed; apparently this is long enough for some more volatiles to evolve from the sample. In addition to heat transfer being more efficient due to the vigorous circulation of particles in the bed, the longer sample residence time at or near peak temperature in the fluidised-bed thus turns out to lead to somewhat increased volatile release.

In Fig. 3.6b, the points marked as (●) represent data for 1000 s hold time in the wire-mesh reactor. The total volatile yield at 500°C increased sharply, but results at 600°C and 700°C remained unchanged. Clearly, 30 s at 400–500°C in the wire-mesh reactor was not sufficient for pyrolysis reactions to reach completion. Subsequent work by Li et al. (1993a) presented in Table 3.3 shows this effect more clearly. At 400°C, the main changes for Linby coal occurred between 30 and 100 s. Later work by Fukuda showed variations from 30 to 400 s between different coals, regarding the length of time required in the wire-mesh reactor for pyrolysis reactions to reach completion at temperatures below 500°C (Fukuda, 2002; Fukuda et al., 2004). The effect appears to depend, at least in part on the structural makeup of particular coals. By contrast, the analogous length of time needed at 700°C for completion of volatile release – for all coals so tested – was less than 1 s.

In the wire-mesh reactor, the longer times required for reactions to reach completion at low temperatures are probably due to overlapping effects of slow reaction kinetics (just discussed), compounded by poor heat transfer from the mesh to the sample particles at these low temperatures. Above 500°C, the mesh can be observed to glow with the naked eye. Radiative heat transfer clearly plays an increasingly important role in heating the sample particles. It is also likely that thermal contact between mesh and sample improves if/when coals soften, usually in the vicinity of 500°C during fast heating experiments. In any case, some care seems necessary in the evaluation of results obtained in wire-mesh reactors at temperatures between 400–500°C, due to the sensitivity of the yields to small variations in the final experimental temperature attained.

The difference between yields from the two reactors may also have been somewhat exaggerated by the larger estimated error inherent in the char yield determinations in the fluidised-bed (Table 3.1). The measurement is made by tipping out all the contents

Table 3.3 Linby vitrinite concentrate total volatile and tar yields (% w/w daf basis) as a function of holding time at 400°C in the wire-mesh reactor. Heating rate: 1000°C s^{-1}

Holding time (s)	30	100	200	250
Tar yield (% daf)	6.7	13.1	12.3	14.3
Total volatiles (% daf)	10.1	20.8	19.9	22.1

Source: Reprinted from Li, C.-Z., Bartle, K.D., Kandiyoti, R., 1993a. Fuel 72, 3. Copyright 1993, with permission from Elsevier.

of the fluidised-bed and comparing the weight with the sum of the original weight of the sand bed added to that of the sample. With the best of operator care, this still turns out to be a difficult experiment to perform accurately.

Tar cracking in fluidized beds: In Fig. 3.6b, the tar yields determined in fluidised-bed experiments were observed to trace a maximum with increasing temperature and to diminish above about 580–590°C. This is the other major difference between the two reactors. When significant secondary charring and/or cracking reactions occur, pyrolysis tar yields usually trace a maximum and decline sharply at higher temperatures (Fig. 3.6b; also see Figure 3.8). Tyler (1979, 1980) has pointed out that the monotonic increase of the *total volatile* curve with increasing temperature suggests that a significant proportion of tar is 'lost' by cracking to gaseous products. For biomass samples and lower rank coals, the position of the maximum usually shifts to lower temperatures, as a result of the greater thermal sensitivity of tars evolving from highly oxygenated samples. For cellulose and silver-birch (a soft-wood) tars/oils, the maximum occurred between 400°C and 425°C, while for a lignite, it was observed nearer 530°C (Stiles and Kandiyoti, 1989). During pyrolysis experiments using semi-tropical banagrass, Morgan et al. (2015a) reported observing the tar yield maximum at around 450°C.

The ability to change freeboard residence times of volatiles enables the calculation of tar cracking kinetics. It also allows estimating the amount of tar destroyed in the bed itself, as a function of reactor temperature. The procedure has been described by Gonenc et al. (1990). During experiments with Linby coal, ~31% of the original sample mass was estimated to have entered the freeboard at 580°C as tar, while at 750°C, the figure was down to 26%. The difference represents the amount of tar destroyed within the bed itself at the higher temperature, before tar vapours reach the freeboard.

By contrast, the relative freedom from secondary reactions of evolving tars in the wire-mesh reactor enables tar yields to remain constant, within experimental scatter, once the temperature for maximum tar production has been reached. However, in the case of thermally more sensitive cellulose tars, or very high heating rates (Peters et al., 1980; Griffin et al., 1993), some tar loss has been observed in wire-mesh reactors, showing a shallow decline in tar yield. In wire-mesh reactors developed at Imperial College, the flow of gas sweeping through the sample holder has served to minimise this effect. However, when peak temperatures above 1000°C are used, some tar loss has been observed – particularly for long hold-times, when tars/oils deposited on the ceiling of the tar-trap (near the entrance to the off-take tube; see Fig. 3.1B) 'see' radiation from the glowing mesh. When tar yield determinations are intended, the effect can be minimised by reducing the hold time at high peak temperatures.

3.6.4 Results from an entrained-flow ('drop-tube') and a wire-mesh reactor

These two reaction types have all but occupied centre-stage in most combustion related research during the past several decades. Data from both techniques have been used in mathematical simulations of pf combustion.

Hindmarsh et al. (1995) have undertaken a comparison of results from the two reactors at atmospheric pressure, using a common set of coal samples. Table 3.4 presents pyrolysis data from the two reactors using similar, but not quite identical, experimental conditions. Two different particle size ranges were used: a 38–75 μm fraction in the EFR and the usual 106–152 μm size fraction in the wire-mesh reactor. Furthermore, the entrained-flow ('drop-tube') reactor was operated with nitrogen rather than helium and at a temperature 50°C higher than the peak temperature used in the wire-mesh reactor. Nominal residence times were on the order of 1 s and sample weight loss in the EFR was calculated by the ash tracer method.

The results in Table 3.4 show systematically lower total volatile yields measured in the EFR experiments. The differences were large for the three softening coals: Linby and two samples of Illinois No. 6 coal. Columns 3 and 6 in Table 3.4 report the level of residual volatile matter remaining in the *chars*. The 3–9% range of values recorded for the EFR chars suggests that pyrolytic reactions have not run to completion. The data suggest that the 1 s nominal residence time of particles in the EFR was not sufficient for heating all sample particles to 1000°C and for the pyrolytic process to be completed for all the particles. It is likely the results are due to a distribution of residence times that developed around the 1-s nominal residence time. When working with the wire-mesh reactor at 1000°C, we found sample weight loss to be largely completed during heatup. Table 3.4 shows a marginal difference in total volatiles in the wire-mesh reactor, when longer hold times were used for 'Illinois No. 6 (SBN)'.

The problem of incomplete pyrolysis reactions in the entrained-flow ('drop tube') reactor could probably be overcome by constructing longer drop-tubes. That, however, raises the prospect of constructing progressively longer drop tube reactors for higher temperature experiments. The entrained-flow ('drop-tube') reactor constructed at the British Gas research station at Solihull (UK) for coal hydropyrolysis–hydrogasification was some 6 m in length.

Meanwhile, several further experiments indicated that the properties of the gases used in the two sets of experiments may account for some of the differences observed between the two sets of results in Table 3.4. Table 3.5 shows that operation with nitrogen in the wire-mesh reactor has the effect of reducing the weight loss by about 3%. This is likely to be due to the lower thermal conductivity of nitrogen compared to helium. It would appear that somewhat longer residence times in the 'drop-tube' reactor coupled with the use of helium would go some way toward aligning results more closely between the two reactors. The relative combustion reactivities of the chars determined by TG analysis seemed in reasonably close agreement (Hindmarsh et al., 1995). However, the far greater scatter in data from EFRs appears endemic to the nature of the design and is probably also associated with difficulties relating to complete char recovery.

3.6.5 Results from different pyrolysis reactors: an overview

We have observed that the level of contact between heated solid particles and evolved volatiles in fixed-bed reactors have measurable effects on results from pyrolysis experiments. Compared to yields from the wire-mesh reactor, the fixed-bed ('hot-rod')

Table 3.4 **Comparison of pyrolysis data from an EFR and a wire-mesh reactor, using common samples**

	Entrained-flow (drop-tube) reactor pyrolysis results (wt% daf) at 1000°C under nitrogen. Estimated residence time: 1 s		Wire-mesh reactor pyrolysis results (wt% daf) at 950–5000°C s^{-1} under helium 2 s holding at peak temperature		
	Total volatiles	**Residual volatile matter in char**	**Total volatiles**	**Tar**	**Residual volatile matter in char**
Taff Merthyr	16.0	3.6	17.2	9.5	1.7
Emil Maryrisch	20.0	3.7	21.2	11.6	1.9
Linby	39.1	8.2	49.6	29.9	2.3
Illinois No. 6 (SBN[b])	46.8	9.3	53.6 (53.4)[a]	28.9 (29.2)[a]	3.7 (3.8)[a]
Illinois No. 6 (APCS[b])	48.0	4.9	59.4	n.d.	2.4

Source: Reprinted from Hindmarsh, C.J., Thomas, K.M., Wang, W., Cai, H.-Y., Güell, A.J., Dugwell, D.R., et al., 1995. Fuel 74, 1185. Copyright 1995, with permission from Elsevier.
[a]Values in parentheses are for 5 s hold; char VM at zero hold time, 4.0 wt% (daf).
[b]*SBN*, Steinkohlebank, Netherlands; *APCS*, Argonne Premium Coal Sample program (Vorres, 1990).

Table 3.5 Pyrolysis of Illinois No. 6 (SBN) Coal; 1000°C in different atmospheres

Reactor	Atmosphere	Total volatiles (wt% daf)	Tar (wt% daf)
EFR	N_2	46.8	n.d.
WMR	He	51.4	27.2
	N_2	48.2	n.d.
	N_2 (O_2 free)	48.1	n.d.

Source: Reprinted from Hindmarsh, C.J., Thomas, K.M., Wang, W., Cai, H.-Y., Güell, A.J., Dugwell, D.R., et al., 1995. Fuel 74, 1185. Copyright 1995, with permission from Elsevier.
EFR, entrained-flow reactor; *WMR*, wire-mesh reactor.

experiments gave less tar and volatiles, when working at similar temperatures, pressures and heating rates. Moreover, tar losses in the 'hot-rod' reactor were found to be more sensitive to sample bed depth than to carrier gas superficial velocity. This may be understood in terms of the flow rate not being the primary factor in determining the frequency of solids-volatiles collisions, which lead to additional gas and char formation.

Greater consistency was observed between tar and total volatile yields from the fluidised-bed operated in flash heating mode, and rapid heating experiments in the wire-mesh reactor. At temperatures below 500°C, divergences observed between the two reactors could be accounted for by the relatively short exposure of samples at peak temperature in the wire-mesh reactor, coupled to poor heat transfer, prior to the onset of radiative heat transfer, at temperatures near and above 500°C. At higher temperatures, tar yields declined due to secondary tar destruction reactions within the fluidised bed itself and in the reactor freeboard. Tar cracking reactions within the bed itself were found to be more significant above about 650°C. By contrast, tar yields in the wire-mesh reactor reached a steady level between 600°C and 700°C and remained constant as higher final experimental temperatures were reached.

Compared to the entrained-flow ('drop-tube') reactor, the wire-mesh reactor appears as the more reliable instrument for measuring sample weight loss. Some of the problematic aspects of the EFR data may be improved by extending residence times through the use of longer reactor tubes. However, avoiding – or narrowing – the distribution of residence times for exiting sample particles does not seem entirely possible. Moreover, difficulties encountered with regard to char recovery and mass closure appear inherent to the configuration of the apparatus. Finally, EFRs were not intended for the accurate measurement of tars released from sample particles. With increasing tube length, the amount of surviving tars would be expected to decline further and the structures of surviving tars to thermally degrade. We would expect tar structures from EFRs to differ substantially from those of primary tars.

Wire-mesh reactors are capable of operating over wider ranges of reaction conditions than other reactor configurations. They require small amounts of sample and enable the recovery of products for further characterization, in a state relatively uncontaminated by secondary reactions. These advantages make the wire-mesh

reactor the instrument of choice in characterising samples of special interest, or scarcity, such as macerals and kerogens. However, wire-mesh reactors present two distinct disadvantages compared to fluidised-bed and entrained-flow ('drop-tube') reactors.

First, fluidised-bed and EFRs can be operated using a range of particle sizes, whereas the wire-mesh reactor is limited in the sizes of particles it can handle, due to the fixed sizes of holes in the mesh. In particular, the wire-mesh reactor configuration would prove clumsy in experiments aimed at determining the behaviour of particles much larger than several hundred micro-metres in diameter. At the other extreme, coal particles below about 60 μm are difficult to handle because of static electricity related effects: particles adhere to feeder and reactor walls and make it difficult to carry out quantitative experiments, although these difficulties are not specific to wire-mesh reactors.

The other limitation of wire-mesh reactors concerns the inherently small sample sizes that are required. Fluidised-bed and EFRs are normally designed to handle variable quantities of sample and are capable of producing tars in the fluidised bed reactor, and chars in both reactors in adequate quantities for tests requiring larger sample sizes, e.g., for surface area determinations and for examination by NMR. Sample sizes in the wire-mesh reactor are of the order of ~5–6 mg. While this is a distinct advantage when working with samples that are relatively scarce (e.g., coal macerals or kerogens), the amounts of chars and tars recovered from wire-mesh experiments are clearly small. The small amounts of liquid products collected at the end of experiments do not allow some of the more standard tests, such as boiling point distribution determinations, to be carried out.

3.7 Pyrolysis of coal macerals and kerogens: a brief excursion

The rest of this chapter will focus on studies carried out using some of the tools and concepts relating to pyrolysis experiments developed in the foregoing sections. Section 3.7 will outline results from experiments on coal macerals and kerogens and introduce a version of the wire-mesh reactor equipped for use at reduced pressures.

3.7.1 Pyrolysis of coal maceral concentrates: Northern Hemisphere coals

In Chapter 2, Solid fuels: origins and characterization, we touched upon the botanical origins of coals and briefly reviewed the organic geochemistry of coal constituents called macerals. The technological interest in diverse coal constituents arises from differences in their behaviour under particular processing conditions, particularly during coke making.

The effect of heating rate on product distributions: In a wide-ranging review, Taupitz (1977) suggested that '…only vitrinite is susceptible to the speed of heating …' Most Northern Hemisphere coals are predominantly vitrinitic and show some sensitivity to 'the speed of heating'. We have since quantified the levels of

sensitivity of different coals to changes in heating rate and, as will be explained below, found that while the response of vitrinites to heating rate is usually significant, coals respond to changes in heating rate for a variety of reasons.

Apart from shifts in product distributions, 'sensitivity' to heating rates may also be observed in terms of the plastic behaviour of some coal samples, which explains the interest by coke makers. The quality and scope of the work by Hamilton and coworkers in mapping the evolution of the morphology of coals by means of photomicrographs, as a function of coal rank, maceral content and heating rate, has yet to be matched (Hamilton et al., 1979; Hamilton, 1980). The work described below presents product distributions (tar, char, total volatiles) along the same three axes: coal rank, maceral content and heating rate. We will also observe below that lignocellulosic biomass samples display similar trends: woods, lignins and lignites display plastic behaviour at high heating rates as well as release increasing yields of tars and volatiles as heating rates increase.

Coal maceral separation: The separation of macerals in coals relies on relatively small density differences between finely ground particles (e.g., Pandolfo et al., 1988 and references therein). Most maceral separation methods therefore require the very fine subdivision of sample particles – to several microns (μm) or less. In the wire-mesh reactor, where sample particle sizes normally need to be greater than 60–70 μm at its finest, this creates a problem. At Imperial College, the solution arrived at was to re-constitute pellets from maceral concentrates recovered in the form of fine particles, using a hydraulic press. The pellets were then reground and sieved, to obtain particles in the requisite size range. However, problems arise with inertinites, which do not compact very tightly. The detachment of fine dust from sample particles tends to alter the weight of the sample after weighing and contributes to experimental scatter.

Despite fine grinding, maceral sample purities vary between different batches. Samples are rarely 100% pure. It is important therefore to distinguish between actual macerals in coals and the maceral concentrates that most experimenters are constrained to work with. For laboratories other than those specialised in maceral separation, the choice of maceral concentrates to be examined is largely a matter of sample availability.

Results from experiments at atmospheric pressure: The work outlined below was performed using the atmospheric-pressure wire-mesh reactor described in Fig. 3.1B. The first set of experiments compares the sensitivity of macerals to changes in heating rate between 1°C s^{-1} and 1000°C s^{-1}. The second set compares product distributions from different macerals during pyrolysis at atmospheric pressure and under reduced pressures. The reader is referred to the brief introduction to coal maceral geochemistry presented in Chapter 2, Solid fuels: origins and characterization, for the definitions of coal components mentioned below.

Table 3.6 shows that, liptinites gave the highest and inertinites the lowest volatile matter yields. The vitrinite data were numerically close to results from predominantly vitrinitic whole-coal samples. All liptinites melted upon heating and most inertinites did not. Linby coal and its vitrinite concentrate are interesting because they melt only upon rapid heating (1000°C s^{-1}) and *not* if heated slowly (1°C s^{-1}). Among the samples tested, Linby (a typical vitrinitic) coal also showed the greatest sensitivity to changes in heating rate. In Chapter 6, Elements of thermal breakdown: heating

Table 3.6 Pyrolysis of coals and their maceral concentrates as a function of heating rate in atmospheric pressure helium. 30 s holding at 700°C

	Carbon content	Heating rate (1000°C s^{-1})	Heating Rate (1°C s^{-1})		
		Tar yields	Total volatiles	Tar yields	Total volatiles
Point of Ayr					
Whole Coal	85.2	26.1	42.4	20.7	33.6
Clarain	82.6	24.4	40.8	18.1	34.7
Durain	84.9	30.1	44.2	26.8	40.5
Vitrinite conc.	84.8	24.6	40.1	20.5	33.9
Liptinite concentration 1	85.7	47.1	62.0	43.4	56.8
Liptinite concentration 2	84.8	47.9	62.5		
Inertinite concentration	84.2	16.1	31.3	15.4	30.4
Linby					
Whole Coal	82.3	30.7	46.6	24.2	40.2
Vitrinite concentration	77.6	29.5	45.2	20.3	37.8
Liptinite concentration	79.1	48.9	64.9	45.5	59.9
Inertinite concentration	78.2	26.3	42.4	19.6	35.8
Cortonwood					
Whole coal	86.5	29.8	40.9	26.7	37.6
Vitrinite concentration	85.9	26.5	42.1	24.7	39.2
Liptinite concentration	85.1	53.7	70.7	54.9	65.5
Intertinite concentration	85.7	22.5	35.8	21.0	33.4
Freyming					
Whole coal	82.3	28.4	44.2	20.3	36.7
Vitrinite concentration	83.5	26.3	43.0	18.2	34.4
Dinnington					
Vitrinite concentration	81.4	21.2	34.2	14.3	31.0
Liptinite concentration	84.3	48.8	63.1	47.3	58.9

Source: Reprinted from Li, C.-Z., Madrali, E.S., Wu, F., Xu, B., Cai, H.-Y., Guell, A.J., et al., 1994. Fuel 73, 851. Copyright 1994, with permission from Elsevier. See Table 3.9 and Li, C.-Z., Bartle, K.D., Kandiyoti, R., 1993a. Fuel 72, 3; Li, C.-Z., Bartle, K.D., Kandiyoti, R., 1993b. Fuel 72, 1459 for the elemental and petrographic compositions of these samples.

rate effects and retrogressive reactions, we will present evidence suggesting how the transitional melting behaviour of certain coals is related to their marginal deficiency in hydrogen content. We will see that such coals may be heated rapidly, to help make stronger cokes from weakly coking coals.

The data in Table 3.6 show that clear-cut generalisations about maceral concentrate behaviour are difficult to make. Above 500°C, many of the samples showed some sensitivity to changes in heating rate, with liptinite and inertinite concentrates

Table 3.7 Sensitivity of total volatile yields to changes in heating rate. Pyrolysis at 20 bar; 10 s holding at 1000°C

Sample	Volume yield (10°C s^{-1} %, daf basis[a])	Volume yield (1000°C s^{-1} %, daf basis[a])	Maceral purity
Liptinite No.11	66.5	67.0	91.2
Repeat run	65.6	67.1	91.2
Inertinite No. 18	18.9	20.3	97.8
Repeat run	20.3	22.5	97.8

Source: Data collected from Messenböck, R.C., 1998. Ph.D. Thesis. University of London; Messenböck, R.C., Chatzakis, I.N., Megaritis, A., Dugwell, D.R., Kandiyoti, R., 1999. Fuel 78, 871–882; Messenböck, R.C., Paterson, N., Dugwell, D.R., Kandiyoti, R., 2000. Fuel 79, 109–121.
[a]daf, dry ash free basis.

broadly showing less sensitivity than vitrinite concentrates. As already observed, however, the maceral samples are never quite pure. In evaluating results presented in Table 3.6, therefore, some suspicion remains that unintended vitrinitic inclusions may have contributed to the unexpected sensitivity to heating rates of the liptinite and inertinite concentrate samples. The compositions of the samples are presented in Table 3.9 (also see Li et al., 1993a,b). In experiments conducted under 20 bar He, with relatively pure liptinites and inertinites from two different coals, Messenböck (1998) again found the sensitivity of these two macerals to the heating rate to be limited (Table 3.7).

Thus after much toil and over a quarter of a century of speculation, we seem able to add to Taupitz's dictum about vitrinites that some liptinites and some inertinites may also be 'susceptible to the speed of heating', albeit generally to a lesser extent than the corresponding vitrinites.

Pyrolysis of maceral concentrates under vacuum: Early work summarised by Howard (1963) and Howard (1981) indicated that tar and other volatile evolution during pyrolysis should be enhanced when the external pressure is reduced. The effect is related to faster mass transfer out of the particles, due to steeper outward pressure gradients (Suuberg, 1985 on mass transfer effects). In this process, tar precursors that normally act as binder in coals that normally soften upon heating, are removed from the pyrolyzing mass. Residual chars from pyrolysis under 'vacuum' are, therefore, less agglomerated. It is still possible, however, to depress volatile yields by hasty reactor design. Working at reduced pressures ('2–200 mm Hg'), Roy et al. (1985) reported not much more than ~36–37% total volatiles at temperatures between 322°C and 1000°C, using a coal with a 'proximate analysis' volatile matter content of 34%. The experiments were done in a 50 mm diameter cylindrical tube, where 120 g of sample particles had been stacked in the form of a fixed bed.

Wire-mesh reactors have proved particularly adaptable to work under vacuum. An early wire-mesh reactor (Jüntgen and van Heek, 1968) was in fact designed to operate at about 10^{-7} bar and the volatiles passed directly into a mass spectrometer.

Howard and coworkers worked between 10^{-4} and about 100 bars (Howard, 1981; Anthony et al., 1975; Suuberg et al., 1978a,b). They found sample weight loss could be increased by about 7% above the weight loss at atmospheric pressure, by reducing the pressure. The effect appears associated with competition between tar precursor transport out of coal particles and intraparticle secondary char formation and cracking reactions. Large increases in yields at high heating rates were also reported by workers at Princeton University when operating at reduced pressures. When the pressure was increased from about 10^{-4} to 2 bars, the sensitivity of coal samples to increasing heating rates was reported to have diminished markedly (Niksa et al., 1982a,,b, 1984).

Winans and coworkers have analyzed vacuum pyrolysis tars, released from a probe attached to the inlet of a mass spectrometer, or alternatively, prepared separately 'in batch mode' (Winans et al., 1986, 1991; Winans and Neal, 1990; Winans, 1991; Hunt et al., 1991). No yield data were reported from the samples nor would it have been possible to determine product distributions using the probe configuration within the mass spectrometer. The attendant mass spectrometric work was capable of identifying relatively small hydrocarbon molecules.

Tar recovery during 'vacuum' pyrolysis: The recovery of tars during pyrolysis experiments under reduced pressures, in wire-mesh reactors presents peculiar challenges. One common difficulty is the recirculation of evolving tars in the vicinity of the heated mesh:'…a certain amount of carbon deposition from cracked volatiles occurred on the stainless steel screen sample holder, particularly at lower pressures…' (Howard, 1981). Suuberg et al. (1978a,b) recovered tars by solvent washing of inner surfaces and linings of the wire-mesh cell. In later work, Suuberg and coworkers (Unger and Suuberg, 1984; Suuberg et al., 1985), using similar procedures, reported greater concentrations of large molecular mass components in tars produced under vacuum compared to atmospheric pressure, while suggesting that their tar recovery procedure was 'somewhat inefficient'.

As explained above, tar capture in the wire-mesh reactor shown in Fig. 3.1 was achieved by sweeping evolving volatiles away from the reaction zone, into a liquid-N_2 cooled 'quench zone'. However, there seemed to be no practical way of setting up an externally imposed flow field under reduced pressures. In the absence of a preferential direction for flow, volatiles could diffuse downward from the mesh as well as upward. Meanwhile, quantitative tar capture in the wire-mesh reactor depended on minimising the recirculation of tar vapours within the cell, and in particular, in the vicinity of the heated mesh. Another constraint was the necessity to minimise the cracking of tars deposited on cold surfaces by the heated, glowing wire mesh, which radiates intensely at temperatures above 500°C.

In arriving at a tar-trap design suitable for operation under reduced pressures, a compromise had to be reached between two extremes:

1. Placing flat parallel cold plates very close to the sample holder, as in the 'short-path vacuum still' (Sun et al., 1958), carried the attendant risk of inducing tar degradation and cracking by radiation from the mesh.
2. At the other extreme, washing tars off the reactor walls would not allow suppressing tar recirculation, with attendant dangers of charring and cracking on the mesh itself.

Fig. 3.7 presents a schematic diagram of the tar trap assembly eventually designed for the recovery of tars in the wire-mesh reactor operating under reduced pressures (Li et al., 1993b). This design aimed to condense evolved tars on exposed trap surfaces, to minimise tar recirculation and simultaneously reduce the exposure of condensed tars to radiation from the mesh. The top part of the trap configuration in Fig. 3.7 was similar to the atmospheric pressure trap (see Fig. 3.1B). As before, the 'chimney' was packed with wire-mesh, cooled with liquid-nitrogen and connected directly to the vacuum pump. The bottom trap was a shallow cup mounted directly underneath the mesh, intended to capture tars released *below* the mesh and, as much as possible, to block tar recirculation. Tiny holes in the cup were used for threading through thermocouple wires and for equilibrating the pressure. In order to limit losses due to cracking by radiation, holding times at peak temperature were reduced from 30 to ~5 s at 700°C. Previous experiments at atmospheric pressure have shown volatile release at 700°C to be virtually completed within about 1 s (see Section 3.3.1). Following initial trials with the new set of traps, it was concluded that the design provided the best working compromise to yield the largest tar yield identifiable under the circumstances.

Table 3.8 shows that, with the exception of the inertinite concentrates, all samples gave enhanced yields when the pressure was reduced from ambient. Under vacuum, as well as at atmospheric pressure, total weight loss and tar yields were greatest for liptinites and smallest for inertinites:

liptinites > *vitrinites* > *inertinites*.

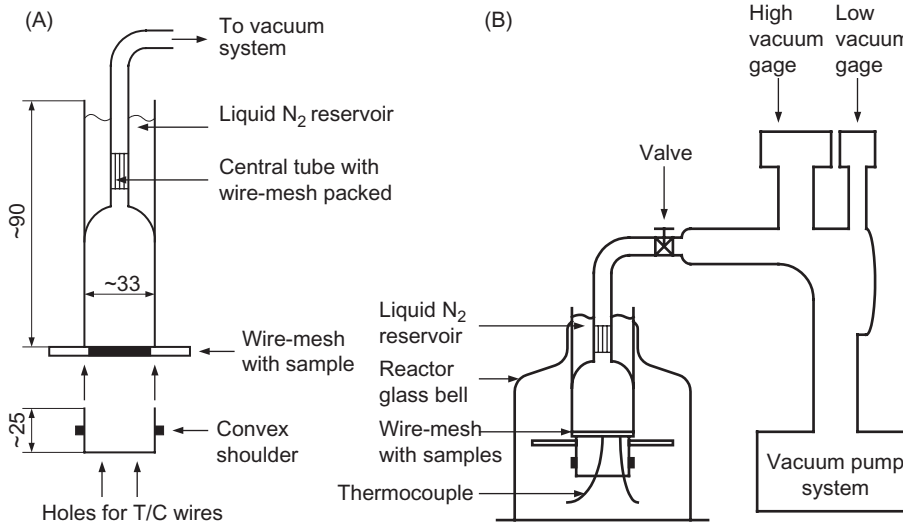

Figure 3.7 Schematic diagram of tar traps designed for use in vacuum pyrolysis experiments. (A) Off take tube above the mesh and 'shallow cup' underneath. (B) Sketch of assembled system showing the positioning of the cell and the vacuum pump. All dimensions are given in millimetres.

Source: Reprinted from Li, C.-Z., Bartle, K.D., Kandiyoti, R., 1993b. Fuel 72, 1459. Copyright 1993, with permission from Elsevier.

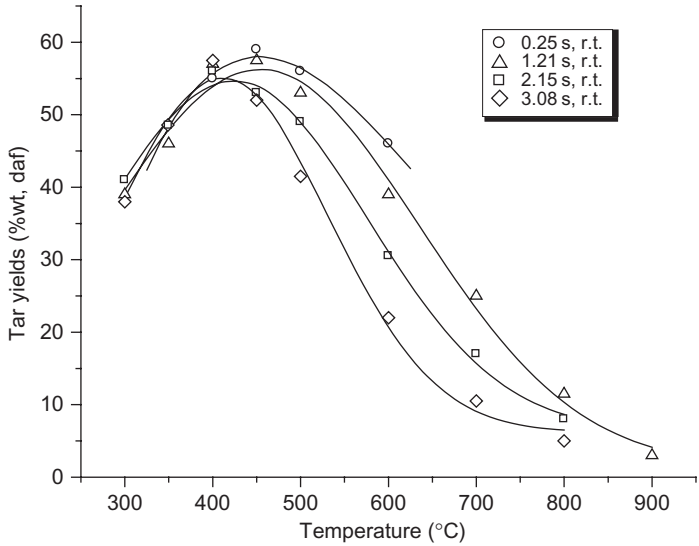

Figure 3.8 Silver Birch pyrolysis tar yields as a function of temperature and freeboard residence times. Operation at atmospheric pressure.
Source: Reprinted from Stiles, H.N., Kandiyoti, R., 1989. Fuel 68, 275. Copyright 1989, with permission from Elsevier.

Comparing yields from vacuum and atmospheric pressure pyrolysis experiments, Table 3.8 shows that observed increases in tar yields under vacuum were greater than corresponding increases in total volatile yields. About 5% more tar was recorded compared to a corresponding increase in total volatile yields of ~1–2%. The result indicates that enhanced volatilisation at reduced pressures primarily affects the devolatilisation of tars. 'Vacuum' appears to facilitate the escape of tar precursors, which at atmospheric pressure would have cracked and given about 5% more gaseous product. It is likely that the effect is associated with both enhanced bubble transport within particles and enhanced evaporation due to a greater driving force at the external particle boundary.

One further point seems worth mentioning before closing the discussion on 'vacuum' pyrolysis. Howard's (1963) description of the 'short-path vacuum still' (Sun et al., 1958) contains a fascinating note regarding the amber colour of material initially condensed onto cold surfaces. This material gradually darkened upon exposure to air. The observation was made possible by the large size of the apparatus and of the relatively large amount of sample used. The low experimental temperature (up to 500°C) would perhaps explain the lightness of the oil. Relatively little attention has been paid in the literature, however, to the possible oxidative re-polymerisation of freshly produced coal liquids. The darkening 'upon exposure to air' certainly raises questions about whether our current methods of tar recovery lead to the polymerisation of tars after collection, with attendant increases of molecular mass distributions and other changes in structural features during handling. More recently, similar

Table 3.8 Pyrolysis tar and total volatile yields from Linby, Point of Ayr and Freyming *whole*-coals and maceral concentrates at atmospheric pressure and under vacuum. Heating at 1000°C s^{-1} to 700°C with 30 s holding at atmospheric pressure and 5 s holding under vacuum. These values represent the average of between 2 and 7 determinations. The data were presented on a w/w % daf basis. Corresponding petrographic compositions may be found in Table 3.9 and Li et al. (1993a,b)

Sample	Atmospheric pressure		Vacuum	
	Tar yields	Total volatiles	Tar yields	Total volatiles
Linby				
Whole coal	30.7	46.6	37.9	49.7
Vitrinite concentrate	29.5	45.2	36.8	47.4
Liptinite concentrate	48.9	64.9	58.2	67.4
Inertinite concentrate	26.3	42.4	31.5	41.3
Point of Ayr				
Whole coal	26.1	42.4	33.1	41.8
Vitrinite concentrate	24.6	40.1	31.3	42.8
Liptinite concentrate	47.1	62.0	62.7	72.6
Inertinite concentrate	16.1	31.3	18.7	29.5
Freyming				
Whole coal	28.4	44.2	35.6	45.4
Vitrinite concentrate	26.3	43.0	30.7	43.5
Liptinite concentrate	42.7	55.1	47.5	57.3

Source: Reprinted from Li, C.-Z., Bartle, K.D., Kandiyoti, R., 1993b. Fuel 72, 1459. Copyright 1993, with permission from Elsevier.

observations were made during the fast pyrolysis of biomass in a fluidised-bed reactor (Morgan et al., 2015a). When the liquid nitrogen cooled tar/oil traps were opened after an experiment, the condensed oils looked like a gel-like solid with a pale yellow colour. The material melted after several seconds, into a pale yellow-orange liquid. By the time the oils were recovered from the traps by washing with methanol-acetone solution, the colour changed to a deeper yellow-orange. However, no attempt was made to study these changes.

Meanwhile, the yields, size exclusion chromatograms and other properties of pyrolysis tars normally change in a fashion that is consistent with changes in reaction conditions (Suuberg et al., 1985; Li et al., 1993a,b). Such trends suggest that the fundamental characteristics of the tars could not have been radically altered by current methods of tar handling. Nevertheless, the image of the amber coloured coal tar is compelling and the subject may be worth revisiting.

3.7.2 The reactive inertinites of the Southern Hemisphere

In the Southern Hemisphere, vast deposits of coal are thought to have common depositional origins in Gondwanaland, the paleo-continent that eventually fragmented into parts of southern Africa, India, eastern Australia, Madagascar, South America and Antarctica. For present purposes, the more intriguing aspect of these coals is the different maceral distribution patterns compared to Northern Hemisphere coals. Vitrinite occurrences of Southern Hemisphere coals occasionally drop below 50% and never quite exceed 80%. Liptinite contents rarely exceed 1–3%. The high inertinite concentrations in these coals include material classed as 'semi-fusinites', which are thought to have formed under cold, dry depositional environments with more than the usual level of peat oxidation. They are more reactive than would have been expected from their classification by the usual microscopic techniques. Much discussion has focused on the exceptional reactivity of 'semi-fusinites' in Gondwanaland coals during coking and liquefaction (Given, 1984).

Gondwanaland coals of the Permian age are mostly bituminous coals. The occurrence of anthracites is rare. Their generally thicker coal seams are cheaper to mine compared to Northern Hemisphere Carboniferous deposits. Furthermore, they have comparatively low sulphur contents. Much of the mineral matter in Gondwanaland coals is finely divided within the carbonaceous matrix, making it difficult to reduce mineral matter contents by usual colliery washing procedures; in power generation, this leads to more severe slagging and fouling.

The high proportion of inertinites often found in Gondwanaland coals is also a source of commercial concern because of their relatively low volatile matter content. In near burner zones of pulverised-fuel combustors, low levels of volatile release during the pyrolytic stage may have adverse effects on flame stability.

In other respects, the structural properties of Gondwanaland coals are similar to coals of the Carboniferous age of the Northern Hemisphere: (1) When their vitrinite reflectances are plotted against carbon content, the plots follow the same curves as other Palaeozoic, Mesozoic and Tertiary coals (Chandra, 1965a,b). (2) Correlations between H/C ratios of Australian coals and their pyrolysis yields appear to accommodate Northern Hemisphere coals (Tyler 1979, 1980). (3) The optically identifiable morphologies and chemical properties of individual macerals are reported to be indistinguishable from their Carboniferous counterparts. Physical and physico-chemical changes that accompany increases in rank appear to be analogous to those of Northern Hemisphere coals (Stach et al., 1982).

Returning to the matter of reactive 'semi-fusinites', inertinite rich Southern Hemisphere coals are considered to provide value for money, in terms of their coking behaviour. Given (1984), citing Roberts (1982) and Diessel (1983), has summarised these observations as follows: '…in predicting the strength and reactivity of cokes made from Northern Hemisphere Carboniferous coals by petrographic analysis, conventionally one third of the semi-fusinite is added to the total of "reactive macerals". Use of the same methods – for evaluating Northern Hemisphere coals – does not lead to useful predictions with Australian coals, which produce better cokes than would be expected from their performance in dilatometer or plastometer tests or their petrographic analyses'. The data of Cudmore (1978) quoted by Durie (1980) indicated

a greater dependence of *liquefaction* conversions on vitrinite reflectance (i.e., rank) than on maceral composition. This suggests that the greater inertinite contents did not imply lower extractabilities, as would have been usual for Northern Hemisphere coals (also see chapter: Liquefaction: thermal breakdown in the liquid phase).

These findings have allowed apparently quite legitimate claims that rank-related effects might provide a better guide to the coking and liquefaction performance of Gondwanaland coals, compared to their petrographic compositions. However, analogous claims have occasionally been made, regarding the *combustion reactivities* of Australian coals (Jones et al., 1985; Thomas et al., 1989; Phong-anant and Thomas, 1990). The debate was reviewed by Cai et al. (1998). Put simply, what needs to be resolved is whether it is warranted to extend observations from coking and liquefaction to the combustion performance of inertinite rich Gondwanaland coals?

In order to achieve a measure of clarity relating to combustion properties, it is necessary to compare both volatile yields and char reactivities of Northern and Southern Hemisphere coals directly. It also seemed useful to compare volatile yields and char reactivities of vitrinites and inertinites found within the same Southern Hemisphere coals. To this end, experiments were conducted using two sets of inertinite-graded South African coals and a set of maceral concentrates from a Northern Hemisphere coal (Point of Ayr; UK). The first set of inertinite-graded South African samples was prepared from Vryheid Coronation Colliery (VCC) coal of 87.5% elemental carbon content. Sub-samples were prepared containing 73.5, 59 and 43.5% vitrinites, the balance being largely inertinites. The second South African coal was a lower rank sample from the Durban Navigation Colliery (DNC), with 83.5% elemental carbon, similarly graded to give samples containing 86.5, 71 and 57% vitrinites, the balance once again being largely made up of inertinites. The pyrolysis experiments were carried out in the atmospheric pressure wire-mesh reactor (Fig. 3.1B), by heating the samples at 5000°C s^{-1} to temperatures up to 1500°C (Cai et al., 1998).

The results from these experiments were much as would be expected from any set of maceral concentrates. For samples of similar elemental carbon content, total volatile release was found to decrease in the order: liptinite > vitrinite > inertinite. Despite the wide variation in origins - elemental carbon content was found to be the dominant parameter. Tar and total volatiles from the South African samples decreased with increasing inertinite concentration, reflecting results from maceral concentrates of Point of Ayr and other Northern Hemisphere coals. Samples from the higher rank (87% carbon) Vryheid Coronation Colliery coal showed less variation in pyrolysis yields with inertinite content. This is consistent with observations based on Northern Hemisphere coals, suggesting that properties of individual macerals tend to converge with increasing rank and elemental carbon content. As in the case of Linby and other coal samples, the data showed no evidence of synergistic effects between vitrinites and inertinites during pyrolysis.

The relative combustion reactivities of chars from these experiments were determined, using a standard TG method at 500°C. For the higher rank Vryheid Coronation Colliery coal, char reactivities were found to be essentially independent of original inertinite content. Once again, this result is consistent with diminishing differences generally observed between macerals of increasingly higher rank coals. However, the

Table 3.9 Petrographic analyses of Linby and Point of Ayr maceral group concentrates

	Vitrinites (% v/v, dmmf)	Liptinites (% v/v, dmmf)	Inertinites (% v/v, dmmf)
Linby (whole) coal	73	15	12
Linby vitrinite concentrate	85	6	9
Linby liptinite concentrate	16	70	14
Linby inertinite concentrate	35	4	61
Point of Ayr (whole) coal	84	6	10
Point of Ayr vitrinite concentrate	91	5	4
Point of Ayr liptinite concentrate	30	61	9
Point of Ayr inertinite concentrate	17	3	80

Source: Reprinted from Li, C.-Z., Bartle, K.D., Kandiyoti, R., 1993b. Fuel 72, 1459. Copyright 1993, with permission from Elsevier.

lower rank Durban Navigation Colliery chars prepared at 1500°C clearly exhibited increasing reactivity with increasing inertinite concentration:

inertinites > *vitrinites* > *liptinites.*

This ordering was the reverse of the order established for volatile matter yields. Taken together, these results show that it is clearly possible for chars from low volatile coals or from high inertinite coals, to be relatively reactive, provided the chars are formed at sufficiently high temperatures, in this case at 1500°C. In this respect, Southern Hemisphere coals may hold their own, when compared with other coals. It is worth noting that the temperature at which the chars are formed is critical. For chars formed at 700°C, inertinite chars were found to be less reactive than the corresponding vitrinite chars (Cai and Kandiyoti, 1995).

However, when properties of Southern Hemisphere coals relevant to ignition and flame stability are compared with those of coals containing less inertinite, the usual observations have to be made: There is no evidence to suggest that 'reactive inertinites' from the Southern Hemisphere might release any more volatile matter than any other inertinite of similar maturity (Cai et al., 1998). In any case, judging by current power station practice, the low volatile content of South African coals is considered as a disadvantage that must be compensated for. In practice, this is normally rectified by judicious blending with higher volatile coals, just as one would have done with inertinite rich Northern Hemisphere coals.

3.7.3 Probing for synergistic effects between maceral components of coals during pyrolysis

Table 3.9 presents maceral analyses for Linby and Point of Ayr coal–derived samples used in the study. The maceral concentrate samples are not pure. However, combined

Table 3.10 Calculated tar and total volatile pseudo-yields for the pyrolysis of Linby and Point of Ayr coal derived 'pure' maceral groups at atmospheric pressure and under vacuum. Heating at 1000°C s^{-1} to 700°C with 30 s holding (atmospheric pressure) and 5 s (vacuum)

Sample	Atmospheric pressure		Vacuum	
	Tar yields	Total volatiles	Tar yields	Total volatiles
	(w/w %, daf sample)			
Linby				
Vitrinites	28.2	44.0	35.6	46.4
Liptinites	59.1	75.1	69.7	78.5
Inertinites	23.1	39.3	26.7	35.9
Point of Ayr				
Vitrinites	22.5	38.8	29.0	40.7
Liptinites	64.2	78.4	86.5	95.4
Inertinites	12.9	27.9	14.0	24.6

with the data from Tables 3.6 and 3.8, it is possible to back-calculate the would-be tar and volatile yields corresponding to the 'pure' macerals of these coals. The calculation is straightforward (Li et al., 1991), requiring three equations and three unknowns. Table 3.10 presents the hypothetical yields calculated for the hypothetical 'pure' macerals of these two coals.

The results largely reflect trends already observed in the data of Table 3.8. Compared to atmospheric pressure pyrolysis, greater yields were observed under vacuum in the case of whole coals, and of vitrinite and liptinite concentrates. However, inertinite concentrates gave smaller increases in tar yield under reduced pressures, and the total volatile yields actually decreased. The latter result appears counter-intuitive; repeated experiments with the present samples produced similar results and did not help clarify the reasons for this observation. Analogous observations on an inertinite concentrate derived from Treeton–Barnsley coal had been reported by Li et al. (1991). It is possible that reduced heat transfer from mesh to sample due to the poor inertinite melting behaviour is exacerbated under vacuum, through the absence of heat transfer by the ambient gas.

When combined with the maceral compositions of the coals (Table 3.9), the tar and volatile yields reported in Table 3.10 allow the calculation of yields from the corresponding whole coals, as a weighted sum of pyrolysis yields from individual 'pure' macerals. The calculation may be likened to "reconstituting" the pyrolysis yields of "whole" coals from those of individual maceral components present in each coal.

Table 3.11 Comparison of experimental and calculated tar and total volatile yields, for the pyrolysis of Linby and Point of Ayr *whole*-coals. Operation at atmospheric pressure and under vacuum. The calculated results are based on assuming additivity of yields from individual pure maceral groups. Heating at 1000°C s^{-1} to 700°C with holding 30 s (atmospheric pressure) or 5 s (vacuum)

Substrate	Atmospheric pressure		Vacuum	
	Tar yields	Total volatiles	Tar yields	Total volatiles
	(w/w%, daf sample)			
Linby whole coal				
Calculated Experimental	32.2 30.7	48.1 46.6	39.6 37.9	50.0 49.7
Point of Ayr whole coal				
Calculated Experimental	24.0 26.1	40.1 42.4	30.9 33.1	42.3 41.8

Source: Reprinted from Li, C.-Z., Bartle, K.D., Kandiyoti, R., 1993b. Fuel 72, 1459. Copyright 1993, with permission from Elsevier.

Table 3.11 compares experimental pyrolysis yields measured using ordinary Linby and Point of Ayr coal samples (from Table 3.8), with those of the calculated ('reconstituted') yields for the same samples given in Table 3.10. For both vacuum and atmospheric pressure data, the level of agreement in Table 3.11 between calculated and experimental values was well within experimental repeatability. In view of errors inherent in the pyrolysis experiments themselves and the usually larger errors common in petrographic analyses, the level of agreement is even a little surprising. In any case, the results showed no evidence of identifiable, experimentally significant synergistic effects between different maceral groups, during the pyrolysis of whole coals. This finding is particularly interesting, when contrasted with data on the pyrolysis of lignocellulosic biomass, showing clear evidence of synergistic effects (Section 3.9).

3.7.4 Using wire-mesh reactors to characterise kerogens

Kerogens are solid organic occlusions found in sedimentary rocks. Depending on the original composition of deposited material and the history of maturation, they may release oil and gas that then migrates from the source rock toward reservoir areas. Kerogens are defined as the fraction of the organic deposit insoluble in common solvents such as dichloromethane. Type I kerogens have high atomic H/C and low

O/C ratios and are classed as oil-prone. They are often composed of algal material, e.g., botryococcus algae. Type II kerogens are also considered as oil-prone, with intermediate atomic H/C and O/C ratios. They normally contain mixed macerals, including nonvascular phytoplanktons and terrestrial liptinites: sporinites, cutinites and resinites. Type III kerogens with lower atomic H/C ratios and higher O/C ratios are considered as gas-prone. Typical components of these kerogens are vascular terrestrial and humic macerals. Oil generation is expected to commence when kerogens have a maturity equivalent to a vitrinite reflectance of between 0.4% and 0.6% and is at its peak at about 1.3, passing to gas production by about 1.7% vitrinite reflectance (Madrali et al., 1994).

Kerogens are usually characterised by determining product distributions during pyrolysis. The standard Rock-Eval test (Tissot and Welte, 1984; Tyson, 1995) is widely used in work related to oil exploration, in the field as well as in the laboratory. The method is empirical in nature and does not distinguish between tars and lighter combustible volatiles. Furthermore, all combustible volatiles are consumed during the test, so the recovery of tar samples for structural characterization is not possible. While the Rock–Eval test seems sensibly designed for use in field conditions, kerogen characterization is an area where care in designing laboratory-based pyrolysis experiments may be of assistance to the organic geochemist.

Pyrolysis tar/oil and volatile yields from the samples shown in Table 3.12 were determined in the atmospheric pressure wire-mesh reactor (Fig. 3.1B). Two samples each from Type I, Type II and Type III kerogens were selected. All six samples were of low maturity, with vitrinite reflectances below 0.5% (Madrali et al., 1994). FT-ir analyses of the samples showed that within each pair of samples, the geologically younger kerogen showed higher overall aliphatic and hydroaromatic content. FT-ir also showed the geologically younger kerogens and their tars to contain greater concentrations of O-bearing groups. The geologically younger samples gave higher pyrolysis tar/oil and total volatile yields, which correlated well with the Rock-Eval–derived Hydrocarbon Index (Rahman et al., 2000). The volatile-yield trends did not, however, correspond closely with results expected from the elemental analyses, as understood in terms of the van Krevelen diagram. On its own, elemental analysis turns out to be a blunt instrument for evaluating the oil potential of individual kerogen samples.

Thus, the level of accuracy available to wire-mesh instruments appears quite adequate for distinguishing between geologically younger and older kerogen samples. A wider range of samples needs to be tested, to explore the extent to which the agreement found between wire-mesh tar yields for this set of samples and the Hydrocarbon Index may be considered as more generally valid. Tar characterization, combining spectroscopic methods with size exclusion chromatography (see chapter 7: Analytical techniques for low mass materials: method development and chapter 8: Analytical techniques for high mass materials: method development), is likely to prove rewarding in linking the molecular structures and molecular mass distributions of kerogen tars with parameters relevant to oil exploration as well as providing a more fundamental understanding of maturation processes.

Table 3.12 Wire-mesh pyrolysis yields as wt%, on dry basis. Pyrolysis conditions: heating rate 1000°C s^{-1}; final temperature 700°C; hold time 30 s; sweep velocity 0.1 m s^{-1}

Sample	Geographic origin	Sedimentary basin	Kerogen type/ deposition environment	Geological age (Ma)	Tar yield (%)	Total volatile yield (%)
A	Philpstoun, Scotland	Midland Valley	Type I/lacustrine	Lower Carboniferous 330 ± 5	48.1	73.5
B	Queensland, Australia	Lowmead	Type I/Lacustrine	Eocene 50 ± 5	61.8	82.1
C	Salt Range, Pakistan	Kohat-Potwar	Type II/Marine	Lower Triassic 240 ± 5	41.5	64.8
D	Lurestan, Iran	Zagros	Type II/Marine	Palaeocene 60 ± 5	48.6	73.0
E	East Midlands, England	East Midland	Type III/Deltaic	Upper Carboniferous 305 ± 5	17.7	36.7
F	Isle of Wight, UK	Wessex	Type III/Deltaic	Lower Crateceous 125 ± 5	18.4	42.9

Source: Reprinted from Madrali, E.S., Rahman, M., Kinghorn, R.R.F., Wu, F., Herod, A.A., Kandiyoti, R., 1994. Fuel 73, 1829. Copyright 1994, with permission from Elsevier.

3.8 Pyrolysis of lignocellulosic biomass

In principle, most of what has already been said about the design of pyrolysis reactors in this chapter applies directly to the thermochemical characterization of lignocellulosic biomass. The designs of experimental reactors for coal and biomass are, or should be, pretty much interchangeable. Even so, much past research has been conducted with relatively little reference to the many common aspects and shared challenges.

A relatively recent review of biomass pyrolysis research provides a good example for how possible synergies are overlooked through compartmentalisation. A recent review by Mettler et al. (2012) correctly pointed out the potential significance of a transient fluid phase, observed during the rapid pyrolysis of wood. The review suggested that further research would be useful. However, no mention was made of the accumulated body of evidence about transient plastic phases previously observed during the pyrolysis of lignites, coals and coal maceral concentrates. Sample softening during heatup, as well as the related effect of heating rates on tar/oil yields, are areas where prior research on a range of sample types provides clues regarding thermal breakdown mechanisms in lignocellulosic biomass. We will return to these key aspects of thermochemical reactions of solid fuels below and in Chapter 6, Elements of thermal breakdown: heating rate effects and retrogressive reactions.

Meanwhile, there are several important differences between the pyrolytic behaviour of biomass and coals. First, conversions of lignocellulosic biomass to volatile products may be considerably higher than coals. During fast (1000°C s^{-1}) heating to temperatures above 600°C, the conversion of silver birch wood to volatiles in a wire-mesh reactor exceeded 95% (Table 3.13) (Fraga-Araujo et al., 1991). 'Slow' heating

Table 3.13 Tar and total volatile yields from the atmospheric pressure pyrolysis of silver birch wood, determined using the wire-mesh reactor. Helium was used as ambient gas in all experiments

Temperature (°C)	Total volatiles (% daf basis)		Tar/oil yield (% daf basis)		Gas (by difference) (% daf basis)	
	Heating rate					
	1°C s^{-1}	1000°C s^{-1}	1°C s^{-1}	1000°C s^{-1}	1°C s^{-1}	1000°C s^{-1}
400	77	89	43	56	33	33
500	89	96	49	58	40	39
700	93	99	54	57	39	43
900	93	99	52	57	41	43

Source: Reprinted from Fraga-Araujo, A.-R., Gaines, A.F., Kandiyoti, R., 1991. Fuel 70, 803. Copyright 1991, with permission from Elsevier.

experiments (1°C s^{-1}) in the same reactor produced about 85% total volatiles, still quite high, when compared with weight loss from coals and coal related materials (e.g., Li et al., 1993a,b). Furthermore, compared to coal pyrolysis, the onset of thermal breakdown in lignocellulosic biomass and the release of tars/oils takes place at significantly lower temperatures.

These observations reflect the more highly oxygenated, thermally labile, and reactive makeup of plant-derived biomass. Moreover, the properties of the original biomass are reflected in the chemical structures of the tars/oils, which are generally more volatile than coal tars and thermally crack at lower temperatures (see below). The greater reactivity of lignocellulosic biomasses and their tars/oils tend to make product distributions more sensitive to changes in sample and reactor configuration, justifying the attention paid to experimental design.

Plastic behaviour during biomass pyrolysis: Boutin et al. (1998) reported evidence for a short-lifetime liquid species formed during the pyrolysis of pure cellulose. Transient plastic deformation is also observed during the pyrolysis of a variety of coals as well as low-rank samples such as lignites (Solomon et al., 1986) (oxygen content of ~25–28%) and a Kraft lignin (estimated oxygen content: 37–38%) (Fraga-Araujo, 1990). As discussed by Morgan and Kandiyoti (2014) (also see chapter: Elements of thermal breakdown: heating rate effects and retrogressive reactions), the transient fluid (plastic) phases observed during biomass and coal pyrolysis are likely to be related to a transient local abundance of native hydrogen. These effects provide an example of how undertaking pyrolysis research on biomass and coals with attention to shared problems may help interpret experimental observations and take advantage of useful synergies.

3.8.1 Product distributions and experiment design: char yields

Experiments with pure cellulose: We next review data showing the extreme sensitivity of cellulose pyrolysis product distributions to experimental design. These experiments were undertaken as part of a wider investigation aiming to examine how charcoal yields may be increased by altering reaction conditions (Zaror et al., 1985).

Initially, samples of pure cellulose were pyrolyzed in two reactors with different geometries. A McBain TG balance was used for heating strips of filter paper (pure cellulose) at 14°C min^{-1} to 480°C under a stream of flowing nitrogen. In a parallel set of experiments, similar samples were heated in a Gray-King retort (British Standard, 1016, Part 12) at 5°C min^{-1} to the same temperature (480°C), again under a stream of flowing nitrogen. Table 3.14 shows that broadly similar char yields (about 12%) were observed in the two sets of experiments. However, when the nitrogen flow sweeping over the sample was interrupted during experiments in the Gray-King retort, with other experimental parameters remaining unchanged, the char yield in the resulting stagnant atmosphere more than doubled to 26%. In the absence of a carrier gas stream, a significant proportion of tar vapours (aerosols), which would have otherwise been removed from the vicinity of the pyrolyzing solids, appear to have remained in situ and reverted to char: there was no visible change in the shape of the filter paper strip. Table 3.14 also shows that using rapid heating and a stream of inert

Table 3.14 Cellulose pyrolysis char yields in four different reactor configurations[a]

Reactor configuration	References	Char yield (% w/w)	Temperature programme
Gray-King retort (without carrier gas)	Zaror et al. (1985)	26	5°C min^{-1} to 480°C
Gray-King retort (without carrier gas)	Zaror et al. (1985)	12.5	5°C min^{-1} to 480°C
McBain TG balance	Zaror et al. (1985)	12.0	14°C min^{-1} to 480°C
Fluidised-bed reactor	Stiles and Kandiyoti (1989)	<3%[b]	Fast (est. > 1000°C s^{-1}) to 450°C
Wire-mesh reactor	Fraga-Araujo (1990)	<1.5[b]	1000°C s^{-1} to 600°C

Source: Adapted with permission from Morgan, T.J., Kandiyoti, R., 2014. Chem. Rev. 114, 1547. Copyright 2014 American Chemical Society.
[a]100 µm thick strip of pure cellulose filter paper was used as sample in the McBain TG balance and the Gray-King retort; 106–152 µm particles were used in the fluidised-bed and wire-mesh reactors.
[b]Below the limit of the determination.

gas to remove volatiles from the reaction zone, the outcome of cellulose pyrolysis experiments could be radically altered. Less than 2% char residue was recovered in the wire-mesh reactor at 500°C and 600°C (Fraga-Araujo, 1990). Stiles and Kandiyoti (1989) reported similar small and diminishing char yields above 400°C in a fluidised-bed pyrolysis reactor (Fig. 3.5B).

At the other end of the product spectrum, Antal et al. (2003) and Yoshida et al. (2008) have shown that when biomass pyrolysis is performed at elevated pressures and with large particle sizes, char yields are increased. However, when *cellulose* was pyrolyzed at elevated pressures, there was no significant change in the char yield (~28 wt%) as a function of increasing pressure (Antal et al., 2003). These researchers found that the pyrolytic yield of carbon from biomass approaches the thermochemical equilibrium 'limit' for the carbon yield from below (Antal et al., 2003; Yoshida et al., 2008). It has also been shown that when banagrass (~9 wt% ash dry fuel basis, ~2 wt% potassium, dry fuel basis) is leached with water to reduce its ash content (removing ~90% of its potassium content) no change in the char yield was observed after flash carbonisation at elevated pressure compared to the untreated banagrass (Yoshida et al., 2008). Similarly, nearly no change in the char yield was observed during the flash pyrolysis of untreated and *pre*-treated banagrass and energy cane in a fluidised-bed reactor, although tar and gas yields were altered significantly (Morgan et al., 2015b).

The very different outcomes encountered during the pyrolysis of cellulose, a thermally sensitive biomass component, underlines the critical role of reactor and sample configuration and the selection of reaction conditions during pyrolysis experiments. In the next several subsections, we review the behaviour of various types of lignocellulosic biomass in three different reactor configurations.

3.8.2 Pyrolysis of biomass in a wire-mesh reactor

Tables 3.13 and 3.15 present tar/oil and total volatile yields from the atmospheric pressure pyrolysis of silver birch wood (Fraga-Araujo et al., 1991) and sugar cane bagasse (Fraga-Araujo, 1990) particles (106−152 μm diameter), respectively. These experiments were done in the wire-mesh reactor shown in Fig. 3.1B. Overall, results changed in predictable ways as a function of increasing heating rate and temperature. Larger tar/oil yields were obtained with faster heating. Near total conversion to gases and liquids was observed with fast heating to between 500°C and 700°C. Experiments with pure cellulose gave less than 2% char from about 500°C onward (Fraga-Araujo, 1990).

Examining the results in a little more detail, Table 3.13 shows that silver birch gave char yields of less than 5% during fast heating (1000°C s^{-1}) to 500–600°C. At 700°C, the amount of char residue recovered was below the limit of detection of the determination. Nominally, 0.2% char could be recovered. Even slow (1°C s^{-1}) heating rate experiments in the same apparatus produced just short of 90% total volatiles (i.e., conversion from a solid to volatiles) of silver birch wood. Tar/oil yields from silver birch wood during fast heating experiments to a temperature of 400°C were 56−58%, compared to 43% for slow heating. Analogous experiments with sugar cane bagasse gave qualitatively similar results; for the latter sample, both volatile and tar yields were slightly lower. Taken together, the results presented in Tables 3.13 and 3.15 highlight the sensitivity of tar/oil yields to the heating rate and show that under carefully selected reaction conditions, the amount of solid product (char) may be reduced to near extinction.

The pyrolytic behaviour of middle-rank *coals* differs significantly from these results. Middle-rank coals rarely release more than 5−7% volatiles at up to 400°C (e.g., Fig. 3.6b). 400°C seems a low temperature for extensive coal thermal breakdown. At these temperatures, reactions are slow; longer holding times (as in the fluidised bed at the same temperature) may release up to 20% volatiles. During rapid heating (1000°C s^{-1}), many coals require temperatures nearer 650−700°C for reaching peak tar yields, which for most coals rarely exceed 28−30% (Fig. 3.6b). Furthermore, even at these higher temperatures, *total volatile* release from middle-rank coals rarely exceeds 45–50%, corresponding to char yields of about 50–55%. Further heating to 1800°C and beyond appears to squeeze out several more percent volatiles (Howard, 1981).

3.8.3 Comparing the pyrolysis and gasification of biomass in a 'hot-rod' reactor

On the face of it, these results suggest there may not be a need to *gasify* lignocellulosic biomass with air or steam for converting biomass to volatile products. This proposition was tested by comparing conversions during the pyrolysis of a biomass sample in helium with conversions from gasification in H_2, CO_2 and steam-helium mixtures, at pressures up to 20 bars (Pindoria et al., 1998a). The version of the fixed-bed ('hot-rod') reactor used in this study was described in Section 3.4 (also see Pindoria et al.,

Table 3.15 Tar and Total volatile yields from atmospheric-pressure pyrolysis of sugar cane bagasse determined using the wire-mesh reactor[a]

Heating rate						
	Total volatiles (% daf basis[b])		Tar/oil yield (% daf basis[b])		Char residue (% daf basis[b])	
Temperature (°C)	1°C s^{-1}	1000°C s^{-1}	1°C s^{-1}	1000°C s^{-1}	1°C s^{-1}	1000°C s^{-1}
400	74.3	88.3	37.0	49.2	25.7	11.7
500	86.1	93.7	42.4	56.4	13.9	6.3
600	89.1	96.1	45.4	54.4	13.9	3.9
700	87.5	96.9	45.6	53.7	12.5	3.1
900	88.8	96.9	45.4	53.7	11.2	3.4

Source: Reprinted with permission from Morgan, T.J., Kandiyoti, R., 2014. Chem. Rev. 114, 1547. Copyright 2014 American Chemical Society.
[a]Helium used as carrier gas in all experiments (Fraga-Araujo, 1990).
[b]*daf*, dry ash free basis.

1997). During these experiments, 50 mg batches of sample were heated at 10°C s^{-1} to 850°C and held at peak temperature for 100 s.

As explained earlier, higher char yields are expected in a fixed-bed reactor configuration, compared to, say, wire-mesh reactors. Even so, at peak temperatures of 850°C in helium, samples of eucalyptus (*Eucalyptus globulus*) sawdust gave 85–88% conversion to volatiles. The greatest difference between heating eucalyptus wood in an inert gas and a reactive gas was 8.5%, observed when comparing weight loss in helium and hydrogen at 20 bars. Furthermore these results were obtained at a relatively slow heating rate (10°C s^{-1}), while using a ~4 mm high fixed-bed of sample. We have already identified both slow heating and sample particle stacking as factors known to *increase* the char yield. At fast heating rates and with no impediment to volatile release by neighbouring sample particles, sample weight loss from pyrolysis alone would have been expected to reach values in the >95% range, leaving even less scope – or need – for reactive gases to make any impact at all.

However, operators of pilot- and plant-scale equipment would likely reject the idea of grinding fibrous lignocellulosic biomass to the range of particle sizes (106−152 μm) used in these experiments, on account of the energy and money costs involved in fine grinding. In fixed beds, excessive pressure drops would not allow using such small particle sizes. Furthermore, operators of pilot and plant scale fluidised bed equipment would normally reject the idea of operating with sawdust, or feedstocks with similar particle size distributions, unless special provision was made to suppress fuel loss through particle elutriation. The standard response to alleviate these problems is to increase the fuel particle size distribution, which, in turn, tends to increase the amount of residual char. Unless reacted rapidly, the resultant char is usually quite unreactive, due to long exposure times at high temperatures (see chapter: High-pressure reactor design: pyrolysis, hydropyrolysis and gasification). These considerations begin to map out the envelope of conditions, where the use of reactive gases would be preferred, to complete the process of biomass conversion to volatile products.

In this context, the link between particle size and char yield is easily explained. Howard and Anthony (1976) have calculated that when heating at 1000°C s^{-1}, the maximum diameter of *coal* particles (which have higher thermal conductivities than wood particles) that could reasonably be expected to show uniform temperature profiles is about 100 μm. Larger particles cannot be pyrolyzed quickly, due to the slower transmission of heat within the body of the particle. The speed of the moving temperature front within larger particles is limited by the usually low thermal conductivity of the biomass – even if the heating rate is large at the outer particle boundary. This effect allows the formation of char precursors at the temperature front and likely provides a barrier to the outward passage of tar vapours generated further inside the particles.

Moreover, when freshly formed chars do not gasify quickly because of large particle sizes, residual solids lose reactivity by exposure to high temperatures. The effect appears akin to the annealing of carbons and chars at high temperature, resulting in the rapid loss of reactivity with increasing times of exposure. In the next chapter, we will present data showing that chars lose nearly 70% of their reactivity within the first 10 s at 1000°C (Zhuo et al., 2000). In pilot or plant scale gasifiers, the presence of

steam, with high heat transfer coefficients between the bulk gas and sample particles – coupled to the reactivity of steam, tends to improve the conversion of larger feedstock particles. As the carbon-steam reaction is endothermic, some air may be introduced for running the reactor in auto-thermal mode. To summarise, the use of reactive gases partially compensates for choices of fluidisation or other reactor related parameters that lead to enhanced char formation. In actual plant design, the combination of all these factors defines a matrix of parameters that must be optimised.

The cracking of evolved tars/oils is another useful action performed by reactive gases such as steam. The absence of tars or tar-derived char in exit streams from the British Coal ABGC pilot fluidised-bed reactor operating at 13 bar, suggests that the action of steam at 900–950°C is useful in destroying residual tar aerosols, provided sufficiently long residence times (~1 s) are allowed (Cai et al., 1996). However, we will see in the next section that the small residue of tar that survives at higher temperatures in inert gas environments at around 900°C is a highly aromatised, chemically stable and toxic mixture.

3.8.4 Biomass pyrolysis in a bench-scale fluidised-bed reactor

We have already reviewed how pyrolysis tar/oil yields in wire-mesh reactors are determined, under conditions minimising the secondary reactions of evolving volatiles. Meanwhile, wire-mesh reactor experiments provide no clues regarding the thermal sensitivity (reactivity) of evolving tars/oils, precisely because the experiment was deliberately designed to suppress extraparticle secondary reactions. We now turn to experiments in the fluidised-bed reactor shown in Fig. 3.5B, which allows manipulating the extents of thermal cracking of volatiles in the reactor freeboard (Stiles and Kandiyoti, 1989).

Much of the early biomass pyrolysis work in laboratory scale fluidised-bed reactors was done by Scott and Piskorz (1982a,b; 1984), who explored product distributions from finely divided (<500 μm) aspen poplar wood particles, mostly between 400°C and 700°C. The basic design of the reactor was similar to but larger than that of Tyler (1979, 1980). The wood powder was introduced into an already heated bed and heating rates were estimated to be quite high. Up to 65% of the original fuel mass could be recovered as tar/oil. The reactivity of lignocellulosic biomass meant that the fluidised-bed itself contained a fuel inventory no larger than several percent of the injected biomass – in the form of char. The rest was made up of inert bed solids that ensured adequate fluidisation.

In these rigs, cracking of volatiles takes place both inside the fluidised bed (in contact with bed solids) as well as in *flight*, as they move up the freeboard section of the reactor. More of the tar/oil cracked to gaseous products with increasing reactor temperature, and the highly oxygenated nature of biomass tars/oils could be observed from increasing CO and CO_2 concentrations in the exit stream. The same researchers scaled up their reactor to pilot scale and led the way in trying to upgrade liquid products from biomass pyrolysis. These liquids are normally corrosive and are unstable during storage, readily forming gums and separating into an aqueous and an organic phase. They turn out to be difficult to convert into more useful fuels and feedstocks.

Early work on the catalytic upgrading of pyrolysis tars/oils has been reviewed by Pindoria et al. (1998b), Furimsky (2000), Huber et al. (2006) and more recently by Sanna and Andrésen (2012), Jones and Snowden-Swan (2013), Jones et al. (2013), Tran et al. (2014), Yang et al. (2014) and Morgan and Kandiyoti (2014).

Pyrolysis in a fluidised-bed with variable freeboard residence times: Conventional fluidised-bed designs do not allow the independent manipulation of the temperature and residence time of volatiles in the reactor freeboard, unless flow rates and fluidising conditions are changed.

As explained in introducing the design of the reactor shown in Fig. 3.5B, the support plate of this particular fluidised-bed may be moved vertically up-or-down between experiments, to allow residence times of volatiles in the reactor freeboard to be altered, in this case between 0.8 and ~4 s. This configuration enables changing the temperature and the volatiles residence time in the freeboard independently, without altering flow rates. It allows the examination of the thermal cracking rates of pyrolysis volatiles as a function of temperature and time.

Fig. 3.5B shows that sample particles were gravity fed into the preheated reactor. Achieving stable bed temperatures was straightforward. Given the high rates of heat transfer in bubbling fluidised beds, the heating rates of sample particles were thought to be high, but could not be measured; they could only be estimated by making relatively inexact assumptions about heat transfer rates to particles.

Fig. 3.8 presents tar yield data from the reactor. Sample from the same batch of finely ground silver birch wood particles was used here as in the wire-mesh experiments by Fraga-Araujo et al. (1991). It may be noted that similar peak tar yields were observed as in Fraga-Araujo's results in the wire-mesh reactor (Table 3.13). As freeboard residence times were increased, Fig. 3.8 shows that the maximum of the tar yield curve receded from a little above 450°C to nearly 425°C. The trend was in line with what could be expect from intensified tar cracking reactions at longer residence times in the reactor freeboard. When freeboard heights were fixed, the temperatures of the tar yield maxima for particular samples provided evidence of the relative thermal stability of evolving tars/oils. The analogous maximum for low rank bituminous Linby coal was observed near 590–600°C. In the case of Çan lignite (Turkey), the maximum of the tar yield at about 530°C was observed between the maxima of the biomass samples and that of the bituminous coal (Stiles and Kandiyoti, 1989).

The second important observation made possible by data in Fig. 3.8 is how fast tar is destroyed in the reactor freeboard, when temperatures and residence times are increased. Compared to coals, lignocellulosic biomasses produce more tar per unit amount of original fuel; however, as reaction severity (time, temperature) is increased, these tars crack to give gaseous products more rapidly than those of coals and lignites.

More recently, Morgan et al. (2015a) at the University of Hawaii have reported the construction of a fluidized bed pyrolysis reactor of similar design where the freeboard residence time could be extended to ~12 s. The new reactor was equipped with more sophisticated instrumentation and was used for assessing the pyrolysis behaviour of locally available tropical biomass species. Despite some operational differences between the two reactors, results on cellulose pyrolysis appear consistent with the earlier work of Stiles and Kandiyoti (1989).

When Morgan et al. first pyrolyzed banagrass (elephant grass; *Pennisetum purpureum*), fairly low bio-oil yields were observed. The authors attributed this to the '…high concentration of alkali and alkali earth metals (totalling ~2.8 wt% relative to the dry feedstock)…' of banagrass. The minerals were thought to act catalytically '…and increase cracking reactions during pyrolysis'. In earlier work, Richards and Shafizadeh (1978) had found higher yields of laevoglucosan when the wood powders they used as sample had been treated with a mild acid washing, compared to the untreated sample. The effect had been attributed to naturally occuring inorganic materials present in the wood samples, particularly to potassium and magnesium species. Oasmaa et al. (2010) have also reported on high amounts of alkali catalysing tar cracking reactions as have Shafizadeh (1985), Fahmi et al. (2008), Mourant et al. (2011), Greenhalf et al. (2013) and Yildiz et al. (2015).

In a subsequent study (Morgan et al., 2015b), the banagrass was water-washed/leached to reduce inorganic content, which led to an increase in 'bio-oil' yields of between 4% and 11%. Moreover, the resulting 'bio-oil' appeared more stable with regard to sample-ageing. Char and total volatile yields appeared unaffected by the washing procedure, suggesting that mineral matter was effective in cracking tars/oils to lighter volatiles. Another tropical biomass species (energy cane) was also pyrolyzed before and after water leaching for comparison. The results confirmed the effect of water-washing on enhanced 'bio-oil' yields (Morgan et al., 2015a,b).

Tar compositions and fluidised bed operating conditions: One major and still largely unresolved problem of biomass gasification in fluidised-beds is the high tar/oil content in the exit stream. The problem is sufficiently severe for catalytic reactors to have been attempted for tar destruction, placed at the exit of an experimental fluidised bed gasifier (Corella et al., 2004). A closely related aspect is the complex composition of biomass tars/oils. Evans and Milne (1987a,b) have attempted to track tar/oil compositions by using molecular beam mass spectrometry (MB-MS). Their work has been seminal, although the instrument used was not able to identify material with molecular masses above the m/z 15–300 range.

Another problematic aspect was the implication that components of wood pyrolyze independently: 'Whole wood appears to behave as the sum of its constituents, with few if any vapour species derived from interaction of the main polymer constituents'. The authors also stated that '…components of wood pyrolyze largely to monomer and monomer-related fragments and give characteristic mass spectral signatures' (Evans and Milne, 1987a). To the extent that the observations focused on surviving fragments, the inventory of compounds identified would reveal little about the structures of parent biomass biopolymers. Isolating '…characteristic mass spectral signatures…' at the end of the chain of pyrolytic reactions does not allow visualising the pyrolytic behaviour of the parent biopolymers and how they interact during thermal breakdown.

Early work by Shafizadeh and coworkers provided fairly conclusive evidence of synergistic effects during pyrolysis, between components of naturally occuring lignocellulosic biomass (Shafizadeh and Fu, 1973; Shafizadeh, 1982, 1985). Section 3.9 reviews a broad range of evidence for identifying and evaluating the extent of

synergistic effects that modify reaction pathways during the pyrolysis of lignocellulosic biomass.

Other researchers (e.g., Güell et al., 1993; Branca et al., 2003), have used GC-MS to study the very large number of chemical components in biomass pyrolysis tars. However, GC-MS can only identify molecules able to pass through the chromatographic column. For most GC-columns, the upper limit for the passage of aliphatic compounds is about 500 u. For aromatic and polar species, this limit would barely reach 300 u. Higher temperature columns have been able to push this limit to about 550–600 u for aliphatics and nearly 400 u for aromatics.

Characterization efforts by size exclusion chromatography and MALDI-mass spectrometry have since indicated that large proportions of biomass tars/oils show up at molecular masses far above the range identifiable by MB-MS or GC-MS. This is because, the rest are not volatile under the conditions of the column. Applications of size exclusion chromatography and MALDI-mass spectroscopy to pyrolysis tars from sugar cane bagasse (Pindoria et al., 1999) and eucalyptus wood (Pindoria et al., 1997) indicate molecular masses up to at least 6000 u and probably some way beyond. We do not, therefore, have direct compound identification for, perhaps, more than 90% of the tars/oils, which simply do not show up in GC-MS. We will return to these matters in Chapter 7, Analytical techniques for low mass materials: method development, and Chapter 8, Analytical techniques for high mass materials: method development.

These developments do not invalidate findings by MB-MS or GC-MS, but enable their evaluation in the wider context of the whole tar/oil sample. Findings from these techniques provide, furthermore, a general framework for visualising the types of structures to be expected in the heavier tars – although, as a rule, direct extrapolations may not be justified. For example, observations by GC-MS on silver birch tars, recovered during experiments in the fluidised-bed reactor of Fig. 3.5B, are relevant in showing the shift in chemical speciation with increasing reactor temperature (Stiles and Kandiyoti, 1989). At the lower range of reactor temperatures (300–400°C) compounds identified in relative abundance included oxygenated species such as dimethoxypropene, tetrahydrofurylmethanol and, of course, laevoglucosan. Phenols and ethoxybenzenes were observed at medium and higher temperatures, while polynuclear aromatic species, such as naphthalenes, acenaphthylenes, 9H-fluorene, and pyrene occurred with greater frequency at higher temperatures (900°C) (Stiles and Kandiyoti, 1989). It is difficult to imagine the latter compounds originating directly from lignocellulosic biomass. Recalling that above 700°C, dehydration and ring closure reactions are intensified, these polynuclear aromatic compounds appear to have formed during the exposure of pyrolysis tar/oils to high temperatures in the reactor freeboard.

The formation of polynuclear aromatic species during biomass gasification signals potential difficulties for product gas clean-up. These species are thermally far more stable than the oxygenated tars/oils recovered during experiments at lower temperatures. If higher freeboard temperatures are used as a single blunt instrument for cracking biomass tars, it appears we are able to decompose and crack *most* of the condensable materials in the product mix, but face the prospect of producing a much reduced but chemically more resilient and toxic residue.

Several contradictory trends need to be reconciled, therefore, before optimum conditions are found for tar destruction in biomass utilisation. In *coal* gasifiers, tars are rarely found to be a problem. The 'bed-solids' streams recovered from an air blown gasifier operating between 900°C and 1050°C, showed no traces of tar or other extractables (Imperial College, unpublished work). Tar destruction appeared complete, presumably due to the presence of steam at around 950°C and probably also to a reactor freeboard, with a residence time of about 1 s. Applications such as steam-oxygen-blown entrained coal gasification reach well above 1800°C and show no trace of tars/oils. Meanwhile, thermal as well as economic efficiency considerations require that biomass gasifiers are operated at relatively low temperatures compared to coal gasifiers. The general solution to the presence of problematic tars/oils in the fuel gas from biomass gasifiers appears to lie in partial oxidation by air or steam injection, perhaps in combination.

Other research teams have resorted to cleaning tars/oils entrained in the fuel gas through devices external to the gasifier. ECN (Energy Research Centre of the Netherlands) have developed an oil-based wet scrubbing system to remove tars from producer gas exiting a demonstration scale biomass gasifier (Zwart et al., 2009). Information on the process can be found in reports published on the ECN website. Meanwhile, Güssing Renewable Energy GmbH has adopted a method where char particles are deliberately entrained in producer gas streams into the baghouse filters to promote tar condensation on chars. These solids are then recycled to the gasifier (Güssing Website).

3.9 Synergistic effects between biomass components during pyrolysis

Most forestry and plant-derived agricultural wastes contain high proportions of cellulose (~35–50%; dry basis), hemicelluloses (~20–35 %; dry basis) and lignins (~10–25%; dry basis) (Huang et al., 2008; Vassilev et al., 2010, 2012). Some North European oak woods reportedly contain up to 35% lignins (Gunther and Mosandl, 2001). Most lignocellulosic biomass normally also contains minor amounts of extractables, such as resins, oils, fats and waxes (Vassilev et al., 2012). Apart from notable exceptions such as wheat straw, rice husks and banagrass, mineral matter contents in most plant-derived material are low, on the order of 1–2% (Vassilev et al., 2010, 2013a,b).

When the linear polymer cellulose is pyrolyzed, covalent bonds holding the 'chain' of rings together (Fig. 3.9) are cleaved, releasing the single-ring compound laevoglucosan (1,6-anhydro-β, D-glucopyranose) as the most abundant primary product. Laevoglucosan is thermally sensitive and may degrade readily if exposed to temperatures above 250–300°C, or contacted with heated surfaces for any length of time. In pioneering work, Shafizadeh and coworkers pyrolyzed various biomass materials by pushing small metallic crucibles filled with sample into a preheated tubular furnace (Shafizadeh and Fu, 1973). When they pyrolyzed pure cellulose, they observed

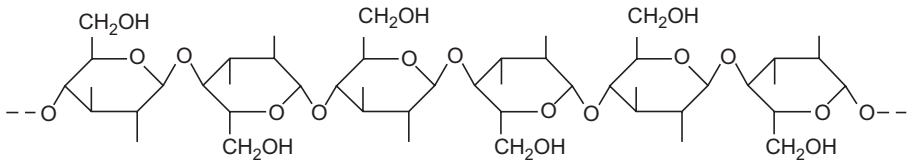

Figure 3.9 The structure of cellulose.

laevoglucosan yields approaching 50%. This was a surprisingly high yield, given the opportunities for secondary thermal degradation and recombination reactions within that particular reactor configuration.

However, when Shafizadeh and coworkers pyrolyzed wood powders that contained between 35–50% cellulose under similar conditions, they found less than 3% of the sample mass in the form of laevoglucosan (Shafizadeh, 1982). Despite the cellulose content of many biomass samples being as high as 50%, low yields of laevoglucosan have been widely reported, during the pyrolysis of naturally occuring lignocellulosic biomass. Fraga-Araujo (1990) using the wire-mesh reactor in Fig. 3.1B, pyrolyzed a sample of sugar-cane bagasse and found virtually no laevoglucosan in the tar/oil. Tars/oils from similar experiments with samples of silver birch wood presented only trace concentrations of laevoglucosan. The yield of laevoglucosan may also be reduced as the content of alkali and alkaline earth metals (AAEM), particularly K and Na increases within the original biomass. Washing with water prior to pyrolysis was shown to increase the yield of laevoglucosan (Shafizadeh, 1985; Fahmi et al., 2007, 2008; Morgan et al., 2015b; Yildiz et al., 2015). Taken together, these preliminary findings provide credible evidence that component parts of lignocellulosic biomass do not pyrolyze independently.

3.9.1 The pyrolysis of lignocellulosic biomass components

The large yields of tars/oils produced when lignocellulosic biomass is pyrolyzed at high heating rates have opened a wide field of possibilities for making transportation and other fuels from renewable feedstocks. A more detailed understanding of the pyrolytic process would be helpful in optimising the *quality* of liquids produced for eventual upgrading.

Recently, excellent progress has been reported in the 'ab-initio' modelling of the decomposition pathways of pure cellulose, based on the stated premise that'…understanding cellulose pyrolysis chemistry is…crucial for developing efficient biofuel production technologies' (Agarwal et al., 2012). Further progress was deemed possible through 'ab-initio' mathematical models, simulating chemical reactions during the pyrolysis of naturally occuring biomass, based on the assumption that this could be done '…analogously from the problems of cellulose…' (Mettler et al., 2012).

Unlike other components of lignocellulosic biomass, the molecular structures of celluloses are well-defined, which helps in reaction modelling. Clearly, however, the extent to which synergistic effects dominate the course of pyrolytic reactions would have a direct bearing on whether and how particular chemical reaction pathways can

be identified and fitted into 'ab-initio' mathematical models. Already cited work by Shafizadeh and coworkers going back to the 1970s and early 1980s provides *prima facie* evidence that differences in composition and composite morphologies of diverse plant components modify pyrolytic reaction pathways.

In this context, some of the experimental work reported in the literature provides a problematic counterpoint. We have already mentioned the work of Evans and Milne (1987a,b), stating that the identification of '…characteristic mass spectral signatures…' provided evidence that '…whole wood appears to behave as the sum of its constituents…' without considering whether tar and char yields from isolated components matched (or not) the tar and char yields of the naturally occuring biomass.

In later work, Yang et al. (2006) recorded the weight loss curves of cellulose, a sample of lignin and 'xylan', using a TG balance. In this context, xylan is often considered as an acceptable representation of hemicellulose present in plants. Despite the shortcomings of TG balances discussed earlier in this chapter, Yang et al.'s data appear useful in pinpointing the temperatures for the *onset* of weight loss for each of the samples, as well as providing qualitative comparisons between the behaviour of the three components, at increasing temperature. However, in their attempted simulation of the pyrolytic behaviour of the three components in a 'synthetic mixture', these researchers loosely mixed the three powders in requisite proportions: '…The biomass samples were synthesised by dry mixing the three components according to the specific ratio'. They reported that '…almost no significant interaction occurs between hemicellulose, cellulose and lignin pyrolysis, although a slight shifting of the peak to a higher temperature (10°C) was observed…' and that '…it could be concluded that pyrolysis of a biomass could be regarded as a superposition of the three components that play individual roles during biomass pyrolysis consistent to previous studies'.

The conclusions arrived at by Yang et al. (2006) seem relevant to a mixture of dry powders charged onto a TG-balance pan. It does not appear possible to generalise from these data to any naturally occuring biomass where the plant components are known to be intimately intermeshed at the macromolecular level. Nonetheless, similar conclusions were reported by Koufopanos et al. (1989), Srivastava and Jalan (1994), Raveendran et al. (1996), Miller and Bellan (1997), Rao and Sharma (1998), Orfao et al. (1999) and Manya et al. (2003). A review on the utilisation of bio-oils from wood and agricultural residues also assumed that lignins, hemicelluloses and cellulose pyrolyzed separately (Oasmaa et al., 2010).

Table 3.16 presents total volatile, tar/oil and char yields from the pyrolysis of a sample of Kraft lignin (Holmen AB, Sweden). The experiments were carried out at two heating rates (1°C s^{-1} and 1000°C s^{-1}), in the wire-mesh reactor described in Section 3.3. As expected, total volatiles increased and char residues decreased with increasing temperature. As commonly observed in data from wire-mesh reactors (Fraga-Araujo et al., 1991; Li et al., 1993b), tar/oil yields tended to increase with temperature to a peak value and then to hold steady with increasing temperature. When the reactor configuration allows significant secondary cracking, however, tar/oil yields go though a maximum [Tyler, 1979; Tyler, 1980; also see Figure 3.8]. Another clearly discernible trend in Table 3.16 was the small but systematic increase in total volatiles and tar/oil yields, when the faster heating rate was used.

In the next sub-section, we aim to develop a clearer view of the nature of synergistic interactions observed during the pyrolysis of lignins embedded within plant-derived biomass, and the effect of these interactions on overall product distributions.

3.9.2 Pyrolysis of isolated lignins and lignocellulosic biomass

Tables 3.13 and 3.15 present data from the atmospheric pressure pyrolysis of silver birch wood and sugar cane bagasse samples, respectively. The data showed similar trends to those of lignin pyrolysis (Table 3.16). In all cases, total volatile and tar/oil yields increased with faster heating. When using rapid heating and effective volatile removal from the reaction zone, small particles of wood (106–152 μm) gave remarkably low char yields: less than 2% between 600°C and 900°C. Char yields from sugar cane bagasse (Table 3.15) were only marginally higher.

However, compared to samples from silver birch and sugar cane bagasse, the Kraft lignin sample (Table 3.16) gave much greater (>30%) yields of char residue, under similar experimental conditions. The sugar cane bagasse and silver birch samples are estimated to contain approximately 21% and 27% lignin, respectively. If lignin, cellulose and other components of lignocellulosic biomass were to *pyrolyze independently*, substantially higher char yields would have been expected from sugar cane bagasse and silver birch pyrolysis – even assuming zero char yields from all other components within the two samples.

Conversely, the data in Table 3.16 showed much higher char yields for the ('pure') isolated lignin samples than would have been predicted, based on the amounts of char produced during the pyrolysis of the silver birch and sugar cane bagasse, given their estimated lignin contents. In other words, *if* the pyrolysis of biomass components takes place independently, the lignin in the plant-derived biomass should have produced more char. On the basis of these experiments, we appear to face a 'char

Table 3.16 Tar and total volatile yields from atmospheric-pressure pyrolysis of kraft lignin determined using the wire-mesh reactor[a]

	Heating rate					
	Total volatiles (% daf basis[b])		Tar/oil yield (% daf basis[b])		Char residue (% daf basis[b])	
Temperature (°C)	1 °C s^{-1}	1000 °C s^{-1}	1 °C s^{-1}	1000 °C s^{-1}	1 °C s^{-1}	1000 °C s^{-1}
400	44.7	50.6	37.6	40.0	55.3	49.4
600	57.2	65.5	42.0	44.9	42.8	34.5
900	58.7	68.3	43.2	45.0	41.3	31.7

Source: Reprinted with permission from Morgan, T.J., Kandiyoti, R., 2014. Chem. Rev. 114, 1547. Copyright 2014 American Chemical Society.
[a]Helium used as carrier gas in all experiments; 30 s holding at peak temperature (Fraga-Araujo, 1990).
[b]*daf*, dry ash free basis.

deficit' in experiments involving the pyrolysis of naturally occuring biomass samples, compared to experiments with chemically isolated lignin.

A survey of lignin pyrolysis experiments: It seems reasonable to expect that the chemical structures and compositions of lignins change from one plant species to another. Similarly, the structures and compositions of chemically isolated 'pure' lignins may vary widely, depending on the chemical isolation method used for preparing the sample. Furthermore, there is no evidence that the structures and compositions of lignins isolated via chemical methods are similar, still less identical, to those embedded within the parent biomass. Strictly, this is a difficulty we cannot eliminate. However, in attempting to test the 'char deficit' hypothesis outlined above, variations in lignin structures may (at least to some extent) be evened out by surveying results from as broad a range of lignin samples and pyrolysis experiments as possible, using isolated (so called 'pure') lignin samples prepared by a wide selection of methods and from a variety of starting biomass materials. By using this admittedly inexact approach, we will seek to observe possible trends in order to arrive at some essentially qualitative conclusions.

Table 3.17 shows a set of results from many different types of pyrolysis experiments, carried out using isolated ('pure') lignin samples prepared via different chemical isolation methods and from a number of distinct plant species.

A more robust comparison would have required data from experiments performed using reactor configurations, which can provide information more closely related to the fundamental pyrolytic behaviour of the materials, such as wire-mesh and fluidised-beds reactors. Nonetheless, results from numerous other experimental configurations are presented in Table 3.17, in order to widen the field of available lignin samples and available pyrolysis experiments. The allure of TG balances for studying the pyrolytic behaviour of biomass seems as undeniable, as are the enduring drawbacks of this type of instrument for performing pyrolysis experiments, as explained earlier in this chapter.

Taken together, the results summarised in Table 3.17 show that the high char yields observed during experiments with the Kraft lignin sample presented in Table 3.16 did not represent an unusual or idiosyncratic outcome. The char yields observed in *all* of these experiments were systematically higher than char yields observed after the pyrolysis of naturally occuring lignocellulosic biomass, performed under experimental conditions minimising secondary reactions. Therefore, compared to chemically isolated lignin samples, we are able to confirm that the pyrolysis of whole lignocellulosic biomass samples show a 'char yield deficit' when considered relative to char yields that might have been anticipated from the (hypothetical) independent pyrolysis of individual biomass components. It seems reasonable to conclude that the pyrolytic reactions of chemically isolated lignin samples take entirely different reaction pathways compared to the pyrolysis reactions of lignins embedded in naturally occuring plant material.

One possible explanation for the 'char yield deficit' is the highly oxidising environment brought about when cellulose and other oxygenated species such as hemicelluloses decompose in close proximity to lignin matrices.

Table 3.17 Selection of pyrolysis char yields, from lignins prepared with diverse methods and pyrolyzed in diverse types of apparatus

Authors (year)	Lignin preparation method	Pyrolysis method	Particle size	Heating rate	Char yield data (Temperature, °C; Char, %)		Comments
Iatridis and Gavalas (1979)	Kraft lignin from Douglas fir	Early version of 'captive sample' technique (wire-mesh reactor)	200 mg	200°C–400°C s^{-1} (approx.)	400 500 600 750	~76–78 ~ 56 ~ 43 ~ 35	Large sample (200 mg) may have contributed to increase char yield (est. <5%)
Chan and Krieger (1981)	Pinewood Kraft lignin	Volume heating by dielectric-loss micro-wave heating	1.5×1.5 cm pellet	20°C s^{-1} (est.)	650–750 (est.)	33%	Pellet size might contribute to some char formation (est. <5%)
Nunn et al. (1985)	Milled wood lignin from sweet gum hardwood	'heated grid' (wire-mesh) reactor	≤100 μm thick flakes	1000°C s^{-1}	307 527 1077	96.9 50 14.5	Result at 1077°C seems low, compared with result at 527°C. Most weight loss expected below 600–650°C
Caballero et al. (1996)	Eucalyptus wood Kraft lignin	Pyroprobe instrument	Powder	Nominal 20,000°C s^{-1}	450 700 900	44[a] 35[a] 33[a]	Sample stacking may have increased char yield by est. several percent
Ferdous et al. (2002)	Alcell and Kraft lignins	Thermogravimetric balance (TGA)	10 mg powder	5–15°C min^{-1}	800 Alcell Kraft	35 43	The lowest char yields observed during heating at 15°C min^{-1} to 800°C.
		Fixed-bed reactor		5–15°C min^{-1}	800 Alcell Kraft	38–42[a] 45–50[a]	Secondary char formation in TGA and fixed-bed reactor; result to be treated as qualitative.[c]

Wang et al. (2009)	MWL[b] from Manchurian ash and Mongolian pine	Thermogravimetric balance (TGA)	Not available	1°C s^{-1}	37% and 26%		Secondary char formation in TGA and fixed-bed reactor; result to be treated as qualitative[c]
De Wild et al. (2009)	**1.** Alcell organosolv process from mixture of hardwoods	Thermogravimetric balance (TGA)	Powder	5°C min^{-1}	Alcell 500	~48[a]	Secondary char formation in TGA and fixed-bed reactor; result to be treated as qualitative[c]
					"GRANIT" 500	~43[a]	
	2. "GRANIT" Precipitation after pulping nonwoody plants	Pre-heated fluidised-bed	1–3 mm pellets	Rapid >1000°C s^{-1}	Alcell 400	35	Higher char yields in TGA compared to fluidised-bed likely due to secondary char formation in TGA
					"GRANIT" 400	30	
Beis *et al.* (2010)	Indulin AT 'Lignoboost' were Kraft lignins. 'Acetocell' lignin from an 'organosolv' process.	Thermo-gravimetric balance (TGA)	10 mg <425 µm particles	5°C min^{-1}	Peak Temperature: 5°C min^{-1}	900°C	Higher char yields in TGA compared to fluidised-bed likely due to secondary char formation in TGA
					Indulin AT	42[a]	
					Lignoboost	38[a]	
					Acetocell	42[a]	
		Fluidised bed All experiments at 550°C	100 g <425 µm particles	Rapid >1000°C s^{-1}	550°C Indulin AT	41	Final char yields in TGA similar for different heating rates
					Lignoboost	29	
					Acetocell	63	Acetocell char yield in fluidised-bed seems inordinately high.
Trinh et al. (2013)	Straw lignin 79% lignin	Pyrolysis centrifuge reactor	<840 µm	200°C–2000°C s^{-1}	500–550°C 27% char		Particle size very large; lignin content low
de Wild et al. (2012)	Alcell lignin	Fluidised bed	2 mm average	Rapid	450–550°C 43% char		Particle size large; would enhance char yield

(*Continued*)

Table 3.17 Selection of pyrolysis char yields, from lignins prepared with diverse methods and pyrolyzed in diverse types of apparatus (Continued)

Authors (year)	Lignin preparation method	Pyrolysis method	Particle size	Heating rate	Char yield data (Temperature, °C; Char, %)	Comments
de Wild et al. (2012)	Granit lignin	Fluidised bed	2 mm average	Rapid	450–550°C 39% char	Particle size large; would enhance char yield
de Wild et al. (2012)	Organosolv lignin A	Fluidised bed	2 mm average	Rapid	450–550°C 36% char	Particle size large; would enhance char yield
de Wild et al. (2012)	Organosolv lignin B	Fluidised bed	2 mm average	Rapid	450–550°C 31% char	Particle size large; would enhance char yield
Nowakowski et al. l(2010)	Lignin from pulp paper plant	Fluidised bed	100–110 μm	Rapid	530°C 48% char	Char yield v. high Ash content may be high

Source: Adapted with permission from George, A., Morgan, T.J., Kandiyoti, R., 2014. Energy Fuels 28, 6918. Copyright 2014 American Chemical Society.
[a]Estimated from graphical data in the publication.
[b]*MWL*, milled wood lignin; cf. e.g., Guerra and Filpponen (2006).
[c]Kandiyoti (2002).

In any case, there seems to be no case for taking forward the proposition that biomass components naturally embedded within lignocellulosic biomass pyrolyze independently.

3.9.3 Synergistic effects during the pyrolysis of composite biomass matrices

Meanwhile, there is a body of contrasting evidence from the pyrolysis of two UK *coals* and their respective maceral concentrates, which we have already reviewed in Section 3.7.3. Tar and volatile yields from the pyrolysis of different 'maceral' constituents of *coal* particles were found to be additive within experimental error (±2%) (Li et al., 1993a,b). These data present an intriguing contrast to the more complex behaviour observed in the case of pyrolyzing biomass components.

Pure or nearly pure (coal) maceral particles tend to have dimensions of several microns or less (Dyrkacz and Horwitz, 1982; Dyrkacz et al., 1984). How would composite particles prepared from powdered cellulose and lignin behave under analogous pyrolysis conditions?

To investigate this latter question, synthesised composite particles made from powders of cellulose and lignin were prepared and pyrolyzed. First, carefully prepared mixtures of fine lignin and cellulose powders were pressed into large pellets. The pellets, each containing different proportions of cellulose and lignin were crushed and sieved to isolate particles in the 106−152 μm size fraction (Fraga-Araujo, 1990; George et al., 2014). Fig. 3.10 presents total volatile yield data from the pyrolysis of the composite particles at two heating rates (1°C s^{-1} and 1000°C s^{-1}). The data have been compared with hypothetical yields calculated by assuming that the two components within the synthetic particles pyrolyze independently; these have been shown as the two straight lines in Fig. 3.10. The measured total volatile yields from pure (100%) cellulose and pure (100%) lignin were used to anchor this latter calculation. In Fig. 3.10, char yields may be calculated by subtracting the value for total volatiles from 100%.

The results presented in Fig. 3.10 revealed a complex picture. The data clearly showed what may be termed synergistic effects between powdered cellulose and lignin, during the pyrolysis of the (synthesised) composite particles. Both the rapid (1000°C s^{-1}) and slow (1°C s^{-1}) heating of the composite particles gave *lower* total volatile yields (*higher char yields*) compared to the case assuming the independent pyrolysis of the two components.

By contrast, data from the two natural biomass samples gave *higher* total volatile yields (lower char yields), compared to the hypothetical case of independent pyrolysis of cellulose and lignin. In Fig. 3.10 silver birch and sugar cane bagasse pyrolysis results were plotted on the basis of their estimated lignin contents (the x axis). In these experiments, it was assumed that hemi-celluloses would leave nearly no char. As a first approximation, this seems reasonable when viewed against the low char yields from the two plant-derived specimens in Tables 3.13 and 3.15, suggesting the already small amounts of char residue would have probably originated from the lignin component.

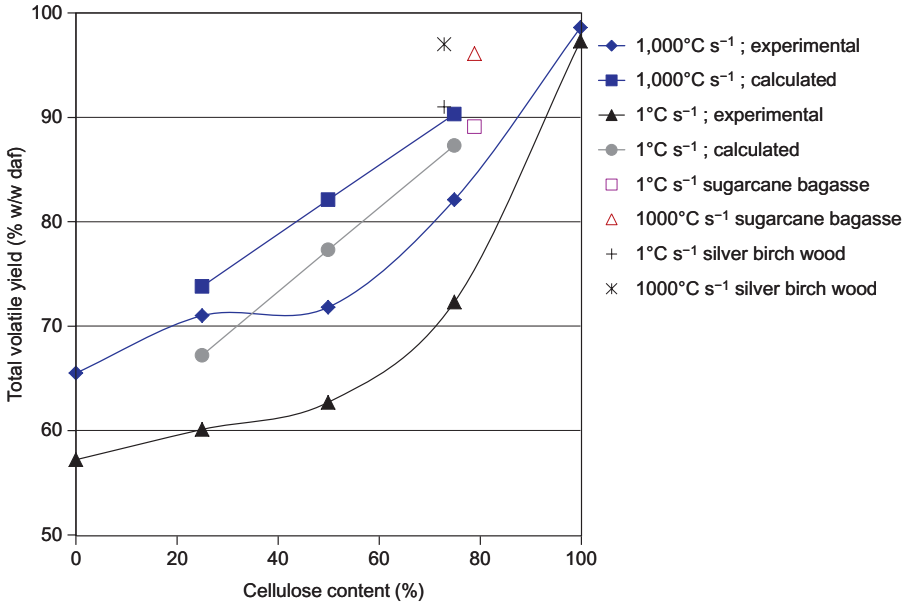

Figure 3.10 Calculated and experimental total volatile yields of composite cellulose–lignin particles, as a function of cellulose content and heating rate (1°C s^{-1} and 1000°C s^{-1}), at 600°C, with 30 s holding at peak temperature. Helium was used as ambient gas in all experiments.
Source: Adapted from Fraga-Araujo, A.-R., 1990. Ph.D. Thesis. University of London, p. 161. Reprinted with permission from Morgan, T.J., Kandiyoti, R., 2014. Chem. Rev. 114, 1547. Copyright 2014 American Chemical Society.

Interpreting Fig. 3.10: The composite particles made from mixtures of cellulose and lignin powders exhibited a trend that differed from the trend observed when pyrolyzing the natural lignocellulosic biomass materials. The composite particles gave more char compared to the hypothetical (*calculated*) values obtained by assuming that no synergistic effects took place. Meanwhile, smaller char residues were observed compared to the hypothetical calculated value, when the *natural* biomass samples were pyrolyzed. It seems clear that the manner in which individual lignocellulosic components are mixed or intermeshed, profoundly influences the pyrolysis behaviour of the sample. It does not seem possible to envisage that these biomass components could pyrolyze independently.

3.9.4 Discussion: data on synergistic effects and the lignin 'char deficit'

In trying to arrive at an explanation for observed synergistic effects between biomass components during the pyrolysis of naturally occuring lignocellulosic biomass, several related factors need to be considered, probably in conjunction: (1) intimate

intermeshing and chemical bonding of biomass components and the resulting physical impediments to the free evaporation of potentially volatile products during thermal breakdown; (2) the onset of decomposition of cellulosic and hemicellulose related structures takes place at lower temperatures compared to lignin, releasing thermally sensitive (i.e., reactive) and highly oxygenated primary products within the heated lignin matrix; with escape pathways mostly blocked, these volatile species are likely to degrade and to react within the pyrolyzing solid lignin matrix surrounding and containing them and (3) the eventual product distribution would be affected by the different reactivities of volatile products released from distinct biomass components. The interactions between these volatiles would in part depend on how these components connect within the molecular architecture of the original plant material.

Let us briefly examine these elements within a likely pyrolytic sequence, ignoring for the time being the role of hemicelluloses, mineral matter and extractable resins, for which we do not have data from purpose-designed experiments. In any case, considering that char yields as low as 2% have been measured, the contribution of these components to the overall char yield would be small.

1. *Intermeshed structures of lignocellulosic biomass components*: Mettler et al. (2012) have presented a detailed conceptual scheme describing the hierarchy of biopolymeric structures that make up lignocellulosic biomass. According to this scheme, elementary 'lignocellulose' macromolecular structures make up wood cells, which combine to make up woody microstructures that in turn combine to constitute wood fibres. Lignin and cellulose present in naturally occuring substrates would be far more intimately linked than the artificially prepared, composite lignin-cellulose particles described above. In other words, contact between distinct components in naturally occuring biomass would take place at the level of macromolecular (Å range) interactions, and not at the level of micron-scale contact taking place within the composite particles used in the set of experiments just described. The tightly packed arrays of biopolymers making up the native woody structures would act to impede the free volatilisation and escape of volatiles produced by the pyrolysis of thermally more sensitive components of the substrate.
2. *Differences in the ranges of decomposition temperatures of biomass components*: An important difference between the behaviour of biomass and coal components during pyrolysis is the differences in temperature intervals, where the thermal breakdown of the different biomass components are initiated. By contrast, corresponding temperature ranges for the onset of pyrolysis of the various coal *maceral groups* have been found to overlap quite considerably (Li et al., 1993a).

   Table 3.18 makes an admittedly qualitative case, showing that when pyrolyzed independently, the pyrolysis of cellulose is completed at a lower temperature interval, compared to the lignin sample. Earlier work carried out in a fluidised-bed reactor provides supporting evidence showing that a sample of cellulose released nearly 70% tar at just above the relatively low temperature of 300°C (Stiles and Kandiyoti, 1989). The corresponding char yield from cellulose at these low temperatures was about 20%.

   Pyrolysis experiments using pure cellulose conducted at rates of 10°C min^{-1} in a TGA (i.e., slow pyrolysis) have shown rapid decomposition at around 320°C (Yang et al., 2007); this is a higher temperature than indicated by data obtained from the fluidised bed, just quoted. Unpublished TG-balance data from recent work at Imperial College suggests that cellulose begins to decompose very near 300°C. Near total decomposition seems to have taken place when *holding* at 300°C for nearly 7 min, which suggests that heat transfer

resistances are affecting results. Heat transfer resistances are a factor that is traditionally and cheerfully ignored in analysing experimental data from TG balances. In the work of Yang and coworkers, when the temperature was ramped, cellulose decomposition appeared completed around 400°C. Yang et al. also examined a sample of lignin; the onset of thermal breakdown of the particular sample was observed to begin at around 300–310°C. However, at 400°C almost 70% of the lignin sample was reported to be present in solid form. As a substitute for hemicellulose, Yang et al. studied a sample of xylan; its decomposition started at around 200°C, although almost 40% of the sample mass remained in solid form at 400°C. This range of values is supported by recent unpublished data from work at Imperial College.

Clearly, the data sets are not complete and agreement on the onset of pyrolysis temperatures rather patchy, probably due to differences in heat transfer efficiencies between TG balances and the fluidised bed described by Stiles and Kandiyoti (1989). Nevertheless, combining information from all the sources cited above with the data in Table 3.18, it seems reasonable to conclude that cellulose would be expected to have lost *all* its solid mass at temperatures around 400°C (if not before) during pyrolysis, whereas the xylan and 'pure' lignin components would still be present as large proportions (>40%) of the solid mass. If we can generalise from the xylan data, it would appear that at 400°C, hemicelluloses would still be in the process of thermal decomposition and probably be quite reactive.

Back to the lignin 'char deficit': In looking for leads to explain synergistic effects between pyrolyzing biomass components, leading to our 'char deficit', the thermal sensitivity of laevoglucosan provides a useful clue. It has a sublimation temperature of 115°C and an onset temperature for decomposition of around 300°C. In the absence of a rapid escape route, the thermal degradation of laevoglucosan at typical cellulose pyrolysis temperatures would be rapid.

We have already seen that much of the lignin microstructure would likely remain intact at these relatively low temperatures – possibly in its initial stages of dehydration and carbonisation. Meanwhile, secondary reactions of laevoglucosan, its secondary products and those of hemicellulose-derived volatiles evolving into the confined spaces of intermeshed microstructures, would probably lead to the extensive oxidation of the pyrolyzing lignin

Table 3.18 Comparison of the pyrolysis temperatures of cellulose and lignin in the atmospheric pressure wire-mesh reactor. Carrier gas: helium. Holding time at peak temperature: 30 s (Fraga-Araujo, 1990; Morgan and Kandiyoti, 2014)

Temperature (°C)	Heating rate (°C s^{-1})	Cellulose total volatiles (% w/w daf[a])	Lignin total volatiles (% w/w daf[a])
400	1	88.2	44.7
	1000	90.4	50.6
600	1	97.3	57.2
	1000	98.6	65.5
900	1	98.4	58.7
	1000	99.4	68.3

Source: Reprinted with permission from Morgan, T.J., Kandiyoti, R., 2014. Chem. Rev. 114, 1547. Copyright 2014 American Chemical Society.
[a]*daf*, dry ash free.

matrix. In other words, the highly oxygenated environment resulting from laevoglucosan and hemicellulose breakdown products are likely to react with pyrolyzing lignin microstructures. Thus, an admittedly speculative likely explanation of the 'lignin char deficit' would go through a highly oxygenated pyrolysis environment leading to the more effective degradation and volatilisation of plant-derived lignin, compared to the pyrolysis of chemically isolated ('pure') lignins, pyrolyzed on their own.

3. *Order of relative tar reactivities*: The design of the fluidised-bed reactor described in Fig. 3.5B allows planning experiments to examine the relative order of sensitivity of tars/oils from particular samples to thermal cracking and thermal degradation reactions. Fig. 3.11 presents tar yields from the pyrolysis of Linby coal at the shortest and longest freeboard residence times practicable in the fluidised-bed reactor. While the shapes of the curves are similar to those for silver birch wood (Fig. 3.8), the data from experiments on Linby coal show far greater proportions of tar survival at higher temperatures. Tar yields showed a maximum around ~580–590°C. For a lignite, the analogous maximum was observed at ~530°C (not shown), while for pure cellulose, silver birch wood (Fig. 3.8) and for banagrass the tar-yield maxima occurred between 425–450°C. A fuller set of data may be found in Stiles and Kandiyoti (1989) and for banagrass in Morgan et al. (2015b). Comparing Figs. 3.8 and 3.11 clearly shows the significant differences between the temperature intervals within which tars from different substrates show reactivity to thermal cracking.

The differences between the pyrolysis onset temperatures of different biomass components (reviewed above) and the differences in the thermal sensitivities of tars/oils from biomass components must be viewed as factors concurrently operating

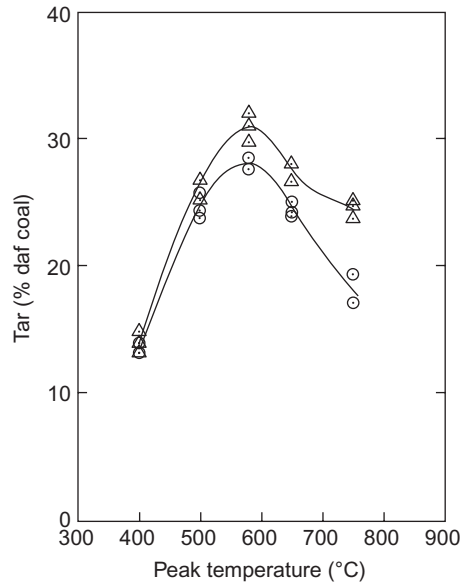

Figure 3.11 Fluidised-bed pyrolysis tar yields as a function of temperature for two different freeboard residence times: (Δ) 0.8 s; (○) 4.5 s Linby (UK) coal.
Source: Reprinted from Gonenc, Z.S., Gibbins, J.R., Katheklakis, I.E., Kandiyoti, R., 1990. Fuel 69, 383. Copyright 1990, with permission from Elsevier.

during the thermal breakdown of lignocellulosic biomass. Once again, the data set is not complete but the demonstrated thermal sensitivity of cellulose tars/oils provides a measure of support for the explanation provided for the absence (or near absence) of laevoglucosan in the product mix from lignocellulosic biomass, compared to the pyrolysis of pure cellulose. These considerations support the idea that the 'lignin char deficit' is associated with lignin volatilisation reactions, intensified by contact with reactive, oxygenated molecular fragments, generated by the prior thermal breakdown of cellulose and hemicelluloses.

Data from differential scanning calorimetry: Some corroboration for the view that the reactive environment in the vicinity of lignin structures alters the course of lignin pyrolysis is found in results from the differential scanning calorimetry (DSC) of cellulose and of the set of samples described in Tables 3.13, 3.15 and 3.16. In these DSC experiments, pure cellulose showed a characteristic single peak between 300°C and 400°C, showing the temperature range over which the sample pyrolyzed. By contrast the 'pure' lignin thermogram showed a broad monotonic rise to 600°C and beyond, with no characteristic breakdown temperature, probably reflecting the reactions of the amorphous mixture of structural features.

However, the two lignocellulosic plant species tested (sugar cane bagasse and silver birch wood) gave broader *single* peaks nearer the zone where the (pure) cellulose decomposition peak had originally appeared. The higher-temperature monotonic rise of heat flow, observed during the decomposition of ('pure') lignin could not be observed at all (Fraga-Araujo, 1990).

By themselves, these observations from differential scanning calorimetry do not represent a conclusive proof of the argument. However, taken together with the 'lignin char deficit' the evidence strongly suggests that the pyrolysis chemistry of lignins is fundamentally altered when thermal breakdown takes place within pyrolyzing matrices of intermeshed biomass components, in an environment where cellulose and hemicelluloses would be releasing reactive oxygenated species.

Other approaches for probing synergistic phenomena during biomass pyrolysis: The observations of synergistic effects outlined thus far have relied on three types of evidence: the 'lignin char deficit', the extents of laevoglucosan survival (or destruction), depending on the complexity of the sample, which defines the chemical environment of the pyrolytic process, and the DSC data just described. Apart for the work of Morgan et al. (2015b), Fahmi et al. (2008) and Mourant et al. (2011), which did not involve changes in char yields, analogous effects pertaining to extractables, mineral matter and hemicelluloses have not been studied. However, char residue from these components appears to be small. Indeed, overall char yields appear to be rather small, when experiments are conducted at higher temperatures (>600°C) and faster heating rates (Tables 3.13, 3.15 and 3.16). Meanwhile, research by other workers has provided valuable additional avenues for investigating synergistic interactions during the pyrolysis of biomass.

Couhert et al. (2009) determined gas evolution in an EFR, during the pyrolysis of a set of five lignocellulosic biomass samples. Similar experiments were performed using xylan (standing in for hemicelluloses), cellulose and several specimens of chemically isolated 'pure' lignins. Their work involved determining total gas evolution from the

pyrolysis of lignocellulosic biomass, and comparing with the gas yields calculated by assuming the independent pyrolysis of the distinct biomass components. This was calculated on the basis of appropriately weighted sums, using gas yields from the isolated biomass components and the estimated contents of the components in each of the lignocellulosic biomass samples. The authors concluded that '…such a simple approach was not successful'. They suggested that the discrepancies might have been caused by the effect of the mineral matter contents of the naturally occuring biomass samples. However, their brief review of work on the subject concluded that '…conclusions are different depending on the authors and on the experimental conditions …'with discrepancies often being explained in terms of '…possible interactions between the components and the likely effect of mineral matter'.

In an earlier study investigating the co-pyrolysis of coal and biomass, observations had been made suggesting that mineral matter contained in biomass might have a catalytic effect on the overall process (Collot et al., 1999). More recent reviews by Vassilev and coworkers have surveyed mineral matter and extractable materials in lignocellulosic biomass (Vassilev et al., 2010, 2012, 2013a,b).

While this approach serves to supplement our descriptive knowledge of biomass composition, sample behaviour under pyrolysis conditions does not necessarily follow from listed compositions. What seems needed is the development of experiments deliberately conceived to elucidate the roles of specific biomass components during pyrolysis. Experiments outlined above regarding the pyrolysis of 'washed' biomass components and the relationship between mineral matter removal and increases in tar yield go some way to elucidating the role of ash components in biomass (Morgan et al., 2015b).

3.9.5 Summary: synergistic effects during biomass pyrolysis

Data have been presented showing that significantly larger char yields were observed when chemically isolated lignin samples were pyrolyzed, compared to the pyrolysis of lignins naturally embedded in plant-derived material. The apparent 'lignin char deficit' has been confirmed by surveying a wide array of lignin pyrolysis experiments. These drew on a variety of original plant materials and a variety of lignin isolation methods. The 'char deficit' may be considered as reflecting the extent of synergistic effects between distinct plant components during the pyrolysis of lignocellulosic biomass. Within this framework, the 'deficit' is consistent with chemical reactions between plant lignin and the reactive and highly oxygenated molecular fragments, generated by the prior thermal breakdown of more labile biomass components, cellulose and hemicelluloses. In the light of these data, there seems to be no question of supporting the proposition that biomass components naturally embedded within lignocellulosic biomass might be pyrolyzing independently.

The observed sensitivity of reaction pathways to plant specific structural features poses added challenges in formulating 'ab-initio' models for tracking the 'detailed pyrolysis chemistry' of lignocellulosic biomass. The complexity of the pyrolysis chemistry of such materials does not appear to justify simple generalisations. The evidence presented suggests that our general level of understanding of the parameters

involved falls well short of predicting trends in product distributions, let alone arriving at quantitative predictions of the detailed chemistry of the pyrolytic processes of naturally occuring biomass. Given the complexities of synergistic interactions during pyrolysis and their probable dependence on species-specific plant morphologies, attempting to develop 'ab-initio' mathematical models (simulations) of the detailed chemistry of biomass pyrolysis, in a manner that would follow '…analogously from the problems of cellulose', do not appear realistic.

However, it is still possible to model the behaviour of larger scale pyrolysis/gasification reactors by combining conventional reactor design concepts with experimental data from experiments that are (1) capable of identifying the fundamental patterns of thermal breakdown, and experiments (2) designed to complement such data by tracking the extra-particle secondary reactions of volatile products.

3.10 Bench-top experiments versus pilot and plant scale design and operation: is there a mismatch?

About a decade ago, data from an experimental 350 kW pf burner showed higher oxygen concentrations in the near-burner zone, compared to levels expected from the calculations of the simulation team within the same research group. To calculate volatile release (weight loss) in the near burner zone, the simulation team were using the system of equations developed by Howard and coworkers (Howard, 1981). All the volatiles were expected to combust in the near-burning zone.

According to their publications, the simulation team assumed that all *volatile matter* evolved in the near burner zone (calculated according to Howard's equations) would combust at the rate of *methane* combustion. Meanwhile, experimentally the group were *observing* 'extra' oxygen in the near burner zone, implying that their volatiles did not combust quite as rapidly as they were assuming.

The coal pyrolysis data outlined earlier in this chapter show that nearly two-thirds of volatiles from the rapid pyrolysis of middle rank coals evolve as *tar* vapours – probably in the form of aerosols. As will be discussed in Chapter 7, Analytical techniques for low mass materials: method development, and Chapter 8, Analytical techniques for high mass materials: method development, condensed coal tars display wide ranges of molecular mass distributions, with the high mass end reaching at least into the low thousands of atomic mass units. There was little likelihood that aerosols packing tar molecules with such large masses would combust at rates similar to those of methane, or indeed present similar *heats of combustion*. At the time, this was pointed out to the modellers of the experimental team, who reportedly adjusted the speeds of gas phase combustion in the near burner zone. The results were said to have 'thrown their calculations off-course'. It seems, the values of some of the adjustable parameters holding the model (indeed all such models) together, might have had to be modified. The modellers were not interested in doing *that*. No further progress could be made.

This episode seems typical of the perennial near-disconnect between experimenters working at bench scale on one hand, and larger-scale plant operators, on the other. Laboratory scale experiments rarely give results that are identical to whatever is happening in larger-scale plants. They are useful in examining trends and exploring relationships between operating parameters. However, the key to the mismatch with larger-scale operations appears to be in the difference of focus. Bench-top experiments enable the manipulation of *one* or a limited number of variables in isolation. In contrast to this mode of work, pilot and plant scale operators usually monitor lumped variables, resulting from a number of events taking place simultaneously. Furthermore, in the cited case, the team were primarily focused on correctly modelling fluid flow. Rates of combustion seemed a secondary issue that could be compensated for by parameter fitting. At other times, perspectives available to operators of larger scale plant appear circumscribed by the availability, sophistication, and even the proper functioning of the instrumentation used for monitoring the plant. Even so, reducing the mismatch between the laboratory on the one hand and pilot and plant scale operation on the other, seems worth striving for.

In the rest of this section, we will explore two cases where bench-scale experiments provided scoping data for larger scale applications, the first for coal injection into blast furnaces, and the second involving modes of tar reduction in fuel gases produced in downdraft biomass gasifiers.

3.10.1 Coal injection into blast furnaces: reactions in tuyeres and raceways

In conventional ironmaking, coke supplied to the blast furnace sustains the burden, while generating the carbon monoxide (by partial gasification), which is necessary for reducing iron oxides. Moreover, a significant part of the coke charged to the blast furnace is eventually consumed by combustion, providing energy to maintain the high temperatures required by the process. However, coke is expensive and its production is rarely free of hazardous emissions. Often, the economics of blast furnace operation is improved by adding a cheaper fuel, through tuyeres at the bottom of the blast furnace, to supply part of the heat and save on coke consumption. Natural gas has been used as a clean and convenient injectant fuel. When natural gas proved expensive, pulverised-fuel grade coal was used for injection into blast furnaces.

In blast furnace operation, the pulverised coal is introduced by means of a lance into a blast of preheated air (or *oxygen-enriched* air), blowing at high velocity through the tuyere into the raceway at the base of the furnace shaft (Geerdes et al., 2015). The raceway is a cavity that forms at the point where the air blast meets the base of the coke bed. It functions as a high-temperature combustion and gasification zone for the injectant coal. One important question facing blast-furnace operators is how much coal to inject without adversely affecting the operation of the blast furnace.

After leaving the coal lance, injectant coal particles are heated rapidly and release volatiles, which tend to form a plume around the particles and burn rapidly, preferentially depleting the supply of air, and limiting the oxygen supply to char surfaces. The

usual blast velocity in the tuyeres approaches 200 m s^{-1}, which limits the residence times of particles in the tuyeres to about 20 ms. By the time coal particles reach the raceways, temperatures normally exceed 1700°C at pressures of 3–6 bars. Any remaining oxygen is quickly consumed in the raceways. The remaining, partially combusted chars are mostly gasified with CO_2, in the raceways (about 50 ms residence time) and as they move up the furnace shaft, where temperatures gradually decrease.

Operational problems are encountered when pf-coal injection rates exceed levels consumed within the blast furnace, usually above about 200–225 kg of coal per ton of pig iron produced. Minimising the proportion of unreacted injectant coal particles and the level of fines moving up, through the furnace is crucial to the correct operation of blast furnaces. High levels of fines can cause blockages leading to poor drainage of molten slag and iron down through the coke bed. Carbon carryover with flue gases leads to fuel loss and undesirable emissions. Numerous studies (e.g., see Maki et al., 1996; Chung and Hur, 1997) have attempted to examine factors that influence the extents of reaction in blast furnace tuyeres and raceways, to clarify possible connections between amounts of coal injection and problems encountered in blast furnace operation.

First try at an experimental design: Examining the fate of injectant coal particles requires an experimental design able to mimic the time–temperature–pressure trajectories of individual fuel particles as they travel through various parts of the blast furnace. A realistic simulation of the conditions in the tuyeres, raceways and finally the blast-furnace shaft would involve, first, pyrolyzing the sample, followed by a short char combustion stage, and ending with CO_2-gasification.

In a preliminary study, the atmospheric pressure wire-mesh reactor (Figure 3.1B) was modified for staged gas injection experiments, mimicking the successive stages coal particles undergo after injection into the tuyeres (Pipatmanomai et al., 2003, 2004). Particles were heated to the peak experimental temperature under an inert atmosphere before a pair of solenoid valves was used to inject short pulses (5–500 ms) of air, or oxygen-enriched air, through the wire-mesh sample holder, thereby simulating the combustion stage. Finally, CO_2 was injected to determine the gasification reactivities of the residual chars.

The pulse-injection system enabled the reactions of injectant coal particles in the raceway to be studied under more representative conditions than had hitherto been possible at bench scale. However, the air injection volume of the system proved limited. Moreover, the system operated at just above atmospheric pressure and temperatures up to 1500°C. Actual blast furnace tuyere and raceway temperatures may reach 2000°C, at pressures in the 3–6 bar range. The pressure limitation in the initial design was partly due to the maximum allowable inlet pressure of the solenoid valves. The large pressure drop across the valves emerged as an additional problem. Nevertheless, the experiment enabled determining the extents of successive pyrolysis, char combustion, and CO_2-gasification reactions, under conditions approaching tuyere and raceway conditions (Pipatmanomai et al., 2003, 2004).

Briefly, by heating at 5000°C s^{-1}, the release of volatiles was found to be completed within the heatup period of somewhat less than 1 s. The results indicated that the residence time available in the tuyeres (~20 ms) was short for the complete

pyrolysis *and* combustion of the injectant coal. When using the subsequent 20-ms air-pulse intervals, the extent of combustion observed was limited by the total amount of oxygen that could be supplied to the experiment, even when oxygen-concentrations in the 21–75% range were used. At these low pressures, all inlet O_2 appeared to have been used up, before the residual char could be consumed.

The residence times in the blast furnace raceways (<50 ms) also appeared short for the complete combustion/gasification of surviving chars. Extents of CO_2-gasification were measured in the 800–1500°C temperature range. Reaction times of tens of seconds were found to be necessary, to achieve measurable extents of CO_2-gasification. Without being conclusive, these findings suggested that a significant proportion of the surviving chars gasify after leaving the raceways, further up the blast-furnace shaft. Unreacted char and soot may then either remain trapped in the coke bed and possibly impede the flow of liquid iron and molten slag, or get entrained in the gas stream, giving rise to the dust related problems observed at high coal injection rates.

Improved system for mimicking conditions in blast-furnace tuyeres and raceways: The experiment was modified, to expose the sample to more accurately controlled quantities of air (or enriched air), over controlled exposure periods (20–100 ms), at pressures up to 6 bars and temperatures up to 2000°C.

Several new elements were introduced to remedy the system's shortcomings. First, the high-pressure wire-mesh reactor described in Chapter 4, High-pressure reactor design: pyrolysis, hydropyrolysis and gasification (Fig. 4.3) was modified for these experiments. A high-pressure gas supply system was constructed, designed for injecting an inert gas through the wire-mesh sample holder, then a controlled pulse of air or enriched air, followed by CO_2, for pre-set time periods, at pressures up to 11 bars.

A schematic diagram of the gas supply system is shown in Fig. 3.12 (Wu et al., 2006, 2007). The system allowed the residence time of the diluted oxygen pulse to be varied, and the oxygen concentration in the mixed gas to be adjusted accurately. Several additional modifications were made to enable operation at temperatures up to 2000°C. The more commonly used stainless-steel mesh would not have withstood the required temperatures. Molybdenum mesh was selected for these experiments. It had been showed to work well during earlier pyrolysis and CO_2 gasification studies up to 2000°C (Peralta et al., 2005; also see chapter: High-pressure reactor design: pyrolysis, hydropyrolysis and gasification). Titanium and tungsten were considered as possible alternatives. However, both these materials have a greater propensity than molybdenum for oxidation under the reaction conditions relevant to the blast-furnace simulation experiments.

Meanwhile, molybdenum itself is not inert in the presence of oxygen. Oxidation may be observed in O_2 concentrations above 3% by volume, at temperatures above 1600°C, and at pressures above about 5 bars. It was found, however, that within the pressure–temperature envelope indicated below, the effect of higher O_2 concentrations on coal samples can be meaningfully studied using sample holders made of molybdenum mesh. Kinetic data could be obtained for char combustion in air (or enriched air) up to about 1600°C; these data were extrapolated, to estimate the extents of char conversion up to 2000°C. These constraints did not apply to experiments performed under pyrolysis or CO_2-gasification conditions. The limitations of using

molybdenum mesh in oxidising environments and the development and verification of the experimental procedure have been discussed in Wu et al. (2006).

In order to raise the temperature ceiling of the experiments, D-type thermocouples were used to monitor the mesh temperature. The 'tungsten/3% rhenium' and 'tungsten/25% rhenium' pair may be used at temperatures up to 2300°C (Peralta et al., 2005).

The modified gas supply system: The aim was to control the volume and pressure of gas in the loop accurately, and inject different gases/mixtures into the system during pre-set time intervals. The solenoid valves (OMEGA SV-1401) had a higher design pressure than those used previously, which enabled replicating the pressure in blast-furnace tuyeres and raceways (3–6 bars). Fig. 3.12 presents a schematic diagram of the gas supply system. V1, V2 and V3 were the fast acting solenoid valves, and N1, N2 and N3, needle valves used for controlling the flow of gas. Before an experiment, the flow rates for the two gas pathways to the wire-mesh reactor (i.e., the N_2-cylinder-V3-N1-V1-WMR (pathway 1) and N_2-cylinder-V3-N2-V2-V1-WMR (pathway 2)) were balanced, using a gas flow metre at the outlet of the wire-mesh reactor and a pressure transducer (P0). This was done to ensure that both pathways have the same

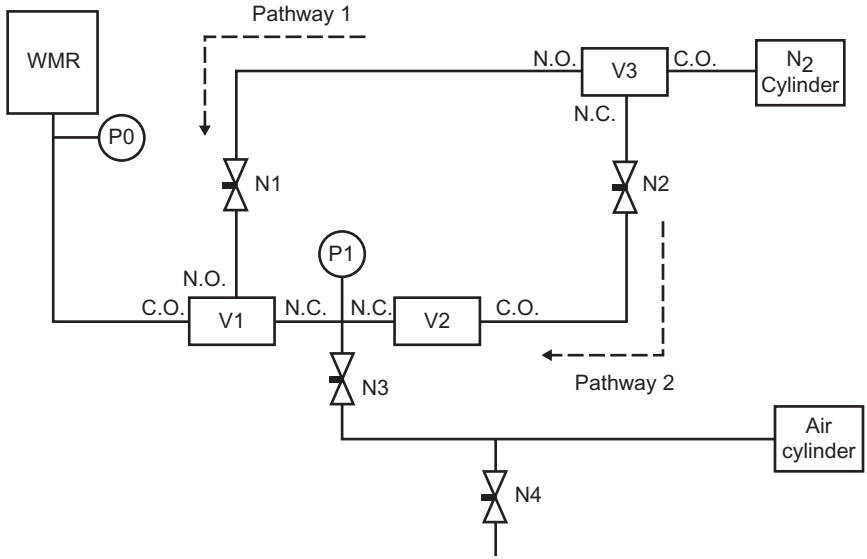

Figure 3.12 Gas supply system for simulating the time-temperature-pressure trajectories of injectant coal particles in blast-furnace tuyeres and raceways and the furnace shaft. V1, V2 and V3 indicate 3-way solenoid valves (SV-1401 OMEGA Company). The normally open port of V2 was blocked. N1–N4 are needle valves. P1 is the precision pressure gauge (0.7 kPa, DPG1001B-100G, OMEGA Company). P0 is the pressure transducer with an accuracy of 1 kPa. *C.O.*, common port; *N.O.*, normally open port; *N.C.*, normally closed port. WMR denotes the high-pressure wire-mesh reactor in Fig. 4.3.
Source: Reprinted with permission from Wu, L., N. Paterson, Dugwell, D.R., Kandiyoti, R., 2006. Energy Fuels 20, 2572. Copyright 2006 American Chemical Society.

pressure drop for the desired gas flow rate; it helped to prevent back mixing when switching from one path to the other. The balance is achieved using needle valves N1 and N2, the pressure transducer (P0), and the flow metre at the exit of the wire-mesh reactor. A known quantity of air (or enriched air) is then trapped in the line between valves V1 and V2, using the needle valve N3 and an accurate pressure gauge, P1, capable of measuring to 0.7 kPa.

At the start of an experiment, nitrogen flows through pathway-1. The computer controlled solenoid valves are set to switch to pathway-2 after a pre-set time interval. At the same time, the inlet and outlet valves of the trapped air loop are opened and the nitrogen flowing into pathway-2 sweeps the accurately known volume of trapped air (or enriched air) out of the loop and toward the wire-mesh reactor. The time interval is calculated and set, so that air reaches the wire-mesh reactor as soon as the peak experimental temperature is reached. The volume of air may be varied by altering the length of the loop between valves V1 and V2 and is set to give the desired air/oxygen-exposure time, usually in the 20–100 ms range. The exposure time may also be varied by altering the gas velocity through the wire-mesh reactor sample holder. For a given loop volume, longer exposure times of sample to the air/oxygen mixture may be achieved by using lower gas velocities.

Wire-mesh reactor data simulation of coal injection into blast furnaces: The effect of holding time at the peak temperature during pyrolysis had previously been investigated by Gibbins-Matham and Kandiyoti (1988) and Pipatmanomai (2002), indicating that volatile release was completed within 1 s when working at peak temperatures between 700°C and 1000°C. At higher temperatures, volatile release appeared to have been completed by the time the peak temperature had been reached. As expected, sample weight loss increased with increasing temperature. Above 1500°C, some of the increase in weight loss, observed in wire-mesh reactor experiments appeared due to the vaporisation of mineral matter in the fuel, since the release of organic volatiles would have been largely completed by the time samples reached 700–1000°C. Within the pressure range studied (1.5–6 bars), the physical effect of increasing pressure tends to supress volatile release. We will return to this in Chapter 4, High-pressure reactor design: pyrolysis, hydropyrolysis and gasification.

Relating the findings from these experiments to fuel injection into blast furnace tuyeres, however, raised some important questions. With particle sizes of pf-grade coal mostly ranging between 40–100 µm, it seems unlikely that all of the injected fuel would complete pyrolysis reactions in anything under 100 ms (Howard, 1981). Since particles go through the tuyeres, typically, in about 20 ms, it is likely the devolatilisation process is completed *after* passage through the length of the tuyeres. The final stages of devolatilisation and partial combustion of the fuel with residual oxygen probably take place in the raceways at the base of the furnace shaft.

Extents of combustion have been measured at 1600°C, with O_2 concentrations in the 3–5% range. Higher O_2 concentrations have been used during experiments at lower temperatures. These limits were imposed by the oxidation reactions of the Mo mesh. The low O_2 concentration is not dissimilar to the concentration 'seen' by char particles *in the raceway*, due to O_2 scavenging by the combusting cloud of volatile matter released by the fuel particles. Moreover, the impact of the temperature

difference on oxidation rates, between our tests (1600°C) and the actual raceway temperatures (estimated ~1800–2000°C) may not be substantial. Kinetic calculations suggests that, at the higher temperatures, combustion reactions take place in a diffusion controlled regime, which would reduce combustion rates and the impact of the higher temperatures (Wu et al., 2007).

Fig. 3.13 shows that the extents of char combustion observed in experimental sequences staged in the wire-mesh reactor were low, mostly less than 5%. These conversions were recorded during exposure times of 100 ms, which is about twice as long as estimated residence times in the raceways, where extents of combustion appear limited by short residence times and probably also by the preferential combustion of volatiles restricting oxygen access to the char. It seems probable, furthermore, that it would be the larger particles in the injectant coal, which get past the raceways in only partially combusted form.

Extents of CO_2-gasification were examined under conditions that represented those in the raceway and the blast-furnace shaft. The results indicated that at 1500°C, complete char gasification may be achieved for contact times of about 10 s. Gasification is therefore capable of completely consuming the char residue formed after coal injection into the raceway. With current designs of blast-furnaces, the major

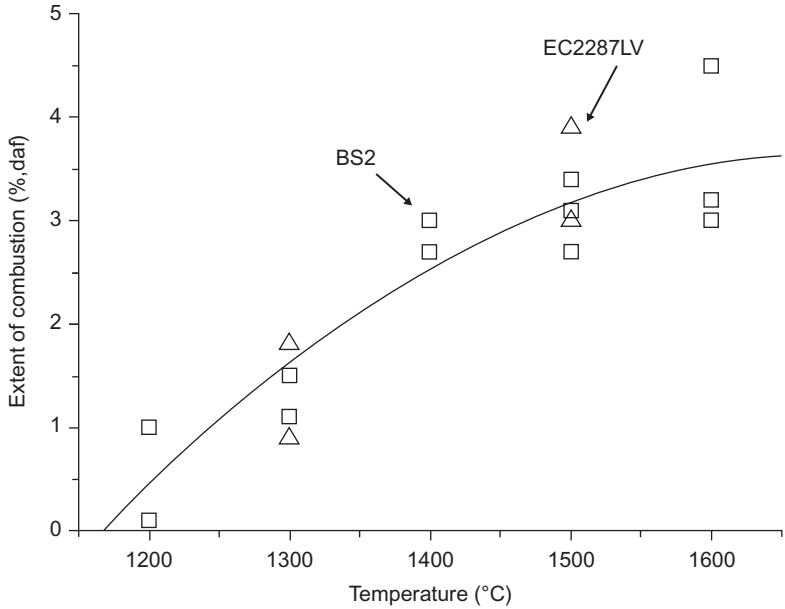

Figure 3.13 Effect of peak temperature on the extents of combustion. Heating rate: 1000°C s^{-1}; Holding time: 1 s; Pressure: 3 bars; oxygen pulse contact time: 105 ms; oxygen concentration: 3% (by volume). BS2 and EC2287LV were two low volatile coals (VM: 13.2% and 21.6%), with 85.9% and 83% elemental carbon content, respectively.
Source: Reprinted with permission from Wu, L., Paterson N., Dugwell, D.R., Kandiyoti, R., 2007. Energy Fuels 21, 2325. Copyright 2007 American Chemical Society.

proportion of the char reaction is thought to occur at progressively decreasing temperatures, as particles move into and up the furnace shaft. However, it is estimated that, in the furnace shaft, contact times with CO_2 in the high temperature zones are far shorter. The presence of char in the collected blast furnace fines shows that the reaction conditions have not been sufficiently intense to allow the complete gasification of all injectant coal.

The effect of particle size has not been assessed during these experiments, due to limitations of the wire-mesh reactor. However, the particle size range used is at the upper end of the range used for pulverised coal injection, and the impact should not significantly alter the conclusions arrived at.

Conclusions: The partial combustion experiments have clearly forced the limits of operation of the high-pressure wire-mesh reactor, equipped with a sample holder made of molybdenum mesh. One of the critical findings was the relatively low carbon conversion through partial combustion. It is thought that the time of exposure of sample to oxygen in the wire-mesh reactor was longer than it would have been in the tuyeres and the raceways. This suggests that the experimental results in Fig. 3.13 might be *overestimating* the extents of combustion taking place at the base of the furnace. Meanwhile, the particle size range used in the present experiments is at the upper end of the size distribution of injectant coals. Thus, extents of combustion of about 5%, arrived at during these experiments appear to represent a reasonable estimate of partial char combustion in the tuyeres and raceways.

Regarding CO_2 gasification, significant conversions may be achieved within a residence time of 5–10 s. Clearly, this is considerably longer than estimated fuel residence times in the tuyeres and raceways, and more typical of residence times in the blast furnace shaft. The wire-mesh reactor data indicate that it is possible to consume most of the char by CO_2 gasification at temperatures close to those of the raceways. However, the *rates* of CO_2 gasification are expected to decrease by the drop in temperature, as particles move up through the furnace shaft. The amount of residual dust thus appears closely related to the temperature distribution within the blast furnace shaft, itself.

3.10.2 Suppression of tar content in product gas from downdraft biomass gasifiers

Agricultural, forestry and domestic wastes mostly present low mass and energy densities. Compared to fossil fuels, therefore, their transport over significant distances is more costly. Proximity to waste processing units reduces transport costs, but entails collecting biomass from relatively small catchment areas, necessitating the processing to be done in relatively small capacity plant. This perspective opens a window of opportunity for downdraft biomass gasification.

One of the attractions of downdraft gasification is the possibility of producing a fuel gas with *relatively* low tar/oil content, compared to updraft fixed-bed or fluidised-bed systems. However, of nearly one-million downdraft gasifiers used in Europe during World War II, *none* have remained in existence (Reed and Das, 1998). Their deployment and use appears to be hindered by numerous factors, which we shall try to examine.

We note first, that downdraft gasification must compete with small scale incineration, possibly winning out where a combustible gas is required for a remote gas burner or for electricity generation, say, in a diesel engine. During World War II, the system clearly found favour in the absence of cheap, convenient fuels like coal, oil or natural gas. The gasifiers in existence would have required constant attention, which was probably accepted with equanimity in wartime. Experience with downdraft gasifiers tells us that fuel feeding systems are capricious. Maintaining the permeability of the bed and suppressing the (albeit low) tar content of the product gas continue to present enduring challenges.

In fact, the 'niche' for downdraft gasifiers to find a place in localised waste disposal, combined with low level energy generation, seems rather restricted. In view of their limited capacity and relatively low grade fuel gas, the new generation of downdraft gasifiers must be cheap to construct and require minimal labour for operation and maintenance. These are severe constraints, delimiting the scope of the design and development effort required.

This section describes experimental work, which seeks to identify conditions for minimising the tar/oil content of the product gas from downdraft biomass gasifiers (Monteiro Nunes et al., 2007, 2008; Dabai et al., 2010, 2014).

Elements of reactor construction: A two-stage fixed-bed reactor was constructed. Biomass was pyrolyzed in the first (upper) stage of the reactor and the evolving volatiles swept into the second stage by means of a stream of carrier gas. The second stage mimicked the action of the throat and exit sections of a downdraft gasifier, where flaming-combustion and gasification take place. Experiments were conducted to study how process variables such as the type of feedstock charged to the first stage, gas composition, temperature and particle size in the second stage, affected the proportion of tar survival in the product gas.

Fig. 3.14 presents a schematic diagram of the reactor assembly. The upper stage (12 mm i.d.; 250 mm long) was constructed as a basic fixed-bed ('hot-rod') reactor, as described in Section 3.4. It was made of AISI 316-grade stainless steel, fitted at the top with connectors to allow for a thermocouple to be inserted into the bed and for gas to be supplied to the reactor in a downdraft configuration.

Originally, the upper section of the reactor assembly was fixed between two rigid electrodes, clamping the top and bottom of the reactor body. However, when peak operating temperatures reach about 1000°C, thermal expansion becomes significant. A similar problem had been encountered in the operation of a high-pressure fluidised-bed reactor (Megaritis et al., 1998; see Chapter 4, High-pressure reactor design: pyrolysis, hydropyrolysis and gasification). In the modified design, the top electrode remained connected to the transformer with rigid copper clamps, and served to fix the reactor in position. However, the *bottom* electrode was connected to the transformer via flexible copper cables, allowing the movement necessary for the thermal expansion of the reactor. The second stage was also heated by direct electrical heating, i.e., by using the tubular reactor body as the resistance heater. It was equipped with two floating electrodes, top and bottom, to allow for thermal expansion during heating to temperatures up to 1000°C.

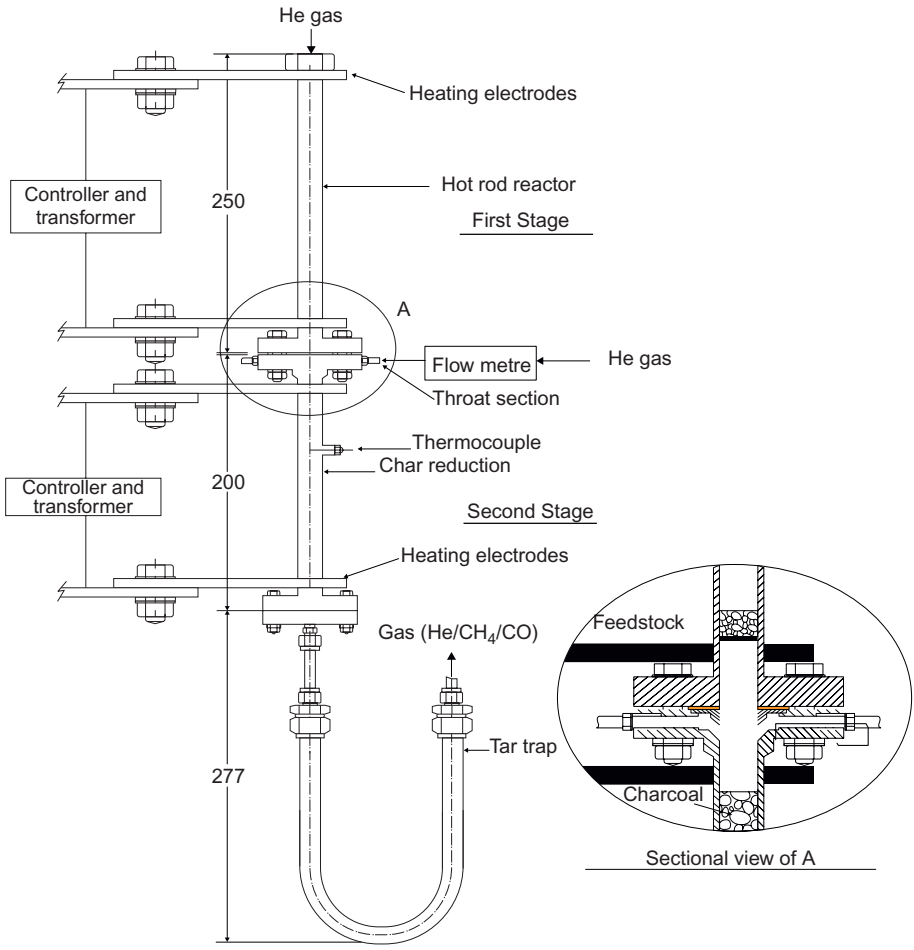

Figure 3.14 Schematic diagram showing component parts of a two-stage reactor for investigating tar destruction parameters in down-draft gasifiers. Operating parameters have been given in the text.
Source: Adapted from Monteiro-Nunes, PhD Thesis, University of London (2007). Adapted with permission from Monteiro Nunes, S., Paterson, N., Dugwell, D.R., Kandiyoti, R., 2007. Energy Fuels 21, 3028. Copyright 2007 American Chemical Society.

Biomass (1 g) was pyrolyzed in the first stage, using a fixed set of conditions to generate a repeatable quantity of volatiles, tars/oils and char. The sample was heated at 10°C s^{-1} to 500°C, at just above atmospheric pressure, and held at 500°C for the duration of the experiment. Helium, at a superficial velocity of 0.1 mL s^{-1} was used to sweep the volatile products of pyrolysis into the second (bottom) stage.

The two stages of the reactor assembly were connected by means of a purpose designed flange assembly (Fig. 3.15). The flange accommodated a V-shaped throat, and was equipped with three equally spaced, lateral inlet nozzles enabling gasification agents (or inert gas) to be injected at the junction of the two stages. The design was intended to simulate the throat of a downdraft gasifier, and allowed controlling the superficial velocity of the carrier gas stream in the second stage, in a manner that was independent of the first-stage flow velocity.

The second stage (12 mm i.d.; 200 mm long), was made of Incoloy 800HT, and served as the tar reduction/destruction zone. It could be operated as an empty tubular reactor to determine tar/oil behaviour under thermal cracking conditions, or could be packed with a fixed amount of char, to mimic tar-cracking conditions in the char reduction zone of the downdraft gasifier. The bottom of the second stage was connected to a tar trap, consisting of a U-tube with an internal diameter of 12 mm, placed in a liquid nitrogen bath. Volatiles exiting the reactor assembly could be condensed and trapped by means of valves placed at either end of the U-tube. The design allowed volatile samples to be withdrawn with a syringe via a septum.

The length of the flaming pyrolysis-gasification zone, where reactive gases contact the char, was about 20 cm long, nearly the length of the analogous section in a full

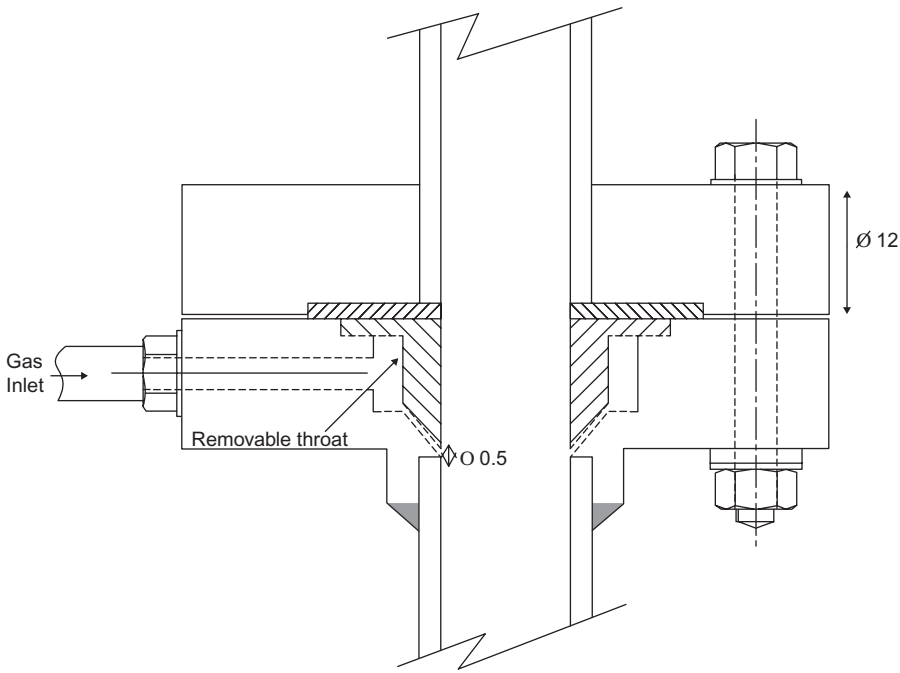

Figure 3.15 Schematic diagram of flanges connecting the two reactor stages. The lower flange contains three gas input nozzles.
Source: Reprinted with permission from Monteiro Nunes, S., Paterson, N., Dugwell, D.R., Kandiyoti, R., 2007. Energy Fuels 21, 3028. Copyright 2007 American Chemical Society.

scale downdraft gasifier (Reed and Das, 1998). Gas temperatures in this zone increase sharply through partial combustion of the chars, so the tars/oils are thermally cracked or partially (or wholly) combusted. In this experimental design, the overall gas temperature was raised by electrical heating, to that required for further tar cracking and gasification of the char.

Summary of results: When, the thermal cracking of tar/oil vapours was investigated using an empty second stage reactor, major extents of tar breakdown were observed at temperatures above 800°C. At 1000°C and a carrier gas velocity of 0.4 m s^{-1}, the tar/oil content of the gas was reduced from an inlet value of 33% of the original biomass sample to 0.7%.

Experiments were also carried out with a packed second stage. The effects of temperature, char particle diameter, the type of char, the gas residence time, and the effect of air injection via the flange-throat were investigated.

Diluted air was used in these experiments, to minimise the combustion of bed char. This is a limitation of the apparatus associated with the static nature of the fixed beds of solids in the two reactors. As expected, packing the second stage with char enhanced tar destruction, by providing heated solid surfaces for repolymerisation and cracking reactions.

Raising the temperature to 1000°C, increasing the sweep-gas residence time, reducing the particle size range in the packed bed of char, and adding diluted air to the throat section all increased the extent of tar destruction. Fig. 3.16 shows that the proportion of tar survival through the second stage rapidly diminished with increasing temperature and the decreasing particle size of the packing. Under these conditions, the presence of char in the second stage decreased the tar/oil content of the exit gas to as low as 0.2% of the input biomass. It was possible to completely remove tars/oils when diluted air was added to the gas mixture.

However, these results do *not* translate directly to the operation of a full-sized gasifier. The use of relatively small particle sizes (up to 2 mm dia.) provided higher surface area solids in the second stage. The small particle size would have enhanced char destruction in the second-stage reactor in a manner not possible in full scale equipment – where the use of larger fuel particles is necessary to avoid grinding costs and large pressure drops. Apart from the particle size, the temperature and the residence time were identified as key parameters in determining the extent of tar destruction.

A selection of biomasses was studied. For all the feedstocks tested, cracking in the presence of char in the second stage decreased the tar/oil discharged from the reactor assembly by more than 98%. Tar destruction was observed to lead to an increase in releases of CO, CO_2, H_2O and light hydrocarbons.

The effect of adding air through the flange at the top of the second stage depended on conditions in the second stage. Working with an empty second stage, added air reduced the tar content at the exit of that stage. With char packed into the second stage, the addition of air did not have much impact at 1000°C, as the extent of tar cracking was already high and the char bed reacted with the oxygen. The amount of CO released increased with temperature, for both empty and packed second stages. However, the CO content was markedly higher at temperatures between 900°C and 1000°C, when a char bed was used, reflecting the effect of the water gas shift reaction,

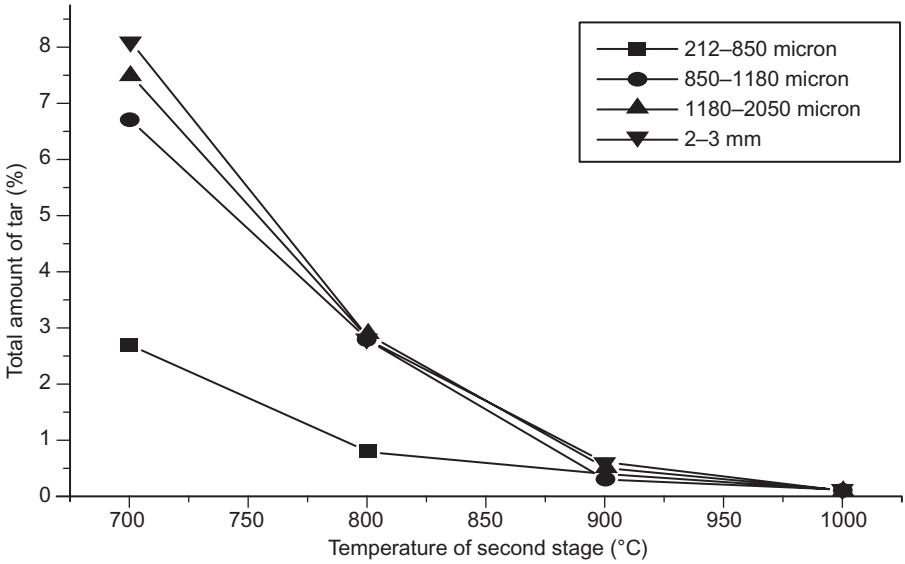

Figure 3.16 Effect of temperature and particle size of charcoal-packing on tar destruction in the second stage of the reactor. Helium atmosphere in both stages. Superficial velocity of first stage was 0.1 m s^{-1}; 0.2 m s^{-1} in the second stage. First-stage tar yield from silver birch wood particles (106–152 µm dia.), at 500°C peak temperature was 47%. Tar yield with an empty second stage at 800°C was 5.2%.
Source: Adapted with permission from Monteiro-Nunes, Ph.D. Thesis, University of London (2007). Copyright 2008 American Chemical Society.

identified by associated reductions in the concentration of CO_2 and H_2O in the exit stream. The amount of light hydrocarbons (C_2-C_5 alkanes and alkenes) showed an initial increase with the temperature in the range of 700–800°C, which then decreased to nearly zero toward 1000°C.

The tars/oils recovered from these experiments have been characterised by GC/MS and by size exclusion chromatography. With more intense reaction conditions in the second stage, a clear transition was observed toward chemically more stable tars/oils. The amounts recovered were reduced, while the proportions of polynuclear aromatic compounds were found to increase.

Conclusions – Experiments with two-stage downdraft biomass gasification: The tar/oil concentration in the product gas was found to decrease with increasing second-stage temperature, decreasing bed particle size, and increasing residence time in the second-stage. The addition of a limited amount of air into the carrier gas stream was observed to help reduce the residual tar/oil content of the product gas. There is clearly scope to minimise the tar/oil content of the product gas from different feedstocks by optimising conditions in the second stage. Overall, the work has shown that the tar/oil content of the product gas from downdraft gasifiers can be reduced to low levels with relative ease but that complete removal will require careful manipulation of reaction parameters, dependent to some degree on feedstock properties.

In other work: A wide range of studies may be found in the literature concerned with cleaning the gas produced in downdraft gasifiers by a variety of methods. Although not meant to be exhaustive, the brief survey presented below may be helpful.

Cracking primary tars/oils from rice straw has been studied in a two stage reactor to clarify stages in its decomposition (Wu et al., 2011). As observed earlier (Stiles and Kandiyoti, 1989; Dabai et al., 2014), at temperatures above 650–700°C, the effects of ring closing reactions tend to convert the predominantly oxygenated open structures of primary/tars oils to noncondensable gases in addition to single ring aromatics and eventually some polynuclear aromatic hydrocarbons (PAHs). Char was found to be effective at capturing PAHs, while steam was found to be an efficient reforming agent for PAH. Hosokai et al. (2011) studied the reforming of tars/oils from woody biomass over charcoal in the presence of steam and air. The near total decomposition observed was attributed to deposition and coking of tars/oils on charcoal surfaces. These reactions were enhanced by the presence of steam, which also helped maintain the activity of charcoal surfaces. Dufour et al. (2011) also used a tubular reactor to study the decomposition of tars formed from wood chips. More recently Zhang et al. (2015) at Shanghai Jiaotong University constructed a reactor system similar to the one described in Figs. 3.14 and 3.15. These researchers identified the conversion of tars/oils to monoaromatic species, and reduced PAH species in product gases, probably through adsorption on char surfaces. Significantly, they identified rapid reductions in the micro-pore volumes of chars as a result of prolonged exposure to tars/oils at the higher temperatures.

References

Agarwal, V., Dauenhauer, P.J., Huber, G.W., Auerbach, S.M., 2012. J. Am. Chem. Soc. 134, 14958.

Anderson, L.L., Hill, G.R., McDonald, E.H., McIntosh, M.J., 1968. Flash heating and plasma processing of coal. Chem. Engr. Prog. Symposium Ser. 64 (85), 81.

Antal, M.J., Mochidzuki, K., Paredes, L.S., 2003. Ind. Eng. Chem. Res. 42, 3690.

Anthony, D.B., Howard, J.B., 1976. AIChE J. 22, 625.

Anthony, D.B., Howard, J.B., Meissner, H.P., Hottel, H.C., 1974. Rev. Sci. Instrum. 45, 992.

Anthony, D.B., Howard, J.B., Hottel, H.C., Meissner, H.P., 1975. 15th Symp. (Int.) Combustion, Pittsburgh, 1303.

Arendt, P., 1980. Ph.D. Thesis. University of Aachen, Germany.

Arendt, P., van Heek, K.-H., 1981. Fuel 60, 779.

Ballantyne, T.R., Ashman, P.J., Mullinger, P.J., 2005. Fuel 84, 1980.

Bautista, J.R., Russel, W.B., Saville, D.A., 1986. Ind. Eng. Chem. Fund. 25, 536.

Beis, S.H., Mukkamala, S., Hill, N., Joseph, J., Baker, C., Jensen, B., et al., 2010. BioResources 5, 1408.

Bennadji, H., Smith, K., Serapiglia, M.J., Fisher, E.M., 2014. Energy Fuels 28, 7527.

Berk, F., 1978. M.Sc. Thesis. Boğazici University, Istanbul, Turkey.

Bolton, C., Snape, C.E., O'Brien, R.J., Kandiyoti, R., 1987. Fuel 66, 1413.

Bolton, C., Snape, C.E., Stephens, H.P., 1988. Fuel 68, 161.

Boutin, O., Ferrer, M., Lede, J.J., 1998. Anal. Appl. Pyrolysis 47, 13.

Branca, C., Giudicianni, P., Blasi, C.D., 2003. Ind. Eng. Chem. Res. 42, 3190.
British Standard 1016, part 12. <http://store.ihs.com/specsstore/controller?event=LINK_DOCDETAILS&getCurVer=false&docId=QGXUCAAAAAAAAAAA&mid=W097>.
Brown, A.L., Dayton, D.C., Nimlos, M.R., Daily, J.W., 2001. Energy Fuels 15, 1276.
Caballero, J.A., Font, R., Marcilla, A., 1996. J. Anal. Appl. Pyrol. 36, 159.
Cai, H.-Y., Kandiyoti, R., 1995. Energy Fuels 9, 956.
Cai, H.-Y., Guell, A.J., Chatzakis, I.N., Lim, J.-Y., Dugwell, D.R., Kandiyoti, R., 1996. Fuel 75, 15.
Cai, H.-Y., Megaritis, A., Messenbock, R., Dix, M., Dugwell, D.R., Kandiyoti, R., 1998. Fuel 77, 1273.
Chan, R.W.-C., Krieger, B.B., 1981. J. Appl. Polym. Sci. 26, 1533.
Chandra, D., 1965a. Econ. Geol. 60, 1041.
Chandra, D. Quart, 1965b. J. Geol. Min. Metal. Soc. India 37, 37.
Chung, J.K., Hur, N.S., 1997. J. Iron Steel Inst. Japan Intl 37, 119.
Collot, A.-G., Zhuo, Y., Dugwell, D.R., Kandiyoti, R., 1999. Fuel 78, 667.
Corella, J., Toledo, J.M., Padilla, R., 2004. Ind. Eng. Chem. Res. 43, 2433.
Couhert, C., Commandre, J.-M., Salvador, S., 2009. Fuel 88, 408.
Cudmore, X.F., 1978. Fuel Proc. Tech 1, 227.
Dabai, F., Paterson, N., Millan, M., Fennell, P., Kandiyoti, R., 2010. Energy Fuels 24, 4560.
Dabai, F., Paterson, N., Millan, M., Fennell, P., Kandiyoti, R., 2014. Energy Fuels 28, 1970.
Desypris, J., Murdoch, P., Williams, A., 1982. Fuel 61, 807.
de Wild, P., Van der Laan, R., Kloekhorst, A., Heeres, E., 2009. Env. Prog. Sustain. Energy 28, 461.
de Wild, P.J., Huijgen, W.J.J., Heeres, H.J., 2012. J. Anal. Appl. Pyrol. 93, 95.
Diessel, C.F.K., 1983. Fuel 62, 883.
Dryden, I.G.C., Sparham, G.A., 1963. B.C.U.R.A. Monthly Bull 7 (1), 1.
Dufour, A., Masson, E., Girods, P., Rogaume, Y., Zoulalian, A., 2011. Energy Fuels 25, 4182.
Durie, R.A., 1980. Coal Liquefaction Fundamentals. In: Whitehurst, D.D. (Ed.), ACS Symp. Ser. No.139, 53.
Dyrkacz, G.R., Horwitz, E.P., 1982. Fuel 61, 3.
Dyrkacz, G.R., Bloomquist, C.A.A., Ruscic, L., 1984. Fuel 63, 1367.
Evans, R.J., Milne, T.A., 1987a. Energy Fuels 1, 123.
Evans, R.J., Milne, T.A., 1987b. Energy Fuels 1, 311.
Fahmi, R., Bridgewater, A.V., Thain, S.C., Donnison, I.S., Morris, P.M., Yates, N., 2007. J. Anal. Appl. Pyrol. 80, 16.
Fahmi, R., Bridgwater, A.V., Donnison, I., Yates, N., Jones, J.M., 2008. Fuel 87, 1230.
Ferdous, D., Dalai, A.K., Bej, S.K., Thring, R.W., 2002. Energy Fuels 16, 1405.
Finn, M.J., Fynes, G., Ladner, W.R., Newman, J.O.H., 1980. Fuel 59, 397.
Fong, W.S., Khalil, Y.F., Peters, W.A., Howard, J.B., 1986a. Fuel 65, 195.
Fong, W.S., Peters, W.A., Howard, J.B., 1986b. Fuel 65, 251.
Fowler, T.G., Kandiyoti, R., Bartle, K.D., Snape, C.E., 1989. Carbon 27, 197.
Fraga-Araujo, A.-R., 1990. Ph.D. Thesis. University of London.
Fraga-Araujo, A.-R., Gaines, A.F., Kandiyoti, R., 1991. Fuel 70, 803.
Freihaut, J.D., Proscia, W.M., 1989. Energy Fuels 3, 625.
Freihaut, J.D., Seery, T.D., 1983. Am. Chem. Soc. Div. Fuel Chem. Preprints 28 (4), 265.
Freihaut, J.D., Seery, D.J., Zabielski, M.E., 1982. 19th Symposium (Intl.) on Combustion. The Combustion Institute, Pittsburgh, PA, 1159.
Freihaut, J.D., Seary, T.D., 1981. Am. Chem. Soc. Div. Fuel Chem. Preprints 26 (2), 133.
Fukuda, K., 2002. Ph.D. Thesis. University of London.

Fukuda, K., Dugwell, D.R., Herod, A.A., Kandiyoti, R., 2004. Energy Fuels 18, 1140.
Furimsky, E., 2000. Appl. Catal. A 199, 147.
Fynes, G., James, R.G., Ladner, W.R., Newman, J.O.H., 1984. Fuel 63, 897.
Gaston, K.R., Jarvis, M.W., Pepiot, P., Smith, K.M., Frederick, W.J., Nimlos, M.R., 2011. Energy Fuels 25, 3747.
Gaur, S., Reed, T.B., 1998. Thermal Data for Natural and Synthetic Fuels. Marcel Dekker, NY.
Geerdes, M., Chaigneau, R., Kurunov, I., Lingiardi, O., Ricketts, J., 2015. Modern Blast Furnace Ironmaking: An Introduction, third ed. IOS Press BV, Amsterdam, The Netherlands.
George, A., Morgan, T.J., Kandiyoti, R., 2014. Energy Fuels 28, 6918.
Gibbins, J.R., 1988. PhD Thesis, University of London.
Gibbins, J.R., Kandiyoti, R., 1989a. Energy Fuels 3, 670.
Gibbins, J.R., Kandiyoti, R., 1989b. Fuel 68, 895.
Gibbins, J.R., Khogali, K., Kandiyoti, R., 1990. Fuel Proc. Tech 24, 3.
Gibbins-Matham, J.R., Kandiyoti, R., 1988. Energy Fuels 2, 505.
Gibbins-Matham, J.R., King, R.A.V., Wood, R.J., Kandiyoti, R., 1989. Rev. Sci. Instruments 60, 1129.
Given, P.H., 1984. In: Gorbaty, M.L. Larsen, J.W. Wender, I. (Eds.), Coal Science, vol. III. Academic Press, NY, pp. 65.
Gonenc, Z.S., Fowler, T.G., Kandiyoti, R., Bartle, K.D., 1988. Fuel 67, 848.
Gonenc, Z.S., Gibbins, J.R., Katheklakis, I.E., Kandiyoti, R., 1990. Fuel 69, 383.
Gong, X., Yu, Y., Gao, X., Qiao, Y., Xu, M., Wu, H., 2014. Energy Fuels 28, 5204.
Graff, R.A., Dobner, S., Squires, A.M., 1976. Fuel 55, 109.
Gray, V.R., 1988. Fuel 67, 1298.
Greenhalf, C.E., Nowakowski, D.J., Harms, A.B., Titiloye, J.O., Bridgwater, A.V., 2013. Fuel 108, 216.
Griffin, T.P., Howard, J.B., Peters, W.A., 1993. Energy Fuels 7, 297.
Griffiths, D.M.L., Mainhood, J.S.R., 1967. Fuel 46, 167.
Güell, A.J., Li, C.Z., Herod, A.A., Stokes, B.J., Hancock, P., Kandiyoti, R., 1993. Biomass and Bioenergy 5, 155.
Guerra, A., Filpponen, I., 2006. J. Agric. Food Chem. 54, 5939.
Gunther, C., Mosandl, A., (2001). The composition of oak and an overview of its influence on maturation (1986) (updated: August 16, 2001). <http://homedistiller.org/oak.pdf>.
Güssing Renewable Energy GmbH; <http://www.gussingrenewable.com/htcms/en/wer-was-wie-wo-wann/wie/thermische-vergasungficfb-reaktor.html>.
Hamilton, L.H., 1980. Fuel 59, 112.
Hamilton, L.H., Ayling, A.B., Shiboaka, M., 1979. Fuel 58, 873.
Hindmarsh, C.J., Thomas, K.M., Wang, W., Cai, H.-Y., Güell, A.J., Dugwell, D.R., et al., 1995. Fuel 74, 1185.
Hiteshue, R.W., Anderson, R.B., Schlesinger, M.D., 1957. Ind. Eng. Chem. 47, 2008.
Hiteshue, R.W., Anderson, R.B., Friedman, S., 1960. Ind. Eng. Chem. 52, 577.
Hiteshue, R.W., Friedman, S., Madden, R., 1962a. USBM Rep. Invest., 6027.
Hiteshue, R.W., Friedman, S., Madden, R., 1962b. USBM Rep. Invest., 6125.
Hosokai, S., Norinaga, K., Kimura, T., Nakano, M., Li, C., Hayashi, J., 2011. Energy Fuels 25, 5387.
Howard, H.C., 1963. In: Lowry, H.H. (Ed.), Chemistry of Coal Utilization Supplementary Volume. Wiley, NY, pp. 340.
Howard, J.B., 1981. In: Elliott, M.M. (Ed.), Chemistry of Coal Utilization Second Supplementary Volume. Wiley, NY. Chapter 12.

Howard, J.B., Anthony, D.B., 1976. AIChE J. 22, 625.
Howard, J.B., Anthony, D.B., Hottel, H.C., 1975. 15th Symposium (Intl.) on Combustion, The Combustion Institute, Pittsburgh, PA, 103.
Howard, J.B., Anthony, D.B., Hottel, H.C., Meissner, H.P., 1976. Fuel 55, 121.
Howard, J.B., Peters, W.A., Derivakis, G.S., 1994. Energy Fuels 8, 1024.
Huang, H.-J., Ramaswamy, S., Tschirner, U.W., Ramarao, B.V., 2008. Sep. Purif. Technol. 62, 1.
Huber, G.W., Iborra, S., Corma, A., 2006. Chem. Rev. 106, 4044.
Hunt, J.E., Lykke, K.R., Winans, R.E., 1991. Prpnt. ACS DFC 36 (3), 1325.
Iatridis, B., Gavalas, G.R., 1979. Ind. Eng. Chem. Prod. Res. Dev. 18, 127.
Jarvis, M.W., Haas, T.J., Donohoe, B.S., Daily, J.W., Gaston, K.R., Frederick, W.J., et al., 2011. Energy Fuels 25, 324.
Jess, A., Andresen, A.K., 2010. Fuel 89, 1541.
Jones, S.B., Snowden-Swan, L.L., 2013. PNNL report no. 22684. Production of Gasoline and Diesel from Biomass via Fast Pyrolysis, Hydrotreating and Hydrocracking: 2012 State of Technology and Projections to 2017.
Jones, R.B., McCourt, C.B., King, K., 1985. Fuel 64, 1460.
Jones S., Tan, E., Jacobson, J., Meyer, P., Dutta, A., Cafferty, K., et al., 2013. PNNL report no. 23053, NREL/TP-5100-61178. Process Design and Economics for the Conversion of Lignocellulosic Biomass to Hydrocarbon Fuels, Fast Pyrolysis and Hydrotreating Bio-oil Pathway.
Jüntgen, H., van Heek, K.H., 1968. Fuel 47, 103.
Kandiyoti, R., 1969. Ph.D. Thesis. University of London.
Kandiyoti, R., 2002. Fuel 81, 975.
Kandiyoti, R., McLaughlin, E., Pittman, J.F.T., 1972. J. Chem. Soc., Farad. Trans. I 68, 860.
Kershaw, J.R., Barras, G., 1979. Am. Chem. Soc. Div. Fuel Chem. Prepr 24 (3), 99.
Kimber, G.M., Gray, M.D., 1967. Combustion and Flame, 360.
Kobayashi, H., Howard, J.B., Sarofim, A.F., 1977. 16 Symp. Combustion. The Combustion Institute, Pittsburgh, 411.
Koufopanos, C.A., Maschio, G., Lucchesi, A., 1989. Can. J. Chem. Eng. 67, 75.
Li, C.-Z., Gaines, A.F., Güell, A.J., Kandiyoti, R., 1991. Proc. Intl. Conf. Coal Sci. 723 Newcastle-upon-Tyne, UK.
Li, C.-Z., Bartle, K.D., Kandiyoti, R., 1993a. Fuel 72, 3.
Li, C.-Z., Bartle, K.D., Kandiyoti, R., 1993b. Fuel 72, 1459.
Li, C.-Z., Madrali, E.S., Wu, F., Xu, B., Cai, H.-Y., Guell, A.J., et al., 1994. Fuel 73, 851.
Loison, R., Chauvin, R., 1964. Chim. Ind. Paris 91, 269. Translation by University of Sheffield (DJB/WBD) May 1964; National Coal Board, Coal Research Establishment Library (Sep 1964).
Madrali, E.S., Rahman, M., Kinghorn, R.R.F., Wu, F., Herod, A.A., Kandiyoti, R., 1994. Fuel 73, 1829.
Maki, A., Sakai, A., Takagaki, N., Mori, K., Ariyama, T., Sato, M., et al., 1996. J. Iron Steel Inst. Japan Intl 36 (6), 650.
Manya, J.J., Velo, E., Puigjaner, L., 2003. Ind. Eng. Chem. Res. 42, 434.
Megaritis, A., Zhuo, Y., Messenbock, R., Dugwell, D.R., Kandiyoti, R., 1998. Energy Fuels 12, 144.
Messenböck, R.C., 1998. Ph.D. Thesis. University of London.
Messenböck, R.C., Chatzakis, I.N., Megaritis, A., Dugwell, D.R., Kandiyoti, R., 1999. Fuel 78, 871–882.
Messenböck, R.C., Paterson, N., Dugwell, D.R., Kandiyoti, R., 2000. Fuel 79, 109–121.
Mettler, M.S., Vlachos, D.G., Dauenhauer, P.J., 2012. Energy Environ. Sci. 5, 7797.

Miller, R.S., Bellan, J., 1997. J. Combustion Sci. Technol 126, 97.
Monteiro Nunes, S., 2007. Ph.D. Thesis. University of London.
Monteiro Nunes, S., Paterson, N., Dugwell, D.R., Kandiyoti, R., 2007. Energy Fuels 21, 3028.
Monteiro Nunes, S., Paterson, N., Herod, A.A., Dugwell, D.R., Kandiyoti, R., 2008. Energy Fuels 22, 1955.
Morgan, T.J., Kandiyoti, R., 2014. Chem. Rev. 114, 1547.
Morgan, T.J., Turn, S.Q., George, A., 2015a. PLoS ONE 10 (8), e0136511. http://dx.doi.org/10.1371/journal.pone.0136511.
Morgan, T.J., Turn, S.Q., Sun, N., George, A., 2015b. PLoS ONE 11 (3), e0151368.
Mourant, D., Wang, Z., He, M., Wang, X.S., Garcia-Perez, M., Ling, K., et al., 2011. Fuel 90, 2915.
Niksa, S.J., Russel, W.B., Saville, D.A., 1982a. Fuel 61, 1207.
Niksa, S.J., Russel, W.B., Saville, D.A., 1982b. 19th Symp. (Intl.) Combustion. The Combustion Institute, Pittsburgh PA, 1151.
Niksa, S.J., Heyd, L.E., Russel, W.B., Saville, D.A., 1984. 20th Symposium (Intl.) on Combustion. The Combustion Institute, 1445.
Nowakowski, D.J., Bridgwater, A.V., Elliott, D.C., Meier, D., de Wild, P., 2010. J. Anal. Appl. Pyrol. 88, 53.
NREL Website: <http://www.nrel.gov/biomass/thermochemical_users_facility.html>.
Nunn, T.R., Howard, J.B., Longwell, J.P., Peters, W.A., 1985. Ind. Eng. Chem. Process Des. Dev 24, 844.
Oasmaa, A., Solantausta, Y., Arpiainen, V., Kuoppala, E., Sipila, K., 2010. Energy Fuels 24, 1380.
O'Brien, J.R., 1986. Ph.D. Thesis. University of London.
Orfao, J.J.M., Antunes, F.J.A., Figueiredo, J.L., 1999. Fuel 78, 349.
Pan, S., Hui, S., Liang, L., Liu, C., Li, C., Zhang, X., 2015. Energy Fuels 29, 520.
Pandolfo, A.G., Johns, R.B., Dyrkacz, G.R., Buchanan, A.S., 1988. Energy Fuels 2, 657.
Peralta, D., Paterson, N., Kandiyoti, R. (2002) 3rd Periodic Report; UK DTI Project No. AEA C/07/00298/00/00.
Peralta, D., Li X., Xu S., Paterson, N., Dugwell, D.R., Kandiyoti, R., 2004. Proc. 2004 Intl. Hi-Tech Symposium on Coal, Chemical Industry and Coal Conversion, 30–31 Oct., Shanghai, China, pp. 136–142.
Peralta, D., Paterson, N., Dugwell, D., Kandiyoti, R., 2005. Energy Fuels 19, 532.
Peters, W.A., Hajaligol, M., Howard, J.B., Longwell, J., 1980. Specialist Workshop on Fast Pyrolysis of Biomass, SERI/CP-622-1096, Solar Energy Research Institute, US Dept. of Energy, Golden CO, USA.
Phong-anant, D., Thomas, C.G., 1990. Fourth Australian Coal Science Conference. Brisbane, Australia, 256.
Pindoria, R.V., Lim, J.-Y., Hawkes, J.E., Lazaro, M.-J., Herod, A.A., Kandiyoti, R., 1997. Fuel 76, 1013.
Pindoria, R.V., Megaritis, A., Messenbock, R., Dugwell, D.R., Kandiyoti, R., 1998a. Fuel 77, 1247.
Pindoria, R.V., Megaritis, A., Herod, A.A., Kandiyoti, R., 1998b. Fuel 77, 1715.
Pindoria, R.V., Chatzakis, I.N., Lim, J.-Y., Herod, A.A., Dugwell, A.A., Kandiyoti, R., 1999. Fuel 78, 55.
Pipatmanomai, S., 2002. Ph.D. Thesis. University of London.
Pipatmanomai, S., Paterson, N., Dugwell, D.R., Kandiyoti, R., 2003. Energy Fuels 17, 489.
Pipatmanomai, S., Herod, A.A., Morgan, T.J., Paterson, N.R., Dugwell, D.R., Kandiyoti, R., 2004. Energy Fuels 18, 68.

Rahman, M., Herod, A.A., Kandiyoti, R., 2000. Fuel 79, 201.
Rao, T.R., Sharma, A., 1998. Energy 23, 973.
Raveendran, K., Ganesh, A., Khilar, K.C., 1996. Fuel 75, 987.
Reed, T.B., Das, A., 1998. Handbook of Biomass Downdraft Gasifier Engine Systems. The Biomass Energy Foundation Press, Golden CO, USA.
Richards, G.N., Shafizadeh, F., 1978. Aust. J. Chem. 8, 1825.
Roberts, O.C., 1982. Published Report 82-8, ISBNNo.0 86722 224 X, Australian Coal Industry Research Laboratories Ltd.
Roy, C., de Caumia, B., Kalkreuth, W., 1985. Fuel 64, 1662.
Sanna, A., Andrésen, J.M., 2012. ChemSusChem 5, 1944.
Sathe, C., Pang, Y., Li, C.-Z., 1999. Energy Fuels 13, 748.
Scott, S.C., Piskorz, J., 1982a. Canad. J. Chem. Eng 60, 666.
Scott, S.C., Piskorz, J., 1982b. Flash Pyrolysis of Biomass. Ann Arbor Science Pub., Ann Arbor, Michigan, Chapter 23.
Scott, S.C., Piskorz, J., 1984. Canad. J. Chem. Eng. 62, 404.
Shafizadeh, F., 1968. Adv. Carbohydr. Chem. 23, 419.
Shafizadeh, F., 1982. Anal. Appl. Pyrol. 3, 283.
Shafizadeh, F., 1985. Pyrolytic reactions and products of biomass. In: Overend, R.P., Milne, T.A., Mudge, L.K. (Eds.), Fundamentals of Thermochemical Biomass Conversion. Springer Netherlands, pp. 183–217.
Shafizadeh, F., Fu, Y.L., 1973. Carbohydr. Res 29, 113.
Solomon, P.R., Serio, M.A., Carangelo, R.M., Markham, J.R., 1986. Fuel 65, 182.
Sonoyama, N., Hayashi, J., 2011. Proc. International Conference on Coal Science & Technology, 9–11 October 2011; Paper No. C43, Oviedo, Spain.
Sonoyama, N., Hayashi, J., 2013. Fuel 114, 206.
Srivastava, V.K., Jalan, R.K., 1994. Energy Convers. Mgmt. 35, 1031.
Stach, E., Mackowsky, M.T., Teichmüller, M., Taylor, G.H., Chandra, D., Teichmüller, R., 1982. Stach's Textbook of Coal Petrology. Gebrüder Borntraeger, Berlin, Stuttgart, pp. 177–198.
Stangeby, P.C., Sears, P.L., 1978. Final Report to Can. Dept. of Energy, Mines and Resources.
Stangeby, P.C., Sears, P.L., 1981a. Fuel 60, 131.
Stangeby, P.C., Sears, P.L., 1981b. Fuel 60, 125.
Stiles, H.N., 1986. Ph.D. Thesis. University of London, UK.
Stiles, H.N., Kandiyoti, R., 1989. Fuel 68, 275.
Sun, B., Ruof, C.H., Howard, H.C., 1958. Fuel 37, 299.
Sun, Q., Fletcher, J.J., Zhang, Y., Ren, X., 2005. Energy Fuels 19, 1160.
Suuberg, E.M., 1977. Sc.D. Thesis. Massachusetts Institute of Technology, Cambridge, Massachusetts.
Suuberg, E.M., 1985. In: Schlosberg, R.H. (Ed.), Chemistry of Coal Conversion, 67. Plenum Press, NY.
Suuberg, E.M., Unger, P.E., 1981. 18th Symposium (Intl.) on Combustion. The Combustion Institute, Pittsburgh, PA, 1203.
Suuberg, E.M., Peters, W.A., Howard, J.B., 1978a. Ind. Eng. Chem. PDD 17, 37.
Suuberg, E.M., Peters, W.A., Howard, J.B., 1978b. 17th Symposium (Intl.) on Combustion. The Combustion Institute, Pittsburgh, PA, 117.
Suuberg, E.M., Peters, W.A., Howard, J.B., 1980. Fuel 59, 405.
Suuberg, E.M., Unger, P.E., Lilly, W.D., 1985. Fuel 64, 956.
Taupitz, K.C., 1977. Hydrocarbon Process. 219.
Thomas, C.G., Holcombe, D., Shibaoka, M., Young, B.C., Brunckhorst, L.F., Gawronski, E., 1989. Proceedings of International Conference on Coal Science, p. 257.

Tissot, B.P., Welte, D.H., 1984. Petroleum Formation and Occurrence. Springer-Verlag, Berlin, NY.509.
Tran, N., Uemura, Y., Chowdhury, S., Ramli, A., 2014. Applied Mechanics and Materials 625, 255.
Trinh, T.N., Jensen, P.A., Sárossy, Z., Dam-Johansen, K., Knudsen, N.O., Sørensen, H.R., et al., 2013. Energy Fuels 27, 3802.
Tsubouchi, N., 2014. Energy Fuels 28, 5721.
Tsubouchi, N., Abe, M., Xu, C., Ohtsuka, Y., 2003. Energy Fuels 17, 940.
Tyler, R.J., 1979. Fuel 58, 680.
Tyler, R.J., 1980. Fuel 59, 218.
Tyson, R.V., 1995. Sedimentary Organic Matter London. Chapman & Hall., Chapter 21.
Unger, P.E., Suuberg, E.M., 1983. Am. Chem. Soc. Div. Fuel Chem. Preprints 28, 278.
Unger, P.E., Suuberg, E.M., 1984. Fuel 63, 606.
Vassilev, S.V., Baxter, D., Andersen, L.K., Vassileva, C.G., 2010. Fuel 89, 913.
Vassilev, S.V., Baxter, D., Andersen, L.K., Vassileva, C.G., Morgan, T.J., 2012. Fuel 94, 1.
Vassilev, S.V., Baxter, D., Andersen, L.K., Vassileva, C.G., 2013a. Fuel 105, 40.
Vassilev, S.V., Baxter, D., Andersen, L.K., Vassileva, C.G., 2013b. Fuel 105, 19.
Vorres, K.S., 1990. Energy Fuels 4, 420.
Wang, S., Wang, K., Liu, Q., Gu, Y., Luo, Z., Cen, K., et al., 2009. Biotechnol. Adv. 27, 562.
Wanzl, W., 1988. Fuel Proc. Tech 20, 317.
Winans, R.E., 1991. J. Anal. Appl. Pyrol. 20, 1.
Winans, R.E., Neill, P.H., 1990. Multiple-heteroatom-containing sulfur compounds in a high sulfur coal. In: Orr, W.L., White, C.M., (Eds.), Geochemistry of Sulfur in Fossil Fuels, ACS Symp. Series 429. Am. Che. Soc., Washington, DC, pp. 249–260.
Winans, R.E., Scott, R.G., Neill, P.H., Dyrkacz, G.R., Hayatsu, R., 1986. Fuel Proc. Tech 12, 77.
Winans, R.E., McBeth, R.L., Hunt, X.E., Melnikov, P.E., 1991. Proc. Intl. Conf. Coal Sci., 44. Newcastle, UK.
Wu, L., Paterson, N., Dugwell, D.R., Kandiyoti, R., 2006. Energy Fuels 20, 2572.
Wu, L., Paterson, N., Dugwell, D.R., Kandiyoti, R., 2007. Energy Fuels 21, 2325.
Wu, W., Luo, Y., Su, Y., Zhang, Y., Zhao, S., Wang, Y., 2011. Energy Fuels 25, 5394.
Yang, H., Yan, R., Chen, H., Zheng, C., Lee, D.-H., Liang, D.-T., 2006. Energy Fuels 20, 388.
Yang, H., Yan, R., Chen, H., Lee, D.-H., Zheng, C., 2007. Fuel 86, 1781.
Yang, H., Yao, J., Chen, G., Ma, W., Yan, B., Qi, Y., 2014. Energy Procedia 6, 1306.
Yildiz, G., Ronsse, F., Venderbosch, R., Duren, Rv, Kersten, S.R.A., Prins, W., 2015. App. Cat. B: Enviro. 168–169, 203.
Yoshida, T., Turn, S.Q., Yost, R.S., Antal, M.J., 2008. Ind. Eng. Chem. Res. 47 (24), 9882.
Zaror, C.A., Hutchings, I.S., Pyle, D.L., Stiles, H.N., Kandiyoti, R., 1985. Fuel 64, 990–994.
Zeng, C., Chen, L., Liu, G., Li, W., Huang, B., Zhu, H., et al., 2008. Rev. Sci. Instrum. 79 (8), 084102. <http://dx.doi.org/10.1063/1.2968714>.
Zhang, S.-F., Xu, B., Herod, A.A., Kandiyoti, R., 1996. Energy Fuels 10, 733.
Zhang, Y.-L., Wu, W.-G., Zhao, S.-H., Long, Y.-F., Luo, Y.-H., 2015. Fuel Process. Technol. 134, 333.
Zhuo, Y., Messenböck, R., Collot, A.-G., Paterson, N., Dugwell, D.R., Kandiyoti, R., 2000. Fuel 79, 793.
Zwart, R.W.R., Van der Drift, A., Bos, A., Visser, H.J.M., Cieplik, M.K., Könemann, H.W.J., 2009. Environ. Prog. Sustainable Energy 28 (3), 324.

High-pressure reactor design: pyrolysis, hydropyrolysis and gasification

4

Chapter Outline

Solid Fuels and Heavy Hydrocarbon Liquids. DOI: http://dx.doi.org/10.1016/B978-0-08-100784-6.00004-7

This chapter continues to outline the development of experimental reactors designed for investigating the behaviour of solid fuels during thermochemical processing. The aim is to evaluate the physical and chemical transformations of solid fuels in response to changes in selected reaction parameters. These measurements must be made, furthermore, in a manner that is, as much as possible, independent of the method of the measurement. In addition to characterising fuel behaviour, we aim to establish some level of comparability between reaction conditions in bench-top reactors and conditions prevailing in larger scale fuel processing plant. This second aim translates into designing reactors that are capable of mimicking the time-temperature-pressure trajectories of individual fuel particles, within designated zones of pilot or plant scale equipment.

The present chapter focuses on experiments carried out at high-pressure. We will review pyrolysis experiments under high-pressure inert gas, hydropyrolysis and hydrogasification experiments under high-pressure hydrogen, and gasification experiments in high-pressure CO_2-steam-air (or oxygen) mixtures. The development of these experiments requires adding new features for pressure containment and reactor safety, to design concepts developed in Chapter 3, Pyrolysis of solid fuels: experimental design and applications. The reactors described in this chapter have been used for solid fuel characterization, and for investigating particular problems encountered during the operation of pilot and plant scale equipment.

4.1 Characterising fuel behaviour under gasification conditions

Gasification is a mature art and vast amounts of experimental work have been performed to investigate the combined pyrolysis–gasification behaviour of solid fuels. Wide-ranging reviews of early work on coal gasification will be found in Chapters 20 and 21 of the 'Chemistry of Coal Utilization; Supplementary Volume' by Lowry (1963) and Chapters 23–26 of 'Chemistry of Coal Utilization: Second Supplementary Volume' by Elliott (1981). A review of coal gasification technologies by Hotchkiss (2003) and the collection of IEA Clean Coal Centre reviews (http://www.iea-coal.org.uk/site/ieaccc/home) provide valuable surveys of the field. Higman and Burgt's 'Gasification' (2008) presents a thorough review of coal and biomass gasification technologies. The more recent 'Technologies for Converting Biomass to Useful

Energy' edited by E. Dahlquist (2013) describes recent work by numerous contributors. On biomass gasification for syngas production, the reader may also refer to Huber et al. (2006), Alauddin et al. (2010), Göransson et al. (2011), and Kirkels and Verbong (2011). Bhavanam and Sastry (2011) have reviewed work on downdraft biomass gasification; Woolcock and Brown (2013) and Abdoulmoumine et al. (2015) have reviewed syngas cleaning methods.

A brief look at gasifier types: In the general scheme of modern gasifier design, laboratory scale experiments performed using slow heating rates are relevant to a limited range of moving-burden ('fixed-bed') type gasifiers. In these reactors, heating rates are usually slow during the pyrolysis step and char residence times in the reaction zone may be long, of the order of tens-of-minutes or longer. Currently operating fixed-bed gasifiers mostly date from the 1980s or earlier. Two arrays of forty gasifiers, each, were constructed in South Africa, in the early 1980s, to serve as the core of SASOL's 'Secunda' synthetic fuels and chemicals production plant. These reactors are SASOL-Lurgi Mark IV fixed-bed, 'dry-bottom' gasifiers, processing over 35 million tons of coal per year. A further fourteen Mark IV gasifiers are operated by the Dakota Gasification Company (USA) for power generation and a clutch of similar gasifiers have been constructed over the past decade at several locations in China (Inner Mongolia, Shanxi and Henan provinces). They are being used as component parts of large scale tests. Finally, an array of twenty-six 'Lurgi type' moving-burden gasifiers have been operating at the world's largest coal fired IGCC power plant in Vresova, Czech Republic (Higman, 2008). However, many of the more recently constructed gasifiers are based on fluidised-bed and, more frequently, higher temperature, short residence-time 'entrained-flow' configurations (NETL, 2010).

An air blown pilot scale spouted bed gasifier operating at 900–950°C was developed and tested by British Coal (Dawes et al., 1993, 1995). A similar spouted-fluidised-bed design (Higginbotham and Motter, 1994) was used in the Piñon Pine Power Project (1998) near Reno, Nevada (USA). In these two gasifiers, residence times for a large fraction of the solid fuel particles were of the order of seconds. However, residual bed solids from both pilot reactors contained some very unreactive chars, probably originating in initially larger diameter particles, which had hardened (annealed) before they could be consumed by gasification (Megaritis et al., 1998b). Fluidised bed gasifiers must be operated below the softening point of fuel-derived mineral matter, to avoid particle agglomeration which may cause loss of fluidisation. This consideration restricts operation to temperatures below the 950–1100°C range for coals and 750–900°C for biomass. Initially developed to process Rheinbraun lignite, the RWE High Temperature Winkler (HTW) gasifier has also been used to gasify municipal solid waste (Adlhoch et al., 2000), operating at 25–30 bar pressure, between 800°C and 900°C, to remain below the ash softening temperature (Radtke, 2011). Meanwhile, the 'U-Gas' gasifier, initially developed by the Institute of Gas Technology (IGT) in Chicago, tolerates particle agglomeration and provides for larger particle removal. The design aims to process a variety of fuels ranging from coals to diverse biomass materials (Synthesis Energy Systems, 2011).

In entrained flow reactors, oxygen blowing replaces air blasts and the fuel is quickly consumed at higher temperatures, between 1400°C and 2000°C under

pressures up to 30 bars. Heating rates in these reactors are high and residence times relatively short at these high temperatures, well above that of ash melting. Provision is made for molten ash removal, usually by allowing the melt to flow down the walls. The slurry-fed downdraft General Electric (formerly Texaco) and dry-feed updraft Shell gasifiers are some of the better known types of entrained flow gasifiers. The NETL Website (NETL, 2015) provides detailed descriptions of these and other well-known commercial entrained flow gasifier types, such as E-Gas, Siemens, PRENFLO as well as some new designs coming out of China and Japan.

Fuel characterization for gasification at high-pressure: There is ample evidence in the literature showing that chars from the same coal or biomass sample can present different reactivities, depending on the way in which the initial pyrolysis step has been carried out (Sha et al., 1990; Ginter et al., 1993; Muhlen et al., 1986; Silveston, 1991; Alvarez et al., 1994; also see below). The relative ordering of reactivities within particular sets of coal or biomass samples may also be affected by the manner in which the pyrolytic step is carried out (Cai et al., 1998; Peralta et al, 2005; Wang et al. 2005). Care is required, therefore, in generating or evaluating data on samples relevant to gasification reactor design and process simulation. Experiments must be designed to distinguish between fuel related and reactor related effects during the pyrolytic step. Moreover, sequences of experiments must be designed to couple the pyrolytic and gasification steps and treat them (as much as possible) as an integral process. This requirement arises from observing that splitting the gasification process into separate pyrolysis and gasification stages may cause measurable changes in fuel reactivities. Experiments must be able to mimic conditions of the actual processing environment, such as flow conditions and residence times; it is necessary to look out for heat and mass transfer resistances.

The acquisition of realistic bench-scale conversion and reactivity data thus requires fuel particles to undergo sequences of conditions akin to those of the processes they aim to simulate. The wider use of fluidised and entrained flow gasifier designs requires that fuel characterization tests be carried out at matching high heating rates and high temperatures. These requirements have effectively changed the face of solid fuel characterization work relating to pyrolysis and gasification.

We note, finally, that for reactors operating at the highest temperatures, fuel reactivity ceases to be a significant factor, since all fuel is completely consumed, and problems relating to ash behaviour, ash-melt viscosity, corrosivity and ash removal, become the major focus of attention for design and operation.

4.1.1 Characterising the gasification behaviour of solid fuels: how to get it wrong?

Before entering into the main body of this chapter, it seems useful to discuss some likely sources of error in procedures commonly used for determining gasification reactivities of solid fuels.

'Two-step-two reactor' methods for determining gasification reactivities: Numerous coal gasification studies have made use of a preliminary pyrolysis step, in order to prepare char samples that would be tested in a subsequent gasification experiment

(e.g., Goring, et al., 1952; Sha et al., 1990; Guo and Zhang, 1986; Haga and Nishiyama, 1988; Nozaki et al., 1991; Ginter et al., 1993; Meijer et al., 1994; Yang and Watkinson, 1994). As already signalled, however, extreme caution is required in cases where samples for laboratory reactivity tests are prepared using procedures that do not reflect the conditions of the actual process.

In one particular case, the aim was to generate background data for an air/steam blown spouted/fluidised-bed gasifier, operating at 13 bars. To prepare char samples for gasification reactivity tests, a laboratory scale atmospheric pressure fluidised-bed reactor was filled with coal particles and the reactor and its charge heated from ambient temperature, i.e., quite slowly. The gasification reactivities of the chars prepared in this fashion were then determined in a high-pressure thermogravimetric (TG) balance. In this example, neither the heating rates of the two reaction steps, nor the dynamics of fluid flow in the vicinity of the sample particles during the gasification step (in the pressurized TG balance) were compatible with the actual process. The ill-defined time-temperature history of the char particles from the pyrolysis step could not be related to those from the actual process, and the data from the pressurised TG balance showed clear evidence of diffusion control rather than chemical reaction control. The resulting data were difficult to interpret.

In other instances, coal samples have been pyrolysed in slow heating furnaces or TG balances. In numerous applications (as in the case cited above), the gasification step following char preparation has involved reactivity measurements in TG balances or differential thermal analysers (DSC), instruments capable of heating, at most, at some hundreds of degrees per minute (Goring, et al., 1952; Sha et al., 1990; Muhlen, et al., 1985; Hurt et al., 1991; Shufen and Ruizheng, 1994; Bota and Abotsi, 1994). In testing for gasification reactivity, tracking effects involving gas diffusion to and from particle surfaces is essential. Where the speed of chemical reactions overtake the speed of diffusional processes (e.g., at high temperatures), the slower rates of mass transfer processes tend to limit the overall reaction rate; at that point mass transfer becomes the rate limiting factor. More generally, it is difficult to interpret reactivity data, unless care is taken to distinguish between kinetics and diffusion related effects (Jess and Andresen, 2010).

Looking for errors: In Chapter 3, Pyrolysis of solid fuels: experimental design and applications, we discussed the effect of reaction conditions, and the role of sample and reactor configuration, on pyrolysis product distributions. We will see below that similar care is necessary in designing gasification experiments.

Experiments reported by Lim et al. (1997) have attempted to examine the effects of gasification reactor design on product distributions. These researchers compared the pyrolysis and CO_2-gasification behaviour of Daw Mill (UK) coal in a wire-mesh and a fixed-bed 'hot-rod' reactor. The experiments were conducted at temperatures between 850°C and 1000°C and pressures up to 30 bars. The reactivities of chars prepared by pyrolysis in helium in the 'hot-rod' (fixed-bed) reactor were found to be systematically and substantially lower than those prepared in the wire-mesh reactor. Clearly, the particular details of the char preparation procedure have a significant effect on char reactivity, which raises questions about the rich variety of char preparation methods reported in the literature. Working with a wire-mesh reactor, a 'hot-rod'

(fixed-bed) reactor and a high-pressure fluidised-bed reactor, Megaritis et al. (1998b) also observed that care must be taken in interpreting reactivity data from 'two-reactor, two-step' procedures. These experiments will be described in Section 4.5.2.

Mass transfer resistances during gasification in TG-balances: The magnitude of gas–solid mass transfer limitations during the gasification step in TG balances may be easily estimated by plotting the relationship between the rate constant (or conversion) and the temperature. As a quick check, mass transfer related effects may be deemed to be affecting measured reaction rates when the straight line ((ln k) vs (1/T), or ln(conversion) vs (1/T)) bends with increasing temperature (e.g., see Kandiyoti, 2009). The disparity in the speeds of mass transfer and intrinsic chemical reaction widens with rising temperature, since mass transfer coefficients increase quasi-linearly with temperature, while reaction rate constants increase exponentially. During CO_2-gasification in a TG balance, calculations have shown that reactant gas diffusion to solid fuel surfaces at temperatures above about 850–900°C was slower than the rate of intrinsic chemical reaction. In other words, in the absence of induced turbulence, mass transfer resistances in TG balances tend to slow down the overall (i.e., apparent) rate of gasification reactions, because reactant gases cannot reach solid fuel surfaces at the speed of the chemical reaction.

As the overall gasification is slowed down by mass transfer effects, the resulting longer residence times at the higher temperatures – required for completing the gasification process, tend to allow the stabilisation of the solid substrate before it can be completely gasified. In effect, the reactivity of the sample decreases as a function of time of exposure at temperature, probably due to some form of annealing. For coal chars, the effect is measurable above 850–900°C (see Section 4.2).

Depending on reactor design, therefore, mass transfer resistances may affect both reaction rates and, indirectly, overall conversions of chars during gasification. Jess and Andresen (2010) have provided a readable treatment of the role of mass transfer resistances in the analyses of combustion and gasification reactivities of 'coke' in TG balances. Inexplicably, the effect of mass transfer resistances on results from gasification experiments performed in pressurised TG balances appears to be near-universally ignored, leading to erroneous calculations of reaction rates and reaction rate constants.

4.2 Rates of char deactivation and implications for reactor design

To the extent that gasifier reactor modelling and design relies on the observed kinetics of gasification, there has been a temptation in the literature to treat chars as if they were well-defined, identifiable compounds – with constant reaction rates at constant temperature – i.e., constant pre-exponential constants and energies of activation. We will next review experiments, which show that rapidly heated char particles lose nearly two-thirds of their combustion reactivity during the first 10 s of exposure at a constant temperature of 1000°C.

4.2.1 Defining a 'relative char combustion reactivity'

Most laboratories find it convenient to use a single standard test to establish relative orders of reactivity between different samples. In general, the combustion reactivity of a fuel depends on the actual combustion conditions, including the hydrodynamics of the process as well as the properties of the fuel. In the work described further, a far simpler 'relative combustion reactivity' test has been adopted.

The measurement is based on the work of Jenkins et al. (1973) and involves the combustion of less than 2 mg of powdered char in a TG balance. A stream of nitrogen (~40 mL min^{-1}) is passed through the instrument during heat up at 25–50°C min^{-1} to 500°C. About 5 min are allowed at this temperature for thermal equilibration. The 'isothermal' combustion of the char is then initiated by switching from pure N_2 to air, flowing at the same rate. The 'relative char combustion reactivity' is calculated from the maximum weight loss rate during the combustion of the sample:

$$R_{max} = -(1/W_0)[dW(t)/dt]_{max}$$

In this equation, t is defined as the time, W_0 the initial and W(t) the time dependent char weight.

In this determination, the (low) experimental temperature of 500°C was selected to ensure that the combustion process is slow and the overall rate of combustion is controlled by the chemical reaction, free of interference from external mass transfer limitations. At this low temperature, effects due to pore diffusion limitations and pore surface accessibility are also expected to be minimised. Clearly, combustion rates are still directly related to the porosity, expressed in terms of total surface area. Indeed, the latter is a key parameter in determining the 'relative combustion reactivities'. To minimise extra-particle diffusion-related effects, sample (pile) sizes need to be limited to around 1.5 mg. The orders of reactivity between chars established using this combustion test were found to be similar to trends found in analogous CO_2 gasification reactivity tests at 950°C (Cai, 1995).

4.2.2 Char deactivation: experiments in the high-pressure wire-mesh reactor

The effect of heating rate and hold time at 1000°C during pyrolysis, on the relative combustion reactivities of Daw Mill (UK) coal chars was investigated, during a set of experiments in atmospheric pressure helium.

Fig. 4.1 presents char reactivity data for samples heated at rates between 1°C s^{-1} and 10,000°C s^{-1} to 1000°C, with 0, 10 and 60 s holding at the peak temperature. The relative combustion reactivities of chars from the series of '0-s holding' runs were observed to increased nearly linearly with increasing heating rate. Pyrolysis at the higher heating rates tend to produce more porous chars, which present greater surface areas to diffused oxygen molecules during the combustion test. On the other hand, Fig. 4.1 shows that when held at 1000°C for a period as short as 10 s, the reactivity of the most rapidly heated chars (10,000°C s^{-1}) dropped to less than a third of the

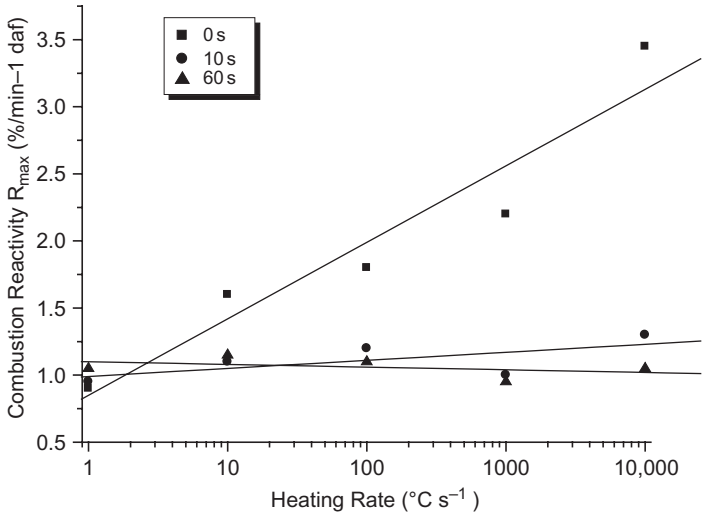

Figure 4.1 Relative char combustion reactivities of chars prepared in atmospheric pressure helium, in a wire-mesh reactor. Daw Mill (UK) coal. The initial pyrolysis experiments were conducted at heating rates between 1°C s^{-1} and 10,000°C s^{-1} to 1000°C, with holding at peak temperature for 0, 10 and 60 s. Rapidly heated chars lose over two-thirds of their reactivity after 10 s at 1000°C.
Source: Reprinted from Zhuo, Y., Messenböck, R., Collot, A.-G., Paterson, N., Dugwell D.R., Kandiyoti, R., 2000a. Fuel 79, 793. Copyright 2000, with permission from Elsevier.

original value. The effect was reproducible and appears to indicate that deactivation has taken place, probably by some form of annealing at the higher temperatures.

These data also indicated that slow heating to 1000°C, even with 0-s holding at peak temperature, causes the chars to deactivate during heatup. In these cases, the holding time has relatively little effect, as most of the deactivation appears to take place during heatup. When heated at 10°C s^{-1}, a sample would spend 10 s between 900°C and 1000°C, which appears sufficient for significantly reducing the reactivity of char.

These results imply that reactivity data obtained using slow-heating TG balances are of questionable value, if results are to be interpreted in relation to gasification in fluidised or entrained bed reactors. The data in Fig. 4.1 also showed that, at temperatures near 1000°C, char reactivity is a function of 'time-at-temperature'. This finding raises direct questions regarding the reliability of kinetic modelling schemes purporting to simulate the gasification or combustion of rapidly heated chars. The present authors have not come across coal or biomass gasification-related kinetic schemes which account for *changes in the values of kinetic constants as a function of time*.

Fig. 4.1 also provides clues for explaining why chars withdrawn from the British Coal air-blown gasifier were found to be so very unreactive. The particle size distribution of the feed coal to this reactor was classed as 'less than 3 mm' and the operating temperature range was mostly between 930°C and 970°C. Parallel experiments have

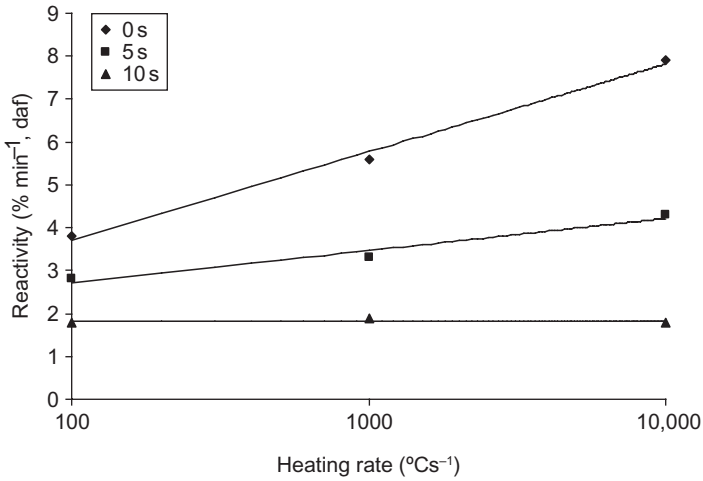

Figure 4.2 Relative char combustion reactivities of chars prepared in 3.5 bar CO_2 in a wire-mesh reactor. Daw Mill (UK) coal with 125–150 mm sized particles. The initial pyrolysis experiments were conducted at heating rates between 100°C s^{-1} and 10,000°C s^{-1} to 1000°C, with holding at peak temperature for 0, 5 and 10 s. Rapidly heated chars lost over two-thirds of their reactivity after 10 s at 1000°C.
Source: D. Peralta; unpublished work. Imperial College (2003).

been conducted in a laboratory-scale high-pressure fluidised-bed reactor at 1000°C (described below), where conversions of the 106–152 µm size particles have been compared with conversions of 600–800 µm particles. The difference in conversion for a reaction time of 60 s was ~14%: about 72% for the smaller particles versus 58% for the larger particles. Clearly, larger particles need more time to achieve total conversion – during which time the carbonaceous material rapidly loses reactivity at these relatively high temperatures. Some of the chars recovered from the British Coal ABGC reactor were thought to have spent more than an hour inside the reactor. Their relative reactivities were found to have very low numerical values, between 0.25 and 0.5 on the scale shown in Fig. 4.1 (Zhuo et al., 2000a).

In the meantime, it seemed useful to ascertain whether the observed effect could be duplicated under matching (but not identical) experimental conditions. A different operator, using a different batch of Daw Mill coal undertook similar experiments in the high-pressure wire-mesh reactor described in the next section. The procedure of Fig. 4.1 was repeated at 3.5 bars in an atmosphere of CO_2. In this second set of runs, the heating rate interval was restricted to between 100°C s^{-1} and 10,000°C s^{-1}, in order to save operator time. Unlike the diagram in Fig. 4.1, therefore, Fig. 4.2 does not show the convergence of the reactivity lines at the low heating-rate end. However, the data were qualitatively similar to those of Fig. 4.1. After heating at the highest available rate (10,000°C s^{-1}) to 1000°C, the relative combustion reactivity was observed to drop to a quarter of its value, during 10 s holding at 1000°C; the drop in reactivity was comparable to the drop observed in Fig. 4.1.

The data presented earlier show that there is no justification for assuming the reactivities of gasifying coals remain constant at temperatures relevant to gasification. The kinetics of char deactivation as a function of time-at-temperature thus plays a role in determining gasification rates. Nevertheless, the rapidly diminishing reactivity of chars as a function of time-at-temperature is a near-universally neglected aspect of mathematical models for gasification kinetics. The only saving grace seems to be the lack of interest in this parameter, for designing high temperature entrained-bed coal gasifiers.

4.2.3 Char deactivation: experiments in a High-pressure spouted-fluidised-bed reactor

The data presented in Fig. 4.1 were generated by pyrolyzing coal particles in a wire-mesh reactor under a variety of experimental conditions, and then determining the 'relative combustion reactivities' of chars from these experiments by using a TG balance–based method outlined in Section 4.2.1. The results of this work were used for explaining the low reactivities of chars withdrawn from an air-blown spouted-fluidised bed pilot reactor, operating at 13 bars and temperatures above 900°C.

Verification of the trends indicated by the data in Fig. 4.1 was sought by designing a new experiment for exploring the aging behaviour of chars in a laboratory scale high-pressure spouted-fluidised-bed reactor (Cousins, 2005; Cousins et al., 2006a,b). The design of the bench-scale, spouted-fluidised bed reactor was similar to the reactor shown in Fig. 4.24 and the experiments were carried out under controlled temperature, pressure, particle size and residence time ranges and several different gaseous environments. The experiments were designed for making and recovering chars, within the operating window of air-blown, spouted-fluidised bed gasifiers and required the development of novel feeding and draining mechanisms. The experiments consisted of pre-heating the reactor and the 'bed material' (acid-washed sand) to the experimental temperature before rapidly injecting a known amount of coal particles (as a 'single slug') into the bed. The sample was kept fluidised in the bed at the experimental temperature for a fixed period of time. At the end of the pre-determined time, all bed materials were rapidly discharged from the reactor and cooled. Coal chars were recovered from the mixture of solids, for characterization and reactivity determinations. Changes in char reactivity with changing reaction conditions were determined using the isothermal TGA method described above (Section 4.2.1); the changes in char structure and morphology were examined by X-ray diffraction and scanning electron microscopy.

The extent of char deactivation was measured for residence times between 2 and 3600 s in the fluidised-bed reactor. As in the case of the wire-mesh reactor based work described earlier, the data showed that the char reactivity declined rapidly when samples were held at the higher experimental temperatures. Temperature, pressure and particle size were all observed to enhance the char aging process. All three parameters tended to affect char reactivity adversely. Over the time scales studied, structural reorganisation tending towards graphitisation was indicated by X-ray diffraction. The low

reactivities of the largest particles formed over the longest times in the fluidised-bed were observed to approach the (lack of) reactivity of the nearly inert particles withdrawn from the pilot-scale, spouted-fluidised bed gasifier. Taken together, the results from the bench scale study were able to explain and confirm mechanisms underlying the low reactivity of chars withdrawn from the pilot-scale spouted-fluidised bed reactor. A more detailed description of the equipment and of the experimental results may be found in the original publications (Cousins, 2005; Cousins et al., 2006a,b).

4.3 Designing a high-pressure wire-mesh reactor

In the decade of high oil prices following the war of 1973 in the Middle East, *hydropyrolysis* emerged as one of the widely investigated coal processing routes. The aim was to react pure hydrogen with coal, to produce primarily methane and some hydropyrolysis tars. It was thought at the time that process economics could be made to 'work' if some credit could be claimed for the tar product, as a source of synthetic fuels and chemicals (Hodrian, 1988).

With the benefit of hindsight and given the cost of hydrogen, it is not clear how this scheme was ever thought to have economic potential. Nevertheless, up to the mid-to-late 1980s, it was actively investigated in North America, in nearly all coal producing European countries, and in Japan. In the UK, British Gas took this work to pilot-plant level in collaboration with a consortium that included several Japanese companies, led by Osaka Gas. At the time, the Japanese gas industry was looking for alternatives to importing LNG, to which they later massively committed themselves. A 2-ton day^{-1}, pilot entrained-flow reactor at Solihull (UK) was followed by a 50-ton day^{-1} facility in Osaka. The Japanese government, having initially pledged some $125 million for this development, eventually abandoned the project early in the new century. At the technical level, however, hydropyrolysis was one of the more successful applications of the wire-mesh reactor configuration.

By the mid-1980s, a handful of major studies of hydropyrolysis had been completed using high-pressure wire-mesh reactors. The initial reactors constructed by Howard and coworkers (Suuberg et al.,1980) operated at heating rates above 200°C s^{-1} and relied for tar yield determinations on deposition onto reactor linings and in the gas filters. At Bergbau Forschung (later Deutsche Montan Technologie – DMT), van Heek and coworkers similarly worked at rates above 200°C s^{-1} and relied on tar deposition on walls and a calculation involving butane concentrations in the product gas to back-calculate the total amount of primary tar released by the sample (Arendt and van Heek, 1981). Data from the work by Stangeby and Sears (1981a,b) suggested that sweeping the wire-mesh with a stream of gas flowing parallel to its plane, tended to give rise to partial tar cracking, particularly at higher heating rates. The work at Princeton University also relied on a design where a stream of gas swept parallel to the surface of the mesh; tar yield determinations at hydrogen pressures up to 25 bars were carried out (Niksa et al., 1982a,b, 1984; Bautista et al.,1986).

4.3.1 A gas-sweep facility for tar capture in the high-pressure wire-mesh reactor

We have seen in Chapter 3, Pyrolysis of solid fuels: experimental design and applications, how the design of the Imperial College wire-mesh reactor evolved along several parallel lines. First, novel (for its time) instrumentation allowed operation at heating rates as low as 0.1°C s^{-1}, giving access to a wider range of heating rates than had hitherto been available. At the time, the data acquisition and control instrumentation required for producing smooth time-temperature ramps at slow heating rates had to be *made in-house*. The system allowed direct observation of the effect of heating rate on product distributions, during coal pyrolysis and hydropyrolysis (Gibbins-Matham and Kandiyoti, 1988; Gibbins and Kandiyoti, 1989a, 1989b; Gibbins-Matham et al., 1989). Circulating water was used to cool the electrodes, particularly necessary during slow heating experiments. The higher end of the heating rates was eventually extended to 10,000°C s^{-1}. In Chapter 3, Pyrolysis of solid fuels: experimental design and applications, we also described how a stream of gas was passed (upwards) through the wire-mesh sample holder, to sweep evolving volatiles away from the heated zone. Evolving tar vapours were directed into a cold-trap for quantitative capture and recovery.

Initially, the wire-mesh configuration used for atmospheric pressure work did not work well at high pressure. The first few commissioning runs quickly showed that the gas sweep through the mesh gave rise to severe lateral as well as temporal (local, time-dependent) *temperature* oscillations, when operating above pressures of 10 bars (Gibbins and Kandiyoti, 1989b). The lateral oscillations were picked up by the two thermocouples placed on the mesh, about 1-cm apart. The magnitudes of these oscillations could be as large as ±150–200°C, sufficient to invalidate results from any experiment. The explanation proved intriguing.

When operating at or near atmospheric pressure, flow distortions caused by the presence of the wire-mesh and the sample particles held within it do not give rise to detectable adverse consequences. At higher pressures, however, gas densities, gas-heat capacities per unit volume, and gas-solid heat transfer coefficients, all take on significantly higher values. As a result, the gas sweeping upwards through the wire-mesh removes far more heat at high pressure, compared to atmospheric pressure operation. It is thought that local variations in gas velocities due to minor turbulence, induced by the presence of the wire-mesh and the sample particles, combine with the greater rates of heat transfer which take place under higher pressures, to give rise to the observed temperature variations. The effect is amplified at increasing pressures.

The initial solution adopted to this problem was to pass a less directed ‘diffuse flow’ through the cell and through and around the mesh. The quartz bell meant to collect tar was also removed. The resulting high-pressure wire-mesh reactor was still able to operate at the pressures required for simulating the hydropyrolysis of coal and to determine total volatile yields, to within several percent accuracy (Gibbins, 1988). However, in the absence of a gas stream directing tar vapours into the traps, tar yields could not be measured reliably.

Eventually, the problem was solved by smoothing the flow of gas passing through the mesh (Güell, 1993; Güell and Kandiyoti, 1993). The Reynolds number for

hydrogen flowing through the 3 cm aperture in the brass plate underneath the mesh was calculated to be about 15 at atmospheric pressure, 950 for operation at 70 bars, and 6850 at 150 bars. At first glance, therefore, the onset of turbulence would have been expected at pressures above 70 bars. However, flow through the wire mesh laden with dispersed sample particles appeared to disrupt streamlines, introducing imbalances in the flow crossing the sample-holding part of the mesh.

It was decided therefore to pass the sweep gas stream through a *vertical* bank of 3 mm-diameter tubes placed below the mesh, to reduce the characteristic flow diameter by a factor of 10. For hydrogen, calculations performed assuming an average gas velocity of 0.15 m s^{-1}, a flow diameter of 3 mm (of individual tubes within the bank of tubes) and a temperature of 357°C, show Reynolds number values increasing from about 1.5 at atmospheric pressure to about 95 at 70 bars and to about 700 at 150 bars. The bank of tubes thus both reduced the Reynolds number and partly suppressed lateral velocity components, helping to even out heat transfer from the wire-mesh to the flowing stream of carrier-gas. These modifications eliminated the temperature fluctuations that had been observed and allowed passing a stream of gas through the sample-holding mesh, similar to atmospheric-pressure operation. It also allowed operation of the tar traps as originally intended, at pressures up to 160 bars (Güell, 1993; Güell and Kandiyoti, 1993).

Fig. 4.3A presents a schematic diagram of the high-pressure reactor, with the flow-smoothing section (bank of 3 mm tubes; Item 14) placed underneath the mesh. The significant difference between this design and the base plate in Fig. 3.1 was the positioning of the gas inlet beneath the mesh. The incoming flow was evened out by passage through two quartz sinter discs (Item 6), the space between them serving as a settling chamber. The bank of tubes (Item 14) intended for smoothing the gas flow was later replaced by a 'flame-trap matrix', which consisted of a rolled up sheet of finely corrugated stainless steel. This arrangement produced conduits of less than 2 mm in diameter for the flow of carrier gas. These design modifications have allowed stabler equilibria to be established between the large energy inputs into the sample holding section of the wire-mesh (Item 16) and the large amounts of heat removed by the gas stream from that section of the mesh, during operation at elevated pressures. The amplitude of the temperature oscillations was much reduced compared to carrier gas flow in the absence of the bank of tubes, but could not be eliminated completely. Fig. 4.3B shows the level of temperature stability, to within ±30°C, that was achieved through the introduction of the bank of tubes, during a run under relatively severe conditions (80 bar H_2 at 850°C).

The tar trap assembly of the high-pressure wire-mesh reactor consisted of a 'quartz bell' (Item 2 in Fig. 4.3A), connected to a steel tube placed at the gas exit (Item 1 in Fig. 4.3A), packed with strips of wire mesh, to improve heat transfer and facilitate condensation. The extension of the tar trap above the pressure case was sealed to the case by tightening a gland nut and cooled externally by liquid nitrogen. Initial attempts to weigh the tar trap before and after the experiment were foiled due to the loss of small amounts of metal as nuts were tightened and loosened, when making and releasing the pressure seals. A procedure was then developed to wash the traps with a 4:1 v/v mixture of chloroform and methanol. The tar sample was recovered by evaporating the solvent (Güell and Kandiyoti, 1993).

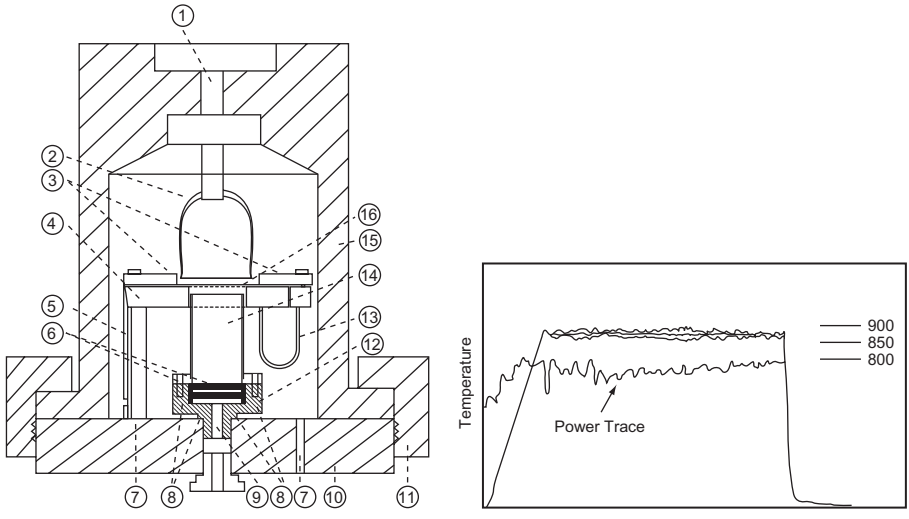

Figure 4.3 (A) The high-pressure wire-mesh reactor: (1) Gas exit; (2) Quartz bell; (3) Electrode clamps; (4) Mesh support plate; (5) Current supply; (6) Sinter disc; (7) Support plate stands, hollow to allow water flow; (8) Copper seals; (9) Gas inlet; (10) Base plate; (11) Throw over sealing ring; (12) Flow smoothing cell; (13) Spring, hollow to allow water flow; (14) Bank of tubes, later replaced by flame trap matrix; (15) Pressure bell; (16) Mesh. (B) Time temperature history from the high-pressure wire-mesh reactor. Pressure 80 bars hydrogen. Heating at 1000°C s^{-1} to 850°C with 10 s holding.
Source: Reproduced with permission: Messenböck, R.C., Dugwell, D.R., Kandiyoti, R., 1999a. Energy Fuels 13, 122. Copyright 1999 Am.Chem.Soc.

4.3.2 High-pressure pyrolysis and hydropyrolysis of coals – general trends

Figs. 4.4A,B show the variation of tar and total volatile yields from Linby (UK) and Pittsburgh No. 8 (US) coals in He and H_2, as a function of pressure. Samples were heated at 1000°C s^{-1} to 700°C with 10 s holding. The Pittsburgh No. 8 coal sample was drawn from the Argonne Premium Coal Sample set (Vorres, 1990).

As expected from trends observed in previous work at high-heating rates (Howard, 1981; Arendt and van Heek, 1981; Niksa et al., 1982a,b; Li et al., 1991), tar and total volatile yields diminished rapidly between 1 and 10 bars, in hydrogen as well as in helium. The effect was first observed and discussed by Howard and coworkers (Howard, 1981). The decline appears to be related to higher ambient pressures physically suppressing the evolution of volatiles from coal particles.

To examine the behaviour of coals more widely at these relatively 'low' high-pressures, the behaviour of eight coals was examined at atmospheric pressure and at 2.5 bars (Table 4.1). All except one of the samples showed behaviour similar to that in Fig. 4.4, with tar yields declining more sharply than the corresponding total

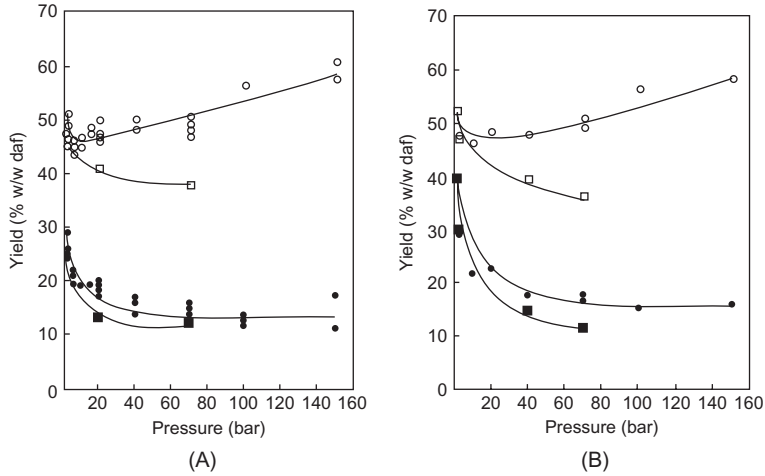

Figure 4.4 (A) Effect of pressure on pyrolysis and hydropyrolysis yields from Linby coal; heating at 1000°C s^{-1} to 700°C, with 10 s holding time: (○) Total volatiles under H_2, (□) Total volatiles under He; (●) Tar yield under H_2, (■) Tar yield under He. (B) Effect of pressure on pyrolysis and hydropyrolysis yields from Pittsburgh No. 8 coal; heating at 1000°C s^{-1} to 700°C, with 10 s holding time: (○) Total volatiles under H_2, (□) Total volatiles under He; (●) Tar yields under H_2, (■) Tar yields under He.
Source: Reprinted with permission from Güell, A.J., Cai, H.-Y., Dugwell, D.R., Kandiyoti, R., 1993. Energy Fuels 7, 943. Copyright 1993 American Chemical Society.

Table 4.1 The effect of a pressure increase from 1 to 2.5 bars on pyrolysis yields in helium (% wt/wt, dry ash free basis). Samples were heated at 1000°C s^{-1} with 10 seconds holding at 700°C

Coal	Elemental carbon	Atmospheric pressure	2.5 bar		
		Total volatiles	Tar	Total volatiles	Tar
Tilmanstone[a]	91.4	20.6	14.0	23.7	11.9
Taff Merthyr[a]	90.0	12.8	10.1	9.1	5.4
Thoresby[a]	84.0	46.8	33.6	42.6	27.0
Hem Heath[a]	83.9	44.6	33.4	42.2	27.4
Pittsburgh No. 8[a]	83.2	50.4	35.2	47.7	28.9
Longannet[a]	82.7	43.4	25.8	43.1	19.1
Linby	81.5	47.4	28.9	45.1	24.4
Gedling[a]	81.3	46.2	29.9	46.2	21.0

Source: Reprinted with permission from Güell, A.J., Cai, H.-Y., Dugwell, D.R., Kandiyoti, R., 1993. Fuel Process. Technol. 36, 259. Copyright 1993 American Chemical Society.
[a]Atmospheric pressure values obtained with 30 s holding.

Table 4.2 Effect of holding time and hydrogen pressure on pyrolysis yields (% w/w daf) from Linby coal heated at 1000°C s^{-1} to 700°C

Pressure (bar)	Holding time (s)	Total volatiles	Tar
2.5	0	30.6	20.3
2.5	1	40.0	27.1
2.5	10	41.9	26.4
70	0	23.2	9.9
70	1	41.0	17.4
70	10	50.3	16.6

Source: Reprinted with permission from Güell, A.J., Cai, H.-Y., Dugwell, D.R., Kandiyoti, R., 1993. Energy Fuels 7, 943. Copyright 1993 American Chemical Society.

volatiles. The only non-softening coal in the present set (Tilmanstone, UK; 91% carbon) showed a small increase in total volatiles alongside the drop in tar yield observed with the other coals. Repeated experiments have confirmed this result. In general, plastic behaviour during pyrolysis is enhanced by increases in experimental pressure. However, under these reaction conditions, Tilmanstone was not observed to soften or melt significantly during pyrolysis (1–2.5 bar; 1000°C s^{-1}). All other samples showed at least some particle softening during rapid heating (1000°C s^{-1}). It is likely that the high carbon-content Tilmanstone coal particles retained their original pore structures to a greater extent than the other coals; the exposure of more pore surface would then allow greater extents of direct hydrogasification to take place.

The data in Table 4.2 show the relationship between weight loss and holding time at 2.5 and 70 bars under hydrogen. They provide evidence of completion of the hydropyrolysis reactions, in the form of tar release, at residence times of the order of 1 s at 700°C. Meanwhile, the steady increase in total volatile yields shows the effect of hydrogasification reactions. Later on, we will use this information in selecting holding times for steam gasification experiments, which are normally carried out at higher temperatures and pressures of 25–30 bars, but where tar yield determinations are difficult.

Fig. 4.4A also shows that, between 20 and 150 bars, hydropyrolysis total volatile yields increased monotonically with pressure. Under these reaction conditions, intense methane formation had already been widely reported, indicating the progress of hydrogasification reactions well beyond the completion of *hydropyrolysis* related volatile release (Howard, 1981; Arendt, 1980; Arendt and van Heek, 1981). The minimum in the hydropyrolysis total volatiles curve was first discussed by Howard and coworkers at the Massachusetts Institute of Technology (Howard, 1981). This minimum appears at the cusp of two opposing trends, the one tending to suppress volatile release by the physical effect of high-pressure and the second, to enhance volatilisation by increasing hydrogasification rates at higher pressures. However, a monotonic rise in weight loss may be obtained (instead of a curve with a minimum) under two related conditions, namely, when the sample is sufficiently reactive and/or if the holding times are sufficiently long (Messenbock, 1998).

Despite important differences between tar yield determination procedures, the trends shown by the data in Fig. 4.4, covering high heating rates, were in broad qualitative agreement with earlier research cited above. Data from slow heating experiments, however, told a different story.

4.3.3 Hydropyrolysis at slow heating rates

Fig. 4.5 shows changes in tar and total volatile yields from Linby coal with increasing hydrogen or helium pressures during slow heating rate experiments (1°C s^{-1}) to 700°C with 10 s holding at peak temperature.

As expected, tar yields in *helium* tended to decrease at first, and to level off around 20 bars onwards, at values well below the atmospheric pressure tar yield. As already explained, this is thought to be due to the physical effect of external pressure. However, the effect of increasing hydrogen pressures produced a somewhat unexpected result. After the initial drop in yields between 1 and 5 bars, there was a small but experimentally significant upward trend in the tar yield with *increasing* hydrogen pressure, up to 70 bars. This result contrasts sharply with the trends observed in Fig. 4.4, showing results from two coals during *fast heating* (1000°C s^{-1}) hydropyrolysis experiments. The observed increase in tar yields in the presence of H_2 appears to show the effect of reactive interactions between hydrogen and the pyrolyzing mass during slow heating. In Fig. 4.5, the differences between tar yields in hydrogen and helium increased with pressure. This latter trend clearly contrasts with that observed at high heating rates and requires clarification. Meanwhile, the longer exposure

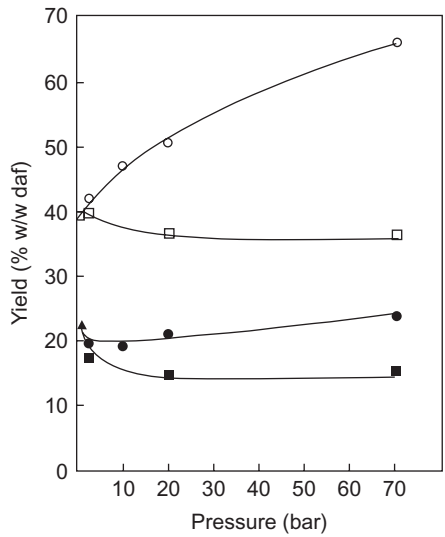

Figure 4.5 Effect of pressure on pyrolysis and hydropyrolysis yields from Linby coal heated at 1°C s^{-1} to 700°C, with 10 s holding at peak temperature. Total volatiles: (○) Hydrogen, (□) Helium. Tar: (●) Hydrogen; (■) Helium.
Source: Reprinted with permission from Güell, A.J., Cai, H.-Y., Dugwell, D.R., Kandiyoti, R., 1993. Energy Fuels 7, 943. Copyright 1993 American Chemical Society.

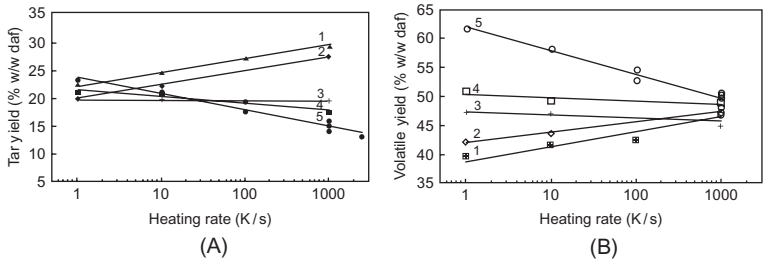

Figure 4.6 (A) Effect of heating rate and pressure on tar yields from Linby coal heated to 700°C with 10 s holding. (1) Atmospheric pressure helium; (2) 2.5 bar H_2; (3) 10 bar H_2; (4) 20 bars H_2; (5) 70 bar H_2. (B) Effect of heating rate and pressure on total volatiles from Linby coal heated to 700°C with 10 s holding. (1) Atmospheric pressure helium; (2) 2.5 bar H_2; (3) 10 bar H_2; (4) 20 bar H_2; (5) 70 bar H_2.
Source: Reprinted with permission from Güell, A.J., Cai, H.-Y., Dugwell, D.R., Kandiyoti, R., 1993. Energy Fuels 7, 943. Copyright 1993 American Chemical Society.

of char to hydrogen during these *slow* heating rate experiments gave total volatile yields that increased sharply compared to heating at 1000°C s^{-1} (also see Fig. 4.6B). As explained earlier, there was no minimum.

Probing differences between slow & fast heating under H_2-pressure: Fig. 4.6A shows the complex relationship that emerged between the effects of heating rate and pressure on tar yield. The data spanned heating rates between 1°C s^{-1} and 2500°C s^{-1} and pressures between 1 and 70 bars. At atmospheric pressure and 2.5 bars, tar yields were observed to increase with increasing heating rate. Based on findings outlined in Chapter 3, Pyrolysis of solid fuels: experimental design and applications, this was the expected trend. It could be repeated with nearly all vitrinitic coals and vitrinite concentrates that were experimented upon. However, at 10 bars, the tar yield appears to be, relatively insensitive to changes in heating rate over the 1–1000°C s^{-1} range, within experimental scatter. Above 10 bars, tar yields were found to decrease with increasing heating rate. To sum up, there was a reversal of the tar release trend with increasing heating rate at pressures above 10 bars.

Cross-reading the data, within the higher heating rate range, tar yields were found to drop rapidly with increasing pressure. This had already been observed in Fig. 4.4A,B. Similar findings for high heating-rates had already been reported in previous work by Howard and coworkers and Niksa and coworkers, cited earlier.

Continuing to cross-read the data, at heating rates below 10°C s^{-1} (1–10°C s^{-1}), tar yields were found to *increase* with pressure, after the initial drop between 1 and 5 bars. Overall, the reversal in the tar yield versus H_2-pressure trend is consistent with slow heating rates affording longer reaction times at temperatures relevant to tar release, allowing better contact between the pyrolyzing mass and the externally supplied hydrogen. As the heating rate is reduced, a larger proportion of tar precursors seems able to react with hydrogen and volatilise as tar.

By contrast, at low pressures, where the reactivity of hydrogen is not great, low heating rates would still lead to lower tar yields – as at atmospheric pressure. However, the volatile suppressing effect of high-pressure prevails across the heating

rate spectrum. The highest tar yields were still observed during high heating rate runs at atmospheric pressure or, indeed, at reduced pressures, as explained in Chapter 3, Pyrolysis of solid fuels: experimental design and applications.

Fig. 4.6B presents total volatiles yields determined during the same set of experiments. In the presence of hydrogen, sample weight loss has a component of volatile release due to hydropyrolysis and one due to hydrogasification. The two processes usually overlap to a certain extent, although tar release and char formation (hydropyrolysis) is generally viewed as preceding the char-hydrogen reaction stage (hydrogasification). These results show that total weight loss was greatest for the combination of high pressures and the long exposures encountered during the slow heating rate experiments. Similar trends were observed during analogous experiments with a sample of Pittsburgh No. 8 coal (Güell and Kandiyoti, 1993; not shown).

4.3.4 *Effect of coal thermoplastic behaviour on hydropyrolysis tar yields*

Table 4.3 presents product distributions from the hydropyrolysis of two Southern Hemisphere (Chilean) coals as a function of pressure and heating rate. During slow-heating hydropyrolysis experiments at the highest pressure attempted, both coals gave greater tar yields than from fast heating rate experiments (1000°C s^{-1}) at both atmospheric pressure and at 70 bars under hydrogen. Previous experience suggested

Table 4.3 Effect of heating rate and pressure on hydropyrolysis tar and total volatile yields of Pecket and Catamutum (Chile) coals. 10 s holding at 700°C. All results are given as % wt/wt, dry ash free basis (daf)

Heating rate (°C s^{-1})		Hydrogen pressure		
		2.5 bar	20 bar	70 bar
Pecket coal				
1000°C s^{-1}	Total volatiles	57.1	69.9	74.3
1000°C s^{-1}	Tar	15.5	11.1	11.1
1°C s^{-1}	Total volatiles	52.8	72.4	n.a.
1°C s^{-1}	Tar	11.3	14.5	24.1
Catamutum coal				
1000°C s^{-1}	Total volatiles	54.3	n.a.	n.a.
1000°C s^{-1}	Tar	20.4	n.a.	n.a.
1°C s^{-1}	Total volatiles	52.4	n.a.	83.3
1°C s^{-1}	Tar	9.7	n.a.	24.7

Source: Reprinted with permission from Güell, A.J., Cai, H.-Y., Dugwell, D.R., Kandiyoti, R., 1993. Energy Fuels 7, 943. Copyright 1993 American Chemical Society.

Table 4.4 Effect of heating rate and pressure on tar yields for coals showing different plastic behaviour. 10 s holding at 700°C. All results are given as % wt/wt, dry ash free basis (daf).

Coal	1°C s^{-1} 70 bar		1000°C s^{-1} 1 bar	1000°C s^{-1} 70 bar	
	H_2	He	He	H_2	He
Tilmanstone	14.1	7.9	14.0	9.1	6.1
Taff Merthyr	8.9	n.a.	10.1	4.8	n.a.
Pittsburgh No8	29.2	20.5	35.2	17.4	11.4
Longannet	20.4	11.8	25.8	15.1	10.6
Linby	23.1	15.0	29.5	15.7	12.2
Pecket	24.1	9.5	14.9	11.1	9.3
Catamutum	24.7	11.6	20.4	n.a.	13.8

Source: Reprinted with permission from Güell, A.J., Cai, H.-Y., Dugwell, D.R., Kandiyoti, R., 1993. Energy Fuels 7, 943. Copyright 1993 American Chemical Society.

that it would be reasonable to expect the highest tar yields for any coal to be observed at low pressures and high heating rates. The indications provided in experiments with the two Chilean coals did not fit the pattern.

There was one obvious difference between these two coals and the other samples examined in this study. The Chilean coals showed no tendency to melt either during rapid heating or under high-pressure hydrogen. Slow heating rates appeared to provide greater opportunity for contact between tar precursors released inside the coal mass and externally supplied hydrogen, within the more open matrix of these non-melting coals. They appear to offer greater surface area to ambient hydrogen and greater porosity for evolving volatiles.

A short investigation of the relationship between the plastic properties of coals and the proportions of tars and volatiles released under hydropyrolysis conditions at different heating rates was then carried out. Table 4.4 presents tars yields for seven coals under the following conditions: (1) 1°C s^{-1} and 70 bars (in helium and H_2), (2) 1000°C s^{-1} in atmospheric pressure helium, and, (3) 1000°C s^{-1} and 70 bars (in helium and H_2). Of these samples, Linby and Pittsburgh No. 8 coals showed the greatest degree of melting when heated under pressure. At all pressures, Longannet, Taff Merthyr, and Tilmanstone displayed little softening during heating at 1°C s^{-1}, but showed limited evidence of melting when heated at 1000°C s^{-1}. The two Southern Hemisphere (Chilean) coals showed no trace of plastic behaviour when heated at 1°C s^{-1} but limited deformation and agglomeration when heated at 1000°C s^{-1}.

Compared to the Northern Hemisphere samples used in this study, atmospheric pressure tar yields from both Pecket and Catamutum were small relative to their corresponding total volatile yields (53.4% and 54.3%, respectively). What makes these two coals atypical, however, is the higher tar yields from slow heating hydropyrolysis experiments, compared to fast heating (1000°C s^{-1}) atmospheric pressure runs. In

this respect they stand out among the other samples, with the possible exception of the high-rank Tilmanstone sample. The findings correlate with the absence of plastic behaviour of these samples upon heating.

There is however another method of evaluating these data, which somewhat anticipates the material presented in Chapter 6, Elements of thermal breakdown: heating rate effects and retrogressive reactions, where we present evidence showing that both the thermoplastic behaviour of coals upon heating and the tar yields (which generally correlate with thermoplastic behaviour) are linked with the availability of hydrogen native to the pyrolyzing material. When we examine the elemental compositions of the set of coals listed in Table 4.4, the two Chilean coals turn out to have the highest elemental oxygen contents: Tilmanstone (0.9%); Taff Merthyr (3.6%); Pittsburgh No. 8 (7.5%); Longannet (10.1%); Linby (9.4%); Pecket (13.0%) and Catamutum (14%) (Güell and Kandiyoti, 1993). It is likely that the high tar yields from the two Chilean coals during slow heating under 70 bar hydrogen pressure are, at least in part, related to the higher oxygen content of these coals being 'scavenged' by the presence of excess hydrogen during the long reaction times available due to the slow heating regime.

However limited the current level of industrial interest in hydropyrolysis-related processes per se, the methods outlined above have provided a platform for developing new wire-mesh reactor configurations suitable for testing the behaviour of coal samples during CO_2 and steam-gasification. We will next describe a high-pressure wire-mesh reactor equipped with a steam injection facility.

4.3.5 Injection of CO_2 and steam into the high-pressure wire-mesh reactor

In the 1970s and early 1980s, most of the research groups that attempted to develop high-pressure wire-mesh reactors were interested in investigating aspects of hydropyrolysis and hydrogasification. Reactor design focused on work with non-condensing gases. They could all operate with hydrogen just as easily as with helium. However, both CO_2 and steam react with the AISI 304 stainless steel mesh used in pyrolysis and hydropyrolysis experiments. A more resistant mesh material was required and molybdenum was selected as the material that was available and reasonably inert under these reaction conditions.

Moreover, CO_2 and steam have higher densities and heat capacities than either hydrogen or helium. They remove more energy from the mesh during experiments and require greater power inputs into the mesh to attain a particular temperature. CO_2 and steam also have lower thermal conductivities, which makes operation more difficult. During experiments with CO_2, this combination of conditions led to overheating in the parts of the mesh not directly cooled by the sweep gas stream. The layer of mica providing electrical insulation between the mesh and the support plate (between Items 4 and 16 in Fig. 4.3) frequently melted, causing short circuits and destroying the sample holder. Whilst CO_2 gasification experiments at 1000°C could still be undertaken below 30 bars and holding times shorter than 10 s (Lim et al., 1997), design changes were required to ensure reliable operation over a wider range of parameters.

The cooling water circulation pattern in the base plate was changed in order to suppress local overheating in parts of the wire mesh not swept by the gas stream, particularly the parts furthest away from the water-cooled electrodes. The new water conduit traced a broadly circular pattern around the aperture in the brass support plate (Fig. 4.2 in Messenbock et al., 1999a,b). In addition, the mica insulation was replaced by a 2-mm thick sheet of ceramic (Macor Machinable Ceramics; Goodfellows, UK), drilled through to open a 30-mm hole mirroring the shape of the support plate. These changes have allowed reliable operation for holding times up to 60 s at pressures up to 30 bars in CO_2. However, the Macor ceramic plates were brittle and were replaced by alumina plates of the same thickness. Alumina tiles worked well and retained their integrity for very many runs.

Steam injection: The basic wire-mesh reactor design operated without complications when noncondensing gases were used. Steam injection inside the wire-mesh reactor vessel posed a new set of challenges, since, when operating with noncondensing gases, all components except the mesh itself were normally 'cold', at or near ambient temperature. For steam-injection to work, it was necessary to prevent condensation on cold surfaces and the possibility of dripping condensed water onto sample particles, the mesh or the electrodes. Prior to this effort, only DMT had attempted to introduce a limited amount of moisture into the system by heating the pressure casing to about 100°C.

In response to these constraints, the carrier-gas flow path of the reactor (Fig. 4.3A), including the mesh and the sample itself, were preheated with a flow of helium, to about 300°C, in order to prevent condensation. All components in the flow-path were redesigned to withstand the higher temperatures and ensure the passage of steam through the flow-smoothing section, the mesh and the quartz bell above the mesh. Teflon seals and other temperature-sensitive components were replaced with others made of copper. The plastic insulation of the thermocouple wires was replaced with drawn glass capillaries (Messenbock, et al., 1999a,b).

Fig. 4.7 presents a schematic diagram of the wire-mesh reactor system equipped with a steam injection unit. The design aimed to introduce the minimum amount of steam into the reaction chamber during a given run. Prior to starting an experiment, the whole of the steam flow-path was preheated by a stream of helium (8), itself heated by passage through a packed-bed heater (11). Meanwhile, carefully metered amounts of water were pumped (3) from the reservoir (1) through a filter (2) into the steam generator operated at about 300°C (4). The steam generator consisted of a 1-in. i.d. AISI 316 stainless steel tube, filled with 3–5 mm glass beads and heated with a resistance heater. Prior to initiating the experimental sequence involving steam-fuel contact, all the generated steam was discharged through the by-pass valve to a condenser (7). This arrangement ensured that a steady supply of steam was ready for diverting into the experimental chamber when the run was actually triggered.

Before initiating an experimental sequence, the reactor pressure was set by adjusting the pressure let down valve (16). At that stage, the flow path would have been preheated, but the temperature of the mesh itself did not normally exceed 150°C. This was due to cooling provided by water circulation through the electrodes and the support plate, which absorbed some of the heat input through the passage of the pre-heated helium. To compensate for this inevitable heat loss, the temperature of the

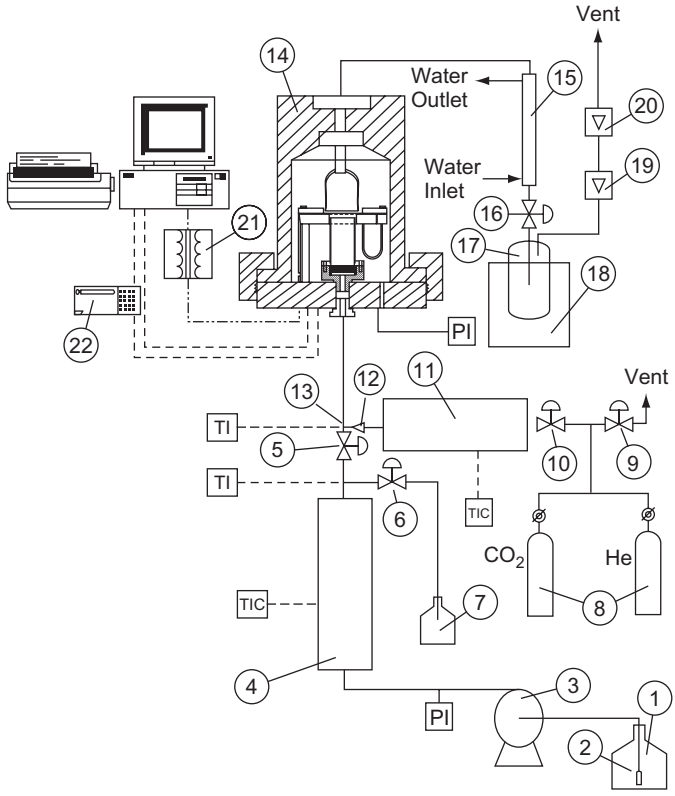

Figure 4.7 Simplified schematic diagram of the steam injection system. Steam is continuously produced and discarded through the by-pass. The steam flow-path is preheated to 300°C before electrical current and steam are simultaneously switched into the high-pressure cell. (1) Water reservoir; (2) Filter; (3) Displacement pump; (4) Steam heater; (5), (6) On/off valves; (7) Steam bypass collector; (8) Sweep gas; (9) Safety valve; (10) Flow control valve; (11) Gas heater; (12) Non-return valve; (13) Mixing point of steam and gas; (14) Wire-mesh reactor; (15) Counter current condenser; (16) Flow control valve; (17) Water collector; (18) Cold trap; (19, 20) Flow-metre; (21) Transformer; (22) Watchdog. (P) Pressure, (T) Temperature, (C) Controller, (I) Indicator. (-) Tubing, (--) Thermocouple lines, (-)Electric current lines. *Source*: Reprinted with permission from Messenbock, R.C., Dugwell, D.R., Kandiyoti, R., 1999a. Energy Fuels 13, 122. Copyright 1999 American Chemical Society.

mesh was boosted to 300°C, by passing a controlled current through the mesh, prior to initiating the experimental sequence.

The possibility that preheating to 300°C for short periods before a run would significantly alter sample behaviour was examined. A pyrolysis run was carried out using the same temperature sequence as a steam-gasification run (but with no steam). At 1 bar and 10- s holding time, the gas and tar yields as well as the combustion reactivity of the char residue were found to be similar to those from a pyrolysis experiment in which the temperature had been directly ramped from ambient temperature.

Steam was allowed to contact the coal sample only as the experiment was initiated. At 'zero-time', the operator switched steam into the cell whilst simultaneously triggering the electrical current to start the heat-up ramp. The temperature of the steam–helium mixture was independently monitored at the exit of the steam generator, where the two steams were mixed (13). The mixture temperature was found to vary between 260°C and 270°C, well above the condensation temperature (212.4°C) of steam at 20 bars, the maximum steam pressure used in this study.

An 80:20 (v/v) mixture of steam and helium was used in the steam gasification experiments and the mass flow rate of the gas was allowed to change with pressure, as the aim was to keep the gas velocity through the mesh constant. Samples were normally heated at 1000°C s^{-1} to 1000°C, with the hold time at peak temperature altered between 0 and 60 s and the pressure from 1 to 30 bars. Temperature stability during steam injection was found to be comparable to levels of stability observed during experiments with any of the non-condensable gases. At the exit of the reactor, the steam/gas mixture was cooled under pressure (15). The water was then collected in a cold trap (17) cooled by liquid nitrogen (18). The gas flow rate was measured by rotameters installed downstream of the condensers. Sample weight loss in steam gasification could be determined with a reproducibility similar to experiments in non-condensable gases of ±1%.

CO_2 and steam gasification of Daw Mill coal: Daw Mill (UK) coal was used as the base-case test sample. It softened only marginally even at high heating rates and had been selected as the standard test coal in gasification trials, including the British Coal Air Blown Gasification Cycle (ABGC) programme. Its elemental composition was (% w/w daf): C: 81.3; H: 4.8; N: 1.3; O: 11.5; S: 1.2; ash: 4.7.

Fig. 4.8A presents total volatile yields from CO_2-gasification experiments in the high-pressure wire-mesh reactor, as a function of pressure (1–30 bars), with 0, 10, 20 and 60 s holding at 1000°C. The conversions for 'zero holding' and data from pyrolysis were close, showing no more than an additional 1–4% conversion by gasification during heatup, above and beyond the weight loss recorded in corresponding pyrolysis experiments. For longer hold times (60 s), a sharp increase in weight loss was observed between 1 and 10 bars; conversions at 30 bars and 60 s holding were found to be as high as 92% (Messenbock et al., 1999a).

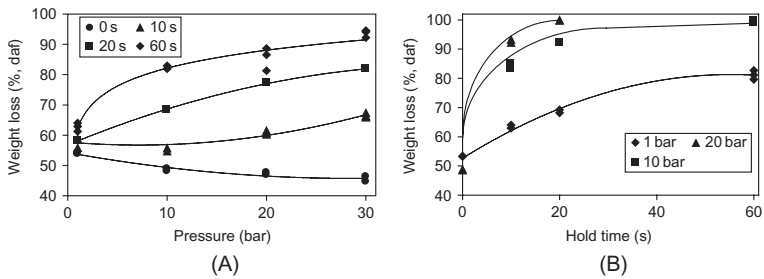

Figure 4.8 (A) Total volatile yields from CO_2-gasification. (B) Total volatile yields from the steam gasification. Daw Mill coal, heated at 1000°C s^{-1} to 1000°C.
Source: Reprinted with permission from Messenbock, R.C., Dugwell, D.R., Kandiyoti, R., 1999a. Energy Fuels 13, 122. Copyright 1999 American Chemical Society.

Fig. 4.8A shows that results from 10-s holding experiments traced a shallow minimum in the vicinity of 10 bars. The trend is familiar from the earlier hydropyrolysis experiments in wire-mesh reactors. In the lower pressure range of 1–10 bars, the physical suppression of devolatilisation by the external pressure caused loss of conversion to volatiles, with repolymerising tars depositing as relatively inert secondary char. At higher pressures, the increasing reactivity of the gas appears to enhance increasing sample weight loss.

At these high heating rates, the gasification process appears to go through several successive stages. As the pressure is increased, volatile suppression (mainly through tar repolymerisation) appears to be followed by gasification of the relatively inert secondary char and finally by the direct gasification of the underlying char residue (Güell et al., 1993). The results in Fig. 4.8A also show that the presence of the minimum at high heating rates depends not only on the pressure (related to the reactivity of the gas and the char) but also on the holding time at the given peak temperature. Experiments with 20 s holding did not show a minimum, suggesting that the secondary-char layer had already been consumed at the end of the 20-s period and that significant gasification of the char particle had already taken place.

Fig. 4.8B presents changes in sample weight loss during steam gasification as a function of holding times up to 60 s, at three different pressures: 1, 10 and 20 bars. Differences between yields at 1 and 10 bars were large, showing a qualitatively similar trend to CO_2 gasification. Differences between 0 and 10 s holding were again large, particularly at the higher pressures. At 20 bars, gasification of the sample (105–152 μm) was virtually completed after 20 s, leaving little except a dusting of ash particles on the sample holder.

The 60-s hold-time CO_2-gasification data in Fig. 4.8A closely matched sample weight loss data from parallel experiments carried out in a high-pressure fluidised-bed reactor. (Megaritis et al., 1998b). At the time of writing, apart from the *hydropyrolysis* data already referred to above, comparable short-time resolution experiments were not available among the vast amount of published data on coal and biomass gasification.

Fig. 4.9A,B present additional types of information that can be generated on sample behaviour, using the high-pressure wire-mesh reactor system, equipped with

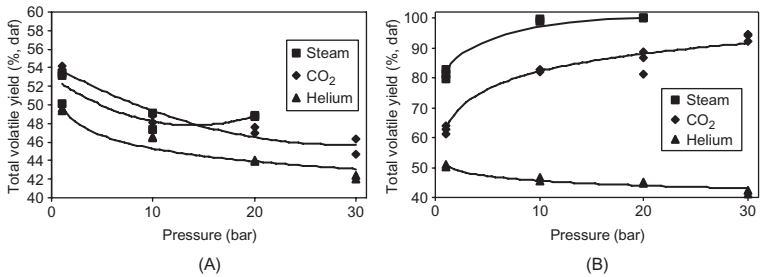

Figure 4.9 Total volatile yields from the pyrolysis, CO_2 and steam gasification of Daw Mill coal, heated at 1000°C s^{-1} to 1000°C. (A) 0 s holding time. (B) 60 s holding time.
Source: Reprinted with permission from Messenbock, R.C., Dugwell, D.R., Kandiyoti, R., 1999a. Energy Fuels 13, 122. Copyright 1999 American Chemical Society.

steam injection (Fig. 4.7). Fig. 4.9A compares sample weight loss data from Daw Mill (UK) coal, from zero-second holding pyrolysis experiments in helium and gasification runs in CO_2 and steam. At atmospheric pressure, a difference of 3–4% was already observed between pyrolysis (in helium) and weight loss during the gasification runs, showing the limited extents of gasification taking place during heatup. Sharp drops were observed in sample weight loss between 1 and 10 bars. In helium and CO_2, the decline was monotonic for 0-s hold times over the 1–30 bar range. However, volatile yields in steam traced a minimum above 10 bars, similar to the one observed earlier for 10 s holding under CO_2 in Fig. 4.8A.

Fig. 4.9B shows that, when samples are exposed to CO_2 or steam for 60 s, the minimum in the conversion versus pressure curves disappears. At the intermediate holding time of 10 s at 1000°C *in steam* (Figure 9 in Messenbock et al., 1999a; not shown), the minimum is also found to disappear. The occurrence of a minimum in conversion versus pressure diagrams, previously observed by numerous researchers in *hydropyrolysis* work, thus appears related to both the reactivity of the gasifying agent *and* the length of the holding-time at peak temperature. In the presence of the more reactive gasifying agent, *steam*, the minimum was observed at shorter holding times compared to experiments in CO_2.

Some of the data presented above reflect the rapid char deactivation discussed in Section 4.1. In Fig. 4.8B, the conversion line for gasification in atmospheric pressure steam tended to flatten out at around 80% conversion for the longer hold-time runs, showing little additional conversion between 40 and 60 s. Similarly, the CO_2 gasification curve in Fig. 4.9B appeared headed for not much more than 90% conversion. At the lower pressure of 10 bars, the CO_2 gasification line flattened out at around 80% conversion (Figure 12 in Messenbock et al., 1999a, not shown). The effect appears due to prolonged exposure of the char to high temperature in a medium not sufficiently reactive for total conversion to be achieved before the onset of deactivation.

The other important outcome of this investigation was the clear observation that in both CO_2 and steam, only a small amount of gasification was observed during heatup. It then becomes relevant to define an ‘extent of gasification’ by subtracting sample weight loss recorded during a pyrolysis experiment from the weight loss observed during a gasification run in a reactive gas, performed under otherwise identical experimental conditions (heating rate, temperature, hold-time, and pressure). With this definition in mind, the data from experiments just described can be recast into the form shown in Table 4.5.

As in the case of atmospheric pressure pyrolysis reactors, the strengths and weaknesses of high-pressure pyrolysis-gasification reactors become clearer when the behaviour of similar samples are compared in reactors of different design. In the next few sections, we will describe the development of a high-pressure, fluidised-bed reactor and compare data obtained from this and the high-pressure wire-mesh reactor, alongside the slower heating, fixed-bed ‘hot-rod’ reactor described in Chapter 3, Pyrolysis of solid fuels: experimental design and applications. As already signalled, the latter reactor configuration can be readily used at high pressures.

Table 4.5 Comparison of the 'extent of gasification' for 0-s and 20-s holding at 1000°C. Sample heating rate: 1000°C s^{-1}

Gas	Extent of gasification (% w/w, daf)		
	Pressure	0-s holding time	20-s holding time
Carbon dioxide	1	4.5	12.1
Carbon dioxide	10	2.0	24.4
Carbon dioxide	20	3.3	34.3
Carbon dioxide	30	3.3	41.9
Steam	1	2.8	20.6
Steam	10	1.7	48.3
Steam	20	4.8	54.4

Source: Reprinted from Messenbock, R.C., Dugwell, D.R., Kandiyoti, R., 1999b. Fuel 78, 781. Copyright 1996, with permission from Elsevier.

4.4 Designing a high-pressure bench-scale fluidised-bed reactor

Compared to wire-mesh reactors, fluidised-bed reactors are able to handle both wider particle size distributions and larger particles as well as greater amounts of sample, providing more char and tar samples for subsequent characterization.

Experimental high-pressure fluidised-bed systems usually consist of a reactor body, heated by a furnace, which is padded with thermal insulation and placed in an outer 'cold' pressure casing. This configuration has the advantage of positioning the pressure containment wall well away from the high temperature zone. At or near ambient temperatures, containment vessels operating at pressures required by the more common gasification tests (10–40 bars) do not require the use of special alloys or indeed, specialised designs. On the other hand, the space requirements and construction costs for such bulky assemblies usually require significant outlays. Furthermore, when constructed, such units incur high running costs, constraining running times and the numbers of experiments that can be carried out. These challenges explain, at least in part, the relatively small number of high-pressure fluidised-bed reactors in operation.

4.4.1 A Survey of small-scale, high-pressure fluidised-bed reactors

Several, relatively large laboratory-scale high-pressure fluidised-bed reactors designed for pyrolysis and gasification experiments have been reported in the literature. Morris

and Keairns (1979) have described a reactor made of Inconel 600 (35 mm i.d., 330 mm long), placed inside a cold pressure casing, together with furnace heaters and the necessary insulation. The bed material (char) was fluidised with nitrogen. The coal sample was held in a horizontal tube attached to a solenoid valve and injected into the reactor using a small cylinder of high-pressure nitrogen. Gas analysis data from experiments up to 982°C and 10 bars have been reported for three different coals. From descriptions, the installation appears relatively large and seems to have required significant maintenance. The schematic diagram of the apparatus in the original publication suggests that the feed tube did not extend into the fluidised-bed of solids. In these reactors, unless a provision is made to introduce the sample directly into the fluidising bed, the trajectories and temperature histories of sample particles remain ill defined.

Adánez et al. (1985) described another stainless steel fluidised-bed reactor (AISI 304 body; 40 mm i.d., 500 mm long), placed in a furnace. Instead of a coal injection system, the reactor was initially charged with 100–630 µm char particles and heated in nitrogen flowing at atmospheric pressure. When the intended reaction temperature was reached, the reactor was pressurised and reactant gases introduced. The temperature was determined by a single thermocouple placed inside the bed and the furnace temperature controlled manually using a variable voltage transformer. Gas pressure was regulated by means of a needle valve. Gasification experiments using a lignite have been reported (1000°C, 25 bar).

Another fluidised-bed pyrolysis-gasification reactor (1000°C; up to 25 bar) has been described by Hüttinger (Hüttinger, 1988; Hüttinger and Nattemann, 1994). Few details of this reactor are available in the open literature. The reactor made of nearly pure alumina ('alsint') was housed in a furnace, within a bronze pressure casing. Coal samples of about ~200 mg were dropped by gravity from a syringe mounted at the top of the assembly into the reactor freeboard. No attempt seems to have been made to guide the sample particles into the shallow (20 mm) fluidised-bed of 60–100 µm alumina particles.

A larger reactor with continuous feeding has been described by Sue-A-Quan et al. (1991, 1995). The main reactor tube (Incolloy; 100 mm i.d.; 1000 mm long) was centrally located and heated electrically inside a refractory-lined steel pressure shell of 305 mm diameter. The coal was fed at 2–5 kg h^{-1} by a star wheel feeder. Water, delivered by a diaphragm pump, was vapourised and superheated in coils immersed in a separate sand fluidised bed heated by a propane burner. Its final temperature was adjusted by heat exchange with product gas from the reactor. The reactor was operated at temperatures up to 900°C and 18 bars. From descriptions, the design and operation of the system appear complex.

4.4.2 The high-pressure fluidized-bed reactor constructed at Imperial College

Fig. 4.10 presents the schematic diagram of a high-pressure, bubbling fluidised-bed reactor, originally conceived for operation by batch sample injection. The reactor was designed for operation by a single researcher, and for a single run to be completed

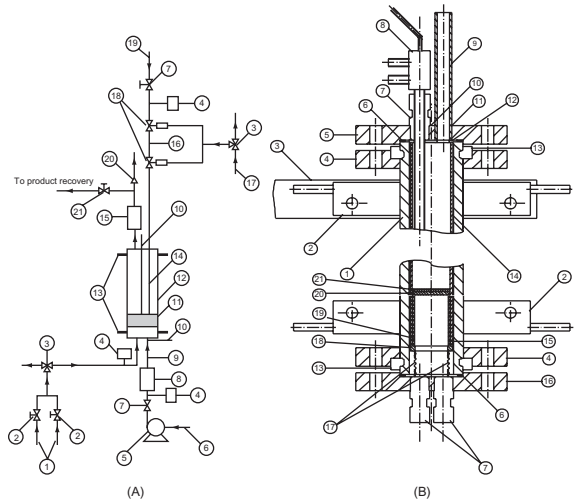

Figure 4.10 (A) Schematic diagram of the high-pressure fluidised-bed system. Below the reactor, a liquid metering pump (5) supplies the steam generator (8). Two non-condensable feed gas lines (1) may also be observed. Before injection into the bed, the sample (16) was held between two air-actuated valves (18). (1) High-pressure gas supply; (2) metering valve; (3) three-way valve; (4) pressure transducer; (5) metering pump; (6) water supply; (7) valve; (8) steam generator; (9) heated line; (10) thermocouple; (11) sand bed; (12) reactor; (13) electrodes; (14) sample injection probe; (15) tar trap; (16) sample; (17) air supply; (18) air-actuated valves; (19) injection probe gas supply; (20) safety valve; (21) gas flow control valve. (B) Main body of the high-pressure fluidised-bed reactor working at up to 1000°C and 30 bars. (1) Reactor tube; (2) Electrode; (3) Copper bar; (4) Flange; (5) Flange; (6) Copper sealing ring; (7) Male weld connector; (8) Sample injection probe; (9) Gas exit line; (10) Position of male weld connector for thermocouple (not shown); (11) Weld; (12) Kaowool-paper sealing ring, wire-mesh plates; (13) 'Half moon' positioning ring; (14) Quartz tube liner; (15) Distributor disc supporting quartz tube; (16) Flange; (17) Springs; (18) Spring loaded ring. (B) Schematic diagram of the system, showing the two valves between which the sample was held for injection. Below the reactor, the steam generator is supplied by a liquid metering pump; two non-condensable gas lines may also be observed.
Source: Reprinted with permission from Megaritis, A., Zhuo, Y., Messenbock, R., Dugwell, D.R., Kandiyoti, R., 1998a. Energy Fuels 12, 144. Copyright 1998 American Chemical Society.

in the course of a normal working day. It did not require a separate high temperature zone and a 'cold' pressure casing for containment. Instead, electrodes were attached directly to the top and bottom of the reactor tube, and the reactor body served as the resistance heater as well as the pressure containment vessel. For safety, the reactor assembly was placed in a steel box with 0.25-in. thick steel walls.

Fig. 4.10A presents the schematic diagram of the reactor system, showing the gas supply train (1), the reactor (12), the coal injection probe (14), the tar trap assembly (15), and the product recovery train. Water was supplied to the steam supply circuit by a calibrated high-pressure liquid metering pump (5). The steam generator

(8) consisted of an electrically heated stainless steel tube packed with ceramic spheres. The concentrations of the feed gas mixtures were controlled by metering valves (2) in the inlet line, where a pressure transducer (4) was positioned for tracking reactor pressure. Exhaust gases passed from the reactor, through a dryer, into the product analysis train. The total flow of fluidising gas was controlled downstream of the reactor by a metering valve (21). The reactor was protected from overpressure by a safety valve (20) connected to the outlet line.

Several materials of construction were considered for the reactor tube. Eventually, the Ni-Fe based Incoloy Alloy 800HT was adopted. It has high tensile strength and good creep resistance combined with resistance to high temperature corrosion. These properties make it useful for applications involving long-term exposure to elevated temperatures and pressures. It was also relatively easy to machine. The creep rupture limit of the reactor body designed for this work (34 mm i.d., 48 mm o.d; 504 mm long) was estimated at about 1000 hours at 1000°C and 40 bars. Some of the Ni-Cr-Fe based heat resistant Haynes Alloys would also have been equal to this relatively exacting task (http://www.haynesintl.com/HTA.html).

During experiments, the reactor tube was lined with a loosely fitting quartz tube, to limit corrosion attack by reactor contents and to block catalytic effects between bed contents and reactor walls. The initial design shown in Fig. 4.10 was intended for operation as a bubbling fluidised-bed, equipped with a sintered quartz support plate, along the lines of Tyler's atmospheric pressure quartz fluidised-bed (Fig. 3.5A). Coal or biomass samples between 50–200 mg, held between two air-actuated valves, were injected batchwise ('single-slug' injection) through a water-cooled probe with its tip *inside* the bubbling fluidised-bed of about 40 g of acid washed sand. Exhaust gases were passed upward through a tar trap and dryer into the gas analysis stage. In addition to product gas analysis, the design of the reactor allowed the determination of tar/oil and char yields with a reproducibility of ±2%. The water cooled the sample injection probe, the tar trap assembly, and other parts of the reactor system have been described in greater detail in the original publication (Megaritis et al., 1998a).

Pyrolysis in the high-pressure fluidised-bed reactor: Fig. 4.11A presents total volatiles data from the pyrolysis of Daw Mill coal in helium. Experiments were conducted at 1000°C, between 1 and 30 bars. Reactor cool-down was initiated after a holding time of 60 s at peak temperature. The results have been plotted alongside high-pressure wire-mesh reactor data from experiments with heating at 1000°C s^{-1} to 1000°C, with 10 s holding.

In Chapter 3, Pyrolysis of solid fuels: experimental design and applications, we observed that during experiments at temperatures of 700°C or above, all recoverable tars are released within the first second following the heatup ramp (Gonenc et al., 1990; Li et al., 1993a). During pyrolysis experiments at 1000°C, therefore, the differences in weight loss and tar yields, due to differences in holding times, between 10 s (wire-mesh) and 60 s (fluidised bed), were expected to be negligible.

Fig. 4.11 shows that, indeed, the differences in total volatile yields measured in the two reactors were similar within experimental scatter. As expected, both sets of yields dropped with increasing pressure, as a result of the physical suppression of

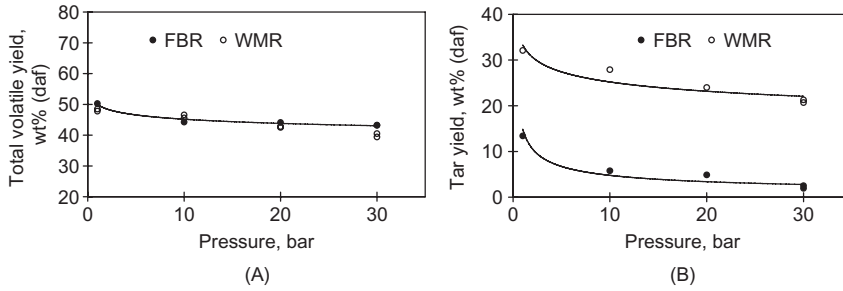

Figure 4.11 (A) Pyrolysis total volatile yields from Daw Mill coal as a function of pressure: Fluidised-bed reactor: 1000°C, 60 s; Wire-mesh reactor: 1000°C, 1000°C s^{-1}, 60 s. (B) Pyrolysis tar yields from Daw Mill coal as a function of pressure: Fluidised-bed reactor: 1000°C, 60 s; Wire mesh reactor: 1000°C, 1000°C s^{-1}, 10 s. *FBR*, fluidised-bed reactor; *WMR*, wire-mesh reactor.
Source: Reprinted with permission from Megaritis, A., Zhuo, Y., Messenbock, R., Dugwell, D.R., Kandiyoti, R., 1998a. Energy Fuels 12, 144. Copyright 1998 American Chemical Society.

volatiles release. Previous work suggests this to be due to suppression of *tar* evolution (Güell and Kandiyoti, 1993). However, the eventual fates of tars released in the two reactors were not the same and reflected the differences in the configurations of the two reactors.

Fig. 4.11B shows that the proportions of tars recovered at the exit of the fluidised-bed reactor were considerably less than those from the wire-mesh reactor. This result could have been anticipated from what we saw of differences between the analogous, atmospheric pressure reactors. In the *wire-mesh reactor*, the stream of carrier gas is intended to sweep tars released by sample particles rapidly out of the shallow reaction zone. In fluidised-bed reactors, on the other hand, tar vapours pass through the length of the freeboard before exiting from the reactor. In the case of the present reactor, before entering the cooled tar trap, volatiles must rise through a 280 mm high freeboard (below the top electrode), where temperatures are high – about the same as those in the fluidised-bed itself.

The temperature of the freeboard was measured as 960°C at a distance of 50 mm below the top electrode. Below that point, the temperature was uniform at about 1000°C. At these temperatures, tars are expected to thermally degrade and partially crack, both during passage through the bed of heated solids, and during passage through the reactor freeboard (Stiles and Kandiyoti, 1989). Moreover, previous work has shown that gas-phase tar cracking to lighter volatiles does not measurably alter total volatile yields (Tyler, 1979, 1980; Stiles and Kandiyoti, 1989).

During pyrolysis experiments in this high-pressure fluidised-bed reactor, considerable agglomeration of bed material was observed by visual examination (after cooldown), although differences with results from the wire-mesh reactor were within experimental error. However, initial CO_2-gasification trials showed that, at

pressures above 10 bars, sample agglomeration affected conversions measurably and adversely. In these initial experiments, sample conversions did not rise above 50% under 20 bar CO_2-pressure, i.e., not much above the weight loss observed during pyrolysis. The difficulty appeared due to the agglomeration of bed solids (sand) and sample particles, reducing sample surface area exposed to the reactive gas. Gasification reactions were slowed down, until the length of exposure at 1000°C led to sample deactivation.

To reduce the extent of agglomeration, (1) the design of the sample injection probe tip was altered to distribute sample particles radially outward, and (2) higher sample injection gas velocities were used alongside (3) larger, (150–300 μm) *sand* particles as fluidising material instead of the more usual 106–152 μm range. Some progress was observed. When a larger sand-particle range (800–1000 μm) was tried, no further reduction in sample agglomeration was observed. Similarly, mixing the coal particles with sand prior to injection was not found to reduce agglomeration significantly. However, less intense agglomeration was observed when *smaller amounts* of coal sample were injected. During subsequent experiments, sample sizes of 50 mg were used rather than the initial 200 mg. Using less sample than 50 mg proved counterproductive, as experimental scatter due to errors in sample recovery increased.

Fig. 4.12 compares total volatile yields from CO_2-gasification experiments at 1000°C, in the high-pressure wire-mesh and fluidised-bed reactors, using samples from the same batch of Daw Mill coal. Extents of agglomeration were monitored by observing the sizes of particle clusters in the fluidised-bed material after the experiments and by comparing results with the wire-mesh reactor. After introducing the corrective measures outlined above, results from the two reactors could be matched closely at 10 and 20 bars. However, at 30 bars, conversions in the fluidised-bed were found little

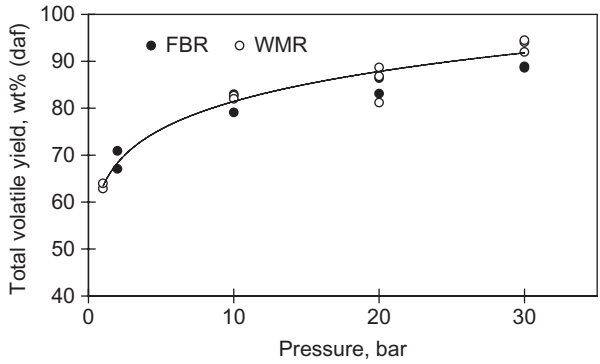

Figure 4.12 Total volatile yields from the CO_2-gasification of Daw Mill coal as a function of pressure. Fluidised-bed reactor: 1000°C, 60 s. Wire-mesh reactor: 1000°C, 1000°C s^{-1}, 60 s holding. *FBR*, fluidised-bed reactor; *WMR*, wire-mesh reactor.
Source: Reprinted with permission from Megaritis, A., Zhuo, Y., Messenbock, R., Dugwell, D.R., Kandiyoti, R., 1998a. Energy Fuels 12, 144. Copyright 1998 American Chemical Society.

changed from those at 20 bars, while the conversion in the wire-mesh reactor continued to rise, indicating the effect of agglomeration in the fluidised-bed. Experiments in the more reactive gasification agent, steam, did not give rise to agglomeration. When operating with steam at up to and including 30 bars, differences in total volatile yields observed in the two reactors were within experimental error (Zhuo et al., 2000a).

These observations fit together reasonably well. We have seen that increasing the pressure of *any* gas will suppress tar evolution and enhance particle plasticity, which promotes particle agglomeration. Tar precursors blocked from evaporating by the effect of rising pressure tend to harden, forming relatively unreactive secondary char. In both reactors, the effect would tend to block pores as well as cover external surfaces of the solid particles. In the fluidised-bed reactor, the passage through the plastic phase appears to have led to agglomeration involving sample particles and (sand) bed particles. Meanwhile, agglomeration in the wire-mesh reactor is prevented by the prior dispersal of sample particles. The agreement between pyrolysis total volatiles from the two reactors suggests that pyrolytic volatile release was mostly completed before the plastic mass had set and hardened into a secondary char.

Meanwhile, extents of gasification in CO_2 would be more closely related (than during pyrolysis) to the actual exposure of reactive surfaces to ambient gas. Agglomerates in the fluidised-bed material indicate that the reactivity of CO_2 was not sufficient to break up the particle clusters, which slowed down the gasification process long enough for the char to begin to deactivate at 1000°C. This explains why increasing CO_2 pressures did not significantly increase conversions. It is also clear from the wire-mesh reactor data (again, no agglomeration) that CO_2 is a less reactive agent for the gasification of residual chars, compared to steam. The data also suggested that *steam* is able to scratch through the secondary char that holds the agglomerates together. Under steam, neither agglomeration nor deactivation took place to the same extent as in the CO_2-gasification experiments. This explains the agreement between the steam gasification data from the fluidised-bed and wire-mesh reactors.

However, there is an additional strand of information that does not quite fit into this scheme. Daw Mill chars from pyrolysis (in helium) and CO_2-gasification, both from the wire-mesh reactor, were compared by scanning electron microscopy (SEM). The chars formed during CO_2-gasification clearly showed greater fluidity. Ordinarily, the reverse would have been expected. Information provided by SEM is inevitably partial and a little subjective. If confirmed as systematic, this observation would suggest chemical activity by CO_2 helping to enhance the plasticity of the pyrolyzing plastic mass (‘mesophase’), alongside the expected gasification reactions. In any case, the observed higher fluidity during CO_2-gasification in the wire-mesh reactor is consistent with greater agglomeration observed in the fluidised bed.

Returning to the design of the high-pressure fluidised-bed reactor, the next step in its evolution was the conversion of the system described in Fig. 4.10 from batch mode to operation with continuous sample injection. The system was next reconfigured for studying changes in ammonia, NO_x and HCN formation, and release during air-blown gasification (Paterson et al., 2002; Zhuo et al., 2002). The subsequent stage of the design and experimental results from it will be presented as a case study in Section 4.8.

4.5 Gasification in three bench-scale reactors with different configurations

We have seen in Chapter 3, Pyrolysis of solid fuels: experimental design and applications, and Section 4.3 how comparing results from different types of reactors can help identify the advantages and shortcomings of each particular reactor configuration. In this section, CO_2 and steam gasification data from the high-pressure wire-mesh reactor will be compared, first, with data from the fixed-bed ('hot-rod') reactor, described in Chapter 3, Pyrolysis of solid fuels: experimental design and applications; results from the high-pressure fluidised-bed reactor will then be added to the comparison. Samples from the same batch of Daw Mill coal were used in all three studies.

4.5.1 Comparing CO_2-gasification results from wire-mesh and fixed-bed reactors

In wire-mesh reactors, the time-temperature history of sample particles is closely controlled. The sweep gas passing through the shallow reaction zone aims to minimize secondary reactions between released volatiles and the finely dispersed sample particles. The fixed-bed ('hot-rod') reactor also provides for a controlled time-temperature history and sweep gas passage through the fixed bed of particles. However, heating rates in this reactor are limited by the thermal inertia of the system and radial heat transfer constraints to less than about 10°C s^{-1}. Moreover, the minimum practicable sample size in this reactor is about 50 mg. Below this sample weight, experimental scatter due to errors in sample recovery tends to grow. In the reactor of Fig. 3.4, a sample weight of 50 mg corresponded to a bed height of about 4 mm, when packed with coal particles (Gonenc et al., 1990). At that bed height, secondary reactions between volatiles and heated solids become inevitable. The reactor was described in Chapter 3, Pyrolysis of solid fuels: experimental design and applications, and results from pyrolysis experiments compared with data from analogous experiments in the wire-mesh reactor in Section 3.6.

Fig. 4.13 compares total volatile yields from experiments at 1000°C between 1 and 30 bars in the two reactors. The steeper drop in yields observed in the wire-mesh reactor pyrolysis data reflected the higher initial starting point, at atmospheric pressure.

During CO_2-gasification, differences in conversion between the two reactors increased with pressure. In contrast to the intimate gas-solid contact in the wire-mesh reactor, the stacking of particles in the fixed-bed ('hot-rod') reactor would tend to partially block the progress of gasification reactions. This is made worse by the onset of plasticity and increasing tar deposition on heated chars (Lim et al., 1997).

Fig. 4.14 compares relative combustion reactivities of chars recovered from 1000°C experiments in the two reactors. Both pyrolysis and CO_2-gasification chars from the fixed-bed ('hot-rod') reactor were less reactive than corresponding chars from the wire-mesh reactor. As outlined above, the slow-heating (10°C s^{-1}) ramp towards higher temperatures in the fixed-bed ('hot-rod') reactor contributes to char

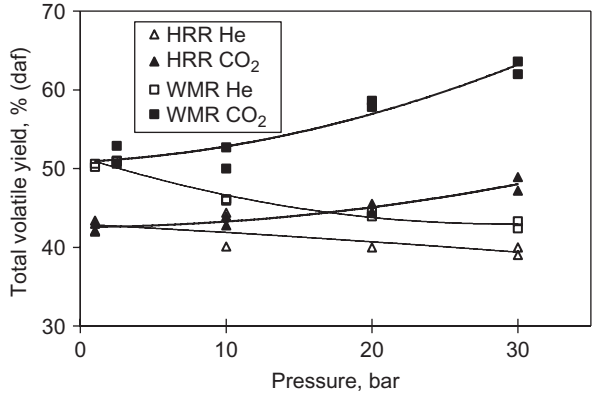

Figure 4.13 Comparison of total volatile yields from the high-pressure pyrolysis and CO_2-gasification of Daw Mill coal in the fixed-bed 'hot-rod' (HRR) and wire-mesh reactors (WMR). Peak temperature: 1000°C with 10 s hold in helium or CO_2. Heating rate 10°C s^{-1} in the fixed-bed ('hot-rod') and 1000°C s^{-1} in the wire-mesh reactor.
Source: Reprinted from Lim, J.-Y., Chatzakis, I.N., Megaritis, A., Cai, H.-Y., Dugwell, D.R., Kandiyoti, R., 1997. Fuel 76, 1327. Copyright 1997, with permission from Elsevier.

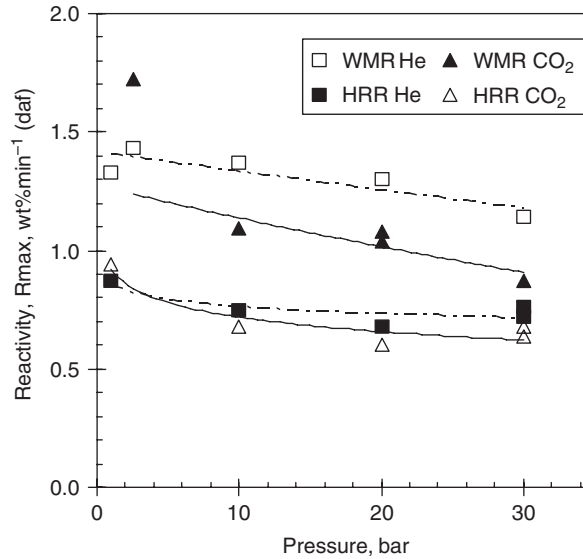

Figure 4.14 Comparison of relative combustion reactivities of chars from the high-pressure pyrolysis and CO_2-gasification of Daw Mill coal in the fixed-bed ('hot-rod') (HRR) and wire-mesh (WMR) reactors. Peak temperature: 1000°C with 10 s hold in helium or CO_2. Heating rate 10°C s^{-1} in the fixed-bed ('hot-rod') and 1000°C s^{-1} in the wire-mesh reactor.
Source: Reprinted from Lim, J.-Y., Chatzakis, I.N., Megaritis, A., Cai, H.-Y., Dugwell, D.R., Kandiyoti, R., 1997. Fuel 76, 1327. Copyright 1997, with permission from Elsevier.

deactivation compared to the rapidly heated wire-mesh reactor chars (1000°C s^{-1}). Moreover, we have already seen how the fixed-bed ('hot-rod') reactor configuration allows more tar deposition on heated particles within the packed bed. The amorphous secondary char formed from deposited tar would be less reactive than the devolatilising solid char matrix (Güell et al., 1993).

Implications for the use of pressurised TG balances: Comparing these results from fast-heating experiments in the wire-mesh and slow-heating in the fixed-bed ('hot-rod') reactor has particular significance in the context of previous comments on experiments done in TG balances. The heating rate in the 'hot-rod' reactor exceeds heating rates practicable in most TG balances: few TG balances would be equipped to operate at 600°C min^{-1} (i.e. 10°C s^{-1}). Moreover, volatiles are swept away more thoroughly and efficiently in the fixed-bed ('hot-rod') reactor used in this study, compared to TG balances, since most TG balances only accommodate a gas flow around *the furnace* within which the sample-bearing pan is held during experiments. The fixed-bed ('hot-rod') reactor configuration is better equipped than TG balances for limiting secondary reactions and attaining *relatively* rapid heating rates. Furthermore, mass transfer limitations are less severe within the fixed-bed reactor due to direct flow of the gasifying agent through the fixed bed and over stacked sample particles. Nevertheless, the data of Fig. 4.14 showed that the fixed-bed ('hot-rod') reactor is clearly inadequate in mimicking fuel behaviour within fast heating process equipment, such as fluidised-bed or entrained-flow reactors. It is necessary to view the utility or otherwise of high-pressure TG balances for assessing sample behaviour during gasification within the framework of these limitations.

4.5.2 Internal consistency of char reactivities from three bench-scale reactors

Broad agreement was found in comparing total volatile yields from pyrolysis and gasification experiments in the high-pressure wire-mesh and fluidised-bed reactors. Lower conversions were observed in the fixed-bed ('hot-rod') reactor, compared to the other two reactors. These differences are to be understood in terms of the basic design features of these reactors: the configurations of the wire-mesh and the fluidised-bed reactors were aimed at minimising interference from neighbouring particles with respect to volatile release and to maximising contact between the sample particles and the reactive gas.

Oxygen-blown gasifiers normally operate at pressures up to 30 bars and are operated at reaction temperatures above 1500°C, where the fuel is rapidly consumed. At these high temperatures, gasifier design becomes less sensitive to the reactivities of the feed coal and its chars, and rather more sensitive to the properties of the resulting molten ash. Nevertheless, we will see further on in this chapter instances where establishing a hierarchy of coal (and char) reactivities may be useful. The present section focuses on experiments intended to simulate coal particle behaviour in air blown gasification systems, where experimental conditions broadly remain within the 1000°C and 25–30 bar envelope (Dawes et al., 1991; Mojtahedi et al., 1991; Motter and Higginbotham, 1993; EPRI Report TR-103367).

The design of bench-scale gasification experiments: There is relatively little work reported in the literature on the relationship between char formation *conditions* and the gasification reactivities of resulting chars (Laurendeau, 1978; Chitsora et al., 1987; Güell and Kandiyoti, 1993; Güell et al., 1993; Cai et al., 1996). Peng et al. (1995) have compared reactivities of directly gasified coals (a lignite, a sub-bituminous and a bituminous coal) with the reactivities of chars from the same coals, pyrolyzed previously under otherwise similar reaction conditions. The work was carried out in a TG balance operated under atmospheric pressure steam-nitrogen mixtures (76 mol% steam), at temperatures between 1000°C and 1400°C. Reactivities of chars generated during direct gasification experiments were reported to be up to six times greater than those of corresponding chars prepared in the same TG balance under nitrogen.

These experiments were reported to have been carried at heating rates that are surprisingly high for a TG balance, *estimated* to be '… between 100 and 1000°C s^{-1} …'. They were reportedly achieved by lowering the sample pan, laden with about 100 mg of 149–210 µm particles, into a heated TG-balance furnace. In fact, such an experimental setup would give rise to a number of potential uncertainties. It is possible that particles near the periphery of the pile were indeed heated rapidly, although the range of heating rates cited ('between 100°C s^{-1} and 1000°C s^{-1}') cannot be verified. Furthermore, it is difficult to visualize how the uniformity of the temperature distribution and the constancy of the heating rate could be maintained within a pile of 100 mg of particles placed on the TG-balance pan. The rate of heat transmission *inside* the pile would be governed by the thermal conductivity of the pyrolyzing mass, rather than the externally imposed temperature gradient. Calculations for the fixed-bed ('hot-rod') reactor described in Chapter 3, Pyrolysis of solid fuels: experimental design and applications, indicated that across a *radius* of 3 mm, heating rates greater than 10°C s^{-1} imposed at the external boundary would lead to severe temperature gradients (O'Brien, 1986). Furthermore, experiments using samples of 50 mg (i.e., half that of Peng et al., 1995) have shown that tar and volatile yields as well as char reactivities are affected by the stacking of coal particles (Gonenc et al., 1990). It is not clear how secondary char formation through tar deposition on pyrolyzing solid surfaces could be ignored in a 100 mg pile of sample particles. Secondary-char deposition in a relatively slow and non-uniform heating environment would be expected to affect char reactivities. The results of this experiment would be difficult to interpret.

The experiments outlined below aimed to clarify some of the uncertainties in the use of single and two-step gasification procedures for char preparation. The effect of char formation conditions was examined at pressures up to 30 bars, using the bench-scale reactors already described. The 'extent of gasification' may be calculated by subtracting mass loss during pyrolysis in helium from mass loss during direct (i.e., one-step) gasification, under otherwise similar reaction conditions. In turn, 'gasification reactivity' has been defined as the 'extent of gasification' divided by the hold time at peak temperature. The 'gasification reactivities' calculated from the CO_2-gasification data have been compared with conversions from two different 'two-step' procedures.

Comparing gasification reactivities: Experiments with untreated coal were carried out in the three reactors under helium and CO_2, at 1000°C, with 60 s holding, at

pressures between 1 and 30 bars (Megaritis et al., 1998b). Heating rates in the fixed-bed ('hot-rod') and wire-mesh reactors were 10 and 1000°C s^{-1}, respectively. No heating rates will be hazarded for the fluidised-bed experiments. It is assumed these were high for most sample particles – probably of the order of 1000°C s^{-1}.

The first set of *char* gasification experiments was carried out by pyrolyzing samples in helium in each of the reactors for 10 s at 1000°C (1, 10, 20 and 30 bars). The carrier gas flows in the reactors were then switched to CO_2 for 60 s. The pyrolysis and gasification steps of these experiments were thus carried out at similar temperatures and pressures. For the second set of char-gasification experiments, a common sample of char was prepared in the fixed-bed ('hot-rod') reactor, by heating under atmospheric pressure helium at 10°C s^{-1} to 1000°C with 60 s holding. The chars were sieved and dried (to drive away adsorbed moisture) prior to the gasification runs. Samples of char prepared in this way were gasified in each of the three reactors, under identical conditions to those used in the *coal* gasification runs (1000°C for 60 s at 1, 10, 20 and 30 bar). Combustion reactivities of the residual chars recovered after these experiments have been determined in an atmospheric pressure TG balance. In what follows, it is useful to remember that combustion and gasification reactivity trends for coal chars measured by TGA are nearly always similar.

Fig. 4.15 presents 'one-step' CO_2-gasification reactivities of Daw Mill coal in each of the three reactors, given in units of 'percent weight loss per minute'. Experiments were carried out between 1–30 bars with 60 s holding at 1000°C. As expected, substantially lower conversions and reactivities were observed in the fixed-bed ('hot-rod') reactor, compared to the wire-mesh and fluidised-bed reactors. The gasification reactivity in the fixed-bed ('hot-rod') reactor was also found to be less sensitive to pressure. Results from the fluidised-bed and wire-mesh reactor were found to be close to each other, except at 30 bars where the reactivity in the wire-mesh reactor was

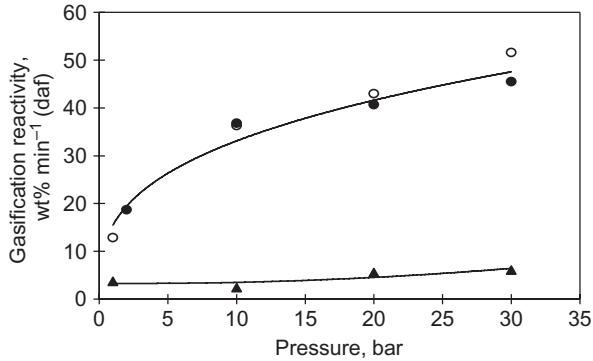

Figure 4.15 CO_2-gasification reactivity of Daw Mill coal as a function of pressure. (▲) Fixed-bed ('hot-rod') reactor: 10°C s^{-1} to 1000°C with 60 s holding in CO_2. (○) Wire-mesh reactor: 1000°C s^{-1} to 1000°C with 60 s holding in CO_2. (●) Fluidised-bed reactor: fast heating to 1000°C with 60 s holding in CO_2.
Source: Reprinted from Megaritis, A., Messenbock, R.C., Collot, A.-G., Zhuo, Y., Dugwell, D.R., Kandiyoti, R., 1998b. Fuel 77, 1411. Copyright 1998, with permission from Elsevier.

higher, by ~5% min^{-1}. This difference is likely to be due to sample agglomeration, observed in the fluidised-bed at the highest CO_2-pressures (see Fig. 4.12).

Two-step gasification sequences: In the first of the 'two-step' sequences, the coal sample was first pyrolyzed in situ, in each of the three reactors, under helium (10 s at 1000°C), before switching over to CO_2 and holding for 60 s *in the same reactor*. This two-step procedure was found to reduce reactivities in the fluidised-bed reactor by up to 4% relative to direct CO_2 gasification, but qualitatively the results did not differ much from Fig. 4.15. However, significant differences were observed in both the wire-mesh and the fluidised-bed reactors between overall conversions from direct CO_2 gasification and those from the gasification of the sample of char prepared in the fixed-bed ('hot-rod') reactor.

Fig. 4.16 compares results from the direct gasification of Daw Mill coal in the fluidised-bed reactor and results from the two 'two-step' procedures. The sharp drop in reactivity observed when using the char prepared in the fixed-bed reactor clearly illustrates the dangers inherent in working with chars under a different regime than the actual gasification stage.

In previous hydropyrolysis work, the lower conversions observed in the fixed-bed ('hot-rod') reactor had been explained in terms of secondary char deposition, leading to low overall char reactivity, as well as poor char-gas contact (Gibbins et al., 1991). On their own, ordinary 'conversion' data do not allow the two effects to be distinguished from each other. Data presented in Fig. 4.16 indicated, however, that low reactivities were observed when the char from the fixed-bed ('hot-rod') reactor was re-ground and gasified in the fluidised bed reactor. This suggests that the *deactivation* of the char during pyrolysis in the fixed-bed ('hot-rod') reactor was significant.

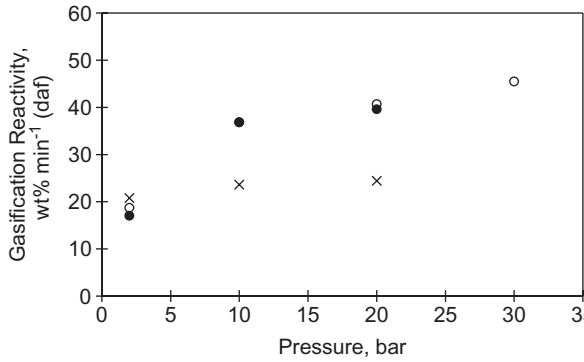

Figure 4.16 Gasification reactivities determined in the fluidised-bed reactor as a function of char preparation conditions. (○) Direct CO_2-gasification of untreated Daw Mill coal. (●) Daw Mill coal, successively pyrolyzed and gasified in the fluidised-bed reactor. (×) CO_2-gasification reactivity in the fluidised-bed of char pyrolyzed in the fixed-bed ('hot-rod') reactor. Char preparation in the fixed-bed ('hot-rod') reactor: 10°C s^{-1} to 1000°C with 60 s holding in CO_2. All runs in the fluidised-bed reactor were carried out by fast heating to 1000°C, 60 s, CO_2.

Source: Reprinted from Megaritis, A., Messenbock, R.C., Collot, A.-G., Zhuo, Y., Dugwell, D.R., Kandiyoti, R., 1998b. Fuel 77, 1411. Copyright 1998, with permission from Elsevier.

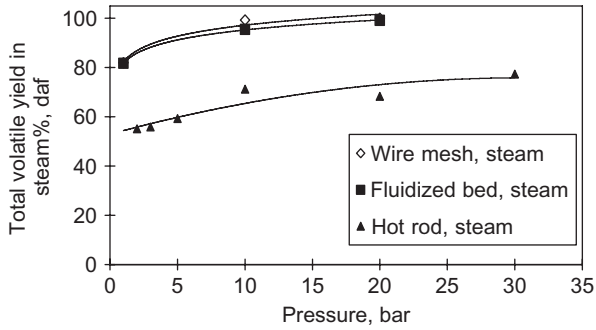

Figure 4.17 Weight loss during the steam-gasification of Daw Mill (UK) coal in the three reactors. 60 s holding at 1000°C.
Source: Reprinted from Zhuo, Y., Messenböck, R., Collot, A.-G., Paterson, N., Dugwell D.R., Kandiyoti, R., 2000a. Fuel 79, 793. Copyright 2000, with permission from Elsevier.

The low reactivity of fixed-bed reactor chars appears to be due to a combination of factors: (1) contact between tar vapours and reacting solids, leading to the repolymerisation of (probably heavier) tar components on char surfaces, leading to the deposition of an amorphous layer of secondary char during the pyrolysis step (Güell and Kandiyoti, 1993), and, (2) char deactivation due to slow (10°C s^{-1}) heating in the fixed bed, which exposes samples to long residence times at temperatures between 850°C and 1000°C, leading to the rapid loss of char reactivity, as observed in Fig. 4.1.

For the Daw Mill coal char tested at 20 bars, the magnitude of the error introduced by adopting the 'two-reactor, two-step' approach was about 20 'wt% min^{-1}'. Sharper char deactivation would be expected with coals that soften when heated slowly. The extent of deactivation would also depend on the amount and properties of tars evolving from particular coals. Even when 'only' aiming to establish *relative* reactivities within a suite of coals, therefore, 'two-reactor, two-step' procedures are likely to lead to erroneous results.

Gasification in Steam: Fig. 4.17 presents conversions during the (one-step) *steam* gasification of Daw Mill coal in the same three bench-scale reactors (Zhuo et al., 2000a). The experiments were conducted with 60 s holding at 1000°C. As in the case of gasification in CO_2, conversions increased monotonically with pressure. However, in the presence of 20 bar steam, a nearly complete conversion of the (106–152 μm particle size) sample was observed in the wire-mesh and the fluidised-bed reactors. These two reactors have been deliberately designed to segregate individual coal particles from one another and operate at high heating rates. In this case, agreement between them was within experimental error. In line with results from hydropyrolysis and CO_2-gasification experiments outlined above, lower conversions were observed in the fixed-bed ('hot-rod') reactor.

Fig. 4.17 clearly suggests, furthermore, an upper limit to the conversion of the char in the fixed-bed ('hot-rod') reactor, under these reaction conditions. Despite operating with a more reactive gas (steam), the maximum attainable conversion does not appear likely to ever reach completion, even at very long holding times. Indeed, long holding times at 1000°C would be expected to exacerbate the deactivation of chars. A similar effect was observed in the chars withdrawn from the British Coal ABGC pilot plant,

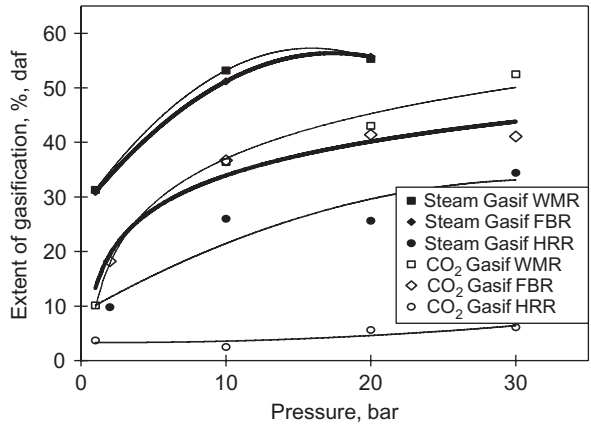

Figure 4.18 Comparison of 'extents of gasification' in steam and CO_2. 60 s holding at 1000°C. *WMR*, wire-mesh reactor; *FBR*, fluidised-bed reactor; *HRR*, hot-rod reactor. *Source*: Reprinted from Zhuo, Y., Messenböck, R., Collot, A.-G., Paterson, N., Dugwell D.R., Kandiyoti, R., 2000a. Fuel 79, 793. Copyright 2000, with permission from Elsevier.

where some of the chars, which probably started as larger particles fed to the reactor, eventually became stable and unreactive.

'Extents of gasification' in coal-steam reactions: The conversions (total volatiles) in Fig. 4.17 correspond to the sum of weight loss through pyrolytic devolatilisation and weight loss due to reactions between the carbonaceous matter and steam. Fig. 4.18 presents 'extents of steam-gasification' calculated by subtracting weight loss during pyrolysis (Figure 4.2 in Zhuo et al., 2000a) from conversions during steam-gasification (from Fig. 4.17). For completeness, corresponding 'extents of CO_2-gasification' have been included in the diagram.

In all reactors, the extent of *steam*-gasification was markedly greater than that in CO_2. Experiments carried out in the fluidised-bed reactor with equal mixtures of steam and CO_2 gave results that were nearly indistinguishable from conversions in pure steam. Furthermore, char agglomeration during CO_2-gasification above 20 bars has been difficult to control and this was reflected in the lower conversion observed in the fluidised bed at 30 bars when compared with the result obtained in the wire-mesh reactor. Measures adopted to reduce agglomeration in the fluidised-bed reactor have been described above (Megaritis et al., 1998a).

4.5.3 Comparison with pilot plant data

Fig. 4.19 compares conversions of five different coals in the 200 kg h^{-1} British Coal ABGC pilot scale gasifier at Stoke Orchard (UK), with direct CO_2-gasification conversions observed in the high-pressure wire-mesh reactor.

Detailed information on the compositions of the coals may be found in Table 4.6 (Megaritis et al., 1998b). The coals and their proximate analysis volatile

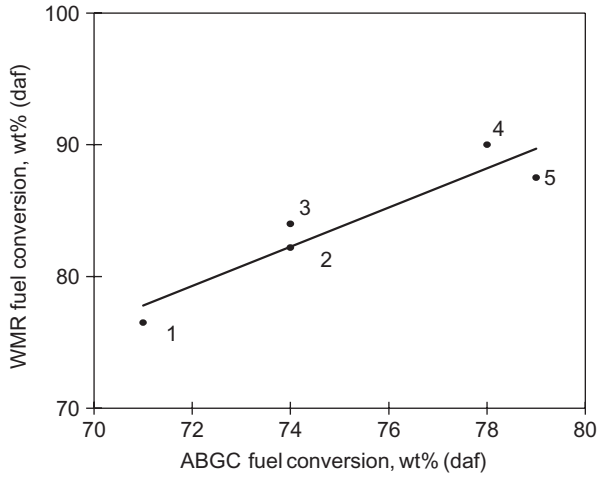

Figure 4.19 Comparison of fuel conversion in the high-pressure wire-mesh reactor and the ABGC pilot scale gasifier. Wire-mesh reactor: 1000°C s^{-1} to 1000°C with 60 s holding at 10 bar CO_2 pressure. ABGC gasifier: 970°C (approx.), 13 bar, air/steam injection. 1, Rietspruit (S. Africa); 2, Daw Mill (UK); 3, Drayton (Aus); 4, Illinois No. 6 (USA); 5, El Cerrejon (Colombia).
Source: Reprinted from Megaritis, A., Messenbock, R.C., Collot, A.-G., Zhuo, Y., Dugwell, D.R., Kandiyoti, R., 1998b. Fuel 77, 1411. Copyright 1998, with permission from Elsevier.

Table 4.6 Proximate and ultimate analyses of the set of coals

	Daw Mill[a]	El Cerrejon	Drayton	Rietspruit	Illinois No. 6	Daw Mill[b]
Volatile matter (%, daf)	39.7	40.7	39.5	32.8	45.5	39.9
Ash (%, db)	14.1	7.2	10.7	12.5	9.5	4.4
Moisture (%, ad)	4.5	5.4	3.1	3.9	7.1	6.1
Swelling number	1	1	2.5	1	6	1
Carbon (%, daf)	80.6	82.4	82.6	82.5	78.2	80.1
Hydrogen (%, daf)	5.4	5.8	5.7	4.9	5.6	4.7
Nitrogen (%, daf)	1.5	1.7	2.0	2.1	1.4	1.3
Sulphur (total) (%, daf)	2.0	0.8	0.8	0.7	4.4	1.1
Vitrinite (%Vol, mmf)	67	84	75	63	92	66
Inertinite (%Vol, mmf)	21	14	21	33	6	21
Liptinite (%Vol, mmf)	12	2	4	4	2	13
Mean vitrinite reflectance	0.60	0.72	0.65	0.73	0.40	0.60

Source: Reprinted from Messenbock, R.C., Paterson, N., Dugwell, D.R., Kandiyoti, R., 2000. Fuel 79, 109. Copyright 2000, with permission from Elsevier.
[a]High ash Daw Mill sample.
[b]Low ash Daw Mill sample.

matter contents (% w/w, dry basis) were as follows: Rietspruit (S. Africa; 28.7); Daw Mill (UK; 34.1); Drayton (Australia; 35.3); 4: Illinois No. 6 (USA; 41.2); El Cerrejon (Colombia; 37.8). They were selected as being representative of the range of coals likely to be used in an eventual commercial application.

In the ABGC pilot reactor, an estimated 30% of the original feed was converted to volatiles through pyrolysis and about 10% by steam and CO_2-gasification. Another (estimated) 30% of the coal mass was consumed by combustion in the auto-thermal reactor, the energy being taken up by endothermic steam and CO_2 gasification reactions. Finally, about 30% of the fuel charged to the reactor was recovered as residual char. In an eventual full-blown process, these chars would have been combusted in a separate unit to raise process steam.

Clearly, conditions in the two reactors were not identical. The ABGC used a mixture of air and steam, with the feed coal crushed to 'less than 3 mm diameter', compared to the use of pure CO_2 and the 100–150 μm particle size range in the wire-mesh reactor. Despite these differences, Fig. 4.19 shows a broadly linear relationship between the pilot-plant gasifier and the bench-scale reactor, suggesting that data from the wire-mesh reactor may be usefully employed to compare *relative* coal reactivities under pilot-plant gasification conditions.

In addition to their ability to predict a correct order of reactivity for this set of coal samples, results presented in this section show the wire-mesh and the fluidised-bed reactors to have been useful in pinpointing reasons for the low reactivity of chars recovered from the pilot-scale spouted bed. Fig. 4.19 thus shows one of the ways in which bench-top experiments may be used in estimating *trends* in pilot or plant scale fuel processing plant.

4.6 Case studies: factors governing coal reactivity in pyrolysis and gasification

4.6.1 Correlating results from coals and coal macerals

This section describes an evaluation of the use of coal maceral analysis for predicting coal reactivity (sample weight loss; conversions) during pyrolysis and gasification. The pyrolysis and gasification reactivities of a suite of six coals and three maceral concentrates were determined. The experiments were done in the high-pressure wire-mesh reactor (Fig. 4.3), between 1 and 30 bars. The coal samples described in Table 4.6 are the same ones used in the ABGC pilot plant trials. The choice of *maceral concentrate* samples was based on availability; the samples used in the study (Table 4.7) were derived from different coals. The proposition tested was that, volatile yields from each coal in the series could be calculated from the weighted sum of (1) the maceral composition of the particular *coal* and (2) the total volatile yields from each of the three available maceral concentrates (Messenbock et al., 2000). The work was viewed as exploratory.

Predicting pyrolysis weight loss from coal maceral behaviour: The pyrolysis and gasification experiments were run in helium and CO_2, respectively, at pressures of 1, 10, 20 and 30 bars. Samples were heated at 1000°C s^{-1} to 1000°C, with 10 s holding

Table 4.7 Properties of the three maceral concentrates used in the calculation of predicted total volatile yields in Fig. 4.20

Maceral group	Vitrinite	Liptinite	Inertinite
Maceral type	Hand picked vitrain	Exinite	Semi-fusinite
Parent coal (Seam)	Markham Main (Barnsley)	Peckfield (Beeston)	Roddymoor (Ballarat)
C (% daf)	81	82	93
H (% daf)	5.5	6.8	4.4
Vitrinite (Vol%, mmf)	98	3	10
Liptinite (Vol%, mmf)	1	92	0
Inertinite (Vol%, mmf)	0.3	5	90

Source: Reprinted from Messenbock, R.C., Paterson, N., Dugwell, D.R., Kandiyoti, R., 2000. Fuel 79, 109. Copyright 2000, with permission from Elsevier.

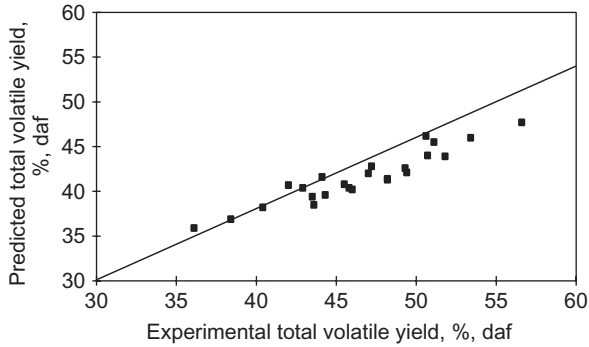

Figure 4.20 Correlation between experimental and predicted results for pyrolysis experiments in 1, 10, 20 and 30 bars helium. Samples were heated at 1000°C s^{-1} to 1000°C, with 10 s holding at peak temperature.
Source: Reprinted from Messenbock, R.C., Paterson, N., Dugwell, D.R., Kandiyoti, R., 2000. Fuel 79, 109. Copyright 2000, with permission from Elsevier.

at peak temperature. The full set of results may be viewed in the original publication (Messenbock, et al., 2000). Weight loss measurements from maceral concentrate samples were combined with the maceral analyses of the six coals, to *calculate* sample weight loss for the six 'whole' coals. These calculated ('reconstituted') weight loss results were compared with the actual weight loss data from pyrolysis and from CO_2-gasification experiments.

Fig. 4.20 shows that predicted values were only marginally lower than experimental values for volatile yields below ~45%. Above that value, the difference between the data and calculated values increased, reflecting the systematic error due to the relatively high rank of the set of 'constituent' maceral concentrates used for the purposes of this calculation. For the approximate calculation that this was meant to be, the predictive value of the correlation appeared to be surprisingly good.

Added to those of Table 3.10, these results indicate that it is possible to predict pyrolysis total volatile and tar yields of individual coals reasonably well from (1) their maceral compositions and (2) pyrolysis weight loss data from their (preferably own) maceral constituents. While it always makes sense to work with many more samples, the indications are that for middle rank bituminous coals, any departures from simple additivity between component macerals during pyrolysis are not experimentally detectable. In other words, any synergistic effects leading to variations in weight loss during pyrolysis are within the scatter in the data. This result is not surprising when taken together with findings outlined in Section 3.7.3 (Li et al., 1993a,b). However, the commercially more significant question would be whether such a predictive method might be applicable to *gasification* conversions.

Predicting gasification reactivity from coal maceral behaviour? The attempted correlation analogous to Fig. 4.20, between experimental and calculated CO_2-gasification conversions showed sufficient scatter to be virtually useless (Messenbock et al., 2000). However, the conversions used in the comparison had been defined as *total weight loss*. In other words, the 'conversion' subsumed sample weight loss by pyrolysis and sample weight loss by gasification. When the predicted and experimental 'extents of gasification' ('total weight loss' minus 'pyrolysis weight loss') were plotted together, the correlation was again found to be weak. In the interest of brevity, the diagrams have not been presented within the present text.

Conclusion: Despite using a single set of disparate maceral concentrates to represent the full spectrum of samples in the set of coals used, it proved possible to estimate the pyrolysis weight loss of coals from data on maceral composition and maceral weight loss during pyrolysis. The experiments covered a pressure range between 1 and 30 bars at 1000°C and the results are in line with those from the atmospheric pressure maceral pyrolysis work described in Chapter 3, Pyrolysis of solid fuels: experimental design and applications (Li et al., 1993a,b). However, the method was not useful in predicting the *gasification* performance of the same coals. There was much scatter in the data for middle-rank coals, although the factors producing this result could not be identified. It seems reasonable to conclude that coal gasification conversions are less dependent on original maceral properties, than was found to be the case for pyrolysis weight loss.

4.6.2 Correlating conversions with FT-IR spectra of coals

The British Coal ABGC pilot-plant runs had produced large amounts of unreactive char, and improving the conversions of feed coals at the gasification stage would have increased overall power generation cycle efficiencies. In a related study, possible correlations between the FT-IR spectra of an array of coals and their pyrolysis and gasification conversions were examined. The work aimed to explore factors which produced differences between the reactivities of coals of nearly similar rank, during the operation of the British Coal pilot-scale air-blown spouted-bed gasifier (Gavin et al., 1997). The core of the study was an attempt to correlate the reactivities of coals with their infrared spectra, with the aim of identifying structural features that affected reactivities in coals. The study was undertaken using a proprietary software package 'QUANT+' for the correlations (Zhuo et al., 2000b).

Table 4.8 Elemental Analyses of the set of 'calibration' coals (% w/w, dry ash free basis)

Coal	C	H	N	S	O
Taff Methyr (UK)	91.5	4.1	1.4	0.7	2.2
Tilmanstone (UK)	91.0	4.3	1.2	1.5	2.0
Emil Mayrisch (Germany)	89.2	4.4	1.4	0.8	4.1
Santa Barbara (Spain)	88.8	5.7	1.9	1.1	3.0
Heinrisch Robert (Germany)	87.7	4.9	1.2	0.9	5.2
Upper Freeport (USA)[b]	85.5	4.7	1.6	0.7	7.5
Candin (Spain)	84.6	4.8	1.7	1.2	7.7
Point of Ayr (UK)	84.5	5.4	1.8	1.5	6.1
Thoresby (UK)	84.0	5.3	1.8	1.0	7.9
WAI (Australia)	84.0	4.0	4.7	0.3	10.0
Hemheath (UK)	83.9	5.4	1.8	0.8	8.1
Bentinck (UK)	83.5	5.6	1.7	2.3	6.9
Pittsburgh No. 8 (USA)[b]	83.2	5.3	1.6	0.9	8.8
Longannet (UK)	82.7	5.0	1.8	1.0	10.1
Lewiston-Stockton (USA)[b]	82.6	5.3	1.6	0.7	9.8
La Jagua (Colombia)	82.1	6.1	1.6	0.5	9.7
Rietspruit (S. Africa)	81.9	4.6	1.6	0.4	9.2
Gedling (UK)	81.3	4.7	1.5	1.0	11.1
Linby (UK)	81.0	5.3	1.7	1.0	11.0
WA2 (Australia)	80.8	5.1	1.9	0.3	11.9
Blind Canyon (USA)[b]	80.7	5.8	1.6	0.4	11.6
Daw Mill (UK)	80.1	4.7	1.3	1.2	11.5
Illinois No. 6 (USA)[b]	79.6	5.0	1.4	4.5	9.5
Illinois No. 6 (SBN)[a]	77.7	5.0	1.4	2.4	13.5
Fording Genesse (Australia)	74.3	4.4	0.7	0.5	20.1
Gardanne (France)	74.2	5.0	1.7	6.2	12.9

Source: Reprinted with permission from Zhuo, Y., Lemaignen, L., Chatzakis, I.N., Reed, G.P., Dugwell, D.R., Kandiyoti, R., 2000b. Energy Fuels 14, 1049. Copyright 2000 American Chemical Society.
[a]Illinois No. 6 (SBN) provided by Steinkohlebank Nederlands (SBN).
[b]Standard samples provided by the Argonne National Laboratories (Vorres, 1990).

Table 4.8 presents the elemental analyses of the 26 coals used in the study. The samples were of diverse geological origins. The pyrolysis and CO_2-gasification conversions of 23 of the coals were determined in the high-pressure wire-mesh reactor (Fig. 4.3). Analogous pyrolysis and CO_2-gasification data on a subset of 16 coals were acquired using the fixed-bed ('hot-rod') reactor. We will see below that the results from the two reactors turned out to be distinct and the comparison instructive.

The wire-mesh reactor experiments were carried out at 10 bars. Samples were heated at 1000°C s^{-1} to 1000°C, with 20 s holding at peak temperature. In the fixed-bed ('hot-rod') reactor, experiments were conducted at 20 bars, heating 50 mg samples of coal at 10°C s^{-1} to 1000°C, with 10 s holding at the peak temperature. A superficial

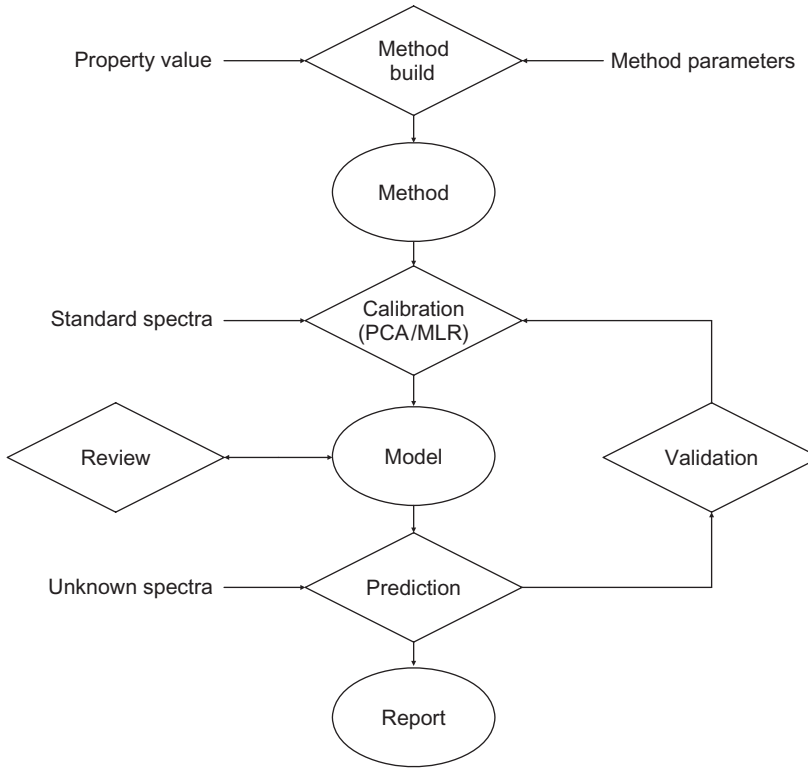

Figure 4.21 Overview of the QUANT+ correlation procedure.
Source: Adapted from Perkin-Elmer Ltd. QUANT+ User's Manual (1991).

gas velocity of 0.1 m s^{-1} was used in all the experiments. The FT-IR spectra of the samples were acquired as described by Li et al. (1994) and Madrali (1994).

The factor analysis and multiple linear regression methods used in the 'QUANT+' correlation procedure have been described by Malinowski and Howery (1980) and Weisberg (1985). The first step in the procedure is to choose a set of 'calibration' coals. Selected properties of each of these samples (e.g., carbon content, weight loss in pyrolysis, etc.) are measured. Their FT-IR spectra are acquired and stored. Relationships between the measured variables and the FT-IR spectra are then explored. The analysis procedure includes three sequential steps: calibration, validation, and prediction. An overview of the steps involved in the 'QUANT+' calculation is presented in Fig. 4.21 (Perkin-Elmer, 1991).

Details of the construction of the 'model' involving the calibration and validation steps have been presented in the original publication (Zhuo et al., 2000b). The aim of the calculation is to estimate the value of an individual property (e.g., elemental carbon content) of an unknown coal from its FT-IR spectrum, by using (1) already-measured properties of the 'calibration' set of coals, and (2) parts of the model's

segments of the FT-IR spectrum, statistically found to be significant in contributing to that particular property.

Cross Validation: A 'cross-validation' procedure is then initiated to test the models generated. The procedure consists of excluding one coal sample at a time from within the calibration set and correlating the FT-IR spectra of the set of samples with their selected properties (minus the excluded sample). The next step is to predict the properties of the sample excluded from the calibration set during the calculation, by using the derived models (using (N − 1) calibration samples). The cross-validation procedure provides a measurement of average prediction error ('standard error of prediction'). These are summed up and the 'model' is then optimized to minimize the cumulative error of prediction. Only the factors (typically, segments of the FT-IR spectrum) with statistical importance are retained in the final regression model.

The final model is thus based on criteria minimising the error of prediction. In what follows, we have confined ourselves to running the cross validation procedures against the existing pyrolysis and gasification data, i.e., taking one sample at a time as the 'unknown', estimating the pyrolysis and gasification conversions of that sample, then moving on to the next sample.

Table 4.9 presents the total volatile yields in He, determined in the *wire-mesh* reactor. The total volatile yields from gasification in CO_2 were also measured and the 'extents of gasification' were then calculated from (Total $Volatiles_{gasification}$ − Total $Volatiles_{pyrolysis}$) on a wt%, dry ash free basis. Table 4.10 presents analogous results from experiments on a subset of 16 coals undertaken in the *fixed-bed* ('hot-rod') reactor.

The data plotted in Fig. 4.22A showed excellent agreement between pyrolysis total volatile yields measured in the high-pressure wire-mesh reactor and weight-loss values predicted by the correlation procedure. Despite the wide diversity in the geological origins of the samples, the calculation procedure was shown capable of estimating the pyrolysis volatile yields of 'unknown' coals once their FT-IR spectra had been recorded and classified within the 'library' of spectra. The level of agreement suggests that the initial structures of coals, as reflected in their infrared spectra, relate closely to their pyrolytic behaviour. The method used in this work thus seems appropriate for estimating, for example, volatile matter yields of 'unknown' power-station coals under pf-combustion conditions. The procedure would require acquiring a complete set of FT-IR spectra and total volatile yields from pyrolysis experiments in a wire-mesh reactor, as the 'calibration' set. The pyrolysis runs would need to be done at atmospheric pressure, probably at some temperature close to 1500°C.

As in the case of the maceral-based correlation discussed in the previous section, however, the predictive value of the correlation procedure for conversions in CO_2-gasification experiments was poor (Fig. 4.22B). Judging by this set of results, measuring FT-IR spectra of coals does not appear as a viable route for reliably predicting CO_2-gasification reactivities. Experimentally, the major part of the actual gasification process takes place between the reactive gas and the post-pyrolysis char. Several char properties relevant to gasification, such as surface area, porosity, the chemical composition and the occurrence of active sites, are all fixed during the intervening

Table 4.9 Total volatile yields from pyrolysis and CO_2-gasification experiments in the wire-mesh reactor and calculated 'extents of gasification'

Coal	Total volatile yields (Pyrolysis in He) (% w/w, daf basis)	Total volatile yields (Gasification in CO_2) (% w/w, daf basis)	'Extent of gasification' TV (gas) – TV (pyr) (% w/w, daf basis)
Taff Methyr (UK)	14.3	16.0	1.7
Tilmanstone (UK)	20.4	24.4	4.0
Emil Mayrisch (Germany)	20.7	22.5	1.8
Santa Barbara (Spain)	37.9	54.9	17.0
Heinrisch Robert (Germany)	31.6	40.3	8.7
Upper Freeport (USA)	35.6	55.5	19.9
Candin (Spain)	40.9	49.8	8.9
Point of Ayr (UK)	41.8	48.5	6.7
Thoresby (UK)	42.2	49.7	7.5
WAI (Australia)	20.7	32.5	11.8
Hemheath (UK)	44.2	81.0	36.8
Bentinck (UK)	42.6	56.6	14.0
Pittsburgh No. 8 (USA)	47.5	58.8	11.3
Lewiston-Stockton (USA)	44.6	75.1	30.6
La Jagua (Colombia)	43.8	57.7	13.9
Gedling (UK)	44.0	49.5	5.5
Linby (UK)	45.9	95.6	49.7
WA2 (Australia)	41.2	52.7	11.5
Blind Canyon (USA)	50.9	74.3	23.4
Illinois No. 6 (USA)	49.2	100.0	50.8
Illinois No. 6 (SBN)	48.1	100.0	51.9
Fording Genesse (Australia)	39.7	82.1	42.4
Gardanne (France)	58.3	82.0	23.7

Source: Reprinted with permission from Zhuo, Y., Lemaignen, L., Chatzakis, I.N., Reed, G.P., Dugwell, D.R., Kandiyoti, R., 2000b. Energy Fuels 14, 1049. Copyright 2000 American Chemical Society.

pyrolytic stage. The original properties of the coal are thus inevitably mediated by the chemistry and physics of the intervening pyrolytic step. In fact, the poor correlation of Fig. 4.22B suggests that the intervening pyrolytic step played the predominant role in determining the gasification reactivity of the chars. When the same FT-IR based method was used to probe the relationship between extents of gasification and mineral matter types and amounts, once again, no systematic trends could be found (Lemaignen et al., 2002).

Table 4.10 Total volatile yields from pyrolysis and CO_2-gasification experiments in the fixed-bed ('hot-rod') reactor and calculated 'extents of gasification'

Coal	Total volatile yields (pyrolysis in He) (% w/w, daf basis)	Total volatile yields (gasification in CO_2) (% w/w, daf basis)	'Extent of gasification' TV (gas) – TV (pyr) (% w/w, daf basis)
Taff Methyr (UK)	4.4	16.3	2.3
Tilmanstone (UK)	19.1	56.8	37.7
Emil Mayrisch (Germany)	17.5	21.8	4.3
Santa Barbara (Spain)	52.9	70.3	17.4
Heinrisch Robert (Germany)	25.0	90.7	65.7
Candin (Spain)	35.2	83.6	48.4
Point of Ayr (UK)	33.7	36.9	3.2
Thoresby (UK)	37.3	80.0	42.7
Hemheath (UK)	36.5	65.8	29.3
Bentinck (UK)	36.3	85.1	48.8
Longannet (UK)	37.3	37.9	0.6
Rietspruit (S. Africa)	34.5	60.9	26.4
Gedling (UK)	40.8	45.3	4.5
Linby (UK)	39.1	40.5	1.4
Daw Mill (UK)	40.0	45.1	5.1
Gardanne (France)	31.0	74.6	43.6

Source: Reprinted with permission from Zhuo, Y., Lemaignen, L., Chatzakis, I.N., Reed, G.P., Dugwell, D.R., Kandiyoti, R., 2000b. Energy Fuels 14, 1049. Copyright 2000 American Chemical Society.

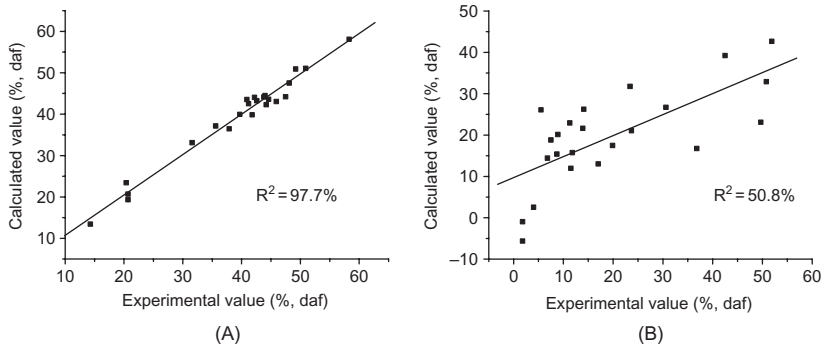

Figure 4.22 (A) Regression for pyrolysis total volatile yields; (B) Regression for the extents of gasification. All data from the high-pressure wire-mesh reactor.
Source: Reprinted with permission from Zhuo, Y., Lemaignen, L., Chatzakis, I.N., Reed, G.P., Dugwell, D.R., Kandiyoti, R., 2000b. Energy Fuels 14, 1049. Copyright 2000 American Chemical Society.

Correlation with data from the fixed-bed ('hot-rod') reactor: Similar correlations were attempted between the FT-IR spectra of a subset of 16 of the coals (Table 4.10) and their pyrolysis and gasification conversions determined in a fixed-bed ('hot-rod') reactor (Zhuo et al., 2000b). That the resulting correlation for gasification would be poor was to be expected. However, the correlation for pyrolysis total volatile yields was also quite poor, giving a correlation coefficient value of 56.6% when using pyrolysis data from the fixed-bed ('hot-rod') reactor, compared to 97.7% calculated when using the wire-mesh reactor pyrolysis data. This result provides a large measure of justification for insisting on developing pyrolysis reactor configurations where product distributions are measured with as little interference as possible from reactor-related effects. This interpretation suggests, furthermore, that the statistical procedure used in this work is capable of leading to predictions of coal pyrolysis yields that may be perceived as physically meaningful.

Conclusion: It is clearly possible to correlate the pyrolysis behaviour of coals with their maceral contents and the pyrolysis yields of their constituent macerals. Useful correlations have also been established between pyrolysis yields of coals and their FT-IR spectra. It would appear that original sample properties allow a level of prediction for weight loss during pyrolysis (total volatiles). However, the outcomes of the 'char gasification' stage could *not* be successfully correlated with the properties of the original coals. It seems facile to say that char gasification reactivities appear dependent on the characteristics of the *char*, rather than those of the original coal. Unfortunately, we have only a superficial grasp of how the intervening pyrolytic process affects the gasification reactivity of the ensuing chars.

4.7 Case studies: simulating entrained-flow gasification in a wire-mesh reactor

There are relatively few bench-scale experimental studies in the literature on the assessment of coal performance under entrained flow gasification conditions. Mamori et al. (1998) used an entrained-flow ('drop-tube') reactor at temperatures up to 1600°C. Other work has focused on pilot-scale rigs and their mathematical modelling (Brown et al., 1988; Hara et al., 2002).

In the first decade of the millennium, the Thermal Power Research Institute (Xi'An, Shaanxi Province, PRC) developed a novel pilot-scale, dry-feed, high-temperature, high-pressure gasifier (Ren et al., 2004). This was done in accordance with the strategic objectives of the Chinese government, and aimed to develop dry-feed entrained flow gasification systems as a component of their new power generation technologies. In this section, we will outline the modification of the high-pressure wire-mesh reactor for operation at temperatures up to 2000°C and pressures up to 30 bars. The aim was to characterize coal particle behaviour under conditions relevant to entrained-flow gasification and to determine the relative reactivities of a set of fourteen Chinese coals, likely to be used for fuelling this and similar gasifiers (Peralta et al., 2004; Wang et al., 2005). The work was carried out within the framework of collaboration with TPRI, supported by the UK and Chinese governments.

4.7.1 Extending the temperature range of the high-pressure wire-mesh reactor

Upgrading the wire-mesh reactor for operation at up to 2000°C and 30 bars required only a minor overhaul of the temperature control instrumentation. The pairs of Pt-PtRh thermocouples used up to about 1500°C were replaced with thermocouples resistant to higher-temperatures. The 'type D' thermocouples used were alloys of 97% tungsten with 3% rhenium and 75% tungsten with 25% rhenium, usable up to 2400°C. The materials harden at the highest temperatures; this need not cause difficulties, so long as fresh thermocouples are used in each experiment. New ports for the new set of thermocouples were installed on the reactor controllers together with the corresponding thermocouple calibration data. In helium, the wire-mesh made of pure molybdenum wire could withstand temperatures up to 2000°C without physical damage or alteration. However, in CO_2, the mesh became brittle near 2000°C. At these higher temperatures, the holding time could be reduced without altering weight loss; this helped to protect the integrity of the mesh.

At temperatures approaching 2000°C, conversions during CO_2-gasification quickly ran to completion (~100%), which was not very informative. When operating in CO_2, therefore, the peak temperature was reduced to 1500°C, which also helped preserve the integrity of the mesh. A 2-mm thick alumina sheet was used to prevent the mesh from contacting the brass support plate and avoid short circuits.

The heating rate used in this work was normally 1000°C s^{-1}. In entrained flow gasifiers, rates are usually calculated to reach higher values. However, previous work with the wire-mesh reactor has shown that changes in heating rates above 1000°C s^{-1} do not significantly affect volatile release. Experiments at 1000°C s^{-1} to 2000°C and pressures between 10 and 30 bars were nevertheless difficult to conduct. Their successful completion reflects the considerable potential of the wire-mesh configuration for studies under variable and, at times, extreme reaction conditions.

4.7.2 Gasification reactivities of a set of Chinese coals

Pyrolysis of the set of coals: Table 4.11 presents the compositions of the set of coal samples used in the study. They ranged from 75.3% (Niemeng) to 92.9% (Yangquan) elemental carbon content with proximate analysis volatile matter contents ranging from the mid-forties down to 9.7%.

The pyrolysis data for 1500°C and 2000°C under 30-bar helium (1 s hold time) are presented in Table 4.12. For some of the coals, there were also significant differences between weight loss at 1500°C and 2000°C. It is known that decomposition and volatilisation of mineral matter in coals begins around 500°C with the escape of water of crystallisation from kaolin and similar components (Taupitz, 1977). Weight loss from mineral matter could be significant at the higher temperatures, particularly since some of the coals contained up to 30% mineral matter. In one case (No. 9; Huating), the mineral matter content reached nearly 40%. The magnitude of the effect normally varies with the composition of the mineral matter. Analogous weight loss experiments have not been run with low temperature ashes to gauge the magnitude of this effect.

Table 4.11 **Compositions of the set of Chinese samples used in the study**

	Sample No.													
	1	**2**	**3**	**4**	**5**	**6**	**7**	**8**	**9**	**10**	**11**	**12**	**13**	**14**
Moisture (% ar)	3.7	3.6	7.6	4.0	7.4	6.2	1.4	9.8	1.1	11.1	1.2	2.0	1.2	0.9
Ash (% db)	15.5	14.4	8.5	8.8	8.0	5.8	29.0	5.9	39.7	12.1	30.0	21.0	28.5	14.3
Volatile matter	44.8	37.2	37.8	31.2	33.3	35.2	23.0	37.5	24.8	42.8	23.4	36.3	34.4	9.7
C	80.4	82.6	79.8	82.4	80.1	80.0	85.2	79.4	78.3	75.3	82.7	85.5	87.0	92.9
H	5.3	4.9	4.7	4.3	4.1	4.4	4.6	4.8	4.2	4.2	4.2	5.1	5.2	3.4
N	1.4	1.5	1.1	0.8	0.8	0.9	1.2	1.0	1.5	1.0	1.1	1.4	1.6	1.5
S	5.0	0.7	0.5	1.2	0.6	0.5	0.6	0.4	1.3	0.3	1.3	0.8	0.6	1.6

Source: Reprinted with permission from Wang, B., Li, X., Xu, S., Paterson, N., Dugwell, D.R., Kandiyoti, R., 2005. Energy Fuels 19, 2006. Copyright 2005 American Chemical Society.
ar, as received; *db*, dry basis; all other data on dry ash free basis. 1, Yanzhuo Beishu; 2, Yanzhuo Yangchun; 3, Shen-Hua Houjitu; 4, Datong mixed; 5, Wujialu; 6, Shen-Mu mixed; 7, Shanxi Beigou; 8, Shen-Mu Daliuta; 9, Huating; 10, Neimeng; 11, Jiangyu; 12, Huangling; 13, Pingdingshan; 14, Yangquan

Table 4.12 **The Performance of the suite of coals in the wire-mesh reactor**

		Carbon content (%, daf)	Pyrolysis 1500°C, 30 bar (%, daf)	Pyrolysis 2000°C, 30 bar (%, daf)	Volatile matter (%, daf)	Gasification 1500°C, 20 bar (%, daf)	Gasification 1500°C, 30 bar (%, daf)	Extent of gasification 1500°C, 30 bar (%, daf)
1	Yanzhuo Beishu	80.4	53.1	61.3	44.8	94.9	99.2	46.1
2	Yanzhuo Yangchun	82.6	48.8	51.9	37.2	85.4	88.6	39.8
3	Shen-Hua Houjitu	79.8	46	51.8	37.8	80.3	83.5	37.5
4	Datong mixed	82.4	40.1	43.1	31.2	62.2	69.3	29.2
5	Wujiala	80.1	44.6	46.2	33.3	89.7	93.2	48.6
6	Shen-Mu mixed	80	43.9	47.1	35.2	81.7	83.4	39.5
7	Shanxi Beigou	85.2	29.2	50.3	23	59.6	71	41.8
8	Shen-Mu-Daliata	79.4	49.4	50.7	37.5	81.9	85.5	36.1
9	Huating	78.3	33.3	54.9	24.8	78.1	88.7	55.4
10	Neimeng	75.3	58.8	59.8	42.8	100.9	103.2	44.4
11	Jiangyou	82.7	30.9	49.7	23.4	66	74.6	43.7
12	Huangling	85.5	44.8	54.7	36.3	71.8	83.2	38.4
13	Pingdingshan	87	44.6	65.5	34.4	76.1	82.8	38.2
14	Yangquan	92.9	18	22.2	9.7	31.5	36.2	18.2

Source: Reprinted with permission from Wang, B., Li, X., Xu, S., Paterson, N., Dugwell, D.R., Kandiyoti, R., 2005. Energy Fuels 19, 2006. Copyright 2005 American Chemical Society.

Table 4.12 shows that weight loss from the set of coals during pyrolysis at 1500°C varied widely, between 20% and 60%, broadly according to the rank ordering of the set of samples. However, after pyrolysis at 2000°C, the rank ordering of sample weight loss was no longer discernible. At these higher temperatures, weight loss from the mineral matter would be expected to come into play as an interfering variable.

Gasification of the set of Chinese coals in CO_2: 'Extents of gasification' have been estimated for each coal by subtracting volatile yields, measured during pyrolysis runs in He, from the total volatile yields determined during experiments in CO_2. Weight loss values for CO_2-gasification experiments at 1500°C and 30 bars are presented in the final column of Table 4.12.

The pyrolysis experiments were run with a hold time of 1 s, whereas the gasification data were obtained with a hold time of 0.5 s. Initial tests in CO_2, done with a hold time of 1 s at 1500°C showed near complete conversion, which made it difficult to differentiate between the relative reactivities of the set of samples. Reducing the hold time to 0.5 s decreased the conversion and enabled differences between coals to be observed. A limited number of pyrolysis tests were repeated with a 0.5 s hold time, to check that it was valid to use the 1 s pyrolysis data set in the estimation of the extent of gasification after 0.5 s. The data obtained in He, at the shorter hold times, were virtually identical to that measured at 1 s and indicated that pyrolysis was completed in less than 0.5 s, when samples are heated to these very high temperatures.

For this set of samples, the values for the extent of gasification, shown in Table 4.12, were in a range from 18% to 55%. Fig. 4.23 shows the extent of gasification plotted as a function of elemental carbon content, on a dry, ash-free basis. The reactivity, as indicated by the extent of gasification, generally decreased with increasing C content, i.e., with increasing rank (maturity) of the coal.

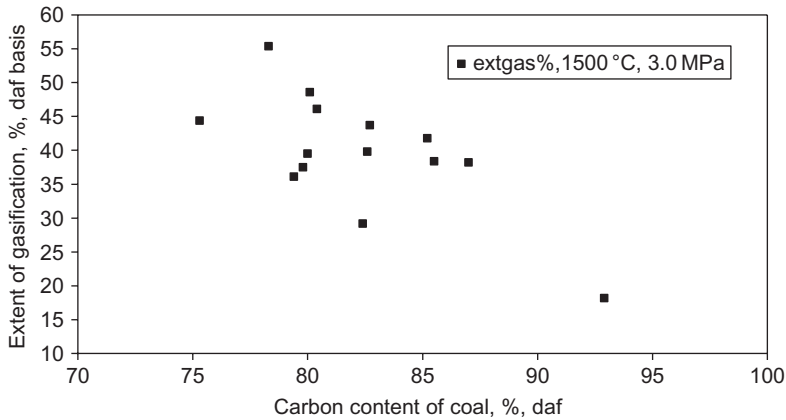

Figure 4.23 The 'extent of gasification' in carbon dioxide as a function of carbon content of the coals.
Source: Reprinted with permission from Wang, B., Li, X., Xu, S., Paterson, N., Dugwell, D.R., Kandiyoti, R., 2005. Energy Fuels 19, 2006. Copyright 2005 American Chemical Society.

While the general trend in Fig. 4.23 is clear, the data did not show the level of coherence needed to provide any hope of serving as a predictive tool. It appears that empirical means will have to be retained for determining the gasification behaviour of unknown coals. As ever, diverse factors could be cited as contributing to the scatter in the data, possibly including the effect of pyrolysis conditions on the distinct mineral matter contents of the coals.

As expected, CO_2-gasification rates at and above 1500°C were sufficiently rapid to gasify much of the coal in the reaction times allowed. As already signalled, coal reactivity is rarely considered an issue in oxygen-blown gasifiers, where complete conversion is achieved provided sufficient residence time is allowed. Meanwhile, the data clearly showed that the residence time in the gasifier that is required for complete conversion will vary with the rank of the coal. This has implications for the design of individual power plants, as the capital cost will be determined by the size and throughput of the gasifier. The aim would be to maximize the throughput for the minimum size of gasifier. An understanding of the reactivity of the candidate coal(s) will be needed to optimize the design. The work outlined above indicates that the high-pressure wire-mesh reactor can provide a relatively low cost method for obtaining information that can be used to gain an insight into how candidate coals perform under various conditions.

4.8 Case studies: by-product formation and trace element problems in a pilot gasifier for coal and biomass

4.8.1 Ammonia formation in a pilot-scale air blown spouted-bed gasifier

High concentrations of NH_3 in fuel gas from gasifiers tend to enhance NOx forming reactions during subsequent combustion. In the operation of the pilot British Coal 'ABGC' gasifier, NH_3 concentrations in the product gas were found to be high, variable and worse, difficult to predict. The removal of NH_3 from fuel gas prior to combustion is technically feasible, but imposes an efficiency penalty on the process. The preferred alternative is to suppress NH_3-formation. That, in turn, required investigating the chemical pathways and reaction conditions conducive to its formation and decomposition.

Open-ended investigations in pilot-plant scale equipment can be expensive, while bench-scale work lends itself to examining reaction parameters in isolation; experiments can be done quickly and relatively inexpensively.

4.8.2 Re-designing the fluidised-bed for semi-continuous operation

In order to clarify mechanisms and assess the impact of individual reaction parameters on NH_3 concentrations in the fuel gas, the laboratory-scale high-pressure fluidised-bed reactor described in Section 4.3 was converted from batch to semi-continuous operation.

The changes to the design and operating procedures of the high-pressure fluidised-bed reactor system have been described by Paterson et al. (2002) and Zhuo et al. (2002).

Although the commercial-scale gasifier planned by British Coal was intended for operation in the 20–25 bar range, conditions in the pilot gasifier were typically 950°C and 13 bars. The 'NH_3-project' undertaken in the bench-scale reactor mimicked conditions in the 200 kg h^{-1} pilot reactor, to compare results between the two systems. Since the gasifier contains oxidising and reducing zones, the nitrogen chemistry in both types of environments had to be considered.

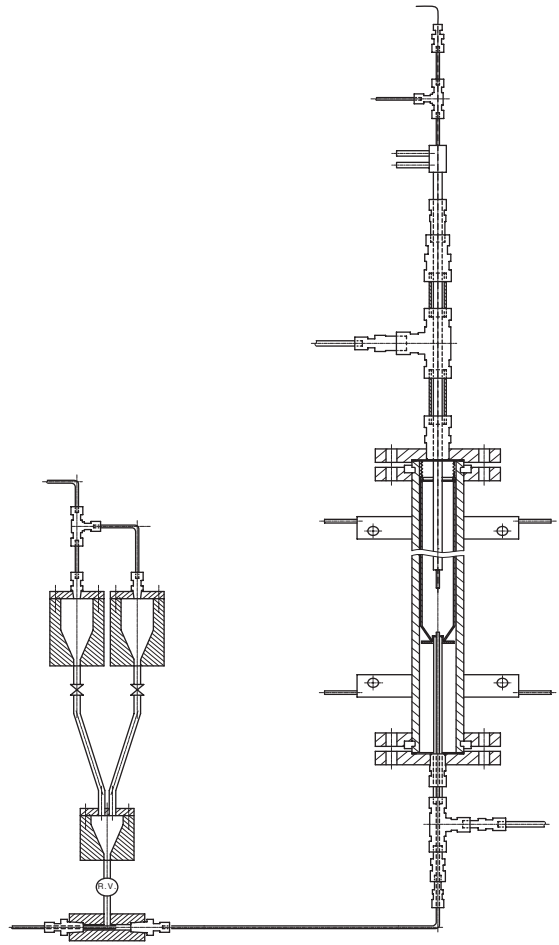

Figure 4.24 Schematic diagram of the continuous sample injection system and the high-pressure fluidised-bed reactor after reconfiguring the system as a semi-continuous, bench-scale spouted bed reactor.
Source: Reprinted with permission from Paterson, N., Zhuo, Y., Dugwell, D.R., Kandiyoti, R., 2002 Energy Fuels 16, 127. Copyright 2002 American Chemical Society.

Fig. 4.24 presents a schematic diagram of the reconfigured reactor system capable of semi-continuous operation. As before, the main body consisted of a 34 mm (i.d), 504 mm tall Incoloy 800 HT tube that served as both pressure shell and resistance heater. Unlike the batch-mode operated bubbling-fluidised bed, the semi-continuous version of the reactor did not make use of a support plate. Instead, the design of the 28 mm (i.d.) quartz liner was altered to have a conical base, with a hole in the bottom to admit the spout jet. The steep angle of the cone was similar to that of the base of the pilot scale gasifier. The coal and spout gas were fed by means of a spout jet, which fitted into the hole at the base of the quartz cone. This configuration was intended to qualitatively reproduce the hydrodynamic behaviour inside the pilot scale gasifier.

The feeding system continuously delivered 1–4 g min^{-1} solids to the reactor, which was operated at temperatures up to 980°C and 30 bars. The system was capable of operating for periods of up to about 30 min before ash sintering at the base interrupted experiments. A sampling probe was installed and attached to the top flange to draw gas samples directly from the spout jet. The probe also housed the exit tube, conveying gas from the reactor through a redesigned cooling section equipped with tar and steam traps. The gas stream was then passed through a small cartridge filter to collect the remaining particulates and exited through a needle valve, used for pressure letdown. As a safety measure, a small incinerator was installed to combust exit gases and vent into the laboratory extraction system. Details of the steam generator unit, fuel gas cleaning and analysis stages and the gas incinerator have been described in the original publications (Paterson et al., 2002; Zhuo et al., 2002).

Feeding the reactor: Fig. 4.24 shows the twin fuel hoppers, with capacities of 60 g of sample, each, feeding into a common hopper. The steep angles of the conical bases were intended to assist slippage and avoid bridging of fuel particles. The hopper and metering valve assembly were mounted on a frame that was vibrated by an eccentric motor, to prevent the bridging of fuel particles inside the hoppers. Before a run, the hoppers were pressurized with nitrogen to approximately 0.2 bars above the reactor pressure. From the common hopper, fuel was fed through to the feeding line by means of a calibrated metering valve, driven by a variable speed DC motor. The metered fuel fell into an ejector, through which, the spout-gas mixture (air/nitrogen) was passed at high velocity. This entrained the fuel and conveyed it through a 1.5 m long, 2 mm (i.d.) line to the spout jet at the base of the gasifier.

The thermocouple and the sampling probe: The sampling probe was designed in the form of three concentric tubes (cf. Figure 5 in Paterson et al., 2002). The inner tube served as the gas outlet and thermocouple conduit, while the outer two tubes carried cooling water (or nitrogen) in and out, through a specially designed head. The height of the probe gas inlet above the spout could be changed between tests, by drawing the tube in or out, when assembling the top flange. Gaseous components analysed included CO, O_2, NH_3 and NO. The amounts of collected NH_3 were determined by ion chromatography; the instrument measured NH_4^+ ion concentrations with a reproducibility of ±2% of the measured value.

The spout-gas temperature was measured using a thermocouple placed down the centreline of the gas-sampling probe, with its tip projecting into the bed by some

5 mm. The design of the top flange and of the spout-gas analysis probe allowed vertical movement between experiments and served to extract gas samples from different heights within the submerged spout jet. It is in this region that the pyrolysis of fresh coal takes place alongside volatile and char combustion, releasing process heat. This is also where nitrogen oxides can potentially form from fuel nitrogen.

4.8.3 Operation of the bench-scale spouted-bed gasifier

Sand had been previously used as bed solids during batch operation, but would not have realistically mimicked the high carbon content of the bed in the British Coal ABGC pilot gasifier. Using char from the pilot reactor was considered and rejected, as the sorbent content would have affected NH_3 release. Calcium oxide and its precursors have been noted to catalyse the formation of both NO_x and NH_3 under conditions relevant to the gasifier (Lin and Johnssen, 1993). Not enough Daw Mill char was available to use as bed material. A low volatile content fuel was necessary for startup, in order to avoid the release of tar and other volatiles during heatup. In the event, it was decided to use a mixture of crushed 'Coalite' (a commercially available 'smokeless fuel') and sand. Coalite has a residual volatile matter content of about 9%, most of which would have been driven off during the start-up sequence.

Reaching gasification temperatures: Due to the continuous input of cold gas, electrical power input was only sufficient to heat the reactor assembly to approximately 750°C at 13 bars. Instead of revamping the power supply, it was found that additional heat generation by combustion in the bed would allow operation at up to 950°C. Accordingly, after the temperature reached a plateau between 700°C and 800°C by electrical heating alone, the fluidising gas composition was changed to approximately a 20% air/80% N_2 mixture. The coal feed was then turned on and the rate adjusted to the desired value using the speed control of the calibrated valve.

In the laboratory-scale reactor, the fuel particle size was in the 200–300 μm range and the superficial fluidising velocity adjusted to between 0.1 and 0.2 m s^{-1}, compared with values of up to 3000 μm and 0.8 m s^{-1} in the pilot-scale gasifier, respectively. The durations of experiments were, typically, between 10 and 15 min. The gas in the spout, as well as the flue gas downstream of the gasifier, were analysed. Reactor stability was monitored by plotting CO_2, CO and H_2S concentrations in the exit gas against time. Due to the small diameter of the reactor, it was not possible to fit a char off-take through the base, so that bed material built up in the gasifier during the test. Some sinter eventually formed on the base during most tests, blocking the spout entry and limiting the maximum run time to less than 30 min. Less sinter formed when steam was used as part of the fluidising gas (Zhuo et al., 2002).

4.8.4 Nitrogen chemistry in the fluidised-bed

When fresh coal is injected into the spout jet of a gasifier, fuel nitrogen–derived pyrrolic and pyridinic compounds are released alongside other pyrolysis volatiles (Burchill and Welch, 1989). At temperatures above 900°C and under fuel rich conditions prevailing in the spout, fuel nitrogen–derived compounds break down, releasing

primarily HCN and smaller quantities of NH_3 (Baumann and Moller, 1991; Kanbara, et al., 1993). The escape of volatiles from fuel particles is normally retarded by the effect of elevated pressures. In fuel-rich conditions, this gives time for the primary HCN produced to be converted to NH_3, through reaction with the hydrogen released during pyrolysis. The proportions of HCN and NH_3 thus depend on the type of reactor used and the conditions of the test. Not all of the fuel-N is released from coal by pyrolysis and the balance (somewhere between 40% and 60% of the initial total) remains embedded within the char structure.

The NH_3 and HCN from pyrolyzing particles are released first into the oxidising environment of the spout and then into reducing environments in the bubbling fluidised bed section above the spout and the reactor freeboard. In the oxidising conditions of the spout, NH_3 and HCN can be oxidized to NO_x and N_2O. HCN oxidation is more efficient at forming N_2O (Hulgaard, 1993). In the spout jet, char-N is thus converted to NO_x, N_2O or N_2. Increasing the pressure increases the N_2O/NO ratio (Haemaelaeinen and Aho, 1996). Increased amounts of N_2O have also been noted in the transition region between oxidising and reducing conditions (Hulgaard, 1992). The NO_x and N_2O formed from char-N compounds are then reduced under the reducing conditions of the bubbling fluidised bed above the spout, to form N_2 or NH_3.

In the fluidised bed, the NH_3 concentration tends toward gas-phase equilibrium according to the reaction, $2NH_3 \leftrightarrow N_2 + 3H_2$. Thermodynamic modelling studies by British Coal have shown that supra-equilibrium NH_3 concentrations were still present in the fuel gas at the point of measurement outside the pilot scale gasifier (Duxbury and Gavin, 1994). This is consistent with other studies (Kilpinen et al., 1991) and shows that equilibrium cannot be reached in the residence times allowed (up to 10 s) inside the reactor. Meanwhile, during the gasification of the residual char, char-N may be released either as N_2 or as NH_3.

NH_3 production in the bench-scale spouted-bed gasifier: When using fluidising gas mixtures of air/N_2, the NH_3 concentrations in the exit gas may be interpreted in terms of the breakdown of volatile fuel nitrogen–derived compounds. Between 35% and 45% of the fuel nitrogen was found in the chars recovered after the experiments.

Table 4.13 shows that the addition of steam resulted in large increases in the NH_3 concentration of the exit gas, compared with operation in mixtures of air/N_2. The amounts of nitrogen in the ammonia were greater than the nitrogen content of *evolving volatiles*. Thus, much of the new NH_3 appears to have been formed by reaction with char-N. The formation of excess NH_3 from char-N in the presence of steam, probably by combining with hydrogen from steam decomposition, was reproducible. A significant effect of steam to form ammonia had not been anticipated in these experiments, even though, the reactivity of char-N in the presence of high-pressure hydrogen had been noted during earlier hydropyrolysis experiments (Wu et al., 1993).

The effect of steam on the char bed was examined further by varying the proportion of inlet steam during tests with a Coalite char bed, in the absence of added coal. The amount of input steam was varied from 0% (Test 61) to 10% (Test 56) and 16% (Test 55) by volume. The amount of NH_3 increased from 50 to 2300 vpm (volume parts per million) over this range of steam injection. Table 4.14 presents nitrogen contents of selected residual char beds, from experiments where coal was used as

Table 4.13 The effect of steam input, operating temperature and coal/air ratio on NH_3 concentrations in the product gas

	Test no.	Percent steam (by vol)	Pressure bar[a]	Cool feed rate (g min^{-1})	Coal: air ratio (mass)	Temperature (°C)	Dilution factor	NH_3 (adjusted for dilution by N_2) vpm, average
No Coal feed	61	0	12.5	0	–	850	6.06	49
	56	10.1	13.2	0	–	860	2.84	1297
	55	16.4	13.0	0	–	890	2.36	2294
Effect of percent steam	48	6.0	13.3	2.1	0.32	795	2.59	2820
	62	14.3	13.1	2.2	0.28	800	2.21	5131
Effect of temperature	48	6.0	13.3	2.1	0.32	795	2.59	2820
	43	6.1	12.6	2.0	0.25	837	2.20	1460
Effect of coal:air	43	6.1	12.6	2.0	0.25	837	2.20	1460
	49	6.5	13.5	2.2	0.46	841	3.10	3720
	47	6.3	13.6	2.2	0.80	830	4.78	5290

Source: Reprinted with permission from Zhuo, Y., Paterson, N., Avid, B., Dugwell, D.R., Kandiyoti, R., 2002. Energy Fuels 16, 742. Copyright 2002 American Chemical Society.
[a]Data corrected for start-up NH3 formed fresh Coalite bed. Gas analysis adjusted for dilution by N_2.

Table 4.14 Nitrogen concentrations in final bed chars

Test no.	Fluidising gas (% vol)	N concentration in final bed char (%wt)
37	Air/N_2	0.8
39	Air/N_2	1.0
48	Air/N_2/steam (6%)	0.7
62	Air/N_2/steam (14%)	0.4

Source: Reprinted with permission from Zhuo, Y., Paterson, N., Avid, B., Dugwell, D.R., Kandiyoti, R., 2002. Energy Fuels 16, 742. Copyright 2002 American Chemical Society.

Table 4.15 Proportions of NH_3 formed by pyrolysis and from char nitrogen

Test no.	Coal:air ratio (mass)	Steam addition % vol	Measured NH_3 vpm (% of total NH_3 during tests with steam)	Difference in NH_3 (with steam-without steam), vpm (% of total NH_3)
43	0.25	6.1	1460 (100)	1173 (80)
18	0.24	0	287 (20)	
49	0.45	6.5	3720 (100)	2336 (63)
19	0.45	0	1384 (37)	

Source: Reprinted with permission from Zhuo, Y., Paterson, N., Avid, B., Dugwell, D.R., Kandiyoti, R., 2002. Energy Fuels 16, 742. Copyright 2002 American Chemical Society.

the feed. The data showed that the presence of steam caused a sharp reduction in the nitrogen contents of bed chars. This finding tends to confirm that steam was instrumental in removing nitrogen from the char.

The complexities of starting operations with a Coalite bed have been detailed in the original publications (Paterson et al., 2002; Zhuo et al., 2002). However the overall effect of added steam on enhancing NH_3 formation, and in particular, its preferential reaction with char nitrogen was clear. Detailed mechanisms of these reactions are of interest and should be studied in further work.

Taken together, these data show that during tests with steam, NH_3 in the exit gas may be formed from both the breakdown of pyrolysis volatiles and from char-N. The proportion of total NH_3 formed via each of these routes can be assessed from the results of tests, with-and-without steam addition (Table 4.15). The table shows data from tests with coal:air ratios of 0.25 and 0.45. The NH_3 content measured at the reactor exit was found to increase substantially as the coal:air ratio was increased during tests in air/N_2. The NH_3 content was also found to increase sharply in air/N_2/*steam* mixtures. Assuming that primary decomposition mechanisms remained unaltered by the presence of steam,

Table 4.16 Ammonia produced in the Daw Mill coal char beda

Test no.	Percent steam (vol)	Coal:air ratio	Temperature (°C)	Pressure (bar)	NH_3(vpm)
80	9.0	0.65	813	13.4	3475
82	14.2	0.72	825	13.7	3617
49	6.5	0.46	841	13.5	4249

Source: Reprinted with permission from Zhuo, Y., Paterson, N., Avid, B., Dugwell, D.R., Kandiyoti, R., 2002. Energy Fuels 16, 742. Copyright 2002 American Chemical Society.

it was calculated that the total NH_3 formed by pyrolysis (i.e., released in the absence of steam) rose from 20% to 37% as the coal:air ratio was raised. The amount of NH_3 formed from char-N by the action of steam also increased with the coal:air ratio.

The data indicated that, during runs with steam in the air blown gasifier, the majority of the NH_3 detected was produced by the interactions of steam with char-N.

In another set of experiments, evidence was sought to confirm how char-N content affected the amount of NH_3 formed. First, Daw Mill coal char was prepared by using the fluidised-bed reactor in pyrolysis mode. Gasification experiments were run using Daw Mill coal as the *feed coal*, but with the fluidised-bed containing either (1) Daw Mill coal *char* as starting bed material (Test numbers 80 and 82 in Table 4.16), or, (2) Coalite as the initial bed material (Test number 49 in Table 4.16).

The Coalite used as initial bed material contained 2% nitrogen and Daw Mill coal char contained 1.1% nitrogen. The Daw Mill coal char bed thus contained less char-N than the Coalite char bed. Each initial bed contained a similar weight of char, although the Coalite char was mixed with an equal weight of sand.

Table 4.16 indicates that the experiments with the coal char bed were run with a higher coal:air ratio and with a higher proportion of steam in the fluidising gas: Runs No. 80 and 82, respectively. Both the higher coal:air ratio and the higher proportion of steam would have tended to raise the amount of NH_3 formed. However, the data in Table 4.16 clearly showed that NH_3 releases from the Daw Mill coal char bed were lower than what was observed with the Coalite char bed. This result confirms that char-N levels have a definite influence on the amounts of NH_3 formed during the steam gasification of coal.

The effect of temperature on NH_3 emissions: Pilot-plant scale tests normally require a significant amount of logistical preparation. By contrast, laboratory-scale experiments can be quick and may be staged at relatively low cost. It is usually possible to alter reaction conditions rapidly and track the physical and chemical transformations taking place in response to changes in selected reaction parameters.

The effect of temperature on NH_3 production during gasification was studied in the high-pressure spouted/fluidised-bed between 850°C and 980°C, in the presence of a sorbent, at a nominal pressure of 13 bars and a coal:air ratio of 0.3. Fig. 4.25 shows the NH_3 concentration measured at the exit of the bench-scale fluidised-bed and the NO concentration in the spout, as a function of temperature. The NH_3 concentration peaked

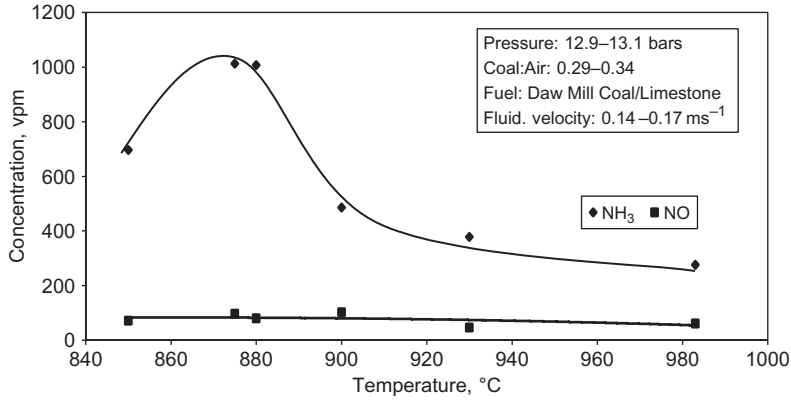

Figure 4.25 NH_3 concentration in the exit gas and the NO concentration in the spout as a function of the temperature, in the presence of sorbent.
Source: Reprinted with permission from Zhuo, Y., Paterson, N., Avid, B., Dugwell, D.R., Kandiyoti, R., 2002. Energy Fuels 16, 742. Copyright 2002 American Chemical Society.

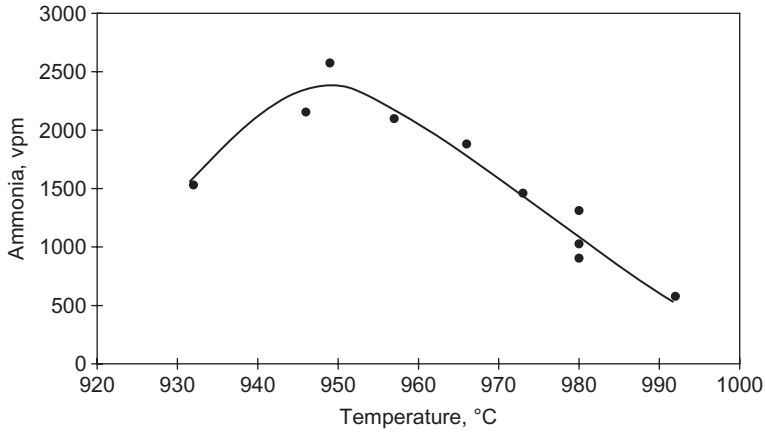

Figure 4.26 The effect of temperature on the ammonia concentration in the fuel gas from the pilot scale gasifier.
Source: Reprinted with permission from Zhuo, Y., Paterson, N., Avid, B., Dugwell, D.R., Kandiyoti, R., 2002. Energy Fuels 16, 742. Copyright 2002 American Chemical Society.

at approximately 880°C, indicating the temperature where the rates of NH_3-formation and destruction reactions were evenly balanced. It would seem that, as the overall composition tended toward gas phase equilibrium values, NH_3 decomposed into N_2 and H_2.

Fig. 4.26 shows the analogous peak in NH_3-concentration in the pilot scale reactor, confirming that trends observed in the bench-scale reactor reflected findings in the much larger gasifier. However, in the pilot-scale gasifier, the peak occurred at approximately 940–950°C. The difference was attributed to the manner of temperature measurement in the pilot-scale gasifier, which was averaged from numerous readings

obtained by several thermocouples, set at different points throughout the bed, over an approximately 24-h mass balance period. By contrast, the value for the laboratory scale reactor was calculated as the average of readings from a single thermocouple over a 10–15 min test period. The latter is likely to reflect the temperature at which NH_3-production and destruction reactions were balanced more accurately.

Summary: In addition to showing sharply rising NH_3 concentrations with increasing steam input, the bench-scale study allowed testing for the effect of several operating parameters on NH_3 formation: char-N content, reactor temperature and coal: air ratio (Paterson et al., 2002; Zhuo et al., 2002). The effect of sorbent addition was discussed in the original publications. In air and oxygen blown gasifiers, steam is used mainly to control the temperature of the bed – since the carbon-steam reaction is endothermic. However, in air-blown gasification, steam injection was observed to lead to rising NH_3 concentrations in the product gas. The main control options to limit NH_3 concentrations in the product stream appear to revolve around the use of an alternative method of bed temperature control. This can be done by accepting higher bed temperatures, with the limit set by ash melting, or by operating at lower pressures within limits set by efficiency considerations for power generation in the downstream gas turbines.

4.8.5 HCN and NH_3 formation during sewage sludge gasification

Analogous data on HCN formation during coal and sewage sludge gasification in the same reactor have been presented by Paterson et al. (2005). In order to identify the effects of temperature and steam on HCN and NH_3 concentrations in the exit gas, dried sewage sludge pellets were gasified in air/N_2 and air/steam/N_2 mixtures. Consistent with the work outlined above, higher concentrations of NH_3 (and HCN) were observed when steam was introduced into the spout-gas mixture. The mechanism of the effect is not obvious, but gives rise to increasing concentrations of potential NO_x precursors. However, the concentration of HCN showed a somewhat different pattern to that of NH_3 formation.

As mentioned earlier, the bench-scale fluidised-bed reactor has no char discharge facility. Instead, the char bed builds up between the beginning and the end of a particular experiment. During sewage sludge processing runs, HCN concentrations were observed to decrease as the experiment progressed and as the depth of the char bed increased. The growing height of the bed appears to have provided an effective environment for the reaction of HCN to form NH_3. This result was consistent with data obtained in the pilot-scale spouted-bed gasifier, where only low concentrations of HCN were measured in the exit fuel gas, after the longer residence times (~10 s) in the char bed, compared to the laboratory scale reactor.

In bench-scale experiments, the concentration of HCN was observed to go through a maximum at around 930°C and to decrease rapidly thereafter (Paterson et al., 2005; not shown). Tar release from the sample would have peaked at or before about 600°C; the rising edge of the HCN concentration curve with temperature probably reflects the intensity of tar cracking reactions taking place in contact with bed solids. The data showed that above about 930°C, HCN destruction by secondary reactions became

increasingly rapid. Meanwhile, NH_3 formation reactions would be further promoted by the increasing amounts of molecular H_2 liberated through the cracking of sewage sludge tars.

The results from sewage sludge gasification indicate that more complete tar cracking may lead to progressively greater proportions of H_2 in the product gas, possibly surpassing the already observed 25% level (Paterson et al., 2005). In this hydrogen-rich environment, very high (supra-equilibrium) NH_3 concentrations, hovering above 9000 vpm, were observed in the presence of steam, at the relatively low temperatures of about 780°C. From these high values, NH_3 concentrations in the exit gas decreased with increasing temperature, both in the presence and absence of steam injection. This outcome appears to result from faster approach to equilibrium values with rising temperature, effectively decomposing NH_3 to N_2 and H_2. The effect was sufficiently large to have masked the increase in NH_3 formation from HCN at higher temperatures.

The concentration of HCN released during the processing of coal in air/N_2 mixtures was also measured in experiments using the bench-scale spouted bed reactor. These tests required an initial char bed in the reactor (for operational reasons), and consequently, the effect of coal (and coal char) residence time in the char bed on HCN concentration could not be monitored. The concentration of HCN in the exit gas was observed to decrease at temperatures above 900°C. This is thought to be a result of the increased H_2 concentration released by pyrolysis, which would enhance the rate of decay of HCN to NH_3.

The work provided useful insights into the reactions of fuel-N in the gasifier and has helped explain why low HCN concentrations were measured in the raw fuel gas from the British Coal ABGC pilot-scale gasifier. It has also identified the significant parameters that would need tracking in a study of the fundamental aspects of fuel-nitrogen reactions.

4.8.6 Trace elements in output solid streams during sewage sludge gasification

Thermochemical processes have attracted interest from water utilities as likely technologies for disposing of sewage sludge. Its gasification would enable waste volume reduction, destruction of pathogenic bacteria and some energy recovery. However, elements such as Ba, Cu, Hg, Pb and Zn are present in sewage sludges at levels significant to the disposal of the residual solid streams from the gasifier. The behaviour of these elements was studied in the air blown laboratory-scale spouted bed gasifier (Fig. 4.24). The fuel consisted of crushed and dried sewage sludge pellets. Trace element concentrations were measured by ICP-AES to determine (1) the retention of selected elements in the solid streams, (2) their relative depletion from the coarser bed residue and (3) any enrichment of these element in fines carried over to the gas cleaning system. The effect of gasifier bed temperature and type of sewage sludge was also investigated.

The results of the study indicated that gasifier bed temperatures in excess of 900°C enhanced the depletion of Ba, Pb and Zn from the bed residue, and showed their

enrichment in the fines. Mercury and selenium capture required low temperature filters operating below 120°C. It was also found that thermodynamic modelling is not always helpful in predicting outcomes of these experiments, due either to limitations of data-bases and problems arising from kinetic constraints. The system rarely reaches equilibrium. Parallel co-combustion experiments have suggested that the presence of chlorine somewhat enhances the volatility of lead and cadmium (Reed et al., 2005).

4.8.7 Calcium-based liquid phase formation in pressurized gasifier environments

Limestone and dolomite are routinely used for retaining sulphur in air blown fluidised-bed coal/waste gasifiers. An intractable deposit was observed to form at the exit of the British Coal ABGC pilot scale gasifier, when limestone was used as sorbent during initial tests after installing a revised base design. The deposit was found to be enriched in Ca and had formed via a melt, which eventually blocked the exit duct. An attempt was made to simulate the formation of melts by sorbent components under laboratory conditions. The detection of melting was done by impedance spectrometry. The technique measures the change in resistivity during the transition from a non-conducting solid to an ionic melt. The validity of the technique was demonstrated by reproducing melt formation that had previously been observed in the CaO/CO_2/steam system under the conditions of the CO_2-Acceptor Process (e.g., see Curran et al., 1967). SEM/EDX and XRD were used to characterize the residues from the present tests.

Among the solid mixtures tested, $CaCO_3/CaSO_4$ was the only system that formed a melt under the experimental conditions corresponding to the pilot-plant trials. Melt formation was observed at 1010°C at pressures in excess of 13 bars. The melting temperature was not affected by the presence of other Ca compounds (e.g., CaS) that would be present in the gasifier. It is thought that $CaSO_4$ formation occurred when CaS in the recirculating solids stream was exposed to the oxidising conditions in the spout of the gasifier. The melt is thought to have formed by the interaction of $CaSO_4$ with as yet uncalcined $CaCO_3$ sorbent particles. Oxidising sulphided limestone (and dolomite) and raising the temperature to above 1010°C caused a melt to form and demonstrated the probable sequence of reactions in the pilot-gasifier. The properties of the melts produced from limestone and dolomite were different. The results also helped explain why using *dolomite* as sorbent did not give rise to deposits during pilot plant trials (Paterson et al., 2001).

4.9 Case studies: 'zero emission carbon (ZEC)' – gasification in steam-hydrogen mixtures

4.9.1 The 'Zero Emission Carbon (ZEC)' concept

'Zero Emission Carbon (ZEC)' is a power generation scheme for producing hydrogen from coal. The scheme was conceived as part of an effort to use modern combustion technologies and gasification systems to minimize the impact on the environment of

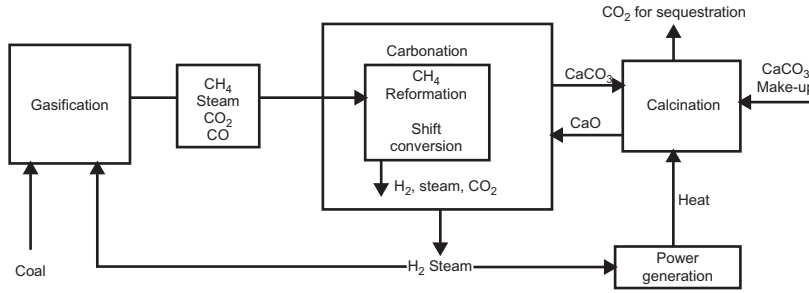

Figure 4.27 Schematic diagram of the ZEC process.
Source: Reprinted with permission from Gao, L., Paterson, N., Dugwell, D., Kandiyoti, R., 2008a. Energy Fuels 22, 463. Copyright 2008 American Chemical Society.

coal use in power generation. Also referred to as the LANL ZEC technology, ZEC was first proposed by researchers at the Los Alamos National Laboratory (LANL) and at Louisiana State University in the United States (OECD/IEA, 2002). The concept of *zero* emissions embraces the capture and disposal of CO_2 and polluting species, such as particulates, mercury, sulphur, nitrogen and volatile organic compounds. The aim was to release only N_2 and water vapour to the atmosphere.

The H_2 produced by this scheme would be used to generate power in fuel cells or gas turbines. Clearly however, pollutant capture systems impose a thermal penalty on the process and reduce overall efficiency. In particular, when coal gasification is adapted for producing H_2, CO_2-sequestration brings about an efficiency penalty of about 20%. In other words, more coal has to be used to generate the same amount of power from a zero-emission process than from a conventional gasification plant. There is, therefore, an incentive to look for ways of raising the efficiency of other component parts of the process to compensate, at least to some extent, for the energy penalty arising from CO_2 removal. Early evaluations of the system concluded that the concept was potentially efficient and viable and that experimental studies were required to test for reaction conditions and outcomes, prior to developing a detailed process flow sheet (Ruby et al., 2002; Ziock et al., 2003).

Fig. 4.27 presents a simplified flow diagram of the ZEC scheme. The first stage involves the gasification of process coal in a steam-hydrogen mixture, at a pressure of about 70 bars. While the aim is to produce primarily CH_4 via the methanation reaction:

$$C + 2H_2 \leftrightarrow CH_4; \quad \Delta H = -74.9\,\text{kJ/mol} \tag{4.1}$$

this first stage produces an impure fuel gas, containing N_2, H_2, H_2O, CO, CO_2, CH_4, H_2S, etc.

Methanation is an exothermic process, and steam is added to moderate the temperature rise to about 900°C. The product gas mixture is then steam-reformed

$$CH_4 + H_2O(g) \leftrightarrow CO + 3H_2; \quad \Delta H = +206\,\text{kJ/mol} \tag{4.2}$$

and passed through a water-gas shift reactor to maximize the H_2-content

$$CO + H_2O(g) \leftrightarrow CO_2 + H_2; \quad \Delta H = -41\,kJ/mol \tag{4.3}$$

and remove environmentally sensitive gases by a combination of absorption and catalytic decomposition. Finally, CO_2 is removed by the carbonation of CaO, to give a nearly pure stream of H_2.

$$CaO + CO_2 \leftrightarrow CaCO_3; \quad \Delta H = -179\,kJ/mol \tag{4.4}$$

In the final stage of the process, the $CaCO_3$ is calcined in a separate reactor to release the CO_2 stream for disposal.

Overall, H_2-producing reactions are endothermic and the heat requirement is provided by Reaction (4.1) and by the carbonation reaction of CaO (Reaction (4.4)). In fact, Reaction (4.4) provides the major portion of the energy required for driving the process, as it removes CO_2 from the product stream. The resulting shift of the equilibrium in Reaction (4.3) ensures that the H_2 concentration is maximized and provides the means to separate a concentrated stream of CO_2.

In all stages of the process, reaction temperatures are limited by the melting properties of coal mineral matter, the need to avoid the formation of eutectic liquid phases with the solid sorbents used for removing CO_2 (Paterson et al., 2001), as well as the equilibrium-controlled inability of CaO to capture CO_2 at temperatures above 900°C at a CO_2 partial pressure of less than 1 bar. To ensure effective energy integration, Reactions (4.2–4.4) must be conducted in a single reactor. Overall, the scheme results in the formation of an *extra* two mols of hydrogen, for each two mols of hydrogen used in the methanation stage. The CO_2 captured in the form of $CaCO_3$, is subsequently released as a concentrated stream for sequestration by the calcination of $CaCO_3$.

On the whole, the same amount of CO_2 is formed when processing coal with the ZEC process or by using conventional technologies. However, the ZEC process potentially has a higher efficiency, because losses are avoided through the integration of several process steps. Moreover, the use of the carbonation/calcination cycle offers the potential to isolate CO_2 as a nearly pure stream for disposal.

Prior to the work summarized below, the integrated ZEC process route had not been studied experimentally, although some component parts of the concept, e.g., hydrogasification, the steam reforming of methane and the water-gas shift reaction to raise the hydrogen concentration were ‘known to work’. Soon after the completion of the experimental work described below, the United States government sponsored laboratories which had initiated the work on the ZEC concept decided not to pursue this process route any further. Meanwhile, the attempt to simulate the gasification conditions required by the ZEC process enabled the ranges of conditions of operation of the high-pressure wire-mesh reactor to be considerably expanded (Gao et al., 2008a,b).

4.9.2 Injecting steam-hydrogen mixtures into the wire-mesh reactor at 1050°C and 80 bars

The conceptual operating pressure for the ZEC gasifier had been selected as 70 bars. Attempting to mimic reaction conditions demanded by the ZEC gasifier necessitated returning the high-pressure wire-mesh reactor to its original hydropyrolysis configuration (Fig. 4.3) and modifying it to accept steam injection at far higher pressures than were required by the work of Messenbock, et al. (1999b). The steam injection system constructed around the wire-mesh reactor (Fig. 4.7) for injection up to 30 bars was modified for operation at up to 80 bars (Gao et al., 2008a).

The steam injection system functioned by evaporating a metered stream of water in a glass-bead packed tube heated to 100°C above the boiling point of water at the required operating pressure. The steam lines were trace-heated to avoid condensation before the steam reached the wire-mesh reactor. The experimental programme required the reactor to operate at pressures up to 80 bars, in atmospheres of pure He, H_2, steam and combinations of these gases. The helium and/or hydrogen stream to be fed to the reactor alongside the steam was preheated to avoid condensation upon mixing. Apart from the installation of higher pressure valves and fittings and CO and H_2 metering equipment, the flow scheme was not significantly altered from what is shown in Fig. 4.7. Rigorous pressure testing was done to ensure the integrity of the pipework and ancillary equipment for withstanding operating temperatures and pressures. CO and H_2 analysers were installed to monitor the atmosphere in the vicinity of the steel cabinet, within which the equipment had been installed. Details of the experimental setup have been described by Gao et al. (2008a,b).

Experimental results using Daw Mill coal: The base case experiments were carried out using Daw Mill (UK) coal (Table 4.17), at a heating rate of 1000°C s^{-1}. In order to calculate extents of gasification in reactive atmospheres, as distinct from total weight loss, volatile yields during pyrolysis in helium were determined first, as a function of pressure. As expected, the weight loss was greatest at atmospheric pressure and declined from about 42–44% to 32–34% as the pressure was raised to 70 bars. These data were used to subtract the effect of pyrolytic weight loss from data obtained during tests in H_2, steam and H_2/steam mixtures.

Experiments were carried out at 70 bars H_2 pressure, in order to calculate the *extents* of *hydrogasification* (weight-loss under hydrogen *minus* pyrolysis weight-loss), which were found to be in the 15–25% range at temperatures between 750°C and 1050°C. After 10 s holding, the extents of gasification under similar pressures of steam were found to be 5–8% lower than gasification in H_2, under otherwise similar reaction conditions. The *extents of gasification* exceeded 35% (in addition to 32–34% volatiles evolution from pyrolysis) when 50–50 mixtures of hydrogen and *steam* were used.

This observation is significant in terms of the sequence of events envisaged. During pyrolysis in helium, as the pressure is raised, sample weight loss progressively decreases. This loss of volatiles appears due to the physical suppression of volatile (in particular, tar) evolution with increasing pressure (Güell and Kandiyoti, 1993). When tar evolution is impeded by the effect of high pressure, repolymerisation of the heavier

Table 4.17 Proximate and ultimate analyses of the set of coals and lignites used in the study

Analysis		Daw Mill bituminous	Illinois No. 6 sub-bituminous	Pittsburgh No. 8 bituminous	Wyodak sub-bituminous	Baag Noor coal lignite	Beulah Zap Lignite
Moisture (% as received)		4.1	8.0	1.7	28.1	6.8	32.2
Ash (% as received)		6.9	14.3	9.1	6.3	11.0	6.6
Volatile matter (% db)		33.7	40.1	37.8	44.7	40.0	44.9
C	%, db	72.7	65.7	75.5	68.4	56.8	65.9
H		4.7	4.2	4.8	4.9	4.6	4.4
N		1.1	1.2	1.5	1.0	0.27	1.0
S		1.1	4.8	2.2	0.63	0.39	0.80
O (by difference)	%, dmmf	na	10.1	6.9	16.9	na	19.1

Source: Reprinted with permission from Gao, L., Paterson, N., Dugwell, D., Kandiyoti, R., 2008a. Energy Fuels 22, 463. Copyright 2008 American Chemical Society.

tar components results in the formation of an amorphous and relatively unreactive char. It is likely, however, that the presence of steam helps remove some of these secondary chars and indirectly promotes reactions between char and *both* hydrogen and steam, by enhancing the reactivity of the char.

Experiments with lignites and several other coals: Beulah Zap lignite from the Argonne Premium Coal Sample set (Vorres, 1990) and Baag Noor, a lignite sample from a weathered and partially oxidized deposit not far from Mongolia's capital Ulaan Bataar, turned out to be the most reactive fuels tested (Gao et al., 2008b). Under 70 bars hydrogen pressure, total conversions in excess of 75% were observed. Both samples gave *extents of hydrogasification* (i.e., volatiles above and beyond pyrolysis yields) in the 38–40% range. Once again, there was scope for maximising the conversion of these fuels by adding steam: the total conversion of Beulah Zap increased from 72% to 86%, when reacted with a 50–50% mixture of hydrogen and steam. In the presence of a similar H_2/steam mixture, the low rank bituminous coal Daw Mill gave a total extent of conversion (i.e., including pyrolysis) of approximately 70%, after 10 s holding at peak temperature.

Similar experiments were carried out with three bituminous coal samples from the Argonne Premium Coal Sample set (Vorres, 1990): Illinois No. 6, Pittsburgh No. 8 and Wyodak (Table 4.17). In planning these experiments, it was considered possible that the more reactive coals might approach complete conversion during 10 s holding at high temperature. The holding time at peak temperature was therefore reduced to 5 s for the current tests, to curtail the levels of conversion and differentiate between the reactivities of the samples. The data are shown in Table 4.18.

Similar orders of reactivity were observed in steam, in hydrogen and in steam/hydrogen mixtures: Pittsburgh > Illinois > Wyodak ≈ Daw Mill. 'Theoretical' conversions for the four coals in H_2/steam have been calculated by adding the extents of reaction measured in steam and pure H_2. The calculated values turned out to be lower than the experimental conversions, suggesting that steam/ H_2 mixtures produce a synergistic effect. As already indicated, the effect has been observed in the case of Daw Mill coal.

The extents of reaction observed in the case of the 5-s holding time runs point to far faster rates of reaction than have been reported from a study carried out for the ZECA Corporation at the Gas Technology Institute (GTI) (Ziock et al., 2003). A high-pressure TG balance had been used in that particular study at similar temperatures and pressures to those used in the high-pressure wire-mesh reactor. However, different samples were used and two of the three samples were charred under unspecified conditions prior to the actual test in the TG balance. In the GTI study, the lignite was reported to have reached about 50% carbon-conversion in approximately 7 min in pure H_2. Similarly, the sub-bituminous and bituminous coals required approximately 8–45 min, respectively, to reach the 50% conversion level in a 50/50 steam/H_2 mixture.

The differences in conversion observed between the two sets of experiments were somewhat large, for a credible explanation to be given in terms of differences between samples. There were several factors to take into account. As already explained in Chapter 3, Pyrolysis of solid fuels: experimental design and applications, TG balances

Table 4.18 Performance of different coals[a]

Sweep gas	Illinois No. 6		Pittsburgh No. 8		Wyodak		Daw Mill	
	Total volatile yield (%, daf)	Extent of reaction (%, daf)	Total volatile yield (%, daf)	Extent of reaction (%, daf)	Total volatile yield (%, daf)	Extent of reaction (%, daf)	Total volatile yield (%, daf)	Extent of reaction (%, daf)
He	42.6		28.5		39.4		35.0	
H_2/He	59.3	16.7	49.3	20.8	52.6	13.2	48.8	13.8
Steam/He	55.7	13.1	44.8	16.3	51.9	12.5	47.1	12.1
H_2/steam, experimental	77.6	35.0	75.1	46.6	68.5	29.1	64.5	29.5
H_2/steam, calculated	72.4	29.8	65.6	37.1	65.1	25.7	60.9	25.9

Source: Reprinted with permission from Gao, L., Paterson, N., Dugwell, D., Kandiyoti, R., 2008a. Energy Fuels 22, 463. Copyright 2008 American Chemical Society.
[a]Temperature, 850°C; Pressure, 7 MPa; Hold time at peak temperature, 5 s; Heating rate, 1000°C s^{-1}; Gas mixtures, 50/50 (by vol).

are not suitable for experiments involving a pyrolytic step (also see Kandiyoti, 2002). Furthermore, the ill-defined flow patterns in the vicinity of the sample pan are likely to introduce external (bulk gas to particle surface) mass transfer resistances, that are usually severe in high pressure applications (Jess and Andresen, 2010). It is also known that heating rates in TG balances are far too low compared to coal heating rates in the wire-mesh reactor. The additional complication introduced by slow heating regimes is that they provide ample time for char deactivation before the required experimental temperature is reached. In addition, two of the fuels used in the GTI study were 'charred' (under unspecified conditions) prior to the TGA test and this would have enhanced the degree of deactivation. Taken together, all of these factors would have tended to reduce the reactivity of the chars and account for the low char conversions observed in the GTI study.

4.9.3 *In closing: the ZEC gasifier*

At the time of writing, the ZEC process was no longer being pursued as a viable route to generate energy from coal. The study has nevertheless allowed developing the high-pressure wire-mesh reactor for steam injection at pressures up to 80 bars. The work also allowed several new insights which may eventually turn out to be useful.

At temperatures in the 900–1000°C range, fairly long residence times would be required to achieve the high conversions demanded by the project. Ten seconds were needed with the relatively fine (106–152 μm) fuel particle size range used in the high-pressure wire-mesh experiments described earlier, to achieve overall conversions above 80%. The original ZEC-flow sheets made no mention of tar formation during hydrogen/steam gasification or, indeed, of char residues. Experience in the ABGC spouted bed pilot gasifier suggests the tars could be destroyed to extinction in this temperature range by exposure to the combination of air and steam and residence times of 1–3 seconds. It is also possible for tar aerosols to adsorb on solid fuel or sorbent particles which circulate for rather longer in the fluidised part of the bed. It seems perfectly possible therefore that a spouted or circulating fluidised bed ZEC-reactor would be capable of producing a tar free gas. However, it seems difficult to avoid the accumulation of relatively stable char residues after 10 s or longer residence times. Provision would have to be made for the disposal of these chars by combustion, possibly for raising process steam.

Finally, retention of sulphur (down to near equilibrium levels) may also be possible by the addition of limestone or dolomite to the reaction mixture. This would minimize the sulphur passing through to the next process stage. It seems likely, however, that some form of finer sulphur capture (such as ZnO-filters) would still be required in order to protect the catalytic reforming and water-gas shift reaction stages from sulphur poisoning.

4.10 Reactor design: pyrolysis, gasification and liquefaction

Chapter 3, Pyrolysis of solid fuels: experimental design and applications, and Chapter 4, High-pressure reactor design: pyrolysis, hydropyrolysis and gasification,

have presented and discussed the capabilities of a range of experimental reactors, designed for tracking the behaviour of solid fuels during thermochemical processing. The focus has been, first, on characterising the fundamental behaviour of the fuels themselves, and second, on mimicking the time-temperature-pressure histories of fuel particles in selected zones of pilot or plant scale equipment – in order to assess how particular fuels respond to changes in selected reaction conditions. Chapter 3, Pyrolysis of solid fuels: experimental design and applications, has focused on atmospheric pressure pyrolysis in inert atmospheres and Chapter 4, High-pressure reactor design: pyrolysis, hydropyrolysis and gasification, has discussed the design and development of high-pressure reactors, for experiments using inert as well as reactive gases such as air (or oxygen), CO_2, hydrogen and steam. The development of the high-pressure wire-mesh reactor design, for accommodating steam injection – and to avoid condensation – has been described.

In Chapter 5, Liquefaction: thermal breakdown in the liquid phase, the attention paid to reactor design thus far will be extended to liquefaction. We will observe that the concepts developed in previous chapters regarding the differentiation between fuel- and reactor-related effects equally apply to the evaluation of product distributions during liquefaction.

References

Abdoulmoumine, N., Adhikari, S., Kulkarni, A., Chattanathan, S., 2015. Appl. Energy 155, 294.

Adánez, J., Miranda, X.L., Gavilan, X.M., 1985. Fuel 64, 801.

Adlhoch, W., Sato, K., Wolff, J., Radtke, K., 2000. High temperature winkler gasification of municipal solid waste. Gasification Technologies Conference, San Francisco, CA; October 8–11, 2000. <http://www.netl.doe.gov/File%20Library/research/coal/energy%20systems/gasification/gasifipedia/Gtc00320.pdf>.

Alauddin, Z.A.B.Z., Lahijani, P., Mohammadi, M., Mohamed, A.R., 2010. Renewable Sustainable Energy Rev. 14, 2852.

Alvarez, T., Fuertes, A.B., Pis, X.X., Parra, X.B., Pajares, J., Menendez, R., 1994. Fuel 73, 1358.

Arendt, P., 1980. Ph.D. Thesis. University of Aachen, Germany.

Arendt, P., van Heek, K.-H., 1981. Fuel 60, 779.

Baumann, H., Moller, P., 1991. Erdol und Kohle, Erdgas, Petrochemie 44, 29.

Bautista, X.R., Russel, W.B., Saville, D.A., 1986. Ind. Eng. Chem. Fund. 25, 536.

Bhavanam, A., Sastry, R.C., 2011. Int. J. Chem. Eng. Appl. 2, 425.

Bota, K.B., Abotsi, G.M.K., 1994. Fuel 73, 1354.

Brown, B., Smot, L.D., Smith, P.J., Hedman, P.O., 1988. AIChE J. 34, 435–446.

Burchill, P., Welch, L.S., 1989. Fuel 68, 100.

Cai, H., 1995. PhD Thesis. University of London, London.

Cai, H.-Y., Guell, A.J., Chatzakis, I.N., Lim, J-Y., Dugwell, D.R., Kandiyoti, R., 1996. Fuel 77, 15.

Cai, H.-Y., Megaritis, A., Messenbock, R., Dix, M., Dugwell, D.R., Kandiyoti, R., 1998. Fuel 77, 1273.

Chitsora, C.T., Muhlen, H.-J., van Heek, K.H., Juntgen, H., 1987. Fuel Process. Technol. 15, 17.

Cousins, A., 2005. PhD Thesis. University of London, London.
Cousins, A., Paterson, N., Dugwell, D.R., Kandiyoti, R., 2006a. Energy Fuels 20, 699.
Cousins, A., Paterson, N., Dugwell, D.R., Kandiyoti, R., 2006b. Energy Fuels 20, 2489.
Curran, G.P., Fink, C.E., Goring, E., 1967. CO_2 acceptor gasification process. ACS Adv. Chem. 69, 141–165. <http://pubs.acs.org/doi/abs/10.1021/ba-1967-0069.ch010>.
Dahlquist, E. (Ed.), 2013. Technologies for Converting Biomass to Useful Energy. CRC Press (Taylor & Francis Group), Boca Raton, FL.
Dawes, S.G., Reed, G.P., Gale, J., Clark, R.K., 1991. Institution of Chemical Engineers Symposium Series No. 123.
Dawes, S.G., Cross, P.J., Minchener, A.J., 1993. UNECE Symposium, Helsinki, 'Development of the British Coal Topping Cycle'.
Dawes, S.G., Mordecai, M., Brown, D., Burnard, G.K., 1995. The air blown gasification cycle. Proc. 13th Intl. Conf. on Fluidised Bed Combustion, Orlando, Florida, May 1995.
Duxbury, J., Gavin, D., 1994. MTDATA Studies ETSU Report R-018.
Elliott, M.M. (Ed.), 1981. Chemistry of Coal Utilization Second Supplementary Volume. John Wiley, NY.
EPRI Report No. TR-103367, 1993. "Gasification of Pittsburgh No. 8 coal" in Rheinbraun's "Pressurised High Temperature Winkler Plant", Final report.
Gao, L., Paterson, N., Dugwell, D., Kandiyoti, R., 2008a. Energy Fuels 22, 463.
Gao, L., Paterson, N., Fennel, P., Dugwell, D.R., Kandiyoti, R., 2008b. Energy Fuels 22, 2504.
Gavin, D., Paterson, N., Duxbury, J., Maxwell, S., Reed, G.P., 1997. Fuel Behaviour in the Air Blown Gasification Cycle, Report No. COAL R1 01, DTI Cleaner Coal Technology Programme.
Gibbins, J.R., Kandiyoti, R., 1989a. Energy Fuels 3, 670.
Gibbins, J.R., Kandiyoti, R., 1989b. Fuel 68, 895.
Gibbins, J.R., Gonenc, Z.S., Kandiyoti, R., 1991. Fuel 70, 621.
Gibbins-Matham, J.R., Kandiyoti, R., 1988. Energy Fuels 2, 505.
Gibbins-Matham, J.R., King, R.A.V., Wood, R.J., Kandiyoti, R., 1989. Rev. Sci. Instrum. 60, 1129.
Ginter, D.M., Somorjai, G.A., Heinemann, H., 1993. Energy Fuels 7, 393.
Gonenc, Z.S., Gibbins, J.R., Katheklakis, I.E., Kandiyoti, R., 1990. Fuel 69, 383.
Göransson, K., Söderlind, U., He, J., Zhang, W., 2011. Renewable Sustainable Energy Rev. 15, 482.
Goring, G.E., Curran, G.P., Tarbox, R.P., Gorin, E., 1952. Ind. Eng. Chem., 1057.
Güell, A.J., 1993. PhD Thesis. University of London, London.
Güell, A.J., Kandiyoti, R., 1993. Energy Fuels 7, 943.
Güell, A.J., Cai, H.-Y., Dugwell, D.R., Kandiyoti, R., 1993. Fuel Process. Technol. 36, 259.
Guo, C., Zhang, L., 1986. Fuel 65, 1364.
Haemaelaeinen, J.P., Aho, M.J., 1996. Fuel 74, 1377.
Haga, T., Nishiyama, Y., 1988. Fuel 67, 743.
Hara, S., Inumaru, J., Ashizawa, M., Ichikawa, K., 2002. JSME Int. J., Ser. B 45, 518.
Higginbotham, E.B., Motter, J.W., 1994. 13th EPRI Conf.: Gasification Power Plants. San Francisco, CA.
Higman, C., 2008. FutureGen Workshop, Tokyo, 25 Feb 2008. <http://www.rite.or.jp/Japanese/labo/choryu/workshop/futuregenws2008/2008FGWS_MrHIGMAN.pdf>.
Higman, C., van der Burgt, M., 2008. Gasification, second ed. Gulf Professional Publishing, Burlington, MA, USA & Oxford, UK.
Hodrian, C., 1988. British Gas; personal communication.
Hotchkiss, R., 2003. Proc. Inst. Mech. Eng., J Power Energy 217 (A1), 27.

Howard, J.B., 1981. In: Elliott, M.M. (Ed.), Chemistry of Coal Utilization Second Supplementary Volume. John Wiley, NY, pp. 665.
Huber, G.W., Iborra, S., Corma, A., 2006. Chem. Rev. 106, 4044.
Hulgaard, T., 1992. Environ. Prog. 11, 302.
Hulgaard, T., 1993. AlChE J 39, 1342.
Hurt, R.H., Sarofim, A.F., Longwell, J.P., 1991. Energy Fuels 5, 290.
Hüttinger, K.J., 1988. NATO ASI Series. Series C: Mathematical and Physical Sciences In: Yürüm,Y. (Ed.), pp. 244, 433.
Hüttinger, K.J., Nattemann, C., 1994. Fuel 73, 1682.
Jenkins, R.G., Nandi, S., Walker Jr., P.L., 1973. Fuel 52, 288.
Jess, A., Andresen, A.K., 2010. Fuel 89, 1541.
Kanbara, S., Takarada, T., Yamamoto, Y., Kato, K., 1993. Energy Fuels 7, 1013.
Kandiyoti, R., 2002. Fuel 81, 975.
Kandiyoti, R., 2009. Fundamentals of Reaction Engineering. Ventus Publishing, Frederiksberg, Denmark, ISBN 978-87-7681-510-3. <http://bookboon.com/uk/student/chemical/fundamentals-of-reaction-engineering>.
Kilpinen, P.; Hupa, M.; Leppaelahti, J., 1991. Nitrogen Chemistry During Gasifications: A Thermodynamic Analysis AAA-KTF/FKF-91/14 (Abo Akademi).
Kirkels, A.F., Verbong, G.P.J., 2011. Renewable Sustainable Energy Rev. 15, 471.
Laurendeau, N.M., 1978. Prog. Energy Combust. Sci 4, 221.
Lemaignen, L., Zhuo, Y., Reed, G.P., Dugwell, D.R., Kandiyoti, R., 2002. Fuel 81, 315.
Li, C.-Z., Gaines, A.F., Güell, A., Kandiyoti, R., 1991. Int. Conf. Coal Sci. 72
Li, C.-Z., Bartle, K.D., Kandiyoti, R., 1993a. Fuel 72, 3.
Li, C.-Z., Bartle, K.D., Kandiyoti, R., 1993b. Fuel 72, 1459.
Li, C.-Z., Madrali, E.S., Wu, F., Xu, B., Cai, H.-Y., Güell, A.J., et al., 1994. Fuel 73, 851.
Lim, J.-Y., Chatzakis, I.N., Megaritis, A., Cai, H.-Y., Dugwell, D.R., Kandiyoti, R., 1997. Fuel 76, 1327.
Lin, W., Johnssen, J.E., 1993. 7th Int. Conf. Coal Sci. (Banff) 554.
Lowry, H.H. (Ed.), 1963. Chemistry of Coal Utilization Supplementary Volume. John Wiley, NY.
Madrali, E.S., 1994. Ph.D. Thesis, University of London.
Malinowski, E.R., Howery, R.G., 1980. Factor Analysis in Chemistry. John Wiley, New York.
Mamori, T., Sagimori, K., Baba, A., Yatani, T., Yasumi, T., Inoue, H., 1998.Souken Houkoku 55, 91 (ISSN: 0285-6697) (in Japanese).
Megaritis, A., Zhuo, Y., Messenbock, R., Dugwell, D.R., Kandiyoti, R., 1998a. Energy Fuels 12, 144.
Megaritis, A., Messenbock, R.C., Collot, A.-G., Zhuo, Y., Dugwell, D.R., Kandiyoti, R., 1998b. Fuel 77, 1411.
Meijer, R., Kapteijn, F., Moulijn, J.A., 1994. Fuel 73, 723.
Messenbock, R., 1998. PhD Thesis. University of London.
Messenbock, R.C., Dugwell, D.R., Kandiyoti, R., 1999a. Energy Fuels 13, 122.
Messenbock, R.C., Dugwell, D.R., Kandiyoti, R., 1999b. Fuel 78, 781.
Messenbock, R.C., Paterson, N., Dugwell, D.R., Kandiyoti, R., 2000. Fuel 79, 109.
Mojtahedi, W., Horrath, A., Salo, K., Gangawal, S.K., 1991. 10th EPRI Conference on Coal Gasification Power Plants, Palo Alto, CA.
Morris, J.P., Keairns, D.L., 1979. Fuel 58, 465.
Motter, J.W., Higginbotham E.B. (1993) 12th EPRI Conference on Coal Gasification Power Plants, San Francisco, CA.
Muhlen, H.-J., Van Heek, K.H., Juntgen, H., 1985. Fuel 64, 944.
Muhlen, H.-J., Van Heek, K.H., Juntgen, H., 1986. Fuel 65, 591.

NETL, 2010. 2010 Worldwide Gasification Database. <http://www.netl.doe.gov/research/coal/energy-systems/gasification/gasification-plant-databases/2010-archive>.
NETL, 2015. Commercial gasifiers. <http://www.netl.doe.gov/research/coal/energy-systems/gasification/gasifipedia/entrainedflow>.
Niksa, S.J., Russel, W.B., Saville, D.A., 1982a. Fuel 61, 1207.
Niksa, S.J., Russel, W.B., Saville, D.A., 1982b. 19th Symp.(Int.) Combustion, The Combustion Institute, Pittsburgh, PA, 1151.
Niksa, S.J., Heyd, L.E., Russel, W.B., Saville, D.A., 1984. 20th Symposium (Intl.) on Combustion, The Combustion Institute, 1445.
Nozaki, T., Adschiri, T., Fujimoto, K., 1991. Energy Fuels 5, 610.
O'Brien, J.R., 1986. PhD Thesis, University of London.
OECD/IEA Technology Status Report, 2002.Solutions for the 21st Century, Zero Emissions Technologies for Fossil Fuels, May, 2002.
Paterson, N., Elphick, S., Dugwell, D.R., Kandiyoti, R., 2001. Energy Fuels 15, 894.
Paterson, N., Zhuo, Y., Dugwell, D.R., Kandiyoti, R., 2002. Energy Fuels 16, 127.
Paterson, N., Zhuo, Y., Dugwell, D., Kandiyoti, R., 2005. Energy Fuels 19, 1016.
Peng, F.F., Lee, I.C., Yang, R.Y.K., 1995. Fuel Process. Technol. 41, 233.
Peralta, D., Li, X., Xu, S., Paterson, N., Dugwell, D.R., Kandiyoti, R., 2004. Proc. '2004 Intl. Hi-Tech Symposium on Coal Chemical Industry and Coal Conversion', 30–31 October 2004, Shanghai, China, pp. 136.
Peralta, D., Paterson, N., Dugwell, D., Kandiyoti, R., 2005. Energy Fuels 19, 532.
Perkin-Elmer Ltd., 1991. *QUANT + User's Manual*.
Piñon Pine Power Project, 1998. <http://www.netl.doe.gov/publications/press/1998/tl_pinon_ded.html>.
Radtke, K., 2011. ThyssenKrupp Uhde's PRENFLO and HTW Gasification Technologies, Gasification Technologies Conference October 9–12, 2011, San Francisco, CA. <http://www.netl.doe.gov/File%20Library/research/coal/energy%20systems/gasification/gasifipedia/16RADTKE.pdf>.
Reed, G.P., Paterson, N., Zhuo, Y., Dugwell, D.R., Kandiyoti, R., 2005. Energy Fuels 19, 298.
Ren, Y., Xu, S., Xu, Y., Chen, C. and Xia, J., Proc. 2004 Intl. Hi-Tech Symposium on Coal Chemical Industry and Coal Conversion, 30–31 October 2004, Shanghai, China, p. 172.
Ruby, J., Johnson, A., Ziock, H., Lackner, K., 2002. Proceedings of the 27th International Technical Conference on Coal Utilization and Fuel Systems, March, 2002, Clearwater, FL, pp. 767–778.
Sha, X., Chen, Y., Cao, J., Yang, Y., Ren, D., 1990. Fuel 69, 656.
Shufen, L., Ruizheng, S., 1994. Fuel 73, 413.
Silveston, P.L., 1991. Energy Fuels 5, 933.
Stangeby, P.C., Sears, P.L., 1981a. Fuel 60, 131.
Stangeby, P.C., Sears, P.L., 1981b. Fuel 60, 125.
Stiles, H.N., Kandiyoti, R., 1989. Fuel 68, 275.
Sue-A-Quan, T.A., Watkinson, A.P., Gaikwad, R.P., Lim, C.J., Ferris, B.R., 1991. Fuel Proc. Tech. 27, 67.
Sue-A-Quan, T.A., Cheng, G., Watkinson, A.P., 1995. Fuel 74 (2), 159.
Suuberg, E.M., Peters, W.A., Howard, J.B., 1980. Fuel 59, 405.
Synthesis Energy Systems, 2011. Gasification Technologies Conference, 10 October 2011, San Francisco, CA. <http://www.netl.doe.gov/File%20Library/research/coal/energy%20systems/gasification/gasifipedia/12PRESTON.pdf>.
Taupitz, K.C., 1977. Hydrocarbon Process. 219.
Tyler, R.J., 1979. Fuel 58, 680.

Tyler, R.J., 1980. Fuel 59, 218.
Vorres, K.S., 1990. Energy Fuels 4, 420.
Wang, B., Li, X., Xu, S., Paterson, N., Dugwell, D.R., Kandiyoti, R., 2005. Energy Fuels 19, 2006.
Weisberg, S., 1985. Applied Linear Regression, second ed. Wiley, New York.
Woolcock, P.J., Brown, R.C., 2013. Biomass Bioenergy 52, 54.
Wu, F., Güell, A.J., Li, C.-Z., Madrali, E.S., Cai, H.-Y.; Dugwell, D.R., et al., 1993. Proc. ICCS, Banff, 307.
Yang, Y., Watkinson, A.P., 1994. Fuel 73, 1786.
Zhuo, Y., Messenböck, R., Collot, A.-G., Paterson, N., Dugwell, D.R., Kandiyoti, R., 2000a. Fuel 79, 793.
Zhuo, Y., Lemaignen, L., Chatzakis, I.N., Reed, G.P., Dugwell, D.R., Kandiyoti, R., 2000b. Energy Fuels 14, 1049.
Zhuo, Y., Paterson, N., Avid, B., Dugwell, D.R., Kandiyoti, R., 2002. Energy Fuels 16, 742.
Ziock, H.-J., Anthony, E.J., Brosha, E.L., Garzon, F.H., Guthrie, G.D., Johnson, A.A., et al., 2003. Progress in the development of zero emission coal technologies. Proceedings of the 28th International Technical Conference on Coal Utilization and Fuel Systems, Clearwater, FL.

Liquefaction: thermal breakdown in the liquid phase

5

Chapter Outline

The history of coal liquefaction in the 20th century has followed a particularly erratic course. Both the direct coal liquefaction process ('Bergius') and the indirect liquefaction route through gasification were invented in Germany during the early part of the 20th century. In the run up to World War II, advances were made to adapt these technologies to produce synthetic fuels and chemical feedstocks from coal. After the war, the accumulated know-how and surviving infrastructure were painstakingly assessed by the Allies. Just at the time, however, the industrialised world was entering a new, long era of cheap and plentiful crude oil. Coal liquefaction was set aside. Following the oil shocks of 1973 and 1979, major oil importing countries returned to evaluating the viability of the (by then) lost arts of coal liquefaction.

During wartime, production had been pursued regardless of cost. In the 1970s, a major new effort was made to look for new pathways, aiming to reduce the costs and the attendant pollution of coal conversion. Much of the new investment for basic research and pilot plant construction took place in the United States. Significant

Solid Fuels and Heavy Hydrocarbon Liquids. DOI: http://dx.doi.org/10.1016/B978-0-08-100784-6.00005-9

advances were made during this period in broadening and deepening the knowledge base on coal processing. However, crude oil prices crashed in the mid-1980s, exposing the economic fragility of the new coal conversion technologies. Although significant new advances were made in the science and engineering of coal processing, relatively little has survived of the process routes piloted during that hectic period.

Crude oil markets have experienced several further major cycles of price fluctuations since the mid-1980s. The markets showed, yet again, that oil prices do not necessarily remain sufficiently high for long enough, to justify the vast capital outlays required for new plant, and indeed the enormous commitment in terms of mining and transportation, that would have been required to turn to very large scale coal utilisation.

It appears we may have finally learned the lesson that, in peacetime, using crude oil is cheaper, even when oil prices are high. In the first decade of the millennium, prices rose to unprecedented levels, in 2008 reaching short-lived peaks above US$140 per barrel, before crashing to about US$40 in early 2009 and eventually stabilising at around US$100–110 per barrel (of Brent crude) between 2011 and 2014. None of this, however, occasioned any further mention of a revival for coal liquefaction. Furthermore, the universal reticence to reopen that particular discussion seems to have been justified. From about the middle of 2014, declining oil consumption levels coincided with renewed struggles between crude oil producers over market-shares, resulting in prices as low as US$28 per barrel in early 2016 (EnerCOM Website, 2016). At the time of writing, prices were lingering just below $50 per barrel.

Thus, there is little current interest in pursuing coal liquefaction as an economically viable process route to make synthetic fuels and chemical feedstocks. Nonetheless, there are several surviving pockets of activity in two countries that rely heavily on their domestic coal resources, South Africa and China. In South Africa, SASOL has been producing some seven million tons per year of synthetic fuels and chemical feedstocks, through an indirect process route via coal gasification, followed by gas conditioning and Fischer–Tropsch synthesis (e.g., Gibson, 2007; Higman and van der Burgt, 2008). Originally established to combat the oil embargo imposed by the United Nations during the apartheid era, SASOL was eventually privatised. At the time, special provisions were made by the Government of South Africa to maintain SASOL as a going concern. In times of high oil prices, the company proved highly profitable.

In China, six SASOL Lurgi Mark IV gasifiers have been constructed by Shanxi Lu'An Group near Changzhi City (Shanxi Province) as part of a demonstration project of SASOL 'coal-to-liquids' (CTL) technology. Several other pilot and small scale demonstration units experimenting with coal liquefaction have also been operating. The Shenhua Group in Inner Mongolia has constructed the largest of these units, making some 20,000 tons of liquid products per year.

Despite the forbidding economic outlook, there are several reasons why it seems useful to retain and develop a chapter on liquefaction in the present volume. Differentiating between the thermal response of solid fuels and reactor specific effects has a direct bearing on current work concerning the hydrothermal processing of biomass. Moreover, examining liquefaction procedures will lead us to a review of methods for liquid product characterization, anticipating some of the analytical methods presented in Chapter 7, Analytical techniques for low mass materials: method development and

Chapter 8, Analytical techniques for high-mass materials: method development. The attempt to discriminate between fundamental fuel behaviour and reactor design will also help achieve a unified understanding of successive, thermally driven events that bring about the processes of thermal breakdown during the pyrolysis and liquefaction of solid fuels. In Chapter 6, Elements of thermal breakdown: heating rate effects and retrogressive reactions, we will juxtapose data from pyrolysis and liquefaction experiments, to highlight structural aspects of thermal breakdown that are common to both process pathways. We will show how this approach might impact on a wide field, ranging from research on coke making to the design of liquefaction reactors, as well as help us develop a broader understanding of the mechanics of thermal breakdown in solid fuels. Early in the chapter, we will also present a general introduction to hydrothermal biomass processing, to signal recent developments in this area and discuss possible future avenues of investigation.

5.1 Introduction: the liquefaction of coal and biomass

Lowry (1963) and Elliott (1981) have provided excellent summaries of early liquefaction research. A brief overview of liquefaction technologies that emerged since the oil shocks of the 1970s and early 1980s may be found in the 'Technology Status Report' by the UK Department of Trade and Industry (CCTP, 1999). Kimber (1997) has reviewed the results of the British Coal Liquefaction Project. Short summaries of the process have been presented by Harrison et al. (1989) and Moore et al. (1989). The massive amount of laboratory research carried out during the same period may be followed through the successive proceedings of International Conference on Coal Science meetings. Furimsky (1998) has reviewed catalysts and reactors for hydroprocessing coal liquids, while Mochida et al. (1998) have presented an overview of progress in coal liquefaction catalysts in Japan, where the commitment to coal liquefaction technologies has been maintained for longer than in Europe and the United States. A comparative analysis of costs of alternative coal liquefaction processes has been provided by Sun et al. (2005). Tekin et al. (2014), Elliott et al. (2015) and several other teams (cited below) have reviewed more recent developments in the hydrothermal processing of biomass.

5.1.1 Hydrothermal processing of biomass

The production of bio-crude by the hydrothermal liquefaction of lignocellulosic biomass, as a replacement for crude-oil, was proposed by E. Berl as early as 1934 (Berl, 1934, 1944). He treated biomass in an alkaline solution at around 230°C and reported that the 'oil' product contained 60% of the original biomass carbon and 75% of its heating value.

In the past, this process route was tested as a route for reducing the oxygen content of the substrate and to produce higher energy density liquids and solid products. More recent work has focused on preparing advanced carbon materials. The basic bench scale experiment consists of heating wet biomass plus added water, and any added

catalyst, in a batch autoclave where system pressure is allowed to rise with increasing reactor temperature. The process obviates the need for a pre-drying step, making it less energy intensive. Furthermore, energy losses from the conversion of liquid water to steam are limited by heating the water under the high pressures generated in the closed vessel.

Product distributions from hydrothermal processing can be changed quite widely, by the selection of reaction conditions. Mainly 'char' is produced when lignocellulosic biomass is heated to between 170°C and 250°C, with pressures ranging up to 50 bars; the sample is heated for 4–15 h, in the presence of a catalyst (e.g., citric acid, $FeSO_4$) (Titirici et al., 2007). Hydrothermal 'liquefaction' requires somewhat higher temperatures, compared to hydrothermal 'carbonisation'. Zhang et al. (2008) collected a phenol-rich oily liquid from heating lignocellulosic biomass in the presence of K_2CO_3 or KOH, to between 250°C and 350°C for 15 min, under pressures between 50 and 200 bars. In these experiments, the state of the liquid phase was deemed to be 'nearing' that of supercritical water. Starting with a biomass feedstock containing 30–50 wt% oxygen and 10–20 MJ kg^{-1} heating value, the oil produced from hydrothermal liquefaction typically presents oxygen contents between 10 and 30 wt% and heating values in the 30–36 MJ kg^{-1} range. Thus, while some upgrading is achieved, the oxygen content of the 'oil' is still high compared to petroleum crudes, which makes these products difficult to utilise (Peterson et al., 2008; Toor et al., 2011; Demirbas, 2010; Elliott et al., 2015).

In another 'near' supercritical water experiment, Ru and Ni based catalysts were used at somewhat higher temperatures (350–380°C); the experiment generated pressures between 180 and 300 bars, producing mainly CH_4 and CO_2 at reaction times of less than 1 h (Elliott, 2008). Above the critical point of water (374.15°C and 221.2 bars), 'hydrothermal gasification' shifts the product distribution towards gasification products (Peterson et al., 2008; Demirbaş, 2010; Toor et al., 2011; Akhtar and Amin, 2011; Elliott et al., 2015). At still higher temperatures (600–700°C), H_2, CH_4 and CO_2 were formed in 15 min, under pressures of 250–300 bars (Matsumura et al., 2005).

Akhtar and Amin (2011) have reviewed the role of process conditions during hydrothermal liquefaction, including the effect of the liquefaction medium, solvent density, temperature, pressure, heating rate, particle size, biomass feedstock, residence time and the effect of reducing gases or hydrogen donors. Short contact hydrothermal processing experiments with woody and herbaceous biomass at 200–230°C were shown to extract nearly 100% of the hemicellulose in just a few minutes, alongside 4–22% of the cellulose and 35–60% of the lignin.

Relatively few studies have been carried out to investigate the continuous flow hydrothermal liquefaction of biomass feedstocks. In a useful review, Elliott (2011) discussed early work on continuous-flow process development at Lawrence Berkeley Laboratory by Schaleger et al. (1982) and at the Albany Biomass Liquefaction Experimental Facility (Thigpen, 1982), as well as later work on the Hydrothermal Upgrading Plant in the Netherlands (Goudriaan et al., 2008). The capacities of these units were reportedly rather limited. Two pilot/demonstration start-up companies in Spain and Switzerland have more recently announced the use of 'semi-continuous'

hydrothermal carbonisation processes. Inevitably, these early stages of process development appear to be rather heavily subsidised. Consequently, not much effort has gone into developing hydrothermal liquefaction technologies at pilot- or demonstration-scale (Peterson et al., 2008; Toor et al., 2011; Elliott et al., 2015).

The further development of hydrothermal processes would probably benefit from determining reaction kinetics and the improved characterization of reaction pathways. Much of the exploratory work to date appears to have made use of closed ('batch') reactors. Further on in this chapter, we will review evidence showing that 'batch' reactors are of little help in either characterising reaction pathways or indeed working out reaction kinetics during coal liquefaction. The challenges provide a direct match with those encountered in using 'batch' reactors for the hydrothermal processing of biomass.

At the time of writing, more work also appears needed for developing overall energy balances. Kruse et al. (2013) have suggested that the efficiency of liquor recirculation and heat recovery are key factors in improving overall energy efficiency. Developing catalysts able to withstand hydrothermal reaction conditions, as well as methods for their recovery and re-use would improve process economics. In addition, novel 'solids management' methods appear to be required, for dealing with the precipitation of inorganic materials, which can lead to 'fouling and plugging' of ancillary equipment (Peterson et al., 2008).

Elliott et al. (2015) have claimed that there was significant potential for the commercialisation of continuous flow hydrothermal technologies. Techno-economic analyses (TEA) are reported to suggest that hydrothermal processes have economic potential, especially for converting algae or wet biomass/waste feedstocks into bio-liquids. However, the cost of constructing, operating and maintaining corrosion resistant, high-pressure, high-temperature reaction vessels and ancillary equipment appears likely to remain as one of the enduring challenges to the long term commercial prospects of hydrothermal processing of biomass. Research focused on making high value advanced carbon materials appears more promising in pursuing the development of thermal hydro-carbonization, against a background of relatively high plant and operating costs (Kruse et al., 2013; Titirici, 2013; Hitzl et al., 2015; Burguete et al., 2016).

Biomass liquefaction in organic solvents – in brief: Liquefaction of biomass with methanol, ethanol and acetone has been examined under supercritical conditions (270–310°C), with and without the use of catalysts (Aysu et al., 2015). In the absence of catalyst, the largest liquids yields were observed in acetone, with conversions increasing as a function of temperature from 50 to 64 wt%. The use of NaOH and $FeCl_3$ as catalysts was tested. When using NaOH, larger liquids yields were obtained with ethanol as solvent. With $FeCl_3$ as catalyst, liquid yields up to 72% were obtained in acetone. In all cases, $FeCl_3$ was found to be a more effective catalyst. The liquids yield was always greater when a catalyst was used except for acetone with NaOH, when the yield decreased.

The character of product bio-oils presents another challenge in developing hydrothermal liquefaction processes. As in the case of biomass *pyrolysis* tars/oils, these liquids are difficult to store and to process. They are corrosive. Gum formation and separation into aqueous and organic phases during storage is common. They often

contain particles of char and/or ash. The viscosity of the organic phase increases with storage time. Problems are also encountered during ignition in engines due to the low volatility of the fuel and the low calorific values due to relatively high oxygen contents, of up to 50% for pyrolysis oils and 10–20% for hydrothermal bio-oils (Peterson et al., 2008; Toor et al., 2011; Brownsort, 2009; Mohan et al., 2006; Huber et al., 2006; Irribaren et al., 2012; Diebold, 2000; Elliott et al., 2012).

5.1.2 The British coal liquefaction process

In what follows, we will observe that some of the experimental methods developed for studying *coal* liquefaction could be usefully applied to the hydrothermal processing of biomass. It therefore seems useful to briefly review one of the more familiar coal liquefaction processes.

The British Coal Liquefaction Project: In the late 1990s, a 2.5 ton day^{-1} pilot plant facility was constructed, commissioned and operated at Point of Ayr, near Prestatyn in North Wales (UK). Much of the work on coal liquefaction *fundamentals* outlined in this chapter was carried out using The British Coal Liquefaction Project as a reference point. A brief description of the process, would be useful for putting the bench-scale experimental research work into context.

Ground coal was slurried with a hydrogen-donor recycle solvent, pressurised to 20 bars, preheated to 410°C and fed to a digester with an average residence time of 1 h. Up to 95% of the coal was dissolved. These high conversions were achieved through the hydrogen-donor properties of the recycle solvent, and no externally added high-pressure hydrogen was used *in the digester*. In the case of 'over-hydrogenation', the donor content of the recycle solvent could be 'trimmed' by the use of a 'saturates cracker', or in case of 'under-hydrogenation', adjusted by mild hydrogenation. The authors explained that, '…an excellent monitor of solvent quality during recycling is (whether) the solvent (dissolves the sample of coal in)… a bomb test, (which) picks up trends *before* plant performance is affected…' (Harrison et al., 1989).

After digestion, the product stream was cooled to 300°C and filtered before entering the two ebullating bed catalytic hydrocrackers (~420°C, 210 bars). The hot-filtration stage developed and successfully tested by British Coal was considered key to the technical and economic viability of the project (Kimber and Davies, 1988; Kimber, 1989). The product mixture from the catalytic hydrocracking stage was distilled to give three main streams: (1) propane and butane (approximating LPG), (2) a naphtha fraction, boiling below 180°C, and (3) 180–300°C boiling middle distillates. Some of the solvent was recovered and a byproduct pitch stream boiling above 500°C was partly bled-off, but mostly recycled into the digestion stage as the donor-solvent. The process was originally designed for a narrow rank range of British coals and subsequently operated using brown coals and lignites (Kimber, 1997).

It seems useful to briefly compare the British Coal 'LSE' process scheme with several other coal liquefaction processes piloted during the same period. The Catalytic Two-Step Liquefaction (CTSL) process, supported by the US Department of Energy (e.g., see Comolli and Zhou, 2000) differs from the LSE process in that, coal is reacted with process-derived recycle solvent *and hydrogen, and* in the presence of a

supported Ni–Mo catalyst in two coupled reactors. The Ruhrkohle AG/VEBA OEL AG Kohleoel process similarly contacted coal with catalyst (a disposable 'red mud' iron catalyst was employed) in the presence of a recycle solvent and hydrogen. The flow sheet of this plant was based on the process used at industrial scale up to 1945 (CCTP, 1999). The 150-tons day^{-1} Japanese NEDOL process (Onozaki et al., 2000) also involved mixing coal with solvent, hydrogen and a synthetic iron-based catalyst. As in the LSE process, the heavier fractions of the product mixture were recycled as donor-solvent after hydrogenation.

In this context, the simultaneous upgrading of coal and petroleum heavy ends ('coprocessing' – see, e.g., Bartle et al., 1994), would have seemed attractive, at least in principle. Feedstock compositions would have been altered in response to market-price trends, and the expectation was that the higher hydrogen contents of petroleum resids might have given rise to useful chemical synergies. However, the generally low concentrations of hydrogen *donors* in petroleum resids did not give rise to significant synergies during coprocessing, despite their higher hydrogen contents. Experimental results did not allow devising convincing coprocessing schemes, largely because of the differing chemical natures of coal and petroleum resids, which necessitated markedly different processing conditions.

5.2 Liquefaction fundamentals: two stages in the solvent extraction of coals

This chapter continues the discussion focused on discriminating between the thermal response of solid fuels and reactor specific effects during experiments on solid fuels. As already mentioned, liquefaction experiments performed in 'batch' reactors do not allow identifying reaction pathways or working out the kinetics of the process. In Section 5.3, the design of a semi-continuous 'flowing-solvent reactor' will be presented, which attempts to overcome these shortcomings. Data from this reactor will be reviewed alongside observations from electron spin resonance (ESR) spectrometry (see chapter 6, Elements of thermal breakdown: heating rate effects and retrogressive reactions), to explore some of the chemical transformations underlying thermal breakdown in coals.

Coal extraction and covalent bond cleavage: Extraction at temperatures below the onset of thermal breakdown may be carried out with several different objectives in mind: (1) to study the chemical structures of coals and coal-derived materials; (2) to investigate relationships between amounts and structures of extractables and the coking behaviour of coals, and (3) to probe the relationship between extractable contents and pyrolysis tar yields, or indeed the levels of conversion during liquefaction (e.g., cf. Lowry, 1963; Elliott, 1981).

A useful starting point for describing the solvent extraction of coals is the work of Iino et al. (1988). These researchers contacted an array of coal samples with a 1:1 mixture of CS_2 and 1-methyl-2-pyrrolidinone (NMP) at room temperature. This mixture has provided the strongest solvent combination yet, for extracting coals at

room temperature. Large extraction yields (30–66%) were reported for 29 of the 49 bituminous coals examined, with elemental C-contents ranging between 76.9% and 90.6% (daf basis). Extract yields were reported to trace a maximum for middle rank bituminous coals. Coal extraction at the boiling points of common solvents such as chloroform and pyridine also represent the dissolution of relatively smaller molecular mass material in coals, prior to the onset of massive covalent bond cleavage.

ESR spectroscopy (Fowler et al., 1988, 1989a,b) is another tool at our disposal, for evaluating transformations taking place when coals are heated. ESR spin populations of stable free radicals begin to increase from about 300–310°C and rise rapidly *after* about 350–375°C, providing (indirect) evidence for the onset of extensive bond cleavage reactions at and above the 350–375°C band.

Solvent extraction of coals prior to thermal breakdown: When coals are preheated to increasing temperatures below the *onset* of covalent bond rupture (i.e., below ~310–350°C) before extraction, extract yields are found to increase gradually. However, major proportions of the coal remain in solid form. During straightforward liquefaction experiments, sample dissolution at temperatures *below* the characteristic depolymerisation band near 350°C precedes extensive thermal breakdown. In batch reactors, extraction products from these two distinct stages inevitably get scrambled together.

When using strong solvents, the proportions of coal extracted at temperatures up to about 350°C are not inconsiderable. In tetralin (tetrahydronaphthalene), a set of selected coals released amounts of extract representing between 30% and 58% of the original sample mass (Xu and Kandiyoti, 1996). These experiments were conducted by heating at 5°C s^{-1} to 350°C, with 1600 s holding in the 'flowing solvent reactor' described in Section 5.3.

Two stages of coal liquefaction: In view of experimental uncertainties (Fowler et al., 1989a) and the likely distributions of bond strengths within complex coal structures, the 350–375°C band cannot be treated as a precise dividing line for deeper extraction to begin. Results presented (e.g., see Fig. 5.1) suggest that the characteristic temperature band may shift up or down by 10°C or 20°C, depending on the properties of individual coals. It seems possible, nevertheless, to broadly distinguish between mass loss taking place prior to and following the onset of extensive covalent bond scission. We will see in Section 5.7, below, that it makes sense to treat these two phases of extraction as distinct, since the energies of activation turn out to be quite different.

The foregoing does not pretend to contribute to debates on the description of coal structure in terms of a 'mobile' and a 'macromolecular' phase. Cumulative extract yields at temperatures up to 350°C change significantly depending on the nature of the solvent. In the flowing-solvent reactor, with a 400 s hold at 350°C, the extract yield from Point of Ayr coal changed from 24.6% in tetralin, to 39.5% in quinoline (Xu et al., 1994). Multi-step extraction (Nishioka, 1991) or the use of more powerful solvents, such as NMP (Takanohashi and Iino, 1990) is likely to give higher extract yields, at temperatures *below the onset of extensive covalent bond scission*. It does not therefore appear possible to distinguish between the presumed *distinct* phases in coals, often described in terms of a 'host-guest' model.

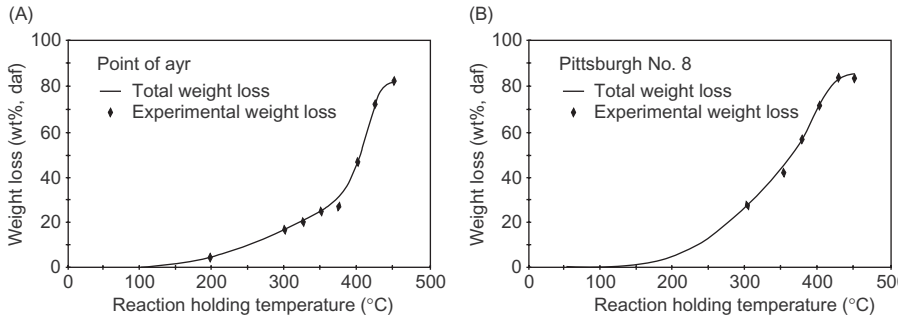

Figure 5.1 Sample weight loss from (A) Point of Ayr and (B) Pittsburgh No. 8 coals as a function of temperature in the flowing solvent reactor. Samples were heated at 5°C s^{-1} to 450°C with 400 s hold. Tetralin flow rate: 0.9 mL s^{-1} at 70 bars.
Source: Reprinted with permission from Xu, B., Kandiyoti, R., 1996. Energy Fuels 10, 1115. Copyright 1996 American Chemical Society.

Returning to liquefaction, once temperatures reach levels where extensive covalent bond cleavage is initiated, the remaining solid mass begins to break down into solvent soluble material. Evidence will be presented below, showing that, unless hydrogen is quickly supplied to materials freshly released from the solid matrix, retrogressive recombination reactions may significantly affect eventual product distributions. When that happens, the already 'liquefied' products begin to increase in molecular mass and viscosity and eventually solidify to a char.

In the laboratory, hydrogen donor solvents such as tetralin have often been used to quench free radicals and stabilise liquefaction products. At pilot or plant level, hydrogenated recycle liquids have been used for the same purpose. It is important to note, however, that donor-solvents may not be the strongest *solvents* for coal-derived materials, and that strong solvents for coal-derived materials may not necessarily be good hydrogen donors or indeed have any hydrogen-donating ability at all (e.g., NMP or quinoline).

Fig. 5.1 shows that between 30% and 40% of the mass of Point of Ayr (UK) and Pittsburgh No. 8 (USA) coals may be extracted in tetralin, at temperatures up to about 350°C. For Point of Ayr coal, the amount of liquefaction product released rose sharply from about 360–375°C. This temperature range corresponds therefore to the onset of extensive depolymerisation of the coal. In the case of Pittsburgh No. 8 coal (Fig. 5.1B), the transition was not as sharply defined. For some coals, however, the transitional temperature band for thermal breakdown may occur at higher temperatures (375–400°C), and in the unusual case of 'K-9 coal' described in Chapter 6, Elements of thermal breakdown: heating rate effects and retrogressive reactions, at about 425–450°C (Fukuda et al., 2004).

The data in Fig. 5.1 show, moreover, that up to 85–90% of the mass of suitable coals may be dissolved by the application of heat in the presence of hydrogen donor solvents. These extracts may be recovered in solution, but are not immediately usable.

They are normally viscous and consist of large-molecular mass materials that need to be hydrocracked and refined before use. Reduction of molecular mass and heteroatom content normally requires severe reaction conditions, with attendant high costs for producing saleable fuels and chemical feedstocks. Process stages designed for upgrading primary coal extracts thus tend to require a larger proportion of the total effort and expense. During pilot-plant tests at the British Coal Liquefaction Facility, hydrogen costs alone were calculated to make up as much as ~25% of total operating costs (Kimber, 1997).

5.3 On the design of bench-scale liquefaction experiments

In the laboratory, liquefaction experiments are ordinarily carried out in 'batch' reactors. These are usually small sealed autoclaves or 'bomb' reactors (e.g., see Clarke et al., 1980). Solid fuel, solvent and catalyst, if required, are charged to the reactor at the start of an experiment. High pressure hydrogen may be used to help the liquefaction process. The reactor is usually heated electrically, or by dipping into a heated sand-bath for 'rapid' heating. After a pre-set time period, the reactor is cooled and emptied and the contents examined.

In principle, the design of liquefaction experiments ought to require as much discrimination between reactor-induced effects and the thermochemical response of the fuel, as was the case for pyrolysis and gasification experiments. In this section, we will first examine the design of conventional 'batch' liquefaction experiments, where product distributions appear to be largely determined by the reactor configuration. We will discuss an alternative reactor design that has proved helpful in revealing key elements of thermal breakdown processes, allowed the identification of some reaction sequences and helped formulate a kinetic model that gave physically meaningful results.

The trouble with 'bomb' reactors…: Conventional autoclaves are heated at several degrees per minute. This means that part of the conversion takes place at lower temperatures than the peak temperature, and at different reaction rates than would have been the case at the peak temperature. Uncertainties involved in taking account of conversion during heat-up and cool-down limits the use of autoclaves, when the aim is to determine *reaction sequences* and *rates* of dissolution (Gorin, 1981).

The introduction of 'micro-bomb' reactors, which have considerably less thermal inertia, has helped improve time resolution during liquefaction experiments. 'Bomb' reactors may be heated and cooled more rapidly than traditional autoclaves. In this mode of heating, the initially high heating rate slows down as the target temperature is approached. We will see below, however, that changes in heating rate do *not* alter coal conversions in batch reactors significantly, so long as a fairly high solvent-to-coal ratio ($\geq$4:1) of hydrogen donor solvent is maintained.

The introduction of 'micro-bomb' reactors thus provided some improvement over the challenges of using massive autoclaves. However, as discussed in relation to the

hydrothermal processing of biomass, 'batch' reactors are not helpful when the objective is to resolve reaction sequences or determine reaction rates. We will see below (Table 5.2) that, depending on the coal selected, more than a quarter of the coal mass usually dissolves during the heatup stage, particularly when target experimental temperatures at or above 400°C are selected. In calculating reaction rates, some researchers have tended to ignore product release during heatup and assigned *all* product formation to the final target temperature. Moreover, many *reaction rate* calculations have come up with a single energy of activation, purporting to represent the liquefaction process as a whole. This has led to the calculation of unrealistically low energies of activation (e.g., Shin et al., 1989). We will see below that it is necessary to calculate reaction rates by assuming physically realistic conversion versus temperature profiles, which take account of a continuously changing time-temperature-conversion relationship.

In search of the sequence of reactions…: The other difficulty associated with conventional batch (closed) liquefaction reactors concerns the fate of the products that are progressively released into solution. During a liquefaction experiment, coal- or biomass-derived materials extracted by the solvent at low temperatures, as well as the products of depolymerisation as a result of covalent bond cleavage reactions, are sequentially released into the liquid phase. In batch reactors, all reactor contents remain exposed to the sequence of reaction conditions during the entire length of the experiment, against a background of rising temperatures and rising product concentrations in the liquid phase.

Depending on the type of experiment intended, batch reactor digestion times may last anywhere from 5–10 to 120 min, or even longer. The procedure provides ample opportunity for reaction products to enter into secondary reactions with any of the materials inside the reactor. The range of possible products formed through the secondary reactions of primary extracts depends largely on the temperature and the local availability of hydrogen. They can form predominantly heavier products and secondary char, or lighter liquid products and gas, with cracking and re-polymerisation reactions being enhanced by catalytically active solids. The mixture recovered from batch reactors might therefore contain primary extraction products, scrambled with products of whatever secondary reactions have occurred in the product mix. It is difficult to see how reaction sequences may be unravelled by examining the final product mixture recovered after experiments staged in 'batch' reactors.

However, investigating the behaviour of fuel particles during liquefaction requires conversion data and information on product compositions, structures and reactivities, as a function of time and in a manner free from the effects of secondary reactions. A measure of clarity may be achieved if we are able to distinguish between sample mass loss and the subsequent fate of the extracts. This particular objective necessitates the removal of products from the reaction zone as soon as they are released into solution. In this respect, the batch reactor configuration is entirely unsatisfactory.

The challenge is not unlike the one faced in designing pyrolysis experiments, where it was desired to recover primary products not affected by secondary reactions and other reactor related effects. To this end, variants of the wire-mesh and of the fixed-bed 'hot-rod' reactors described in Chapter 3, Pyrolysis of solid fuels: experimental design and applications, have been tested in liquefaction mode.

5.3.1 *The* wire-mesh *liquefaction reactor*

Initially, constructing a wire-mesh reactor for liquefaction experiments appeared promising. The coal sample was loaded onto the mesh in a horizontal, cylindrical high-pressure chamber, where the plug at one end of the cylinder carried the two long (horizontal) electrodes, between which the wire-mesh sample holder could be mounted. Thermocouples were fastened, after the sample laden mesh had been fixed between the electrodes, much as described in Chapter 3, Pyrolysis of solid fuels: experimental design and applications, and Chapter 4, High-pressure reactor design: pyrolysis, hydropyrolysis and gasification.

The reactor was then filled with tetralin and the heating sequence triggered; the time-temperature ramp was followed by a variable length holding-time, at 'peak' temperatures between 350°C and 450°C. However, from the first test, sample particles showed evidence of swelling and coking. Such events would have been expected at temperatures far higher than those measured by the thermocouples attached to the mesh. Discoloration of the mesh in the vicinity of coal particles also suggested that higher temperatures than those intended (~350–450°C, max.) had been reached by the mesh and apparently by the sample particles. An explanation was needed for the observed overheating.

When the horizontally positioned wire-mesh is heated, the solvent (in this case, tetralin) in the immediate vicinity of the mesh picks up heat and expands. Natural convection currents are thus initiated within the reactor. The solvent initially below the mesh sweeps through it, removing heat from the mesh as well as removing some dissolution products from the vicinity of the coal particles. The initially cool liquid removes vastly more energy from the mesh than would be the case during experiments in a gaseous atmosphere. This forces the control system to deliver large electrical currents, to keep pace with the pre-programed time-temperature ramp of the sample holder.

It eventually became clear that the points where heat was not withdrawn from the mesh were those points where solvent flow was blocked by the presence of sample particles. The resulting local overheating could not be suppressed even when the total sample was reduced to a *single coal particle*. This precluded the use of a wire-mesh type reactor for coal liquefaction. The attempt was abandoned.

5.3.2 *The design of the 'flowing solvent reactor'*

The use of a continuous stream of gas to sweep products out of the reaction zone has been described in Chapter 3, Pyrolysis of solid fuels: experimental design and applications, and Chapter 4, High-pressure reactor design: pyrolysis, hydropyrolysis and gasification. The 'flowing solvent reactor' described below was developed by adopting a fixed-bed reactor configuration, similar to that of the 'hot-rod' reactor.

This reactor consisted of a length of high-pressure tubing, within which a sample of coal was mounted in the form of a fixed bed. The sample was heated by passing an electrical current through the walls, and was continuously swept through, by a stream of pressurised solvent. However, adapting the 'hot-rod' configuration to liquefaction experiments required several modifications. When operating at the usual

low superficial gas velocities (~0.1 m s^{-1}), it was possible for the carrier gas to reach the reaction section temperature simply by contacting reactor walls. During the few experiments performed at very high superficial gas velocities (~10 m s^{-1}), a wire-mesh plug was inserted into the reactor to help pre-heat the gas stream. However, solvents have far greater heat capacities than the gas stream in the comparable 'hot-rod' reactor, and a new arrangement had to be devised for pre-heating the solvent before it reached the sample bed.

In the flowing-solvent reactor, the sample temperature was ramped linearly up to the target temperature, held there for a pre-set time period, followed by cool-down, by sweeping through with unheated solvent. In order to raise the temperature of the *solvent* to the (continuously changing) temperature of the sample, the bottom half of the reactor tube was left empty, its rate of direct electrical heating being controlled separately, and driven by a thermocouple placed immediately above the plug of sample (Fig. 5.2). This arrangement enabled solvent sweeping through the reactor to reach the temperature of the sample stage, before contacting the fixed bed of sample.

During trial runs with the 'flowing-solvent' reactor, a *surge* of product from the sample-bed was observed, usually between 390°C and 425°C. It was necessary to temper the rush of these viscous extracts, in order to avoid clogging up the interstices

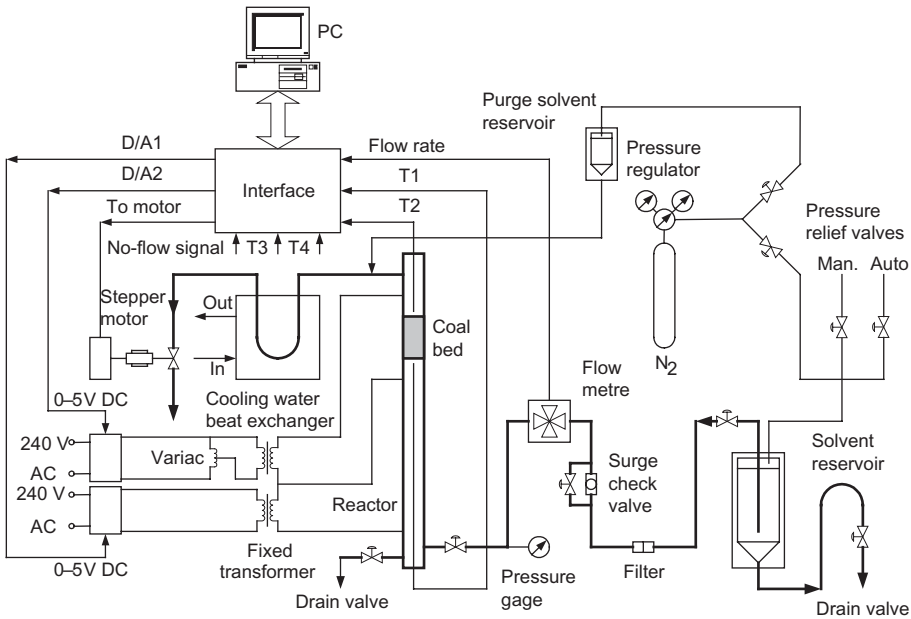

Figure 5.2 Schematic diagram of the flowing solvent reactor system. The thick line from the reservoir traces the solvent flow path. The solvent is forced through the fixed coal bed and sweeps dissolved product into the heat exchanger. The letdown valve is attached to a computer-controlled stepper motor and serves to control the flow rate.
Source: Reprinted from Xu, B., Dix, M., Kandiyoti, R., 1995. Rev. Sci. Instrum. 66(7), 3966 with the permission of AIP Publishing.

between coal particles and blocking the flow of solvent through the fixed bed of sample. The solution adopted was to dilute the coal sample with sand particles. This expedient reduced the *local* concentration of extract released during the temperature interval of interest. The arrangement was similar to that of Kershaw and Barras (1979), who used it in their 'hot-rod' reactor, constructed for *hydropyrolysis* experiments.

The 'flowing-solvent' configuration allowed extraction and liquefaction products to be removed from the reaction zone within 6–10 s after being released from parent coal particles. In contrast to (closed) 'batch' reactors, this configuration avoided 'cooking' products in the presence of reacting fuel particles. Moreover, by forcing an excess of solvent through the bed of particles, it was possible to extract coal particles against a virtually 'zero' external product concentration within the solvent. This helps reduce diffusive resistances that build up when (as in a batch reactor) the concentration of product dissolved in the solvent increases continuously. By virtue of the extraction process taking place against a virtually 'zero' product concentration, this feature has the advantage of nearly standardising extraction conditions between different samples.

There were several antecedents of the reactor constructed at Imperial College. Koll and Metzger (1978) installed a fixed bed reactor in a gas-chromatographic oven and swept it with a stream of supercritical acetone to remove the degradation products of cellulose and chitin. Squires and coworkers (Squires et al., 1983; Aida et al., 1985; Slomka et al., 1985, 1986) used a similar reactor configuration, mostly for studying the supercritical extraction of coals with benzene and other light hydrocarbons. Interestingly, they attached an UV-absorption detector at the exit of the reactor to monitor changes in product composition. McPherson et al. (1985a,b) used a fixed-bed reactor immersed in a heated sand-bath. The coal bed mounted inside the reactor was swept with tetralin. These researchers reported on the morphology of solid residues and the reactions of *tetralin* during coal liquefaction.

The reactors mentioned in relation to these studies have all used various types of external heating: a GC oven and a sand fluidised bed have already been mentioned. Due to their high thermal inertia, these systems can only apply limited rates of heating or cooling. In the work of Squires and coworkers, even with supplementary heating from electrical heating tape wound around the reactor, peak heating rates were limited to a maximum of about 2.5°C s^{-1}.

The flowing solvent reactor constructed at Imperial College was similar in conception to the 'hot-rod' reactor, constructed for pyrolysis and hydropyrolysis experiments. The basic device was a tubular reactor with an empty inlet (solvent-preheating) zone making up the bottom section. A fixed bed of coal was mounted above this zone, between two porous wire-mesh plugs. Both sections were heated directly by clamped copper electrodes. The temperatures of the upper (sample holding) and lower (solvent pre-heating) sections were controlled separately. With the thermal inertia of the system thus kept to a minimum, heating rates well in excess of 10°C s^{-1} could be achieved. The time-temperature histories of the samples were pre-programed and controlled by an online computer. The original apparatus described by Gibbins and Kandiyoti (1990, 1991a,b) was subsequently revised and equipped with a 'Mark-II' computer controlled system (Xu et al., 1995; Xu and Kandiyoti, 1996).

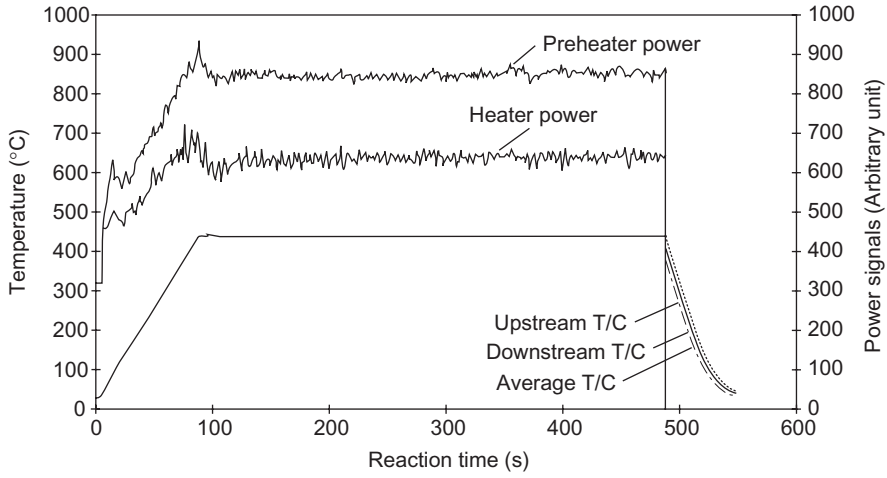

Figure 5.3 Flowing-solvent reactor time-temperature and power-control histories. The sample was heated at 5°C s^{-1} to 450°C with 400 s hold. Solvent flow rate: 0.9 mL s^{-1} at 70 bars.
Source: Reprinted with permission from Xu, B., Kandiyoti, R., 1996. Energy Fuels 10, 1115. Copyright 1996 American Chemical Society.

Fig. 5.2 presents a schematic diagram of the flowing-solvent reactor system. The reactor tube made of Haynes 230 alloy (Ni with 22% Cr, 14% W, 2% Mo, 3% Fe, 5% Co) had an outside diameter of 3/8-in. (0.95 cm), with 0.036-in. (0.091 cm) wall thickness and was capable of withstanding the intended pressure of 70 bars at up to 1000°C. It was packed with a mixture of ~200 mg coal and 2800 mg acid-washed sand (106–150 μm), mounted as an (approx.) 50 mm deep fixed bed between the two wire-mesh plugs. The temperature was measured by 1 mm diameter, mineral-insulated sheathed thermocouples positioned immediately above and below the bed.

The use of pumps was avoided, in order to maintain a steady flow of liquid. Instead, solvent was forced from a pressurised reservoir (0.9 mL s^{-1} at 70 bars) through a surge check-valve and flow metre, into the lower section of the reactor tube, which served as the solvent pre-heater stage. Power to both sections of the reactor was supplied and controlled separately. Temperature control in the pre-heater (lower) section was set for delivering solvent to the reactor (upper) section, at the temperature of the latter. Samples were ordinarily heated at 5°C s^{-1} to the intended peak temperature and held for between 100 and 1600 s. Fig. 5.3 presents a typical time-temperature profile, showing a heatup ramp, a 400-s holding period and the cool-down ramp. The power-input versus time traces for the two reactor stages have been plotted against arbitrary units. Details of the heating and temperature control system, including the designs of the purpose built electronic circuit cards have been described by Xu et al. (1995).

The reactor was operated without a gaseous medium (e.g., hydrogen), other than the N_2 used for pressurising the liquid reservoir. A large excess of solvent (600–1000 mL) was passed through the sample bed during a run, where no more

than ~200 mg of coal were being reacted. Products released by the coal were diluted by solvent and the mixture rapidly swept out of the reaction zone into a cooler-heat exchanger unit. The interval between the dissolution of product and its arrival in the cooling zone was estimated to be between 6 and 10 s.

At the exit of the reactor, the product stream was cooled in the heat exchanger to near ambient temperature, causing coal extracts to precipitate out of solution; this tended to block the letdown valve and slow down the solvent flow rate. To counter this effect, a computer-controlled pressure letdown valve was placed at the reactor exit. The flow-control system was designed to open the valve until the blockage was removed and then to restore the flow rate to pre-set levels. The reproducibility of sample weight-loss measurements was usually better than ±1.5%. Conversions were not found to be sensitive to solvent pressure changes between 50 and 100 bars and flow rate changes between 0.9 and 2.4 mL s^{-1} (Gibbins and Kandiyoti, 1990, 1991b; Xu and Kandiyoti, 1996).

Had it worked as intended, the 'liquefaction wire-mesh' reactor described in Section 5.3.1 would have allowed the measurement of changes in conversion over a wide-range of heating rates. The thermal inertia of the flowing-solvent reactor system did not allow such wide variations in heating rates to be applied. Nevertheless, some variation in heating rate was possible. It was found that changes in heating rate between 0.3 and 10°C s^{-1} had no measurable effect on coal conversion, when operating with tetralin as the liquefaction medium (Gibbins and Kandiyoti, 1990). We will return to this observation in Chapter 6, Elements of thermal breakdown: heating rate effects and retrogressive reactions.

5.3.3 Liquefaction trends in the flowing solvent reactor

Fig. 5.1A, B show the type of conversion versus temperature data that are normally obtained from the flowing-solvent reactor. Each point on the diagram represents the weight loss from a single experiment. The set of experiments described below was carried out with seven samples drawn from the Argonne Premium Coal Sample (APCS) Program (Vorres, 1990) and a Point of Ayr (UK) coal sample provided by the Point of Ayr Coal Liquefaction Project. Table 5.1 presents elemental analyses for the set of samples ranging from a lignite to a semi-anthracite.

Table 5.2 presents experimental weight loss data from the flowing-solvent reactor, as a function of temperature. Comparing results between 350°C with 1600 s holding and 375°C with 400 s holding, all samples showed significant increases in weight loss over the temperature interval, except for Point of Ayr (UK), Upper Freeport, and Pocahontas No. 3 coals. The data suggest that for these three coals the transition temperature band, delineating simple extraction from the depolymerisation stage, was probably somewhat higher than 350°C. In the kinetic model calculations outlined below, 375°C was used as the characteristic transition temperature, T_d, to delimit Stage A (extraction) and Stage B (depolymerisation) processes for these three coals.

Several points arise from an inspection of data in Table 5.2. The large conversions of Upper Freeport coal at relatively low temperatures were consistent with the 59.4% extraction yield from this sample in a mixture of CS_2 and 1-methyl-2-pyrrolidinone at room temperature (Takanohashi and Iino, 1990). The next largest extraction yield reported by Takanohashi and Iino was 39.2% for Pittsburgh No. 8 coal.

Table 5.1 Elemental Analysis of the Argonne (APCS) coals (Vorres, 1990) and Point of Ayr (UK) coal (Xu, 1995)

Cool Sample	C (daf)	H (daf)	N (daf)	S (daf)	O (by diff)	ash (dry basis)
Beulah-Zap	72.9	4.8	1.2	0.7	20.4	9.7
Wyodak Anderson	75.0	5.4	1.1	0.5	18.0	8.8
Illinois No.6	77.7	5.0	1.4	2.4	13.5	15.5
Blind Canyon	80.7	5.8	1.6	0.4	11.5	4.7
Pittsburgh No. 8	83.7	5.3	1.6	0.9	9.0	9.3
Upper Freeport	85.5	4.7	1.6	0.7	7.5	13.2
Pocahontas No. 3	91.0	4.4	1.3	0.5	2.8	4.7
Point of Ayr (UK)	84.5	5.4	1.8	1.5	6.8	9.6

Table 5.2 Primary liquefaction yields from eight coals in the flowing-solvent reactor

Holding temperature (°C) Holding time (s)	300 400	350 400	*350* *1600*	375 400	400 400	425 400	450 400	*450* *1600*
Coal sample	Weight loss (w/w, %, daf)							
Beulah-Zap	17.4	31.1	*40.6*	46.7	55.2	68.3	75.0	*84.0*
Wyodak-Anderson	25.0	35.0	*38.6*	45.2	62.0	73.1	82.0	*88.6*
Illinois No. 6	24.6	47.3	*54.7*	61.6	79.8	89.0	90.0	*94.7*
Blind Canyon	22.9	35.4	*37.9*	48.6	73.0	84.4	91.0	*92.0*
Pittsburgh No.8	26.6	41.5	*55.2*	56.4	71.6	84.7	84.2	*89.0*
Point of Ayr (UK)	17.0	24.6	*36.0*	27.0	47.0	72.5	82.5	*84.0*
Upper Freeport	39.7	51.9	*57.9*	58.7	67.0	75.0	81.8	*86.0*
Pocahontas No. 3	9.0	24.0	*29.8*	27.3	32.7	39.8	43.5	*70.0*

Source: Reprinted with permission from Xu, B., Kandiyoti, R., 1996. Energy Fuels 10, 1115. Copyright 1996 American Chemical Society.
Samples were heated in tetralin at 5°C s^{-1}, to the holding temperature. Solvent flow rate: 0.9 mL s^{-1} at 70 bars (g).

In Table 5.2, the conversions of most coals for 400-s holding at 450°C were close to the 'ultimate' conversion observed at the same temperature with 1600 s holding. At 450°C, only the conversion of Pocahontas No. 3 coal increased quite substantially during holding between 400 and 1600 s, probably reflecting the more highly crosslinked structure of this coal.

The two stages of coal liquefaction: The foregoing suggests that coal liquefaction in the flowing-solvent reactor may be described, principally, in terms of two successive stages:

1. Extraction of material soluble in the particular solvent, at up to the transitional temperature band, *prior to extensive depolymerisation*, followed by dilution and transport of extract molecules out of the reaction zone,

2. Extraction of material released by the coal matrix *during extensive depolymerisation*, taking place above the transitional temperature band.

The conversion *data* in Table 5.2 do not allow an estimation of the temperature of the onset of covalent bond scission, likely to take place at lower temperatures, but provide clear indications for the onset of generalised product release due to extensive bond rupture. We will return to this point in Chapter 6, Elements of thermal breakdown: heating rate effects and retrogressive reactions, and try to locate the transition between the extraction and depolymerisation stages more precisely, with the aid of data from ESR spectroscopy.

Conversion during heatup: Fig. 5.5A shows an additional effect, which is important in trying to understand the *kinetics* of coal liquefaction. The figure clearly shows that substantial amounts of product (~ 30–35%) was released by Point of Ayr coal during *heatup*, before the liquefaction temperatures of 400°C or 425°C were reached (also see Figures 1 and 5 in Gibbins et al., 1991). In the past, many calculations of kinetic constants have made use of the relationship between conversion in a batch reactor and the final (highest) temperature reached in the reactor (e.g., see Shin et al., 1989). In such calculations, the material released during heatup, i.e., over a wide band of temperatures from ambient to peak temperature, are assumed to have taken place at the *final* temperature. Apart from scrambling the rates at which products are released over the spread of temperatures, this approach tends to mask the distinct dissolution rates governing the extract release and the depolymerisation stages of coal liquefaction.

5.4 Comparing liquefaction in the 'flowing-solvent' reactor and a 'mini-bomb'

The advantages of the flowing-solvent reactor may be restated as the largely intact removal of primary liquefaction products from the reaction zone, in the relative absence of secondary reactions. During the initial phase of the work, it was also anticipated that the new reactor would possibly give higher conversions and show what effect changes in heating rates would have on coal conversions. As explained in Section 5.3, however, no differences in conversions were observed for changes in heating rates between 0.3–10°C s^{-1}, when operating with tetralin as the liquefaction medium (Gibbins and Kandiyoti, 1990).

The proposition that higher conversions might be obtained compared to 'batch' reactors, was put to the test by parallel experiments in a batch reactor. Conversions and liquid product properties were compared. The extractions were carried out using tetralin and 1-methylnaphthalene, the former a known hydrogen-donor solvent and the latter, a stronger solvent for coal-derived materials, but at best, a poor hydrogen-donor (Gibbins et al., 1991). The parallel 'mini-bomb' reactor experiments were carried out at the Point of Ayr Coal Liquefaction Facility, with samples drawn from the same batch of Point of Ayr coal. A solvent to coal ratio of 4:1 was used in experiments between 385°C and 460°C. The bombs were sealed under nitrogen at atmospheric

pressure (cold). A heat up period of three minutes in the sand fluidised bed was allowed for reaching the target temperature. The mini-bombs were held at peak temperature for contact times of 100, 400 or 1600 s, after which the contents were Soxhlet extracted with tetrahydrofuran (THF).

It was also observed that, when the mini-bomb reactor contents were extracted with *quinoline*, instead of cold THF, the apparent conversions increased by about 10–20%. These higher conversions were less sensitive to the reaction temperature. This particular washing procedure was not considered relevant to the pilot-plant operating conditions, and was set aside. It seems useful to note, however, that for any given set of coal liquefaction experiments, the procedure for washing residual solids is one of the parameters that determines what is meant by 'conversion'.

5.4.1 Two reactors: comparison of conversions in tetralin

The temperature versus conversion data from the two reactors showed similar trends, although, at first glance, conversions in the flowing-solvent reactor appeared larger by about 10%. Fig. 5.4 shows that differences between conversions in the two reactors (the two solid lines) for 100 s contact time were systematic over the temperature range.

However, the procedure for determining conversions in the flowing-solvent reactor involved washing the solid residue in *boiling* THF. To bring the procedures used in the two sets of experiments into line, (1) the cold-THF solubles extracted from the reaction residue from the flowing solvent reactor were counted as 'product', and (2) the mass difference between cold-THF solubles and hot-THF solubles was counted as 'unconverted material'. The experimental procedures have been described in greater detail by Gibbins et al. (1991). When conversions in the flowing-solvent reactor were recalculated on the same basis as in the mini-bomb experiments, differences between conversions observed in the two reactors diminished significantly.

The corrected results from the two reactors were quite similar, once allowance was made for other minor variations between procedures employed in product isolation. It seemed reasonable to conclude from the foregoing that, when a tetralin-to-coal ratio of about 4:1 was used in the mini-bomb reactor, only minor differences emerged when compared with conversions in the 'flowing-solvent reactor'. An altogether different picture emerged, however, when conversions in the two reactors were compared in the presence of 1-methylnaphthalene.

5.4.2 Two reactors: comparison of conversions in 1-methylnaphthalene

1-Methylnaphthalene is an essentially non-donor solvent, but one known to have greater solvent power for coal-derived materials compared to tetralin. Fig. 5.5A, B presents conversions from liquefaction experiments in the two reactors, using tetralin and 1-methylnaphthalene at 400°C and 450°C.

The conversion versus temperature *trends* observed in the flowing-solvent reactor broadly reflected those observed when using tetralin, although the actual conversions

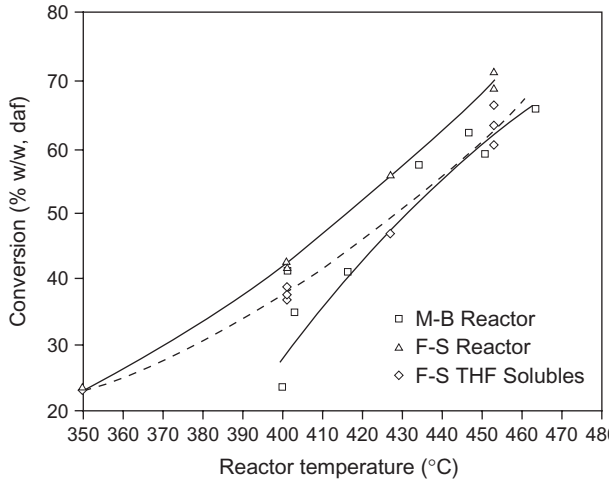

Figure 5.4 Comparison between overall conversions in tetralin, in the flowing solvent and mini-bomb reactors for 100 s holding at peak temperature. When procedures for calculating conversions were brought in line, differences between conversions in the two reactors were relatively minor. *M-B*, mini-bomb reactor; *F-S*, flowing-solvent reactor; F-S THF solubles (broken line ---): the recalculated conversion after the conversion was defined as cold-THF solubles as in the case of the 'mini-bomb' experiments.
Source: Reprinted from Gibbins, J.R., Kimber, G., Gaines, A.F., Kandiyoti, R., 1991. Fuel 70, 380. Copyright 1991, with permission from Elsevier.

were lower than in tetralin by about 10–12% (Fig. 5.5A). However, Fig. 5.5B shows major departures in the 'mini-bomb' reactor, from trends previously observed when using tetralin. Conversions at 400°C were lower by more than 20% when compared with conversions in tetralin. They were also considerably lower than values observed in *1-methylnaphthalene* experiments in the flowing-solvent reactor. Finally, at 450°C, Fig. 5.5B showed clear evidence of retrogressive char forming reactions in the 'mini-bomb' reactor. At contact times longer than 100 s, conversions *diminished* in the presence of 1-methylnaphthalene.

The latter trend was consistent with data from earlier work in a larger batch ('maxi-bomb') reactor. Clarke et al. (1980) found that conversions remain fairly constant at and above donor-solvent:coal ratios of 4:1. During experiments in which a solvent-to-coal ratio of 4:1 was used, extraction yields for Annesley (low rank UK bituminous) coal were observed to drop from 86% in tetralin to 48% in 1-methylnaphthalene. Experiments were also carried out in a 3:1 solvent-to-coal ratio with phenanthrene, another non-hydrogen donor but a strong solvent for coal-derived materials. When measured as a function of time in the presence of phenanthrene, sample weight loss for both Annesley and Beynon coals initially increased, and went through a maximum between 10 and 20 min contact time; the total solids in the vessel then sharply increased with time.

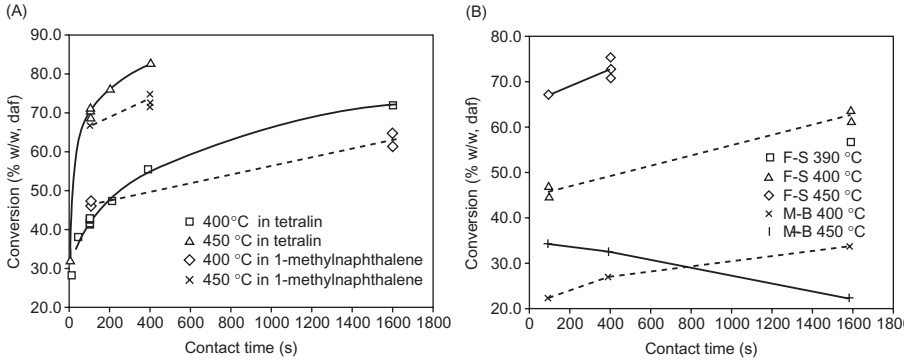

Figure 5.5 (A) Effect of solvent type on conversions in the flowing-solvent reactor. Heating rate: 5°C s^{-1}; solvent flow rate: 0.9 mL s^{-1} at 70 bars. (B) Flowing-solvent reactor and mini-bomb reactor comparison using 1-methylnaphthalene as the liquefaction medium; solvent/coal ratio in mini-bomb reactor: 4/1 by weight.
Source: Reprinted from Gibbins, J.R., Kimber, G., Gaines, A.F., Kandiyoti, R., 1991. Fuel 70, 380. Copyright 1991, with permission from Elsevier.

Shin et al. (1989) also reported small but identifiable increases in solid residue with increasing hold time, for three out of the five Argonne coals liquefied in their micro-bomb reactor with 1-methylnaphthalene. The latter experiments had been carried out under hydrogen pressure, confirming the expected relative inertness of 1-methylnaphthalene regarding hydrogen transfer reactions, but the data also showed some effect of the externally added hydrogen.

Higher flowing-solvent reactor conversions in 1-methylnaphthalene: It is perfectly possible that some of the impurities contained in the batches of 1-methylnaphthalene used (~98% purity) could have been performing a hydrogen-donating function. Due to the larger total volumes of solvent used in the flowing solvent reactor, compared to the 'mini-bomb', a small concentration of donor-material passing through the reactor could have made a measurable difference in conversion. However, gas chromatographic analysis did not show the presence of tetralin at or above the detection limit of the instrument, and no other hydrogen-donor materials could be identified in the solvent phase recovered from flowing solvent reactor experiments. The dimerisation of 1-methylnaphthalene has also been offered as a possibility for hydrogen release (Gibbins et al., 1991). It is likely, however, that the amount of hydrogen liberated into the reaction mixture by this route would be small.

On purely reactor design considerations, the difference between results from the two reactors (in the presence of 1-methylnaphthalene) may be explained in terms of two likely factors. First, the far greater dilution of products in the flowing solvent reactor, and the far shorter residence times in the reaction zone. During a single run, nearly 1 L of solvent passed through the fixed bed of sample of (initially) no more than about 200 mg. The dissolved coal-derived species would be diluted by excess solvent sweeping through

the fixed bed, and removed from the reaction zone into the cooling section in about 6–10 s. Comparing, the *hundreds* of seconds of residence time in the 'bomb' reactor would offer far more time for retrogressive recombination reactions to take place.

Fig. 5.5A shows that, compared to extraction in tetralin, the *absence* of externally (i.e., solvent) supplied hydrogen gives rise to product loss of about 10% of the coal mass, presumably through retrogressive reactions. It is likely that this loss is primarily due to relatively rapid retrogressive reactions taking place within the parent coal particles, i.e., before product molecules diffuse out of parent coal particles and are diluted by the solvent. In the flowing-solvent reactor, data for other coals showed similar small drops in conversion compared to liquefaction in tetralin (Gibbins et al., 1994).

5.4.3 The effect of reactor design on product quality

In Sections 5.4.1 and 5.4.2, we compared *conversions* from the two reactor configurations during liquefaction in two types of liquid phases. This section attempts to address the effect of reactor design on product quality.

Gibbins et al. (1991) compared size exclusion chromatograms (SEC) of liquefaction products recovered in the two reactors. In the initial phases of the work, THF was used as eluent. This solvent was subsequently shown to have several disadvantages when used as mobile phase in size exclusion chromatography. After the adoption of NMP (1-methyl-2-pyrrolidinone) as eluent, the work was repeated, confirming the original conclusions. Although SEC and its applications have been described in Chapter 8, Analytical techniques for high mass materials: method development, it seems useful to quickly review some observations regarding the comparison of product distributions from the two reactors.

The initial product characterization work was useful in distinguishing between the mechanisms operating in the two types of reactors. In the flowing solvent reactor, progressively larger molecular mass materials were released by the coal mass, as the peak experimental temperature was raised. Broader mass distributions were also observed when progressively longer hold times were used at peak temperature. These findings were interpreted in terms of the deepening of depolymerisation and extraction, as the temperature was raised and/or the hold time at a given temperature was prolonged. The opposite trend was observed when products from the 'mini-bomb' reactor were examined. The molecular mass distributions of products progressively narrowed with increasing temperature, and with exposure time at temperature. Overall, the flowing-solvent reactor gave products with broader molecular mass distributions under comparable holding times and temperatures.

It seems reasonable to assume that *primary* products detaching from the coal matrix in the two reactors initially had similar structures and molecular mass distributions. The observed differences in molecular mass distributions may thus be interpreted as reflecting the effect of secondary, cracking and repolymerisation reactions taking place in the mini-bomb reactor.

Fig. 5.6 compares SEC using NMP as eluent, of Point of Ayr coal extracts produced under four different sets of conditions. The samples shown in this diagram were prepared (1) in the flowing-solvent reactor, (2) in the mini-bomb (MB) reactor, using

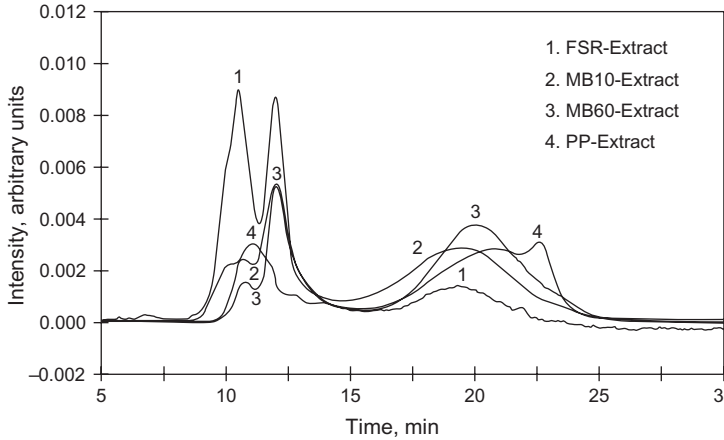

Figure 5.6 Size exclusion chromatograms (NMP eluent) point of Ayr coal extracts prepared in different reactors, detection by UV-absorption at 450 nm. Samples extracted in 1, flowing-solvent reactor; 2, mini-bomb 10 min; 3, mini-bomb 60 min; 4, Point of Ayr liquefaction pilot-plant (~1 h average digester time).
Source: Reprinted from Zhang, S.-F., Xu, B., Moore, S.A., Herod, A.A., Kandiyoti, R., 1996. Fuel 75, 597, 1996. Copyright 1996, with permission from Elsevier.

10 min reaction time at peak temperature, (3) in the mini-bomb (MB) using 60 min reaction time at peak temperature. Sample (4) was the filtered extract from the Point of Ayr coal liquefaction pilot-plant (~1 h average digester time) and was known to contain coal-derived recycle solvent.

Without going into details of size exclusion chromatography, it may be observed that the extract from the flowing solvent reactor gave more intense signal at short elution times. In SEC, larger size (and mass) molecules are expected to elute at shorter retention times compared to smaller molecular mass materials. The twin peaks appearing at shorter elution times thus represent a broader molecular mass distribution compared to the other samples. The diagram presents a qualitative picture of the extent of molecular size reduction, caused by extended residence times at reaction conditions in the mini-bomb reactor and in the pilot-plant digester (Zhang et al., 1996).

5.5 Effect of solvent type on conversion, in greater detail

We have already observed in Fig. 5.5A that in the flowing-solvent reactor, about 10–12% higher conversions were obtained in tetralin compared to liquefaction in 1-methylnaphthalene. We have also indicated that solvents could be classed according to their hydrogen-donor ability as well as their solvent power. Effective hydrogen-donors (e.g., tetralin) are not necessarily as powerful solvents for coal-derived

materials as some non-donor solvents (e.g., quinoline, phenanthrene). We will next describe a set of experiments designed to distinguish between the effects of the two functions on conversions during liquefaction.

Similar experiments were undertaken with tetralin, quinoline, a mixture of quinoline and phenanthrene (both effective solvents for coal-derived materials) and finally hexadecane, a straight chain aliphatic compound, which is neither a hydrogen-donor, nor known for its solvent power for dissolving coal-derived materials. The Point of Ayr coal sample used in these experiments had already been extracted at 350°C, without the onset of extensive depolymerisation reactions being observed. In Chapter 6, Elements of thermal breakdown: heating rate effects and retrogressive reactions, data from ESR spectroscopy will be used to confirm this observation.

The experiments described in Table 5.3 were designed to distinguish between the effects of the hydrogen-donor ability of tetralin and the high solvent power of two essentially non-donor solvents, quinoline and phenanthrene. On its own, phenanthrene is a solid at room temperature and would not have flowed through the tubing upstream of the reactor, unless mixed with another solvent that was liquid at room temperature, in this case quinoline.

Table 5.3 shows that at up to ~350°C, both quinoline and the mixture of quinoline and phenanthrene extracted greater proportions of the coal mass, compared to tetralin. The result is consistent with the known greater solvent power of these materials for dissolving coal-derived materials. At 450°C, however, the two non-donor solvents

Table 5.3 Comparing conversions between solvents and with a pyrolysis experiment. Liquefaction experiments with solvent flow rate of 0.9 mL s^{-1} at 70 bar (g). Pyrolysis experiments done with heating at 1000°C s^{-1} to 350 or 450°C.

	Heating rate (°C s^{-1})	Holding time (s)	Ambient medium	Weight loss	
				350°C	450°C
POA Vitrinite	1000 (pyrolysis experiment)	150	Helium	3.3	20.5 (2)[a]
	5	400	Tetralin	28.8[b]	77.6 (2)
	5	400	Q/P[c]	38.0	73.8 (2)
	5	400	Quinoline	—	72.7 (2)
	5	400	Hexadecane	12.5	27.3 (2)
POA Whole coal	5	400	Tetralin	24.6	82.5 (4)
	5	400	Quinoline	39.5	74.7 (2)
	5	400	Hexadecane	—	24.0 (1)

Source: Reprinted with permission from Xu, B., Madrali, E.S., Wu, F., Li, C.-Z., Herod, A.A., Kandiyoti, R., 1994. Energy Fuels 8, 1360. Copyright 1994 American Chemical Society.
All data are given on % w/w dry ash free basis.
[a]Number of repeated runs used for calculating the average value.
[b]Holding time, 500 s. The weight loss from 100 s experiments under the same conditions was 29.2%, within experimental error.
[c]Q/P, quinoline/phenanthrene (2.5:1 w/w) mixture.

gave lower conversions compared to tetralin; the results were consistent with those from 1-methylnaphthalene, another non-donor solvent (Fig. 5.5A).

Potentially important clues are provided by a comparison of liquefaction conversion data at 450°C, in tetralin and in the two more powerful solvents. As a first approximation, it seems safe to assume that the extent of coal depolymerisation is primarily a function of the temperature alone. In other words, with comparable coal samples at the same temperature, we expect approximately similar amounts of coal matter to detach from the parent solid matrix, irrespective of the surrounding medium – whether liquid or gas. In the case of a gaseous medium, pyrolysis data show that rapid char formation may be expected at temperatures above 450–470°C (depending on the coal – see chapter: Elements of thermal breakdown: heating rate effects and retrogressive reactions), through recombination reactions between reactive free radicals released by the coal matrix. In liquefaction, the temperature normally remains below this range and the use of a donor-solvent partially suppresses fast retrogressive reactions. That is why less volatile matter is released during pyrolysis to, say, 700°C, compared to the amount of product dissolved during most, but not all, attempts at coal liquefaction (see below).

We have also observed that retrogressive, char-forming reactions take place during 'liquefaction', in the non-donor solvent 1-methylnaphthalene, in the 'mini-bomb' reactor. It may be noted, however, that the rate of retrogressive reactions indicated by the downward slope of the (reversing) conversion line in Fig. 5.5B (after 100 s contact time) was clearly slow: the amount of solids increased, on a scale of *hundreds of seconds*.

During liquefaction in 1-methylnaphthalene in the flowing solvent reactor, there would have been insufficient time for extensive levels of these apparently slow retrogressive reactions to develop. This is because, less than 10 s elapses, between the dissolution of extract molecules in the solvent and the extracts reaching the cooling section of the reaction system (Fig. 5.2). Although the non-donor solvent would have been carrying dissolved material with ability to repolymerise, the level of dilution (~150–180 mg solute in 700–1000 mL solvent) appears to have largely helped suppress these reactions, as the mixture was swept out of the reactor.

On the basis of this evidence, it seems reasonable to postulate two distinct speeds for the occurrence of retrogressive reactions during liquefaction: (1) rapid retrogressive reactions due to short range interactions within the coal particles, taking place immediately following bond scission, in the absence of (or before the intervention of) donatable hydrogen, and, (2) slower radical recombination (retrogressive) reactions of less reactive material, if/when present in a concentrated phase, as in the 450°C mini-bomb reactor experiments of Fig. 5.5B. The *pyrolysis-based* data of Fukuda (2002), examined in Chapter 6, Elements of thermal breakdown: heating rate effects and retrogressive reactions, are similarly consistent with the occurrence, in successive stages, of fast and slow recombination reactions, within the same coal mass.

The strange case of liquefaction in hexadecane: In the absence of both solvent power and of hydrogen donor-donor ability, Table 5.3 shows that extractions (in the flowing-solvent reactor) in *hexadecane* gave results closer to those obtained during *pyrolysis in the wire-mesh reactor*. Heating in helium at 1000°C s^{-1} to 350°C with 150 s holding, the pyrolysis weight loss from Point of Ayr vitrinite concentrate was

3.3% (% w/w daf basis); at 450°C, the weight loss improved to 20.5%. Meanwhile in hexadecane, sample weight loss in the flowing solvent reactor at up to 450°C did not exceed 27%.

This result is a little counterintuitive; it might have been expected that mass transfer between a solid and a liquid (coal-to-hexadecane) would have been far more efficient than a mass transfer from coal to an inert gas stream. However, in the absence of solvent power for coal-derived materials, the presence of hexadecane appears to have made relatively little difference from pyrolysis in helium. Results presented in Table 5.3 may therefore be understood in terms of the coal (or its vitrinite concentrate) sample depolymerising quite substantially during heating to (and at) 450°C. The outcome of the experiment then appears to depend on whether a fraction of the depolymerised material can be chemically quenched by a hydrogen-donor and/or moved out of the reaction zone by dissolving in a suitable solvent. In the case of liquefaction in hexadecane, the occurrence of extensive repolymerisation was confirmed by the negligible amounts of extra material extracted from the solid residues, upon subsequent refluxing in a 4:1 mixture of chloroform and methanol. The FT-IR spectra of hexadecane extracts showed greater aliphatic and hydroaromatic content than tetralin or quinoline extracts, suggesting a degree of preferential, if limited, extraction by the long-chain compound (Xu et al., 1994).

5.6 Flowing-solvent reactor: successive extract fractions released from coal

Pre-asphaltenes represent a usually significant proportion of primary coal extracts that turn out to be resistant to upgrading. The refractory nature of these materials has led, in the past, to questions about whether products released during *shorter extraction time* runs may be more amenable to subsequent upgrading (Moroni, 1991). At bench scale, it is possible to attempt short duration experiments in micro-bomb reactors. However, in a batch reactor, only the cumulative (scrambled) extract mixture released between the beginning of the experiment and its endpoint is available for characterization. It is not possible to recover extract fractions released during specific time- or temperature-intervals. Moreover, the length of heat-up and cool-down periods of batch reactors (order of minutes), introduces uncertainties in the time resolution of extracts released from the coal sample. We have already observed, furthermore, that the closed ('batch') reactor configuration allows extraparticle secondary reactions of extracts to take place.

The continuous flow of dissolved extracts out of the flowing-solvent reactor makes it suitable for identifying and comparing successive product fractions released from coal during the liquefaction process. However, the 'flowing-solvent' reactor has its own peculiar shortcomings: characterising product fractions is made difficult by the high level of dilution by the flowing solvent, as well as by the possible reactions of the solvent itself.

In earlier work, products from the thermal reactions of tetralin have been examined by gas chromatography–mass spectrometry (GC–MS). Tetralin–tetralin dimers

and tetralin–naphthalene adducts, mainly of mass 258 u and 262 u were identified within the spectrum of products. The total concentration of this class of compounds did not exceed about 1% of the total solvent recovered from the flowing-solvent reactor. Greater concentrations of relatively more stable dimers and adducts including naphthalene, butylbenzene and 1-methylindane, have been identified within products from a stirred micro-autoclave (residence time: 1 h) (Brodzki et al., 1994a, b; 1995).

In assessing structural differences between successive extract fractions, effects due to products derived from the solvent used for liquefaction have to be eliminated or mitigated. The boiling points of the tetralin dimers and related adducts identified were above 350°C, and it was not possible to remove them by distillation without unduly altering the composition of the sample itself. Furthermore, preparing samples for characterization by distilling off the solvent, followed by drying, suffers from masking effects due to the possible presence of larger molecular mass, solvent-derived byproducts.

However, unlike the coal sample, solvent residence times are constant in the flowing-solvent reactor. *Changes* in the structural features of the reaction mixtures can serve, therefore, as a more reliable guide to changing extract properties in successive fractions recovered from the flowing solvent reactor (Xu et al., 1994; Li et al., 1995). Table 5.4 presents the temperature-time intervals used for collecting time-resolved product fractions released by the fuel during the course of a single experiment. FT-infrared spectroscopy of product fractions showed decreasing extents of aromatic substitution and increasing product polarity with increasing extents of reaction, i.e., the deepening liquefaction of the coal.

In terms of size exclusion chromatography, *solvent-derived* products appeared at relatively longer elution times and could be blanked out, enabling the comparison of the larger molecular mass fractions of the extracts. In both tetralin and quinoline, liquefaction products showed broadening molecular mass distributions with progressively intensifying reaction conditions, i.e., increasing reaction temperatures, and

Table 5.4 Temperature intervals corresponding to time-resolved product fractions

Fraction number	Time interval (s)	Temperature interval (°C)
1	0–70	ambient-350
2	70–80	350–400
3	80–90	400–450
4	90–100	450
5	100–140	450
6	140–190	450
7	190–490	450
8	From 490 s until reaching ambient temperature	450-ambient

Source: Reprinted with permission from Xu, B., Madrali, E.S., Wu, F., Li, C.-Z., Herod, A.A., Kandiyoti, R., 1994. Energy Fuels 8, 1360. Copyright 1994 American Chemical Society.
Samples were heated at 5°C s^{-1} to 450°C and held for 400 s. A tetralin flow of 0.9 mL s^{-1} was maintained under 70 bars pressure.

longer holding times at the target temperatures. In both solvents, the SEC of fractions released at 450°C indicated the presence of material at the high-molecular mass limit of the calibration of the SEC column. Thus, the proposition that fractions released from coal during earlier stages of liquefaction might require less severe catalytic hydroprocessing appeared to merit attention.

During efforts to characterise these extract fractions, a UV-*fluorescence* spectrometer was used for the first time, as detector in SEC, *in series* with the usual UV-absorption detector. However, the sensitivity of the UV-fluorescence spectrometer was found to diminish with increasing sample molecular mass (i.e., at shorter elution times). Above about 3000 u, where intense signal could be observed from the UV-absorption spectrometer, the quantum yields and detector sensitivity of the UV-*fluorescence* spectrometer were reduced to near zero (Li et al., 1995; Herod et al., 1996).

5.7 A Two stage kinetic model of primary coal liquefaction

The formulation of a realistic kinetic model for coal liquefaction requires a description of the process reflecting its basic features. Fig. 5.5A shows that about 30% of sample weight loss took place as Point of Ayr coal was heated to the target temperature. Relatively few mathematical models in the literature take account of weight loss during sample heatup. One notable exception is the kinetic model for coal *pyrolysis*, due to Howard and coworkers (Howard, 1981). By assuming a Gaussian distribution of activation energies, the same model contributed an additional feature, reflecting the variety of structures undergoing thermal breakdown and the multiplicity of different chemical bond cleavage reactions likely to be taking place.

Another key element to consider is whether the same activation energy, or the same *distribution* of activation energies, might apply to all stages of the liquefaction process. This is another way of asking whether, the same mechanism may be assumed to predominate during all stages (temperature levels, conversion levels) of the liquefaction process. Assuming a multiplicity of successive reaction mechanisms would lead to models of increasing complexity. In the case of coal liquefaction, the model presented below simplifies the process, by assuming that two distinct and successive stages take place: the solvent extraction of material that is readily extractable followed by the release of extractable material formed through the depolymerisation of the coal matrix.

5.7.1 Elements of the two-stage kinetic model for coal liquefaction

The following strands of information will be incorporated into the relatively simple global kinetic model described below.

1. *Reactor-Related Effects*: We have already observed that apparatus with specialised configurations such as the flowing-solvent reactor are not absolutely necessary, for determining

coal conversions at a given temperature. When using tetralin as the 'vehicle', similarities between coal mass loss in the flowing-solvent and the 'mini-bomb' reactors suggest that it is possible to determine coal conversions from batch reactor data, so long as an efficient hydrogen-donor solvent is used in sufficient abundance. In tetralin, solvent-to-coal ratios of about 4:1, or higher, would appear to suppress significant extents of recombination reactions between coal-derived free radicals. Ratios as high as 1:8 had been suggested by Hill et al. (1966) to suppress retrogressive reactions. Thus we may consider that data from 'mini-bomb' reactors could be deemed relatively free of reactor-related effects, as far as determining conversions are concerned.

Several additional factors need to be considered, however, in calculating liquefaction *reaction rates*. In batch reactors, the outward diffusion of extract molecules from coal particles takes place against a continuously increasing concentration of extract molecules in the liquid phase surrounding liquefying coal particles. The *rates* of extract release into solution (sample weight loss) are slowed down by decreasing rates of outward diffusion of product molecules. Unpublished data from the Point of Ayr Pilot Plant (British Coal) (Moore, 1994) showed that 10-min extractions of Point of Ayr coal in the mini-bomb gave about 15% *lower* conversions than the flowing-solvent reactor, in which sample exposure at the target temperature was about 400 s. Meanwhile, 60-min extraction results in the 'mini-bomb' were comparable with conversions in the flowing-solvent reactor.

Thus, the design of the flowing-solvent reactor enables the diffusion of extract molecules out of coal particles into a flow of fresh solvent, against a nearly zero concentration of dissolved coal extracts in the solvent phase. This allows the calculation of kinetic constants that are *relatively* independent of external (i.e., particle to bulk liquid) diffusion resistance effects. The fact that sample weight loss was not found to be sensitive to solvent flow rate changes between 0.9–2.4 mL s^{-1} (Gibbins and Kandiyoti, 1990, 1991b; Xu and Kandiyoti, 1996), tends to support the contention that observed reaction rates were free of particle-to-bulk mass transfer resistances.

2. *Effect of non-donor solvents*: In both reactors, lower conversions were observed in the presence of non-hydrogen-donor solvent, 1-methylnaphthalene. However, the drop in conversion was greater in the 'mini-bomb' reactor. Thus, reaction pathways in coal liquefaction appear to depend, to some degree, on the interrelationships between the role of the reactor configuration and the composition of the solvent. It seems reasonable to conclude that these parameters affect both the rates and extents of the liquefaction process.

   It is important to note, finally, that in the absence of abundant H-donor solvent (e.g., in the presence of 1-methylnaphthalene), kinetic expressions describing coal liquefaction processes in batch reactors would (in addition to sample dissolution) need to reflect product loss through retrogressive radical recombination reactions, char formation, etc. In the flowing-solvent reactor, such retrogressive reactions appear to be partially suppressed, but not totally eliminated. This may be observed from experiments with 1-methylnaphthalene, quinoline, and mixtures of quinoline and phenanthrene (all non-donor solvents), for which conversions were at least ~10% lower than those observed in tetralin under otherwise similar experimental conditions (Table 5.3).
3. *Processes preceding and following the onset of extensive covalent bond scission*: Describing coal dissolution in terms of a single activation energy assumes that successive events taking place over the entire temperature range may be described in terms of a single process. This effectively masks significant differences between processes taking place above and below the temperature band delineating purely extractive processes from dissolution following depolymerisation. Several early workers have shown that activation energies of processes taking place prior to the onset of extensive depolymerisation reactions were

significantly lower than those of processes taking place above that temperature threshold (Hill et al., 1966; Han and Wen, 1979). We have already signalled that ESR spectroscopy makes it possible to distinguish between coal mass loss taking place prior to and following the onset of extensive covalent bond scission reactions. We will return to this point in Chapter 6, Elements of thermal breakdown: heating rate effects and retrogressive reactions. Meanwhile, the model outlined below assumes that dissolution of products at temperatures below the characteristic band around 350°C may be reasonably considered as taking place as simple extraction, prior to extensive coal depolymerisation.

4. *Non-isothermal mass loss during heatup*: In the flowing-solvent reactor, coal conversion during heatup can be determined with relative ease. The linear time-temperature ramp may be interrupted at any desired temperature. Then, rapid cool-down is made possible by allowing a flow of cold solvent to wash over the fixed bed of sample. Experiments conducted in tetralin at 5°C s^{-1} to 450°C with 'zero-seconds' holding at peak temperature gave about 20% weight loss for Pocahontas No. 3 and about 30% weight loss for Point of Ayr coal (Xu et al., 1994; Xu, 1995).

For most bomb reactors, average heating rates over the temperature interval are usually of the order of 2–5°C s^{-1}. Using an autoclave with a heatup period of 1.5–2 hours, Hill et al. (1966) reported that '80% of the total possible extraction' was achieved 'before the system reached the reaction temperature'. In such a reactor, the rates of heating would continuously diminish with rising temperature, while sample weight loss takes place over a continuum of temperatures, making it difficult to calculate *rates of reaction*. To summarise, events in the autoclave during heatup between ambient temperature and 420–450°C encompass (1) two distinct stages of the process with different activation energies and (2) significant levels of product release during heatup, taking place over a range of temperatures, presumably at increasing rates with rising temperature.

We note that the amount of extract released during the overall process is a sensitive function of the holding time at peak temperature, where some 400 s appear to be required in the case of most samples to reach an 'ultimate' conversion value.

We have already described the relative insensitivity of liquefaction conversions to changes in heating rates between 0.1°C s^{-1} and 10°C s^{-1}, in the presence of the efficient hydrogen-donor tetralin (Gibbins and Kandiyoti, 1991b). Mechanisms underlying changes in yields with changes in heating rates appear to involve competition between *recombination reactions* on the one hand, and quenching of coal-derived free radicals by locally available hydrogen, on the other (Li et al., 1994). The high conversions observed in the presence of an efficient hydrogen donor as well as the absence of heating rate effects during liquefaction suggest that competition between recombination reactions seem to be swamped by the abundant supply of donor solvent and seems to explain why under these conditions, the heating rate is not a significant parameter.

In the next section, we will describe a set of equations enabling the calculation of reaction rate parameters for coal weight loss during coal liquefaction. The model explicitly accounts for product release during heatup, and the assumption that distinct processes are taking place before and after the onset of extensive covalent bond scission (around 350°C).

5.7.2 Two-stage kinetic model of primary coal liquefaction: the assumptions

1. The process is assumed to take place in two stages.
   a. *Stage A processes*: This first stage consists of sample weight loss prior to the onset of extensive covalent bond rupture, taking place between ambient temperature and approximately 350°C. The model was formulated without explicit reference to the nature of physical and chemical phenomena occurring in this temperature interval. It is thought, however, that these processes include ordinary dissolution of more soluble (smaller molecular mass and/or less polar) species possibly occluded or held by weak interactions such as hydrogen bonding and van der Waals forces. In what follows, Stage A will be modelled, first, as a single-activation energy, irreversible, first-order process and, second, as a set of parallel independent first-order processes with a Gaussian distribution of activation energies characterised by the standard deviation, σ_A (see Howard, 1981). In the latter case, a common pre-exponential constant was used to characterise the set of parallel, independent reactions.
   b. *Stage B processes*: The second stage is defined as the process of weight loss following the onset of extensive covalent bond cleavage, broadly corresponding to weight loss above approximately 350°C. Once again, the model makes no explicit reference to the nature of chemical and physical phenomena occurring in this temperature interval. It is thought, however, that weight loss happens due to depolymerisation of the coal matrix and the dissolution of the depolymerised material in the solvent. Stage B will also be modelled, first, as a single, irreversible, first order process and, second, as a set of parallel independent first order chemical reactions with a Gaussian distribution of activation energies, characterised by the standard deviation, σ_B. A common pre-exponential constant will be used to characterise the set of parallel, independent reactions.
2. The coal is considered to behave as a homogeneous material. For ease of calculation, a single temperature is selected to distinguish between Stages A and B, defined as T_d. While this value was set at 350°C for most coals, in calculations involving the dissolution of Point of Ayr, Upper Freeport, and Pocahontas No. 3 coals, the liquefaction data suggested 375°C to be a more appropriate value.
3. The effect of intraparticle mass transport as a significant resistance or as a rate-determining step has been neglected. This assumption is treated as a first approximation and facilitates the development of the present model. The following experiments suggest that internal diffusion may, in the first instance, be neglected, at least for some coals. A set of liquefaction experiments were carried out with a sample of larger (250–500 μm) Point of Ayr (UK) coal particles, over the 300–450°C range. Differences in weight loss were found to be within experimental error of data obtained using 106–150 μm particles (Xu, 1995). In particular, no experimentally significant differences could be observed between the behaviour of different sized particles at temperatures below the onset of extensive covalent bond scission. The evidence presented here is not thought to be conclusive and a separate study of the effect of intraparticle diffusion effects would be desirable to evaluate the effect in greater detail.
4. For both Stage A and Stage B processes, the concentration driving force in all first order reaction terms has been expressed in terms of an 'ultimate' (equilibrium) weight loss value. For Stage A, equilibrium values have been estimated from sample weight loss determined by heating samples at 5°C s^{-1} to 350°C (or 375°C – depending on the coal – see below) with 1600 s holding, followed by washing the solid residue with a 4:1 chloroform-methanol solution at ambient temperature. 'Ultimate' conversions at 450°C were similarly determined by 1600 s holding at peak temperature. Clearly, 'ultimate' (equilibrium) weight loss may assume different values if the coal, the vehicle, or the solid residue washing procedure is changed.

5.7.3 *Description of the two-stage,* single-reaction *model*

In formulating the simplified model, both Stage A and Stage B processes were assumed to have single activation energies that could be represented by irreversible, first-order reactions. $x_A(t)$ was defined as the time-dependent weight loss variable for Stage A. This variable had an experimentally determined ultimate (equilibrium) value of x_{mA}, defined as the conversion after 1600 s at T_d – the transition temperature between the two weight loss regimes. The kinetic constants for Stage A processes at up to the temperature T_d were calculated first.

Sample weight loss due to Stage B processes was defined as $x_B(t)$. The overall ultimate (equilibrium) conversion for Stage B processes, x_m, was defined by the equation

$$x_m = x_{mA} + x_{mB}.$$

x_m was determined as the total weight loss from heating samples at 5°C s^{-1} to 450°C and holding for 1600 s. x_{mB} was calculated from the experimental determinations of x_m and x_{mA}.

Weight loss during heatup: To account for sample weight loss during heatup, it was necessary to integrate mass loss over the heatup period, as a function of the linearly changing temperature. With the initial (ambient) temperature defined as T_0 and the heating rate during the heatup period defined as k_h, the temperature T(t) at any time was calculated from

$$T(t) = T_0 + k_h t.$$

The total weight loss 'x(t)' at any time thus included weight loss during heatup and weight loss during the subsequent holding period. When the final (holding) temperature was lower than T_d (the transition temperature), total sample weight loss was calculated using rate constants for Stage A processes only. When a run with holding temperature above T_d was being simulated, conversions from the two successive stages were calculated separately and added together. It was thus necessary to calculate three parameters for Stage A (x_{mA}, k_{0A}, E_A) processes and another three for Stage B (x_{mB}, k_{0B}, E_B) processes.

The first step of the calculation, for Stage A parameters, made use of sample weight loss vs. temperature data at up to T_d, as listed in Table 5.2. k_{0A} and E_A values were calculated using a two-dimensional surface-fitting nonlinear regression algorithm and sample-mass vs. time expressions, described in the original publication (Xu and Kandiyoti, 1996).

The values of the starting parameters used in the iterative calculation have not been found to influence the final values obtained either in these, or in the multiple-reaction model calculations described below.

Discussion – Results from the Two-Stage Single-Reaction Model: Table 5.5 presents kinetic parameters calculated using the single-reaction model (Eqs. 4 and 5 in Xu and Kandiyoti, 1996). In Table 5.5, k_{0A} and k_{0B} denote the pre-exponential factors calculated for Stage A and Stage B, respectively, while E_A and E_B denote

Table 5.5 Comparison of kinetic parameters of the set of coal samples in Table 5.1

	Stage A				Stage B		
Coal Sample	**X_m[a] (w/w, daf)**	**X_mA (w/w, daf)**	**k_{0A} (s^{-1})**	**E_A (kj mol^{-1})**	**X_mB (w/w, daf)**	**k_{0B} (s^{-1})**	**E_B (kj mol^{-1})**
Beulah-Zap	0.84	0.41	1.52×10^2	55.4	0.43	4.12×10^6	124.0
Wyoming	0.89	0.39	0.50×10^2	47.2	0.50	1.67×10^7	130.4
Illinois No. 6	0.95	0.55	3.06×10^3	69.3	0.40	2.26×10^8	142.5
Blind Canyon	0.92	0.38	7.44×10^2	60.5	0.54	2.50×10^8	142.7
Pittsburgh No. 8	0.89	0.56	0.16×10^2	44.0	0.31	8.25×10^9	161.2
Upper Freeport	0.86	0.58	0.51×10^2	46.8	0.28	6.23×10^7	139.4
Pocahontas No. 3	0.70	0.30	2.05×10^4	80.5	0.4	9.40×10^7	150.0
Point of Ayr (UK)	0.84	0.36	0.21×10^2	35.0	0.48	4.65×10^{15}	238.0

Source: Reprinted with permission from Xu, B., Kandiyoti, R., 1996. Energy Fuels 10, 1115. Copyright 1996 American Chemical Society.
Single-Reaction Model.
[a]X_m, Total mass loss after 1600 s at 450°C.

the energies of activation calculated for the two stages. As would be expected from primarily desorption- and diffusion-driven phenomena, activation energy values for Stage A processes, E_A, were found to be considerably smaller than those for Stage B processes, E_B (Table 5.5).

With the exception of Pocahontas No. 3 coal, E_A values (Stage A) were found to vary within a relatively narrow band with no discernible pattern, suggesting a degree of similarity between rate-limiting steps in this temperature range. Most of the E_A values were low even for diffusion-limited processes. These energies of activation are attributable to processes involving desorption and dissolution of smaller molecular mass and/or less polar materials. It may be noted, however, that the lowest E_A value in Table 5.5 was found for Point of Ayr coal, the sample for which conversions were found not to change when the particle size was more than doubled (see above). The two elements of information appear consistent, in the sense of indicating weak resistances to desorption and/or the outward intraparticle diffusion of extract molecules.

Energies of activation for the higher temperature range (from T_d up to 450°C) Stage B processes were found to lie between 124 and 238 kJ mol^{-1} (Table 5.5). This is the temperature range where extensive covalent bond scission is expected to contribute massively to the dissolution of the coal mass. The sharp difference between the ranges of E_A and E_B values found in these calculations confirm the validity, and indeed the necessity of the added complication involved in introducing a two-stage model. Descriptions of coal liquefaction in terms of a single activation energy, expected to span the range of processes taking place between ambient and peak temperature, clearly conceal at least one distinct and important transition. Nevertheless, values at the lower end of the E_B range were smaller than would have been expected, compared to bond dissociation energies and activation energies calculated in previous pyrolysis related work (Burnham et al., 1989; Gavalas et al., 1981). The next section introduces the adoption of a multiple reaction model, which seems a more realistic representation of coal liquefaction processes.

5.7.4 Description of the two-stage multiple-reaction model

Early work on coal pyrolysis by Jungten and van Heek (1970) has shown that when a process consisting of *multiple, parallel independent reactions* is modelled in terms of a single reaction, the apparent activation energy of the imaginary lumped process turns out to be lower than the actual activation energies of the individual reaction pathways. To test the relevance of this proposition to coal liquefaction, both Stage A and Stage B of the liquefaction process were considered to proceed by means of multiple, parallel, independent, irreversible first-order processes. The approach was adapted from the work of Howard and coworkers on volatile release during coal pyrolysis (Howard, 1981).

It is assumed, once again, that weight loss during a particular liquefaction experiment includes weight loss during heatup, as well as the weight loss during the holding period. For simplicity, weight loss during the *cooling* period has been neglected. In the multiple-reaction model, in addition to the pre-exponential term and the average activation energy, the standard deviation of the distribution of activation energies (σ)

must be calculated. As before, Stage A parameters (k_{0A}, E_{0A} and σ_A) were calculated first, using weight loss data obtained between ambient temperature and the transition temperature, T_d, for the particular coal.

To reduce the new three-dimensional non-linear regression problem to a two-dimensional search, the third variable σ_A was pre-set at a series of fixed values ($E_{0A}/10$, $E_{0A}/25$, $E_{0A}/50$, $E_{0A}/100$ and $E_{0A}/200$) and the (k_{0A}, E_{0A}) values corresponding to the best fit were calculated with the same two-dimensional surface-fitting algorithm used for the single reaction model calculations. As before, when the peak experimental temperature exceeds T_d, weight loss due to Stage B processes is added to that due to Stage A processes (Eqs. 15 and 16 in Xu and Kandiyoti, 1996). A similar algorithm was then used for calculating values of k_{0B}, E_{0B} and σ_B. Listings of the computer codes have been given in Xu (1995).

Results from the two-stage multiple-reaction model: Table 5.6 presents kinetic parameters calculated using the multiple parallel independent reaction model. Comparing the parameters calculated from the single and multiple reaction models (Tables 5.5 and 5.6), it may be observed that activation energies for Stage A processes ($T < T_d$), calculated using the multiple, parallel independent reaction model were only slightly larger than those calculated from the single reaction model. The spread of activation energies, characterised by the standard deviations of the distributions, σ_A, were found to be correspondingly narrow. This result suggested that the number and nature of independent pathways involved in Stage A processes are fairly limited. The steady decline of absolute σ_A values with increasing coal rank (with the exception of the two low-rank samples) may be interpreted in terms of the simplification of structural features with increasing coal maturation.

Activation energies for Stage B processes for $T>T_d$, however, differed sharply from results calculated using the single-reaction model. The average activation energy values were found to be systematically greater, with an overall range between 160 and 275 kJ mol^{-1}. Pullen (1981) reported the activation energy for the bibenzyl cracking reaction as 201 kJ mol^{-1} while quoting a somewhat higher value (235 kJ mol^{-1}) by Vernon (1980) for the same reaction. The E_{0B} values calculated for the present set of coals thus appear within the range that can be said to represent thermally induced bond cleavage (Nishioka, 1991).

In view of the multiplicity of parallel independent reaction pathways expected at temperatures above 350–375°C, it seems physically reasonable that the single-reaction model (Table 5.5) should underestimate the average energy of activation for Stage B processes and that the absolute values of σ_B in Table 5.6 should be significantly greater than σ_A values. The trend of *decreasing* σ_B values (Table 5.6) with increasing coal rank may be viewed in terms of increasing structural uniformity and possibly increasing degrees of cross-linking accompanying coal maturation.

In Table 5.6, the E_{0B} value for Pocahontas No. 3 was lowest, while the value for Upper Freeport turned out to be unexpectedly high. For these two coals, the values of E_{0A} and E_{0B} are probably linked more closely than in other cases. The greater extent of *extraction* from Upper Freeport coal at lower temperatures has already been mentioned. The high E_{0B} value for temperatures greater than T_d may be viewed in terms of the more difficult (possibly more polar or more densely cross-linked) fractions of the coal

Table 5.6 Comparison of kinetic parameters of the set of coal samples

		Stage A				Stage B				Parameters from pyrolysis experiments[a]	
Cool sample	**X_m (w/w, daf)**	**X_mA (w/w, daf)**	**k_{0A} (s^{-1})**	**E_{0A}**	**σA**	**X_mB (w/w, daf)**	**k_{0B} (s^{-1})**	**E_{0B}**	**σ_B**	**E_0**	**σ_B**
				(kJ mol^{-1})				**(kJ mol^{-1})**		**(kJ mol^{-1})**	
Beulah-Zap	0.84	0.41	3.07×10^2	58.9	$E_{0A}/25$	0.43	2.23×10^{12}	200.0	$E_{0B}/25$	232	E0/38
Wyodak-Anderson	0.89	0.39	0.92×10^2	50.0	$E_{0A}/25$	0.50	4.32×10^{11}	188.4	$E_{0B}/25$	263	E0/45
Illinois No. 6	0.95	0.55	3.55×10^4	81.3	$E_{0A}/25$	0.40	2.32×10^{12}	194.1	$E_{0B}/50$	210	E0/45
Blind Canyon	0.92	0.38	9.41×10^2	64.5	$E_{0A}/25$	0.54	6.08×10^{13}	210.9	$E_{0B}/50$	196	E0/49
Pittsburgh No. 8	0.89	0.56	0.25×10^2	46.5	$E_{0A}/25$	0.31	1.97×10^{12}	191.0	$E_{0B}/50$	205	E0/54
Upper Freeport	0.86	0.58	0.93×10^2	49.5	$E_{0A}/25$	0.28	2.09×10^{16}	252.5	$E_{0B}/50$	262	E0/84
Pocahontas No. 3	0.70	0.30	3.70×10^4	83.6	$E_{0A}/100$	0.40	4.94×10^8	160.0	$E_{0B}/100$	222	E0/57
Point of Ayr (UK)	0.84	0.36	0.25×10^2	35.6	$E_{0A}/25$	0.48	1.97×10^{18}	275.0	$E_{0B}/100$	n/a	n/a

Source: Reprinted with permission from Xu, B., Kandiyoti, R., 1996. Energy Fuels 10, 1115. Copyright 1996 American Chemical Society.
Multiple-Reaction Model.
[a]From Burnham et al. (1989).

residue remaining behind for depolymerisation. The opposite trend may be attributed to the case of Pocahontas No. 3 coal. However, the high E_{0B} value found for Point of Ayr coal does not fit the same pattern. This last result does reflect, however, the consensus at the Pilot Plant that this particular coal was not, after all, an 'easy' one to liquefy.

For all coals in the study, good internal agreement was obtained between simulated results and conversion data *not* used in the calculation of the kinetic constants (Xu, 1995). If the kinetic procedure described in this study survives the test of time, the E_{0B} values calculated by this method may be useful for investigations of coal structure, as well as help in determining the suitability of individual coals for conversion by liquefaction.

5.7.5 Comparison with previous studies of coal liquefaction kinetics

The present calculation takes into account weight loss during heatup, distinguishes between two distinct stages in coal liquefaction with different activation energies and shows that modelling the thermal breakdown step as a set of parallel independent reactions leads to more realistic energies of activation. The inclusion of parallel independent reactions in the model was shown (Tables 5.5 and 5.6) to have a significant effect on calculated activation energies for Stage B (thermal breakdown) processes. Clearly, a direct comparison with results of calculations from other work assuming (1) a single energy of activation and/or (2) isothermal kinetics for the whole process is not entirely appropriate. The findings from this model need nonetheless to be placed in the context of previous work by comparison with activation energies calculated during different investigations. Table 5.7 presents a short literature review of activation energies arrived at for coal liquefaction. The review was not meant to be exhaustive.

A number of investigations have reported activation energies that seem unacceptably low (e.g., Shin et al., 1989; Curran, et al., 1967; Brunson, 1979; Wiser, 1968; Cronauer et al., 1978; Morita et al., 1979). Differences in model formulation outlined above (i.e., modelling coal liquefaction as an isothermal process and/or in terms of single reactions) may help explain some of these results. However, a small number of studies, using models similar to those used in the latter studies, have reported energies of activation similar to or greater than those found in the present work. These studies will be briefly reviewed.

Weller et al. (1951a,b) worked with a rotating autoclave, which had a 1-h heatup time. These researchers used an isothermal kinetic scheme for their calculations, based on the peak temperature alone. Heating and cooling periods were assumed to add another 20 min to reaction time at peak temperature. During the catalytic 'hydrogenolysis' in the absence of liquid solvent of an 'anthraxylon' (vitrinite) fraction of Bruceton coal, '…reaction was so rapid…' that '…no accurate value for the activation energy… can be deduced…' suggesting that '…the simple Arrhenius relation … does not hold …' The authors calculated an activation energy of 150 kJ mol^{-1} for the hydrogenation of an 'asphalt' fraction, from results at 430°C and 440°C, '…for which the greatest accuracy in k' was observed…'.

Table 5.7 Summary of results from a selection of previous studies on coal dissolution kinetics

Coal	Solvent/coal ratio	Temperature (°C)	Definition of conversion[a]	Activation energy (kJ mol^{-1})	References
Utah HV	Tetralin (10:1)	409–497 (Pyrolysis) 350–450 (Liquefaction)	Wt. loss (Pyrolysis) Benzene solubles	149 (2nd-order initial) 17.2 (1st-order later) 120.5 (2nd-order initial) 54.8 (1st-order later)	Wiser (1968)
Pittsburgh seam (Ireland mine)	Tetralin (4:1)	324–387	Xylenol Cyclohexane, Benzene, cresol	E_a=125.5 (fast) E_a=159.0 (slow)	Curran et al. (1967)
Belle Ayr (sub)	HAO[b] HPH[b]	400–470	Pentane, benzene, pyridine	Coal→product E_a=70.0 (HAO) Coal→product E_a=85.8 (HPH)	Cronauer et al. (1978)
Pittsburgh seam (Bruceton mine)	None	400–440	Benzene	'Asphalt' hydrogen E_a=150	Weller et al. (1951a,,b)
Miike	Recycle stream MoO_3 catalyst	350–450 330–380	Hexane Benzene	Coal→asphaltene E_a (calcd) = 68.6 Asphaltene oil E_a (calcd) = 67.0	Morita et al. (1979)
Utah Spring Canyon	Tetralin (10:1)	350–450	Benzene	E_a=134 from 0 to 90% reacted ΔH = 155.6–358	Hill et al. (1966)
Big Horn	Process (3:2)	413–440	Boiling ranges (Heavy oil >343°C)	Coal→oil E_a = 230 Coal→furnace oil E_a = 169.5	Shah et al. (1978)
Makum	Tetralin (1:1)	380–410	Benzene	Initial rxn = E_a=330.5 Step 2 E_a = 196.6 Step 3 E_a = 146.4	Gun et al. (1979)
Argonne PCS	I-MN[b]	375–425	Toluene THF	E_a = 18–112 E_a = 31.4–123.4	Shin et al. (1989)

Source: Reprinted with permission from Xu, B., Kandiyoti, R., 1996. Energy Fuels 10, 1115. Copyright 1996 American Chemical Society.
[a]Solid residue washed (extracted) in stated solvent.
[b]*HAO*, hydrogenated anthracene oil; *HPH*, hydrogenated phenanthrene; *I-MN*, I-methylnaphthalene. E_a, Energy of activation.

In another early study, Hill et al. (1966) used a 1-L autoclave into which Spring Canyon (Utah) coal was injected at the intended reaction temperature. The estimated 1-2 min heatup time quoted in their paper corresponds to a heating rate of between 3.5°C s^{-1} and 7°C s^{-1}. The authors stated that '… at the initial stage of the experiment, *the reaction is under diffusion control* (emphasis added)… this process has a very low activation energy'. This sentence could be interpreted as referring to what we have described as the solvent extraction phase prior to the onset of covalent bond rupture. A little disappointingly however, for purposes of the kinetic calculations, the coal was assumed to have reached the reaction temperature instantaneously. The calculations did not take account of weight loss during heatup. Instead, these researchers assumed a first-order dissolution process to be taking place in parallel with a second-order 'extraction of interspersed materials' at the peak experimental temperature. Activation energies of 212 and 109 kJ mol^{-1}, respectively, were reported.

In a second model developed within the same report, the 'first order reaction velocity constant' was found to vary with the fraction extracted at constant peak temperature. A gradual increase in the 'enthalpy of activation' from 156 to 358 kJ mol^{-1} with increasing conversion (nearly 90%) was reported. The activation energy for the rate constant characterising the initial rate at each temperature was found to be 134 kJ mol^{-1}. Despite the simplifications, the work clearly identified a sequence of process stages with corresponding distinct energies of activation. In this sense, it may be said to have foreshadowed the more detailed kinetic approach outlined earlier.

In modelling coal liquefaction and the subsequent reactions of extracts in a 'segmented-bed' reactor, Shah et al. (1978) reported a coal-to-gas energy of activation of 357 kJ mol^{-1}. It is straightforward to show that if intervening steps within a set of *consecutive* reactions are ignored (and provided that the pre-exponential constants are of comparable magnitude), calculated apparent energies of activation for the overall process may approach or even exceed the sum of the energies of activation for the intervening reaction steps. The same study found energy of activation values closer to those in Table 5.6, of 230 and 169.5 kJ mol^{-1} for coal to 'heavy oil', and coal to 'furnace oil' conversion, respectively. In these calculations, isothermal kinetics and a single-stage coal dissolution step had been assumed. However, the results are more difficult to interpret than most, since the presence of a preheater was indicated, operating at a temperature that was unspecified in the cited reference.

During coal liquefaction experiments in tetralin, Gun et al. (1979) also reported observing that the reaction order and the energy of activation changed with time. These workers used a 2-L stirred autoclave and assumed isothermal kinetics at peak temperature. The *order* of the reaction rate was reported to have increased from initial values of 1.0–1.2 to 2.0–2.2 and then to decrease to between 0.6 and 1.0. Activation energies during this three-step process were given as 332.5, 196 and 146 kJ mol^{-1}, respectively. Energies of activation were thus reported to have decreased with increasing reaction time. In view of the large thermal inertia of their reactor and the assumption that 'experimental zero time' was assigned to the time when reaction temperature had been reached, it seems difficult to comment on these results in any detail.

Comparison with Kinetic Parameters Calculated from Pyrolysis Experiments: Similarities and differences between coal thermal breakdown during the initial stages

of coal pyrolysis and liquefaction have been previously discussed (Li et al., 1994; Zhuo et al., 2003; also see chapter: Elements of thermal breakdown: heating rate effects and retrogressive reactions). Generally, pyrolysis yields are even more sensitive than liquefaction conversions to reactor design. Not surprisingly, activation energy values reported in the literature cover a very wide spectrum (e.g., see Howard, 1981). Total volatile yields from pyrolysis are also considerably lower than conversions normally expected from liquefaction. A comparison of energies of activation between pyrolysis and liquefaction experiments is only defensible (1) if it can be assumed that thermal breakdown constitutes the rate-limiting step in product release during pyrolysis and (2) to the extent that Stage B processes represent thermal breakdown in the liquefaction of coals. Within the present context, the first of these assumptions is not entirely justifiable. In addition to extensive recombination reactions, internal tar migration and diffusive resistances to tar release from external particle surfaces may be cited as significant resistances to product release from coal particles (Suuberg, 1985). Recombination reactions and diffusion limitations do not appear to affect liquefaction conversions, in any case not to the same extent as in pyrolysis. It seems reasonable to conclude that the two processes are not readily comparable. It may nevertheless be instructive to compare activation energies from the present liquefaction work and pyrolysis experiments from a study on similar coal samples, which were calculated using a multiple parallel independent reaction model.

The last column of Table 5.6 presents energies of activation and σ values (with units adapted to the present study) from the pyrolysis of the set of coals from the Argonne Premium Coal Sample Programme (Vorres, 1990). A Rock–Eval reactor was used in these experiments (Burnham et al., 1989). The latter apparatus is not thought to be as free from extraparticle secondary reactions as 'drop-tube' or 'wire-mesh' instruments (Howard, 1981; Li et al., 1993). A comparison of results with those from the present liquefaction study indicates somewhat higher pyrolysis E_0 values and some individual differences, notably for Wyodak and Pocahontas No. 3 coals. The results nevertheless appear to show the energies of activation from the two studies to be within the same range of values. σ values calculated from the pyrolysis data covered a narrower range, but progressively diminished with increasing rank, in line with the trend observed in the liquefaction results (Table 5.6).

5.8 Overview: designing liquefaction experiments

In coal liquefaction, it seems necessary to distinguish between solvent extraction prior to and following the onset of extensive covalent bond cleavage. For any given coal, the amount of extractable material recovered prior to extensive covalent bond rupture was found to depend on the solvent used for extraction and the extraction temperature. The results suggest that coals are made up of materials within some sort of continuum of molecular masses. Prior to the depolymerisation stage, a more powerful solvent may extract more of the coal mass. On the other hand, a rise in temperature may change the rules. Some coal-derived material may become soluble at higher temperatures – without necessarily breaking many covalent bonds.

In the next chapter, we will review findings from ESR spectroscopy, showing the onset of covalent bond scission reactions occurring as early as about 310–340°C. The increase observed in the intensity of the ESR-derived 'spin-population' signal occurs in the same temperature band as the thermally induced breakdown of coals, at or above the 350–375°C band. The temperature interval between the 'onset' of bond cleavage (310–340°C) and more rapid depolymerisation above 350°C is thought to represents a gestation period, where several bonds are cleaved before larger molecular mass fragments are released from the coal matrix.

We have also observed that even in the flowing-solvent reactor, the presence of a hydrogen donor solvent leads to higher conversions, compared to non-donor solvents. The availability of a sufficient supply of hydrogen-donor solvent serves to quench reactive free radicals and chemically stabilise extract molecules. In our experiments, some 10% less conversion was observed in the presence of non-donor solvents, presumably due to short-range retrogressive interactions taking place within the parent coal particles. In the flowing-solvent reactor, extracts reaching the solvent stream were quickly diluted and carried out of the reaction zone. However, when the process was carried out using a non-donor (albeit powerful) solvent in a 'batch' (i.e. closed) reactor, increasing char residues were observed at higher temperatures and longer residence times. Thus the outcome of a liquefaction experiment is determined by the configuration of the reaction vessel and the nature as well as the relative abundance of the liquid medium.

In general, the formulation of mathematical models requires identifying key variables and rate determining steps. We have observed, however, that the conceptual modelling of liquefaction experiments is also closely bound up with the type of experiment being staged. The ability of the flowing-solvent reactor to separate reactant from product provided a convenient fit with the liquefaction model outlined above. The configurations of batch reactors do not allow tracking reaction sequences or working out reaction kinetics, for either coal liquefaction or indeed for the hydrothermal processing of biomass.

The liquefaction model outlined above was defined, as a first approximation, in terms of a two-stage process. The resulting calculations gave distinct energies of activation for the two successive stages, providing a measure of justification for the approach. Not surprisingly, the magnitude of the energies of activation for the 'extraction' phase turned up values closer to those associated with diffusion, whereas energies of activation for the 'depolymerisation' stage turned out to be closer to values associated with covalent bond rupture. The points of correspondence between the model and the physical and chemical processes observed to be taking place were apparent.

In the next chapter, we will attempt to draw together elements from our discussions on pyrolysis and liquefaction, to attempt a more detailed understanding of thermal breakdown in coals. We will also attempt to identify common points with thermal breakdown in lignocellulosic biomass, although the available data for biomass are far less detailed. We will attempt to explain how heating rates affect the behaviour of both coal and lignocellulosic biomass during *pyrolysis*. However, in the presence of a donor-solvent, product distributions from coal *liquefaction* have appeared to be relatively insensitive to heating rates. The attempt to explore the fundamental processes

underlying these multifaceted trends will help clarify several aspects of solid fuel processing, and explain something of the behaviour of poorly coking, as well as of premium coking coals.

References

Aida, T., Slomka, B., Shei, J.C., Chen, Y., Squires, T.G., 1985. Am. Chem. Soc. Div. Fuel Chem. Prepr. 30 (4), 274.
Akhtar, J., Amin, N.A.S., 2011. Renewable Sustainable Energy Rev. 15, 1615.
Aysu, T., Demirbaş, A., Bengü, A.Ş., Küçük, M.M., 2015. Process Safety Environ. Protection 94, 339.
Bartle, K.D., Bottrell, S., Burke, M.P., Jones, C., Louie, P.K., Lu, S.L., et al., 1994. Int. J. Energy Res. 18, 299.
Berl, E., 1934. Science 80, 227.
Berl, E., 1944. Science 99, 309.
Brodzki, D., Djega-Mariadassou, G., Li, C.-Z., Kandiyoti, R., 1994a. Fuel 73, 789.
Brodzki, D., Abou-Akar, A., Djega-Mariadassou, G., Li, C.-Z., Xu, B., Kandiyoti, R., 1994b. Fuel 73, 1331.
Brodzki, D., Abou-Akar, A., Djega-Mariadassou, G., Kandiyoti, R., 1995. Fuel 74, 407.
Brownsort, P.A., 2009. UKBRC Working Paper 5. <www.biochar.org.uk >; UKBRC: 2009.
Brunson, R.J., 1979. Fuel 58, 203.
Burguete, P., Corma, A., Hitzl, M., Modrego, R., Ponce, E., Renz, M., 2016. Green Chem. 18, 1051.
Burnham, A.K., Oh, M.S., Crawford, R.W., Samoun, A.M., 1989. Energy Fuels 3, 42.
CCTP, 1999. Technology Status Report 010; Coal Liquefaction. Cleaner Coal Technology Programme, Department of Trade and Industry/Pub URN 99/1120, London, UK.
Clarke, J.W., Kimber, G.M., Rantell, T.D., Shipley, D.E., 1980. ACS Symp. Ser. No. 139. In: Whitehurst, D.D., (Ed.), p. 111.
Comolli, A.G., Zhou, P., 2000. Hydrocarbon Technologies Inc. Final Report to US DOE, AC22-92PC92148. US Department of Energy, Pittsburgh, PA.
Cronauer, D.C., Shah, Y.T., Ruberto, R.G., 1978. Ind. Eng. Chem. Process Des. Dev. 17, 281.
Curran, G.P., Struck, R.T., Gorin, E., 1967. Ind. Eng. Chem. Process Des. Dev. 6, 167.
Demirbas, A., 2010. Energ Source Part A: Recovery Utilization Environ. Effects 32, 1100.
Diebold, J.P., 2000. A Review of the Chemical and Physical Mechanisms of the Storage Stability of Fast Pyrolysis Bio-Oils. National Renewable Energy Laboratory, Golden, Colorado.
Elliott, D.C., 2008. Biofuels Bioprod. Bioref. 2, 254e65.
Elliott, D.C., 2011. Thermochemical Processing of Biomass. John Wiley & Sons Ltd., Chichester. p. 200.
Elliott, D.C., Lee, S.-J.; Hart, T.R. Stabilization of fast pyrolysis oil: post processing. Report 21549; Pacific Northwest National Laboratory: Richland, Washington, 2012.
Elliott, D.C., Biller, P., Ross, A.B., Schmidt, A.J., Jones, S.B., 2015. Bioresour. Technol. 178, 147.
Elliott, M.M. (Ed.), 1981. Chemistry of Coal Utilization Second Supplementary Volume. John Wiley, NY.
EnerCOM, 2016, <http://www.oilandgas360.com/analytics/wti-brent-prices.pdf?utm_source=Crude+Oil+%2F+Natural+Gas&utm_campaign=ee484da50c-Crude+Oil+Cuttings_February_3_2016&utm_medium=email > .

Fowler, T.G., Bartle, K.D., Kandiyoti, R., 1988. Fuel 67, 173.
Fowler, T.G., Kandiyoti, R., Bartle, K.D., Snape, C.E., 1989a. Carbon 27, 197.
Fowler, T.G., Bartle, K.D., Kandiyoti, R., 1989b. Energy Fuels 3, 515.
Fukuda, K., 2002. PhD Thesis. University of London.
Fukuda, K., Dugwell, D.R., Herod, A.A., Kandiyoti, R., 2004. Energy Fuels 18, 1140.
Furimsky, E., 1998. Appl. Catal. A General 171, 177.
Gavalas, G.R., Cheong, P.H.-K., Jain, R., 1981. Ind. Eng. Chem. Fundam. 20, 113.
Gibbins, J.R., Kandiyoti, R., 1990. Fuel Proc. Tech. 24, 237.
Gibbins, J.R., Kandiyoti, R., 1991a. Rev. Sci. Instr. 62 (9), 2234.
Gibbins, J.R., Kandiyoti, R., 1991b. Fuel 70, 909.
Gibbins, J.R., Kimber, G., Gaines, A.F., Kandiyoti, R., 1991. Fuel 70, 380.
Gibbins, J.R., Gaines, A.F., Li, C., Kandiyoti, R., 1994. Intl. J. Energy Research 18, 215.
Gibson, P., 2007. Kentucky Energy Security Summit, October 11, 2007. <http://www.caer.uky.edu/podcast/Gibson-KESummitOct2007r.pdf > .
Gorin, E., 1981.. In: Elliott, M.A. (Ed.), Chemistry of Coal Utilisation-Supplementary Volume II. J. Wiley, NY. 1485.
Goudriaan, F., van de Beld, B., Boerefijn, F.R., Bos, G.M., Naber, J.E., van der Wal, S., et al., 2008. Progress in Thermochemical Biomass Conversion. Blackwell Science Ltd, Oxford.1312.
Gun, S.R., Sama, J.K., Chowdhury, P.B., Mukherjee, S.K., Mukherjee, D.K., 1979. Fuel 58, 171.
Han, K.W., Wen, C.Y., 1979. Fuel 58, 779.
Harrison, J.S., Kimber, G.M., Gray, M.D., 1989. Intl. Conf. Coal Sci., Tokyo, II, 655.
Herod, A.A., Zhang, S.-F., Johnson, B.R., Bartle, K.D., Kandiyoti, R., 1996. Energy Fuels 10, 743.
Higman, C., van der Burgt, M., 2008. Gasification, second ed. Gulf Professional Publishing, Burlington, MA, and Oxford.
Hill, G.R., Hariri, H., Reed, R.I., Anderson, L.L., 1966. Coal science. In: Gould, R.F. (Ed.), Advances in Chemistry Series 55. American Chemical Society, Washington, DC, pp. 427.
Hitzl, M., Corma, A., Pomares, F., Renz, M., 2015. Catal. Today 257, 154.
Howard, J.B., 1981.. In: Elliott, M.A. (Ed.), Chemistry of Coal Utilization Second Supplementary Volume. Wiley, New York, pp. 665.
Huber, G.W., Iborra, S., Corma, A., 2006. Chem. Rev. (Washington, DC, U S) 106 (9), 4044.
Iino, M., Takanohashi, T., Ohsuga, H., Toda, K., 1988. Fuel 67, 1639.
Irribaren, D., Peters, J.F., Dufour, J., 2012. Fuel 97, 812.
Jungten, G., van Heek, K.H., 1970. Reaktion-ablaufe unter nichtisothermen Bedingungen, vol. 13. Fortschritte der chemischen Forschung; Springer-Verlag, Berlin601–699, translated by Belov and Associates, Denver, CO, APTICTR-0776. Quoted by Howard [1981].
Kershaw, J.R., Barras, G., 1979. Am. Chem. Soc. Div. Fuel Chem. Prepr. 24 (3), 99.
Kimber, G.M., 1989. Proc. Conf. Am. Filtration Soc., Pittsburgh (USA).
Kimber, G.M., 1997. A history of UK coal liquefaction, ETSU/DTI Report No. Coal R078.
Kimber, G.M., Davies, G.O., 1988. Proc. symp. energy production processes. Inst. Chem. Eng., London.
Koll, P., Metzger, J., Angew, 1978. Angew. Chem. Int. Ed. Engl. 17, 754.
Kruse, A., Funke, A., Titirici, M.-M., 2013. Curr. Opin. Chem. Biol. 17, 515.
Li, C.-Z., Bartle, K.D., Kandiyoti, R., 1993. Fuel 72, 3.
Li, C.-Z., Madrali, E.S., Wu, F., Xu, B., Cai, H.-Y., Guell, A.J., et al., 1994. Fuel 73, 851.
Li, C.-Z., Wu, F., Xu, B., Kandiyoti, R., 1995. Fuel 74, 37.
Lowry, H.H. (Ed.), 1963. Chemistry of Coal Utilization Supplementary Volume. John Wiley, NY.

Matsumura, Y., Minowa, T., Potic, B., Kersten, S.R.A., Prins, W., van Swaaij, W.P.M., 2005. Biomass Bioenergy 29, 269e92.
McPherson, W.M., Foster, N.R., Hastings, D.M., Kalman, J.R., Okada, K., Heng, S., 1985a. Fuel 64, 454.
McPherson, W.M., Foster, N.R., Hastings, D.M., Kalman, J.R., Gilbert, T.G., 1985b. Fuel 64, 457.
Mochida, I., Sakanishi, K., Suzuki, N., 1998. Catal. Surv. JPN 2 (1), 17–30.
Mohan, D., Pittman Jr., C.U., Steele, P.H., 2006. Energy Fuels 20, 848.
Moore, S.A., 1994. Unpublished data. Point of Ayr Coal Liquefaction Pilot Plant, British Coal.
Moore, S.A., Jones, M.A., Kimber, G.M., 1989. Intl. Conf. Coal Sci., Tokyo, II, 663.
Morita, M., Sato, S., Hashimoto, T., 1979. Am. Chem. Soc., Div. Fuel Chem. Prepr. 24, 63.
Moroni, E.C., 1991. Prepr. Am. Chem. Soc., Div. Fuel Chem. 36 (2), 433.
Nishioka, M., 1991. Fuel 70, 1413.
Onozaki, M., Namiki, Y., Ishibashi, H., Takagi, T., Kobayashi, M., Marooka, S., 2000. Energy Fuels 14, 355.
Peterson, A.A., Vogel, F., Lachance, R.P., Froling, M., Antal Jr., M.J., Tester, J.W., 2008. Energy Environ. Sci. 1, 32.
Pullen, J.R., 1981. Solvent Extraction of Coal. IEA Coal Research, London.65.
Schaleger, L.L., Figueroa, C., Davis, H.G., 1982. Biotechnol. Bioenergy Symp. 12, 3–14.
Shah, Y.T., Cronauer, D.C., McIlvried, G.G., Paraskos, J.A., 1978. Ind. Eng. Chem. Process Des. Dev. 17, 288.
Shin, S.C., Baldwin, R.M., Miller, R.L., 1989. Energy Fuels 3, 193.
Slomka, B., Aida, T., Squires, T.G., 1985. Am. Chem. Soc. Div. Fuel Chem.Prepr. 30 (2), 368.
Slomka, B., Aida, T., Chen, Y., Junk, G.A., Squires, T.G., 1986. Am.Chem.Soc.Div. Fuel Chem. Prepr. 31 (1), 238.
Squires, T.G., Aida, T., Chen, Y., Smith, B.F., 1983. Am. Chem. Soc. Div.Fuel Chem. Prepr. 28 (4), 228.
Sun, Q., Fletcher, J.J., Zhang, Y., Ren, X., 2005. Energy Fuels 19, 1160.
Suuberg, E.M., 1985.. In: Schlosberg, R.H. (Ed.), Chemistry of Coal Conversion. Plenum, New York, pp. 67.
Takanohashi, T., Iino, M., 1990. Energy Fuels 4, 452.
Tekin, K., Karagöz, S., Bektaş, S., 2014. Renew. Sustainable Energy Rev. 40, 673.
Thigpen, P.L., 1982. Final report: an investigation of liquefaction of wood at the Biomass Liquefaction Facility. Battelle Pacific Northwest Laboratories, U.S. Department of Energy, Wheelabrator Clean fuel Corporation. Contract.
Titirici, M.-M. (Ed.), 2013. Sustainable Carbon Materials from Hydrothermal Processes. Wiley, West Sussex.
Titirici, M.M., Thomas, A., Yu, S., Muller, J.O., Antonietti, M.A., 2007. Chem. Mater. 19, 4205e12.
Toor, S.S., Rosendahl, L., Rudolf, A., 2011. Energy 36, 2328.
Vernon, L.W., 1980. Fuel 59, 102. quoted in Pullen [1981].
Vorres, K.S., 1990. Energy Fuels 4, 420.
Weller, S., Pelipetz, M.G., Friedman, S., 1951a. Ind. Eng. Chem. 43, 1572.
Weller, S., Pelipetz, M.G., Friedman, S., 1951b. Ind. Eng. Chem. 43, 1575.
Wiser, W.H., 1968. Fuel 47, 475.
Xu, B., 1995. Ph.D. Thesis. University of London.
Xu, B., Kandiyoti, R., 1996. Energy Fuels 10, 1115.
Xu, B., Madrali, E.S., Wu, F., Li, C.-Z., Herod, A.A., Kandiyoti, R., 1994. Energy Fuels 8, 1360.

Xu, B., Dix, M., Kandiyoti, R., 1995. Rev. Sci. Instrum. 66 (7), 3966.
Zhang, B., von Keitz, M., Valentas, K., 2008. Appl. Biochem. Biotechnol. 147, 143e50.
Zhang, S.-F., Xu, B., Moore, S.A., Herod, A.A., Kandiyoti, R., 1996. Fuel 75, 597.
Zhuo, Y., Herod, A.A., Kandiyoti, R., 2003. The thermochemical reactions of middle rank coals. In: Ikan, R. (Ed.), Natural and Laboratory Simulated Thermal Geochemical Processes. Kluwer Academic Publishers, Dordrecht Boston London, pp. 53.

Elements of thermal breakdown: heating rate effects and retrogressive reactions

6

Chapter Outline

In Chapter 5, Liquefaction: thermal breakdown in the liquid phase, we considered evidence showing that chemical changes observed during the early stages of pyrolysis and liquefaction follow similar pathways. In this chapter, we first evaluate data from electron spin resonance (ESR) spectroscopy, which shows how spin populations change during the early stages of pyrolysis. The work tries to address several fundamental questions regarding thermal breakdown in middle-rank coals: When does thermal breakdown actually begin? What are the similarities between reaction pathways during pyrolysis and liquefaction? When and how do these reaction pathways begin to diverge? The discussion will lead us to explore reasons why changes in heating rates affect pyrolysis-product distributions and, crucially, how the outcomes (e.g., product distributions) of thermal breakdown processes relate to the way retrogressive reactions work. Observable differences between rates of free-radical recombination reactions will be reviewed and an attempt will be made to distinguish between the

Solid Fuels and Heavy Hydrocarbon Liquids. DOI: http://dx.doi.org/10.1016/B978-0-08-100784-6.00006-0

extremes of fast and slow recombination reactions in both pyrolysis and liquefaction. In the process, we will try to answer some questions thrown up by research on modern coke making, and broaden the discussion to explore the role of the heating rate and retrogressive reactions during biomass pyrolysis.

The line of investigation outlined in this chapter has led to several previous attempts to collate and examine available evidence on thermal breakdown in coals (Li et al., 1994; Zhuo et al., 2003; Fukuda et al., 2004; Kandiyoti, 2011).

6.1 The ESR spectrometry of thermal breakdown

In their natural state, coals contain large numbers of free radicals, reflecting the stable populations embedded within coals during coalification. Population densities of free radicals in untreated coals increase with rank, typically from about 0.3×10^{19} spins gm^{-1} for a lignite, to about 1.7×10^{19} spins gm^{-1} in the case of an anthracite (Fowler et al., 1989b).

Much of the early fundamental work on the ESR spectrometry of carbonaceous materials was carried out by Singer and coworkers (Singer, 1963; Singer and Lewis, 1978; Lewis and Singer, 1981). These researchers were able to show that the stable paramagnetic species observed in products of low-temperature pyrolysis were indeed free radicals. Among other advances, they made use of ESR spectroscopy to study the kinetics of transformations from pitch to coke and discussed the relevance of free radicals observed by ESR to the carbonisation process (Singer and Lewis, 1982).

When a pyrolysis experiment is performed in situ within the spectrometer cavity, ESR spectroscopy allows observing changes in the population of unpaired electrons resulting from covalent bond-cleavage reactions during heatup. It is important to note that the changes observed in these experiments represent the number of stable free radicals, left over from completed pyrolytic processes. With appropriate corrections, changes in spin populations may be plotted as a function of the temperature. Meanwhile, observing reactive free radicals in coals by ESR spectroscopy has not proved possible, due to the shorter lifetimes of reactive free radicals and their low concentrations at any given time, relative to the much higher background count of stable free radicals (Fowler et al., 1989a). What can be monitored with relative ease, however, are changes in the populations of stable free radicals. Indeed, the methods used for calculating free radical populations assume the spin populations to be stable (Fowler et al., 1987a,b; 1988a; 1989a).

6.1.1 The ESR spectrometry of coal pyrolysis

As in the case of ordinary pyrolysis experiments, results from the ESR spectrometry of pyrolyzing coals partially reflect the design of the experimental reactor and the configuration of the sample (Fowler et al., 1987b, 1989a). Early pyrolysis studies of coals by in situ ESR spectrometry made use of vacuum cells placed within the spectrometer cavity (Austen, et al., 1958; Smidt and van Krevelen, 1959), where evolving

volatiles were continuously removed from the reaction zone. In later work, coal samples were heated in sealed (i.e., closed) quartz ampoules (Petrakis and Grandy, 1983; Sprecher and Retcofsky, 1983). Their data showed spin concentrations going through well-defined maxima, a little above 400°C, and appeared to suggest that the populations of free radicals had first increased with temperature and eventually declined at higher temperatures.

Fowler et al. (1987b; 1989a) have reviewed the set of assumptions that underpin the theoretical basis of spin population calculations based on measurements by ESR spectrometry. Among other factors, the validity of the calculations depends on the conformity of the residual chars with Curie's Law, which requires the temperature dependence of the ESR signal from char residues to be linear. Experimentally, Curie's Law was found to be poorly obeyed by samples pyrolyzed in sealed tubes (Fowler et al., 1987a,b). It may not surprise the reader that the problem appeared yet again to involve artifacts due to secondary interactions between evolved volatiles and residual solids, within the confined spaces of the sealed tubes.

To put this proposition to the test, a shallow fixed-bed flow reactor was constructed of quartz for carrying out pyrolysis experiments inside the spectrometer cavity. The design deliberately emulated that of the 'hot-rod' reactor, described in Chapter 3, Pyrolysis of solid fuels: experimental design and applications. A continuous stream of inert gas was used to sweep evolving volatiles out of the reaction zone and out of the ESR cavity. During these experiments, the fixed-bed of sample was heated at 10°C min^{-1} to 480–500°C.

Fig. 6.1 presents a schematic diagram of typical spin population versus temperature curves observed when coal samples were heated in the quartz fixed-bed reactor, placed inside the cavity of the ESR spectrometer. Three distinct types of thermally induced processes have been identified during coal pyrolysis experiments (Fowler et al., 1989b). In this diagram, spin populations (S) were defined as free radicals per gram of initial sample.

Region I ($T_1 > T$): S increased to a relatively shallow maximum (T_1 near 200°C in Fig. 6.1), due to the recovery of signal through desorption of gases adsorbed on sample surfaces. These gases, primarily moisture and oxygen, would have been adsorbed on coal surfaces by previous exposure to air.

Region II ($T_2 > T > T_1$): S decreased to a minimum. This decline is thought to be associated with recombination reactions, resulting from the thermally induced mobility of free-radical-bearing material with sufficiently high reactivity, already residing within the coal matrix.

Region III ($T > T_2$): Above the temperature T_2, S increased monotonically, signalling an increase in the free-radical population as the temperature rises and coal thermal breakdown commences. It is thought that the temperature T_2 marks the onset of covalent bond-cleavage reactions. Generally T_2 in Fig. 6.1 is found to be above 300°C (Table 6.1).

Above the 'onset' temperature T_2, observed increases in stable free radical concentrations were interpreted as representing the accumulating 'debris' left over from completed bond-scission reactions. Evolving volatiles were swept away from the vicinity of the fixed bed of sample by means of the carrier gas stream, and the change

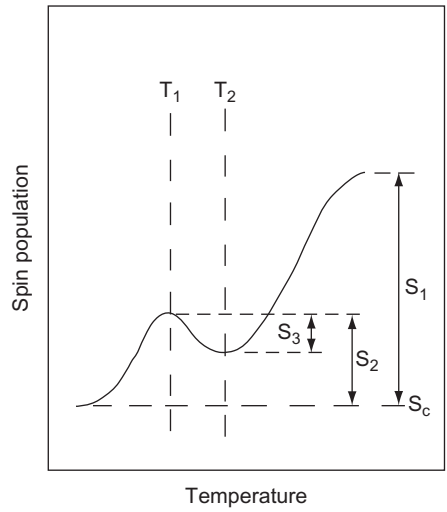

Figure 6.1 Schematic diagram of spin populations versus temperature, defining parameters in. *Source:* Reprinted from Fowler, T.G., Kandiyoti, R., Bartle, K.D., Snape, C.E., 1989b. Carbon 27, 197. Copyright 1989, with permission from Elsevier.

in signal above T_2 (i.e., in Region 3) was interpreted as reflecting changes in the concentration of stable free radicals embedded in the residual char matrix.

Overall, the experiments in the in situ quartz flow-cell gave larger spin populations than those observed in sealed ampoules, with the signal becoming more intense as the carrier gas flow rate was increased. The results confirmed that the removal of pyrolysis volatiles from the reaction zone at least partially suppressed the quenching of char free-radicals by evolving volatiles (Gonenc et al., 1988). The maxima observed around 400°C when using sealed tubes were no longer observed, suggesting that these were artefacts of the closed cell configuration (Fowler et al. 1987b; Gonenc et al., 1988). The subsequent observation of maxima above 400°C when using extremely high gas velocities through the flow-cell were found to be unrelated to char-volatile interactions, but to be due to interference by conducting electrons (see further).

Comparing chars from the in situ and a stand-alone 'hot-rod' reactor: Increasing velocities of inert gas were forced through the in situ quartz fixed-bed reactor. This gave rise to progressively greater spin populations throughout the temperature range. In a parallel set of experiments undertaken in the metallic 'hot-rod' reactor described in Chapter 3, Pyrolysis of solid fuels: experimental design and applications, it was observed that tar yields increased with increasing sweep gas velocity (Gonenc et al., 1988). When the residual chars from the two reactors were checked for Curie Law behaviour, the results were qualitatively similar. At the lower flow rates, the samples conformed to Curie law behaviour and the temperature dependence of the ESR signal was linear.

However, for the highest carrier gas flow rates used in both reactors, the low-temperature regions showed Curie-law conformity, while reproducible departures

Table 6.1 **ESR parameters of coals given as 'spin populations $\times 10^{-19}$' in the flow cell under slow sweep velocity conditions**

Coal	Elemental C (%, daf)	Temperature, T_1 (°C)	Temperature, T_2 (°C)	Spin population S_C (g^{-1})	Spin population S_1 (g^{-1})	Spin population S_2 (g^{-1})	Spin population S_3 (g^{-1})
Can[a]	54.2	250	310	0.3	0.8	0.46	0.12
Burning Star	75.5	220	310	0.8	2.9	0.54	0.23
Linby	83.0	205	310	1.07	3.26	1.19	0.33
Point of Ayr	85.4	220	325	1.37	1.98	0.58	0.3
Cortonwood[b]	87.2	250	340	1.36	3.21	0.67	0.23
Cynheidre[c]	95.2	–	–	1.72	–	–	–

Source: Reprinted from Fowler, T.G., Kandiyoti, R., Bartle, K.D., Snape, C.E., 1989b. Carbon 27, 197. Copyright 1989, with permission from Elsevier.
[a]The three-region behaviour not well developed.
[b]Swelling forced part of the sample out of the cell.
[c]Three region behaviour not apparent with this coal.

from linearity of signal from the chars were observed at the higher temperatures. The curvature, observed for chars from both reactors, closely correlated with a sharp drop in measured spin populations above 400°C for the highest gas flow rates (2.1–2.5 m s^{-1}). In earlier work, Singer and Lewis (1982) had pointed out that unpaired spins detected in higher temperature carbons and graphites primarily show the presence of conduction electrons (Singer and Lewis, 1982). This observation was useful for interpreting the maxima observed in spin populations at the higher temperatures for large gas-flow rates and appeared to arise from the high conductivity of the chars produced when large gas-flow rates were used. Under these more extreme conditions, signal due to the unpaired spins of free radicals (resulting from covalent bond-cleavage reactions) appear to overlap with signal from free conduction electrons.

To summarise, the increasingly rapid removal of pyrolysis volatiles from the reaction zone was found to give rise to increases in observed spin populations. The effect appears due to the sweep gas removing pyrolysis volatiles from the reaction zone more rapidly, which results in the partial suppression of recombination reactions between tar free-radicals and free-radicals of the pyrolyzing char matrix. The corresponding increase in tar yield with increasing gas-flow rate, observed in the stand-alone metallic reactor, was consistent with this interpretation of the data. Qualitative agreement was also observed between the Curie Law behaviour of chars produced in the stand-alone, metallic 'hot-rod' pyrolysis reactor and the quartz in situ ESR flow cell. This provided confirmation that the observations resulted from interplay between sweep gas velocities and tar-char interactions within the reaction zone.

Designing an experiment that would allow the direct observation of free radical recombination reactions between volatilised tars and a pyrolyzing mass of coal does not seem a straightforward task. The removal of volatiles from the reaction zone at increasing carrier gas velocities provided a 'second-best' experiment. It afforded evidence for the suppression of recombination reactions between pyrolyzing coal particles within the ESR cavity and evolved pyrolysis volatiles through their more rapid removal from the reaction zone at increasing carrier gas velocities.

6.1.2 Temperatures associated with product release: pyrolysis and liquefaction

For most coals, raising the temperature to about 300°C does not appear to break many covalent bonds (Fowler et al., 1989b). Instead, small amounts of gases are released by the coal mass, including some hydrogen, methane, ethane, H_2S and small amounts of light hydrocarbons (e.g., see Neuburg et al., 1987). At these temperatures, thermally induced mobility within the coal mass appears to allow some free-radical recombination reactions to take place ($T_2 > T_1$, in Fig. 6.1).

In situ ESR pyrolysis experiments undertaken in the presence of a donor-solvent suggest that similar processes are initiated when sample temperatures are raised to about 300°C during 'dry' pyrolysis and during liquefaction (Fowler et al., 1988b). Nonetheless, some differences may be identified early on. When heated in a suitable solvent, many coals tend to swell. It is also possible to extract significant proportions of many coals in appropriate solvents after pre-heating to temperatures below the

onset of covalent bond-cleavage reactions. Swelling and solubility in coals are often related; solvents that swell coals often prove effective in extracting them.

Table 6.1 presents data from ESR experiments using six coal samples, spanning a broad range of coal ranks. In this series, T_2 increased from 310°C for the lignite to 340°C for 'Cortonwood Silkstone' coal, the highest rank coal for which a result could be obtained (87.2% C content). The Welsh anthracite Cynheidre turned out to be rather inert. While many more samples need to be tested for establishing definitive trends, Table 6.1 suggests that the characteristic onset temperatures for covalent-bond-cleavage reactions, labelled as T_2 in Table 6.1, are rank dependent. As the temperature is raised above the characteristic onset temperature, the ESR data showed rising spin populations, as a result of intensifying covalent bond-cleavage reactions (Region III in Fig. 6.1).

Comparing these results with data from coal liquefaction experiments is revealing. The data presented in Fig. 5.1, from experiments in the flowing-solvent reactor, show that it was possible to extract up to one-third of the mass of both Point of Ayr (UK) and Pittsburgh No. 8 (USA) coals, at temperatures below 300–325°C. According to Table 6.1, these are temperatures below or near the onset of covalent bond cleavage. It seems reasonable to expect that any weight loss observed up to these temperatures would be due to simple solvent extraction of the more mobile, relatively low molecular mass material present within the coals.

In fact, for most middle-rank coals, sample weight loss at temperatures up to 350°C could be explained in terms of extracting small(er) molecular mass and more soluble material native to the coal (Xu and Kandiyoti, 1996). Fig. 5.1 also shows that above 350–375°C, the rate of weight loss accelerated with increasing temperature. The data on Point of Ayr (UK) coal show this more graphically than many other coals. As the temperature rose to between 375°C and 400°C, coal extract yields from the two middle-rank coals reached and exceeded 40%. This increase was accompanied by a broadening of the molecular mass distributions of the extracts (Xu et al., 1994; Li et al., 1995). These threshold temperatures depend on the structures of particular coals; below, we will encounter a coal, which displayed extensive depolymerisation behaviour nearer 450°C.

The temperature gap between the onset of bond cleavage and extensive depolymerisation: Fig. 5.1 shows that extensive coal depolymerisation took place at temperatures that were clearly above the temperatures where the onset of covalent bond cleavage (310–340°C) was observed. This temperature gap suggests that coal samples need to climb a long way up the ESR curve in Region III (Fig. 6.1), before more intense mass release is actually observed. This observation is consistent with the proposition that more than one bond must be cleaved before large molecular fragments – attached to the solid matrix by more than one covalent bond – may be released as large free radicals, within the coal particles. This description would explain limited nature of extract release from the coal particles above 300°C up to the temperature band (>350–375°C).

Thus, provided a suitable solvent is used for dissolving and sweeping the extractable material away, solvent-extraction/liquefaction allows the recovery of a large proportion of the coal mass as a solvent-soluble extract at temperatures up to 400°C. This temperature was sufficient for extracting about 50% of the Point of Ayr and nearly

70% of the Pittsburgh No. 8 coals, in the flowing solvent reactor. Meanwhile, sample weight loss during the *pyrolysis* of low-to-middle rank Linby coal (UK) at the same temperature (400°C) was less than about 5% (Fig. 3.3B).

Compared to pyrolysis, the removal of tar/extract precursors from parent coal particles into the surrounding solvent during coal extraction or liquefaction presents a far less steep (solid-to-liquid) mass transfer barrier, that needs to be overcome (Suuberg, 1985). However, not all classes of liquids behave in similar ways. Hexadecane (*n*-hexadecane) is neither a hydrogen donor nor a good solvent for most coal-derived materials. Table 5.3 showed that in the absence of hydrogen-donor properties and/or adequate solvent power, the mass transfer barrier between the solid and liquid phases was nearly as difficult to overcome as the case of 'dry' pyrolysis. For material chemically released from the coal matrix, the major distinguishing feature between pyrolysis and liquefaction thus turns out to be the mass transfer step between external coal particle surfaces and the surrounding fluid medium.

The effect may also be described as follows. Assuming that covalent bond cleavage is primarily a function of temperature, similar proportions of extractable material would be expected to detach from the solid matrix, during liquefaction and during 'dry' pyrolysis. These extractables would be released into the mass of individual coal particles. However, during 'dry' pyrolysis (in the absence of solvent), no mechanism exists for their removal, apart from a small amount that might evaporate. The rest of the 'tar-precursors' remain trapped within heated coal particles. We will see below that these 'trapped' tar-precursors are chemically fairly stable at 400°C for up to 120 s and perhaps longer.

As the temperature is raised above the 400−450°C range in (dry) pyrolysis, tar-precursors trapped within pyrolyzing coal particles become more reactive. They may evaporate or repolymerise, or undergo cracking reactions, producing some light gases and some smaller molecular mass tar-precursors. In turn, these species may evaporate or undergo further pyrolytic degradation. With rising temperatures, the rates of cracking, evaporation and repolymerisation all increase sharply. The competition between these reactions determines the eventual product distribution. Experiments show, however, that above 450°C, a larger part of the residual extractable materials within solid particles rapidly solidify, thus reducing the amount of potentially volatile (or potentially soluble) coal-derived material (Fukuda et al. 2004). This is why much higher proportions of residual chars are observed during the 'dry' pyrolysis of coal, compared to the larger proportions of extracts recovered during liquefaction in a donor solvent.

6.2 Extractables as a diagnostic tool for pre-pyrolysis phenomena

6.2.1 Solvent extracts and coal plasticity

The solvent extraction of unheated coals is known to release soluble extracts. The amounts of coal mass extracted reflect something of the makeup of the coal as well as the properties of the solvent (Friedel et al., 1968; Kessler et al., 1970). Solvent

extracts of diverse coals have been analysed by practically every available technique. Early work on coal extraction has been reviewed by Howard (1963) and Wender et al. (1981).

Relationships between the proportions of material extracted from coals after heating and their plastic behaviour during heating have also been widely discussed (Orchin et al., 1951; Dryden and Pankhurst, 1955; Brown and Waters, 1966a; Brown and Waters, 1966b). Dryden and coworkers (Dryden and Pankhurst, 1955; Dryden and Joy, 1961), and, a decade later, Brown and Waters (1966a,b), described the recovery of increasing amounts of chloroform-soluble material when, prior to extraction, coals were heated (slowly) to temperatures between 300°C and 400°C. For any given coal, the amount and composition of extracts was reported to change as a function of the heat-treatment temperature and the time-at-temperature. It was observed, furthermore, that extracting bituminous coals with chloroform prior to thermal treatment had a detrimental effect on their subsequent softening and coking behaviour. The softening and agglomerating behaviour of particular coals (indicators of coking properties) were thus observed to correlate with the amounts of chloroform extractable material that was found in pre-heated samples.

Howard and coworkers experimented with Pittsburgh No. 8 coal and observed clear relationships between the temperature, the duration of the plastic state at a given temperature, and the extractable content of coal particles at that temperature (Fong et al., 1986a). These researchers monitored the development of coal plasticity and its retrogression (i.e., loss of plasticity) with a fast response plastometer. They observed that the plasticity of the coal could be closely correlated with the inventory of pyridine extractables within the sample. They showed that plasticity could be quantified in terms of the rates of generation and destruction of pyridine extractables (labelled as 'metaplast') within the coal particles.

The rest of this section explores how changing the heating rate can affect the extractable content and the plasticity of coals and the impact of these parameters upon the amounts of tar released during pyrolysis. The analysis will lead us to a more detailed view of retrogressive recombination reactions and how they affect the course, and eventual outcome of coal thermal breakdown.

6.2.2 A novel approach to coke making

Prime coking coals are usually more expensive than other coals, e.g., steam coals, and are becoming less readily available. Research on coke making seeks to take advantage of insights that may help to reduce the proportion of prime coking coals utilised in coke blends and to expand the range of coals that could be used in these operations (Sasaki et al. 1998). Shifting the coke blend composition toward weakly coking coals is therefore commercially attractive. Useful summaries of the vast literature on conventional coking operations may be found in standard texts (e.g., Elliott, 1981; Kumar et al., 2009; Speight, 2012).

Meanwhile, some low-rank bituminous coals remain morphologically unchanged when heated slowly (~1°C s^{-1}), but soften or melt under rapid heating conditions (e.g., 1000°C s^{-1}) (Hamilton, et al., 1979; Hamilton, 1980; Gibbins-Matham and

Kandiyoti, 1988). In searching for ways to improve coke-making, Aramaki et al. (1996) demonstrated at bench scale that when weakly coking coals were first 'pre-heated' rapidly to temperatures up to 400°C, and then heated slowly to temperatures of 900°C or higher, a coke of increased strength could be obtained. Ohtsuka et al. (1996) also reported that the swelling ability and softening properties of coals could be improved by rapid pre-heating to their softening temperatures; the heating rates used in that work ranged between 5°C and 500°C min^{-1}.

At Nippon Steel Corporation, experimental observations showing links between heating rates and coal plasticity led to a pilot-scale application aimed at improving the coke production process. The concept involved rapidly pre-heating crushed coal in a riser to about 400°C. The resulting mass of sticky particles collected in a retort was then slowly heated to 800−900°C. The overall effect was to form a stronger coke than would have otherwise been possible by heating the same coal (or blend) in the same retort slowly from ambient temperature (Aramaki et al., 1996). The procedure was found to be effective for improving the coking properties of weakly coking coals. For prime coking coals, however, the initial rapid-heating step provided no significant improvement in the amount or strength of the coke product.

6.2.3 Exploring pre-pyrolysis phenomena in coals

In a study that followed on from the pilot work at Nippon Steel, extractable materials accumulating within coal particles prior to full-blown pyrolysis were studied as a diagnostic tool (Fukuda, 2002; Fukuda et al., 2004). The aim was to explore how the extractable contents of heated particles could be altered by changing the heating rate and the holding time at the target temperature. Experiments were designed for identifying (1) the temperature interval within which fast heating was instrumental in causing discernible changes in the extractable content and (2) the range of 'fast' heating rates, which were effective in enhancing the formation and survival of extractables within the coal mass.

Samples from three coal blends, already studied at Nippon Steel were used. Weakly coking Newcastle Blend Coal (NCBC) is labelled below as Coal A, strongly coking Goonyella as Coal B, and the very strongly coking K-9 Blend as Coal C. Table 2 presents the properties of the three sample blends. As will be explained below, K-9 was a blend with some rather peculiar properties.

The atmospheric-pressure wire-mesh reactor used in these experiments (Fig. 3.1) was capable of programmed multistage heatup between several pre-set temperatures, and of variable hold times during intervals between the time-temperature ramps. The initial set of experiments followed one of two sequences (Fukuda et al., 2004).

Sequence I: Step 1: Fast heating (1000°C s^{-1}) to 400°C. Step 2: 30 s holding at 400°C. Step 3: Slow heating (1°C s^{-1}) to a target temperature between 400°C and 500°C. Step 4: 30 s holding at the target temperature, followed by cooling and extraction with NMP (1-methyl-2-pyrrolidinone).

Sequence II differed from Sequence I only by application of slow (1°C s^{-1}) heating up to 400°C during Step 1.

Sequence II: Step 1: Slow heating (1°C s^{-1}) to 400°C. Step 2: 30 s holding at 400°C. Step 3: Slow (1°C s^{-1}) heating to a target temperature, between 400°C and 500°C. Step 4: 30 s holding at the target temperature, followed by cooling and extraction with NMP.

The 106–150 μm particle size range was used for volatile and tar yield measurements in the wire mesh reactor. This size range was partly determined by the smallest size of stainless steel mesh able to accommodate the relatively easy to handle 50 μm diameter thermocouple wires. However, when chars from coals ground to 106–150 μm were extracted in NMP, some of the solid sample escaped through the holes in the mesh (63 μm × 63 μm aperture size). The problem was side stepped by using a larger sample size fraction, 212–250 μm, in experiments where heating in the wire-mesh reactor was followed by extract yield determinations.

Using a 25 μm diameter thermocouple wire would have allowed the use of mesh with smaller aperture sizes. However, compared to 50 μm, handling 25 μm diameter thermocouple wires turns out to be disproportionately difficult, requiring manipulation under a microscope, which was impractical for performing a large number of experiments.

Fig. 6.2 compares the amounts of extractable material recovered from Coal A particles heated to 400°C rapidly (1000°C s^{-1}) and slowly (1°C s^{-1}) during Step 1. In both sets of experiments, the samples were held at 400°C for 30 s, heated slowly (at 1°C s^{-1}) from 400°C to target temperatures between 400°C and 500°C, and held for 30 s before cooling to ambient temperature.

The key finding from these experiments was the large difference between extract yields from chars recovered after fast and slow heating to 400°C. Samples rapidly heated to 400°C at 1,000°C s^{-1} gave about 66% extract, compared to about 33% extract from the samples heated slowly (1°C s^{-1}) to 400°C. The extract yield from untreated (unheated) Coal A was about 35%. As the temperature was raised from 400°C at 1°C s^{-1}, the amount of extractable material accumulated within the particles that had been initially heated rapidly, increased slowly to about 80% near 450°C. Above that temperature, the plastic mass quickly resolidified. Meanwhile, the extractable material within initially slowly heated particles appeared to be surprisingly inert between 400°C and 500°C. The slow upward drift of extractable content observed in Fig. 6.2 was not much greater than experimental scatter.

These findings raised two questions regarding how these differences arise during heat up to 400°C. First, was there a critical target temperature above which differences between fast (1000°C s^{-1}) and slow (1°C s^{-1}) heating particles became apparent and below which differences in the extractables contents of chars were not pronounced? Second, how fast did the fast heating need to be for differences to begin to emerge between slow and fast heating?

6.2.4 Critical temperature for fast heating to begin making a difference

To answer the first question, Coal A particles were heated at 1000°C s^{-1} to temperatures between 350°C and 400°C, followed by cooling and extraction with NMP. Fig. 6.3A shows that a fairly clear transition to greater extractable accumulation

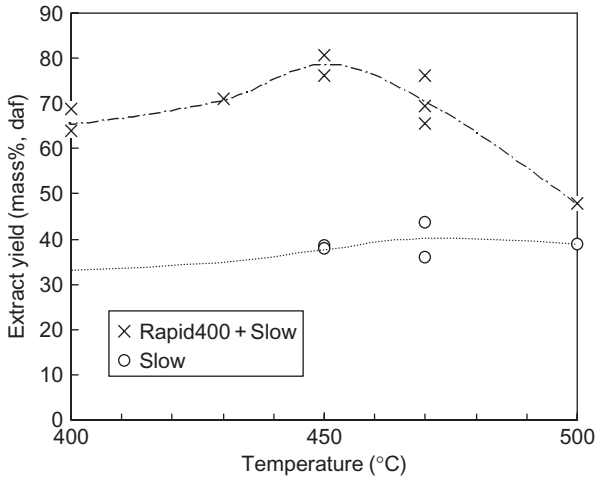

Figure 6.2 Comparison of NMP-extract yields between 'rapid400 + slow' and simple 'slow' heating (NCBC coal).
Source: Reprinted with permission from Fukuda, K., Dugwell, D.R., Herod, A.A., Kandiyoti, R., 2004. Energy Fuels 18, 1140. Copyright 2004 American Chemical Society.

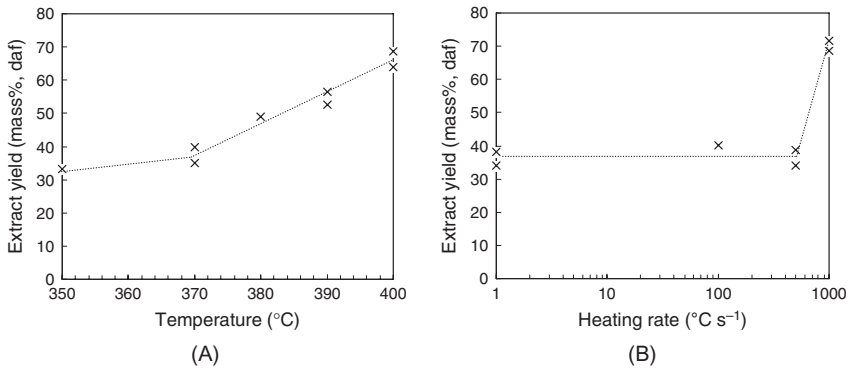

Figure 6.3 (A) Relationship between peak temperature and NMP-extract yield; heating rate: 1000°C s^{-1}. (B) Relationship between heating rate and NMP-extract yield (370–400°C).
Source: Reprinted with permission from Fukuda, K., Dugwell, D.R., Herod, A.A., Kandiyoti, R., 2004. Energy Fuels 18, 1140. Copyright 2004 American Chemical Society.

occurred between 370°C and 400°C. Near 400°C, the extractable yields rose toward the same point (~65%) reported in Fig. 6.2, showing satisfactory internal consistency within the data (Fukuda et al., 2004).

The faster rise in extractables above 370°C was also consistent with the temperature for the onset of massive depolymerisation inferred from ESR-spectroscopy-based observations discussed above and from the liquefaction data in Fig. 5.1.

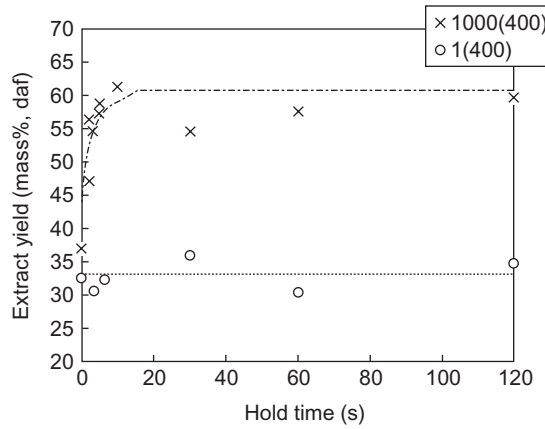

Figure 6.4 Effect of holding time at 400°C on NMP-extract yields for NCBC samples heated at 1°C and 1,000°C s^{-1}.
Source: Reprinted with permission from Fukuda, K., Dugwell, D.R., Herod, A.A., Kandiyoti, R., 2004. Energy Fuels 18, 1140. Copyright 2004 American Chemical Society.

Recalling the assumption that covalent bond cleavage reactions are functions of the temperature alone, the smaller extractable yields from particles heated slowly to 400°C (Fig. 6.2) suggests that a greater number of free-radical recombination reactions must have taken place during slow heatup to 400°C, compared to fast heating to 400°C. The greater extractable inventories within the rapidly heated particles indicate that during rapid heating, recombination reactions must have taken place to a lesser extent, compared to slow heating. Meanwhile, the less reactive free radicals that survived the heat-up process to 400°C (at either heating rate) within the extractable mass are observed to be stable at 400°C for at least 120 s (Fig. 6.4). These observations give us a preliminary handle on how to distinguish between fast and slow free-radical recombination reactions and by inference, on the reactions of the more reactive and less reactive free radicals during coal pyrolysis. We will return to this point.

Meanwhile, the larger pool of extractables (tar-precursors) contained in rapidly heated particles goes some way toward explaining the higher tar yields from middle-rank coals during rapid heating. As temperatures are raised by rapid heating above 400–450°C, e.g., to 700–800°C, some tarry material begins to evaporate directly while heavier tar precursors may crack to produce more volatile tar precursors and gas as well as forming some secondary char. As first suggested by Gray (1988), it is likely that some tarry material may be ejected due to steep internal pressure gradients generated by the high speeds of heating. This suggestion is consistent (1) with the larger tar yields observed, and, (2) with data from size exclusion chromatography (SEC), showing broader molecular mass distributions for tars recovered from faster heating rate experiments (Li et al., 1993a,b). The broader molecular mass distributions would correspond to heavier tars, rapidly ejected from coal particles, presumably before some of these tar precursors could undergo further cracking and/or charring reactions.

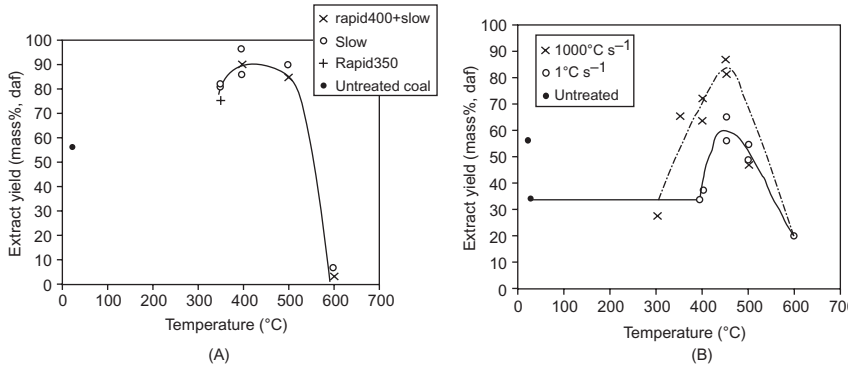

Figure 6.5 Relationship between NMP-extract yield and temperature for samples of (A) Goonyella (Coal B) and (B) K-9 (Coal C), both prime coking coals, heated at 1°C s^{-1} and 1000°C s^{-1} to 400°C, followed by heating at 1°C to a variable peak temperature up to 600°C (30 s holding at peak temperature).
Source: Reproduced with permission from Reprinted with permission from Fukuda, K., Dugwell, D.R., Herod, A.A., Kandiyoti, R., 2004. Energy Fuels 18, 1140. Copyright 2004 American Chemical Society.

We note that tar yield enhancement through rapid heating is not a large effect. Tests on many coals have shown that maximum differences observed in tar yields between slow and fast heating are in the 4–8% range (Table 3.6). This is not a large difference, compared to the greater than 30% difference in extractable (tar precursor) accumulation, observed between the slow and fast heating of samples from the same coal to 400°C (Fig. 6.2). Even greater accumulations of plasticising mass have been observed in 'good' coking coals (cf. Fig. 6.5A, B). Meanwhile, Fig. 3.3C shows that for Linby coal, which was more heating-rate sensitive than most of the coals tested, the difference in tar yields between heating at 1°C and 1000°C s^{-1} was about 6% (Gibbins and Kandiyoti, 1989). Thus, when temperatures were raised above 500°C, char formation rather than tar evaporation or explosive ejection appears to have remained the dominant (but clearly not the only) reaction pathway for tar-precursors, irrespective of the heating rate.

Returning to Fig. 6.4, the extractables accumulated within Coal A particles showed remarkable stability for up to 2 min and possibly beyond. With the benefit of hindsight, the duration of the experiment should have been prolonged. This level of chemical stability of the extractables appears consistent with the work of Fong et al. (1986b). For the higher temperature interval of 540–800°C, these researchers reported a depletion rate for pyridine extractables ('metaplast depletion') characterised by the first-order reaction rate constant:

$$k = 1.9 \times 10^{10} \exp(-21{,}200/T), \quad (s^{-1}).$$

The numerical value of this rate constant, calculated for the depletion of extractable materials at 400°C is small, indicating the relative absence of char-forming radical recombination reactions within this 'extractable' phase at 400°C.

6.2.5 The heating rate: how fast must 'fast heating' be?

Experiments were carried out to determine how fast 'fast heating' had to be for measurable differences in the extractables content to become apparent. In this set of experiments, sample particles were heated to 400°C at increasing heating rates between 1°C s^{-1} and 1000°C s^{-1}, while holding all other parameters constant. The solid residues from these experiments were then extracted with NMP. Fig. 6.3B shows the percentage of extractables (tar precursors) accumulated in the heated particles as a function of increasing heating rate. The transition near 500°C s^{-1} was sharp and repeatable. The total weight loss (total volatiles) data from these experiments (not shown) qualitatively presented a similar trend, including the transition at and above 500°C s^{-1} (Fukuda et al., 2004).

The level of accumulation of extractables within the particles was thus observed to be directly affected by the heating rate. While we should be hard put to explain why the particular heating rate threshold value of 500–1000°C s^{-1} turns out to be the critical one, it seems sufficient for present purposes to note that a heating rate above 500°C s^{-1} is required for recovering larger amounts of extractables from Coal A particles. Moreover, the effect only became apparent at temperatures of 375°C or above for this particular blend.

These findings made it possible to arrive at a working explanation of the results from the pilot-plant work at Nippon Steel. We know from previous work that coal plasticity and extractable contents are linked. Earlier work on coal extracts had shown that minimum viscosity and maximum pyridine-extractable contents occurred within the same temperature interval (Fong et al., 1986b). Characterization work within the Nippon Steel project also showed that the temperature of maximum extractables accumulation in Coal A was near its temperature of maximum thermoplasticity, between 400°C and 430°C (Aramaki et al., 1996). Finally, the stability of extractables during at least 2 min (Fig. 6.4) and possibly longer, appears to allow sufficient time for particles emerging from the riser tube in a plastic state, to form coherent lumps of coke when stacked within the retort and heated slowly to 800–900°C.

Thus, rapid heating is observed to lead to improved coke strength via the related increase in extractables content and the resulting enhanced thermoplasticity of Coal A. However, we still need to clarify how and why faster heating rates (>500°C s^{-1}) gave rise to the formation of greater amounts of extractable material. To explore this further, let us recall that coal A was a 'weakly' coking coal. At this stage, it is of interest to examine how the 'good' coking coals behaved during analogous experiments.

6.2.6 Pre-pyrolysis behaviour of strongly coking coals

Coal B was a prime coking coal with a volatile matter content of 24.1% and a maximum Gieseler fluidity of 3.0 (Table 6.2). Extract yields from Coal B chars were determined following one of three time–temperature profiles: (1) slow (1°C s^{-1}) heating directly to the target temperature, (2) rapid (1000°C s^{-1}) heating to 350°C followed by slow heating to the target temperature, and, finally, (3) rapid (1000°C s^{-1}) heating to 400°C followed by slow heating to the target temperature.

Table 6.2 Characteristics of the three Australian coal blends used in the study

		NCBC	Goonyella	K-9
Elemental composition (% dry basis)	Carbon	83.6	87.7	90.7
	Hydrogen	5.6	5.0	4.6
	Sulphur	0.6	0.6	0.2
	Nitrogen	1.8	1.7	0.8
	Oxygen	8.3	4.8	3.3
Maceral composition	Vitrinites	72.6	61.5	82.3
	Liptinites	3.1	1.0	0.0
	Inertinites	26.8	37.9	20.8
Proximate analysis	TM	3.4	1.5	0.9
	VM	35.2	24.1	17.9
	FC	52.4	65.1	72.3
	Ash	9.0	9.3	8.9
	CSN	3.5	6.5	8.0
Gieseler plastometre	Softening	392.0	399.0	444.0
	Max. temp.	430.0	455.0	485.0
	Resol. temp.	457.0	493.0	505.0
	MF	2.0	3.0	1.3

Source: Adapted from Fukuda, K., Dugwell, D.R., Herod, A.A. and Kandiyoti, R. (2004) *Energy & Fuels* 18, 1140; copyright 2004 American Chemical Society.
TM, Total moisture (%); *VM*, Volatile matter (%); *FC*, Fixed carbon (%); *CSN*, Crucible swelling number (—); *Softening*, Softening temperature (°C); *Max. temp*., Maximum fluidity temperature (°C); *Resol. temp.*, Resolidification temperature (°C); *MF*, Maximum fluidity; *NCBC*, Newcastle Blend Coal.

Fig. 6.5A shows that as the target temperature was raised, the extractables yields from Coal B chars increased, reaching a maximum between 400°C and 450°C, and then declined, giving near-total resolidification at about 600°C. When heated to 400°C, the coal displayed highly plastic (fluid) behaviour, where more than 85% of the sample mass could be dissolved in NMP, irrespective of the heating rate. In other words, no measurable effect of the heating rate on extractables yields was observed.

This finding contrasts with the behaviour of Coal A, which only gave significantly larger extractable yields when heated at or above 500°C s^{-1} and not when heated at 1°C s^{-1}. On the basis of the behaviour of Coal A, we would have expected to observe more char-forming recombination reactions in the 350–400°C interval during the slow (1°C s^{-1}) heating of Coal B to 400°C, compared to rapid heating. Whatever the internal processes of Coal B, however, such repolymerisation of solvent-soluble material to secondary char was not observed.

It appears possible to arrive at a more general tentative observation when pyrolysis tar-yield data from a wider range of samples is considered (see chapter: Pyrolysis of solid fuels: experimental design and applications). Taken together, the body of data shows that high heating rates improve the plastic behaviour of ordinarily nonmelting coals, i.e., coals that do not melt at slow heating rates. However, little difference in tar yields was observed for coals showing good plastic behaviour at low as well as high

heating rates. Below, we will examine evidence suggesting that the melting behaviour of coals is associated with the local availability of hydrogen, serving to quench (cap) reactive free radicals. The process appears to be helped along when the contents of hydrogen scavengers, such as oxygen and sulphur, are relatively low within the pyrolyzing mass.

The Coal C blend, the second 'good' coking coal sample used in the study, showed similar but not identical behaviour to Coal B. Despite a relatively low volatile matter content of 17.9% and a (low) maximum Gieseler fluidity of 1.3, Coal C behaved as a 'good' coking coal, albeit with somewhat peculiar properties. It was observed to have a relatively high softening temperature (~450°C) compared to ~400°C for the two other blends considered in the study. The elemental carbon content of this blend (90.7%) was high, but the contents of potential hydrogen scavengers, sulphur (0.15%) and oxygen (3.3%), were low relative to most coals.

A small but measurable effect of heating rate could be observed for this unusual coal from approximately its softening point onward. The long (~400 s) holding times required at 450°C for these effects to become apparent are consistent with slow depolymerisation of a highly cross-linked coal blend of 90.7% overall carbon content.

Fig. 6.5B presents extractable yields from Coal C chars heated at 1°C s^{-1} and 1000°C s^{-1} directly to the target temperature. For a heating rate of 1°C s^{-1}, the extractable yield at 400°C was similar to that from untreated Coal C. Above 400°C the extractable yield traced a sharp maximum at about 450°C, with resolidification reaching completion somewhat above 600°C.

By contrast, when samples were heated at a rate of 1000°C s^{-1}, the extractable yield remained similar to that of unheated Coal C up to 300°C but increased sharply from 350°C onward, reflecting a little of the behaviour of Coal A. The shape of the curve was similar to that obtained for heating at 1°C s^{-1} in Fig. 6.5B, tracing a sharp maximum at about 450°C and declining rapidly at higher temperatures. However, extractable yields were enhanced by ~30% of the coal mass in response to rapid heating. Meanwhile, almost identical results were obtained when NMP-extractable yields from rapid heating to 400°C followed by slow heating and the slow heating programs were investigated (Fukuda, 2002).

Taken together, the pyrolytic behaviour of Coal C seemed to be intermediate between Coal A and Coal B, with the added peculiarity of a high softening temperature and the slow development of pyrolytic reactions at 450°C. Recalling that Coal C was a proprietary blend of several coals, there was insufficient evidence to comment further.

6.3 How does fast heating work?

A brief summary of observations: According to Gray (1988), the higher tar yields observed during fast heating may be explained in terms of the 'explosive ejection' of tar precursors (i.e., 'extractables') from pyrolyzing coal particles. However, explosive ejection can only give increased tar yields if the coal mass already holds enough 'tar

precursor' within the fluid/plastic mass. Working with a high-pressure plastometre, Howard and coworkers (Fong et al., 1986a,b) have showed links between coal plasticity and the inventory of extractables (metaplast) within coal particles.

Moreover, observations summarised in Figs. 6.2–6.5 indicated that a larger pool of tar precursors developed when coals with marginal coking ability were heated rapidly. We next explore how this larger pool of extractable material came into being (and remained as 'extractable') when particles of the marginally coking Coal A were heated rapidly.

The plastic state in coals: Clarification of the links between faster heating, greater extents of 'extractables' formation and higher tar yields, requires examining what we know of the plastic state in coals. The discussion goes back to earlier investigations of coking phenomena (Brown and Waters, 1966a,b; Wiser, 1968).

The consensus view of plasticity articulated by Neavel (1981) may be paraphrased as follows: pyrolytic processes prior to tar evaporation may be viewed as a hydrogen-donation stage, during which, the hydrogen-donating activity of the plastic phase provides a medium analogous to liquefaction in a hydrogen-donor solvent such as tetralin. The hydrogen donating action of the plastic phase would tend to block some (but not all) free-radical recombination reactions. Within this framework, the coal itself is viewed as supplying the solvating and hydrogen-donating vehicle.

According to Neavel, the hydrogen donor ability within the pyrolyzing mass was held to reside in the hydroaromatic (alicyclic) component of the plasticising phase. Broadly, the 'plasticising phase' term corresponds to the term 'extractables' ('tar precursors') used in this work, and to 'metaplast' in the work of Howard and coworkers' (Fong et al., 1986a,b). Within this formulation, the extent of coal plasticity and the magnitude of tar yields are thought to depend on the local availability of hydrogen that is directly proportional to the hydroaromatic hydrogen content of the pyrolyzing coal.

Neavel's model and the role of high heating rates: Neavel's conceptual model takes no account of how changes in heating rate affect reaction pathways during thermal breakdown. However, it provides a useful framework for explaining the observed role of heating rates.

During fast heating experiments, we observe that pyrolytic events, such as tar evaporation, are compressed into a shorter time frame and pushed up the temperature scale. Experiments with Linby (UK) coal showed that the level of weight loss achieved by heating at 1°C s^{-1} was matched during rapid heating (1000°C s^{-1}) at temperatures that were about 100°C higher (Figure 4 in Gibbins and Kandiyoti, 1989). This difference continued up to 600°C, after which volatiles evolution from slowly heated samples tended to slow down. Temperature differences between analogous pyrolytic events during the fast and slow heating of Pittsburgh No. 8 coal were closer to 130−140°C (Gibbins-Matham and Kandiyoti, 1988).

When middle-rank coals are heated, small amounts of hydrogen are released from about ~285−300°C (e.g., see Neuburg et al., 1987). The telescoping together of pyrolytic events and shifting to higher temperatures during faster heating would tend to improve the probability that internal hydrogen release should overlap with extensive covalent bond-cleavage taking place at higher temperatures. Both the donatable alicyclic hydrogen and the internally released molecular hydrogen are thus more likely

to enter the pyrolyzing mix and quench (cap) freshly formed free radicals, blocking more of the recombination reactions, compared to slow heating.

The model formulated here suggests that the hydrogen transfer process within the coal mass overlaps more completely with covalent bond cleavage, when coals are heated rapidly and pyrolytic processes are telescoped closer together in time.

While we have no direct proof for this sequence of events, this model is able to explain several observations, as well as some of the data presented above. (1) Fig. 6.2 shows Coal A particles maintain larger inventories of extractable material during heat up to 400°C at 1000°C s^{-1} compared to heatup at 1°C s^{-1}. (2) Fig. 6.4 shows the greater inventory of extractable materials to be chemically stable for at least 120 seconds, strongly suggesting that the more reactive free radicals had been mostly capped (quenched). (3) Fig. 3.3C shows increasing tar and volatile yields with increasing heating rate. (4) The model is able to provide an explanation for observations on marginally hydrogen-deficient coals such as Linby (UK), NCBC blend (Australia), and Pittsburgh No. 8 (US), which do not melt when heated slowly (~1°C s^{-1}) but show plastic behaviour when heated rapidly (1000°C s^{-1}).

It appears, therefore, that no strict dividing line exists between melting and non-melting coals. Low- to middle-rank bituminous coals appear to be transitional between subbituminous and high-volatile bituminous coals (less mature coals that would melt with greater difficulty) on the one hand and the readily melting and swelling, 'coking' coals on the other. At the higher end of the rank scale, anthracites might partially respond to very fast heating rates by marginally softening, if they respond at all.

It now becomes possible to explain the behaviour of coals like Goonyella (Coal B, above) or indeed the behaviour of other H_2-rich specimens such as liptinites (see chapter 3: Pyrolysis of solid fuels: experimental design and applications), which show far less sensitivity to changes in heating rate, compared to Linby coal or the NCBC blend.

Liptinites and Goonyella coal present relatively high elemental hydrogen contents and relatively low contents of hydrogen scavenging species (oxygen and sulphur). These properties tend to provide an environment capable of swamping the internal 'liquefaction' process with sufficient hydrogen to block some of the recombination reactions, regardless of the heating rate. The more abundant supply of hydrogen allows these samples to show melting and swelling behaviour during both slow and fast heating. By comparison, marginally hydrogen-deficient vitrinites show more pronounced heating rate sensitivity during pyrolysis, with regard to both plastic behaviour and tar yields (Li et al., 1993a,b, 1994; Aramaki et al., 1996) due to their greater dependence on the hydrogen-enhancing effects brought about by rapid heating.

6.3.1 Tar yields and hydrogen donors in coals

We have already encountered the concept that hydrogen-donor ability in pyrolyzing coals during the internal liquefaction process resides in the hydroaromatic component (Brown and Waters, 1966a,b; Neavel, 1981). Hydroaromatic content in coals generally decreases gradually with increasing rank, or elemental carbon content, up to about 87–88% carbon. Above this level, it is observed to decrease rapidly with increasing coal rank.

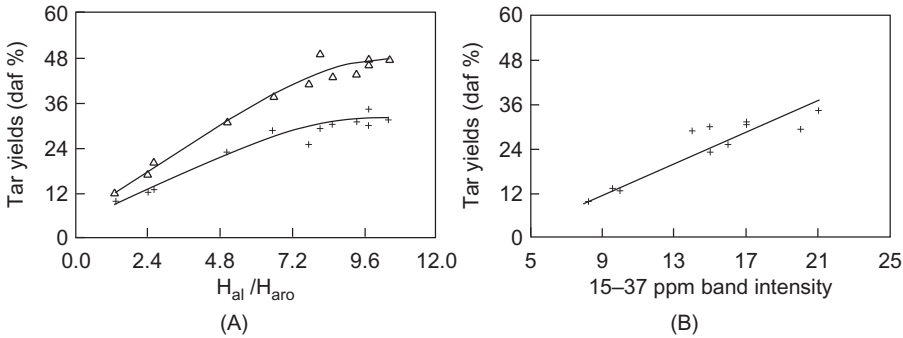

Figure 6.6 (A) Pyrolysis yields as function of FT-IR–derived aliphatic: aromatic hydrogen ratio for a rank-ordered series of Northern Hemisphere coals: (+) tar, (Δ) total volatile. Pyrolysis in atmospheric pressure helium, with heating at 1000°C s^{-1} to 700°C with 30 s holding time. Non-melting coals: Taff Merthyr, Emil Mayrisch, Tilmanstone; melting coals: Heinrich Robert, Santa Barbara, Longannet, Candin, Bentinck, Thoresby, Gedling, Linby, Illinois No. 6. (B) Pyrolysis tar yields as a function of ^{13}C-NMR–derived 15–37 ppm aliphatic band intensity for a rank-ordered series of Northern Hemisphere coals. Coals and pyrolysis conditions as in (A).
Source: Reproduced with permission: Reprinted from Li, C.-Z., Madrali, E.S., Wu, F., Xu, B., Cai, H.-Y., Güell, A.J., et al., 1994. Fuel 73, 851. Copyright 1994, with permission from Elsevier.

Fig. 6.6 presents pyrolysis tar yields from a set of coals, plotted against (A) FT-IR–derived aliphatic/aromatic hydrogen ratios (H_{ali}/H_{aro}) and (B) ^{13}C-NMR–derived aliphatic (15–37 ppm) band intensities of a set of sample coals. In both cases, the samples consisted of a rank-ordered but otherwise nearly randomly selected set of Northern Hemisphere specimens. Both sets of data showed reasonably smooth trends of increasing tar yields with increasing aliphatic content in the coal samples. We note that both sets of data lumped together signal that tars form from alkyl and hydroaromatic (alicyclic) structures.

There is an ongoing need for a reasonably direct and preferably practical method for determining hydroaromatic contents in coals. Estimates of hydroaromatic carbon content based on the dehydrogenation of coals using benzoquinone indicated about 29−30% hydroaromatic carbon for vitrinites of 82.5% C content, declining to 20% for 87.5% C content coals (Peover, 1960). Using a broadly similar approach, Reggel et al. (1968, 1971, 1973), catalytically dehydrogenated vitrinites in an organic vehicle (phenanthridine) with various formulations of palladium and rhodium catalysts mounted on $CaCO_3$, alumina or charcoal supports. The latter results were broadly in line with hydroaromatic contents reported by using the benzoquinone-based method of Peover (1960).

Both past and some more recent work aiming to quantify hydroaromatic content in coals has focused on coal-derived liquids rather than on solid coals. In solution-state ^{1}H-NMR, the difficulty consists in distinguishing between the α-hydrogens of hydroaromatic (alicyclic) structures and the α-hydrogens of alkyl substituents of

aromatics in the 2.45–4.45 ppm chemical shift region. Studies based on solution-state ^{13}C-NMR have not provided new routes for distinguishing between $C_{\alpha 2}$ carbons in bridging structures from $C_{\alpha 2}$ carbons in hydroaromatic groups (Álvarez et al., 2013). The lines of approach and challenges faced are similar to the characterization of hydroaromatic structures in petroleum-derived heavy fractions (Gould and Wiehe, 2007; Guo et al., 2010).

In Chapter 8, Analytical techniques for high mass materials: method development, we will review relatively recent attempts to resolve this enduring problem. Meanwhile, what can be shown with reasonable clarity is the absence of any contribution to hydrogen donation by long chain aliphatic species when used as the liquid medium during coal liquefaction. The data presented in Table 5.3 and discussed in Chapter 5, Liquefaction: thermal breakdown in the liquid phase, showed that the straight chain alkane, hexadecane (n-$C_{16}H_{34}$), contributed little to the coal liquefaction process in terms of either solvent power or hydrogen-donor activity. In fact, when coal samples were liquefied in hexadecane, conversions differed only marginally from pyrolysis in an inert gas environment.

Returning to the data in Fig. 6.6, we do not yet appear to have a direct method for distinguishing with any degree of accuracy between the presence of cyclic and alkyl groups in solid coals during pyrolysis. That said, we do not expect alkyl groups within the plasticising mass to donate hydrogen to reactive free radicals. It would therefore seem reasonable to assume provisionally, but difficult to prove, that the observed increases in tar and total volatile yields in Fig. 6.6 correspond to the progressively increasing hydroaromatic component within the coal sample sequence.

6.4 Fast and slow recombination reactions in pyrolysis and liquefaction

As already noted, the shorter lifetimes of reactive free radicals and their consequently low concentrations make them difficult to observe by ESR against the far greater background count of stable free radicals (Fowler et al., 1989a). In the absence of direct measurements, it is necessary to rely on indirect evidence when attempting to distinguish between fast and slow retrogressive free-radical recombination reactions.

6.4.1 Fast and slow retrogressive reactions in pyrolysis

Fast retrogressive reactions during pyrolysis: Table 6.3 presents data from an earlier study comparing sample weight loss during pyrolysis and liquefaction (Li et al., 1994), using samples of the already familiar Linby and Point of Ayr (UK) coals. The pyrolysis runs were done under standard fast heating conditions in helium (see caption). The liquefaction runs were similarly done under standard conditions in tetralin (see caption). The data show that Linby coal gave about 36% more weight loss during liquefaction compared to pyrolysis; Point of Ayr coal gave over 42% more extract than total pyrolysis volatiles. The pyrolysis data also showed that nearly 15% of the

Table 6.3 Sample weight loss in pyrolysis and liquefaction of Linby and Point of Ayr coals. Pyrolysis: 1000°C s^{-1} to 700°C with 30 s holding time in atmospheric pressure helium. Liquefaction: 5°C s^{-1} to 450°C with 400 s (Point of Ayr) or 100 s (Linby) holding time. Tetralin flowing at 0.9 mL s^{-1} under 70 bar pressure

	Linby coal (% w/w daf)		Point of Ayr coal (% w/w daf)	
Liquefaction	83		85	
Pyrolysis	**Tar**	**Total Volatiles**	**Tar**	**Total Volatiles**
	30.7	46.6	26.1	42.4

Source: Reprinted from Li, C.-Z., Madrali, E.S., Wu, F., Xu, B., Cai, H.-Y., Güell, A.J., et al., 1994. Fuel 73, 851. Copyright 1994, with permission from Elsevier.

original mass of either coal did not condense during the tar capture procedure (see chapter: Pyrolysis of solid fuels: experimental design and applications), suggesting that anything up to 10–15% of extractables (tar precursors) have cracked to lighter volatiles, presumably at temperatures above 450–500°C.

Assuming, once again, that covalent bond cleavage reactions take place primarily as a function of the temperature, similar extents of covalent bond cleavage would be expected to have taken place during heatup in pyrolysis and liquefaction – in each of the two coals. It seems safe to conclude therefore that during the 'dry' *pyrolysis* of these two coals, nearly 40% of 'tar-precursors' that had been released during heatup, repolymerised to secondary char through retrogressive reactions between 450°C and 700°C. When heating at 1000°C s^{-1}, this temperature interval represents some 250 ms, although some of the retrogressive reactions may have spilled over into the 1-s holding time at peak temperature after the heatup ramp.

In this example, the difference in outcomes between the pyrolysis and liquefaction experiments was useful in showing the extent of secondary char formation during pyrolysis, within the short, rapid-heating interval between 450°C and 700°C. Reexamining Fig. 6.3B, however, we are reminded that samples heated at 500°C s^{-1} to 400°C gave low extractable yields (~35%), while heating at 1000°C s^{-1} produced extractable yields of about 65%. In other words, at 500°C s^{-1}, the recombination reactions regime operated as at the lower heating rates – even though the heating rate was fairly high. It is likely that working with more samples would elucidate the significance of the 500–1000°C temperature interval as the transition heating rate between the two regimes. These reactions provide an example of *fast retrogressive reactions* during pyrolysis.

Slow retrogressive reactions during pyrolysis: The speed of these retrogressive reactions contrasts sharply with data from Fig. 6.2, where all ('dry') heating above 400°C took place at 1°C s^{-1}. The data show that the proportion of tar precursors that had survived heatup and reached 400°C slowly increased up to 450°C. The tar precursor ('extractable') content then declined by 30% when the sample was heated at

1°C s^{-1} to 500°C, an interval corresponding to 50 s. These latter data show that the sample underwent relatively slow char-forming reactions when the temperature was raised 'slowly' above 450°C.

These two examples underline the role of the temperature and of the heating rate in determining the reactivity of the pyrolyzing coal mass. However, the role of the temperature and of the heating rate tend to mask any differences between the *intrinsic reactivities* of particular types of free radicals. A direct comparison of free-radical reactivities would require matching experiments with similar time-temperature ramps, or comparing the progress of retrogressive reactions under isothermal conditions.

6.4.2 Fast and slow retrogressive reactions in liquefaction

Table 5.3 shows that at 350°C, greater amounts of coal had been extracted by the non-donor solvents, compared to extraction in tetralin. This was explained in terms of the process at up to 350°C mainly representing simple extraction, where quinoline and phenanthrene, stronger solvents for coal-derived materials, could dissolve more of the sample compared to tetralin. Table 5.3 also showed that when the peak experimental temperature was raised from 350°C to 450°C, systematically higher conversions were recorded in the presence of tetralin, compared to conversions in the non-donor strong solvents.

In a separate set of flowing-solvent reactor experiments, about 10–12% higher conversions were obtained in tetralin compared to liquefaction in the strong (but) non-hydrogen-donor solvent 1-methylnaphthalene at 400°C and 450°C (Figure 5.5A) (Gibbins et al., 1991). We will next examine the reasons why the trend in Table 5.3 was reversed between 350°C and 450°C and why the donor-solvent tetralin gave systematically higher conversions at the higher temperature compared to the three strong (but) non-donor solvents.

Rapid Retrogressive Reactions in Liquefaction: Much of the present discussion is based on the premise that covalent bond cleavage reaction rates during thermal breakdown depend primarily on the temperature. In this instance, the experiments consisted of heating similar coal samples to similar temperatures. We expect therefore broadly similar rates of covalent bond cleavage and the release by the solid matrix of similar amounts of extractables into sample coal particles, irrespective of whether the liquid medium is a hydrogen-donor or a non-hydrogen-donor solvent.

In the flowing-solvent reactor the solvent stream sweeps away all extractable materials that have dissolved in the liquid medium and diffused out of the coal particles. When operating to 450°C, we found higher conversions in the presence of tetralin, the hydrogen-donor solvent with less solvent power, despite bond-cleavage reactions releasing broadly similar amounts of extractables. We are led to think that any extractables not carried away by the stronger (non-H-donor) solvents must be no longer soluble. In other words, data in Table 5.3 suggest that short-range (and probably rapid) retrogressive reactions occurred (compared to heating in tetralin) during heatup in the non-donor solvents, between 350°C and 450°C, before the extractables were able to diffuse out of the coal particles.

The higher conversions in tetralin at 450°C are therefore consistent with the hydrogen-donor ability of tetralin being better able to block what appear to be rapid

retrogressive reactions during heatup compared to the non-donor solvents that are unable to provide this function. The analogy between the role of tetralin in these experiments and the internal liquefaction process posited for coal pyrolysis is clear.

It must be noted that the design of liquefaction reactors plays a key role in determining the course of the liquefaction process. In the flowing-solvent reactor, high conversions may still be maintained in the presence of non-H–donor solvents, as products are diluted and rapidly removed from the reaction zone, within about 10 seconds. The contrast with 'batch' reactors, where extracts are exposed to 'scrambled' reaction pathways, must raise questions about the persistent widespread utilisation of non-flow reactors, not least in biomass hydroliquefaction studies.

Slow retrogressive reactions during liquefaction: During experiments in the batch ('mini-bomb') reactor, operating with a tetralin to coal ratio of about 4:1, only minor differences were found compared to conversions observed in the flowing-solvent reactor (Gibbins et al., 1991; also see chapter: Liquefaction: thermal breakdown in the liquid phase). Conversions in the non-donor 1-methylnaphthalene were also compared in the two reactors (see Fig. 5.5B). In the flowing-solvent reactor, conversions increased monotonically with contact time at both 400°C and 450°C. At 400°C, conversions in the mini-bomb also increased monotonically with time, but were nearly 30% lower than conversions in the flowing-solvent reactor. This conversion loss in the mini-bomb reactor at 400°C appears due to relatively rapid recombination reactions in the batch reactor, where the configuration does not allow product removal from the reaction zone before the termination of the experiment.

At 450°C, however, data in Fig. 5.5B showed clear evidence of retrogressive char-forming reactions in the mini-bomb reactor, at contact times longer than 100 seconds. The net conversion diminished (and residual solids increased) by some 12–13% over the time interval between 100 and 1600 s. This aspect of the data was consistent with trends observed during earlier work (e.g., see Clarke et al., 1980). The relevance of these results in the present context is the demonstration of the slow speed of char-forming reactions, when the reaction mixture was held at the constant temperature of 450°C.

Even Slower Retrogressive Reactions-Sample Ageing: On the face of it, coal extracts that have been catalytically hydrocracked in tetralin under high-pressure hydrogen should be quite stable during storage. In order to test this proposition, a sample of Point of Ayr (UK) coal extract was hydrocracked for 10 min in distilled tetralin at 440°C under 190 bar H_2 pressure, in the presence of a pre-sulphided NiMo/Al_2O_3 catalyst.

As soon as the liquid product was filtered from the solid material in the reactor, a sample was drawn for characterization by size exclusion chromatography (SEC) and UV-fluorescence spectroscopy. The rest of the sample was separated into two parts. One part was kept under nitrogen in a freezer at −22°C. The second part of the sample was kept exposed to air at room temperature. Samples were examined by SEC and UV-fluorescence spectroscopy every 2 h during the first day, once a day during the first week, once a week during the first month, and then once a month for the rest of the year. Sample ageing was assessed in terms of shifts to shorter elution times (broader molecular mass distributions) in SEC and indications of 'red shift' in

the UV-fluorescence spectra. Both stored products showed significant structural evidence of ageing over the first week of storage. Subsequent changes observed in the samples were within the range of variability of the polystyrene standards, routinely used for checking internal consistency in SEC. Ageing was attributed to the presence of low-reactivity free-radical species undergoing fairly slow recombination reactions during storage – during the first week after the hydrocracking of the samples (Begon et al., 2000).

Ageing in Biomass Tars/Oils: Similar ageing tests were carried out on tars/oils from the pyrolysis of samples of beech wood and rice husks. Tar/oil samples were stored under several different sets of conditions: (1) at 5°C with nitrogen-filled headspace; (2) laboratory ambient temperature with a nitrogen-filled headspace; (3) laboratory ambient temperature with air-filled headspace; and (4) 40°C with nitrogen-filled headspace. Structural changes in the samples were followed by SEC and UV-fluorescence spectrometry (Somrang, 2011). Shifts of SEC chromatograms to shorter elution times, corresponding to broadening molecular mass distributions, was observed during the first four days after the pyrolysis experiments. The changes were observed to level off after that period and no experimentally significant structural changes were observed during the following three months during which the samples were periodically examined. The changes in the SEC chromatograms of the rice husk bio-oils showed only slight differences from those of beech wood tars/oils. These results were in qualitative agreement with earlier work based on viscosity measurements (Czernik et al., 1994). Higher storage temperatures tended to accelerate the ageing process, although ageing could also be observed in bio-oils stored at relatively low temperatures. Oxygen in air did not seem to affect the ageing processes of these samples. A related account of sample ageing reactions in tars/oils from coal-biomass coprocessing has been given by George et al. (2013).

6.5 Summary: What we know about thermal breakdown in coals

6.5.1 Initial stages of thermal breakdown

Data from ESR proved useful in observing the onset of covalent bond-cleavage reactions. For a lignite, these processes were initiated near 310°C, rising to 340°C with increasing coal rank. Above the 350−375°C temperature band, the depolymerisation of coals tends to accelerate. Above these temperatures, enhanced weight loss during liquefaction was matched by sharply increasing spin populations in ESR spectroscopy. It was also matched by the accumulation of larger amounts of extractables (‘tar precursors’) during ‘dry’ heating of coal particles to temperatures below 450°C.

The temperature interval between the ‘onset’ of covalent bond cleavage and enhanced depolymerisation above 350−375°C was consistent with the need for several bonds to rupture before larger molecular mass fragments could detach from the solid matrix to be released within the coal particles. In this work, this material has been labelled as ‘extractables’ or ‘tar precursors’. The terms ‘plastic phase’,

and ‘metaplast’ commonly refer to broadly the same solvent-soluble mass, although nuances of meaning are found in diverse approaches to analysing coal thermal breakdown.

The pathways of pyrolysis and liquefaction diverge during the accumulation of extractables (tar precursors) within coal particles. In liquefaction, the solvent (vehicle) serves to remove the extractables from reacting coal particles; at 400°C, examples of weight loss ranging from 32% to nearly 80% have been observed (Table 5.2). During the early stages of pyrolysis in an inert gas medium, however, there is no mechanism for ‘tar-precursor’ removal; the accumulated extractables remain mostly trapped inside coal particles. At 400°C, weight loss by evaporation in ‘dry’ pyrolysis rarely exceeds several percent of the initial coal mass. The extractables (‘tar-precursors’) content of particles that were ‘dry’ heated to 400°C was found to be as high as 65−80%, depending on the coal.

During pyrolysis, the proportions of extractable materials present in coal particles tend to affect the plasticity of the pyrolyzing mass. Greater pre-pyrolysis extractable (tar-precursor) contents and the resulting greater plasticity of coal particles closely correlated with larger tar yields, observed when fast pyrolysis experiments were driven to 700–800°C. Observations on middle-rank coals indicated that high heating rates (>500°C s^{-1}) enhanced all three effects, namely, the proportion of solvent extractables (tar-precursors) formed within coal particles, the plasticity of the coal mass, and, as the temperature was raised, the eventual tar yields.

6.5.2 Effect of rapid heating

We have surveyed clear and consistent experimental evidence showing that far larger proportions of the initial mass of weakly coking coals end up as extractable material during ‘dry’ pyrolysis, if the sample is heated rapidly to 400°C, compared with slow heating to the same temperature. As covalent bond cleavage is primarily a function of the temperature, broadly similar temperature extents of bond cleavage are expected to occur during fast and slow heating. We expect therefore that similar amounts of potential extractables are initially released inside coal particles, irrespective of the heating rate. It appears, therefore, that the observed differences in extractable yields (found inside the particles) between fast and slow heating may be explained in terms of many more char-forming recombination reactions taking place during slow heating to 400°C.

On their own, however, these observations do not explain why fewer retrogressive reactions take place during rapid heating. Fast heating tends to telescope the sequence of pyrolytic events into a narrower time frame and shifts the temperature scale of pyrolytic events to higher temperatures. For the few coals tested, this upward temperature shift was observed to be between 90°C and 140°C. It is thought that the internal release of hydrogen may temporally overlap more extensively with processes of covalent bond-cleavage during rapid heating. The pyrolyzing mass may thus be able to assimilate internally released hydrogen more effectively and quench (cap) more of the reactive free radicals during fast heating. This action would effectively block more of the potentially rapid recombination reactions.

We have already mentioned two likely sources for internally released hydrogen. First, the low-level release of molecular hydrogen from pyrolyzing coals can be measured relatively easily from about 285°C to 300°C, during slow-heating experiments. During fast heating, the hydrogen release would overlap with coal depolymerisation, and the hydrogen would be more likely to remain in contact with the pyrolyzing mass at higher temperatures. Second, according to the sequence of events described by Neavel (1981), internally released 'donatable' hydrogen plays a role that is analogous to donor-solvents during liquefaction, blocking potentially char-forming free-radical recombination reactions. Donatable hydrogen in coals and coal-derived materials is thought to reside in the hydroaromatic component of the plastic phase. Such hydrogen transfer would block some free-radical recombination reactions more effectively, when thermally activated hydrogen-donor activity and covalent bond-cleavage overlap more extensively. This is more likely to occur during rapid heating. More efficient hydrogen release to the pyrolyzing coal mass during rapid heating would explain (1) the larger 'extractable content,' (2) the enhanced plasticity of weakly coking coals, and (3) the relative chemical stability of 'tar precursors' at temperatures up to 450°C. It would also explain the higher tar and total volatiles yields from pyrolysis, as temperatures were raised to 700–800°C. Experimental results showing good correlation between hydroaromatic content in untreated (unheated) coals and increasing tar and total volatile yields during pyrolysis have been presented.

6.5.3 Fast and slow free-radical recombination reactions in thermal breakdown

As thermally induced bond-cleavage reactions and the depolymerisation of coals accelerate above 350–375°C, the more reactive of the free radicals have greater potential to undergo either retrogressive or quenching (capping) reactions. The evidence presented suggests that the outcomes of these processes during pyrolysis are determined by the relative abundance (or not) of locally available, internally released hydrogen.

In Fig. 6.2, fast heating was shown to give rise to a larger pool of extractable ('tar-precursor') material, observable at the end of the heatup ramp. Assuming bond-cleavage to be a function of temperature alone, the reactions that served to quench and stabilize over 30% of the coal mass (which remained as extractables) must have been relatively rapid. These reactions would have taken place during the temperature rise at 1000°C s^{-1} to 400°C. The interval consists of about 375 ms. This observation is in glaring contrast to the demonstrated chemical stability of extractables still found to be present at temperatures between 400°C and 450°C, in the same coal particles. Fig. 6.4 clearly shows the extractables remaining intact for over 120 s at 400°C. The stability of these extractables appear to demonstrate the effectiveness of the free-radical capping that must have taken place during fast heatup to 400°C.

Fast recombination reactions in pyrolysis: For any given coal, experiments show that far larger proportions of the sample mass may be dissolved in a donor-solvent during liquefaction at 450°C, than may be converted into volatiles during fast heating to 700°C. About 40% of the coal mass reverts to char, between 450°C and 700°C,

by which stage no further volatiles and very little extractables may be produced from the recovered residue. At a heating rate of 1000°C, the retrogressive reactions would have produced the 40% char within 250 ms – plus possibly some overspill into the 1-s holding time at 700°C, before cooldown was initiated.

Another way of observing fast recombination reactions would be to heat the coal to 400°C at 500°C s^{-1}. At this relatively high heating rate, Fig. 6.3B showed nearly 30% less extract accumulation compared to heating at 1000°C.

Slow Recombination Reactions in Pyrolysis: During pyrolysis, some of the extractable mass survived the heat-up stage to 400°C. For weakly coking Coal A, this was found to be about 35% after slow heating and about 65% after fast heating. At 400°C, the extractables content identified within the coal particles remained remarkably stable for 120 s and possibly longer. Slow recombination reactions making fresh char were observed to proceed only slowly above 450°C. Fig. 6.2 shows that about 30% of the coal mass reverted to char over a time span of 50 s, between 450°C and 500°C.

Rapid Recombination Reactions in Liquefaction: Coal liquefaction experiments in the flowing-solvent reactor showed that about 10% more extract could be produced in tetralin compared to the strong non-hydrogen-donor solvent 1-methylnaphthalene (Table 5.3). In other words, despite the presence of excess strong solvent, 1-methylnaphthalene could not prevent some 10% more of the coal mass undergoing retrogressive reactions (Fig. 5.5A). The difference in conversion between donor and non-donor solvents is thought to arise from the outcome of short-range interactions, as extractables detach from the coal matrix within the coal particles. In the absence of sufficient locally available hydrogen, such short-range interactions would preferentially produce char-producing recombination reactions. These repolymerisation reactions appear to be taking place prior to 'extractables' exiting from the particle into the flowing solvent stream, suggesting that retrogressive char-forming reactions must be relatively rapid.

Slow Recombination Reactions in Liquefaction: At 450°C, Fig. 5.5B showed how extracts already dissolved in 1-methylnaphthalene repolymerised to form solids at the rate of 12−13% over a time span of 1500 s. These reactions appear distinct from and slower than the rapid recombination reactions taking place during heat up in the flowing-solvent reactor. It appears we are able to differentiate between some very fast and very slow retrogressive reactions taking place during coal liquefaction.

It is not surprising that free radicals generated by a multiplicity of covalent bond-cleavage reactions of complex structures should display a range of reactivities. However, in many of the examples from pyrolysis cited above, the differences in intrinsic free-radical reactivity were largely masked by the effect of the temperature and the heating rate.

6.5.4 A unified outlook for coal and biomass

It would be useful to work with a wider array of coal and biomass samples, to confirm and expand observations presented in this and in previous chapters. Nonetheless, the picture emerging from the work outlined thus far appears to be a coherent one.

ESR spectroscopy showed that the (pre-pyrolysis) onset of covalent bond cleavage reactions and the extensive release of 'extractables,' or 'tar precursors,' by the coal matrix are sequential phenomena. The temperature gap between the onset of bond cleavage and massive depolymerisation suggests that a number of bonds must break before relatively large molecular mass free-radicals are released from the solid matrix. The analogous effect might yet be observed in the thermal breakdown of lignocellulosic biomass.

The effect of heating rate in coal pyrolysis: The sensitivity of pyrolysis tar yields of some coals to changes in the heating rate had previously been explained by greater tar survival through the rapid, 'explosive' ejection of 'tar precursors'. The observation (Fig. 6.2) that fast heating gave rise to a larger pool of nearly 30% more extractables ('tar precursors') tended to complement this proposition, while raising questions regarding how the larger pool of extractables was formed in the first place.

In trying to answer this question, it was observed that fast heating tends to telescope the sequence of pyrolytic events into a narrower time frame and shifts the temperature scale of pyrolytic events upwards. It was proposed that sample-derived hydrogen may be incorporated into the pyrolyzing mass more effectively during fast heating. The greater availability of hydrogen would help quench and stabilise the more reactive 'tar-precursor' free radicals.

It was also found that only coals that are marginally deficient in donatable hydrogen and contain more sulphur and oxygen appear to show sensitivity to heating rates. Neither the plastic behaviour of, nor the pyrolysis product distributions of premium coking coals (and of similarly hydrogen-rich liptinite fractions), showed sensitivity to changes in heating rate.

We do not have 'proof' for a model describing the mechanisms by which hydrogen is transferred within the pyrolyzing mass to reactive free-radicals. However, the data are consistent with a chain of events that culminates in the capping (quenching) some of the reactive free radicals, and is consistent with changes in product distributions, as well as the plastic behaviour of the samples during pyrolysis.

The identification of similarities between the early stages of pyrolysis and liquefaction has also helped pin-point when and how the courses of the two classes of processes diverge. We have observed, however, that eventual product distribution in both the pyrolysis and liquefaction of coals are determined primarily through competition between covalent bond cleavage, free-radical capping ('quenching'), and retrogressive char-forming reactions.

A far wider pool of information and insight seems available for discussing aspects of thermal breakdown in coals, compared with *biomass* pyrolysis and liquefaction. It is nevertheless possible to identify analogous trends in biomass pyrolysis, from admittedly sparse yet internally consistent sets of data.

Thermal breakdown in lignocellulosic biomass: The obvious starting point is the widely known sensitivities of lignocellulosic biomass to heating rates during pyrolysis. It is essential to identify the link between sensitivity to heating rates and the (infrequently) observed tendency of woody biomass to soften and melt during fast heating. The two effects need to be explored together within the framework of analogous processes involving covalent bond cleavage, free-radical capping ('quenching'),

and retrogressive char-forming reactions. The examination of thermal breakdown in lignocellulosic biomass must take account, however, of the fiercely hydrogen-scavenging environment resulting from the far higher oxygen content (~40%) of these materials.

A variety of researchers have identified changes in product distributions or the softening behaviour of biomass materials upon fast heating. An outline of work linking changes in product distributions to increasing heating rates has been provided in Chapter 3, Pyrolysis of solid fuels: experimental design and applications. Mettler et al. (2012) have summarised earlier reports about the softening of woody biomass during ablative pyrolysis (Lede et al., 1987), reports on the melting behaviour of cellulose during rapid pyrolysis (Boutin et al., 1998), and on the observation of 'short-lived (<100 ms) intermediate liquids by using high-speed photography during ablative pyrolysis' (Dauenhauer et al., 2009).

Curiously, none of these sources have referred to similarities with transient plastic or fluid phases observed during the pyrolysis of many coals. It seems reasonable to expect that comparing fluid phases of heated coals with those of pyrolyzing biomass would have provided clues about mechanisms of thermal breakdown in lignocellulosic biomass. Moreover, the relatively widely reported heating rate sensitivity of product distributions from biomass pyrolysis has rarely been considered in relation to the plastic behaviour of rapidly heated samples of biomass. Nor have these two related effects been studied in the context of the analogous knowledge base deriving from coal pyrolysis.

There are other highly oxygenated materials that also display plastic behaviour during pyrolysis at high heating rates. Solomon et al. (1986) reported the transient plastic deformation of North Dakota Zap lignite particles (oxygen content: 26.5%), during pyrolysis in the high heating rate environment of an entrained flow reactor. They noted '... This behaviour is not observed at lower heating rates …' and speculated that '… the high heating rate may have reduced the cross-linking reactions responsible for lack of fluidity.' Fraga-Araujo (1990) presented photomicrographs of solidified fluid-like residues deposited on wire-mesh lattices, taken after pyrolysis experiments with Kraft lignin at 1000°C s^{-1}, in an atmospheric pressure wire-mesh reactor. The residues showed clear evidence of melting of the pyrolyzing Kraft lignin sample, which had an (estimated 'by difference') initial oxygen content of 37–38% (carbon content: 53.5%; hydrogen content: 6.0%).

Within this framework it is quite conceivable that the fluid (plastic) phase identified during biomass pyrolysis is related to a transient local abundance of native hydrogen, as in the case of pyrolyzing coals, discussed earlier in this chapter. Reports of such melts in biomass have suggested the softening phase to be of very short duration (Dauenhauer et al., 2009), which would be consistent with the vastly more effective hydrogen-scavenging, oxygen-rich environment of pyrolyzing biomass compared to coals.

While these short-lived plastic stages observed during biomass pyrolysis clearly require further careful examination, the body of related knowledge developed within the sphere of coal pyrolysis research looms large as a resource that has yet to be fully exploited. This potential resource extends to the greater range of reactors that could be made available for research on the thermal breakdown of biomass. We have

already indicated in Chapter 5, Liquefaction: thermal breakdown in the liquid phase, a possible link between the general lack of understanding of reaction sequences and reaction rates in research on the hydrothermal processing of biomass and the types of reactors used for such work, namely autoclaves and bomb reactors operated in batch mode. Using flow reactors to overcome this knowledge barrier would seem a useful starting point. 'Hot-rod' reactors used in trickle-bed mode as well as variants of the flowing-solvent reactor (see chapter: Liquefaction: thermal breakdown in the liquid phase) would appear as suitable types of equipment to explore.

Thus far, relatively little has been said about the molecular structures and mass distributions of tars and extracts encountered in the course of the thermal breakdown of solid fuels. The next two chapters will attempt to address some of the issues involved in unravelling the structures and estimating the molecular mass distributions of these complex samples.

References

Álvarez, P., Díez, N., Blanco, C., Santamaría, R., Menéndez, R., Granda, M., 2013. Fuel 105, 471.
Aramaki, T., Arima, T., Yamashita, Y., Inaba, A., 1996. Tetsu to Hagane 82 (5), 34.
Austen, D.E.G., Ingram, D.J.E., Tapley, J.G., 1958. Trans. Faraday Soc. 54, 400.
Begon, V., Suelves, I., Herod, A.A., Dugwell, D.R., Kandiyoti, R., 2000. Fuel 79, 1423.
Boutin, O., Ferrer, M., Lede, J., 1998. J. Anal. Appl. Pyrolysis 47, 13.
Brown, H.R., Waters, P.L., 1966a. Fuel 45, 17.
Brown, H.R., Waters, P.L., 1966b. Fuel 45, 41.
Clarke, J.W., Kimber, G.M., Rantell, T.D., Shipley, D.E., 1980. ACS Symp. Ser. 111 (139)
Czernik, S., Johnson, D.K., Black, S., 1994. Biomass Bioenergy 7, 187.
Dauenhauer, P.J., Colby, J.L., Balonek, C.M., Suszynski, W.J., Schmidt, L.D., 2009. Green Chem. 11, 1555.
Dryden, I.G.C., Joy, W.K., 1961. Fuel 40, 473.
Dryden, I.G.C., Pankhurst, K.S., 1955. Fuel 34, 363.
Elliott, M.A. (Ed.), 1981. Chemistry of Coal Utilization, Second Supplementary Volume. John Wiley & Sons, NY.
Fong, W.S., Khalil, Y.F., Peters, W.A., Howard, J.B., 1986a. Fuel 65, 195.
Fong, W.S., Peters, W.A., Howard, J.B., 1986b. Fuel 65, 251.
Fowler, T.G., Bartle, K.D., Kandiyoti, R., 1987a. Fuel 66, 1407.
Fowler, T.G., Bartle, K.D., Kandiyoti, R., 1987b. Carbon 25, 709.
Fowler, T.G., Bartle, K.D., Kandiyoti, R., 1988a. Fuel 67, 173.
Fowler, T.G., Kandiyoti, R., Bartle, K.D., 1988b. Fuel 67, 1711.
Fowler, T.G., Bartle, K.D., Kandiyoti, R., 1989a. Energy Fuels 3, 515.
Fowler, T.G., Kandiyoti, R., Bartle, K.D., Snape, C.E., 1989b. Carbon 27, 197.
Fraga-Araujo, A.R., 1990. Ph.D. Thesis. Imperial College, University of London.
Friedel, R.A., Shulz, J.L., Sharkey, A.G., 1968. Fuel 47, 403.
Fukuda, K., 2002. PhD Thesis. University of London
Fukuda, K., Dugwell, D.R., Herod, A.A., Kandiyoti, R., 2004. Energy Fuels 18, 1140.
George, A., Lorente, E., Berrueco, C., Alvarez, P., Millan, M., Ungeheuer, J., et al., 2013. Energy Fuels 27, 3786.

Gibbins, J.R., Kandiyoti, R., 1989. Fuel 68, 895.
Gibbins, J.R., Kimber, G., Gaines, A.F., Kandiyoti, R., 1991. Fuel 70, 380.
Gibbins-Matham, J.R., Kandiyoti, R., 1988. Energy Fuels 2, 505.
Gonenc, Z.S., Fowler, T.G., Kandiyoti, R., Bartle, K.D., 1988. Fuel 67, 848.
Gould, K.A., Wiehe, I.A., 2007. Energy Fuels 21, 1199.
Gray, V.R., 1988. Fuel 67, 1298.
Guo, A., Wang, Z., Zhang, H., Zhang, X., Wang, Z., 2010. Energy Fuels 25, 3093.
Hamilton, L.H., 1980. Fuel 59, 112.
Hamilton, L.H., Ayling, A.B., Shibaoka, M., 1979. Fuel 58, 873.
Howard, H.C., 1963. In: Lowry, H.H. (Ed.), Chemistry of Coal Utilization Supplementary Volume. John Wiley and Sons, New York, p. 342.
Kandiyoti, R., 2011. Thermal breakdown in middle rank coals. Paper A00, Intl. Conf. Coal Sci. & Tech., 9–13 October 2011, Oviedo, Spain.
Kessler, T., Friedel, R.A., Sharkey, A.G., 1970. Fuel 49, 222.
Kumar, R., Jaivir, V., Ray, K., Tirkey, S., 2009. Coking Coals and Coke Making. Steel Authority of India Ltd, New Delhi, ISBN 10: 8130912058, ISBN 13: 9788130912059.
Lede, J., Li, H.Z., Villermaux, J., 1987. J. Anal. Appl. Pyrolysis 10, 291.
Lewis, I.C., Singer, L.S., 1981. In: Walker, P.L. Thrower, P.A. (Eds.), Chemistry and Physics of Carbon, 17. Marcel Dekker, New York and Basel, p. 1.
Li, C.-Z., Bartle, K.D., Kandiyoti, R., 1993a. Fuel 72, 3.
Li, C.-Z., Bartle, K.D., Kandiyoti, R., 1993b. Fuel 72, 1459.
Li, C.-Z., Madrali, E.S., Wu, F., Xu, B., Cai, H.-Y., Güell, A.J., et al., 1994. Fuel 73, 851.
Li, C.-Z., Wu, F., Xu, B., Kandiyoti, R., 1995. Fuel 74, 37.
Mettler, M.S., Vlachos, D.G., Dauenhauer, P.J., 2012. Energy Environ. Sci. 5, 7797.
Neavel, R.C., 1981. In: Gorbaty, M.L. Larsen, J.W. Wender, I. (Eds.), Coal Science, vol. I. Academic Press, New York, pp. 1–19.
Neuburg, H.J., Kandiyoti, R., O'Brien, R.J., Fowler, T.G., Bartle, K.D., 1987. Fuel 66, 486.
Ohtsuka, Y., Wu, Z., Tomita, A., Itagaki, S., 1996. Tetsu to Hagane 82 (5), 28.
Orchin, M., Golumbic, C., Anderson, J.E., Storch, H.H., 1951. Bulletin No. 505. U.S. Bureau of Mines: Washington, DC.
Peover, M.E., 1960. J. Chem. Soc., 5020.
Petrakis, L., Grandy, D.W., 1983. Free Radicals in Coals and Synthetic Fuels. Elsevier.
Reggel, L., Wender, I., Raymond, R., 1968. Fuel 47, 373.
Reggel, L., Wender, I., Raymond, R., 1971. Fuel 50, 152.
Reggel, L., Wender, I., Raymond, R., 1973. Fuel 52, 162.
Sasaki, M., Komaki, I., Matsuura, M., Sato, K., Fukuda, K., 1998. Proc. ICSTI Ironmaking Conference, 803.
Singer, L.S., 1963. Proc. 5th Carbon Conf. 1961, Pergamon, NY, 37.
Singer, L.S., Lewis, I.C., 1978. Carbon 16, 417.
Singer, L.S., Lewis, I.C., 1982. Appl. Spectrosc. 36, 52.
Smidt, J., van Krevelen, D.W., 1959. Fuel 38, 355.
Solomon, P.R., Serio, M.A., Carangelo, R.M., Markham, J.R., 1986. Fuel 65, 182.
Somrang, Y., 2011. PhD Thesis. Imperial College London.
Speight, J.G., 2012. The Chemistry and Technology of Coal, third ed. CRC Press; Taylor & Francis Group, New York.
Sprecher, R.F., Retcofsky, H.L., 1983. Fuel 62, 473.
Suuberg, E.M., 1985. In: Schlosberg, R.H. (Ed.), Chemistry of Coal Conversion. Plenum, NewYork, p. 67.

Wender, I., Heredy, L.A., Neuworth, M.B., Dryden, I.G.C., 1981. In: Elliott, M.A. (Ed.), Chemistry of Coal Utilization Second Supplementary Volume, 1981. John Wiley and Sons, New York, p. 479.

Wiser, W., 1968. Fuel 47, 475.

Xu, B., Kandiyoti, R., 1996. Energy Fuels 10, 1115.

Xu, B., Madrali, E.S., Wu, F., Li, C.-Z., Herod, A.A., Kandiyoti, R., 1994. Energy Fuels 8, 1360.

Zhuo, Y., Herod, A.A., Kandiyoti, R., 2003. In: Ikan, R. (Ed.), Natural and Laboratory-simulated Thermal Geochemical Processes. Kluwer Academic Publishers, Dordrecht, Boston, London, p. 53.

Analytical techniques for low mass materials: method development

7

Chapter Outline

Solid Fuels and Heavy Hydrocarbon Liquids. DOI: http://dx.doi.org/10.1016/B978-0-08-100784-6.00007-2

In this book, we focus on the examination of solid fuel behaviour and liquid fuel properties, emphasising the conceptual integration of sample characterization, reactor design, and evaluation of product distributions. This chapter presents a systematic overview of methods for analysing smaller molecular mass (MM) materials, while Chapter 8 outlines procedures for characterising high-mass samples not amenable to analysis by GC-MS or probe-MS. We will attempt to show how properties of fuel-derived samples need to be matched to the capabilities and ranges of available analytical techniques. In this chapter, we describe the use of chromatographic, mass spectrometric and other supporting methods for the *analysis* of materials, broadly below molecular masses of about 500 u.

The introduction of thin layer (planar) chromatography is attributed to the work of Michael Tswett (1872–1919) (see Lederer (1994), for a brief biography). Gas chromatography (GC) dates from the work of Martin and Synge on partition chromatography, for which they received the Nobel Prize in Chemistry in 1952 (see Bartle and Myers (2002) for a brief history). Other forms of chromatography were devised from these developments. Liquid chromatography and supercritical fluid chromatography (SFC) were later developments that took advantage of improved solvent properties, compared with GC that depends only on the volatility of the analytes for its operation.

Thin layer chromatography (TLC), also called 'planar chromatography', involves a layer of particles of relatively uniform size (usually silica, alumina or cellulose) stuck onto a backing plate of glass or metal. A complex mixture applied to the plate, in a suitable solvent as a spot or as a band, is dried and the chromatogram developed by allowing solvent to spread along the plate as a sharp front from one edge toward the opposite edge of the plate. A selection of solvents can be used in any order so long as the previous solvent is dried off before the next one is applied. Components of the sample usually have different affinities for the separating medium. For example, over a silica bed, the sample mixture would separate according to the polarity of the solvents used. The technique is particularly useful with samples containing heavy material. Larger and more polar molecules in the initial sample mixture may be isolated by their lack of mobility, nearer the origin, after smaller molecules are removed by appropriate solvents. Smaller volatile components may be lost during solvent evaporation. Many of the components covered by the current discussion can be isolated according to MM and polarity by using an appropriate solvent sequence. Touchstone (1992) and Hamilton and Hamilton (1987) have provided instructive texts. Morlock (2012) has reviewed the combination of high-performance TLC-mass spectrometry for the analysis of small molecules.

Column chromatography involves more cost than TLC because the volumes of solvent are greater. GC is relatively expensive both in instrumentation and in the cost of (expendable) columns. HPLC is even more expensive to set up because the pumps and detectors as well as the (expendable) columns involve significant capital expenditure. Once these chromatography methods are interfaced with mass spectrometry, however, the costs of installation and maintenance as well as the need to have an operator who understands the mass spectrometric instrumentation become relatively high.

The chemical complexity of coal and other fuel-derived materials requires detailed characterization of their constituents to be carried out by a combination of separation

Table 7.1 Chromatographic methods in coal science

Mobile phase	Method	Spectroscopic method	
Gas	GC	Coupled MS (IR, UV)	Off-line
Supercritical fluid	Supercritical fluid chromatography	MS, IR, UV fluorescence	
Liquid	Thin layer chromatography	MS, UV, UV-fluorescence,	NMR
	HPLC	HPLC, (SEC) MS, IR, UV-fluorescence	

and spectroscopic methods (Bartle, 1989). Given the wide molecular mass range, a variety of chromatographic methods is required to separate coal derivatives with gas, supercritical-fluid, or liquid mobile phases. Many of these have been used in tandem with a spectroscopic identification method, either coupled or off line (Table 7.1).

7.1 Gas chromatography

7.1.1 Capillary-column GC

For the relatively small molecules present in coal products, ranging from permanent gases to hydrocarbons and their derivatives with molecular masses up to approximately 400 u, GC is often the method of choice (Lee et al., 1984; Bartle, 1985; Handley and Adlard, 2001).

The complexity of fuel derivatives demands the greatest possible resolution capability. Fused silica columns are used universally (Bartle and Myers, 2002) for these samples, and if the surface activity is controlled by silanisation treatments, trace compounds can be eluted as sharp peaks. For most analytical work, columns 10–25 m in length are suitable, with internal diameters of 0.2–0.3 mm (although see Section 7.1.3). Column performance may be evaluated from the separation of isomer pairs such as anthracene/phenanthrene and chrysene/benz[*a*]anthracene. In the past decade the routine availability of small diameter, durable, thermostable-fused silica columns coated with a wide range of stationary phases has been increased and consolidated to a large extent driven by the demands of multidimensional GC.

Increased understanding of the retention mechanism and use of MS detection means that (single) capillary column GC can be confidently described as a mature technique, capable of major feats of analysis, such as the analysis of coal-derived products. The non-polar or slightly polar stationary phases-methylsiloxanes (0V-1, 0V-101) or 'small content' phenyl siloxanes (SE-52 and SE-54) have generally been used, especially after free radical cross-linking, to improve thermal stability. Poly-(mesogenmethyl) siloxanes are gum phases which show high column efficiencies and stabilities but retain a high selectivity for polycyclic aromatic hydrocarbon compounds (PAC) isomers of coal origin (Fig. 7.1). They have a wide nematic temperature range

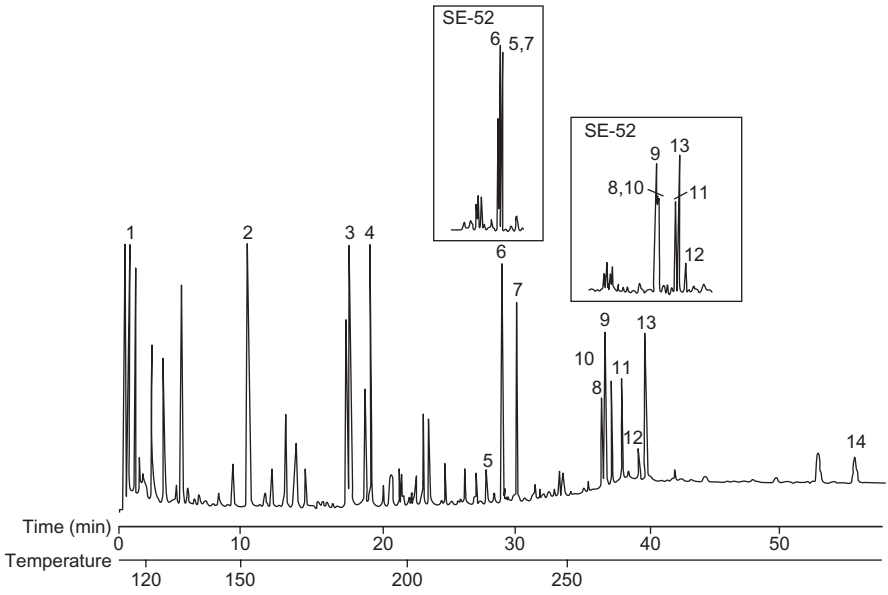

Figure 7.1 GC chromatogram of coal tar on a 20-m-long column coated with a mesogenic stationary phase. Inset are portions of the chromatogram on an SE-52 methylphenyl stationary phase. Peak assignments: 5, triphenylene; 6, benz[*a*]anthracene; 7, chrysene; 8, benzo[*j*]fluoranthene; 9, benzo[*b*]fluoranthene; 10, benzo[*k*]fluoranthene; 11, benzo[*e*] pyrene; 12, perylene; 13, benzo[*a*]pyrene and 14, indeno [1,2,3-*cd*] pyrene.
Source: Reproduced with permission from Lee, M.L., Yang, F.J., Bartle, K.D., 1984. Open Tubular Column Gas Chromatography, Wiley, New York. Copyright © 1984 John Wiley & Sons, Ltd.

(70–300°C) (King et al., 1982). The shape selectivity of smectic liquid-crystal GC phases has proved useful in the separation of a number of PAC isomer groups present in standard reference materials, e.g., those with molecular mass 228, 252 and 278.

Fig. 7.1 shows components of the tar volatiles identified using a 20-m-long column coated with a mesogenic stationary phase. The analysis showed signal up to benzopyrenes, $C_{20}H_{12}$ of mass 252 u, after which peak intensities fall toward zero. The MM range of this tar is likely to extend much further but the higher mass components were presumably too involatile or decayed to char in the injection system and were not observed. Where tars are produced in the relative absence of secondary reactions, as in a wire-mesh reactor (see Chapter 3: Pyrolysis of solid fuels: experimental design and applications), the tar sample dried at 50°C showed few low-mass components that could be detected using GC methods. The technique would be of little use for the structural analysis of such samples, apart from demonstrating the absence of low mass components.

A similar result was arrived at when liquefaction extracts from a 'flowing-solvent' reactor (see Chapter 5: Liquefaction: thermal breakdown in the liquid phase) was examined by GC-based techniques. This reactor was designed to suppress secondary

reactions of coal extracts released from coal particles. While GC appears of little use for analysing even small fractions of primary tars and extracts released from coals, it is a powerful technique for analysing coal-derived samples which have been thermally or chemically degraded, as well as for biomass, petroleum, and other fossil fuel-derived materials. As described in Section 7.6, GC with mass spectrometric identification is often the final step of combined procedures in which open-column LC and HPLC are used to separate coal liquids, with hundreds of compounds being identified. What must always be remembered, however, is that the proportion of the total sample that shows up in the analysis may be unknown.

Capillary-column flame-ionisation (FID) chromatograms may be used for identifications, after GC-MS calibration, by making use of retention indices – systems of reproducible retention parameters. The use of a retention index, 'I', based on a homologous series of retention standards, is useful in handling variations in chromatographic conditions and column-film thickness. For PAC, the Kovats system, which uses n-alkanes as reference standards, is less reliable than that of Lee et al. (1979), which is based on the internal standards naphthalene, phenanthrene, chrysene and picene:

$$I_Z = 100\,Z + 100(T_{RX} - T_{RZ})/(T_{RZ+1} - T_{RZ}),$$

where T_{RX} is the elution temperature of compound x in the linear temperature programed GC, and Z and Z + 1 are the number of rings in the bracketing standards.

The original system (Lee et al., 1979) has been critically evaluated by Vassilaros et al. (1982) and the effects of variations in programing rate, column internal diameter, and initial temperature have been discussed. Values of 'I' for 310 PAC compounds were listed by Romanowski et al. (1983), with standard deviations (generally less than 0.10 unit) and 95% confidence limits. This system has the advantage that most of the reference standards are generally present in coal-derived oils. Lai and Song (1995) have described similar retention indices for coal- and petroleum-derived mixtures.

The wide volatility range of coal-derived mixtures means that care is necessary to exclude discrimination against higher MM compounds when using split-less injection. Only cold on-column injection completely avoids fractionation during sample vapourisation.

Simple GC-FID still finds a use for analysis of PAHs emitted from coke ovens (Kozielska and Konieczynski, 2015) where particulate matter was collected around a Polish coke oven battery, extracted and concentrated before injection into a non-polar capillary column; concentrations of 13 PAHs from fluorene to benzo[*ghi*]perylene were quantified. Similarly, GC-FID was used to assess catalytic hydrocracked products of Maya vacuum residue (Purón et al., 2013) with boiling points below 450°C.

While the FID is still used in the GC of fuel-derived mixtures, mass spectrometry is now very commonly employed in both total-ion current (universal) and selective ion modes. The high concentrations of nitrogen- and sulphur-containing compounds and increasing interest in their toxicity (Eisentraeger et al., 2008) makes selective detection especially useful in GC analysis of coal liquids using dual trace nitrogen (nitrogen and phosphorus detector-NPD) and sulphur (by flame photometric

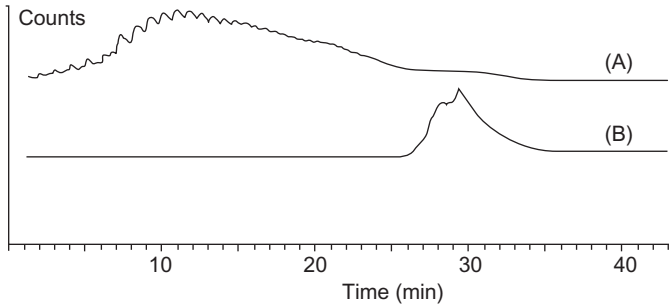

Figure 7.2 (A) Carbon (248 nm) and (b) Vanadium (292 nm) AED chromatograms of an extract of crude oil. Data from Atiku and Bartle (2016, unpublished). Five-metre-thin film column with temperature programme 150°C for 5 min, then 10°C min^{-1} for 20 min.

detector-FPD) for enriched fractions. The increased number of structural isomers created from each aromatic molecule by incorporating a nitrogen atom (as pyrrolic or pyridinic nitrogen) makes the identification of particular isomers difficult without a specific detector or without a selective fractionation to isolate basic or neutral nitrogen compounds. Concentrations of individual components tend to be around 1% of the intensity of unsubstituted aromatics. Limited use has also been made of infrared and UV detection (Lee et al., 1984).

A recent development is the use of positive and negative ion electrospray mass spectrometry at high resolution, for the qualitative detection of N- and O-containing compounds in liquids without chromatographic separation (see Section 8.6.9), but the most versatile selective detector for GC (Quimby and Sullivan, 1990) of fossil fuel–derived materials is the atomic emission detector (AED) in which the carrier gas flow is directed into a microwave-induced plasma and the resultant atomic emission monitored by a photodiode array for up to four elements across the periodic table. Numerous applications in the fuel area have been reported, especially for the selective detection of the usual N and S, but also O (Bartle et al., 2009). Analyses for metals such as V, Ni, Fe, etc. present in, for example, thermostable porphyrins in crude oil (Fig. 7.2) have been reported (Zeng et al., 1992; Al-Rabbiah, 2000).

Graphs of gas-chromatographic peak area against element concentration for carbon, sulphur, oxygen and nitrogen are approximately linear and indicate that the AED is a highly sensitive detector for the heterocyclic compounds present in heavy liquids (Holden, 1999; Bartle et al., 2009). The sequence of AED response carbon > sulphur > oxygen > nitrogen was found to be in the approximate ratios 1:0.33:0.07:0.02 and in principle the very high temperature of the plasma should result in complete atomisation of the analyte molecules so that the AED response should be independent of molecular structure. In fact compound – independent calibration has not proved reliable (Schafer, 1993) for electron-rich aromatic molecules with high dissociation energies because of their incomplete decomposition and/or formation of small molecular species (Janak, 1995). Thus, the AED response per unit mass of oxygen

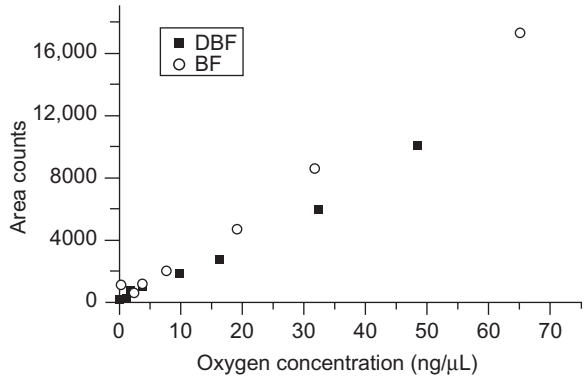

Figure 7.3 Variation of oxygen AED elemental response (777 nm) for benzo[*b*]furan (BF) and dibenzofuran (DBF).
Source: Reprinted from Bartle, K.D., Hall, S.R., Holden, K., Ross, A.B., 2009. Fuel 88, 348–353. Copyright 2009, with permission from Elsevier.

for benzo[*b*]furan and dibenzofuran determined under the same conditions (Fig. 7.3) differed slightly and at relatively high concentrations deviated from linearity. Similar results were observed for the AED response of sulphur and nitrogen isosteres of the above compounds. Calibration of the detector with a compound of similar structural type is necessary during the analysis of heteroatom-containing PAC with the AED; in definitive determinations of polycyclic aromatic sulphur heterocycles (PASH) in fossil fuel standard reference materials, Mossner and Wise (1999) found similar response factors for a wide range of alkylated PASH but used perdeuterated PASH as internal standards. The combination of AED with concurrent MS detection is a particularly powerful detection system (Mol et al., 1999).

7.1.2 High-temperature GC

The increase in thermal stability necessary to extend the working temperature of stationary phases was achieved by in situ free radical cross-linking. Such columns are stable at temperatures above 300°C (Bartle, 1985) and allow the elution of compounds with MM above 450 u in coal tar and combustion products. For example, high temperature GC-MS of a fraction separated from coal tar by liquid chromatography allowed the presence of compounds containing 8–9 aromatic rings and molecular masses up to 456 to be determined (Romanowski et al., 1983). Similar results were obtained in a comparison of 5% diphenyl-substituted polysiloxane and biphenyl-substituted silarylene-siloxane polymers. The latter showed high separation efficiency, but retention times for PAC were longer (Bemgard et al., 1993). Examples of the use of HT-GC-MS for analysing a coal tar pitch, a petroleum residue and a low-temperature coal tar are presented in Figs. 7.7, 7.16 and 7.17, respectively. Distillation data are of obvious importance in the characterization of petroleum feedstocks and coal liquids, and are commonly obtained by simulated distillation (SIMDIST) by GC,

rather than by actual distillation tests (Abbott, 1995). The principle is that hydrocarbons and their heterocyclic isosteres elute from a column with a non-polar stationary phase, during a temperature-programed run, in a sequence of increasing boiling temperatures. Calibration with a set of n-alkanes enables retention times to be converted to a boiling-temperature scale.

Such procedures should be applicable to coal-derived oils of low and intermediate MM. Two standardised American Society for Testing Materials (ASTM) GC methods for SIMDIST of petroleum fractions designated ASTM D2887 and D3710 have been used for this purpose. ASTM method D5307 was established in 1992 for crude- oil boiling ranges. However, these methods are only applicable to materials boiling up to 538°C because they use packed columns which are susceptible to stationary-phase loss at high temperatures. Thermally stable capillary columns have been used for SIMDIST of higher-molecular mass oils (Trestianu et al., 1985). Reddy et al. (1998) have shown that an upper temperature, equivalent to an atmospheric boiling point of 847°C, could be achieved by using a temperature programme to 425°C, eluting alkanes in excess of n-C_{92}. Ultra-fast SIMDIST may be achieved by use of a specially designed low-thermal mass GC instrument (Aybar et al., 2014).

Higher resolutions and better reproducibility were obtained with capillary columns than with packed columns, and hydrocarbons boiling up to 750°C have been successfully eluted using this technique. When using aluminium coated (Lipsky and Duffy 1986) and stainless steel (Takagama et al., 1988) capillaries, the high temperature exposes analytes to the possibility of thermal degradation. Complex molecules such as hydroaromatics may decompose at these high temperatures (Bartle et al., 1992), and evidence from comparison of probe-MS and GC-MS of coal tar pitch fractions indicates that the polycyclic aromatics of mass greater than 278 u are present and detected by probe-MS but not detected by GC-MS in similar abundance. Boeker and Leppert (2015) have described a novel heating and cooling system for improving the separation of labile compounds in GC columns. This concept can greatly reduce the cycle time of high-resolution GC and can be integrated into hyphenated or comprehensive GC systems. It can lead to peak sharpening when a cooling region is configured appropriately.

7.1.3 Fast GC

Recent advances have emphasised ‘Fast GC’, reducing analysis time by the use of small diameter columns and fast temperature programming. Column lengths may also be cut by using selective stationary phases to reduce the number of theoretical plates required for given separations (Cramers et al., 1999). In comparison with analysis on more conventional 250 µm i.d. capillaries, separations are more rapid and efficient on 100 µm i.d. capillaries (Table 7.2) (Boden et al., 2002). Optimisation of injector volumes is necessary, and the column oven must be capable of temperature programming rates up to 20°C min^{-1}. Even faster analysis may be achieved if hydrogen is employed as mobile phase but specific safety measures must be used (Grob, 2015). At the time of writing the increased cost of helium is a further incentive to using hydrogen as carrier.

Table 7.2 Comparison of properties of capillary GC columns in PAC analysis.

Parameter	Fast GC	Column standard GC	Fast GC
Column length, m	10	30	20
Internal diameter, μm	100	250	100
Film thickness, μm	0.1	0.25	0.1
Theoretical plates, m^{-1}	8600	3300	8600
Total theoretical plates	86,000	99,000	172,000
Relative column efficiency	0.93	1	1.32
Relative analysis time[a]	0.38	1	0.55

Source: Reproduced with permission from Boden, A.R., Ladwig, G.E., Reiner, E.J., 2002. Polycyclic Aromatic Compounds 22, 301. Copyright 1 2002 Taylor & Francis.
[a]For benzo[*ghi*]perylene.

7.1.4 Two-dimensional gas chromatography

The single most rapidly expanding area in the chromatographic analysis of lower MW fossil fuel fractions is two-dimensional gas chromatography (2D GC), with numerous technical developments and applications (Mogollon et al., 2014). In conventional capillary GC of complex mixtures such as coal oils, many compounds co-elute at a single given retention time and must therefore be interpreted with care. However, in comprehensive 2D GC such overlapping peaks in the first dimension are subjected to a second separation with a different basis (e.g., polarity or polarizability). The technique is capable of achieving much greater resolution of components from neighbouring compounds (Phillips and Venkatramani, 1993). In practice, fractions from the first column are introduced into a second column by modulated injection; the computer software needed to process the data is included with the instrumentation; but the combination of 2D GC with a time-of-flight mass spectrometer provides a good solution when examining mixtures of unknown compounds. Column 1 is typically a 20 min low-polarity phase column, while Column 2 is typically a more polar phase column of short length (1–2 min) joined by a sleeve. Thermal modulation of the output from column 1 is necessary and involves alternately freezing and heating two points near the end of the column, on say, a 10 sec cycle so that a discreet pulse of material from the column enters the second column every 10 seconds. Because of the different polarities of the two columns, co-eluting mixtures of aliphatic and aromatic molecules behave differently on the second column than on the first with aromatics delayed more than aliphatics. The second column must produce a gas chromatogram every 10 s compared with a total elution time for a chromatogram from the first column of 0.5–1 h. This is achieved by a combination of faster linear flow through the second narrow column combined with a much shorter length. An example is given in Fig. 7.11. The modulated injection procedure described earlier, termed thermal modulation, can also be carried out by valve-based interfaces (Marriott, 2001).

A second advantage accrues in 2D GC: in many regions of a single-column GC chromatogram of coal, biomass, or petroleum oils no one compound is present at sufficient concentration to be detected above the 'baseline'. This is due to the elution of many (literally hundreds) of low-concentration species. This situation is shown below in Figs. 7.17A,B and 7.18. However, in 2D GC the high speed of analysis in the secondary GC column also brings about a considerable improvement in peak amplitude, and hence in sensitivity (Lee et al., 2001). Consecutive fractions of the primary peak are processed through the modulation to produce a series of much sharper peaks, which then pass into the detector. Data manipulation procedures such as the construction of difference ratio and addition chromatograms may be applied (Eiserbeck et al., 2014). Reviews of the method have been given (Shellie et al., 2003; Marriott et al., 2004; Beens et al., 2004; Górecki et al., 2004). Detection in 2D GC is usually by time-of-flight MS, but selective GC detectors may also be employed. Examples of the application of this technique are given in Section 7.6.2.

7.2 Supercritical fluid chromatography (SFC)

7.2.1 SFC of coal derivatives

The application of GC in the analysis of coal derivatives is limited by the low volatility of PAC of relatively modest MM at temperatures at which chromatographic columns can be routinely operated (about 350°C) without significant degradation. Applications of GC are also limited by the possibility of decomposition of the constituents of coal oils held at high temperatures for periods of minutes typical of GC analysis. Chromatography with a supercritical fluid as mobile phase (SFC) should in principle extend the MM range amenable to high resolution analysis (Sharriff et al., 1997).

Above the critical point, substances have density and solvating power approaching that of a liquid but viscosity similar to that of a gas and diffusivity intermediate between those of a gas and of a liquid. Hence, above the critical temperature, fluid properties become very favourable for use as a chromatographic mobile phase. Extraction and solvation effects allow the migration of materials of higher MM than in the more usual GC. The low viscosity means that the pressure drop across the column is greatly reduced for given flow rates. High linear velocities can be achieved and high diffusivity confers very useful mass-transfer properties so that higher efficiencies in shorter analysis times are possible than could be achieved in HPLC. The density of the supercritical fluid and hence the solubility and chromatographic retention of different substances can be easily changed by varying the applied pressure. SFC with pressure programing is done by slowly increasing the mobile phase density and decreasing solute retention; equivalent to temperature programing in GC and gradient elution in HPLC. The much-reduced operating temperatures in SFC compared with GC allow high-resolution chromatography to be applied to mixtures which would normally be separated by HPLC, but only after considerable investment of time to determine the appropriate mobile phase composition.

In general, the separating power of SFC is midway between that of GC and HPLC. The separation achieved by SFC on a 34 m × 50 µm internal diameter capillary column falls little short of that obtained by GC with the same stationary phase on a 20 m × 300 µm i.d. capillary for a coal tar mixture. Standard HPLC columns are suitable for SFC, and many applications in the separation of polycyclic aromatic compounds have been reported (Sharriff et al., 1997). Efficient and rapid analysis of coal-derived oils is possible with CO_2 as mobile phase at low temperatures. The SFC chromatogram of an anthracene oil (within 5 min) on a conventional HPLC packed *octa*-decylsilane bonded-phase (ODS) column gave a separation of benzopyrenes and benzofluoranthenes similar to that obtained by capillary GC of the same mixture (Bartle et al., 1987). The 16 toxic PACs on the list of the United States Environmental Protection Agency containing 2–6 rings were separated within 6 min by SFC with a CO_2/methanol mobile phase with simultaneous temperature, pressure and composition gradient (Heaton et al., 1994).

The greater permeability of capillary columns allows column lengths to be greatly increased, with subsequent high efficiency. The advent of new column technology has made small-diameter fused-silica columns for SFC widely available. The stationary phase, usually a polysiloxane, must be subjected to free radical cross-linking to prevent extraction by the mobile phase. Capillary columns offer a number of further advantages in SFC: high sensitivity, the maximum use of density programing, and compatibility with a variety of detectors including the universal flame ionisation detector. The use of the last section of the capillary as a detector can help eliminate band spreading. Capillary columns also permit low flow rates of flammable, dangerous mobile phases, such as n-pentane (critical temperature 196.6°C) to be used which is able to elute larger coal-derived molecules than can be eluted using CO_2 alone. UV absorption or the selective fluorescence detector may give chromatograms (Figs. 7.4 and 7.5) in which molecules beyond ovalene (MM 398 u) are eluted with high resolution (Bartle, 1989). On a liquid-crystal stationary phase, isothermal density programing at 90°C gave acceptable resolution of PAC up to indeno [1,2,3-*cd*] pyrene on the basis of molecular shape (e.g., length to breadth ratio), but higher mass PACs gave very broad peaks. On the other hand, slow simultaneous density temperature programing gave better resolution for the compounds eluting beyond coronene (MW 300) with good peak shapes because of increased solute diffusion in the mobile phase (Kithinji et al., 1990). However, the upper mass range of the chromatogram still falls short of the upper mass range of the actual sample.

7.2.2 SIMDIST by SFC

The greater solubilities of PAC in supercritical fluids at much lower temperatures than in gases have led to a number of attempts to replace GC by SFC for simulated distillation (SIMDIST). Sharriff et al. (1997) noted that capillary SFC under mild conditions (column temperatures as low as 100°C) could be used to characterise heavy petroleum oils with true boiling temperatures extending beyond 700°C, thus eliminating possible sample decomposition. The accessible boiling range has been extended to 750°C, but problems of sample capacity and loadability have been cited. The composition of high-boiling temperature mixtures has been determined by SFC using packed

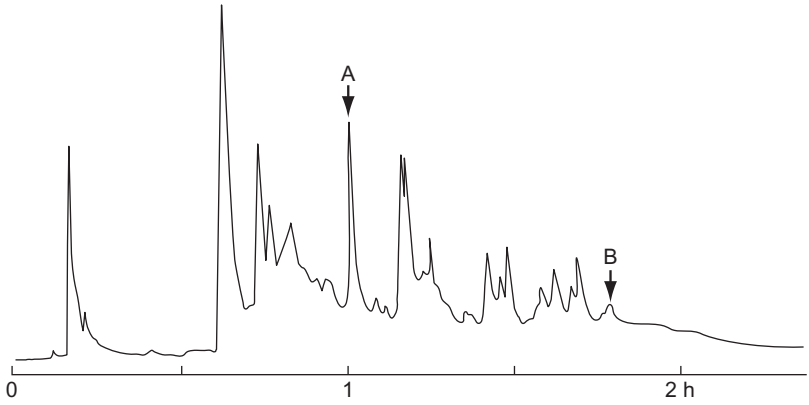

Figure 7.4 SFC chromatogram of coal tar pitch on 10-m long capillary column. Mobile phase pentane at 220°C with fluorescence detection. Peak assignments: A, coronene; B, ovalene.
Source: Reprinted from Bartle, K.D., 1989. Spectroscopic Analysis of Coal Liquids. In: Kershaw J.R., (Ed.), Elsevier Amsterdam, Chapter 2. Copyright 1989, with permission from Elsevier.

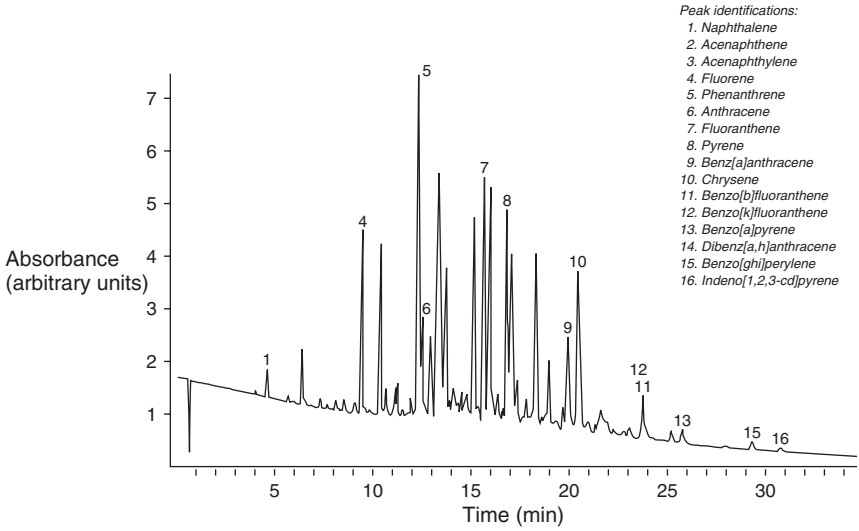

Figure 7.5 SFC chromatogram of a coal tar oil on a 30-m-long packed capillary column in a unified chromatograph. Mobile phase carbon dioxide with programmed methanol content and pressure programming. Detection by UV absorption.
Source: Reprinted with permission from Bartle, K.D., Clifford, A.A., Myers, P., Robson, M.M., Sealey, K., Tong, D., et al., 2000. Unified chromatography. In: Parcher, J.F., Chester, T.L., (Eds.). ACS Symp. Series 748, Amer. Chem. Soc., Washington DC, p. 142, copyright 2000 American Chemical Society.

Table 7.3 Deviations between the true boiling points and the predicted boiling points of PAC

		Deviations (°C)			
Compound	**True boiling point (°C)**	**High temperature GC[a]**	**SFC (open tubular)[a]**	**SFC (packed octylsilyl)**	**SFC (packed hexylsilyl)**
Naphthalene	218	0	+24	+25	+19
Fluorene	293	–11	+20	+18	**+7**
Phenanthrene	338	–19	+4	+12	**+2**
Pyrene	393	–25	0	+5	0
Chrysene	447	–38	–14	+2	–2
Benzo[*e*]pyrene	493	–48	–11	–4	–10

[a]Values from Shariff et al. (1994).

capillary columns (Sharriff et al., 1994). SIMDIST was carried out at 120°C with carbon dioxide as mobile phase with pressure programing from 100 to 350 atmospheres using flame ionisation detection and calibration by n-alkanes (polywax polyethylene) standards. At the limit of the technique, using the hexylsilyl bonded silica, hydrocarbons boiling beyond 800°C (n-C_{130}) can be eluted and detected. Excellent agreement was obtained with SIMDIST by high-temperature GC.

Sharriff et al. (1997) pointed out that there may be discrepancies between true boiling points of PAC and those calculated on the basis of a calibration of an SFC method with n-alkanes. Deviations of boiling temperatures in simulated distillation are tabulated in Table 7.3.

The greatest deviation for SIMDIST is by GC, but the deviation is reduced for SIMDIST by capillary column SFC and is minimised when packed capillary SFC is applied, especially for aromatic compounds containing three or more aromatic rings. This procedure was found to be particularly effective in determining the progress of the corefining of coal and petroleum from the boiling temperature distribution of products (Bartle et al., 1994), but, in general, the main influence of SIMDIST by SFC has been in providing impetus to the use of high-temperature GC in this context.

7.2.3 Aromatic content of fuels by SFC

A more productive area and a niche application for SFC is the rapid determination of the content of aromatics in fuels, with high precision and reproducibility. The standard method (ASTM Method D5186–91) replaces the old fluorescent indicator adsorption (FIA) method, and employs a packed silica column, of length 25 cm, with CO_2 as mobile phase and an FID as detector – clearly not possible in a liquid chromatographic separation. A hydrocarbon group separation on a packed capillary column may be used to determine contents of mono-, di- and PAC in coal-derived fuels. The aromatic content of a variety of fuels (17–88%) was in good agreement with that

determined by the FIA method (Shariff et al., 1998). In a detailed examination of the ASTM method, Berger (1995) concluded that resolution increased with decreased temperature and that the conditions corresponded to sub-critical chromatography.

Similar approaches have been made to the aromatic group-type separation of fuels on columns ranging from semi-prep to capillary scale packed with different particle and pore size silicas (Campbell and Lee, 1986; Li et al., 1995). Smit et al. (2015) applied GC with FT-ICR-MS to diesel fuels to give an analysis similar to a hydrocarbon group type analysis. This technique is discussed further in Chapter 8, Analytical techniques for high mass materials: method development.

7.2.4 Fractionation of fuel-derived mixtures by SFC

The solubility of hydrocarbons and other constituents of complex coal-derived mixtures and high-boiling petroleum residues varies with CO_2 density (Clifford, 1998) so that fractionation is possible by simple supercritical fluid extraction (SFE) (Rudzinski and Aminabhavi, 2000). However, elution with supercritical CO_2 from columns packed with a variety of stationary phases such as (Lundanes and Greibrokk, 1985) cyano (aromatics by ring number), silica and silver on silica (saturated from unsaturated compounds) (Ni et al., 2013) was more selective. Skaar et al. (1990) were able to include asphaltenes and maltenes by including back flushing in a similar separation scheme. Andersson et al. (1993) employed a system of this type but with MS detection in the analysis of diesel fuels, although many applications of this type were carried out with packed capillary columns to minimise flow rates and hence facilitate the use of flame-based detectors. Heavy petroleum distillates such as vacuum gas oil may be separated on a group type basis by SFC with the resulting fractions stored in sample loops and subject to detailed analysis by 2D GC (Dutriez et al., 2013).

In applications to petroleum materials, advanced analytical methods have been applied to fractions separated by SFE and SFC. Zhang et al., (2014) subjected Venezuela Orinoco extra-heavy-crude-oil-derived vacuum residuum to SFE and fractionation (SFEF) to prepare multiple narrow fractions. The SFEF fractions were analysed by Fourier transform (FT) ion cyclotron resonance mass spectrometry (FT-ICR MS) with various ionisation techniques. The results showed that the SFEF separated the vacuum residuum species by their molecular weights and degrees of molecular condensation. The FT-ICR MS data were in agreement with the elemental analysis and molecular weight determined by gel permeation chromatography (GPC) and vapour pressure osmometry (VPO) for the extractable fractions. The molecular compositions of SFEF fractions determined by FT-ICR MS provided important clues for the understanding of the molecular composition of the unextractable end-cut (asphaltenes). A thorough characterization of species in heavy petroleum fractions cannot be achieved by using one ionisation technique but must involve different ionisation techniques.

SFC has recently undergone a resurgence, with developments in instrumentation leading to greater reliability and reproducibility (Berger, 2014). Either hyphenated or as part of the unified chromatographs described below, or in an individual instrument, SFC can be expected to play a greater role in fuels analysis in the future.

7.3 High performance liquid chromatography

Since its inception in the early 1970s, HPLC has been widely used in the separation of PAC. The small particle sizes, necessitating the pumping of the liquid mobile phase through the column, result in much more efficient separations than can be achieved on open columns (Wise, 1983). Unless microcolumns with very small internal diameters are used, the high separation efficiency of capillary GC and SFC is not achieved in HPLC. However, HPLC does offer a variety of stationary phases capable of providing unique selectivity both for functional group types and for difficult-to-separate isomers because of interactions of the solute with both stationary and mobile phases. HPLC thus provides a useful fractionation technique and the means of high-resolution analysis for compounds with molecular masses up to 600 u (Bartle et al., 1981). In principle, the greater solubilities of PACs in liquid solvents should extend the applicable MM range over those achievable in GC and SFC.

Unusual amongst HPLC techniques, size exclusion chromatography (SEC) is an example of HPLC where separation is achieved through penetration of the porosity of the packing. Smaller molecules penetrate the porosity of the column packing and are delayed to a greater extent than larger molecules, which elute earlier. Interaction of sample with column packing surfaces is avoided. As discussed below, SEC has been found useful in resolving aliphatic as well as aromatic species (also see Chapter 8, Analytical techniques for high mass materials: method development).

Columns used for HPLC are normally packed with particles of uniform size, often with a chemically bonded surface modifier, such as amino-groups for normal phase or alkyl groups for reverse phase operation. These surface-bonded groups allow samples to adhere to the surface until a sufficiently polar solvent can displace them, allowing a more effective separation of chemical types. Column technology is driven by the need to carry out specific separations of critical components, which are needed in pollutant detection. Column performance will thus be classified on the basis of the separation of particular isomers or compound types, possibly PAC standards.

The early years of the present century have seen significant improvements in the technology available for HPLC. New small diameter (less than 2 µm, hence requiring very high pressures) or superficially porous ('core-shell') particles both bring about improved separation efficiency and speed of analysis; this approach, is termed 'Ultra High Performance Liquid Chromatography' (UHPLC) (Hudalla and McDonald, 2012).

7.4 Unified chromatography

Many mixtures of interest in coal or petroleum chemistry are made up of constituents with a very wide range of volatilities that are difficult to analyse by a single chromatographic procedure. GC, SFC and HPLC may be applicable to different series of compounds and separations may be carried by any of the above techniques, either alone or in sequence on the same instrument, termed the 'unified chromatograph' (Ishii and Takeuchi, 1989; Tong et al., 1995). The appropriate mobile phase is supplied to either a small-diameter capillary column or a micro-packed column. Detection is

either by FID or UV absorption. Independent optimisation of mobile phase (helium and carbon dioxide respectively) flow rates is made possible in GC and SFC. Hybrid (or 'universal') commercial chromatographs are now available which permit GC, SFC or HPLC to be carried out on the same instrument (Tong et al., 1995), but the wide-boiling mixtures encountered in the energy industries are conveniently analysed by using first helium (GC) and then supercritical CO_2 (SFC). Light oils (GC), heavy oils (SFC) and pitches (SFC and HPLC) may be analysed on the unified chromatograph (Tong et al., 1993). The detection of the contamination of diesel fuel with a heavy lube oil was achieved by GC (He mobile phase) with temperature programming up to 240°C, followed by SFC at 120°C and pressure programming of the CO_2 mobile phase.

Fig. 7.5 shows the chromatogram of a coal tar recorded on this instrument, with GC and HPLC with simultaneous mobile phase composition and pressure programing. Hybrid SFC/ HPLC instruments are usually configured to allow flexible switching between supercritical CO_2 and a liquid mobile phase that may also contain modifiers and additives. However, in the example shown (Fig. 7.5), the largest aromatic detected is of mass 278 u and is still within the range of GC using normal GC-columns and equipment. At the time of writing, the approach seems to be at the stage of 'proof of concept' initial development and not yet ready for routine application to the analysis of coal or petroleum-derived. More probably applicable is 'convergence' chromatography in an UHPLC.

The modern UHPLC chromatograph enables true unified or 'convergence' chromatography (marketed as 'UltraPerformance Convergence Chromatography'), which involves the use of SFC to bridge the gap between GC and HPLC; it employs CO_2 as the initial mobile phase and then simultaneous programming of composition, temperature and pressure (and hence density) of the mobile phase up to 100% liquid – thus making possible any of the different modes of chromatography during the same run. Remarkable selectivity of separation is possible with short run times and the replacement of expensive and environmentally unfriendly organic solvents by CO_2. Mobile phases proposed for convergence chromatography include methanol/water/CO_2 for SEC; n-hexane/CO_2 for normal phase HPLC; and methanol/water/CO_2 for reverse phase HPLC.

7.4.1 Normal phase HPLC

In normal phase HPLC, when silica or amino-group bonded phase columns are used with an alkane as eluent, saturated hydrocarbons exit the column first, followed by aromatics. Polar compounds are eluted by back-flushing. An alternative procedure involved solvent programing to a more polar solvent with elution of some more polar components (Herod et al., 1988) as determined by LC-MS. Class fractionation of coal liquids by functional group has also been investigated for a wide variety of other normal-phase columns (chemically bonded NO_2, CN, diol, sulphonic acid), and NH_2 and NO_2 found to be the most selective for fractions containing hetero-functions (Bartle et al., 1979). Normal phase HPLC is commonly used to separate PAC on the basis of ring number (Fig. 7.6).

The data of Fig. 7.6 shows that the chromatographic intensity fell away markedly as the 5- and 6-ring aromatic components eluted. It seems unlikely that the sample did not contain larger aromatic systems. Clearly, elution using an alkane cannot possibly

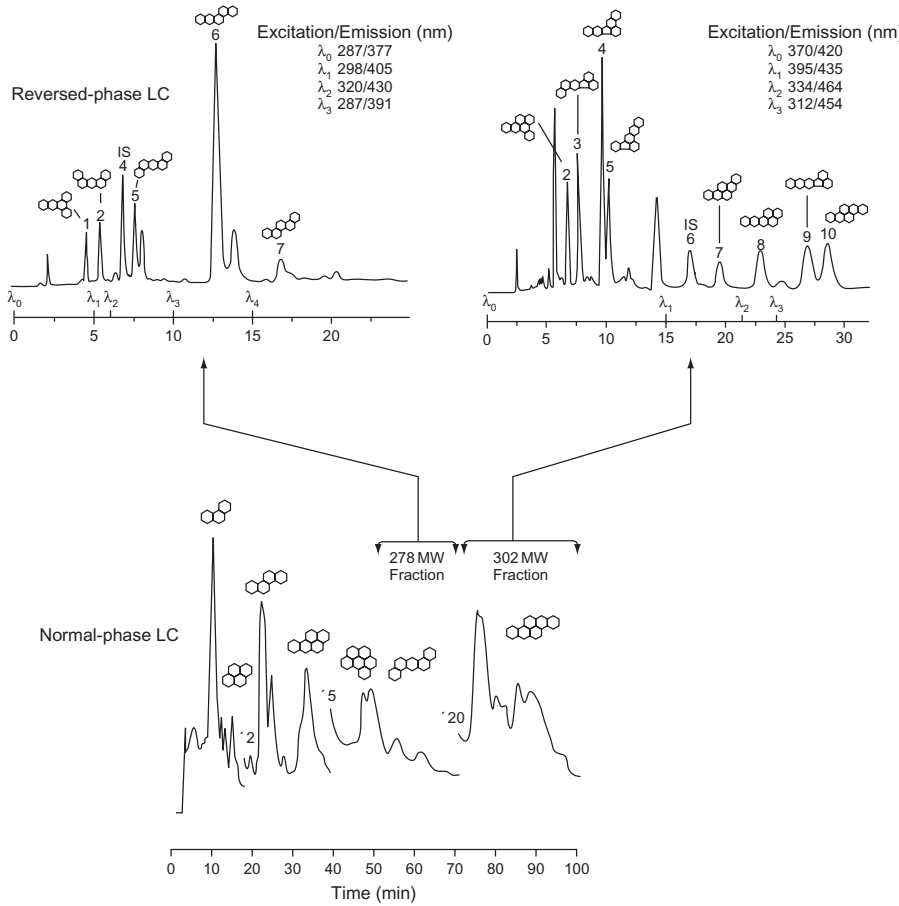

Figure 7.6 Sequential normal phase (lower) and reverse phase (upper) HPLC chromatograms of structurally isomeric 5 and 6 ring aromatic compounds in coal tar.
Source: Reproduced with permission from Wise, S.A., 2002. Polycyclic Aromat. Compd. 22, 197. Copyright © 2002 Taylor & Francis.

elute all the aromatics of a coal tar since many of the higher mass aromatic components are not soluble. Solvent programing to introduce a more polar solvent might improve the situation. Table 7.4 indicates that significant proportions of three coal tars were not soluble in pentane.

7.4.2 Reverse phase HPLC

High resolution HPLC is generally achieved on reverse-phase columns, such as octadecylsilane (C_{18}) with a polar solvent as mobile phase (methanol, acetonitrile, etc., in water), often with its composition changed continuously during the run, termed

Table 7.4 Fraction weights recovered from column chromatography using a sequence of solvents.

	Petrox flash column residue	Pitch	Coal digest	Low temperature tar
Fractions[a]	*%*	*%*	*%*	*%*
Pentane first	50.67	3.77	12.41	10.5
Pentane second	17.96	17.38	29.64	25.71
Toluene	5.72	26.52	10.12	19.55
Acetonitrile	1.74	5.20	3.14	13.72
Pyridine	2.52	15.29	17.50	4.01
NMP	6.16	15.09	8.54	4.25
Water	11.26	2.84	5.08	6.64
SUM	*97.03*	*86.09*	*86.43*	*84.38*

Source: Reprinted with permission from Al-Muhareb, E.M., Karaca, F., Morgan, T.J., Behrouzi, M., Herod, A.A., Bull, I.D., et al., 2006. Energy Fuels 20, 1165–1174. Copyright 2006 American Chemical Society.
[a]Pentane first and second fractions are from successive elutions of the columns with 50 mL each of pentane.

'gradient programing'. Increasing the proportion of organic solvent decreases retention. Methyl and other alkyl derivatives are usually separated from parent compounds (Table 7.4). Numerous separations of PAC and polycyclic aromatic sulphur heterocycle (PASH) fractions from coal have been reported (Wise, 1983), which show the excellent selectivity for the separation of PAC isomers and alkyl derivatives. The great advantage of reverse phase packings is their compatibility with a variety of mobile phases and with gradient elution. Selective separations are achieved on the basis of the length-to-breadth ratio of solutes: the more nearly linear molecules are retained longer (Wise, 1985).

Not all C_{18} stationary phases provide the same selectivity for PAC separations. The selectivity depends on the method of stationary phase preparation, and there are clear differences between separations achieved on 'monomeric' (prepared by reaction of mono-functional silanes) and 'polymeric' (prepared using trifunctional silanes) C_{18} packings. The separation of PAC isomers is vital in studies of coal-derived mixtures. Thus, the selectivity of 'polymeric' phases is especially marked, e.g., in the separation of isomers with MW 302. Other factors influencing the separation include the pore size of the packing and the phase coverage, as well as column temperature during HPLC (Wise, 2002).

A major advantage of HPLC in the analysis of coal liquids is the availability of sensitive and selective detectors. The UV detector is universal for PAC. The sensitivity and selectivity may be increased by monitoring at specific wavelengths for given compounds. For example, benzo[*a*]pyrene exhibits nearly maximum absorbance at 290 nm with very little interference from perylene (Wise, 1983). A scanning UV detector or photodiode array detector allows the possibility of identifying chromatographic peaks either from complete spectra or absorbance ratios at several

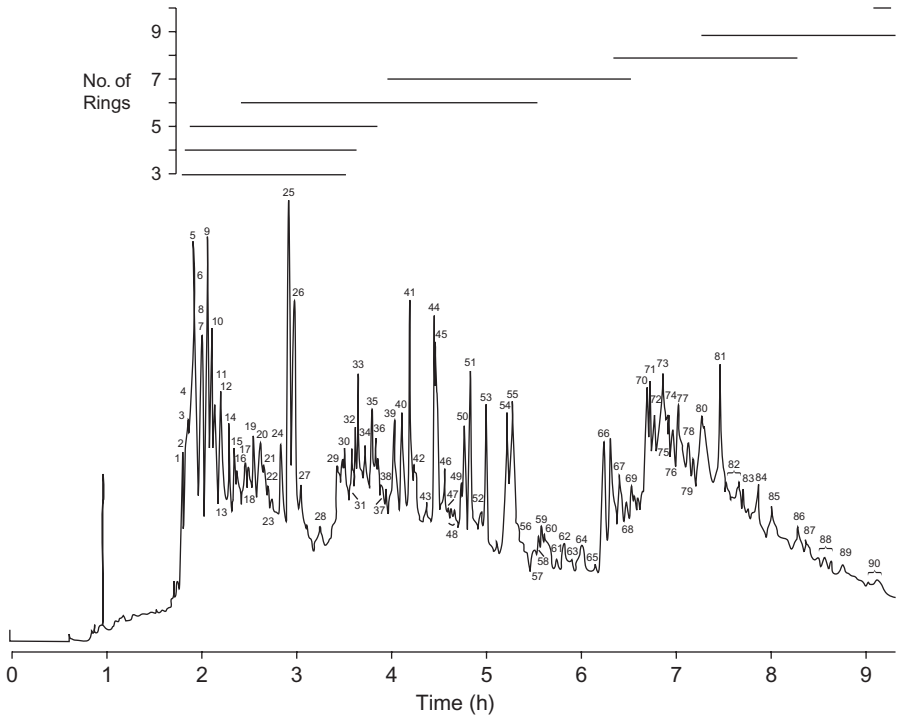

Figure 7.7 Microcolumn HPLC chromatogram of solvent-refined coal fuel oil.
Source: Reprinted with permission from Novotny, M., Hirose, A., Wiesler, D., 1984. Anal. Chem. 56, 1243. Copyright 1984 American Chemical Society.

wavelengths. Compositional changes in coal liquids as a function of process conditions have been demonstrated by this approach (Klatt, 1979).

Fluorescence detection provides unique selectivity in the identification of individual compounds separated by HPLC. For example, six isomeric PACs of MM 252 (perylene, benzopyrene, etc.) are generally found in coal-derived mixtures and are not completely resolved in HPLC with ODS columns, but all may be determined by varying the emission and excitation wavelengths (Bartle et al., 1981). Combination of HPLC with mass spectrometry has provided the most useful results, particularly in the analysis of higher MM constituents of coal liquids. For example, HPLC-MS allowed identification and qualification of PAC with masses up to 450 with an acetonitrile-dichloromethane mobile phase gradient (Caslavsky and Kotlarikova, 2003).

Microcolumn HPLC has been proposed as a method of improving the efficiency of LC separations and has proved capable of resolving many constituents of coal-derived materials containing between five and nine rings. The columns are typically 200 µm i.d. and, when packed with 3 µm C_{18} particles, can generate over 200,000 theoretical plates, although very long analysis times are necessary (Fig. 7.7) (Novotny et al., 1984).

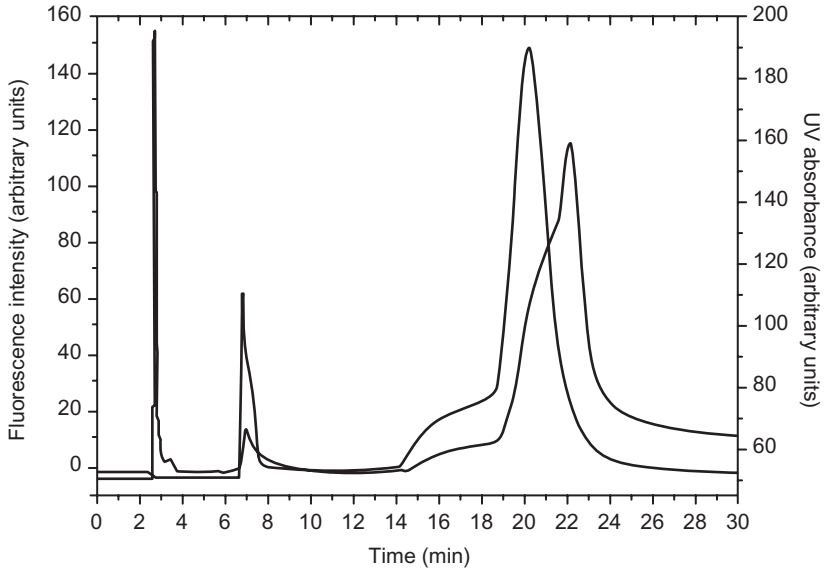

Figure 7.8 Overlay of UV absorbance and fluorescence analytical scale chromatograms of a single 20 µL injection of 0.02 g L^{-1} solution of asphaltenes at 0.5 mL min^{-1}. Fluorescence: excitation wavelength 340 nm; emission wavelength 450 nm. UV absorbance at 340 nm. The first larger peak at 3 min and the two smaller peaks at 7 and 22 min correspond to the UV chromatogram.
Source: Reprinted with permission from Loegel, T.N., Danielson, N.D., Borton, D.J., Hurt, Kentamaa, H.I., 2012. Energy Fuels 26, 2850–2857. Copyright 2012 American Chemical Society.

Attempts at applying HPLC to asphaltenes with weak solvents such as alkanes have been, of course, unsuccessful, but the desorption of these materials from bare silica surfaces by low (2–10%) concentrations of NMP in toluene proved possible (Pernyeszi and Dekany, 2001). Similarly, it was observed by Loegel et al. (2012) that a strong solvent such as NMP might allow reverse phase HPLC of asphaltenes if the surface of the silica particles were uniformly end-capped by silanisation, and a separation (Fig. 7.8) was achieved with fluorescence detection on a cyanopropyl column with a solvent gradient of water/acetonitrile added to a mixture of NMP and tetrahydrofuran (THF).

Sim et al. (2015) also used a cyanopropyl column with THF and acetonitrile to obtain fractions from two deasphalted samples – a conventional crude oil and an oil shale pyrolysate. Molecular-level characterization of the oil fractions was obtained by reversed-phase HPLC coupled with high-resolution mass spectrometry. Analyses of the fractions showed that the carbon number of alkyl chains and the double bond equivalent (DBE) value were the major factors determining elution order.

Arboleda et al. (2015) achieved a hydrocarbon-type analysis in seven chromatographic regions with quantitative recovery on gas oil resins using a hyper-cross-linked-polystyrene

stationary phase with elution by a four solvent gradient (hexane, chloroform, THF and methanol). This system was an improvement over an amino-cyano column in terms of stability over time and in retention of large aromatics.

In Chapter 8, Analytical techniques for high mass materials: method development, we compare fractionation methods used with crude petroleum materials and in the case of Sim et al. (2015), upper mass levels reached m/z 2000, beyond the remit of this chapter, but indicating that reversed phase HPLC has the capability of eluting a wide range of molecular sizes.

7.5 Combined chromatographic methods

The coupling of chromatographic techniques can provide particular advantages in the analysis of mixtures as complex as coal and biomass derivatives. The most powerful of these comprises one or more separations by liquid chromatography into fractions based on chemical type, followed by a high-resolution analysis of the constituents of the fraction by capillary GC, usually with mass spectrometric identification. Alternatively, two sequential liquid chromatographic dimensions may be employed (Saini and Song, 1994). In one example, a coal extract was fractionated by first separating aliphatic and PAC fractions using adsorption chromatography on neutral alumina (Campbell and Lee, 1986). The aliphatic fraction was separated into branched/cyclic alkanes and n-alkanes using a 5 Å molecular sieve. The neutral PAC fraction was further fractionated by normal-phase HPLC into sub-fractions based on aromatic ring number. The numerous constituents of these subfractions were identified by capillary column GC-MS.

A direct reverse-phase HPLC analysis provides precise, reliable quantitative results for only 10–12 major PAC in complex mixtures of fossil fuel origin. This limitation has been partially overcome by using a multidimensional HPLC procedure in which a normal phase separation on an aminopropyl phase was used to produce fractions based on the number of aromatic carbon atoms. These fractions were analysed by reverse phase HPLC with fluorescence detection to quantify the various isomers (Wise, 1985). Off-line HPLC uses relatively large volumes of solvent and requires intermediate reconcentration steps prior to GC analysis. The use of microbore HPLC columns, with internal diameter 1 mm, can reduce the volume of solvent containing the various separated fractions so that these are contained within 100 µL of HPLC eluent (Davies et al., 1987); the fraction solutions may be transferred directly to an analytical GC capillary column.

Online HPLC-GC is a rapid and highly reproducible method for the analysis of complex samples such as coal liquids (Kelly and Bartle, 1994); coupled normal phase HPLC-GC was applied in the analysis of lignite liquefaction products using two approaches. In the first, aminosilane/silica columns were used in series to provide an aliphatic/aromatic separation and a ring size separation of the aromatic fraction. To resolve alkenes from alkanes, a silver-impregnated silica stationary phase located after the silica column was used to retain the alkenes selectively.

7.6 Mass spectrometric methods

General descriptions of mass spectrometric procedures and ionisation methods are available (Chapman, 1993; Hamming and Foster, 1972) as are methods for interpreting mass spectra (Chapman, 1993; Hamming and Foster, 1972; McLafferty and Turecek, 1993; Eight Peak Index, 1992; Watson and Sparkman, 2005). Applications of mass spectrometric methods to petroleum chemistry and coal have been described (Genuit, 2005; Herod, 2005; Herod et al., 2012). In what follows, we propose to limit the discussion to aspects of mass spectrometry relevant to samples derived from the several major classes of fuel already described.

Mass spectrometric methods most suitable for the detection of low mass components of complex mixtures are based on vapourisation of the sample in a gas stream or under vacuum. In these applications, the method of introduction of the sample to the mass spectrometer becomes more important than the type of mass spectrometer (magnetic sector, quadrupole, ion trap, time-of-flight, cyclotron or some combination of different sectors). The mode of operation of the mass spectrometer is one of repetitive scans over a range of masses. The frequency of the scans is adjusted, such that the period of one scan is appreciably smaller than the rate of change of sample concentration at the sample inlet of the mass spectrometer. During input from a gas chromatograph, the mass spectrometer must be capable of several complete scans over the duration of the chromatographic peak of a pure compound, to minimise distortion of the mass spectrum. This may be arduous for fast GC but can be achieved by time-of-flight instruments as used in 2D GC-MS. Under such conditions, the determination of nominal mass (measurement of the mass to charge ratio of each ion to the nearest integer mass) is often adequate.

An alternative method of using the mass spectrometer is to utilise multiple ion detection with accurate mass measurement for the detection of specific compounds of known mass spectrum. In this method, the mass spectrometer steps in sequence over a set of predetermined accurate values of m/z characteristic of the analyte. The concept of accurate mass is based on the ^{12}C relative mass (mass 12.00000) scale of isotopic atomic mass with ^{1}H of mass 1.00782, thus operating with mass measurement to at least a few parts per million of the mass of the ion. The atomic composition of the ion may then be calculated. Whereas a double-focusing mass spectrometer used to be required, in the past, to achieve accurate mass measurement, it is now possible to use FT–mass spectrometers and time-of-flight mass spectrometers equipped with advanced electronic data systems. A high resolution mass spectrometer using a quadrupole-orbitrap system for GC applications has been developed (Peterson et al., 2014) to allow accurate mass measurement of analytes emerging from GC columns and avoid ambiguities that result from nominal mass measurement and library matching of spectra.

When the sample for analysis can be entirely vapourised and held in a reservoir and leaked slowly into the mass spectrometer with an unchanging composition, repetitive scans over a wide mass range using accurate mass measurement becomes possible, giving a wealth of information on the small molecules since their atomic compositions can be determined directly from the accurate masses of their molecular

ions. The method can also be applied to samples partially volatile in the reservoir. The increasing availability of FT-ICR mass spectrometers with sample feed in solution has made this instrumentation, with a range of ionisation methods, into a very important source of information for petroleum distillate fractions as well as partially volatile asphaltenes; further discussion is in Chapter 8, Analytical techniques for high mass materials: method development.

Methods of ionisation commonly used in the mass spectrometry of volatile molecules include electron ionisation, chemical ionisation and field ionisation, atmospheric pressure chemical ionisation, atmospheric pressure photon ionisation and laser ionisation methods. Electron ionisation involves the production of electrons in the mass spectrometer ion source with energies sufficient to induce ion formation in neutral gas-phase molecules of sample, through electron repulsion. Because molecular ion formation and fragmentation of molecular ions are functions of the energy of the ionising electron, it is common to use relatively high energy electrons, of 70 eV, to yield ionisation and fragmentation patterns which are independent of the ion source configuration. An alternative approach is to select an electron energy low enough to avoid ionising aliphatic molecules but to form relatively intense molecular ions from aromatics without extensive fragmentation. Aliphatic molecules have ionisation potentials of around 14 eV while aromatic molecules have ionisation potentials of around 7–8 eV, and by selecting an ionising energy of about 10 eV, it is possible to focus on forming only aromatic molecular ions.

Chemical ionisation methods involve the production of a reagent gas mixture in the ion source using electron ionisation of a relatively high-pressure gas such as methane. Ions form through electron ionisation and ion-molecule reactions to give a set of ions which cannot react further with the reagent gas, but which can react by proton transfer to analyte molecules of lower ionisation potential than the reagent gas itself. Field ionisation is a method of ionisation, which avoids extensive fragmentation. The ionisation is effected by passing volatile sample through an intense electrical field, produced by applying a voltage of several kV to a sharp edge such as a razor blade or a sharp point.

In the following sections, examples of the different sample introduction methods are discussed.

7.6.1 Gas chromatography-mass spectrometry (GC-MS)

This method involves the use of one GC column with the effluent passing into the mass spectrometer through some interface held at an elevated temperature. The components of highest mass eluting from the column should neither condense nor thermally crack in the interface. For many interfaces, the operating pressure at the column outlet is reduced pressure because of proximity to the mass spectrometer vacuum. Under these conditions, the GC column performance may differ somewhat from operation at atmospheric pressure with a flame ionisation detector or with a mass spectrometer with an atmospheric pressure inlet system.

The proportion of sample that can be identified by this technique is not readily quantifiable. Menéndez et al. (2002) have suggested that this could be as high as 20% of a coal tar pitch, with the upper limit normally around m/z 300–350 corresponding

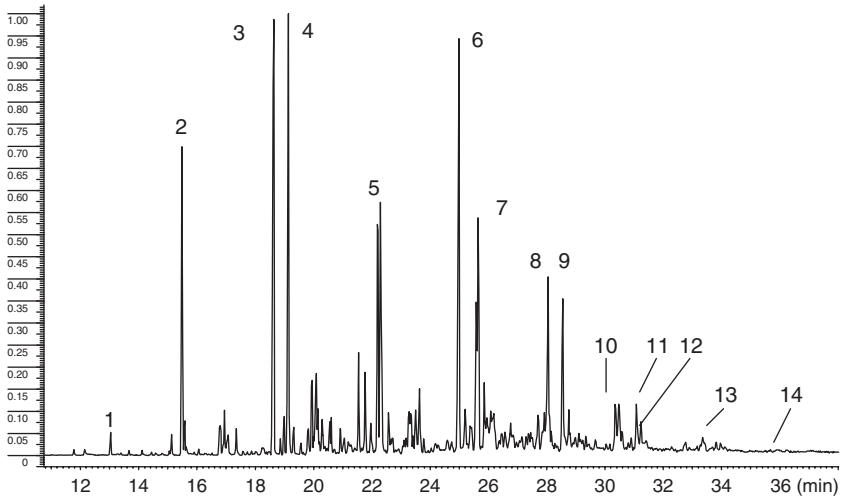

Figure 7.9 HT GC-MS of second pitch pentane soluble fraction. Peaks are: 1, m/z 166 fluorene; 2, m/z 178 phenanthrene; 3, m/z 202 fluoranthene; 4, m/z 202 pyrene; 5, m/z 228 chrysene isomers; 6, m/z 252 benzofluoranthenes; 7, m/z 252 benzopyrenes; 8, m/z 276 and 278 indenopyrene and dibenzanthracene; 9, m/z 276 benzo[*ghi*]perylene; 10, and 11, m/z 302 dibenzopyrene isomers; 12, m/z 300 coronene isomers; 13, m/z 326 rubicene isomers; 14, m/z 352 tribenzopyrene isomers.
Source: Reprinted from Herod, A.A., 2005. Mass spectrometry of coal liquids, p790 in Chapter 8, determination of organic compounds by methods using mass spectrometry. In: Nibbering, N.M.M., (Ed.), Encyclopedia of Mass Spectrometry, vol. 4. Elsevier. Copyright 2005, with permission from Elsevier.

to coronene and benzocoronene. Components described for creosotes and coal tars range from indan and naphthalene to benzo[*ghi*]perylene (creosote) and to coronene (tar) and consist mainly of unsubstituted polycyclic aromatics (PAC) (Howsam and Jones, 1998; Herod, 1998).

Fig. 7.9 shows a chromatogram of the pentane soluble fraction of a coal tar pitch (Herod, 2005); identities of the main peaks are given in the Figure caption. This sample is the second pentane soluble fraction of Table 7.4. The reason for examining this sample by GC-MS was to look for aliphatic components that might have survived the coke oven and subsequent tar distillation processes usual for isolating the pitch; all the components detected were aromatics and no aliphatics were evident.

Fig. 7.10 shows the chromatogram of a Polywax 500 sample (a mixture of even-carbon number polyethenes) extending up to C_{56} on the same column as used for Fig. 7.9. Although known to be present from probe-mass spectra, aromatics above m/z 350 decayed or otherwise failed to pass through the column under conditions able to pass much higher mass alkanes. This inability to pass through normal or HT columns appears to be a problem of the higher aromatics. Extrapolation of the structures known in pitch to components at higher masses by sequential addition of benzo

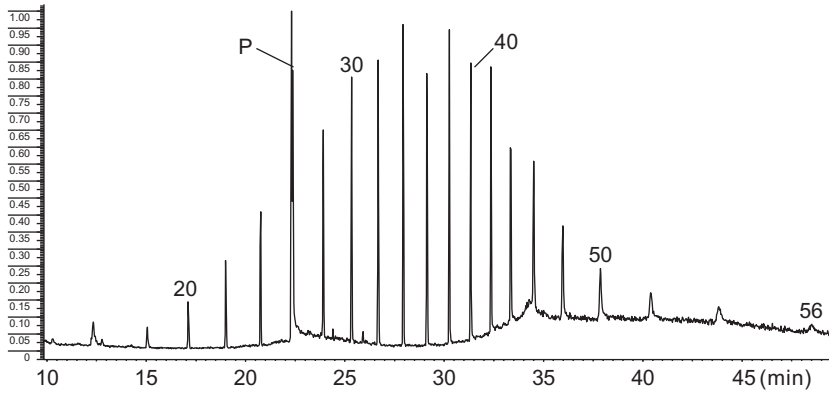

Figure 7.10 High-Temperature GC-MS chromatogram of Polywax 500. The peaks are of even-carbon number alkanes, C_nH_{2n+2}, carbon numbers as shown above peaks (P is a phthalate impurity co-eluting with C_{26} alkane).
Source: Reprinted with permission from Al-Muhareb, E.M., Karaca, F., Morgan, T.J., Behrouzi, M., Herod, A.A., Bull, I.D., et al., 2006. Energy Fuels 20, 1165–1174. Copyright 2006 American Chemical Society.

groups does not produce molecules within the C/H ratios of tars (Parker et al., 1993) and therefore some structural changes must occur at higher masses.

GC-MS has been applied to tars and extracts from wide ranges of coals, kerogens, and macerals, as well as from biomass and waste materials. Some examples are given here. An oil shale from Mongolia (Avid et al., 2004) gave a tar after pyrolysis and gasification at 800°C consisting of PACs, phenols, aza-aromatics, furans, thiophenes, and alkylated aromatics up to benzopyrene isomers. Sewage sludge gave a tar after pyrolysis and gasification in a bench scale reactor (Adegoroye et al., 2004) consisting of PACs and their aza-derivatives with some furans and carbazole, up to mass 228. Pyrolysis tars from animal bones (at 700°C) and milk casein (at 550°C) in a retort contained alkanenitriles, alkanes and amides (bone tar), and alkyl benzenes, phenols, alkanes and alkylnitriles (casein tar) (Purevsuren et al., 2004a,b). Both sets of products were quite unlike coal- or petroleum-derived tars. The pyrolysis of wood and lignin samples gave tars that contained components based on the three oxygenated structural groups typical of biomass, derived from terpenes: syringol, guaiacol and coniferol (Evershed et al., 1985; Robinson et al., 1987; Guell et al., 1993a,b).

P-coumaryl alcohol from grasses extends the spectrum of materials identified toward more aromatic, less oxygenated molecules as the pyrolysis temperature is increased (Bocchini et al., 1996). Sun et al. (2015) have examined a high temperature distillate (>300°C) sample of a low-temperature coal tar by reaction with formaldehyde followed by fractionation into toluene solubles and THF soluble and insoluble fractions. The toluene and THF solubles were examined by GC-MS but only the toluene solubles gave any GC-able materials – mainly aliphatics and alkyl PACs.

Wood waste tars have been examined by Challinor (1995) (and by Evans and Milne (1987a,b) in Section 7.6.4). Wood and cellulose tars from the atmospheric pressure wire-mesh reactor described in Chapter 3, Pyrolysis of solid fuels: experimental design and applications, have been analysed by GC-MS (Fraga et al., 1991). Total ion chromatograms of wood and biomass tars from GC analysis differ for the different feedstocks and the molecular structures of the main components have not always been determined from the mass spectra (Fraga et al., 1991; Pindoria et al., 1997b), in part because libraries of mass spectra did not contain the required spectra. Many of the compounds generated by the wire-mesh and hot-rod reactors are unlikely to be in the mass spectral libraries because the pyrolysis conditions do not match those used for the more usual wood pyrolysis products, such as the Stockholm tars (Evershed et al., 1985; Robinson et al., 1987). One of the issues when using GC-MS to analyse biomass fast pyrolysis oils/tars is the low concentration of individual compounds and their polydispersity. This means that relatively highly concentrated samples are required to obtain reliable quantitative data (~50 mg mL^{-1}) (Mohan et al., 2006). The polydispersity of bio-oils and the use of MS for detection also make quantification difficult. The high variability in GC-MS response factors for bio-oil compounds means it is not possible to obtain a useful estimate of the concentrations of uncalibrated compounds through a comparison to the internal standard (Eom et al., 2013).

Quantification via GC-MS is less reliable (significantly greater uncertainty) than by GC-FID for biomass gasification tars (Chapman, 1993) and samples in general because relative sensitivities are more variable by ionisation methods than in FID response. An example is shown in comparison of Fig. 7.12A,B, with ionisation by 10 eV electron ionisation and chemical ionisation, respectively, where relative intensities are markedly different for the same sample. GC-MS analysis of fast pyrolysis oils from banagrass produced in a fluidised bed (residence time ~1.4 s) showed that less than ~10 wt% of the oil was accounted for in the GC range (Morgan et al., 2015). The amount of material detected by GC-MS is often only a minor portion of the original biomass feedstock (dry basis), less than 10 wt% of the feedstock or at the upper extreme, possibly ~50 wt% of the pyrolysis oil (Mohan et al., 2006; Olcese et al., 2013; Le Brech et al., 2016). Often the results from GC-MS analysis of bio-oils are lists of compounds detected (identified by library matching) along with the percent area of each peak relative to the total ion chromatogram, or to an internal standard. This type of information is not quantitative. The upper mass limit that can be routinely detected by GC-MS for bio-oils is m/z ~220 (Morgan and Kandiyoti, 2014).

The role of GC-MS in the petroleum industry has been described by Genuit (2005). Components of petroleum products identified range from alkanes, through mono- to hexa-cyclo alkanes and aromatics from benzenes to chrysenes, including benzo-, dibenzo- and naphthobenzo-thiophenes to nitrogen substituted aromatics. Extensive alkylation with up to C_{10} groups has been encountered in all cases. The vacuum residues of petroleum crudes are extremely complex and it is generally beyond the capability of GC-MS to resolve most of the components of the mixture. Techniques such as hydrocarbon type analysis were developed to simplify the analysis. GC-MS chromatograms of two Petrox Refinery (near Concepcion, Chile) flash-column residue fractions are shown in Fig. 7.16A,B. An underlying broad peak of unresolved material may be observed in each chromatogram of the pentane soluble material.

GC has been combined with high resolution mass spectrometry (FT-ICRMS) by Barrow et al. (2014) to examine ground waters associated with the Athabasca Tar Sands for environmental reasons. Acids from the tar were methylated before analysis by GC with the effluent passing to an APCI source before sampling to the mass spectrometer. Ortiz et al. (2014) carried out a similar study of Athabasca tar sands extractive waters and ground waters associated with the area by methylating the acids and examining by electron and chemical ionisation methods with a high resolution triple quadrupole FT-ICR MS.

7.6.2 Two-dimensional GC-MS

This method was developed during the past two decades and relies for its operation on access to a fast scanning mass spectrometer such as a time-of-flight instrument. The reproducibility of the method appears to be good (Shellie et al., 2003; Marriott et al., 2004). The gas chromatographic part of the method has been discussed in some detail in Section 7.1.4.

The elution time on the second column is arranged to be the same time as the frequency of injection to this column. The mass spectrometer must be able to collect spectra sufficiently fast to characterise all the components eluting from the second column after a single injection. Using proprietary software, the mass chromatograms corresponding to the separate injections into the second column may be plotted orthogonally to the direction of the chromatogram emerging from the first GC column. This constitutes the second dimension and allows components co-eluting from the first column to be separated by the second column. The mass spectra are linked to the separated spots and can be manipulated in the normal ways to show specific ions or particular fragment ions or molecular ions. In 2D GC-MS, the spectra of individual components are much less prone to overlap from other components. For complex mixtures, individual mass spectra are much cleaner than spectra from 1D GC-MS. Furbo et al. (2014) have provided a 'tutorial' for the analysis of comprehensive 2D GC with examples of petroleum fractions, by a pixel-based approach. A set of data from 75 petroleum samples – light gas oils, light cycle oils and kerosenes – was considered.

The 2D chromatogram of Fig. 7.11 is from a coal-derived process stream from the Point of Ayr coal liquefaction pilot plant: the feed to the hydrocracker (Hamilton et al., 2007). Differences attributable to the process can be distinguished between the feed to and product (not shown) from the hydrocracker. These relatively small molecules are mostly associated with the process-derived recycle oil and are involved in the production and destruction of hydrogen-donor species and their isomerisation into non-hydrogen donor structures. In Fig. 7.11, the series of n-alkanes is evident. The scatter of points of the more aromatic types indicated a very complex mixture of hydroaromatics. Pyrene and fluoranthene are identified in the Figure; their position on the diagram indicated that these components exceeded the elution time allowed for the second column (8 s) and appeared at very early elution times in a later scan. In the Figure, the spot density increased with the concentration of the component. The method has not been used extensively for coal tars, but a petroleum fraction has shown the presence of benzothiophenes that co-eluted with naphthalenes (Genuit, 2005). Zoccali et al. (2015) directly coupled LC with 2D GC-MS and demonstrated

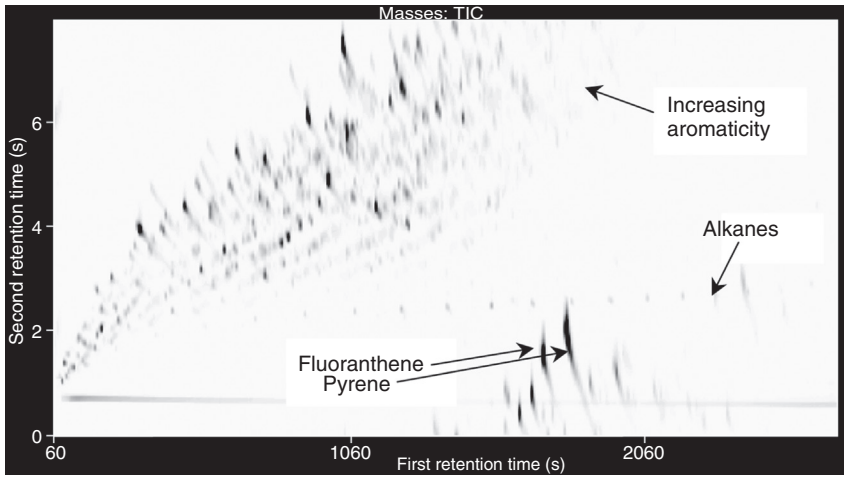

Figure 7.11 Point of Ayr coal liquefaction plant, feed to hydrocracker by 2D GC-MS. *Source:* Reprinted with permission from Hamilton, J.F., Lewis, A.C., Millan, M., Bartle, K.D., Herod, A.A., Kandiyoti, R., 2007. Energy Fuels 21, 286–294. Copyright 2007 American Chemical Society.

the combination using a coal tar; the normal-phase LC process allowed the separation of three classes of coal tar compounds: (1) non-aromatic hydrocarbons, (2) unsaturated compounds (with and without S), and (3) oxygenated constituents.

Coal oils contain very many individual species; Franck (1955) estimated that as many as 10^4 separate compounds may be present in the multicomponent mixture comprising coal tar which imposes impossible demands on any single chromatographic technique. However, Koolen et al. (2015) showed how coal tar is ideally suited to analysis by 2D GC. In remarkable agreement with the above estimate they identified 6600 individual peaks in the chromatogram from 2D GC–TOF MS, in contrast to the 200–300 peaks separated by one dimensional GC. Antle et al. (2013) devised an algorithm for the quantitative analysis of PAC and polycyclic aromatic sulphur heterocycles (PASH) in soil contaminated by coal tar from the full-scan 2D GC data collected by TOF MS.

Fractions of crude petroleum contain similarly huge numbers of individual compounds and 2D GC-MS has been applied to petroleum-derived materials. Ruddy et al. (2014) used 2D GC-MS in the investigation of the oil spilled from the Macondo well disaster. Hourani et al., (2015) examined five highly naphthenic base oils by 2D GC, HPLC and FT-ICRMS with APCI and APPI. They considered that none of the studied analytical techniques was by itself sufficient to provide comprehensive information on the complex samples. Avila et al. (2012) obtained several gas oil cuts from an atmospheric petroleum residuum by molecular distillation at different temperatures; these samples were investigated using 2D GC with time-of-flight mass spectrometry (TOF MS) and ESI FT-ICRMS. Compound classes identified included tri-, tetra- and

pentacyclic terpanes, steranes, and secohopanes, several PACs such as fluorene, phenanthrene, pyrene and benzo[*ghi*]perylene, the sulphur compounds alkylbenzothiophenes, alkyldibenzothiophenes and alkylbenzonaphthothiophenes and alkylphenols. The use of MS for detection is standard but selective GC detectors such as the nitrogen-phosphorus thermionic (NPD) (da Silva, 2014) and sulphur-chemiluminescence (SCD) (Blomberg et al., 2004) detectors add further power to the 2D GC analysis of fossil fuel fractions (von Muhlen, 2007). An example of multiple detectors following 2D GC is that of Dijkmans et al. (2015) where information from flame ionisation, SCD, nitrogen chemiluminescence and TOF MS on three different GCs was combined in the analysis of a shale oil sample to reveal 20 different chemical classes: paraffins, isoparaffins, olefins/mononaphthenes, dinaphthenes, monoaromatics, naphthenoaromatics, diaromatics, naphthenodiaromatics, triaromatics, thiols/sulphides, benzothiophenes, napthenobenzothiophenes, dibenzothiophenes, pyridines, anilines, quinolines, indoles, acridines, carbazoles and phenols.

Bartha et al. (2015) combined 2D GC with flame ionisation detection and MS on samples of known provenance, to develop an understanding of the primary factors controlling asphaltene content and viscosity in a reservoir, the Llanos basin in Colombia. Forsythe et al. (2015) investigated a large Saudi Arabian oilfield which has been shown to be in vertical and lateral equilibrium. 2D GC and stable isotope analysis (δ D and δ ^{13}C) were used to determine the consistency of the liquid-phase components with equilibration and the effects of biodegradation or thermal maturity on the observed asphaltene gradient. Knorr et al. (2013) have published a method based on automated compound identification in complex matrices from 2D GC to give quantitative structure-property relationships with computer aided structure interpretation to predict three specific parameters to enhance the confidence for correct compound identification: Kovats Index for the first dimension separation, relative retention time for the second dimension, and boiling point.

Wilde and Rowland (2015) examined naphthenic acids following their conversion to hydrocarbons by methylation to methyl esters, followed by reduction to alcohols, followed by formation of the tosyl esters which were finally reduced to hydrocarbons and analysed by 2D GC-MS. This procedure led to the identification of more than 30 individual bicyclic naphthenic acids as the bicyclane hydrocarbons. Tranchida et al. (2015) have developed a flow modulated 2D GC with high resolution TOF MS, applied to the analysis of a heavy gas oil. The system was targeted to determine the presence of benzothiophenes and dibenzothiophenes. Collin et al. (2015) have fabricated a micro GC × GC system and demonstrated it in application to alkanes and small hydrocarbons and oxygenated molecules, with the output to a FID.

Applications to biomass oils are few but growing rapidly; several examples are given, but the list is not intended to be comprehensive. Pyrolysis products from lignin, cellulose, and sewage were studied by 2D GC-TOF MS (m/z 40–300) by Fullana et al. (2005), more than 1000 compounds were detected. Amador-Munoz and Marriot (2008) reviewed quantitative 2D GC methods and proposed a new approach to quantification. Marsman et al. (2007, 2008) proposed a simplified approach to quantify and identify components from biomass pyrolysis using 2D GC-FID for quantification and a standard GC-MS for group type identification, thus avoiding the need for an

expensive MS. The analytical approach was demonstrated by comparing a raw biomass pyrolysis oil with its hydrotreated product; after upgrading organic acids, sugar concentrations in the oil decreased and hydrocarbons, alcohols, and alkyl-benzenes increased. GC-MS on its own was not the best technique for the analysis of biomass pyrolysis oil. Sfetsas et al. (2011) examined the influence of the analytical procedure on quantitative and qualitative results from GC-FID and 2D GC-TOF MS, i.e., choice of solvent for analysis, column types and chromatographic conditions, as well as the data processing and classification methods for three biomass pyrolysis oils. All the samples contained at least 300 compounds when detected by 2D GC-TOFMS; only 11 compounds were quantified by GC-FID.

Djokic et al. (2012) used 2D GC-TOF MS to identify components in a raw biomass pyrolysis oil and used 2D GC-FID for quantification. Approximately 150 compounds were tentatively identified and quantified by the method, which account for ~80% of the peak volume of the chromatogram. Tessarolo et al. (2013) pyrolysed empty palm fruit bunches and pine wood, with oils characterised by 2D GC-TOF MS and GC-MS. Significant differences in the GC range compounds were indentified in the two pyrolysis oils, with more than 600 compounds detected for the palm bunches and ~850 compounds from pine wood. Both samples contained ketones, cyclopentenones, furanones, furans, phenols, benzenediols, methoxy and dimethoxy-phenols and sugars. The palm bunches also contained esters, aldehydes and pyridines, while the oil from pine wood contained alcohols and cyclopentanediones.

Da Cunha et al. (2013) analysed solubility fractions from a sugarcane straw pyrolysis oil by 2D GC–quadrupole MS. Olcese et al. (2013) reported a detailed characterization of biomass pyrolysis oil before and after upgrading using 2D GC-FID for the low MM compounds (<250 u) and FT-ICRMS to examine higher MM species; they also provided a short review of previous studies on biomass pyrolysis oils using FT-ICR-MS and examined the influence of different ionisation sources on the results. The total amount of material detected in the raw pyrolysis oil by the 2D GC analysis was ~9 wt% of the dry feedstock; after upgrading this fell to ~6 wt%. This drop in detectable material after upgrading was attributed to significant losses of material as char formed on the catalyst. FT-ICR-MS was able to detect species up to O_8 and C_{37} compared to O_4 and C_{14} by GC.

Hartman and Hatcher (2015) applied hydrothermal liquefaction (HTL) to cuticular materials from *Agave americana* and *Capsicum annuum* for extended periods of time (72 h) at 360°C in attempting to simulate long-term maturation of the organic matter. Analysis by 2D GC-MS indicated that the Agave bio-oil was dominated by a homologous series of n-alkanes, whereas cyclic and aromatic compounds were the major compounds identified in the Capsicum bio-oil. Analysis using ESI-FT-ICRMS revealed the bio-oil samples were predominantly lipid-like in character, showing that highly aliphatic biopolymeric components of certain plant materials can produce bio-oils with potential as alternative fuels.

In summary of the above discussion, although 2D GC coupled to a FID or MS detector is an extremely powerful tool for analysing biomass pyrolysis oils it cannot provide complete information. 2D GC methods have the capability of identifying close to 1000 compounds in pyrolysis oils; however, the amount of material this

represents relative to the original feedstock (dry basis) is often small, accounting for less than 10 wt% of the feedstock (Mohan et al., 2006; Olcese et al., 2013; Le Brech et al., 2016; Morgan et al., 2015). Clearly, other methods are required that can provide information on the less volatile and higher MM species present in pyrolysis oils as will be discussed in Chapter 8, Analytical techniques for high mass materials: method development.

2D GC-MS must be considered a routine analytical tool, rather than a promising technique in the process of development. It has been applied to the characterization of extraterrestrial organic matter, such as that found in the Murchison chondrite and synthetic tholins (complex organics formed in the atmosphere of Titan (Saturn's largest moon) by photolysis but formed in the laboratory by cold plasma discharge in a methane–nitrogen mixture) using a variety of methods to release the organic matter (Watson, 2012).

7.6.3 2D LC-MS

Tomasini et al. (2014) have demonstrated a two-dimensional (reversed phase) LC system with analysis by either electron ionisation or APCI for the characterization of the aqueous phase from pyrolysis of lignocellulosic biomass materials. Biomass materials used were coconut fibres, sugar cane straw, and sugar cane bagasse. Tran et al. (2013) have prepared fullerene-modified silica and demonstrated its application to 2D LC of oxygenated molecules, possibly of relevance to biomass pyrolysis liquids.

7.6.4 Pyrolysis GC-MS

The pyrolysis GC-MS method involves placing a pyrolysis stage in the GC carrier gas stream. Volatiles may be fed into GC-columns from several types of pyrolysis stages, including resistively heated filaments such as platinum, laser pyrolysis and Curie point pyrolysis stages, where ferromagnetic metals or alloys are heated to a particular temperature by inductive heating, achieved by exposure to a high frequency field in an induction coil. The mass range limitations of the pyrolysis products are the same as for GC-MS. Involatile material remains behind as char in the pyrolysis stage, or deposits onto the inlet system or parts of the column. The method is useful in identifying structural elements of involatile samples that cannot themselves pass though the GC-column. The technique has been used in investigations of coal tars and petroleum residue fractions as well as for biomass tars that do not give a direct response in ordinary GC-MS.

Ross et al. (2011) and Lea-Langton (2012) developed a microflow cell reactor Py-GC-MS system in which a commercial pyrojector was coupled to a pyrolysis unit. This allowed more complete pyrolysis and hence a simpler product profile than that observed with a filament because of a longer residence time and was applied (Bartle et al., 2013) to heavy fuel oil asphaltenes. In keeping with TGA analysis the resulting chromatograms at 300°C contained peaks from volatile aliphatic and monocyclic aromatic hydrocarbons occluded in the asphaltene particle pores. At temperatures between 400°C and 500°C the compounds evolved were alkane/alkene pairs from the

β-bond scission of bonded long chain alkyl groups, alkanoic acids and alkyl aromatics (benzenes, and 2- to 4-ring PACs along with hydroaromatics). These results are consistent with the thin-film pyrolysis experiments of Karimi et al. (2011) and with an 'archipelago' structure for the asphaltenes in which small aromatic and naphthenic clusters ('building blocks') are present with substituent alkyl groups, some of which are in long chains. Pyrolysis at temperatures of 600°C and above gave similar products, but also evidence of secondary reactions.

Valuable ancillary information was provided by pyrolyses in which the MS detector was replaced (Ross et al., 2001) by an AED detector. Complementary py-GC-AED allowed identification of a range of numerous alkylated, mainly methyl, benzo[*b*], – and dibenzothiophen isosteres of the liberated PACs, suggesting an important contribution of sulphur heterocyclic groups to asphaltene structure.

Py-GC-MS is often used to characterise the pyrolysis behaviour of biomass samples despite the inherent limitations of the method for this type of study, as discussed elsewhere (Morgan and Kandiyoti, 2014). Typically, the gas yield is quantified by the MS detector, char yield by weighing the sample holder after pyrolysis, and the oil/tar by difference (or through partial quantification of compounds in the GC range, up to m/z ~220 u). This method of characterising biomass samples has obvious appeal in comparison to custom built fixed or fluidised bed reactors due to simplicity of use and speed of analysis. However, the results are not comparable to those obtained under conditions more representative of industrial processes or conditions that reveal the fundamental behaviour of the solid fuels (i.e., through minimising the effects of heating rate, secondary reactions, and reactor and sample geometry on results). This can result in misleading conclusions although, py-GC-MS can be useful to fingerprint samples, compare sample chromatograms and to quantify permanent gases released during pyrolysis.

In pyrolyzing polymers, it is expected that they break down thermally into their characteristic monomers to reveal the chemical nature of the polymer. In the samples of interest for fuel characterization work, however, the notion of monomers is not useful. Instead, the method aims to identify pyrolysis fragments from large complex molecules of unknown but probably irregular structures. We describe later in this Chapter some examples where no detectable fragment molecules were released by samples being studied.

Py-GC-MS of coals indicates the main volatile fragments to be aliphatic rather than aromatic in nature, with biomarker molecules from original depositional material in evidence (Scott and Fleet, 1994). Experiments with Curie point pyrolysis – GC has shown how the aromatic groupings and aliphatic materials released by several coals change with coal rank (Tromp et al., 1988, 1989). Under mild pyrolysis temperatures, homologous series of alkanes from C_{12} up to C_{30} were observed alongside a range of aromatics up to phenanthrenes. Phenols up to xylenols were detected at high pyrolytic temperatures. Yan et al. (2015) investigated the release of PACs and phenols from three coals of different ranks using pyrolysis temperatures of 400°C, 600°C, 800°C, 1000°C and 1200°C with a nominal heating rate of 10,000°C s^{-1}, using GC-MS to analyse the products. PACs up to benzo[*ghi*]perylene and phenols up to 2-naphthol were detected.

Results from the pyrolysis GC-MS of coal tar and extract fractions have been widely reported (Herod et al., 1999; Islas et al., 2000, 2002, 2003a; Song et al., 1992); identified components closely resembled pyrolysis products from unfractionated liquids or the parent coals. However, only those low-mass fractions soluble in acetonitrile or THF gave significant amounts and numbers of individual products. Fractions of material insoluble in acetonitrile and pyridine gave virtually no signal. This suggests fundamental structural changes in material with increasing molecular masses (as identified by SEC and MALDI-MS) and increasing polarity. It appears these largest molecules either form char at the pyrolysis stage and/or their pyrolytic fragments condense somewhere within the GC-system.

However, the parallel increases of molecular masses and associated increasing sizes and complexities of PAC groups observed for coal liquids are not applicable to samples of different origins. Solvent extracts of a Baltic amber were examined by pyrolysis-GC-MS (Islas et al., 2001). The components detected in pyrolysis products from the pentane-solubles, toluene-solubles, the NMP-extracts and the NMP-insoluble residue were all relatively similar to each other and to the products from the pyrolysis of the whole amber. The range of masses detected by py-GC-MS, up to m/z 270, was exceeded by the probe mass spectra of the amber solubility fractions which reached m/z 700; this difference exposes the limitation imposed by the GC column. Despite the wide spread of molecular masses, units making up the amber structure appear not to differ greatly from one another. This similarity of products from the different solubility fractions contrasts markedly with observations on coal-tar–derived solubility fractions displaying very different properties. In this sense, the behaviour of amber is more closely related to those of polymers with known regular structures.

Py-GC-MS can thus be used to investigate whether high mass, relatively intractable molecular units can be readily broken up into smaller structural units or whether these structural units themselves evolve and become more intractable with increasing MM and polarity. We have observed how the pyrolysis of toluene, acetonitrile, pyridine and NMP insoluble fractions of coal liquids and a petroleum vacuum residue (Table 7.4) did not give molecules detectable by GC-MS. The larger mass molecules from coal-derived fractions appear therefore to have different structures from smaller molecules ordinarily identifiable by GC-MS. The *characterization* of these larger MM materials is the subject of Chapter 8, Analytical techniques for high mass materials: method development.

Applications of py-GC-MS to other hydrocarbon sources include the analysis of Murchison chondrite material using a CDS Pyroprobe to reveal aromatics up to pyrene (Watson, 2012). The demethylation of PACs in diesel fuel has been investigated both by using a diesel engine and analysing the exhaust particulates, and by a flow-cell pyrolysis reactor attached to GC-MS (Lea-Langton et al., 2015) using PAC molecules with ^{13}C labelled methyl groups. Pyrolysis with GC-FID-MS has been used to evaluate tars from briquettes made from coals, tar and biomass (chestnut sawdust waste) and to quantify the 16 EPA priority PACs (Montiano et al., 2015) as well as identifying components from furfural to coronene; no synergy was evident between biomass and coal tars. He et al. (2015) have coupled thermogravimetric analysis to GC through an autoinjector system to capture gas evolved over different temperature

ranges from room temperature to 1200°C, with subsequent analysis by GC-MS; they pyrolyzed a lignite sample.

Pyrolysis-Mass Spectrometry Evans and Milne (1987a,b) developed a pyrolysis MS method in which the products of pyrolysis were directed into a quadrupole mass spectrometer as a molecular beam. The products from wood waste passed through a system of skimmers to reduce the pressure to that of the mass spectrometer. The maximum mass detected was up to m/z 220 and structural isomers could not be distinguished. Changes in mass spectra as pyrolysis temperature increased were attributed to increasing pyrolysis of the released volatiles. Jarvis et al. (2011) and Gaston et al. (2011) have coupled the molecular beam technique with small scale pilot plant – an entrained flow pyrolyser and a fluidised bed respectively. Temperatures up to 1000°C were applied but mass spectra were only shown up to m/z 270 from a mass scan range from m/z 20 to 450. In view of the lack of restraint by having no GC column, the upper mass detected would appear very low; in addition, there is no mention of tar formation. It remains unclear whether the mass range detected in these studies represents the entire mass range of volatile species formed during pyrolysis or is an artifact of the sampling method. Condensed pyrolysis oils contain much broader mass distributions, ranging to at least 3000 u.

At present only a few studies by FT-ICRMS on biomass pyrolysis or gasification oils/tars have been reported. FT-ICRMS was used to study biomass-derived samples: biomass char, where the sample was introduced to the MS using desorption atmospheric pressure photoionisation (DAPP) (Podgorski et al., 2011). The aim of the work was to develop a method capable of providing structural information for samples currently limited by solubility and sample preparation issues. Samples of the parent (uncharred) oak, after combustion (250°C) and pyrolysis (400°C) were examined. Useful information was obtained on H/C and O/C ratios which revealed clear differences between the samples related to aliphatic and aromatic contents. Olcese et al. (2013) have reported a detailed account of the benefits and limitations of the FT-ICR-MS and 2D GC-MS techniques in relation to the study of biomass pyrolysis oils. In particular the high resolution provided by FT-ICR-MS was useful in understanding the mechanisms related to catalytic upgrading of bio-oil. High resolution FT-ICR-MS has also been used to study the ageing of biomass pyrolysis oils. It was concluded that issues related to stability (ageing reactions) are mainly due to oligomerisation of lignin-derived compounds (Smith et al., 2014). Liu et al. (2014) detected molecules up to C_{45} and O_9 in hydro-liquefaction oils from sawdust in petroleum ether by FT-ICR-MS. A useful and detailed account of the FT-ICR-MS method in relation to studying pyrolysis oils from biomass has been reported by Bai et al. (2014).

A recent development is the coupling of thermal analysis to APCI FT-ICR-MS (Rüger et al., 2015) with the ability to raise the thermobalance temperature at a slow rate to match the scan of the MS. The concept was demonstrated using the thermal behaviour of different fossil fuels: heavy fuel oil, light fuel oil, and a crude oil, and different lignocellulosic biomass, namely, beech, birch, spruce, ash, oak and pine as well as commercial available softwood and birch-bark pellets with components detected in the mass range m/z 100–500.

7.6.5 Heated glass inlet

The heated glass inlet allows the sample to be evaporated without fractionation, giving hydrocarbon-type analysis through the summation of ions characteristic of various hydrocarbon types. Low ionising voltages may be used to suppress the formation of doubly charged ions and the fragmentation of aromatic molecules by loss of alkyl side chains. The ionisation potentials of aliphatic molecules are higher than those of aromatics; at 10 eV, any ions observed are normally molecular ions of aromatic molecules. In high-resolution mass spectrometry, the definition of aromatic types by accurate molecular ion mass provides a formidable, semi-quantitative analysis tool.

The concept of the Z number from the general hydrocarbon formula C_nH_{2n+Z} (N.S.O) is essential for the understanding of type analysis results. N.S.O represents the possible inclusion of nitrogen, sulphur, or oxygen atoms and does not alter the Z number. It reflects the total number of rings and double bonds in a structure defined by the carbon number (n), and is used as an index of hydrogen deficiency, compared with the corresponding alkane, where Z = +2. The number of heteroatoms N, S and O indicate that their structural configuration is not specified; they may be present in rings or as parts of pendant groups (Aczel, 1972; Aczel and Lumpkin, 1979; Herod, 1989). Distillate samples can be analysed by GC-MS and the data evaluated to give the equivalent of type analysis. Methods were initially developed by ASTM for petroleum middle distillates using 70 eV electron impact (ASTM, 1972). Applications of hydrocarbon group–type analysis methods using both complete evaporation (with electron ionisation at 70 and 10 eV) and GC-based methods in petrochemistry have recently been described by Genuit (2005).

The method is not now much used because (1) quantification was not accurate since assumptions had to be made concerning the make-up of the structural isomers of each type of compound based on available standard materials, and (2) relatively high mass resolution was needed for the low eV work, requiring a double-focusing mass spectrometer. An effective replacement for this method of sample introduction is the thermospray system where a dilute solution of sample in toluene with or without methanol and additives such as formic acid or ammonium hydroxide (for +ve or –ve ion formation respectively) is nebulised at atmospheric pressure in association with a variety of ionisation methods before sampling into a very-high resolution mass spectrometer such as the FT-ICRMS, TOFMS or Orbitrap systems. The method is discussed further in Chapter 8, Analytical techniques for high mass materials: method development, but the limitations of the glass inlet system still apply in that there is no separation of structural isomers and assumptions must be made as to relative sensitivities of the different isomers. In compensation, the range of mass detected by newer MS instruments has increased and sensitivity and accurate mass measurement allow the collection of immense volumes of data.

7.6.6 Solids probe

Solids probe mass spectrometry may be considered as an extension of hydrocarbon type analysis into the volatility region beyond that accessible by the heated glass

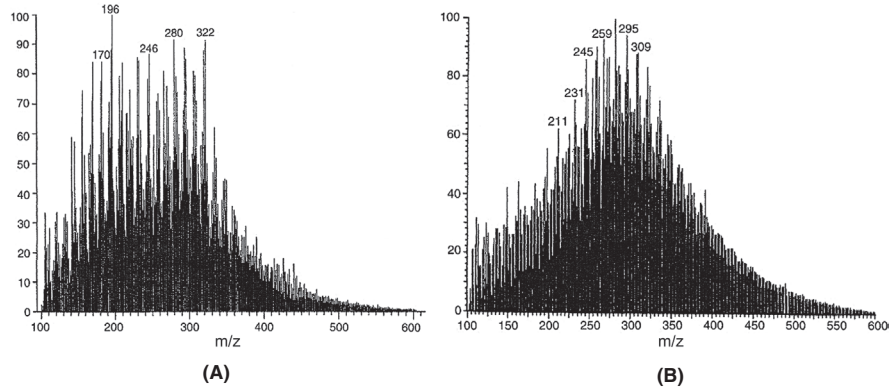

Figure 7.12 (A) Probe mass spectrum at 10 eV of a hydropyrolysis tar from coal. (B) Chemical ionisation mass spectrum of the same tar using isobutane gas.
Source: Reprinted from Herod, A.A., Ladner, W.R., Stokes, B.J., Berry, A.J., Games, D.E., Hohn, M., 1987. Fuel 66, 935–946. Copyright 1987, with permission from Elsevier.

inlet system. It is a method for detecting components not amenable to GC due to high polarity or low volatility (see Section 7.6.6). Distillation of the sample into the ionising region at low pressure, with increasing probe temperature permits the examination of a series of components with increasing MM. High or low mass resolutions and ionising voltages may be used. In terms of scanning a range of masses, the use of nominal mass rather than accurate mass permits faster scans over a wider range and may be necessary to evaluate the components of a complex mixture. Since very small sample quantities are required, the possibility exists of repeated runs with different mass spectrometric conditions to investigate aspects of the sample.

In this configuration, samples may be part pyrolyzed if the maximum probe temperature is high enough. The presence of char on the probe after the experiment is an indication of incomplete volatility. The mass range of SEC fractions of the asphaltenes (benzene insolubles) of a hydropyrolysis tar (Herod et al., 1993) extended to m/z 500. Fig. 7.12A shows a probe-mass spectrum at 10 eV summed over a range of scans and showing only molecular ions in the aromatic fraction of a hydropyrolysis tar. The spectrum shows a very complex mixture. For instance, around m/z 322, at least seven components can be seen in the cluster of peaks, ranging from m/z 316 to 328 and corresponding to aromatics of decreasing Z number. At m/z 316, we can propose a structure derived from benzofluorene (m/z 216) by addition of two benzo groups, as $C_{25}H_{16}$. Thus, the other components of the group may correspond to molecular ions of $C_{25}H_{18}$ (m/z 318), $C_{25}H_{20}$ (m/z 320), $C_{25}H_{22}$ (m/z 322), $C_{25}H_{24}$ (m/z 324), $C_{25}H_{26}$ (m/z 326) and $C_{25}H_{28}$ (m/z 328). Accurate mass measurement would be required to verify these suggestions. A pyridine-insoluble fraction of a coal tar pitch (Begon et al., 2000) gave no significant ions when examined by probe mass spectrometry because the lighter materials had been removed. However, after catalytic hydrocracking, a wide range of aromatic molecular ions was observed, typical of a coal-derived

material. This evidence indicated that the molecules of the pyridine-insolubles were very large and broken down by hydrocracking into relatively small molecules.

A sample of Baltic amber was pyrolyzed in the wire-mesh reactor described in Chapter 3, Pyrolysis of solid fuels: experimental design and applications, (Pipatmanomai et al., 2001) and extracted to give solvent extract fractions (Islas et al., 2001). The product pyrolysis tar and solvent extracts were examined by probe mass spectrometry. The mass spectra of the pyrolysis tar and the solvent extracts contained many common ion fragments; the mass range of the spectra of the solvent extracts extended to m/z 700 and indicated homologous series of components in the mass range above m/z 500. These probe-mass spectra showed material far beyond the range covered by GC-MS.

Probe-mass spectra of sample spots recovered from thin layer (planar) chromatography plates have shown sample aromaticity increasing with decreasing mobility in solvents like pentane, toluene and pyridine. Increasing solvent polarities were required to move components with increasing polarity and increased heteroatom content. In another application, fractions of coal tar pitch collected from an analytical SEC column as successive 1 min time fractions and examined by probe-MS showed little signal for the early eluting fractions. Components of the early-eluting fractions were of too large MM (and too involatile) to ionise by this method, and were clearly not aggregated small molecules. Ions characteristic of pitch were observed only in the last few fractions (Lazaro et al., 1999).

Desorption chemical ionisation provides a method of evaporating material from a heated probe by a relatively gentle ionisation method which may be selective for particular types of compounds, depending on the ionisation reagent gas used. The limitation is the volatility of sample components. Fig. 7.12B shows the DCI mass spectrum using isobutane reagent gas, of the same aromatic fraction as in Fig. 7.12A, showing a different mass range than the low voltage probe, possibly because the relative sensitivities of aromatics and alkylated aromatics differ in the two ionisation methods. Here too, the method is not readily available on new instruments, and similar analyses can be done using a solution of the sample pumped to a nebuliser for an atmospheric pressure inlet to a high resolution mass spectrometer, and involatile samples on TLC plates after development can be inserted directly into LDI-MS instruments.

7.6.7 Field ionisation

Field ionisation mass spectrometry depends on the tunnelling of an electron from a molecule in the gas phase on passage through a steep electric field to an electrode. The method detects those molecules which are volatile in vacuum or which form on pyrolysis in vacuum. High resolution FIMS may allow determination of atomic compositions of peaks, but the complexity of mass spectra observed for asphaltenes and pre-asphaltenes tends to limit the unambiguous use of this technique. In addition, the relative intensity of odd-mass peaks to even-mass peaks in spectra of asphaltenes tends to be greater than in spectra of aromatics or oil fractions, indicating that the molecular complexity has increased by the introduction of heteroatoms, further reducing the ability of high resolution mass measurement to give unambiguous results. The

upper mass limit of the technique, defined by the requirement of volatility under the operating conditions, appears to be about m/z 1200, but that need not correspond to the largest masses present in any given sample. Mass spectra of aromatics extended to m/z 1100 (Herod et al., 1993). FIMS and pyrolysis FIMS have been used to analyse coal liquids (Malhotra et al., 1993; Cagniant et al., 1992). Type analysis of a base oil using FIMS showing types ranging from alkanes to benzodicycloalkanes (Z number range from +2 to −10) has been presented by Genuit (2005). Pyrolysis-FIMS has been applied to the examination of volatiles from oil shales (Oja, 2015) where shale samples were heated slowly to 710°C at 10°C min^{-1}. The kerogen in the shale formed volatiles from m/z 50 up to 700 approximately, with peak intensity around m/z 4–500 at a temperature of 4–500°C.

The best application of FIMS is probably to distillate samples likely to be entirely volatile in the vacuum of the mass spectrometer. The technique has been used to examine the volatile components of coal liquids, as described earlier, but the limitations are clear. Examination of the sample holder after an experiment can be useful in indicating the proportion of sample that remained involatile.

7.6.8 Isotope ratio mass spectrometry

This method of operation requires a mass spectrometer set to measure ions of different mass, e.g., m/z 44 $^{12}CO_2$ and m/z 45 $^{13}CO_2$; the intensity of the m/z 46 ion beam is also monitored simultaneously since both $^{13}C^{16}O^{16}O$ and $^{12}C^{17}O^{16}O$ contribute to mass 45, but the contribution of the latter is corrected for from the intensity of mass 46 (mainly $^{12}C^{18}O^{16}O$) and the known ratio of ^{18}O to ^{17}O. An oxidation stage is necessary to convert the carbon of the analyte to carbon dioxide, and if the sample elutes from a chromatography column, the oxidation must be rapid and complete. The ratio of ^{13}C to ^{12}C in coal liquids has been measured by GC-MS to show that the ratio differs from that of petroleum liquids and the source of environmental pollution from the two types of material can be distinguished (McRae et al., 2000). The method has not yet been applied to the intractable fractions of coal tars or vacuum residues. It may be useful in revealing differences in isotopic compositions between such fractions and provide clues relating to the origins for large and small molecules. The method has not reached the stage of routine operation for characterising relatively heavy fractions but clearly presents novel analytical options and has been applied (Bottrell et al., 1991; Louie et al. 1993) to determine the degree of incorporation of coal and petroleum into the products of coprocessing (Wallace et al.,1990) The incorporation of coal carbon into the different fractions determined from stable isotope ratio measurements of products from coprocessing under hydrocracking conditions was assessed after corrections for catalytic reaction of the end members and for retrogressive reactions (Louie et al., 1993).

Stable isotope (^{13}C (Lea-Langton et al., 2015; Eveleigh et al., 2014) and ^{2}H (Lombaert et al., 2006)) tracers have been employed in place of ^{14}C radioactive tracers (Tancell et al.,1996) to determine the contribution of fuel PAH to emissions from diesel engines. Pyrolytic reactions of ^{13}C-labelled methyl arenes were studied

(Lea-Langton et al., 2015) in a micro-pyrolysis-GC-MS apparatus (Ross et al., 2011) and confirmed de-alkylation as the predominant reaction.

7.6.9 Tandem mass spectrometry

Tandem mass spectrometry is a method in which an ionisation source and a mass selective device, such as a quadrupole or magnetic sector is used to select a particular ion from the initial ion source for study in one or more subsequent analytical mass selection detectors.

The aim of such work may be to determine either the characteristic fragments from the selected ion after collision-induced dissociation or the fragments resulting from the specific loss of a neutral fragment. The possibilities of this instrument configuration have been summarised by Chapman (1993). Sample introduction by probe or reservoir is needed to maintain constant pressure. Preasphaltenes from liquefaction extracts of coals (Wood et al., 1985) have been examined to identify homologous series of hydroxy- and dihydroxy-aromatics that would not pass through a GC column.

The tandem mass spectrometry approach is one able to pick out specific components or types of component in complex mixtures. It is necessary to understand what is being looked for at the outset so that the instruments may be set up to search for either the neutral mass loss characteristic of fragmentations of a chemical type or the specific ion fragments that may identify a compound class. The experiment can be achieved using quadrupole analysers or even an ion trap mass spectrometer by using appropriate software normally supplied with the instrument. Given the complex mix of chemical types found in coal and petroleum-derived samples, the scope for experimentation is almost endless. The method is a research tool rather than a routine analytical method as far as fossil fuel–derived liquids are concerned. It has been used in the search for 'archipelago'-type asphaltene molecules, as discussed in Chapter 8, Analytical techniques for high mass materials: method development.

7.6.10 MALDI and LD-mass spectrometry

MALDI and LD-MS are methods normally used to generate molecular ions from large MM, thermally labile molecules, described in Chapter 8, Analytical techniques for high mass materials: method development. However, MALDI-MS can be used at low laser power to produce mass spectra of small aromatic molecules, showing aromatics in acetone and pyridine-soluble fractions of pitch up to m/z 400 (Millan et al., 2005). Small aromatic molecules have also been ionised by laser-desorption mass spectrometry (Herod et al., 1994). These applications of MALDI- and LD-MS approximate to the solids probe method described above. The low-mass spectrum of a pyridine-soluble fraction of a coal tar pitch is shown in Fig. 7.13. The processing of polydisperse hydrocarbon samples by laser desorption methods has been reviewed (Herod, 2012) and in conclusion, the need for supporting information from independent analytical methods was emphasised.

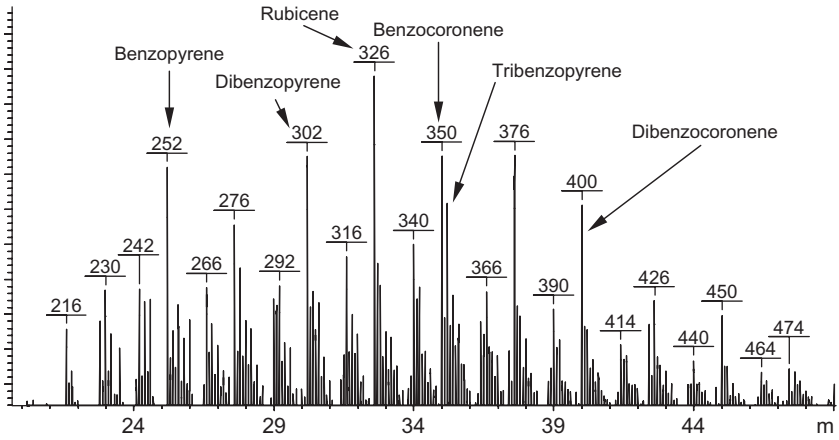

Figure 7.13 LD-MS of pitch pyridine soluble fraction of pitch at low laser energy showing low mass aromatic molecules.
Source: Reproduced with permission from Millan, M., Morgan, T.J., Behrouzi, M., Karaca, F., Galmes, C., Herod, A.A., et al., 2005. Rapid Commun. Mass Spectrom. 19, 1867–1873. Copyright © 2005 John Wiley & Sons, Ltd.

7.6.11 LC-MS

Lababidi et al. (2013) achieved the coupling of normal-phase high performance liquid chromatography (HPLC) with a polar aminocyano column to an FTICR mass spectrometer to analyse a maltene fraction of a crude oil. Atmospheric pressure laser ionisation was used as an ionisation technique to analyse the nitrogen-containing aromatic compounds in a deasphalted crude oil because of its unique selectivity toward aromatic compounds.

7.7 Aliphatic materials from coal and from petroleum

7.7.1 Introduction

When a coal is pyrolyzed and the products examined by GC-MS, the major components detected are n-alkane series and multicyclic terpane structures (see for instance, articles in Scott and Fleet 1994). Alkanes and alkenes up to about C_{33} were observed in pyrolysis and hydropyrolysis tars from coals (Snape et al., 1985). Aliphatic materials are thus known components of coals, with methane (firedamp) as a volatile and dangerous hazard of coal mining (ICS Ref Lib, 1920). Higher alkanes can be evaporated at low temperatures from coals and peat when used as a gas chromatographic column packing (Herod et al., 1983, 1991). The gas products from the high-temperature coking of coals (Owen, 1979) include methane and small alkanes (17% weight of dry coal), often considered to result from the pyrolysis of alkyl groups attached to the

coal structure, with liquor (2.5%), light oils (0.8%), and tar (4.5%) as the other components of the volatiles leaving behind the coke product (75%). Alkanes and cyclic aliphatics (mono-, di-, tri- and tetra-cyclics) have been detected in a saturate fraction of a coal liquefaction recycle solvent (Wilson et al., 1987) and by GC-MS of a coal digest (Islas, 2001). Series of alkanes have also been detected through LC-MS work on hydro-pyrolysis tars (Herod et al., 1987, 1988) showing alkanes up to C_{60} together with cyclic alkanes including pentacyclic triterpanes.

Alkanes have been detected by GC-MS in coal-liquefaction fractions (Walton, 1993; Herod et al., 1995a), in a low-temperature coal tar (Islas, 2001), but not in a coal tar pitch from high-temperature coking. MM ranges of technical waxes and paraffins have been compared using SEC (with *O*-dichlorobenzene as eluent), SFC and MALDI-MS and found to agree reasonably well up to a mass (M_n) of about 2000 u (Kühn et al., 1996) but the methods have not been applied to coal waxes.

7.7.2 SEC methods for alkanes in coal liquids and petroleum fractions

Investigations and applications of SEC have involved the solvent 1-methyl-2-pyrrolidinone (NMP) in order to examine the polar and large-sized molecular material of coal-liquids, petroleum residues and humic acids (Herod et al., 1995b). It proved possible to examine material insoluble in pyridine that could not be examined by SEC using a solvent less powerful than NMP. However, NMP is a poor solvent for aliphatic materials and the examination of petroleum vacuum residues using NMP, only allowed the examination of aromatic materials with aliphatic material remaining insoluble.

Accordingly, a method for the examination of mixtures of aliphatics and aromatic materials was sought. A solvent that dissolves both aliphatics and aromatics was considered desirable as eluent in SEC. THF can dissolve both types of material and in principle, SEC could be done with THF as eluent. Since aliphatic materials do not absorb UV-light, the tandem use of UV-absorbance and a universal 'evaporative light scattering' detector would provide an element of distinction between aromatic and aliphatic species. However, fractions containing larger aromatics are only partially soluble in THF. This is easily ascertained by observing increasing pressure drops across guard columns as sample progressively precipitates out from THF onto column packing. Because of the relatively low solvent power of THF, the true size exclusion mechanism for aromatics is partially lost during the SEC of some of the heavier coal and petroleum-derived materials; this will be discussed again in Chapter 8, Analytical techniques for high mass materials: method development, (Herod et al., 1995b). In the absence of solvents able to carry all classes of materials through the SEC column, possibilities of analysing different classes of compounds separately had to be considered.

Carbognani (1997) performed SEC using toluene as eluent, in silica columns operated at 45°C. The injection valve and transfer lines were held at 60°C. This system would probably elute *most* (but not all) aromatics together with the aliphatics. Large alkanes ($>C_{30}$) are soluble in hot toluene but not in cold toluene. Thus, toluene might enable a level of isolation of alkane concentrates. Another alternative was to use heptane as eluent. In contrast to the application of NMP as eluent in SEC, which

minimised the surface interaction between aromatics and the column packing, the use of heptane as eluent tended to maximise the surface interaction between aromatics and the polymer packing. The elution of aromatics was delayed until well after the permeation limit for aliphatics, allowing a complete separation of the types and an unambiguous identification of aliphatic material.

Accordingly, heptane was selected as eluent in the SEC of aliphatic materials. The SEC column was calibrated using standard alkanes with carbon numbers 13, 14, 16, 20, 22, 25, 30, 40, 44, 50, 60 and branched-C_{19} as well as Polywaxes 500, 655 and 1000 (consisting of even-numbered-carbon alkanes from about C_{20}–C_{100} in different ranges) with detection by an evaporative light scattering detector. Pentane and toluene soluble fractions isolated by column chromatography from a petroleum residue, a coal tar pitch, a coal digest and a low temperature tar, where aliphatics were concentrated, were examined (Islas, 2001; Islas et al., 2003b). High temperature GC-MS using a 25-m HT-5 column was used to identify some of the aliphatic standards. Fig. 7.10 presents elution times of standard n-alkanes contained in Polywax 500 from this GC column.

Fig. 7.14 shows the calibration of the SEC column in heptane solvent using standard n-alkanes from C_{13} to C_{50}; larger alkanes do not appear to be readily soluble in heptane. Detection of the alkanes was by ELS since they do not absorb UV-light. The elution times of the alkanes up to C_{50} follow a linear trend against log (MM).

The SEC chromatograms in heptane showed a shift in elution times from Polywax 500 to 655, but insufficient Polywax 1000 sample dissolved in heptane to give a signal at the detector. The range of alkanes in the Polywax samples given by the suppliers

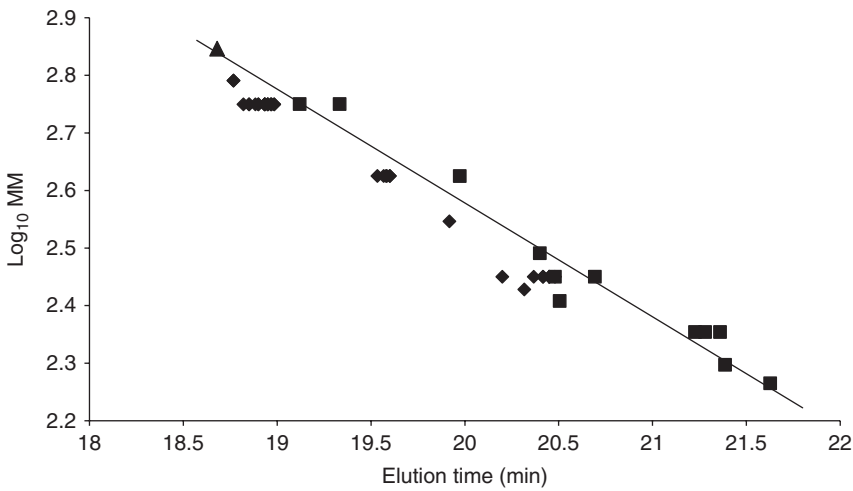

Figure 7.14 Calibration of the 'Mixed-E' column using alkane standards up to n-C_{50} (triangle); squares and diamonds represent calibration at different times. Detection by an evaporative light scattering detector.
Source: Reprinted with permission from Al-Muhareb, E.M., Karaca, F., Morgan, T.J., Behrouzi, M., Herod, A.A., Bull, I.D., et al., 2006. Energy Fuels 20, 1165–1174. Copyright 2006 American Chemical Society.

was: Polywax 500 $C_{20–60}$, Polywax 655 $C_{40–60}$ and Polywax 1000 $C_{40–80}$. No aliphatic materials eluted later than the small-molecule permeation limit, at about 24 min for this column. However, the small aromatics, benzene and toluene, did not elute before the permeation limit and did not appear until about 45 min later as a broad peak. Similarly, polystyrene standards eluted much later than the permeation limit. The exclusion limit of the column has not been defined using alkanes, but the colloidal silicas of diameters 9, 12 and 22 nm *all* eluted at about 11 min.

When the pentane and toluene soluble fractions from the fractionation of the Petrox petroleum residue were examined by using n-heptane as eluent, only the pentane soluble fractions gave signal in SEC. Analysis by GC-MS however showed a familiar picture. The first pentane solubles fraction showed a series of n-alkanes superimposed on a broad peak of aliphatic material with no discernible molecular ions, the broad peak presumably reflecting the presence of branched and cyclic aliphatics. The second pentane fraction showed only the broad peak of aliphatic material with some alkyl-substituted phenanthrenes. The analysis of the toluene solubles fraction by GC-MS gave no signal, confirming the presence of larger mass materials than could be handled by the GC columns. The mass balances for the fractionation of four samples by column chromatography using pentane, toluene, acetonitrile, pyridine, NMP and water are shown in Table 7.4. The heptane soluble fractions of six samples (Vac Bottoms A, B, C, Forties vacuum residue, Petrox residue and Sample 2) were examined using the mixed-E column and their ELS chromatograms are shown in Fig. 7.15. There are clear differences amongst the six chromatograms reflecting the

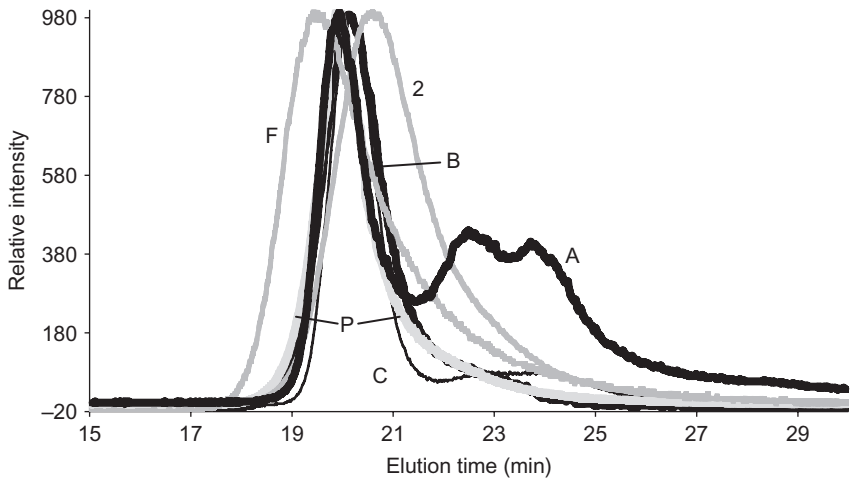

Figure 7.15 Heptane soluble fractions of several vacuum bottoms on Mixed-E, ELS detector. Samples are A—vacuum bottoms A; B—vacuum bottoms B; C—vacuum bottoms C; F—Forties vacuum residue; P—Petrox residue, 2-residue sample 2.
Source: Reprinted with permission from Al-Muhareb, E.M., Karaca, F., Morgan, T.J., Behrouzi, M., Herod, A.A., Bull, I.D., et al., 2006. Energy Fuels 20, 1165–1174. Copyright 2006 American Chemical Society.

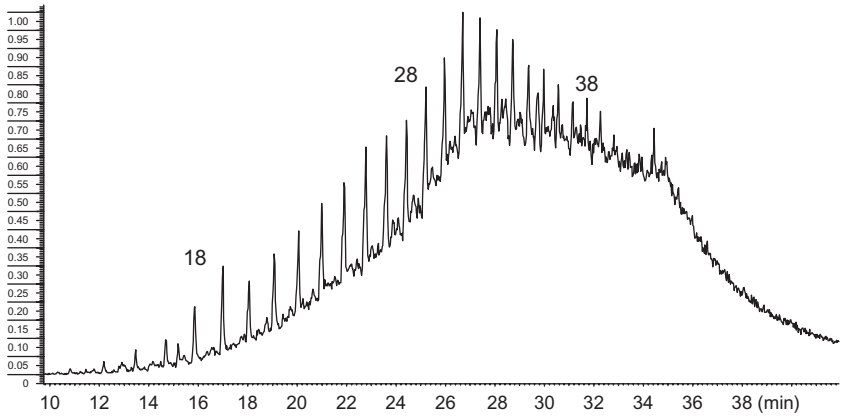

Figure 7.16 HT-GC-MS of first pentane-soluble fraction of Petrox residue; carbon numbers of n-alkanes shown and the unresolved hump corresponds to branched alkanes.
Source: Reprinted with permission from Al-Muhareb, E.M., Karaca, F., Morgan, T.J., Behrouzi, M., Herod, A.A., Bull, I.D., et al., 2006. Energy Fuels 20, 1165–1174. Copyright 2006 American Chemical Society.

alkane contents of the samples. However, the range of elution times for these samples did not exceed the range of the calibration samples. The peaks in Fig. 7.15 for samples A and C from 23 to 26 min may correspond to multicyclic alkanes since these elution times correspond to alkanes smaller than C_{12} and such small alkanes are too volatile to register with the ELS detector.

7.7.3 HT-GC-MS of petroleum and coal liquid fractions

Fig. 7.16A,B presents chromatograms of two pentane soluble fractions of the Petrox refinery flash column residue, examined by HT-GC-MS. The first pentane fraction gave a series of alkanes from C_{16} to C_{44}, superimposed on a broad underlying peak of aliphatic material. There was no light material in this sample of flash distillation residue. The second pentane fraction showed very few alkanes and some aromatics, but the underlying unresolved peak of aliphatic material shifted to later scans than that observed for the first fraction. The toluene fraction showed very little signal, indicating that the fraction contained very little material able to pass through the high temperature column.

Aliphatics in coal-derived samples: SEC using heptane as eluent has indicated that both pentane soluble fractions of the low temperature tar (Table 7.4) contained aliphatics, which presented peaks in the retained region. The toluene soluble fraction gave no signal in this column. The coal digest gave a similar distribution of SEC peaks. In contrast, the pitch fractions showed no aliphatic signal in SEC with heptane as eluent. When analysed by GC-MS, the first pentane fractions of the low temperature tar and the coal digest gave series of alkanes. Chromatograms for the two fractions of the low

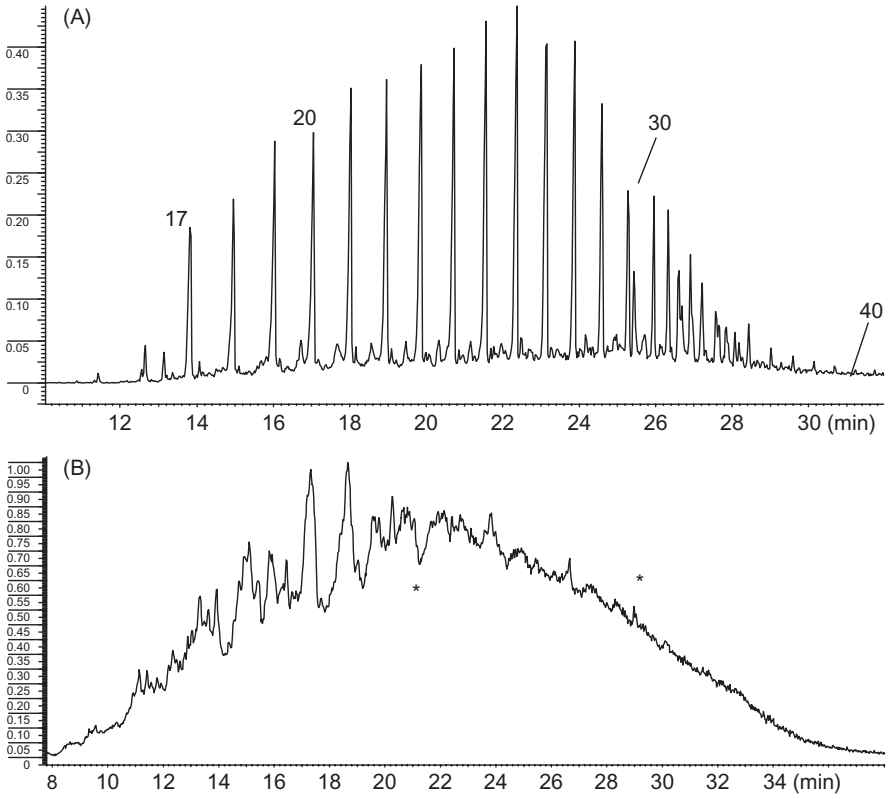

Figure 7.17 (A) HT GC-MS of first pentane-soluble fraction of low temperature tar; n-alkane carbon numbers as marked. (B) HT GC-MS of second pentane-soluble fraction of low temperature tar; all the components were aromatic with no detectable alkanes. *Source*: Reprinted with permission fro m Al-Muhareb, E.M., Karaca, F., Morgan, T.J., Behrouzi, M., Herod, A.A., Bull, I.D., et al., 2006. Energy Fuels 20, 1165–1174. Copyright 2006 American Chemical Society.

temperature tar are shown in Fig. 7.17A,B. In contrast, the pitch gave no aliphatic peaks in GC-MS, even though the range of aromatics detected was up to m/z 352, tribenzopyrene. The range of alkanes observed in the Polywax 500 sample was up to C_{56}. In two of the coal-derived samples (low temperature tar and coal digest), GC-MS detected the presence of aliphatic species when there was an SEC peak with n-heptane as eluent. The SEC method can provide an unambiguous indication of the presence of alkanes in a complex mixture, but high-temperature GC-MS must remain the method of choice for the examination of alkanes, particularly when MM measurements are required. Fig. 7.18 shows one mass spectrum taken from the chromatogram of Fig. 7.17B at 22 min; another spectrum from the same chromatogram at about 30 min indicated molecular ions from m/z 280 up to 372 but with no prominent fragment ions, indicating the complexity of the mixture at the points marked by stars.

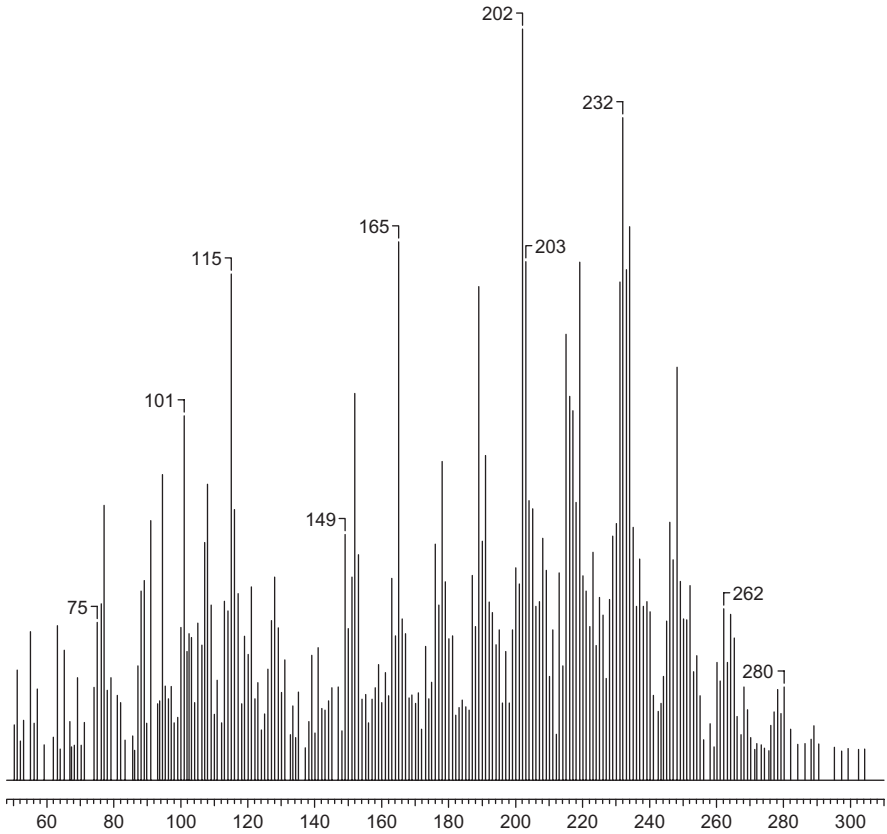

Figure 7.18 Mass spectrum from the chromatogram of Fig. 7.17b at about 22 min. The major components of the spectrum in the valley shown have molecular ions from m/z 200–230 with minor components to m/z 300. While some of these components might be known, the overlap of individual mass spectra in this mixture is too complex for meaningful identification. *Source:* Reprinted with permission from Al-Muhareb, E.M., Karaca, F., Morgan, T.J., Behrouzi, M., Herod, A.A., Bull, I.D., et al., 2006. Energy Fuels 20, 1165–1174. Copyright 2006 American Chemical Society.

Coal tar pitches as in Fig. 7.10 present a much simpler problem of resolution of components by GC-MS. The spectrum of Fig. 7.18 indicated that the low temperature tar contains many overlapping types of aromatic molecule even after simplification by fractionating by column chromatography. 2D GC-MS could, in principle, be used to resolve the overlapping spectra if it was considered necessary to identify all the minor components. The complexity of the whole sample can be illustrated by comparing mass spectra from direct mass spectrometry methods, such as shown in the complex mass spectra of Fig. 7.12 for an unfractionated hydropyrolysis tar.

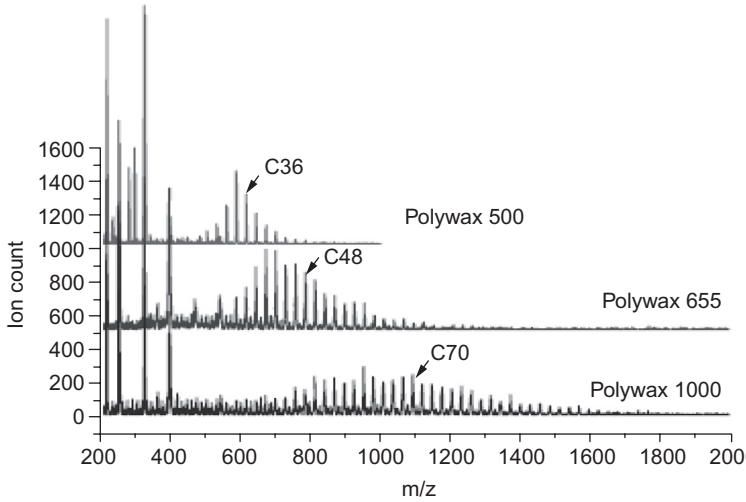

Figure 7.19 Maldi mass spectra of the Ag derivatives of the three polywax samples. *Source:* Reproduced with permission from Lorente, E., Berrueco, C., Herod, A.A., Millan, M., Kandiyoti, R., 2012. Rapid Commun. Mass Spectrom. 26(14) 1581–1590. Copyright © 2012 John Wiley & Sons, Ltd.

7.7.4 Alkanes in petroleum crudes by TLC and MALDI-MS as silver adduct ions

An alternative method to detect n-alkanes in petroleum was developed (Lorente et al., 2012) that did not involve SEC but relied on derivatisation of alkanes as urea adducts. Two crude oils, alkanes and polywax standards (500, 655 and 1000), were examined. The method avoided the sample recovery step with hot toluene in the conventional alkane isolation procedure, also provided an effective sample preparation route before analysis by MALDI-MS. Urea-alkane adducts were formed by mixing sample and urea solutions on chromatographic paper or silica coated plates. Unreacted hydrocarbons were removed by developing the plates with chloroform. In a second development with water, adducts were broken up in situ and the liberated urea removed, leaving bands of isolated alkanes behind. For MALDI-MS, strips of paper or plates, carrying the isolated alkanes, were fixed on metal target plates. The samples were treated with matrix ($AgNO_3$) and analysed by MALDI-MS. The spectra represented silver ion adducts of the isolated alkanes. Much improved MALDI-MS detection sensitivity and a wider range of masses was observed when samples were ablated from paper/plate surfaces, than by ablation from bulk samples spread over a smooth metal surface. Chromatographic paper gave better resolution and a broader range of masses than silica-coated plates. The analytical sequences were confirmed using standard alkanes (C_{20}–C_{60}) and Polywax standards. The method was useful in detecting n-alkanes to m/z 1500 (C_{100}) and required relatively small quantities of sample and reagents. It provides a promising qualitative analysis and Fig. 7.19 shows

the MALDI-mass spectra of polywax alkanes as silver adducts. The mass spectra of the derivatised alkanes from paper chromatography of the crude oil sample in comparison with the direct mass spectra of the non-adduct forming fraction indicated that some ions form from the non-adduct forming fraction and from the crude, but the derivatised alkanes are easily distinguished.

Saturates in vacuum gas oils and vacuum residues have been investigated by silver nitrate cationisation (Mennito and Qian, 2013). Standard polywaxes and saturate fractions from in-house materials were mixed with silver nitrate and cobalt powder for laser desorption silver ion (FT-ICRMS). The mass ranges of saturates were from m/z 400 to 1300 equivalent to alkyl bridged polynaphthenes with Z numbers from +2 to −24. Zhou et al. (2014) examined the saturate compounds in heavy petroleum fractions that have rarely been analysed using advanced mass spectrometry methods. The compositions of saturate fractions derived from six vacuum residua by SARA fractionation (saturates, aromatics, resins, asphaltenes), of different geological origins were determined and compared. The results showed that the saturates derived from vacuum residues consisted of n-paraffins, isoparaffins and naphthenes with 1–10 rings. Tose et al. (2015) have shown that chemical ionisation MS using iso-octane as reagent can produce high resolution mass spectra from paraffin samples up to m/z 1000, including when in the presence of crude oil; ions formed were the $(C_n H_{2n+1})$ + species.

Conclusions

GC remains pre-eminent in the chromatographic analysis of lower MM complex materials derived from fossil and biomass fuels. It gives the greatest resolution. Recent advances in column technology have both increased analysis speed and extended the MM range of possible analyses, while 2D GC offers unparalleled resolution. The inherent limitation of GC is that at temperatures at which higher MM compounds have sufficient volatility both column and analyte may be thermally degraded. The method will remain important for the determination of those lighter PACs considered to indicate the carcinogenic properties of coal-derived liquids.

Because of greater solubilities in supercritical fluids compared with those in gases, MM ranges of SFC should be greater than those attainable by GC. However, in practice, such advantages have been smaller than anticipated for PAC. The accessible MM range has increased by approximately 200 mass units. Separations are, of course, carried out at much lower temperatures in SFC than in GC (raising the temperature reduces the fluid density at a given pressure, and reduces solubility) so that thermal decomposition of analytes is not an issue. SFC analysis is more rapid than HPLC because of the greater diffusivity of supercritical fluids in comparison with gases. Future developments may require mobile phases other than carbon dioxide. Nor has HPLC greatly extended the available MM range of PAC analysis. Higher MM PACs are not soluble in the hydrocarbon solvents used in normal phase HPLC but some advances have been reported by using more polar solvents such as dichloromethane. New stationary phases are also required for which partition on to the column packing is less marked. Similar considerations apply to reverse-phase HPLC.

None of the gas or liquid chromatography methods has given sufficient resolution to allow unambiguous identification of many of the numerous components present in the complex coal, biomass or petroleum-derived liquids we have examined. GC-MS is directly useful for the estimation of the individual PAC molecules that are generally considered to present a carcinogenic hazard, such as the EPA 16. Also, the method quickly provides indications of the probable processing temperature of coal tars. The higher the temperature, the fewer the peaks and these tend to be unsubstituted aromatics with few alkyl derivatives. Tars produced at lower temperatures tend to show an underlying unresolved peak of material, as in Figs. 7.16 and 7.17B and the spectrum of Fig. 7.18. In addition, the data of Section 7.7.3 on the search for alkanes using HT-GC-MS showed that only those components soluble in pentane could pass through the GC column. Therefore all the material of these samples insoluble in pentane but soluble in toluene, acetonitrile, pyridine or NMP, could not be detected by GC methods. Mass balances for four samples shown in Table 7.4 reinforce this argument.

In these circumstances, two methods can give significant information: GC-mass spectrometric detection and 2D GC with mass spectrometry. HPLC methods have given MM information over wider ranges of mass than by GC, but compounds larger than those commonly available as standards are difficult to identify. The low-mass MALDI-MS gave mass values, shown in Fig. 7.13 and the structures likely to represent those mass values were guessed from masses of smaller standards. This is not a positive identification of molecular types for which accurate mass measurement of molecular ions is necessary. The variety of structural isomers making up each of the particular molecular ions cannot be determined by MALDI-MS and some chromatographic separation would be needed to achieve resolution of structural isomers. In Fig. 7.13 for instance, the peak at m/z 252 can be assumed to correspond to a collection of 7 isomers.

Mass spectrometric methods give valuable information on MM and molecular type either when used directly in sequence with GC, SFC or HPLC, or when used off-line in the analysis of fractions prepared by other methods, including distillation, chromatographic methods or by use of different methods of ionisation. The limitations applicable to mass spectrometric methods are generally those associated with the thermal volatility of sample. Volatility does not appear to be a problem in the case of LD-MS at low laser power. In general, off-line mass spectrometry is able to generate molecular ions for coal and petroleum-derived materials in excess of those achieved by using chromatographic methods on-line with mass spectrometry.

In view of these considerations, a chromatographic approach based on a separation principle other than partition is required for the higher MM constituents of coal derivatives. High-performance SEC satisfies this criterion since molecules of different sizes are separated according to their degree of penetration into the pores of a gel packed into a column in the form of small-diameter spheres. Elution is in reverse sequence of molecular weight. Choice of mobile phase is vital in SEC. The work described in this chapter has shown that heptane can be used to elute aliphatics with enhanced interaction of column packing and aromatic solutes, thereby allowing the unambiguous identification of aliphatics in the presence of aromatics. In contrast in the next chapter, application of more powerful solvents to SEC has allowed SEC of petroleum asphaltenes as well as coal liquids.

References

Abbott, D.J., 1995. In: Adlard, E.R. (Ed.), Chromatography in the Petroleum Industry. Elsevier, Amsterdam, p. 41.
Aczel, T., 1972. Rev. Anal. Chem. 1, 226.
Aczel, T., Lumpkin, H.E., 1979. Chapter 2 in refining of synthetic crudes. Adv. Chem. Series 179, American Chem. Soc. p.13.
Adegoroye, A., Paterson, N., Morgan, T.J., Herod, A.A., Dugwell, D.R., Kandiyoti, R., 2004. Fuel 83, 1949–1960.
Al-Muhareb, E.M., Karaca, F., Morgan, T.J., Behrouzi, M., Herod, A.A., Bull, I.D., et al., 2006. Energy Fuels 20, 1165–1174.
Al-Rabbiah, H., 2000. Thesis University of Leeds. UK.
Andersson, P.E., Demibuker, M., Blomberg, L.G., 1993. J. Chromatogr. A 641, 347–355.
Antle, P.M., Zeigler, C.D., Gankin, Y., Robbat Jr, A., 2013. Anal. Chem. 85, 10369.
Arboleda, P.H., Dettman, H.D., Lucy, C.A., 2015. Energy Fuels 29, 6686–6694.
Amador-Munoz, O., Marriott, P.J., 2008. J. Chromatogr. A 1184, 323.
ASTM, 1972. American Society for Testing Materials, Methods in Annual Year Books.
Atiku, F., Bartle, K.D., 2016. Unpublished work.
Avid, B., Purevsuren, B., Paterson, N., Zhuo, Y., Peralta, D., Herod, A.A., et al., 2004. Fuel 83, 1105–1111.
Ávila, B.M.F., Azevedo, D.A., 2012. Energy Fuels 26, 5069–5079.
Aybar, J., Firor, R. Godina, L., 2014. Proceedings 38th International Symposium on Capillary Chromatography. Paper N.10.
Bai, X., Kim, K.H., Brown, R.C., Dalluge, E., Hutchinson, C., Lee, Y.J., et al., 2014. Fuel 128, 170–179.
Barrow, M.P., Peru, K.M., Headley, J.V., 2014. Anal. Chem. 86, 8281–8288.
Bartha, A., Peters, K.C., Mullins, O.C., 2015. Energy Fuels 29 (8), 4755–4767.
Bartle, K.D., 1985. In: Bjorseth, A. Ramdahl, T. (Eds.), Handbook of Polycyclic Aromatic Hydrocarbons, vol. 2. Marcel Dekker, New York. Chapter 6.
Bartle, K.D., 1989. In: Kershaw, J.R. (Ed.), Spectroscopic Analysis of Coal Liquids. Elsevier, Amsterdam. Chapter 2.
Bartle, K.D., Myers, P., 2002.) Trends Anal. Chem. 21, 547.
Bartle, K.D., Collin, G., Stadelhofer, J.W., Zander, M., 1979. J. Chem. Tech. Biotech. 29, 531.
Bartle, K.D., Lee, M.L., Wise, S.A., 1981. Chem. Soc. Review 10, 113.
Bartle, K.D., Barker, I.K., Clifford, A.A., Kithinji, J.P., Raynor, M.W., Shilstone, G.F., 1987. Analyt. Proc. 24, 299.
Bartle, K.D., Burke, M., Mills, D.G., Pape, S., Lu, S.L., 1992. Fuel Sci. Tech. Int. 10, 1071.
Bartle, K.D., Bottrell, S., Burke, M.P., Jones, C., Louie, P.K., Lu, S.L., et al., 1994. Int. J. Energy Res 18, 299.
Bartle, K.D., Clifford, A.A., Myers, P., Robson, M.M., Sealey, K., Tong, D., et al., 2000. In: Parcher, J.F., Chester, T.L. (Eds.), Unified Chromatography; ACS Symp. Series 748. Amer. Chem. Soc., Washington DC, p. 142.
Bartle, K.D., Hall, S.R., Holden, K., Ross, A.B., 2009. Fuel 88, 348–353.
Bartle, K.D., Jones, J.M., Lea-Langton, A.R., Pourkashanian, M., Ross, A.B., Thillaimuthu, J.S., et al., 2013. Fuel 103, 835–842.
Beens, J., Brinkman, U.T., 2004. Anal. Bioanal. Chem. 378, 1939.
Begon, V., Islas, C.A., Lazaro, M.-J., Suelves, I., Herod, A.A., Dugwell, D.R., et al., 2000. Eur. J. Mass Spectrom. 6, 39–48.
Bemgard, A., Colmsjo, A., Lundmark, B.O., 1993. J. Chrom. A 630, 287.

Berger, T.A., 1995. Packed Column SFC. Royal Society of Chemistry. Ch. 11. p. 212.
Berger, T.A., 2014. J. Chrom. A 1364, 249–260.
Blomberg, J., Riemersma, T., van Zuijlen, M., Chaabani, H., 2004. J. Chromatogr. A 1050, 77–84.
Bocchini, P., Galletti, G.C., Seraglia, R., Traldi, P., Camarero, S., Martinez, A.T., 1996. Rapid Commun. Mass Spectrom. 10, 1144–1147.
Boden, A.R., Ladwig, G.E., Reiner, E.J., 2002. Polycyclic Aromatic Compounds 22, 301.
Boeker, P., Leppert, J., 2015. Anal. Chem. 87, 9033–9041.
Bottrell, S.H., Bartle, K.D., Louie, P.K.K., Taylor, N., Kemp, W., Steedman, W., et al., 1991. Fuel 70, 742–746.
Cagniant, D., Gruber, R., Lacordaire-Wilhelm, C., Schulten, H.-R., 1992. Energy Fuels 6, 694–701.
Campbell, R.M., Lee, M.L., 1986. Anal. Chem. 58, 2247–2251.
Carbognani, L., 1997. J. Chromatography A 788, 63–73.
Caslavsky, J., Kotlarikova, P., 2003. Polycyclic Aromatic Compounds 23, 327.
Challinor, J.M., 1995. J. Anal. Appl. Pyrol. 35, 93–107.
Chapman, J.R., 1993. Practical Organic Mass Spectrometry, second ed. Wiley, London.
Clifford, A.A., Ramsay, E.D. (Eds.), 1998. Analytical Supercritical Fluid Extraction Techniques. Kluwer. Ch. 1, pp. 1–42.
Collin, W.R., Bondy, A., Paul, D., Kurabayashi, K., Zellers, E.T., 2015. Anal. Chem 87, 1630–1637.
Cramers, C.A., Janssen, H.-G., van Deursen, M.M., LeClerq, P.A., 1999. J. Chromatogr. A 856, 315.
da Cunha, M.E., Schneide, J.K., Brasil, M.C., Cardoso, C.A., Monteiro, L.R., Mendes, F.L., 2013. Microchem. J. 110, 113.
da Silva, J.M., Machado, M.E., Maciel, G.P.S., et al., 2014. J. Chromatogr. A 1373, 159–168.
Davies, I.D., Raynor, M.W., Williams, P.T., Andrews, G.E., Bartle, K.D., 1987. Anal. Chem 59, 2579.
Dijkmans, T., Djokic, M.R., Van Geem, K.M., Marin, G.B., 2015. Fuel 140, 398–406.
Djokic, M.R., Dijkmans, T., Yildiz, G., Prins, W., Van Geem, K.M., 2012. J. Chromatogr. A 1257, 131–140.
Dutriez, T., Thiebaut, D., Curtiade, M., Dulot, H., Bertoncini, F., Hennion, M.-C., 2013. Fuel 104, 583–592.
Eight Peak Index of Mass Spectra, 1992. Fourth ed., Royal Society of Chemistry, Cambridge, UK.
Eisentraeger, A., Brinkmann, C., Hollert, H., Sagner, A., Tiehm, A., Neuwoehner, J., 2008. Environ. Chem. Toxicol. 27, 1590–1596.
Eiserbeck, C., Nelson, R.K., Reddy, C.M., Grice, K., 2014.. In: Grice, K. (Ed.), Principles and Practice of Analytical Techniques in the Geosciences. Royal Society of Chemistry, Cambridge. Ch. 12.
Eom, I.-Y., Kim, J.-Y., Lee, S.-M., Cho, T.-S., Yeo, H., Choi, J.-W., 2013. Bioresour. Technol. 128, 664–672.
Evans, R.J., Milne, T.A., 1987a. Energy Fuels 1, 123–137.
Evans, R.J., Milne, T.A., 1987b. Energy Fuels 1, 311–319.
Eveleigh, A., Ladommatos, N., Balachandran, R., Marca, A., 2014. Combust. Flame 161, 2966–2974.
Evershed, R.P., Jerman, K., Eglinton, G., 1985. Nature 314 (6011), 528.
Forsythe, J.C., Pomerantz, A.E., Seifert, D.J., Wang, K., Chen, Y., Zuo, J.Y., et al., 2015. Energy Fuels 29 (9), 5666–5680.

Fraga, A.R., Gaines, A.F., Kandiyoti, R., 1991. Fuel 70, 803–809.
Genuit, W.J.L., 2005. Chapter 8 Determination of organic compounds by methods using mass spectrometry. In: Nibbering, N.M.M. (Ed.), The Encyclopedia of Mass Spectrometry vol. 4 Fundamentals of and Applications to organic (and organometallic) compounds. Elsevier, Oxford, UK, pp. 781–790.
Franck, H.-G., 1955. Brennst. Chemie 36, 12–20.
Fullana, A., Contreras, J.A., Striebich, R.C., Sidhu, S.S., 2005. J. Anal. Appl. Pyrol. 74, 315.
Furbo, S., Hansen, A.B., Skov, T., Christensen, J.H., 2014. Anal. Chem. 86, 7160–7170.
Gaston, K.R., Jarvis, M.W., Pepiot, P., Smith, K.M., Frederick, W.J., Nimlos, M.R., 2011. Energy Fuels 25, 3747.
Górecki, T., Harynuk, J., Panić, O., 2004. J. Sep. Sci. 27, 359.
Grob, K., 2015. Working Safely with Hydrogen as Carrier Gas/Chromatography Information. <Restek.com>.
Guell, A.J., Li, C.-Z., Herod, A.A., Stokes, B.J., Hancock, P., Kandiyoti, R., 1993a. Proc. advances in thermochemical biomass conversion. Interlaken, Switzerland, 11–15 May 1992. Blackie, London, 2, 1053–1067.
Guell, A.J., Li, C.-Z., Herod, A.A., Stokes, B.J., Hancock, P., Kandiyoti, R., 1993b. Biomass Bioenergy 5 (2), 155–171.
Hamilton, R., Hamilton, S., 1987. Thin layer chromatography ACOL. John Wiley & Sons, Chichester, UK.
Hamilton, J.F., Lewis, A.C., Millan, M., Bartle, K.D., Herod, A.A., Kandiyoti, R., 2007. Energy Fuels 21, 286–294.
Hamming, M.C., Foster, N.G., 1972. Interpretation of Mass Spectra of Organic Compounds. Academic Press, NY.
Handley, A.J., Adlard, E.R., 2001. Gas Chromatography Techniques and Applications. Sheffield Academic Press.
Hartman, B.E., Hatcher, P.G., 2015. Fuel 156, 225–233.
He, Q., Wan, K., Hoadley, A., Yeasmin, H., Miao, Z., 2015. Fuel 156, 121–128.
Heaton, D.M., Bartle, K.D., Clifford, A.A., Myers, P., King, B.W., 1994. Chromatographia 39, 607.
Herod, A.A., 1989. Institute of Petroleum, Quarterly Journal of Technical Papers, April–June, 15–53.
Herod, A.A., 1998.. In: Neilson, A.H. (Ed.), PAHs and Related Compounds Part 3I. Springer-Verlag, Berlin, pp. 271–323. Chapter 7.
Herod, A.A., Hodges, N.J., Pritchard, E., Smith, C.A., 1983. Fuel 62, 1331–1336.
Herod, A.A., Ladner, W.R., Stokes, B.J., Berry, A.J., Games, D.E., Hohn, M., 1987. Fuel 66, 935–946.
Herod, A.A., Ladner, W.R., Stokes, B.J., Major, H.J., Fairbrother, A., 1988. The Analyst 113, 797–804.
Herod, A.A., Stokes, B.J., Radeck, D., 1991. Fuel 70, 329–340.
Herod, A.A., Stokes, B.J., Schulten, H.-R., 1993. Fuel 72, 31–43.
Herod, A.A., Stokes, B.J., Hancock, P., Kandiyoti, R., Parker, J.E., Johnson, C.A.F., et al., 1994. J. Chem. Soc. Perkin 2, 499–506.
Herod, A.A., Hellenbrand, R., Zhang, S.F., Xu, B., Kandiyoti, R., 1995a. Fuel 1995 (74), 1739–1752.
Herod, A.A., Kandiyoti, R., 1995b. J. Chromatogr. A 708, 143–160.
Herod, A.A., Islas, C.A., Lazaro, M.-J., Dubau, C., Carter, J.F., Kandiyoti, R., 1999. Rapid Commun. Mass Spectrom 13, 201–210.

Herod, A.A., 2005. Mass spectrometry of coal liquids, p790 in Chapter 8, Determination of organic compounds by methods using mass spectrometry. In: Nibbering, N.M.M. (Ed.), Encyclopedia of Mass Spectrometry, vol. 4. Elsevier.

Herod, A.A., 2012. Hydrocarbon processing: MALDI-MS of polydisperse hydrocarbon samples; Chapter 33. In: Lee, M.S. (Ed.), Mass Spectrometry Handbook. John Wiley & Sons Inc, Hoboken, NJ, pp. 725–747.

Herod, A.A., Bartle, K.D., Morgan, T.J., Kandiyoti, R., 2012. Chem. Rev 112, 3892–3923.

Holden, K., 1999. Thesis University of Leeds, UK.

Hourani, N., Sarathy, S., 2015. Energy Fuels 29 (5), 2962–2970.

Howsam, M., Jones, K.C., 1998.. In: Neilson, A.H. (Ed.), *PAHs and Related Compounds* Part 3.I. Springer-Verlag, Berlin, pp. 137–174. Chapter 4.

Hudalla, C.J., McDonald, P.D., 2012. Chromatogr. Today 5, 18–20.

ICS Reference Library, vol 33A, 1920. Properties of Gases, Mine Gases, Mine Ventilation, Geology of Coal, Rock Drilling, Explosives and Shot-Firing, Mine-Air Analysis, Geological Maps and Sections, Section 31, International Correspondence Schools Ltd., London.

Ishii, D., Takeuchi, T., 1989. J. Chromatogr. Sci. 27, 71.

Islas, C.A., Suelves, I., Carter, J.F., Herod, A.A., Kandiyoti, R., 2000. Rapid Commun. Mass Spectrom. 14, 1766–1782.

Islas, C.A., 2001. PhD Thesis. University of London.

Islas, C.A., Suelves, I., Carter, J.F., Herod, A.A., Kandiyoti, R., 2001. Rapid Commun. Mass Spectrom. 15, 845–856.

Islas, C.A., Suelves, I., Carter, J.F., Li, W., Morgan, T.J., Herod, A.A., et al., 2002. Rapid Commun. Mass Spectrom. 16, 774–784.

Islas, C.A., Suelves, I., Carter, I.E., Apicella, B., Herod, A.A., Kandiyoti, R., 2003a. Comb. Sci. Technol. 175, 775–791.

Islas, C.A., Suelves, I., Li, W., Morgan, T.J., Herod, A.A., Kandiyoti, R., 2003b. Fuel 82, 1813–1823.

Janak, J., 1995. J. Chrom. A 715 (2), 385–386.

Jarvis, M.W., Haas, T.J., Donohoe, B.S., Daily, D.W., Gaston, K.R., Frederick, W.J., et al., 2011. Energy Fuels 25, 324.

Karimi, A., Qian, K., Olmstead, W.N., Freund, H., Yung, C., Gray, M.R., 2011. Energy Fuels 25, 3581–3589.

Kelly, G., Bartle, K.D., 1994. J. High Res. Chromatogr. 17, 390.

King, R.C., Lee, M.L., Tominaga, R., Pratap, R., Iwao, M., Castle, R.N., 1982. Anal. Chem. 54, 1802.

Kithinji, J.P., Raynor, M.W., Egiu, B., Davies, I.L., Bartle, K.D., Clifford, A.A., 1990. J. High Res. Chromatogr. 13, 27.

Klatt, L.N., 1979. J. Chromatogr. Sci. 17, 225.

Knorr, A., Monge, A., Stueber, M., Stratmann, A., Arndt, D., Martin, E., et al., 2013. Anal. Chem. 2013 (85), 11216–11224.

Koolen, H.H.F., Swarthout, R.F., Nelson, R.K., 2015. Energy Fuels 29, 641–648.

Kozielska, B., Konieczynski, J., 2015. Fuel 144, 327–334.

Kühn, G., Weidner, St, Just, U., Hohner, G., 1996. J. Chromatogr. A 732, 111–117.

Le Brech, Y., Jia, L., Cissé, S., Mauviel, G., Brosse, N., Dufour, A., 2016. J. Anal. App. Pyrolysis 117, 334–346.

Lai, W.-C., Song, C., 1995. Fuel 10, 1436.

Lababidi, S., Panda, S.K., Andersson, J.T., Schrader, W., 2013. Anal. Chem. 85, 9478–9485.

Lazaro, M.J., Islas, C.A., Herod, A.A., Kandiyoti, R., 1999. Energy Fuels 1999 (13), 1212–1222.
Lea-Langton, A.R., 2012. J. Anal. Appl. Pyrol. 103, 119–125.
Lea-Langton, A.R., Andrews, G.E., Bartle, K.D., Jones, J.M., Williams, A., 2015. Fuel 158, 719–724.
Lederer, M., 1994. Chromatography for Inorganic Chemistry. John Wiley & Sons, Chichester, UK.
Lee, A.L., Bartle, K.D., Lewis, A.C., 2001. Anal. Chem. 73, 1330.
Lee, M.L., Vassilaros, D.L., White, C.M., Novotny, M., 1979. Anal. Chem. 51, 768.
Lee, M.L., Yang, F.J., Bartle, K.D., 1984. Open Tubular Column Gas Chromatography. Wiley, New York.
Li, W., Malik, A., Lee, M.L., Jones, B.A., Porter, N.L., Richter, B.E., 1995. Anal. Chem. 67, 647–654.
Lipsky, S.R., Duffy, M.L., 1986. J. High Res. Chromatogr. 9, 376.
Liu, D., Song, L., Wu, P., Liu, Y., Li, Q., Yan, Z., 2014. Bioresour. Technol. 155, 152–160.
Loegel, T.N., Danielson, N.D., Borton, D.J., Hurt, Kentamaa, H.I., 2012. Energy Fuels 26, 2850–2857.
Lombaert, K., LeMoyne, I., Tardieu, J.D.M., Amoureux, J., 2006. Combust. Sci. Technol. 178, 707–728.
Lorente, E., Berrueco, C., Herod, A.A., Millan, M., Kandiyoti, R., 2012. Rapid Commun. Mass Spectrom 26 (14), 1581–1590.
Louie, P.K.K., Bottrellm, S.,H., Steedman, W., Kemp, W., Bartle, K.D., Taylor, N., 1993. Fuel 72, 1507–1513.
Lundanes, E., Greibrokk, T., 1985. J. Chromatogr. 349, 439–446.
McLafferty, F.W., Turecek, F., 1993. Interpretation of Mass Spectra, fourth ed. University Science Books, Mill Valley, CA.
Malhotra, R., McMillen, D.F., Watson, E.L., Huestis, D.L., 1993. Energy Fuels 7, 1079–1087.
Marriott, P.J., 2001. In: Mondello, L., Lewis, A.C., Bartle, K.D. (Eds.), Multidimensional Chromatography. Wiley, Chichester, pp. 77–108. Chapter 4.
Marriott, P.J., Massil, T., Hugel, H., 2004. J. Sep. Sci. 27, 1273–1284.
Marsman, J.H., Wildschut, J., Mahfud, F., Heeres, H.J., 2007. J. Chromatogr. A 1150, 21.
Marsman, J.H., Wildschut, J., Evers, P., de Koning, S., Heeres, H.J., 2008. J. Chromatogr. A 1188, 17.
McRae, C., Sun, C.G., McMillan, C.F., Snape, C.E., Fallick, A.E., 2000. Polycycl. Aromat. Compd 20, 97–109.
Menéndez, R., Blanco, C., Santamaría, R., Domínguez, A., Blanco, C.G., Suelves, I., et al., 2002. Energy Fuels 16, 1540–1549.
Mennito, A.S., Qian, K., 2013. Energy Fuels 27 (12), 7348–7353.
Millan, M., Morgan, T.J., Behrouzi, M., Karaca, F., Galmes, C., Herod, A.A., et al., 2005. Rapid Commun. Mass Spectrom. 19, 1867–1873.
Mogollon, N.G.S., Prata, P.S., Agosto, F., 2014. Chromatogr. Today, 3–6.
Mohan, D., Pittman Jr., C.U., Steele, P.H., 2006. Energy Fuels 20, 848–889.
Mol, H.G.J., Hankemeier, T., Brinkman, U.A.T., 1999. LC-GC Intern. 12, 108–111.
Montiano, M.G., Fernández, A.M., Díaz-Faes, E., Barriocana, l C., 2015. Fuel 154, 261–267.
Morgan, T.J., Kandiyoti, R., 2014. Chem. Rev. 114 (3), 1547–1607.
Morgan, T.J., Turn, S.Q., George, A., 2015. PLoS ONE 10 (8), e0136511.
Morlock, G.E., 2012. High performance thin-layer chromatography-mass spectrometry for analysis of small molecules. Chapter 49. In: Lee, M.S. (Ed.), Mass Spectrometry Handbook. John Wiley & Sons, Hoboken, NJ, pp. 1181–1206.

Mossner, S.G., Wise, S.E., 1999. Anal. Chem. 71, 58–69.
Ni, H., Hsu, C.S., Shi, Q., Xu, C., 2013. Energy Fuels 27, 5069–5075.
Novotny, M., Hirose, A., Wiesler, D., 1984. Anal. Chem. 56, 1243.
Oja, V., 2015. Fuel 159, 759–765.
Olcese, R., Carré, V., Aubriet, F., Dufour, A., 2013. Energy Fuels 27, 2135.
Ortiz, X., Jobst, K.J., Reiner, E.J., Backus, S.M., Peru, K.M., McMartin, D.W., et al., 2014. Anal. Chem. 86, 7666–7673.
Owen, J., 1979. In: Pitt, G.J., Millward, G.R. (Eds.), Coal and Modern Coal processing: An Introduction. Academic Press, London. Chapter 9.
Parker, J.E., Johnson, C.A.F., John, P., Smith, G.P., Herod, A.A., Stokes, B.J., et al., 1993. Fuel 72, 1381–1391.
Pernyeszi, T., Dekany, I., 2001. Colloid Surf 194, 24–39.
Peterson, A.C., Hauschild, J.-P., Quarmby, S.T., Krumwiede, D., Lange, O., Lemke, R.A.S., et al., 2014. Anal. Chem 86, 10036–10043.
Phillips, J.B., Venkatramani, C., 1993. J. Microcolumn Sep. 5, 511–516.
Pindoria, R.V., Lim, J.-Y., Hawkes, J.E., Lazaro, M.-J., Herod, A.A., Kandiyoti, R., 1997b. Fuel 76, 1013–1023.
Pipatmanomai, S., Islas, C.A., Suelves, I., Herod, A.A., Kandiyoti, R., 2001. J. Anal. Appl. Pyrol. 58, 299–313.
Podgorski, D.C., Hamdan, R., McKenna, A.M., Nyadong, L., Rodgers, R.P., Marshall, A.G., et al., 2011. Anal. Chem. 84 (3), 1281–1287.
Purevsuren, B., Herod, A.A., Kandiyoti, R., Morgan, T.J., Avid, B., Gerelmaa, T., et al., 2004a. Fuel 83, 799–805.
Purevsuren, B., Herod, A.A., Kandiyoti, R., Morgan, T.J., Avid, B., Davaajav, Ya, 2004b. Eur. J. Mass Spec. 10, 101–108.
Purón, H., Luis Pinilla, J., Berrueco, C., Montoya de la Fuente, J.A., Millán, M., 2013. Energy Fuels 27, 3952–3960.
Quimby, B.D., Sullivan, J.D., 1990. Anal. Chem. 62, 1027–1033.
Reddy, K.M., Wei, B., Song, C., 1998. Catal. Today 43, 187–202.
Robinson, N., Evershed, R.P., Higgs, J., Jerman, K., Eglinton, G., 1987. The Analyst 112, 637.
Romanowski, T., Funcke, U., Grossman, I., Konig, I., Balfanz, E., 1983. Anal. Chem. 55, 1030.
Ross, A.B., Junyapoon, S., Bartle, K.D., Jones, J.M., Williams, A., 2001. J. Anal. Appl. Pyrol. 58–59, 371–385.
Ross, A.B., Lea-Langton, A.R., Fitzpatrick, E.M., Jones, J.M., Williams, A., 2011. Energy Fuels 25, 2945–2955.
Ruddy, B.M., Lobodin, V.V., Bythell, B.J., McKenna, A.M., Rodgers, R.P., 2014. Energy Fuels 28 (6), 4043–4050.
Rudzinski, W.E., Aminabhavi, T.M., 2000. Energy Fuels 14, 464–475.
Rüger, C.P., Miersch, T., Schwemer, T., Sklorz, M., Zimmermann, R., 2015. Anal. Chem. 87, 6493–6499.
Saini, A.K., Song, C., 1994. Amer. Chem. Soc. Div. Fuel Chem. 39 (3), 796.
Schafer, W., 1993. J. High Res. Chromatogr. 16 (11), 674–676.
Sfetsas, T., Michailof, C., Lappas, A., Li, Q., Kneale, B., 2011. J. Chromatogr. A 1218, 3317.
Sharriff, S.M., Tong, D., Bartle, K.D., 1994. J. Chromatogr. Sci. 32, 541.
Sharriff, S.M., Robson, M.M., Bartle, K.D., 1997. Polycyclic Aromat. Compd. 12, 147.
Shariff, S.M., Robson, M.M., Myers, P., Bartle, K.D., Clifford, A.A., 1998. Fuel 77, 927–931.
Shellie, R., Marriott, P., Leus, M., Dufour, J.-P., Sun, K., Winniford, B., et al., 2003. J. Chromatogr. A 1019, 273–278.

Scott, A.C., Fleet, A.J. (Eds.), 1994. Coal and Coal-bearing Strata as Oil-prone Source Rocks? The Geological Society, London. Geological Society Special Publication no. 77.
Sim, A., Cho, Y., Kim, D., Witt, M., Birdwell, J.E., Kim, B.J., et al., 2015. Fuel 140, 717–723.
Skaar, H., Norli, H.R., Lundanes, E., Greibrokk, T., 1990. J. Microcol. Sepn. 2, 222–228.
Smit, E., Rüger, C.P., Sklorz, M., De Goede, S., Zimmermann, R., Rohwer, E.R., 2015. Energy Fuels 29 (9), 5554–5562.
Smith, E.A., Thompson, C., Lee, Y.J., 2014. Bull Korean Chem. Soc. 35 (3), 811.
Snape, C.E., Ladner, W.R., Bartle, K.D., 1985. Fuel 64, 1394–1400.
Song, C., Schobert, H.H., Hatcher, P.G., 1992. Amer. Chem Soc. Div. Fuel Chem 37 (2), 638–645.
Sun, M., Ma, X.-x, Lv, B., Dai, X.-M, Yao, Y., Liu, Y.-Y, et al., 2015. Fuel 160, 16–23.
Takagama, Y., Takeichi, T., Kawai, S., 1988. J High Res. Chromatogr. 11, 732.
Tancell, P.J., Rhead, M.M., 1996. J. Chromatogr. A 787, 181–192.
Tessarolo, N.S., dos Santos, L.R.M., Silva, R.S.F., Azevedo, D.A., 2013. J. Chromatogr. A 1279, 68.
Tomasini, D., Cacciola, F., Rigano, F., Sciarrone, D., Donato, P., Beccaria, M., et al., 2014. Anal. Chem. 86, 11255–11262.
Tong, D., Bartle, K.D., Robinson, R.E., Altham, P., 1993. J. Chromatogr. Sci. 31, 77–81.
Tong, D., Bartle, K.D., Clifford, A.A., Robinson, R.E., 1995. Analyst 120, 2461.
Touchstone, J.C., 1992. Practice of Thin Layer Chromatography, third ed. John Wiley & Sons Inc, New York.
Tose, L.V., Cardoso, F.M.R., Fleming, F.P., Vicente, M.A., Silva, S.R.C., Aquije, G.M.F.V., et al., 2015. Fuel 153, 346–354.
Tran, T.A., Gibbs-Hall, I., Young, P.J., Thompson, J.D., Stoll, D.R., 2013. Anal. Chem. 85, 11817–11825.
Tranchida, P.Q., Salivo, S., Franchina, F.A., Mondello, L., 2015. Anal. Chem. 87, 2925–2930.
Trestianu, S., Zilioli, G., Scironi, A., Saravelle, C., Munari, F., Galli, M., et al., 1985. J. High Res. Chromatogr 8, 771.
Tromp, P.J.J., Moulijn, J.A., Boon, J., 1988. In: Yurum, Y. (Ed.), New Trends in Coal Science. Kluwer Academic Publishers, pp. 241–269.
Tromp, P.J.J., Moulijn, J.A., Boon, J., 1989. J. Anal. Appl. Pyrolysis 15, 319–331.
Vassilaros, D.L., King, R.C., Later, D.W., Lee, M.L., 1982. J. Chromatogr. 252, 1.
von Muhlen, C., Ecole, E., Oliveira, P.C., Morrison, P.D., 2007. J. Sepn Sci, 3223–3232.
Wallace, S.H., Bartle, K.D., Kemp, W., Steedman, W., Flynn, T., Burke, M.P., et al., 1990. Fuel Proc. Technol. 24, 225–230.
Walton, S.T., 1993. Fuel 72, 687.
Watson, J.T., Sparkman, O.D., 2005. Chapter 7, Rules for mass spectral interpretation: the standard interpretation procedure. In: Nibbering, N.M.M. (Ed.), The Encyclopedia of Mass Spectrometry vol 4 Fundamentals of and Applications to Organic (and organometallic) Compounds. Elsevier, Oxford, UK, pp. 719–731.
Watson, J.S., 2012. Application of GC x GC-TOFMS to the characterization of extraterrestrial organic matter. Chapter 18. In: Lee, M.S. (Ed.), Mass Spectrometry Handbook, 2012. John Wiley & Sons, Hoboken, NJ, pp. 407–415.
Wilde, M.J., Rowland, S.J., 2015. Anal. Chem. 87, 8457–8465.
Wilson, R., Johnson, C.A.F., Parker, J., Herod, A.A., 1987. Organic Mass Spectrom. 22, 115–116.
Wise, S.A., 1983. In: Bjorseth, A. Ramdahl, T. (Eds.), Handbook of Polycyclic Aromatic Hydrocarbons, vol. 1. Marcel Dekker, New York. Ch 5.

Wise, S.A., 1985. In: Bjorseth, A. Ramdahl, T. (Eds.), Handbook of Polycyclic Aromatic Hydrocarbons, vol. 2. Marcel Dekker, New York. Ch 5.
Wise, S.A., 2002. Polycyclic Aromatic Compounds 22, 197.
Wood, K.V., Albright, L.F., Brodbelt, J.S., Cooks, R.G., 1985. Analytica Chimica Acta 173, 117–127.
Yan, L., Bai, Y., Zhao, R., Li, F., Xie, K., 2015. Fuel 145, 12–17.
Zhang, Y., Zhang, L., Xu, Z., Zhang, N., Chung, K.H., Zhao, S., et al., 2014. Energy Fuels 28 (12), 7448–7456.
Zeng, Y., Seeley, J.A., Dowling, T.M., Uden, P.C., 1992. J. High Res. Chromatogr. 15 (10), 669–676.
Zhou, X., Zhang, Y., Zhao, S., Chung, K.H., Xu, C., Shi, Q., 2014. Energy Fuels 28, 417–422.
Zoccali, M., Quinto Tranchida, P., Mondello, L., 2015. Anal. Chem. 87, 1911–1918.

Analytical techniques for high-mass materials: method development

8

Chapter Outline

Solid Fuels and Heavy Hydrocarbon Liquids. DOI: http://dx.doi.org/10.1016/B978-0-08-100784-6.00008-4

8.1 Introduction

In Chapter 7, Analytical techniques for low mass materials: method development, we examined techniques available to analytical chemistry for examining coal, petroleum and biomass-derived oils, tars and extracts. Typically, these are materials recovered during the pyrolysis, gasification, and liquefaction experiments described in Chapter 3, Pyrolysis of solid fuels: experimental design and applications, Chapter 4, High-pressure reactor design: pyrolysis, hydropyrolysis and gasification, Chapter 5, Liquefaction: thermal breakdown in the liquid phase, Chapter 6, Elements of thermal breakdown: heating rate effects and retrogressive reactions. Large proportions of such samples are of molecular masses above the ranges amenable to analysis by the methods reviewed in Chapter 7, Analytical techniques for low mass materials: method development.

In this chapter, we consider analytical methods able to characterise materials, which lie beyond the range of such standard techniques, with masses greater than 500 u. We first outline developments in bulk methods for mass estimation, starting with size exclusion chromatography (SEC).

We will next describe mass spectrometric methods likely to ionise and detect materials with molecular masses above the m/z 500 range, normally beyond the working range of mass spectrometric methods of the previous chapter. Methods described in the present chapter are usually applied following sample fractionation and involve several different combinations of sample introduction methods into the mass spectrometric system (e.g., liquid chromatography, thin layer chromatography (TLC)). The ionisation techniques involved include desorption chemical ionisation (DCI), field ionisation (FI), field desorption (FD), fast atom bombardment (FAB), plasma desorption (PD), matrix assisted laser desorption/ionisation (MALDI)—and laser desorption (LD) mass spectrometry, and electrospray ionisation (ESI). Units of molecular mass based on the unified atomic mass scale (^{12}C) are shown as u (Mills et al., 1993) rather than the alternative Dalton (Da), while masses determined by mass spectrometric methods are shown as mass to charge ratio (m/z).

Structural features of these larger molecular mass materials have been examined with methods such as UV-fluorescence spectroscopy, NMR and FT-IR. Examples presented below have been selected from the examination of coal liquids, soots, petroleum products and distillation residues, biomass tars and kerogens. Previous reviews include Zhuo et al., 2003; Herod et al., 2003, 2012; Herod 2005; Zubkova, 2011; Morgan and Kandiyoti, 2014.

8.2 The SEC of complex mixtures

SEC has been the subject of periodic reviews (Barth et al., 1996, 1998; Zubkova, 2011; Herod et al., 2012; Morgan and Kandiyoti, 2014). Kostanski et al. (2004) have reviewed calibration methodologies. SEC depends for its action on the absence of interaction with the surface of the column packing material and only depends on the ability of material with different molecular sizes to penetrate the porosity of the column-packing. The largest size molecules elute first because they cannot penetrate the porosity and elute through the inter-particulate voids of the column; the smallest molecules that can penetrate the smallest porosity of the packing elute last and define the permeation limit of the column. No part of any sample should elute after the permeation limit in true SEC. The measure of molecular size is the hydrodynamic volume in the solvent used to elute the column, which depends on solvation effects and this may not necessarily equate with molecular mass. The solvent used must be able to completely dissolve the sample and be sufficiently polar to minimize surface interactions between sample and column packing material.

Parameters that define SEC include the void volume (the earliest possible time or elution volume that corresponds to the elution of the largest size molecules through the column void volume), the permeation limit (the latest time or greatest elution volume required for elution of small molecules), number average molecular weight (M_n), weight average molecular weight (M_w) and peak average molecular weight (M_p). Polydispersity is defined as M_w/M_n and serves as an index of the breadth of the molecular weight distribution. For a sample of narrow polydispersity ($M_w/M_n < 1.1$) it may be expected that $M_n \sim M_w \sim M_p$.

The following equations define M_n and M_w:

$$M_n = \Sigma_i n_i M_i / \Sigma_i n_i \text{and } M_w = \Sigma_i n_i M_i^2 / \Sigma_i n_i M_i,$$

where n_i is the number of molecules in the ith elution volume interval of mass M_i.

SEC is the liquid chromatographic method most suitable for this purpose but has the drawback that calibration of the relation between molecular size and elution time or elution volume must be achieved by using standard molecules. The method also assumes that the calibrant and analyte molecules have the same relation between molecular size and molecular mass. For tar and asphaltene components of mass greater than 500 u, this presents difficulties because the molecular structures are not generally known. The extrapolation of molecular structures from aromatics known from gas chromatography, by addition of successive benzo groups (replacement of 2 H by $-C_4H_4-$, net mass increase 50 u), a methene bridge (replacement of 2 H by $-CH_2-$, net addition of 12 u), ethylene bridges (replacement of 2 H by -CH = CH-, net addition of 24 u) or ethyl bridges (replacement of 2 H by $-CH_2-CH_2-$, net addition 26 u), leads to structures too highly aromatic in relation to the bulk atomic composition of the sample. In the case of the coal tar pitch used for some of the work described below, the C/H ratio is 1.9, whereas for structures such as coronene, the C/H ratio is 2. For ovalene the ratio is 2.28 and increases for more

condensed structures. This has also been discussed in the context of NMR studies described in Section 8.8.

Distributions of molecular masses in coal- and petroleum-derived liquids are relevant to research in fields as diverse as catalytic hydrocracking and environmental pollution diagnostics. Recent work (Herod et al., 2000a, 2012; Morgan et al., 2005c, 2008a, 2009, 2010a; Morgan and Kandiyoti, 2014) has developed tools for the characterization of 'heavy' coal liquids and petroleum asphaltenes through the parallel use of SEC and laser-desorption mass spectrometry. Progress in the parallel use of these two independent techniques has provided evidence for the presence of high-mass materials in coal and petroleum derived samples. The mass spectrometric work is described below in Sections 8.6 and 8.7, with evidence from supporting techniques in Section 8.9.

The use of SEC in the estimation of molecular mass ranges of hydrocarbon mixtures relies on the assumption that the sizes of standard molecules or polymers relate to the sizes of the sample molecules of similar molecular masses. The general principles of the method have been given (Wu, 1995; Kostanski et al., 2004). For a fraction of narrow molecular mass range, the peak mass (M_p) in SEC approximates to both M_n and M_w. Polymer standards of narrow polydispersity ($M_w/M_n < 1.1$) tend to show linear relations between $\log_{10}$ molecular mass and elution time (or elution volume) over wide ranges of mass. In principle, a universal calibration can be applied to SEC where a graph of log 10 ([ή]M_n) against elution time or volume ([ή] is the intrinsic viscosity) should account for the elution behaviour of all polymers in a given solvent. Malawer (1995) and Kostanski et al. (2004) have given detailed discussions of the method.

The major problem with the estimation of molecular mass ranges of coal liquids or petroleum distillation residues is that the upper mass limit is undefined and unknown. Accordingly, it is necessary to assemble evidence from as many sources as possible to enable comparisons to be made with the intent of reaching some indication of what the upper limits may be. SEC is not limited by volatility considerations but is limited by sample solubility in the chosen solvent.

8.2.1 Summary of previous SEC work in solvents (eluents) other than NMP

Much of the early SEC work on coal-derived materials was carried out using tetrahydrofuran (THF) as eluent (Bartle et al., 1983, 1984, 1986). Solutions of coal extract subfractions in THF had intrinsic viscosities very close to that of the solvent and the procedure of universal calibration for SEC in THF was considered experimentally unreliable (Bartle et al., 1984). Characterization work on pyrolysis tars and liquefaction extracts (Bartle et al., 1983, 1984, 1986) by SEC, using THF as eluent, indicated that the upper limit of molecular masses (MMs) was in the range 4000–6000 u (Li et al., 1993a,b, 1994a). These results were comparable with those from similar research involving the use of SEC coupled to calibrations based on the vapour pressure osmometry (VPO) of coal-derived liquid fractions. The use of pyridine as eluent (Boenigk et al., 1990) led to average mass values up to 2500 u, while Larsen and coworkers (Larsen and Wei, 1988; Nishioka and Larsen, 1990) reported average MM-values of 5050 u, with indications of masses up to possibly 15,000 u.

However, neither THF nor pyridine completely dissolve many common coal-derived liquids. When using either THF or pyridine as eluent, the progressive increase in back pressure across SEC-columns has been widely recognised as a symptom of partial sample precipitation out of solution. Clearly, some of the higher molecular mass and/or most polar materials were not observed by SEC in THF and in pyridine. Insufficient solvent power leads to adsorption effects between solute and column packing, known to distort chromatograms (Yau et al., 1979) and lead to smaller apparent MM-distributions. The shortcomings of still weaker solvents, such as toluene, chloroform, dichloromethane, benzonitrile and dimethylformamide, have been reviewed by Johnson et al. (1998) and Paul-Dauphin et al. (2007). It does not appear possible to dissolve coal tars or extract samples in these solvents completely. Results from any solution-based technique, obtained with samples dissolved in the latter solvents, must therefore be regarded as reflecting only the more soluble parts of the samples. For asphalts however, THF solvent dissolves all the material and SEC in THF (Davison et al., 1995) showed an excluded peak, which concentrated the material of the high molecular mass fractions. The association of the sample in solvents used for VPO was clearly demonstrated by an increase of apparent molecular mass in less polar solvents (Davison et al., 1995). The dissociation with time in solution in dichloromethane of asphaltene aggregates has been observed in SEC as the shifting of the relative intensities of peaks from early- to late-eluting (Strausz et al., 2002). Sato et al. (2005) have shown that chloroform in use as SEC eluent and calibrated using polystyrene (PS) standards, significantly underestimated the molecular masses of asphaltene molecules reported as below m/z 800.

These necessarily incomplete data from SEC suggested that coal tars or extracts contained significant proportions of material with MMs above 1000 u and that smaller amounts of these materials could have molecular masses well above 5000 u. However, results from SEC using THF or pyridine as eluent have often (and justly) been criticised for the structure-dependence of measured retention volumes, inaccuracies inherent in VPO-based calibrations at high MMs and the scarcity of model compounds above 300 u that could be used as calibrants. Confirmation of results from SEC by independent techniques was also clearly necessary, but much of the early work based on mass spectrometric methods did not show molecular masses much above 1000–1200 u (e.g., cf. Larsen and Wei, 1988).

Problems encountered with THF included surface interactions between packing and sample molecules and partial precipitation of sample with attendant gradual increases in column back pressure (Herod et al., 1995a, 1996b). These problems with THF led to its replacement by NMP (1-methyl-2-pyrrolidinone) for coal-derived samples, and mixed with chloroform for petroleum asphaltenes (Herod et al., 1995a, 1996b, 2012; Paul-Dauphin et al., 2007; Morgan and Kandiyoti, 2014).

8.2.2 SEC using NMP as solvent

NMP was first used as eluent in SEC by Lafleur and Nakagawa (1989) using a polydivinylbenzene column at ambient temperature, which allowed the detection of a large peak near the exclusion limit of the column in the pyridine extracts of coals.

The conclusion from the work was that materials observed at or near the exclusion limit of the column were aggregates of smaller, polar molecules, held together by ionic forces and not as evidence of large molecular mass materials. Subsequent work outlined below has shown that this is not the case.

The solids that had precipitated in and were blocking a guard column during use with THF were recovered by solution in NMP, giving a black solution that contained mainly large molecules in SEC with NMP as eluent (Herod et al., 1995a). Meanwhile, NMP appears to completely dissolve most coal-derived 'liquids' investigated, including a coal tar pitch, which is normally a solid at room temperature (Guillen et al., 1991; Morgan et al., 2008b). Extended periods of column use with NMP have not led to the buildup of backpressure in the SEC columns utilized.

The SEC columns used in work outlined below include Polymer Laboratories (Church Stretton, UK) Mixed-Bed columns labelled as 'Mixed-E', 'Mixed-D' and 'Mixed-A'. The columns were packed with progressively larger (3, 5 and 20 μm diameter, respectively) particles of PS/polydivinylbenzene copolymer with different ranges of porosity (not specified by the manufacturer). These porosity ranges give linear relations between $\log_{10}$ molecular mass of polystyrene (PS) standards and elution time (min), from low-mass to 30,000 u (Mixed-E), from 200 to 400,000 u (Mixed-D), and from 1000 to 40 million u (Mixed-A) when using THF as eluent. Meehan (1995) has described the behaviour of these columns in use with THF.

When using NMP as eluent, the Mixed-E column was operated at 85°C and a flow rate of 0.45 mL min^{-1}. The Mixed-D column was operated at 80°C and a flow rate of 0.5 mL min^{-1}, while the Mixed-A column operated at ambient temperature and a flow rate of 0.5 mL min^{-1}. Detection was by UV-absorbance at 280, 300, 350, 370 and 450 nm. The use of an evaporative light scattering (ELS) detector and other details of operation have been given elsewhere (Zhang et al., 1997b, Lazaro et al., 1999b, Herod et al., 2000a, Islas et al., 2001c, 2002b; Morgan et al., 2009).

An important feature of SEC results described below (e.g., Islas et al., 2003b; Morgan et al., 2009) as well as in the original work (Lafleur and Nakagawa, 1989) was the appearance of an early-peak eluting by exclusion from the porosity of the column, with a second peak consisting of material able to penetrate the porosity of the column packing. This bimodal distribution is a standard feature of SEC using NMP and raises two important questions: (1) is the early peak formed by very large molecules or by aggregates of small polar molecules or is there another mechanism at play? (2) What is the significance of the valley between the two peaks? These questions are addressed below, in sections on calibration and aggregation.

PS molecular mass standards up to 15×10^6 u, polymethyl-methacrylate standards up to 1×10^6 u, and polysaccharide (PSAC) standards up to 788,000 u have eluted in NMP with apparently minimum interference from surface effects (Islas et al., 2001b). The PSAC standards eluted at earlier times than PS or polymethylmethacrylates (PMMA) standards of similar mass, presumably due to differences in hydrodynamic volumes in solution. In some preliminary work with NMP, the use of a triple detector has been attempted (courtesy of Viscotek UK). However the viscosity detector element of the system failed to produce any signal for coal tars or their high-mass fractions including pitch, coal extract, and a low-temperature tar, or for asphaltenes from

petroleum residues, biomass tars, amber extracts or from soots although a signal was detected from PS standard polymers. In this unpublished work (Herod and Kandiyoti, 2000) one element of the detector system was a refractive index detector and because this is insensitive relative to UV-absorbance, highly concentrated solutions (5–20 mg mL^{-1}) were injected onto the SEC column to signal on the RI detector.

In this type of work, the initial aim is to obtain a calibration, which provides reasonable estimates of molecular mass distributions of heavy hydrocarbon liquids, irrespective of their origins and of the structural features of their components. To the extent that such samples contain multiplicities of molecules with different and largely ill-defined structural features, it is important to minimize the level of structure dependence of elution times. The aim of the work described below was to obtain calibration curves for two SEC-columns, using NMP as eluent, and to test the level of dependence of the calibrations on chemical structures.

Calibration with polymers: In SEC, a calibration curve is prepared by measuring the elution times of a set of polymer standards of known molecular mass and of low polydispersity such as a set of PS standards (Vander Hayden et al., 2002). The curve is obtained by plotting the logarithms of the known molecular masses ($\log_{10}$MM) against their elution times.

Fig. 8.1 presents calibration data ($\log_{10}$MM vs elution time) for the Mixed-A column; analogous calibration data for the Mixed-D column was qualitatively similar and is not shown. Three sets of polymer standards with known MMs were used to calibrate both the Mixed-D and Mixed-A columns: PS, PMMA and PSAC, the latter with masses up to 788,000 u. An ELS detector was used when working with the PMMA and PSAC samples, which do not contain UV-absorbing chromophores. The linear part of the calibration plot corresponds to the molecular size range resolved by the particular SEC-column. At the high-mass end, the void volume represents the shortest possible elution time. Exclusion limits of the two columns are indicated by

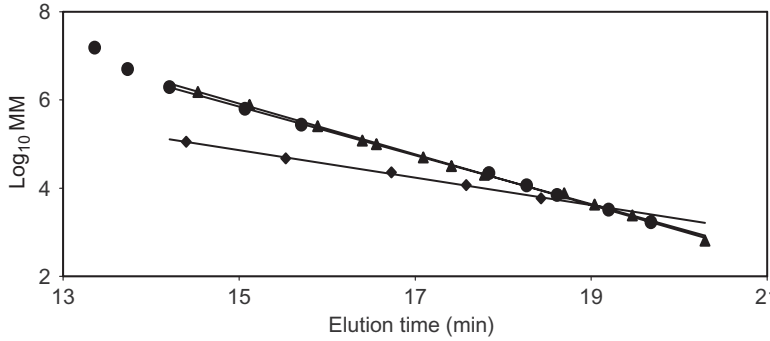

Figure 8.1 Calibration of Mixed-A column using polymers: (●) polystyrene; (▲) polymethylmethacrylates; (♦) polysaccharides.
Source: Reprinted with permission from Karaca, F., Islas, C.A., Millan, M., Behrouzi, M., Morgan, T.J., Herod, A.A., et al., 2004. Energy Fuels 18, 778–788. Copyright 2004 American Chemical Society.

the onset of departure from linearity at the short elution time end of the straight line. This occurred at ~14 min for the Mixed-A column, just short of the largest commercially available PS standard of 15 million u (Fig. 8.1) and ~10 min for the Mixed-D column at a mass between ~200,000 and 400,000 u (not shown) (Lazaro et al., 1999b; Herod et al., 2000a; Apicella et al., 2002).

These data show that in both columns, the elution times of PS and PMMA standards up to masses of ~1.5 million u were statistically nearly indistinguishable (Islas et al., 2001b). In view of the structural differences between PS and PMMA standards, these findings were encouraging. However, the elution times of the highly oxygenated PSAC samples traced a different curve. To the extent that elution times reflected structural differences between PSAC and the other two sets of standards, the present column/eluent combination cannot be said to have operated in a fashion independent of chemical structure. Considering Fig. 8.1 in detail, closer agreement was observed between the three calibration lines at longer elution times (smaller MMs). The data were nearly indistinguishable at 19–20 min, but differed by a factor of ~1.8 at 18 min (~15.5×10^3 u vs 8.5×10^3 u) and by a factor of between 12 and 15 at 14.5 min: ~1.34×10^6 u for PS and 1.61×10^6 u for PMMA compared to 0.104×10^6 u for PSAC. To put these elution times into context, 18 min corresponded to the forward edge of the resolved peak in pitch (see discussion in Section 8.4.1 for pitch fractions), while 14.5 min was on the low-mass tail of the excluded peak. System specific calibration equations (not shown) may be formulated to provide estimates of the masses for unknown materials, based on the molecular masses of the standard polymer eluting at the same time.

These results show the necessity for caution in the levels of confidence attached to quantitative estimates of molecular masses of structurally less well-defined samples when using the PS-PMMA calibration line. However, the structural differences between hydrocarbon liquids (the main focus in much of this work) and the PSAC-polymers are quite marked. The results also show that below 15×10^3 u, even the MMs of PSACs, may be estimated to within a factor of ~2–2.5. Clearly, quantitative determinations appear subject to increasing uncertainty with increasing MM. These low levels of precision of mass measurement bear no relation to the mass measurement achieved by working with GC-MS and other high precision methods of analysis. However, many materials lie outside the reach of these well-known techniques and SEC is useful in attempting to assess and compare the ranges of MMs of heavier samples.

Calibration with standard polymer molecules: Fig. 8.2 presents plotted elution times determined using the Mixed A column for several different types of polymers of wider polydispersity than the calibration standards that have already been discussed. These standards were characterised by peak average molecular weight M_p: polyethylene oxide (M_p 58,400 polydispersity 1.03) and polyethylene glycol (M_p 4120, polydispersity 1.02) from Polymer Laboratories; poly-N-vinylcarbazole (M_p 90,000), two different samples of polyvinylpyrrolidinone (M_p 3500 and 58,000), polyvinylacetate (M_p 170,000), and polyethylene adipate (M_p 10,000) from Acros Organics, supplied by Fisher Scientific of Loughborough, UK. Polydispersities of the latter samples were not supplied but were expected to be greater than the polydispersity (1.04) of the PS and PMMA standards. Fig. 8.2 shows the elution times of these

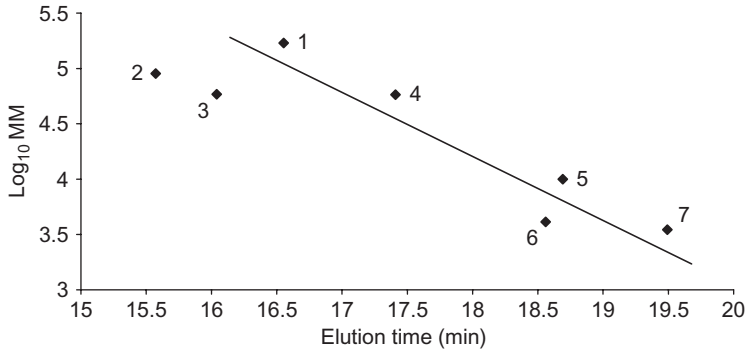

Figure 8.2 Miscellaneous polymers and polystyrene calibration line on Mixed A column; (1) Polyvinylacetate, Mp 170,000; (2) Poly(N-vinylcarbazole), Mp 90,000; (3) Poly(ethylene oxide), Mp 58,400; (4), Poly(vinylpyrrolidinone), Mp 58,000; (5) Polyethylene adipate, Mp 10,000; (6) Poly(ethylene glycol), Mp 4120; (7) Poly(vinylpyrrolidinone), Mp 3500.
Source: Reprinted with permission from Karaca, F., Islas, C.A., Millan, M., Behrouzi, M., Morgan, T.J., Herod, A.A., et al., 2004. Energy Fuels 18, 778–788. Copyright 2004 American Chemical Society.

seven polymeric MM-standards plotted alongside the PS-PMMA calibration line of the Mixed-A column.

The interest in these samples arises because of their considerable structural differences from PSs, PMMAs and PSACs. Of the seven polymer standards, four eluted within half a minute of the calibration line, despite polydispersities greater than those of the PSs and PMMAs. Only poly-N-vinylcarbazole (90,000 u) eluted ~1.2 min early, indicating nearly an order of magnitude difference with the calibration line, between ~100,000 and 1×10^6 u. The two oxygenates, polyethylene-oxide and polyethylene-glycol also eluted early compared to the straight line, the first by nearly a minute, and the second by less than half a minute. Comparing Fig. 8.1 to results for these polymers of different structures helps put differences between the PS-PMMA and the PSAC calibration lines into a broader context. The smaller deviations observed in Fig. 8.2 suggest that to a first approximation, we might consider deviations between the PSAC and PS-PMMA lines in both Mixed A and D columns as an upper limit to levels of error arising from the structure dependent variations in the elution behaviour of these samples. In other work (Apicella et al., 2003b) using a Mixed-D column, NMP eluent and PS calibration, showed that polyacenaphthylene of mass 5000–10,000 eluted very close to the PS calibration line.

Calibration with small molecules: The linear mass range quoted for the Mixed-A column by the manufacturers is between 1000 and 10 million u. This column would not normally be selected for resolving mixtures of relatively small molecules. It is necessary to understand the elution behaviour of small molecules in order to interpret signal observed at long elution times during the characterization of complex mixtures.

Fig. 8.3 shows the elution times of 11 model compounds plotted alongside the PS calibration line for the Mixed A column. Consistent with the behaviour of highly

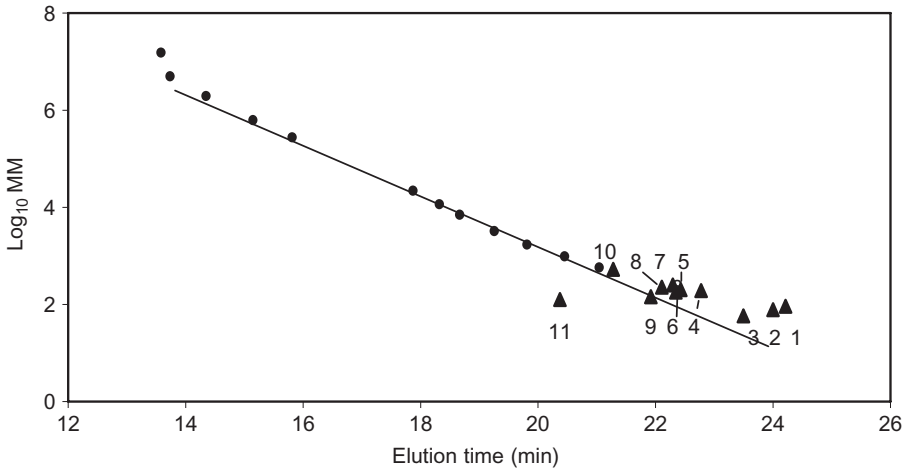

Figure 8.3 Elution times of small molecules on Mixed-A column versus polystyrene calibration; compounds are: 1—Toluene (92); 2—Benzene (78); 3—Acetone (58); 4—9-Methyl anthracene (192); 5—Fluoranthene (202); 6—5,6-Benzoquinoline (179); 7—Perylene (252); 8—Chrysene (228); 9—2,3-Dimethylindole (145); 10—Rubrene (532); 11—Pyrogallol (126). Molecular masses in parentheses.
Source: Reprinted with permission from Karaca, F., Islas, C.A., Millan, M., Behrouzi, M., Morgan, T.J., Herod, A.A., et al., 2004. Energy Fuels 18, 778–788. Copyright 2004 American Chemical Society.

oxygenated PSAC samples, pyrogallol eluted earlier than expected. Many of the other samples eluted at about 0.5 min longer than predicted by extrapolating the PS-calibration line. Acetone and anthracene eluted with slightly less than ~1 min delay. The largest deviations of nearly 2 min delay were observed for the smallest two aromatic compounds, benzene and toluene.

Analogous data for three sets of model compounds (PAC compounds, oxygenated compounds and nitrogen bearing compounds) compared with the PS-PMMA calibration line of the Mixed-D column are shown in Table 8.1, arranged by increasing molecular mass (Lazaro et al., 1999b). The PAC standards (including cataannelated/cata-condensed, peri-condensed, non-planar and some alkyl-substituted species) were found to behave much as they did in the Mixed-A column, systematically eluting at slightly longer times than expected from their molecular masses. The effect appears related to greater diffusivities due to the compact shapes of these molecules. Thus, in calculating average MMs of complex mixtures, the deviation from linearity of smaller PAC species needs to be taken into account. The nitrogen bearing compounds (ranging from pyridine to the dye, alcian blue, of MM 1086 u) showed more symmetric scatter about the PS-PMMA calibration line than the PAC-group, while elution times of oxygenates, ranging from acetone to stearyl alcohol, MM 270 u were more heavily weighted toward shorter elution times, reflecting the behaviour of the PSAC standards and other oxygenates. Only the mixtures of C60 and C70 fullerenes with their rigid

Table 8.1 Calibration of Mixed-D column using standard compounds, showing experimental and calculated elution times (based on PS calibration) and time differences

Compound name	MW	t_{exp}	t_{calc}	Δt_{calc}
Acetone	58	21.5	21.4	+0.1
Benzene	78	22.2	21.0	+1.2
Pyridine	79	21.9	21.0	+0.9
Toluene	92	22.7	20.8	+1.8
Phenol	94	19.9	20.8	−0.9
Indole	117	20.2	20.5	−0.5
Benzoic acid	122	19.6	20.4	−0.8
Pyrogallol	126	18.8	20.4	−1.5
Quinoline	129	21.2	20.4	+0.9
Cyanuric acid	129	18.7	20.4	−1.7
Benzo[*b*]thiophene	134	21.5	20.3	+1.2
Salicylic acid	138	16.9	20.3	−3.4
1-Methyl naphthalene	142	21.9	20.2	+1.6
2,3-Dimethylindole	145	20.2	20.2	0.0
3-Phenylpropenoic acid	148	19.4	20.2	−0.8
3-Nitrobenzyl alcohol	153	19.6	20.1	−0.5
3-Dimethylaminobenzoic acid	165	19.5	20.0	−0.5
Fluorene	166	21.6	20.0	+1.6
Carbazole	167	19.9	20.0	−0.1
2-Mercaptobenzothiazole	167	20.7	20.0	+0.7
Dibenzofuran	168	21.4	20.0	+1.4
Anthracene	178	21.2	19.9	+1.3
Phenanthrene	178	21.2	19.9	+1.3
5,6-Benzoquinoline	179	20.9	19.9	+1.0
Phenanthridine	179	20.9	19.9	+1.0
Coniferyl alcohol	180	18.6	19.3	−1.3
2-Aminofluorene	181	19.4	19.9	−0.5
Hydrocaffeic acid	182	18.3	19.9	−1.6
3,5-Dimethoxybenzoic acid	182	19.2	19.9	−0.7
3,5-Dimethoxy-4-hydroxycinnamic acid	182	18.3	19.9	−1.6
4,4-Dimethyl 2,2 bipyridyl	184	21.3	19.9	+1.4
9-Methylanthracene	192	20.4	19.8	+0.6
Fluoranthene	202	21.0	19.8	+1.2
Anthraquinone	208	20.7	19.7	+1.0
Sinapyl alcohol	210	18.6	19.7	−1.1
9-Anthracene carboxylic acid	222	16.4	19.7	−3.2
Chrysene	228	20.8	19.6	+1.2
Triphenylene	228	20.7	19.6	+1.1
2,6-Diphenylpyridine	231	20.1	19.6	+0.5

(*Continued*)

Table 8.1 Calibration of Mixed-D column using standard compounds, showing experimental and calculated elution times (based on PS calibration) and time differences (Continued)

Compound name	MW	t_{exp}	t_{calc}	Δt_{calc}
n-Phenylcarbazole	243	20.6	19.5	+1.1
2-Aminochrysene	243	19.1	19.5	−0.4
9-Aminochrysene	243	19.1	19.5	−0.4
Perylene	252	20.8	19.5	+1.3
Benzo[*a*]pyrene	252	20.8	19.5	+1.3
1,1-Binaphthyl	254	20.4	19.5	+1.0
9-Phenylanthracene	254	20.6	19.5	+1.1
1,2-Benzanthraquinone	258	20.5	19.4	+1.1
1-Acetaminopyrene	259	19.3	19.4	−0.1
Stearyl alcohol	270	19.4	19.4	0.0
Benzo[*ghi*]perylene	276	20.8	19.3	+1.5
Picene	278	20.2	19.3	+0.8
20-Methylcholanthrene	286	20.8	19.3	+1.5
Rubicene	326	20.2	19.1	+1.1
Dibenzopentacene	378	20.6	18.9	+1.7
3,4,9,10-Perylen tetracarboxylic dianhydride	392	19.4	18.9	+0.5
Rubrene	532	19.1	18.5	+0.6
N,N′-bis(3-aminophenyl)-3,4,9,10-perylenetetracarboxyldiimide	573	17.6	18.4	−0.8
Fullerene	720–840	9.0	17.5–17.8	−8.5–8.8
Alcian yellow	838	18.0	17.9	+0.1
Alcian blue (pyridine variant)	1086	21.2	17.5	+3.7

Source: Reprinted with permission from Lazaro, M.J., Islas, C.A., Herod, A.A., Kandiyoti, R., 1999b. Energy Fuels 13, 1212. Copyright 1999 American Chemical Society.
t_{exp} is the measured elution time (min); t_{calc} is the elution time calculated from the polystyrene calibration; Δt_{calc} is the difference between t_{exp} and t_{calc}.

three-dimensional structures showed anomalous behaviour, eluting near the exclusion limit of both the Mixed-A and the Mixed-D columns (Lazaro et al., 1999b; Karaca et al., 2004). This constituted the greatest single departure from the PS-PMMA line and will be discussed below. Apicella et al. (2003b) using a Mixed-D column and NMP eluent, showed that dicoronylene (596 u), a mixture of PACs of average molecular mass 200 and toluene all eluted close to the PS calibration line.

Calibration with pitch fractions of narrow polydispersity; MALDI-mass spectrometry of successively eluting SEC fractions of a coal tar pitch: Two sets of samples have been prepared using the same coal tar pitch by collecting fractions exiting from a preparative scale SEC column (details below). The first set consisted of successively eluting 3-min fractions. The second set was made up of fractions of 10 s collected every 3 min. The elution times of these fractions were determined in the analytical

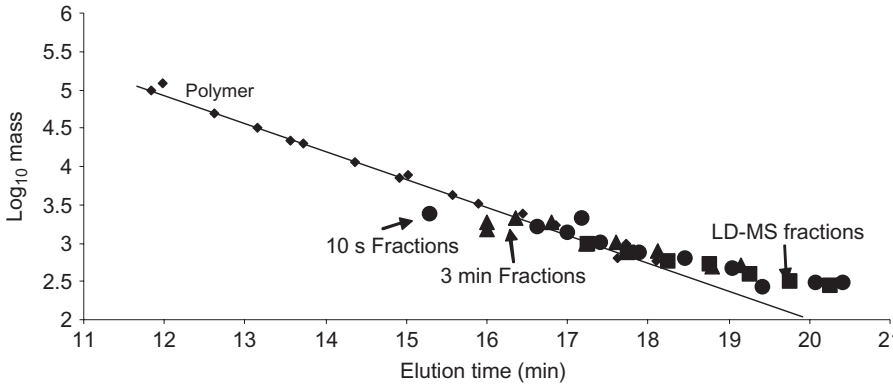

Figure 8.4 Plots of log10 Mp from MALDI-MS and LD-MS of narrow-time fractions of pitch from SEC versus elution times measured on Mixed-D column.
Source: Reprinted with permission from Karaca, F., Islas, C.A., Millan, M., Behrouzi, M., Morgan, T.J., Herod, A.A., et al., 2004. Energy Fuels 18, 778–788. Copyright 2004 American Chemical Society.

Mixed-D column. A third set of fractions was prepared using 30-s fractions eluting from the same analytical Mixed-D column. MMs of all three sets of fractions were evaluated by their masses at peak intensity (M_p) in MALDI and LD-mass spectra (MS). Mercaptobenzothiazole was used as matrix for the 3 min samples, and sinapinic acid for the 10-s fractions. The third set was examined by LD-MS (i.e., no matrix).

Fig. 8.4 presents plots of $\log_{10}$ (Mp) versus elution time in the Mixed-D column, for all three sets of fractions. The data were internally consistent and reproducible, despite the acquisition of the data at different times, from three separate SEC-experiments, using two different matrices, two different mass spectrometers, and several spectrometer operators. Later-than-expected elution times were observed for smaller molecular mass samples in all three sets, in parallel with shifts observed for known model compounds in Fig. 8.3.

Above 3000 u, the MALDI-derived M_p values were observed to flatten out for samples eluting at shorter elution times, i.e., larger MMs. For molecular masses of pitch fractions up to about m/z 3000, reasonably good agreement was found between the PS-PMMA calibration of the Mixed-D column and M_p values arrived at by MALDI and LD-MS.

We have thus noted that (1) the largest deviations from the PS-PMMA line were found in the case of oxygenated samples, (2) that even for these samples, MMs may be estimated to within a factor of ~2–2.5 below about 15 k u and that (3) other structural features (e.g., ring-embedded nitrogen) are likely to give rise to smaller departures from the PS-PMMA calibration line. Put in this context, the agreement observed between findings from SEC and MALDI/LD-MS up to about 3000 u in Figs. 8.4 and 8.26 suggests that up to this limit and perhaps a little beyond, SEC as defined in the sections above may be considered as a quantitative tool, the accuracy of the measurement being subject to greater uncertainty with increasing molecular mass.

Three-dimensional standards: solid or rigid samples with known diameters: In Table 8.1, we noted that a sample of mixed C60 and C70 fullerenes eluted near the exclusion limit of the column (Fig. 8.5). Fullerenes of mass 720 and 840 u and diameters of ~1 nm, are two major outliers with respect to *all* the calibration curves described earlier, with the greatest discrepancy between molecular *mass* and molecular *size*.

Previous reports (Herod et al., 2000b; Apicella et al., 2002; also see Section 8.4.2) indicated that soot samples could be caught by a 20-nm filter, and after being redissolved or re-dispersed in NMP the earlier chromatograms could be reproduced. The higher mass components of the samples analysed using these SEC-columns contain material with diameters in tens of nm, suggesting that there might be a direct relationship between elution times and the sizes of more fully 3-dimensional objects in these columns. Colloidal silica samples (Nissan Chemical Industries Ltd. of Houston, Texas, USA) of diameters 22, 12 and 9 nm were used to test the relationship between particle diameters and elution time. Fig. 8.5 shows plots of log 10 (particle diameter) versus elution times, in the Mixed-A and Mixed-D columns. Both plots are linear and are independent of particle density or molecular mass. The data points for 1 nm

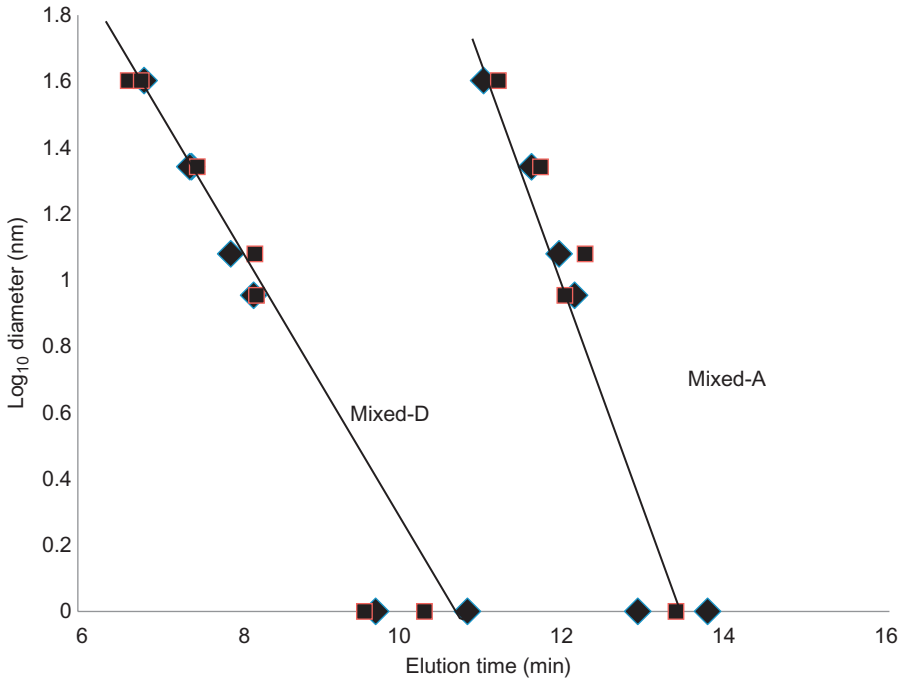

Figure 8.5 Three dimensional standards (soot, colloidal silica and fullerenes) on Mixed-D and Mixed-A columns. Diamonds and squares represent replicate determinations.
Source: Reprinted with permission from Karaca, F., Islas, C.A., Millan, M., Behrouzi, M., Morgan, T.J., Herod, A.A., et al., 2004. Energy Fuels 18, 778–788. Copyright 2004 American Chemical Society.

diameter are for the mixture of C60 and C70 fullerenes, eluting at ~13.5 min in the Mixed-A and ~10.5 min in the Mixed-D columns. The void volume changes slightly as column flow is stopped overnight and started the following day, the elution time within the exclusion region may vary by 15–30 s; replicate determinations on the same day showed much smaller variations.

Fig. 8.5 indicates that the sample of fullerenes eluted according to molecular *size* rather than molecular *mass*. The possibility of reaction between NMP and fullerene in solution has been raised by Yevlampieva et al. (2002) and it is not clear what effect this would have on the elution time of fullerene.

Behaviour of steam-distilled samples: the behaviour of chemicals from natural sources and known to consist of small molecules was investigated (Morgan et al., 2005b) to show that they behaved as small molecules and produced no excluded peaks. Three essential oils produced by steam distillation of plant materials were examined by the Mixed-A and Mixed-D columns using NMP as eluent. The results showed that these samples did indeed elute as small molecules and showed no evidence of an excluded peak. The three essential oils, Tea Tree Oil from leaves of the tree *Melaleuca alternifolia* and two lavender oils (*Lavandula angustifolia* and *Lavandula intermedia lavandin*) produced by steam distillation were examined by GC-MS. The molecular components of these oils are diterpenes, sesquiterpenes, and oxygenated derivatives of terpenes of relatively low mass. All three oils were completely soluble in NMP and the chromatograms gave only late eluting peaks and no excluded 'aggregate' peaks were detected.

Summary: The calibration data presented in this section cover a wider range of PS standards compared to previous work and have been overlaid with elution times of a set of PMMA standards. The resulting PS-PMMA calibration has been compared against elution times of standards: (1) PSAC, (2) known high-mass polymers of various origins and narrow polydispersity, (3) model compounds, (4) colloidal silica spheres and (5) samples known to consist of only small molecules. The level of agreement between SEC and MALDI/LD mass spectrometry has also been examined, using narrow SEC elution fractions of a coal tar pitch and a Maya crude oil asphaltene (see Section 8.7) and elution times matched against mass values observed in MALDI-MS (and LD-MS). The two techniques are independent and the level of agreement between them provides a yardstick with which to evaluate the SEC results.

In SEC, problems may arise from two further sources: (1) solvent flow rates should be low to avoid shear degradation of polymers and (2) covalent bonds of polymers may break during extensive ultrasonication to get the polymers into solution (Aust, 2003; Strlic and Kolar 2003). The largest MM materials found in coal tars, biomass tars, lignin, petroleum asphaltenes, and tar sands elute at similar times as the PS standard of mass 20 million u and could possibly suffer from degradation (George et al., 2011; Herod et al., 2012; Sathitsuksanoh et al., 2014; Morgan and Kandiyoti, 2014). However, where early-eluting material has been collected at the exit of the UV-absorbance detector and reinjected, the elution times have been observed to remain unchanged (Islas et al., 2003c; Morgan et al., 2009). In one case, shorter times were observed because in the initial injection, the capacity of the excluded region of

the column was exceeded (i.e., overloaded). Another problem seems to arise when the oxygen content of the analyte is high, as in humic and fulvic acids. These materials are polyelectrolytes, soluble in NMP in the protonated form but insoluble in NMP when in the neutral state in soil or peat.

8.2.3 SEC using a mixed solvent NMP/chloroform

Although pure NMP may be routinely used as SEC eluent for coal-derived materials, it is not a good solvent for aliphatic compounds, predominantly aliphatic alkylaromatics or their mixtures. Ascanius et al. (2004) reported finding proportions of NMP-insolubles (MNIs) ranging between 9 and 53 wt% in a series of petroleum asphaltenes. Thus, NMP as an eluent cannot be used to completely characterize petroleum crudes or mixtures containing both aromatic groups and significant aliphatic content. Chloroform dissolves most crude oil fractions, although it is not a strong solvent for coal-derived heavy fractions. In one set of experiments, SEC of known aromatic standards in chloroform eluent gave the opposite of the trend expected from a size exclusion mechanism, with smaller standard molecules eluting at shorter times than their larger mass counterparts (Paul-Dauphin et al., 2007). One solution to the problem is the use of mixtures of NMP and chloroform as the eluent. NMP insoluble fractions of petroleum-derived material were found to be entirely soluble in NMP-chloroform mixtures, in volume ratios of 5:1 and 6:1 (NMP:$CHCl_3$), with detection by SEC using UV-absorbance (Paul-Dauphin et al., 2007; Berrueco et al., 2008).

The petroleum asphaltenes insoluble in NMP appear to be largely aromatic in character and of a larger molecular mass than the NMP-soluble (MNS) fractions. When using mixtures of NMP and chloroform as eluent, the excluded peak observed in chromatograms of asphaltene samples became more intense, compared to SEC using NMP alone, indicating that more of the heavier material went into solution. Compared to the MNS fractions, UV-F spectra of MNIs appear at longer wavelengths, suggesting the presence of larger chromophores, presumably attached to large aliphatic structures that render the material insoluble in NMP (Paul-Dauphin et al., 2007; Berrueco et al., 2008). Indeed, an asphaltene fractionated by washing with NMP produced an MNI fraction that had limited fluorescence but was detected in SEC using the NMP-chloroform mixture with UV-absorbance and a higher proportion of material in the excluded region than the more soluble fractions (Al-Muhareb et al., 2007). Fig. 8.6 shows synchronous UV-F spectra of vacuum residue C in NMP and chloroform.

Standard PS-polydivinylbenzene packed SEC columns have been calibrated, using the mixed solvent as eluent, with polymeric molecular mass standards, including sets of PS and PMMA as well as model polycyclic aromatic (PAC) and heterocyclic compounds (Paul-Dauphin et al., 2007; Berrueco et al., 2008). As in the case of NMP eluent, the PS and the PMMA calibration lines were statistically indistinguishable. Other polymeric standards, including a set of PSAC standards, which had (in NMP as eluent) shown the greatest divergence from the PS-PMMA line, were found to elute at times much closer to the PS-PMMA line. The solvent mixture reduced the structural dependence of elution times of all sample polymers tested, compared to elution in NMP (Paul-Dauphin et al., 2007; Berrueco et al., 2008). However, the elution times

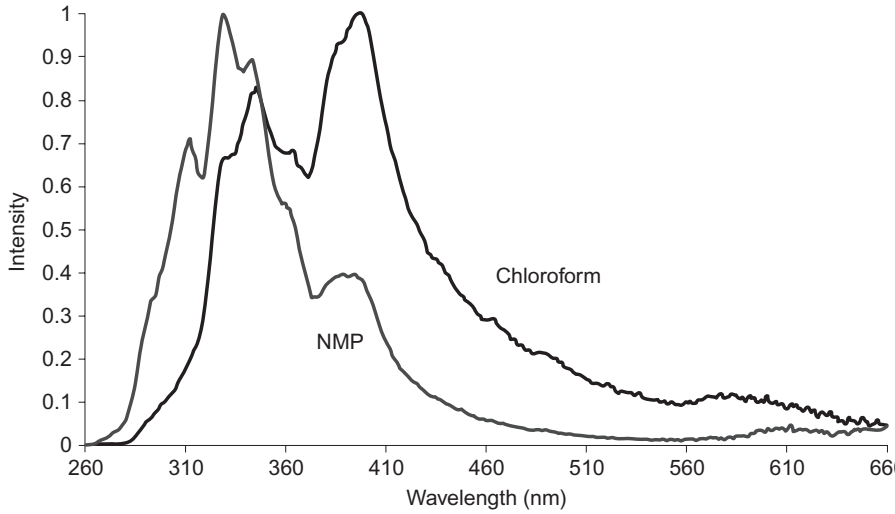

Figure 8.6 Synchronous UV-F spectra of Vac residue C in NMP and chloroform.
Source: Reprinted with permission from Paul-Dauphin, S., Karaca, F., Morgan, T.J., Millan-Agorio, M., Herod, A.A., Kandiyoti, R., 2007. Energy Fuels, 21(6), 3484–3489. Copyright 2007 American Chemical Society.

for the set of smaller mass (<500 u) model polycyclic aromatic and heterocyclic compounds gave a calibration line with a less steep slope than the PS-PMMA calibration line. Mixing $CHCl_3$ with NMP appears to extend the elution times of these aromatic and polar compounds, possibly due to promotion of surface effects (Berrueco et al., 2008), compared to when 100% NMP was used as eluent.

Fig. 8.7 presents SEC chromatograms obtained using a 6:1 mixture (v/v) of NMP/$CHCl_3$ as eluent (Morgan et al., 2010b). The samples were solubility fractions prepared from Maya crude oil, a heavy Mexican crude. Chromatograms are shown of the 'whole' asphaltene prepared from Maya crude and its MNS and MNI fractions. The strong absorption of UV light indicated that both fractions contained significant proportions of aromatic structures as was confirmed by subsequent NMR analysis (Morgan et al., 2010a), as discussed further in Section 8.8.1.

As expected, the molecular mass range of the maltene fraction (MM) was observed to be far narrower and of smaller molecular size than that of the asphaltene (MA). The MNS and MNI fractions of the asphaltene bracketed the molecular size range of the whole asphaltene. The data clearly show the mass range of the MNI asphaltene fraction to be broader than that of the MNS fraction. At the extreme dilutions used in the SEC system ($0.15 - 0.35\,g\,L^{-1}$ before injection with 20 µL eluted through the column using 15 mL of solvent, a further dilution factor of approximately 10^3 on column), it seems unlikely that the higher mass material, showing up under the early eluting peak, might be composed of aggregates.

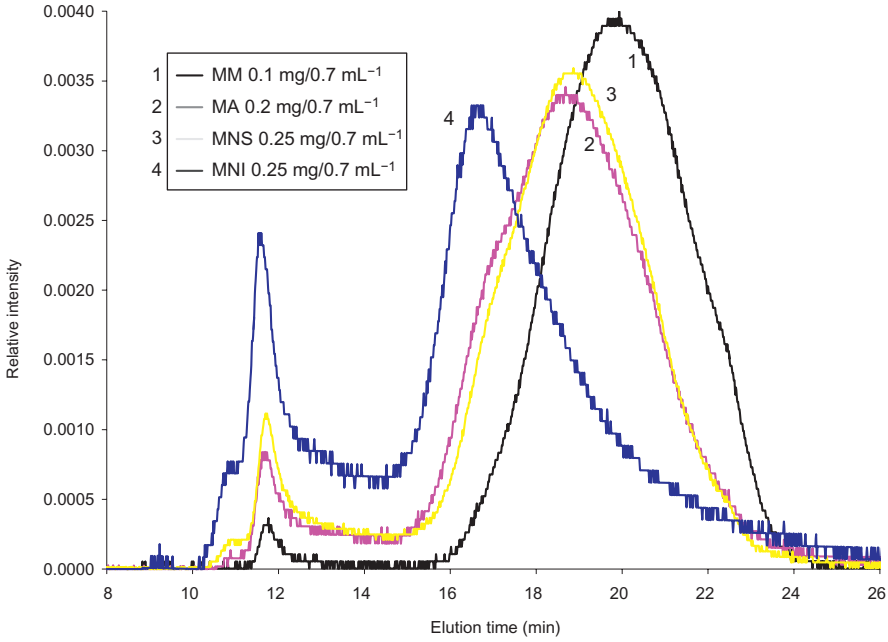

Figure 8.7 Area normalized SEC chromatograms of Maya solubility fractions. Detection by UV-absorbance at 300 nm. Mixed-D column eluent 6:1 mix of NMP and $CHCl_3$, samples dissolved in 6:1 mix. *MM*, Maya maltene fraction (heptane soluble); *MA*, Maya asphaltene fraction (heptane insoluble, toluene soluble); *MNS*, NMP soluble fraction of the Maya asphaltene; *MNI*, NMP insoluble fraction of the Maya asphaltene.
Source: Reprinted and adapted from Figure 1 in Morgan, T.J., George, A., Alvarez-Rodriguez, P., Millan, M., Herod, A.A., Kandiyoti, R., 2010a. J. Chromatogr. A 1217(24), 3804–3818. Copyright 2010, with permission from Elsevier.

As a further check, narrow elution time fractions (60 s) have been collected from the outlet of the SEC system and reinjected (effecting higher levels of dilution). These SEC elution fractions were also analysed by LD-MS which showed good correlation between increasing elution times from SEC with decreasing average mass (m/z) observed by LD-MS, see Sections 8.2.2. and 8.3.4 (Morgan et al., 2009). When using UV-absorbance detection in series with UV-F detection (see Sections 8.4.3 and 8.9), the extreme dilutions needed to avoid overloading the fluorescence detector failed to cause any significant difference in the UV-absorbance chromatograms compared with chromatograms at higher, more usual concentrations (Morgan et al., 2005a). There was no evidence of molecular aggregation at the high levels of dilution used in these analyses. The NMP – chloroform eluent mixtures provide the most widely usable single eluent/solvent combination identified to date; manipulating solvent properties has made the same SEC setup useful in characterising structurally very different samples—light and heavy coal- or biomass-derived oils and pitches, as well as petroleum- and bitumen-derived fractions.

8.3 Fractionation methods to isolate molecules of large mass or size

In view of their high polydispersity, it is necessary to fractionate many fuel-derived samples (Herod and Kandiyoti, 1995c; Herod et al., 1995b, 2012; Morgan et al., 2008a; Zubkova, 2011; Morgan and Kandiyoti, 2014). The results obtained from the fractions recovered are in part defined by the fractionation method used, particularly for the larger mass or more polar fractions. Fractionation methods used in this context include planar chromatography, column chromatography, preparative SEC, ordinary solvent solubility separations and ultrafiltration (UF).

8.3.1 Planar chromatography (TLC)

Planar chromatography is the subject of many reference and teaching books (Touchstone, 1992; Hamilton and Hamilton, 1987) as well as regular reviews in Analytical Chemistry (Sherma, 1996, 1998, 2000). The advantage of the technique is the ability to recover the heavier fractions that are immobile in the set of solvents used. By contrast, other chromatographic methods lose the heavier components either as involatiles in the injection system in gas chromatography or by remaining immobile on the column in HPLC when using inadequate solvents. Fraction recovery in TLC is usually not quantitative, but the method is rapid and cheap to operate; any combination of volatile solvents can be used to develop the chromatogram. Acetonitrile and pyridine have been used in TLC on silica, to generate fractions equivalent to those from the solvent solubility method. After drying, the separated fractions may be recovered by dissolving in NMP (Herod et al., 1996b,d, 1999; Lazaro et al., 1999d; Deelchand et al., 1999; Herod and Kandiyoti, 1996; Herod and Lazaro, 2000; Suelves et al., 2001a; Morgan et al., 2008a; Morgan et al., 2010a,b; Herod et al., 2012). However, fraction sizes are usually small for analytical methods such as NMR and some of the of the heavier material cannot be recovered from the silica into NMP.

Solvents were used with and without added salts to investigate claims that salts added to the eluent in SEC could disaggregate the material excluded in SEC using NMP as eluent (see Section 8.5). Fractions were recovered from the plates by scraping the appropriate area of silica from the plate into NMP, exposing the mixture in an ultrasonic bath for a short time and filtering to remove silica particles. The heaviest fraction remains on the plate and can be examined in situ if necessary. Almost any analytical method can be applied to the separated fractions. Somsen et al. (1995) have reviewed methods for combining TLC with other spectroscopic methods. The method has been used to prepare fractions of a coal digest for examination of the iron content by Mössbauer spectroscopy (Herod et al., 1995c, 1996c; Richaud et al., 2000b).

In more recent work, TLC has played a vital role in the development of a LD-MS method which can provide more accurate estimates of the molecular mass distributions present in polydisperse hydrocarbon mixtures, such as coal-, biomass-, and petroleum-derived liquids/tars and heavy fractions (Morgan et al., 2008a, 2010a; Herod et al., 2012; George et al., 2013; Morgan and Kandiyoti, 2014). This development work is described in Section 8.6.8.

8.3.2 Column chromatography

A column chromatography method was developed, eluting fractions of the sample successively with acetonitrile and pyridine. NMP was used to sweep the remaining material immobile in pyridine (Islas, 2001; Islas et al., 2003b; Suelves et al., 2001a). This method allows a quantitative estimation of fractions and provides sufficient material for further analyses by a variety of methods. Some material could not be recovered and the silica remained coloured; sample losses were about 10% overall as volatiles and insolubles. The method was developed to fractionate up to 1 g of sample and initially used silica gel with sequential elution using acetonitrile, pyridine and NMP. In subsequent work, pentane and toluene were added to the sequence. A total volume of 100 mL of each solvent was used, 50 mL with gravity elution and the 50 mL under vacuum and then NMP (100 mL) with vacuum elution. Water (100 mL) was added to wash out the NMP. Some loss of material in each fractionation was through a combination of high-mass material retained on the silica and low mass material lost with evaporation of solvent during distillation and in the vacuum oven; an approximate mass balance was achieved.

8.3.3 Solvent solubility

The traditional method consists of separation by solvent solubility into oils (pentane solubles), asphaltenes (pentane-insolubles, benzene-solubles) and preasphaltenes (benzene insolubles) (e.g., see Suelves et al., 2001b). In much of the work described in this chapter, acetonitrile (or acetone) and pyridine were used to produce analogous solubility fractions, to concentrate the larger molecules in the acetonitrile insoluble-pyridine soluble and the pyridine insoluble fractions (Lazaro et al., 1999d; Herod and Lazaro, 2000; Morgan et al., 2008b; Herod et al., 2012). NMP was also used to isolate the largest molecules from a pyridine insoluble fraction of coal tar pitch by working at high sample loadings to produce an NMP insoluble pitch fraction (Morgan, 2008; Morgan et al., 2009). Solubility in heptaneisolatedheptane-insoluble materials from several heavy petroleum fractions (Suelves et al., 2001a,b; Al-Muhareb et al., 2006, 2007; Morgan et al., 2010b). NMP has also been used to produce NMP-soluble and -insoluble fractions from petroleum asphaltenes (Morgan et al., 2010a,b).

Sample was mixed with the least polar solvent, acetonitrile (or acetone) in excess, shaken and stood in the dark. The solution was then decanted off the residual solid. The extraction was repeated several times, with collection of the acetonitrile (or acetone) solubles. The residual solid was dried and extracted using pyridine in the same way. The solvent-soluble and -insoluble fractions were dried to give a mass balance. The method uses large quantities of solvent and gives a less clear separation than either TLC or column chromatography but has the advantage that no large mass material is lost on the filtration or separation media. Mass balances were usually slightly greater than 100% because of the difficulty of completely removing the solvents. A process for removing NMP from coal- and petroleum-derived samples while avoiding polymerisation and oxidation products from NMP has been reported (Berrueco et al., 2009; Morgan et al., 2009, 2010b).

8.3.4 Preparative and analytical SEC

A Perkin-Elmer LC 250 isocratic pump maintained an NMP flow rate of 2 mL min^{-1} through the preparative SEC column (600 mm; 25 mm ID packed with PS/polydivinylbenzene beads) held at 85°C and connected to a Perkin-Elmer LC 290 UV-absorbance detector at 450 nm. A single run of 100 min gave enough sample for subsequent analyses. Two sequences of collection were used. In the first, fractions were collected at consecutive 3 min intervals. In the second sequence, narrow fractions corresponding to about 10 s elution periods were obtained with 3 min intervals between the fractions. This method minimized overlap between different fractions and restricted the total number of samples collected (Islas 2001; Islas et al., 2001a, 2002a). A Mixed-D analytical column was also used to prepare fractions, with collection of eluting material at consecutive 0.5 min intervals (Karaca et al., 2004; Millan 2005) and 10 consecutive 1.0 min elution-time fractions that were subsequently analysed by LD-MS (Morgan, 2008; Morgan et al., 2009).

8.3.5 Ultrafiltration

UF is an established technique commonly used for purifying and concentrating protein solutions (Marshall et al., 1993; Rodríguez et al., 1999; Huisman et al., 2000). More recently UF (nanofiltration) has been used to separate oil water emulsions (Tsang Mui Ching et al., 2010 and references therein). UF membranes can effectively act at the molecular level to remove larger molecules from solution on the basis of size. Suspended solids and solutes of high molecular mass (size) are retained by the membrane, while solvent and lower molecular mass sample molecules pass through the membrane (Millipore, 2015; Marshall et al., 1993; Smith, 1998; Rippe and Haraldsson, 1999).

Permeability through the membrane depends on a number of factors such as the composition of the solute, its molecular size distribution, solubility properties and the chemical and physical properties of individual molecules, in addition to solvent properties and the properties of the solution as a whole. These factors cannot be readily isolated and quantified.

When the difference in mass between solvent and solute is greater than 10-fold, a separation of >90% can be achieved (Millipore, 2015). The use of UF has generally been restricted to the separation of simple solutions, for example, a light solvent and a large protein. With regard to the use of UF in the study of complex mixtures such as coal- and petroleum-derived liquids, tars and asphaltenes, it is known that the technique cannot provide discrete separations. To date, it has been rarely used for studying complex samples. Only a few reports may be found in the literature for its application to coal- or petroleum-derived complex mixtures. Nonetheless, some useful insights on molecular sizes have been put forward (Duong et al., 1997; Lai and Smith, 2001; Zhao and Shaw, 2007; Fulem et al., 2008; Marques et al., 2008; Anwarul Hasan et al., 2009; George et al., 2010; Tsang Mui Ching et al., 2010; Yarranton et al., 2013). UF is particular useful when used in parallel with thin layer or column chromatography (see Section 8.4.1) (George et al., 2010).

8.4 Application of SEC and fractionation methods to samples

8.4.1 Coal-derived materials

Samples that have been characterised by these methods include a coal tar pitch (Parker et al., 1993; Herod et al., 1999, 2000a; Lazaro et al., 1999d; Menéndez et al., 2001; Begon et al., 2000; Islas et al., 2001a,b, 2001a, 2003b; Morgan et al., 2008b, 2009; George et al., 2010), coal extracts prepared using different solvents and thermal treatments (Islas et al., 2000; Suelves et al., 2001b; Begon et al., 2002; Bodman et al., 2002, 2003), a low-temperature coal tar (Islas, 2001; Islas et al., 2002b), direct solvent extracts of coal (Richaud et al., 2000a), pyrolysis tars (Avid et al., 2004; Morgan et al., 2008a) and tars from the copyrolysis of coal and waste lubricating oil (Lazaro et al., 2001). Much of the method development work has been done using a sample of coal tar pitch because of its chemical stability and availability in quantity (Herod et al., 2012; Morgan and Kandiyoti, 2014). Analytical SEC profiles of fractions (Islas et al., 2001b) obtained by sample collection from a preparative SEC column showed regular small shifts to smaller size molecules with increasing elution time (Islas 2001; Islas et al., 2002a; Morgan et al., 2009).

Discussion of the shape of the SEC chromatogram: Fig. 8.8 shows SEC profiles of three coal-derived samples, a pitch, a coal extract and a low temperature tar eluted using the Mixed-D column. The SEC chromatograms of fractions from these samples have been shown elsewhere (Herod et al., 1999; Islas, 2001; Islas et al., 2000, 2002b,c). However, in common, they all exhibit a gap in elution time between about 10 min and 13 min during which no sample is detected. We have noted that the

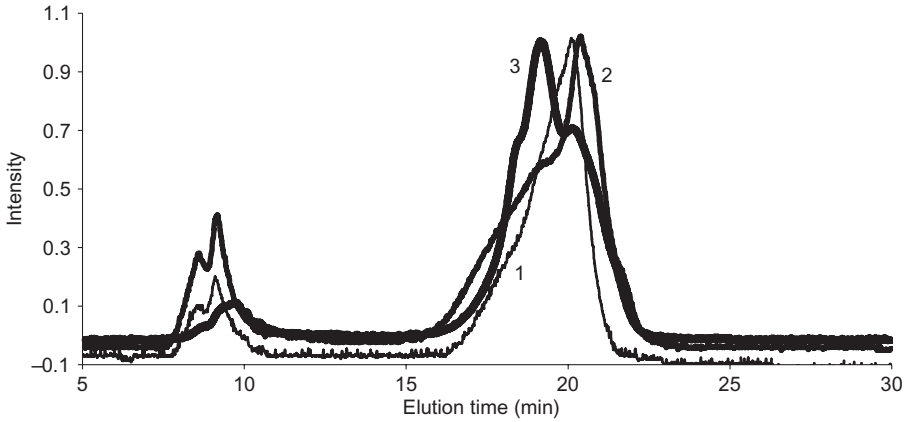

Figure 8.8 SEC chromatograms on Mixed-D of (1) pitch, (2) a coal digest and (3) a low temperature tar; zeros offset slightly; UV-absorbance detection at 350 nm.
Source: Reproduced with permission from Herod, A.A., Islas, C.A., Lazaro, M.-J., Dubau, C., Carter, J.F., Kandiyoti, R., 1999. Rapid Commun. Mass Spectrom. 13, 201–210. Copyright © 1999 John Wiley & Sons, Ltd.

exclusion region of the column, before 10 min, tends to overload before the porosity (retained region) becomes overloaded (Lazaro et al., 1999b) and therefore it is essential to operate the columns with relatively dilute solutions of sample, 1% or 2% by weight at most. When higher concentrations are used, the excluded material cannot pass through the column in the correct time band and elutes at later times, gradually filling the gap. Much of the data generated using the Mixed-E column showed overloading with a non-zero intensity region between material excluded and retained by the porosity (Zhang et al., 1996a,b,c, 1997a,b; Johnson et al., 1997). A similar overloading of the excluded region appears to have occurred in other work, where refractive index detection was used (Chen and Iino, 2001). The RI detector is less sensitive than either UV or ELS detectors and requires greater amounts of sample to be injected.

The excluded peak would be expected to diminish in height or completely disappear on dilution if it were made up of smaller, aggregated molecules; dilution of these samples leads to the sharpening of both peaks. As dilution normally favours disaggregation, these findings tend to suggest that the excluded material is of high-mass rather than being aggregates of small molecules. The relative intensity of UV absorbance over the range of wavelengths used shifts toward 450 nm for the excluded material rather than the 280–300 nm maximum for the retained material, indicating that the two sets of material are structurally different. In another set of experiments, coal samples were extracted in parallel, with nearly boiling NMP and with cold NMP. All SEC chromatograms showed two peaks, the one showing signal for material resolved by column porosity and the other excluded, with a zero-intensity gap. However, the hot extraction gave a more intense excluded peak than the cold extraction, an expected result if dissolving in the hot solvent increases the amounts of larger molecules extracted (Richaud et al., 2000a).

In separate work, a pyridine insoluble fraction of coal tar pitch (PPI) was used to produce a NMP insoluble pitch fraction (PPI-N) by working with a high loading of PPI in NMP. Due to the high sample concentration only part of the PPI sample dissolved and an insoluble fraction was recovered by filtration (Morgan et al., 2009). At the usual low concentrations used for preparing samples for SEC, the PPI sample is completely soluble in NMP. When the PPI-N sample was examined by SEC in NMP solution (the PPI-N sample is soluble in NMP at low concentration) the peak area of the excluded peak increased compared to the PPI sample and the retained peak area decreased. Samples were recovered from the SEC outlet of the excluded and retained region, and analysed by LD-MS (as discussed in Section 8.2.2). LD-MS clearly showed that the material recovered from the excluded region was of higher average molecular mass than the material recovered from the retained region.

In a related study UF was used to produce a series of size-based fractions from the same coal tar pitch (George et al., 2010). SEC analysis of the UF fractions showed a clear trend where the molecules that passed through the UF membranes eluted at later times (smaller molecules) than the larger molecules that were retained on the membranes. The material retained on the largest sized membranes showed the largest peak area in the excluded region by SEC. None of the UF fractions were very discrete groups of molecules according to their SEC profiles, even the apparently largest

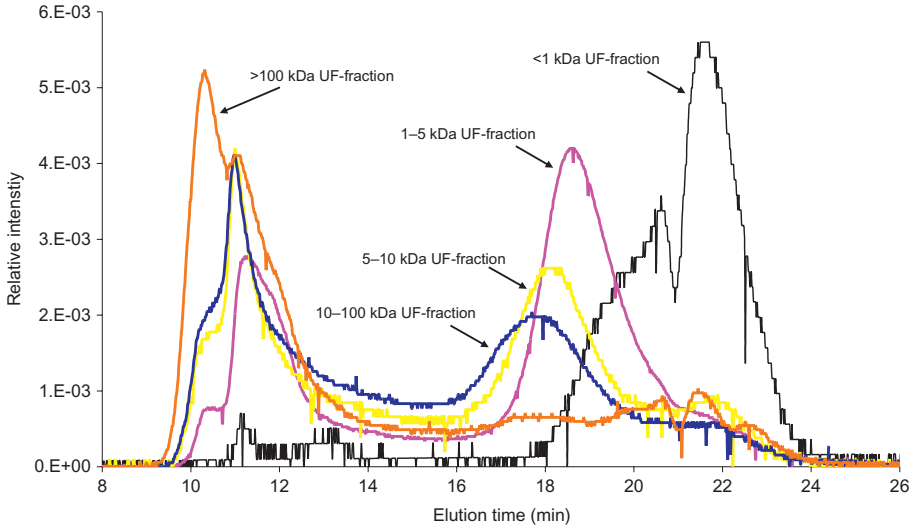

Figure 8.9 Area normalized SEC chromatograms of the pitch pyridine soluble (PPS) sample ultrafiltration (UF) fractions, Mixed-D column operating at 80°C with NMP as eluent, detection at 300 nm UV-A.
Source: Reprinted from George, A., Morgan, T.J., Alvarez, P., Millan, M., Herod, A.A., Kandiyoti, R., 2010. Fuel 89(10), 2953–2970. Copyright 2010, with permission from Elsevier.

molecules (retained on the largest UF membrane) showed some material eluting in the retained SEC region and vice versa for the smaller sized UF fractions. The SEC chromatograms from the UF fractions from the pitch pyridine soluble (PPS) sample are displayed in Fig. 8.9, spectra from UV-F in Fig. 8.10 and LD-MS spectra in Fig. 8.11.

Relatively good agreement was observed between mass estimates based on SEC and LD-MS of the smaller UF-fractions, showing material with molecular masses ranging between 800 and 10,000 u. Examining the largest UF fractions of the pitch-pyridine-insoluble sample also gave clear evidence for material with molecular masses *above* 10,000 u. Taken together, however, the LD-MS data showed progressively *diminishing* differences, as the sizes of the UF membranes, and the likely molecular masses of the sample fractions, increased. One likely explanation is incomplete sampling during the LD procedure. The evidence suggests that the upper mass limit detectable for these and similar samples by LD-MS has been reached. Despite these reservations, LD-MS appears as the best method to date, for investigating the mass ranges of samples derived from coal tar pitch and heavy petroleum fractions; more detail is provided in the original publication (George et al., 2010).

Pitch polymerisation by several different heat treatments showed that the SEC profile shifted to shorter elution times (larger MMs). Extended treatment gradually caused the retained peak (small MMs) to be reduced. The mechanisms of polymerisation varied according to treatment; however, the *initial* pitch or anthracene oil samples were almost entirely soluble in NMP and observable by SEC (Menéndez et al., 2001, 2002; Bermejo et al., 2001a,b; Álvarez et al., 2008; Morgan and Kandiyoti, 2014).

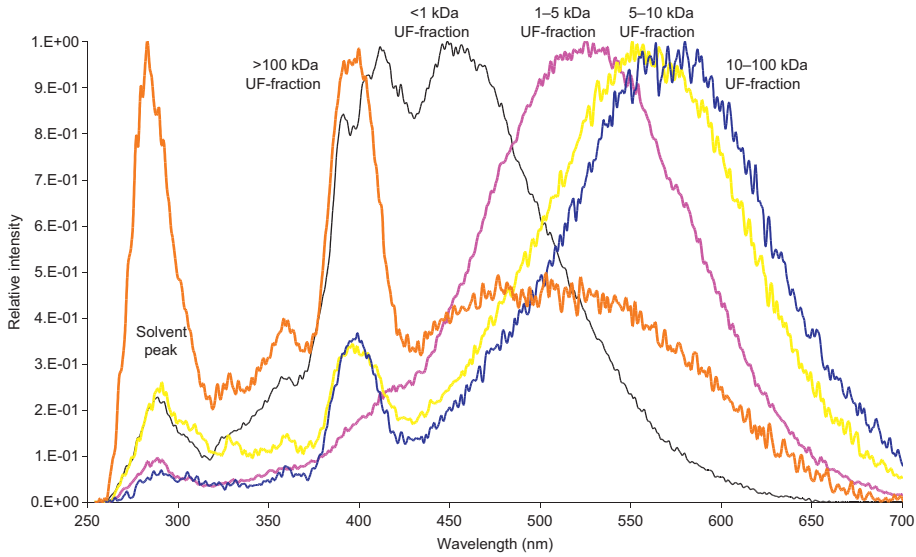

Figure 8.10 Peak normalized synchronous UV-fluorescence spectra of the PPS ultrafiltration (UF) fractions: < 1 k, 1–5 k, 5–10 k, 10–100 k and > 100 kDa NMWL.
Source: Reprinted from George, A., Morgan, T.J., Alvarez, P., Millan, M., Herod, A.A., Kandiyoti, R., 2010. Fuel 89(10), 2953–2970. Copyright 2010, with permission from Elsevier.

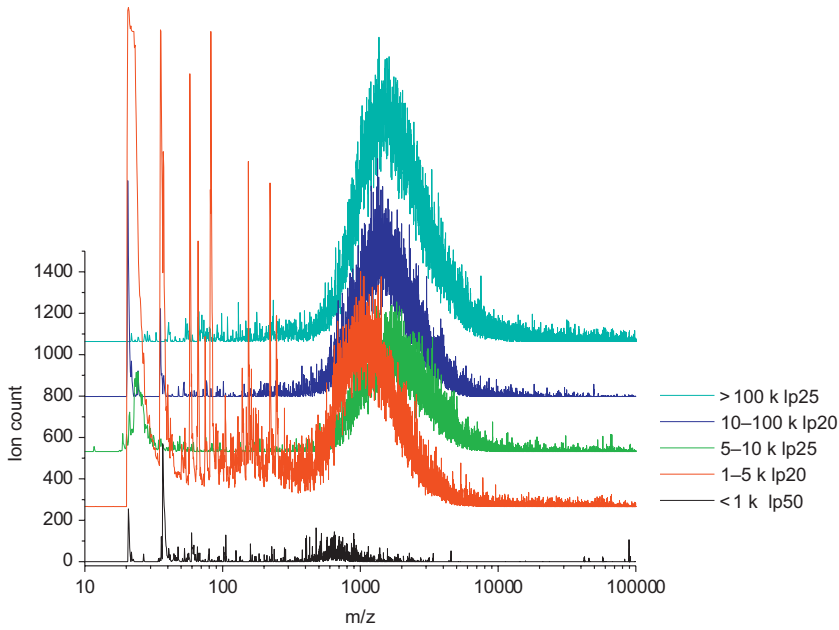

Figure 8.11 LD-mass spectra of the PPS ultrafiltration (UF) fractions, acquired in linear-mode with No DIE and maximum HMA voltage (10 kV). The percent laser power (lp) used to acquire each spectrum is displayed in the caption.
Source: Reprinted from George, A., Morgan, T.J., Alvarez, P., Millan, M., Herod, A.A., Kandiyoti, R., 2010. Fuel 89(10), 2953–2970. Copyright 2010, with permission from Elsevier.

A coal tar pitch and a naphthalene-derived pitch were compared in terms of molecular mass and size (Gargiulo et al., 2015) using SEC in NMP solution, LDI-TOFMS and fluorescence spectroscopy. SEC indicated that the naphthalene pitch had a higher number average molecular mass than the coal tar pitch but without consideration of the material excluded from the column porosity; mass spectrometry indicated smaller mass ranges than SEC. Emission and synchronous UV-fluorescence spectra indicated that the naphthalene pitch had stronger fluorescence than coal tar pitch in the range 450–600 nm and this was attributed to peri-annellation of naphthylenes in naphthalene pitch which were not present in the coal tar pitch. Millan et al., 2005a have shown that the fluorescence intensities of the largest molecules of coal tar pitch decrease significantly as molecular mass increases; this can only be detected by fractionation of the pitch.

Correlation of structural features with changing molecular mass: A sample of coal tar pitch, a coal extract and a low-temperature coal tar were fractionated by column chromatography and examined by SEC as well as by pyrolysis-GC-MS (Herod et al., 1999; Islas 2001; Islas et al., 2000, 2002b). SEC chromatograms of the three coal-derived samples using the Mixed-D column showed significant differences in both the excluded and retained regions of the chromatograms. A common feature of the SEC chromatograms of the fractions of these column-chromatography separations of the three samples was the parallel shifts in molecular size distribution to shorter elution times in increasing order of solvent solubility from acetonitrile to pyridine and NMP-solubles, shown in Fig. 8.12 for the coal digest. The pyridine and NMP soluble fractions gave very little signal by py-GC-MS (mostly residual solvent), indicating that any volatile pyrolytic fragments were too large to pass through the chromatographic column. Only the acetonitrile-solubles fragmented into small molecules detectable through a GC column (Herod et al., 1999; Islas, 2001; Islas et al., 2000, 2002b). Pitch

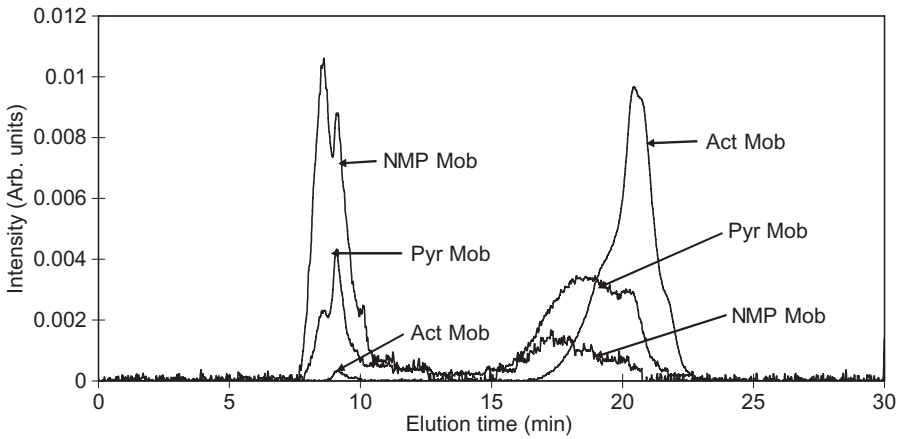

Figure 8.12 Size exclusion chromatography (SEC) on Mixed-D of column chromatography fractions of coal digest.
Source: Reprinted from Islas, C.A., Suelves, I., Li, W., Morgan, T.J., Herod, A.A., Kandiyoti, R., 2003b. Fuel 82,1813–1823. Copyright 2003, with permission from Elsevier.

fractions from preparative SEC using NMP as eluent (Islas et al., 2002a) showed that even those molecules that eluted within the retained region of the Mixed-D column but were too large for GC-MS themselves produced a wide range of fragments and structural isomers when analysed by pyrolysis-GC-MS. These fragments were mostly the usual array of small PACs, readily observed by GC of the whole pitch.

Applications of SEC to liquefaction and hydrocracking: A set of coal macerals, including a vitrinite, a liptinite and two inertinites was liquefied in tetralin at 450°C and the coal extracts examined by SEC in NMP, using the Mixed-E column (Begon et al., 2002). Comparisons of MM-distributions of coal-derived materials at different stages of the liquefaction process showed the expected trends. The subsequent catalytic hydrocracking in tetralin of these (Begon et al., 2002) and other coal extracts (Herod et al., 1996a; Zhang et al., 1996a,b,c, 1997a,b; Bodman et al., 2002, 2003), reduced the proportion of excluded material and produced a shift of the retained material to longer elution times. The pyridine insoluble fraction of pitch was catalytically hydrocracked (Begon et al., 2000); this sample mainly appeared under the excluded peak of the SEC chromatogram and this material reacted rapidly under hydrocracking conditions with loss of the excluded SEC peak and generation of a retained peak at a longer elution time than observed in the starting material. This new peak contained material of molecular masses less than m/z 600 that were detectable by probe mass spectrometry. Part of the material adhering to the catalysts was extracted into NMP and contained relatively high proportions of excluded material by SEC. The synchronous UV-fluorescence spectra of the pyridine insoluble fraction and the hydrocracked product showed a clear shift to smaller molecules and smaller aromatic clusters on hydrocracking, as observed by SEC.

8.4.2 Soots

Several soot samples have been examined including coal and wood soots from domestic open fires, soots, or tars from the combustion of coal in a Bunsen flame and a candle soot from condensation from a burning candle onto a cool glass tube (Herod et al., 2000b, 2003, 2004; Apicella et al., 2002, 2003a,b). A series of soots produced from two fuel-rich burner systems fed by ethylene gas, rape seed oil, diesel oil, and heavy petroleum oil have also been examined. In all cases, a distinguishing feature of the SEC profiles was a very early eluting peak at 6–7 min from the Mixed-D column and a peak in the Mixed-A column eluting well before the elution time of PS of mass 15 million. When the candle soot was examined by transmission electron microscopy (TEM), it showed some material with approximately 50 nm diameter (Herod et al., 2000b). This material could be filtered out of NMP solution using a 20 nm porosity filter, redissolved by ultrasonication into NMP, reinjected into SEC, with no change of elution time and no generation of smaller molecules. A candle soot was analysed at three wavelengths (300, 370 and 450 nm) for comparison with coal injected into a blast furnace (Dong et al., 2007).

Other soots showed the same behaviour after filtration (Apicella et al., 2002, 2003a,b). The soots were assumed to be in colloidal solution, but again, the existence of gaps in the elution profile between dichloromethane soluble small molecules and

the soot peak at 6–7 min points to abrupt changes of molecular size and shape with increasing mass. These findings are in agreement with evidence from other techniques applied to soot formation in flames where diameters of primary soot particles ranged from 20 to 60 nm (Hessler et al., 2002; Choi and Mochida, 2002; Blevins et al., 2002; Pacey and Glasier, 2002). Soot of diameter about 40–50 nm has been detected in the dust from blast furnace operation where coal injection was used to reduce the quantity of high-strength coke needed to support the blast furnace burden (Pipatmanomai et al., 2004). Soot particles from ethylene combustion were reported to have diameters of about 60 nm (Kim et al., 2005), a similar size to those of the other flames while primary soots from diesel engines ranged from 18 to 33 nm (Mathis et al., 2005). Apicella et al. (2003b) have confirmed these observations on soots, using samples filtered above and below diameters of 20 nm, and a carbon black sample. Carbon black and the > 20 nm fraction of soot were excluded from the column porosity and were assumed to be of very large size and similar to the observations described earlier.

8.4.3 Petroleum residues, oil shale and bitumen

A major discussion has centred on the molecular mass ranges of petroleum vacuum residues and asphaltenes because of the importance of this property for the conversion and use of the heavy parts of crude petroleum feedstocks. Strausz et al. (2002) have suggested that asphaltenes in solution exhibit colloidal behaviour and associate into micelles with apparently very large molecular masses but that, nevertheless, the system contains some molecules with relatively large masses. This view has been challenged as being caused by 'ephemeral dynamically fluctuating inhomogenieties' and not a valid diagnostic of aggregation (Sirota, 2005). We show in Section 8.5 that aggregation is most likely a function of inadequate solvent power to completely dissolve the largest molecules of crude petroleums, which remain in suspension. The use of SEC with asphaltenes using various solvents (but not NMP) has been discussed using refractive index detection (Merdrignac et al., 2004). Weight average masses for a Safaniya asphaltene were around 8000 u and the molecular weight profile varied with eluent.

Groenzin and Mullins (2000) and Badre et al. (2006) view asphaltene structures as small molecules as shown by fluorescence depolarisation techniques and that apparently high-mass values are caused by aggregation. However that technique cannot detect the nonfluorescent components of the asphaltenes (Strausz et al., 2002; Ascanius et al., 2004; Morgan et al., 2005a). An example of a vacuum bottoms sample examined by SEC with UV-absorbance and-fluorescence detectors in series is shown in Fig. 8.13, showing poorer sensitivity to fluorescence of the larger molecules. Surface tension measurements (Monte et al., 2004) and atmospheric pressure chemical ionisation mass spectrometry (Cunico et al., 2004) supported the small molecule nature of asphaltenes.

Only NMP (and mixed with $CHCl_3$) appears to produce SEC chromatograms from vacuum residues and asphaltenes with two peaks, one excluded and one within the porosity range of the column (Pindoria et al., 1997a; Deelchand et al, 1999; Suelves et al., 2000, 2001a,b, 2003; Ascanius et al., 2004; Morgan et al., 2005a; Millan et al.,

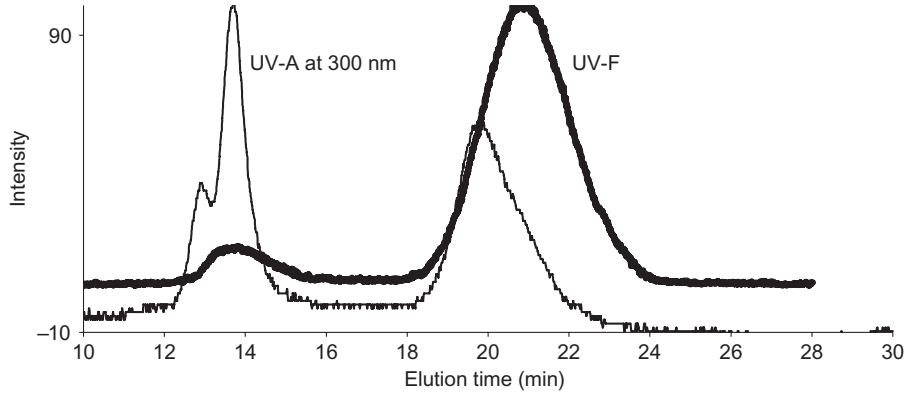

Figure 8.13 Size exclusion chromatography (SEC) of heptane insolubles of vacuum bottoms C. Chromatograms were obtained using UV-absorbance and UV-fluorescence detectors in series. Mixed-A column, both chromatograms show two separated peaks.
Source: Reprinted from Millan, M., Behrouzi, M., Karaca, F., Morgan, T.J., Herod A.A., Kandiyoti, R., 2005b. Catal. Today 109, 154–161. Copyright 2005, with permission from Elsevier.

2005b), apart from the work of Strausz et al. (2002). SEC of three asphaltenes, insoluble in heptane but soluble in NMP, isolated from three vacuum bottoms samples, showed significant differences in terms of relative proportions of excluded and retained peaks (Morgan et al., 2005a). The asphaltenes are only minor components of the whole residues but show a significant shift to larger size molecules for the retained peaks compared with the whole samples and the excluded peaks become a much more significant proportion of the fraction than in the whole sample. A non-fluorescent fraction of asphaltenes was not soluble in NMP (Ascanius et al., 2004) and was considered to consist of waxes. In view of the work above (see Section 8.2.3) using a mixed solvent with SEC, the more likely explanation is that the NMP-insoluble fraction was not wax but molecules with aromatic cores with numerous alkyl pendant groups, giving the outward appearance of an aliphatic molecule.

Petroleum vacuum residues have been examined by SEC using NMP as eluent with the Mixed-E (Pindoria et al., 1997a) and the Mixed-D columns (Deelchand et al., 1999; Suelves et al., 2000, 2001a,b, 2003). The vacuum residues examined on the Mixed-D column showed two peaks: a small excluded peak and a large retained peak that eluted before the retained peaks observed for coal-derived materials (Deelchand et al., 1999).

Athabasca bitumen was fractionated by preparative SEC using THF eluent (Domin et al., 1998) and the fractions examined by analytical SEC using NMP. The THF eluent produced a very poor fractionation, but estimates of peak masses from analytical SEC in NMP agreed reasonably well with estimates from VPO and MALDI-ms. ^{252}Cf plasma desorption mass spectrometry (PDMS) showed similar trends to SEC, MALDI and VPO but underestimated the masses. The masses of PS standards having similar elution times to the peak intensities of the retained peaks of the fractions were

3200, 1005, 480, 390 and 370. The comparison of SEC in THF and NMP indicated that the material excluded in the NMP system had been spread throughout the material retained in THF within the column porosity.

Waste motor oil was examined by the Mixed-E column (Lazaro et al., 2001) and is shown to contain mainly small molecules, with the peak intensity at about 22.5 min, equivalent to PS of mass about 200 u. Some excluded material was observed suggesting that even after use in an engine, the large excluded molecules are not completely degraded.

Fractions of a vacuum residue separated by TLC have been examined by SEC with NMP as eluent (Li et al., 2004). The proportion of material excluded from the column porosity increased with increasing polarity of the solvent used to develop the thin layer chromatographic plates. An oil shale from Mongolia gave an oil by pyrolysis showing the characteristic double peaks observed in SEC for other oil-derived products, with insignificant signal between the peaks; the yield of oil was low (7% wt) following pyrolysis at 800°C (Avid et al., 2004).

Subsequent studies were made to find an eluent that was capable of completely dissolving asphaltene samples while maintaining the SEC mechanism, as described in Section 8.2.3 (Paul-Dauphin et al., 2007; Berrueco et al., 2008). Petroleum asphaltene samples are only partially soluble in NMP but are soluble in a mixed eluent of NMP and chloroform (6:1 by volume). When the NMP soluble and insoluble fractions of an asphaltene from Maya crude oil (Mexico) were examined by SEC with the mixed eluent it was found that the NMP soluble fraction had a narrow MM distribution with most of the material eluting in the retained region, Fig. 8.8 (Morgan et al., 2010a). The NMP insoluble fraction contained more higher molecular-mass molecules with significantly more material eluting in the excluded region. The SEC results correlate with the results from LD-MS analysis of the NMP soluble and insoluble asphaltene samples: the NMP insoluble fraction contained the highest average molecular mass material (Morgan et al., 2010a). Further confirmation of the suitability of the mixed eluent for SEC analysis of asphaltene samples comes from the collection of fractions from the outlet of the SEC system followed by analysis by LD-MS (see Section 8.2.2) (Morgan et al., 2009). For samples recovered from the retained region of the SEC system, the LD-MS results showed a trend of increasing average molecular mass with decreasing elution time. The samples recovered from the excluded region were always of higher MM than those from the retained region, but there was no longer a trend of increasing MM with decreasing elution time within the excluded region.

SEC has also been used to study solubility and planar chromatography fractions of a syncrude (Athabasca tar sands, bitumen) using the mixed eluent SEC and LD-MS; NMR and UV-F were also used for structural characterization (Herod et al., 2012). As with the Maya samples, the syncrude asphaltene showed a greater proportion of material excluded from the SEC column than the maltene fraction. Four fractions separated by PC on silica plates revealed that fraction 1, the least mobile fraction, consisted almost entirely of material excluded from column porosity in SEC; at the other extreme fraction 4, the most mobile fraction, contained almost entirely small molecules that eluted in the retained region. As with the Maya fractions, the UV-F results for the maltenes and asphaltenes show differences in chromophore size which bracket that of the *'whole'* syncrude sample. LD-MS spectra of the unfractionated

syncrude showed ions ranged from m/z 200 to < 2000 with a peak of maximum intensity between m/z 300 and 400, which was similar to PC fraction 4, the most mobile of the PC fractions. The mass range of fractions 2 and 3 ranged from m/z 200 to 4000 with a maximum intensity between m/z 1000 and 2000. PC fraction 1, the least mobile fraction did not given an adequate spectrum, but the ions at low intensity range from m/z 800 to possibly 5000. It seems likely that this fraction has not ionised properly and has only given an indication that the mass range is greater than that of fraction 2. For a discussion of the NMR results see Herod et al. (2012).

Hydrocracking of a petroleum residue using tetralin as solvent and with different catalysts has shown that the SEC chromatogram of the residue shifted to smaller molecular sizes after reaction, with the greatest shift to smaller molecules shown using pillared clay catalysts (Bodman et al., 2002, 2003). In the absence of catalyst, polymerisation of the residue was observed with a marked shift of the peak intensity of the chromatogram to shorter times than observed for the initial residue sample.

NMP/chloroform solvent in SEC has been used to evaluate the effects of catalytic hydrocracking on a Maya vacuum residue (Purón et al., 2013) and showed a clear shift to smaller molecules following reaction. The asphaltene fraction of the residue differed from the maltenes fraction in terms of both excluded material (mainly in the asphaltene) and in molecular sizes of the maltene fractions (maltenes < asphaltenes); after reaction the asphaltene fraction had been reduced in both proportion of excluded material and in a large shift to smaller sized molecules in the product.

8.4.4 SEC of kerogen extracts

Kerogen samples have been pyrolysed using the wire-mesh reactor described in Chapter 3, Pyrolysis of solid fuels: experimental design and applications (Madrali et al., 1994, Rahman et al. 2000). Similar samples have also been extracted in NMP and liquefied in the flowing solvent reactor described in Chapter 5, Liquefaction: Thermal breakdown in the liquid phase (Li et al. 2002). The aim of the work was to correlate tar yields with oil production and the structure and maturity of the kerogen.

Extracts of immature kerogen samples in NMP showed behaviour that could be considered as anomalous and characteristic of soots. In SEC, peaks were observed at the unexpectedly early elution times of 6–7 min, as well as at the 9–10 min and 14–20 min ranges (Herod et al., 1997). The masses of the early eluting 6–7 min peaks cannot be estimated, but may be equivalent to spherical particles of diameter up to 40 nm and similar to the spherical particles found in soots. This peak was more prominent for the younger kerogens than for the older samples. The excluded peaks at 9–10 min eluted as if similar to the largest PS standard available of 15 million u, down to the exclusion limit of around 200,000 u; the material corresponds to very large molecules of unknown mass. The retained peaks (at maximum intensity) were equivalent in mass to PS standards of mass between 1600 and 760 u; signal in the retained region extended up to 15 min, equivalent to PS of mass about 7000 u. Extracts in NMP of the older immature kerogens had proportionally shown more signal in the retained region of the Mixed-D column than was found for younger but also immature kerogens. However, the signal in the retained region from extracts from younger kerogens (Types I and III) was shifted to slightly longer elution times (smaller molecular size) than for the older kerogens.

Three kerogens of type I and different maturities (immature, in the oil-producing window, and mature) have been extracted (Li et al., 2002) using the flowing solvent liquefaction system using NMP. The mass of kerogen extracted in the flowing solvent method using NMP at 300°C varied, with the least in the mature sample (3.4%), the most in the sample within the oil production window (51.2%) and less extract from the immature sample (37.6%). The proportions of material (in direct solvent extracts in NMP) in the excluded and retained regions changed with the most excluded signal from the kerogen within the oil-producing window and the least in the extract from the mature sample. The possibilities of the product characterization methods described remain to be fully explored. However, these initial results suggest far greater possibilities for examining the fundamental properties of kerogens than studies using Rock–Eval tests.

8.4.5 Biomass and amber extracts and tars

Extracts have been obtained using NMP to partially dissolve wood fragments known as 'forest residue' over a period of weeks at ambient temperature and by heating to the boiling point of NMP (Richaud et al., 2000a). The higher temperature extraction showed an increase of excluded material on the Mixed-D column, an expected result if dissolving macromolecules. The excluded material had relatively greater absorbance at 370 and 450 nm than the retained material, particularly when examining the sample recovered after the hot extraction. Peat from different sources has also been extracted using NMP to show that the extracted material was both unlike humic substances and unlike coal-oil contamination of soil (Morgan et al., 2005c).

Samples of amber were pyrolysed using the atmospheric pressure wire mesh pyrolysis reactor described in Chapter 3, Pyrolysis of solid fuels: experimental design and applications (Pipatmanomai et al., 2001). Gases and tars evolved and there was little char residue left on the mesh, suggesting the absence of large polycyclic aromatic systems in amber. The tar recovered from the tar trap was examined by SEC and by GC-MS. The amber tar was similar in GC-MS analysis to the solvent extracts of amber, showing mainly a distribution of small aromatic groups. The amber has also been extracted using pentane, toluene and NMP with the extracts and the insoluble residue being examined by pyrolysis-GC-MS (Islas et al., 2001 d,e). In SEC, the proportion of excluded material increased from pentane to NMP extracts. However, unlike findings for coal liquids, pyrolysis-GC-MS showed that structures observed for each fraction *and* the insoluble residue were practically identical. These data showed that even when molecular masses increased, the structural units (including PAC groups) making up the amber matrix were relatively similar. The absence of large polycyclic aromatic systems in amber is interesting.

Spruce wood was also pyrolysed using the wire-mesh technique at 1000°C in a stream of helium using different heating rates (1, 50, 200 and 1000°C s^{-1}) and the tars analysed on the Mixed-E column (Messenböck, 1998). The excluded material was more intense than the retained material in each case, but greatest in proportion for the fastest temperature rise.

The pyrolysis products of eucalyptus wood in the wire-mesh and a fixed-bed ('hot-rod') reactor (see Chapter 3: Pyrolysis of solid fuels: experimental design and

applications) have been compared by Pindoria et al. (1997b). The hot-rod reactor was heated at slower heating rates, ranging from $10°C\,s^{-1}$ to $10°C\,min^{-1}$. The wire mesh reactor with a rapid temperature rise and a sample bed of dispersed particles would be expected to generate tars with larger molecular sizes than those from a packed bed, where tar cracking through contact with heated solid particles would tend to narrow molecular mass distributions. As expected, the SEC chromatograms indicated that tars from the 'hot-rod' reactor were of smaller molecular size than the tar from the wire-mesh reactor and that molecular size decreased with increasing bed thickness. Hydrocracking of the tar sharply reduced the yield of tar while increasing the gas and char yields (Pindoria et al., 1998). The effect on the recovered tar was to produce some smaller molecular mass material as well as increasing the proportion of excluded material. A sugar cane bagasse sample was also pyrolysed using both wire-mesh and hot-rod reactors (Pindoria et al., 1999) at different pressures. The hot rod reactor tar contained smaller molecules than the wire mesh tar, but tars from both reactors contained large proportions of excluded material. In conclusion, the hydropyrolysis route was not a good method for producing bio-oils for potential use as transport fluids because the catalytic hydrocracking route to deoxygenation of the tars produced increasing quantities of volatiles and gas and little distillate-grade fuels with prolonged use of the catalyst.

Other materials pyrolysed and examined by SEC include silver birch wood alone or in mixtures with coal (Collot, 1999), wood, rice husk, coconut coir, agricultural waste (Vasanthakumar et al., 1998) and various wood tar samples (Tei et al., 1997). A sample of Stockholm tar was examined following fractionation by TLC (Lazaro et al., 1999c). This material formed by destructive distillation of pine wood has been produced for many centuries and used as tar in wooden ships (Robinson et al., 1987). It contained material excluded from the Mixed-E column in all fractions from TLC (Fig. 8.14).

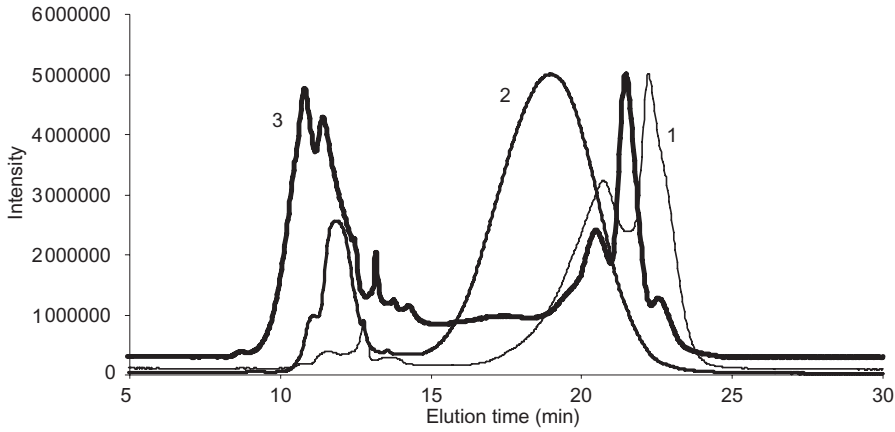

Figure 8.14 Stockholm tar fractions from TLC (1) acetonitrile mobile, (2) pyridine mobile and (3) pyridine immobile, detection by ELS, Mixed-E column.
Source: Reprinted from Lazaro, M.J., Domin, M., Herod, A.A. and Kandiyoti, R., 1999c. J. Chromatogr. A 840, 107–115. Copyright 1999, with permission from Elsevier.

SEC with NMP eluent, LD-MS and UV-F spectroscopy have also been used to determine changes in mass distributions and structural properties of biomass/coal cogasification tars, after storage of these samples as a function of temperature, time, and presence of ambient light (George et al., 2013). The samples examined were tars recovered during cogasification of pine and a sub-bituminous coal (70:30 wt%) in an internally circulating fluidized bed reactor. The results show that detailed information can be obtained on molecular mass distribution and the changes that occur during ageing. The fresh tar contained molecular masses ranging from <200 to >2000 u, with a shift in mass distribution to higher average values after ageing. Precipitation occurred in the tar solutions after <14 h of storage at >5°C (George et al., 2013). The molecules that contained the largest conjugated aromatic systems, rather than the molecules with the greatest masses, were primarily involved in the ageing reactions that resulted in precipitation. Different ageing mechanisms were identified, depending on whether the tar was stored in darkness or in the presence of ambient light.

The pyrolysis of sewage sludge produced a tar that in SEC showed a bimodal chromatogram (Adegoroye et al., 2004). Tars produced by the pyrolysis of animal bones and casein from milk production (Purevsuren et al., 2004a,b) also showed the bimodal pattern in SEC. It seems likely that the pyrolysis of any biomass material might produce some material eluting in the excluded region as well as the range of smaller molecules eluting within the range of porosity of the columns used. Although these molecules have not been defined except in terms of their probable three-dimensional shapes, they are clearly not detectable by GC-MS methods or indeed, by mass spectrometric methods other than MALDI-MS or LD-MS (see below).

8.4.6 Humic and fulvic acids

Much of the organic material of soils, sediments and natural waters remains beyond the molecular range of characterization methods normally applied to such samples such as gas chromatography (Hedges et al., 2000; Poirier et al., 2000). The behaviour of humic and fulvic acids in the SEC system was studied in relation to determining the sources of soil contamination and distinguishing between residues from old coal processing plant and from naturally occurring humic substances.

Humic and fulvic acids obtained from the International Humic Substance Society, have been examined using the Mixed-D and Mixed-A columns (Herod et al., 2003b; Morgan et al., 2005c). The normal characterization method by SEC for these materials uses aqueous solvents. They are however, very soluble in NMP and give clear, dark-coloured solutions after ultrasonic treatment. Their SEC chromatograms showed relatively simple profiles, with a single peak of relatively narrow spread. Using the Mixed-D column, humic acids were excluded from the porosity while the fulvic acids, eluting later than humic acids, were of smaller size. On the Mixed-A column, both humic and fulvic acids eluted within the linear region of the calibration and approximated to PS masses of around 1 million u (humic acids) and 0.5 million u (fulvic acids). Fig. 8.15 presents the SEC chromatograms of humic and fulvic acids. NMP extracts of peat gave solutions quite unlike those of standard fulvic or humic acids prepared from peat by extraction using NaOH solution. The humic materials

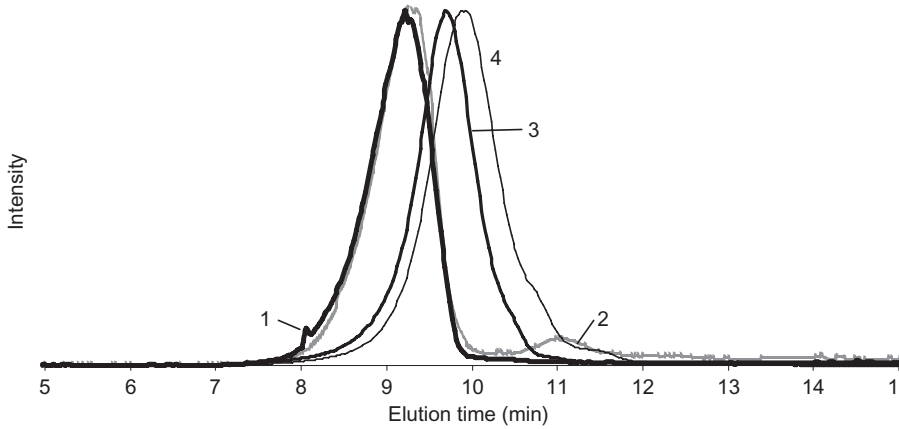

Figure 8.15 Standard humic and fulvic acids on Mixed-D column; curves are (1) Peat standard humic; (2) Peat reference humic; (3) Peat fulvic; (4) Soil fulvic by ELS detection. *Source:* Reprinted from Morgan, T.J., Herod, A.A., Brain, S., Chambers, F., Kandiyoti, R., 2005c. J. Chromatogr. A 1095, 81–88. Copyright 2005, with permission from Elsevier.

purchased as standards were in the protonated polyelectrolyte form whereas the humic substances in the peat were in the native form as polyelectrolyte salts that would not be expected to be soluble in NMP. Estimates of mass using the PSAC calibration suggest average masses of humic and fulvic acids to be 124,000 and 66,000, respectively.

A summary of findings from studies using organic eluents other than NMP has been given by Johnson et al. (1998). In aqueous phase SEC, high molecular masses up to 10^5 u have been observed in alkaline solutions of lignin (Wong and de Jong, 1996). Molecular weights of alkali-solubilised coal were estimated by Polman and Quigley (1991) at about 26,000 u. Alkali-solubles of a THF-insoluble brown coal extract gave molecular masses ranging from 355,000 to 33,000 u, in agreement with values determined by UF techniques (Ralph and Catcheside, 1996).

More recent studies of humic and fulvic acids by mass spectrometry have indicated much smaller molecular mass ranges for these materials. Literature reports of attempts to examine humic and fulvic acids by MALDI-MS and LD-MS have given weak spectra consistent with the detection of only very minor quantities of the sample (Pokorna et al., 1999; Haberhauer et al., 1999, 2000; Ziechmann et al., 2000; Stenson et al., 2002). Aqueous SEC has been coupled to electrospray MS for the analysis of Suwannee River humic and fulvic acids (Reemstma and These 2003). Molecular ions up to m/z 2000 were the highest mass ions detected. Suwannee River fulvic acid examined by ESI (Leenheer et al., 2001) detected ions up to m/z 2500. None of these mass spectrometric examinations of humic substances has defined the upper mass limits of these materials because of the limitations of the electrospray process that has not been shown to ionize the largest molecules of complex mixtures (These and Reemstma, 2003; These et al., 2004). Therefore, the masses of these materials (peak and average masses) remain a source of conjecture.

Humic and fulvic acids have been prepared from a bituminous South African coal (Waterberg) by oxidation at 180°C, at 40 bar pressure in a water slurry with an oxygen flow (Skhonde et al., 2006) for 1 h. The humic acids had an elemental composition (% wt daf): C 49.2; H 3.16; N 1.29; O + S by difference 46.3, with total acid 5.98%, in agreement with the ranges shown by the International Humic Substances Society of wt%C 49–63 and %O 44–63. Although not analysed by SEC, the humic acid was subjected to thermogravimetric analysis up to 1000°C and to FTIR. The results showed that carboxylic acid functions were lost at low temperatures but phenolic groups were more resistant to degradation; total weight loss to temperature was about 55% suggesting that the molecular size was not of only small molecules. Examination of humic acids from soils and Leonardite (North Dakota) by aqueous SEC (Piccolo et al., 2000) with similar elemental analyses as the Waterberg humic acid gave number average molecular weights in the approximate range 20,000–50,000 mass units by UV detection and even higher (up to 100,000 mass units) by RI detection that is independent of chromophores in the acids.

8.4.7 Lignin

In the present context, a brief mention of the SEC of isolated lignin is warranted. The majority of published SEC studies of lignins use THF as eluent (Ringena et al., 2006; Baumberger et al., 2007; Abaecheril et al., 2009; Asikkala et al., 2012) despite there being little evidence that this approach is valid. The general assumption used is that lignin will behave in the same manner as a simple polymer such as polystyrene during SEC chromatography and that useful relative trends may emerge. The use of universal calibrations is also common. These approaches are likely to suffer from the same issues as discussed above for coal tar and petroleum-derived samples: i.e., lignin has a structure more similar to complex coal or petroleum-derived materials than polymers with regular structures. In our studies of lignin, NMP was used as the SEC eluent (George et al., 2011; Sathitsuksanoh et al., 2014). The SEC-NMP chromatograms of various lignin samples showed bimodal distributions with significant signal in the excluded region, similar to those observed from coal tar pitches, compared to a unimodal distribution with SEC using THF as eluent.

In an unpublished work (Morgan and George, 2011), column chromatography (CC) fractions were produced from Organosolv lignin followed by analysis by SEC using three eluents, NMP, THF and H_2O + NaOH as well as MALDI-MS and FT-ICR-MS analyses. The mass distribution estimates from SEC-NMP and H2O + NaOH correlated with MALDI-MS–derived mass estimates better than those from using SEC with THF. When THF was used as SEC eluent all the CC fractions had similar distributions with an upper mass limit of ~1200 u. In contrast, SEC-NMP, SEC-H2O + NaOH and MALDI-MS showed evidence for molecular masses to at least 3000 u (m/z) with clear trends of increasing average molecular mass with decreasing mobility of the CC fractions. There are significant differences in the results obtained when using NMP as eluent versus using H_2O + NaOH, but it was not possible to determine the reason for this; further work is required to understand the observed differences. Nonetheless, the results from NMP and H_2O + NaOH provide credible evidence for

molecular masses greater than 1500 u in Organosolv lignin (to at least 3000 u); the results also call into question the usefulness of THF as a SEC eluent for lignins.

Recently, researchers have turned to derivatising lignin samples to improve their solubility in THF with an aim to improving its SEC behaviour (Guerra et al., 2007; Asikkala et al., 2012). To date we have not seen any evidence from independent techniques (such as MALDI-MS) to confirm that the mass estimates obtained from SEC-THF of derivatised lignins accurately represent all of the sample or that this method is superior to the use of NMP (Herod et al., 2012; Morgan and Kandiyoti, 2014) or H_2O + NaOH (Gidh et al., 2006; de Wild et al., 2012) as eluent. Clearly, further research is required to determine the 'best' SEC method for studying the molecular mass distribution of lignins.

It is more difficult to obtain satisfactory MALDI-MS spectra from lignin samples than from coal- or petroleum-derived materials. Three matrices were tested in the unpublished work mentioned above: sinapinic acid, 2,5 dihydroxybenzoic acid (DHB) and 2–(4 ′ -Hydroxybenzeneazo) benzoic acid (HABA); the HABA matrix was found to be the most effective. Based on previous experience with developing MALDI-MS methods, it is likely that the largest molecules in the lignin samples were not being ionized, and/or certain molecules were fragmenting at the laser power required to ionize/vapourize the molecules. Further work is required to understand the limitations of the MALDI-MS method and to optimize the procedure. To our knowledge, MALDI-MS is the most promising MS technique to obtain information on mass distributions from lignin. FT-ICR-MS can provide detailed information on structure through accurate mass measurements, but this method appears to be limited to compounds with mass less than m/z ~1500 (unpublished work).

8.5 Aggregation of small polar molecules to appear as large molecules – in NMP? A question of solvent power?

Aggregation of small molecules in solution in NMP has been held as the cause of the excluded peak in SEC when using NMP as eluent. Initially, LiBr was held to dissociate these aggregates when added to the eluent NMP (Takanohashi et al., 1994; Masuda et al., 1996; Mori, 1983; Chen and Iino, 2001) by dissipating the ionic forces holding the aggregates together. The observed shift of chromatograms to longer elution times upon LiBr addition to the NMP eluent was explained in terms of disaggregating large polar molecular aggregates (Masuda et al., 1996).

Experiments showed that LiBr ruined the size exclusion mechanism by promoting surface effects and causing even non-polar materials to elute after the permeation limit of the column (Herod et al., 1998). The addition of LiBr to the eluent NMP shifted chromatograms of two nonpolar samples (a naphthalene mesophase pitch and a mixture of C60 and C70 fullerenes) to longer retention times (Herod et al., 1998), even longer than the permeation limits of the analytical columns, although not changing elution times of PS standards. In the same study, excluded peaks were observed in the SEC chromatograms of a naphthalene mesophase pitch, an observation unlikely to

be related to 'aggregates of smaller, polar molecules, held together by ionic forces'. MALDI-mass spectra of the same naphthalene pitch have shown molecular mass distributions with large high-mass limits (Herod et al., 1998). In a separate experiment, LiBr was added to the solution of sample in NMP, which was then injected into the SEC column using NMP as eluent. The profiles of the sample with and without LiBr were identical (Herod et al., 1996b). It is difficult to envisage a disaggregation in the sample solution with added LiBr, which could reconstitute the 'aggregates' exactly as before the addition of salt, upon injection and subsequent dilution in the eluent NMP. Subsequently other salts were claimed to perform a similar disaggregation function (Chen and Iino, 2001; Shui et al., 2002). A new experiment separated the action of the salt from the SEC mechanism (Karaca et al., 2005a,b); the fractionation of pitch using thin-layer chromatography was performed with and without salt additions (LiBr, TBAA, TCAA) to the solvents. Bands of material mobile in pure and salt-added solvents (acetonitrile and pyridine) were examined by SEC. In all cases tested, including some experiments using column chromatographic separation rather than TLC, the salt-added solvent mobilized some sample in addition to that mobilized by the pure solvent and the extra sample was of larger molecular size than that mobilized by the pure solvent. In terms of action at the silica surfaces, the solvent plus salt had greater polarity than, and displaced more material from, the polar sites of silica than the pure solvent.

It seems reasonable to consider that aggregates do not form in NMP under the dilute conditions used (Thiyagarajan and Cody, 1997), but that they can and do form in other, less powerful solvents, or at higher concentrations than those prevailing in the detection stage of the SEC systems. We estimate that sample concentrations (in NMP) in the detector stage of the SEC are lower by more than an order of magnitude from those likely to cause micelle aggregation in nitrobenzene, by petroleum asphaltene molecules (Karaca et al., 2004).

Several additional strands of experimental evidence run counter to the claim that sample under the excluded peak may represent molecular aggregates. Among others, these findings show that fluorescence based methods provide a poor guide to the detection of high mass material.

1. The early-eluting peak of coal tar pitch was fractionated using analytical SEC (Lazaro et al., 1999b); on reinjection, the first two fractions eluted at the times of collection while the third fraction eluted earlier, showing that far from dissociating on dilution, the material had been delayed in elution by overloading the column. None of these fractions gave rise to a late-eluting peak that might have been expected if the 'aggregated' material had been dis-aggregated by dilution.
2. Fluorescence spectroscopy was used as detector in series with UV absorbance on samples and fractions in both static solutions and on SEC effluents. The synchronous fluorescence spectra of late-eluting peaks, of presumably small molecular mass material, tend to be rather intense. When the fractions of tars insoluble in acetonitrile but soluble in pyridine or insoluble in pyridine but soluble in NMP are added to the fluorescence cell at dilutions used for strongly fluorescing molecules, no signal could be detected.
3. When the fluorescence instrument was used as a detector in the SEC, in flow mode, it was necessary to inject very dilute solutions, in order to avoid overloading this detector with the fluorescence of the small, strongly-fluorescing molecules. This requirement means that the UV-absorbance signal was very weak (cf. Fig. 8.13). Under these conditions, the

early-eluting materials of the pyridine-solubles and the pyridine-insolubles showed no significant fluorescence signal, and the fluorescence that was detected came from the smallest molecules of these fractions (Morgan et al., 2005a). Meanwhile, the early eluting material still showed intense UV absorption signal and did not alter by dilution in the SEC detector systems.

4. Pyrolysis of the pyridine-soluble or pyridine-insoluble fractions of pitch, coal extract or low temperature tar using the pyroprobe of the GC-MS system, showed that these fractions gave no significant components able to pass through the GC column (cf. chapter 7: Analytical techniques for low mass materials: method development). In other words, there was no evidence that any of the sample had, or could be, dis-aggregated.
5. When a sample of the pitch pyridine-insoluble fraction was pyrolysed in the atmospheric pressure wire-mesh reactor described in Chapter 3, Pyrolysis of solid fuels: experimental design and applications, little tar was produced (~13% by weight), none of which could be examined by GC-MS. Once again, no evidence of dis-aggregation could be found.
6. Py-GC-MS of a series of fractions of low temperature tar collected from the SEC effluent (equivalent to acetonitrile-solubles) indicated that only the last few fractions (corresponding to the smallest molecular mass fractions of the sample) were able to give any signal in the MS detector.

No examples of chromatograms of coal-derived liquids obtained using THF as eluent have showed any material excluded from the column porosity, except for material dissolved from coal at 450°C (Gibbins et al., 1991; Li et al., 1995), where an extra peak was observed at the earliest elution times. However, chromatograms of masticated natural rubber, obtained using THF as eluent, with refractive index detection (Homma and Tazaki, 1995), have shown excluded material of molecular mass from 1 to 10 million. In this case, the excluded material is likely to have been particulates produced by milling from previously insoluble rubber gels, similar to the colloidal silicas used to calibrate the excluded region in SEC (see above). Strausz et al. (2002) observed three peaks in the SEC of asphaltenes using dichloromethane as eluent and at least a part of the excluded material appear to have corresponded to aggregates in the initial solution that disaggregated on standing; the remaining excluded material did not disaggregate and may have been of large molecular size. In the calibration of SEC columns in NMP, and in heptane, the colloidal silica samples eluted from each one at the exclusion limit, indicating that colloidal particles could be swept through the columns in the interparticulate voids (Karaca et al., 2004, Al-Muhareb et al., 2006). The evidence from the study of Athabasca bitumen discussed next indicates that large molecules are present in THF solution but are not separated from small molecules until examined by SEC with NMP.

In another set of experiments, the fractionation of Athabasca bitumen (into five equal-time fractions) using preparative SEC in THF eluent was followed by analytical SEC in NMP eluent. The work showed that although the THF fractionation gave no evidence of excluded material, all the fractions did show some excluded material when analysed subsequently in NMP solution by SEC (Domin et al., 1999). The proportion of excluded material in a particular fraction decreased with increasing elution time of that fraction on the preparative column. This change was interpreted to indicate that the largest, excluded molecules observed in SEC with NMP were not separated sufficiently by THF solvent and eluted from the SEC column in THF in

part by a surface interaction mechanism, which appears to have delayed their elution well beyond the excluded region. Thus, these materials appeared to have molecular sizes or masses much smaller in THF than observed in NMP solution. The SEC chromatograms of the whole sample in THF and in NMP, and chromatograms of the fractions in NMP are shown in Fig. 8.16 as: (1) the THF SEC repeated several times

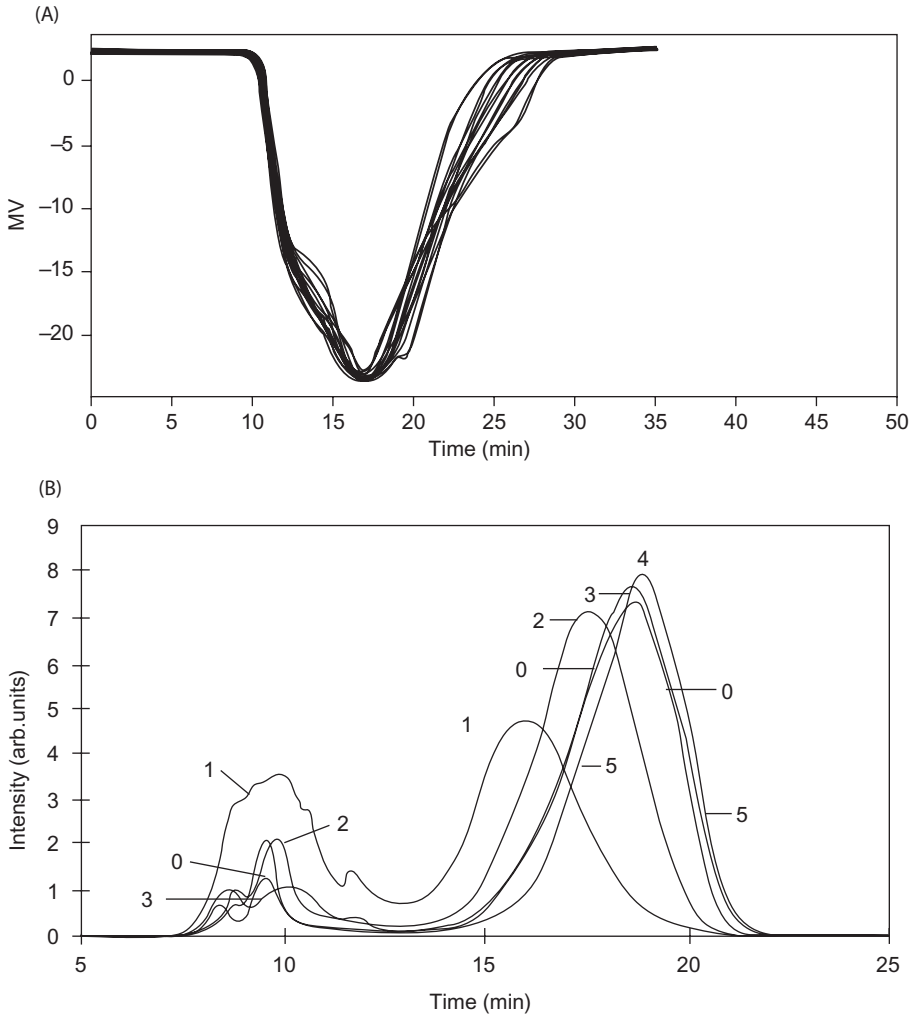

Figure 8.16 (A) Athabasca bitumen, preparative SEC in THF, repeated runs. (B) SEC in NMP of Athabasca bitumen (0) and of five equal time fractions from preparative SEC in THF, one being the earliest and five the last.
Source: Reprinted with permission from Domin, M., Herod, A.A., Kandiyoti, R., Larsen, J.W., Lazaro, M.-J., Li, S., et al., 1999. Energy Fuels 13, 552–557. Copyright 1999 American Chemical Society.

and (2) the NMP SEC of the fractions, "1" being the earliest fraction and "0" being the whole sample.It was concluded that the use of SEC with THF as eluent for these and similar samples prevents the observation of the excluded aromatic material, through lack of separation from the smaller molecular size components. The preparative SEC did produce some fractionation of the small molecules as detected by analytical SEC, with fractions “1” and “2” showing the largest effect. The remaining three fractions, however, indicate that no significant fractionation had taken place later in the preparative column. Hence, we consider that SEC using THF is pointless for samples that are largely aromatic in character.

Summary of evidence against aggregation in NMP: The various attempts to use salts mixed into the SEC solvent to disaggregate the excluded material, described earlier, have shown that salts only have an effect on the mechanism of SEC, resulting in excluded and retained material eluting later than in the absence of salts. The SEC in NMP system has been studied using various approaches to determine whether aggregation has a significant influence on mass estimates, including: recovering narrow elution time fractions from the outlet of the SEC system followed by analysis by MALDI-MS and LD-MS (see Section 8.2.2); the tandem use of UV-A and UV-F as detectors for SEC (see Sections 8.4.3 and 8.9); the use of column or TLC before SEC and LD-MS analyses (see Sections 8.4.1 and 8.6.8); and the use of ultrafiltration followed by SEC and LD-MS analyses (see Section 8.4.1). In all these studies no evidence could be found for aggregation. Perhaps of more significance is that we have not succeeded in did-aggregating any of the excluded material by successive dilutions or by collection of fractions of the excluded material followed by reinjection without concentration of the dilute effluent from the column. Aggregates of asphaltenes form if not completely soluble in the liquid mixture they experience, suggesting that increasing dilution of the excluded material would, if formed by aggregates, lead to disaggregation and the appearance of molecules in the retained region of the chromatogram; this has not been the case. Furthermore, attempts at dis-aggregation by thermal and chromatographic methods has shown no evidence for the breakup of presumed aggregates into smaller molecules.

8.5.1 Aggregates in petroleum asphaltenes

Aggregates in crude oils and in reservoirs have been observed by many groups (Mullins et al., 2007; Tsang Mui Ching et al., 2010; Mullins et al., 2012; McKenna et al., 2013a,b; Barrera et al., 2013; Yarranton et al., 2013; Anisimov et al., 2014; Zhang et al., 2014a; Painter et al., 2015; Morimoto et al. 2015a,b; Dutta Majumdar et al 2015; Mozaffari et al., 2015) and they form naturally because the largest, most polar molecules are not completely soluble in crude oil that may consist predominantly of aliphatic and light aromatic molecular types. Under these circumstances, the partially soluble molecules are likely to aggregate to form a solvated cluster of molecules that can remain suspended but not truly soluble in the crude oil. Ovalles et al. (2015) have studied the effect of temperature on the quantity of asphaltenic material deposited as a function of temperature, using a Teflon-packed column. In the temperature range 35–195°C, the asphaltene content decreased and the maltene

content of several asphaltenes increased with increasing temperature, indicating that solubility increased in hotter liquids. Rogel et al. (2015b) found that an asphaltene deposit in a pump chamber was much more aromatic than those asphaltenes precipitated from heptane solution, indicating that the least soluble asphaltenes tended to deposit first. These clusters vary in size depending on solvent (Leonardo et al., 2011). Mitchell and Speight (1973) showed that an Athabasca bitumen (pentane) asphaltene was completely soluble in alkyl cycloalkanes, alkyl benzenes and common chlorinated solvents; they also precipitated asphaltenes in stages and showed that the heaviest asphaltenes precipitated first and contained the majority of the metallic elements as shown by ashing the fractions. Asphaltenes precipitated from oil with a 3:1 pentane:oil mix were more aromatic and higher molecular weight than those subsequently precipitated using excess pentane (Fossen et al., 2011). Painter et al. (2015) considered that solubility in toluene implied not leaving a precipitate, and asphaltenes of high solubility parameter would not be soluble in toluene. Anisimov et al. (2014) showed that aggregate size depended on concentration of heptane and of the resin fraction (heavy maltene fraction) with resins able to stabilize the aggregate size. Mozaffari et al. (2015) showed that ageing in heptane led to reduction of viscosity as asphaltene aggregation increased, but viscosity did not change in toluene. Soorghali et al. (2015) have shown the role of resins in stabilising asphaltenes to avoid deposition during production. Aguiar and Mansur (2015) also demonstrated that resins stabilize asphaltenes by addition of extra resin to an asphaltic residue. Alfi et al. (2015) found that electron radiation of an ultra-heavy asphaltenic oil during processing helped to reduce viscosity of the cracking product.

Although outside the remit of this Chapter, methods used in laboratory studies of fouling by crude oils, asphaltenes and deasphalted crudes have been described (Crittenden et al., 2015), where fouling of surfaces resulted from thermal reactions of the petroleum material, including maltene fractions, as temperatures reached above 300°C. Application of methods described in this chapter (SEC, UV-fluorescence and FTIR) to deposits recovered from refinery processing of petroleum materials have been reviewed (Chew et al., 2015) in considerable detail.

Given a solvent able to fully dissolve the largest polar molecules in a particular sample, clusters and aggregates would not form and all molecules would be dispersed; this is essentially the case for the maltenes of crude oils that are the major fractions of the oils and not a very good solvent for the heavy asphaltenes. The work at Imperial College described in this **c**hapter has aimed to isolate asphaltenes from maltenes and then fractionate them by different methods to try to identify the molecular mass and size of the asphaltenes.

8.5.2 *Fractionation methods used with crude petroleum materials*

An Athabasca bitumen vacuum gas oil was distilled to give eight fractions with a maximum boiling point of 583°C (McKenna et al., 2010a) and analysed by FT-ICR-MS. Molecular compositions of the fractions were shown to change in a regular and predictable way, with PAH and heteroatom content increasing with BP,

as predicted by the Boduszynski model (cf. chapter 7: Analytical techniques for low mass materials: method development). A similar exercise with a series of Middle Eastern crude distillate fractions with the upper ranges 538–593°C, and >593°C vacuum bottoms fraction followed (McKenna et al., 2010b). The Boduszynski model was considered to apply to the distillate fractions but not to the composition of the residue. In two further papers McKenna et al. (2013a,b) investigated the nondistillable asphaltene and the maltenes and asphaltenes of a Middle Eastern heavy crude vacuum residue (>593°C) by FT-ICR-MS, without fractionation of the involatile fraction. Podgorski et al. (2013) examined a distillate fraction (523–593°C) of a North American crude, fractionated according to number of aromatic rings by HPLC. The heptane-deasphalted whole oil and the pentane soluble/insoluble fractions and each of the ring-number fractions were characterised by APPI-FT-ICR-MS and by tandem MS/MS. The gradual and consistent trends in composition from the pentane soluble and insoluble HPLC fractions were as predicted by the Boduszynski model.

Fossen et al. (2011) prepared asphaltenes by pentane dilution in two sequential steps (3:1 pentane:oil followed by 18:1 ratio) and examined them by analytical techniques: elemental, FTIR, ^{1}H and ^{13}C NMR, NMR-DEPT and LDI-MS. Weight averaged molecular masses for the asphaltene fractions were between 500 and 800 u.

Merdrignac et al. (2004) used SEC with PS/DVB and DVB columns with several solvents (THF, benzonitrile, methanol and mixtures) with RI detection to examine the heptane asphaltene of vacuum residues. In our experience, refractive index detectors are insensitive at the sample loadings needed to avoid overloading the excluded region of the column; the examples shown have two peaks but with no zero-intensity valley between. Hydrotreating of the asphaltenes shifted the relative intensities of the two peaks in favour of the second, later eluting one, as expected. The same SEC method was used by Durand et al. (2010) in their ^{1}H DOSY NMR experiments to investigate the asphaltene macro-structures of Maya, Athabasca and Buzurgan feedstocks in toluene-D_8 at 20°C. The number and weight average masses of the three asphaltenes were of the order of thousands of mass units but roughly 5–8 times smaller than values derived from NMR work.

Loegel et al. (2012) examined Maya asphaltene by reverse phase LC with a cyanopropyl column and a solvent gradient from MeCN and water to NMP and THF with detection by sequential UV and fluorescence. Three peaks were indicated by fluorescence, two resolved; UV revealed another peak weakly retained and free from fluorescence; this was taken as quenched by aggregation. Twelve fractions were collected and selected fractions analysed by APCI-MS with a quadrupole MS. Molecular weight distribution for the 12 fractions was approximately constant indicating that the separation was not by size but by adsorption. Sim et al. (2015) also used reverse-phase chromatography with a similar column and off-line high resolution mass spectrometry. The last fraction of a heavy Arabian crude oil extended to m/z 2000 and provided evidence of the need for fractionation to detect more of the sample.

TLC was used by Strausz et al. (2011) to investigate the volatile aromatic fraction of Athabasca bitumen, using argentation chromatography, followed by alumina column chromatography, into 13 mono-, di- and tri-aromatic subfractions, each of which was subjected to FIMS analysis. Altogether, close to 6000 constituent molecules,

ranging in molecular weight from 200 to ~ 800 Da, were observed. Jarne et al. (2011) applied automated multiple development with high-performance TLC to separate aromatics in bitumens, a heavy crude oil and an asphaltene. Aromatic standards up to 1000 u were used to calibrate the separation. Detection was by fluorescence scanning densitometry using 365 nm UV light. The bitumen and other samples showed a continuous range of aromatics without resolution; the initial sample deposition point on the plates showed different concentrations of sample that had not moved, assumed to represent the most polar aromatics larger in mass than 700 u. Smith et al. (2014) also used TLC separations of petroleum samples, examined by LDI coupled to FT-ICR-MS imaging. The developed plate was stuck to the laser target with sticky tape. LDI of TLC plates selectively ionized condensed aromatic hydrocarbons and facilitated two-dimensional imaging of TLC-separated petroleum compounds.

Gaspar et al. (2012) employed fractionation by solubility and polarity (SARA). Fractions were analysed by APLI–FT-ICR-MS. Without fractionation, the number of components detected in the whole oil was lower than the sum of components detected in the fractions. Cho et al. (2012) fractionated crude oils by the SARA method and analysed the fractions by APPI-FT-ICR-MS. The spectra of the aromatics fractions closely resembled the spectra for unfractionated crudes.

Yarranton et al. (2013) investigated two bitumen samples (Peace River and Athabasca); the asphaltenes were recovered as the pentane or heptane insoluble, with removal of toluene-insolubles by centrifuge before precipitation from toluene solution. Selected fractions were examined by ESI with FT-ICR-MS. Toluene solutions consisted of associating and non-associating species; the associated species were in the densest, highest molecular weight, most polar end of the continuum of aromatic and resin species.

Wiehe (2008) reacted a Cold Lake 1050°F (565°C) vacuum residue for 60 min at 400°C under nitrogen gas pressure in a tubing bomb and separated the products into gas (vented), saturates, aromatics, resins, asphaltenes and toluene-insolubles. VPO measurements in *o*-dichlorobenzene at 130°C indicated a number average molecular weight for the asphaltenes of 2009, whereas values for the saturates (690), aromatics (470) and resins (899) were similar to values derived from FT-ICR-MS.

Tsang Mui Ching et al. (2010) filtered a crude oil through a Gore–Tex membrane with nominal pore sizes as low as 30 nm; asphaltenes were considered to form nanoaggregates with not more than 10 molecules per aggregate. Leonardo et al. (2011) investigated Athabasca asphaltenes and found that aggregate size varied with solvent used to 'dissolve' the asphaltene. Barrera et al. (2013) fractionated heptane extracted asphaltenes into self- and non-self associating components; non-self associating components were estimated at 15% of the asphaltenes.

Hourani et al. (2015) examined naphthenic base oils by 2D GC, HPLC and FT-ICR-MS with APCI and APPI ionisation and concluded that detailed compositional information could only be obtained through a combination of an array of analytical tools. Rogel et al. (2015a) presented a series of correlations between physical and chemical properties of asphaltenes based on extensive characterization of asphaltene solubility fractions from diverse origins. In a further development, Rogel et al. (2015c) deposited asphaltene materials in dichloromethane or toluene, onto a filter cartridge and eluted with heptane (to remove maltenes), then methylene

chloride/methanol (90:10 vol) and finally 100% methanol. This procedure eluted the asphaltenes of lowest solubility, highest aromaticity, last. Average molecular weights of asphaltenes were about 1900 u. Fluorescence shifted to longer wavelengths from maltenes to the least soluble asphaltene fraction (Rogel et al., 2015b) with a decrease in fluorescence intensity as solubility decreased.

In summary, the fractionation methods used in the literature cited reveal extensive details of petroleum asphaltenes and maltene fractions. However, the methods have not been targeted to define the heaviest asphaltene materials that form aggregates in toluene solution. While the FT-ICR-MS analyses undoubtedly gives a detailed description of the material accessible through nebulisation to form ions, the components of aggregated material appear to avoid ionisation. Clearly, the largest molecules require stronger solvents and targeted fractionation for their characterization.

8.6 Molecular mass methods – mass spectrometry of high-mass materials >500 u

There are many different methods for the introduction of high-mass materials into mass spectrometers, ranging from liquid chromatography, through DCI, FI, FD, FAB, PD, LD, matrix assisted laser desorption and ESI. Burlingame et al. (1996) have reviewed many of these applications. All of the sample introduction methods work well for specific applications, often to biological molecules, but their performance when applied to material of relatively wide polydispersity and of unknown upper mass, leaves much to future development. None of the available methods can define an upper mass limit independent of other measurements, and it is necessary to assemble evidence from several techniques to compare data from individual samples or fractions of samples. Experience suggests that an absence of signal from an experimental method cannot necessarily be taken to indicate an absence of material, merely an indication that some method development may be needed to investigate the lack of signal.

The sample introduction (gas chromatography and complete thermal evaporation) and ionisation methods described in the previous chapter are only able to deal with relatively small molecules. In the present Chapter, sharp differences are shown between results from the low-mass techniques and those described below, using MS techniques where ionisation is thought to take place before or during evaporation (e.g., FD, FAB, laser-desorption), where the molecular ions are released into the gas phase by processes other than thermal evaporation (Herod et al., 1993a). As in Chapter 7, Analytical techniques for low mass materials: method development, however, the analyses that can be attempted will depend on the available mass spectrometers, the types of ionisation methods, and sample inlet systems they are able to accommodate and the type of mass analysis systems (quadrupole, time of flight, synchrotron, etc.) they are connected to.

The current trend in biological mass spectrometry to use ESI has superseded the use of FAB methods in that field, to the extent that FAB may not now be available without searching store-cupboards for old equipment. The problems faced in the

analysis of complex fuel-derived liquids are different from those encountered in biomedical or biochemical work. In the former, we search for methods able to detect large molecules in the presence of an excess of small ones. Meanwhile, new developments in mass spectrometric ionisation methods are generally in the biological chemicals field, where the requirement is that of confirming the mass of a molecule of known or suspected structure.

General texts on mass spectrometry include Chapman (1993), Hamming and Foster (1972), McLafferty and Turecek (1993), while papers covering specific topics such as the invention of the MALDI techniques (Hillenkamp et al., 1991) are in the voluminous mass spectrometry literature. The background and evidence of large molecules in coal- and petroleum-derived liquids by mass spectrometry has been reviewed by Herod (2005, 2012), Herod et al. (2012) and Morgan and Kandiyoti (2014). The work described further has shown that material appearing under the 'excluded' peaks in SEC (Herod et al., 1996b) does not correlate with MALDI mass-spectra showing material extending to molecular masses as high as 40,000 u (Herod et al., 1995a; Lazaro et al., 1997; Domin et al., 1997a; Millan et al., 2005a) since this high-mass signal is formed by ablation of cluster ions caused by high laser power onto small molecules in the target sample. This problem highlights the need for fractionation to separate molecular sizes. We next present an outline of sample introduction methods into mass spectrometers, with reference to samples likely to contain high-mass materials.

8.6.1 Liquid chromatography

The requirement for analytes to be volatile in gas chromatography is overcome in liquid chromatography, but sample introduction can still be a significant problem at the mass spectrometer interface. Many different interfaces have been devised to avoid thermal degradation during transfer to the mass spectrometer, including the moving belt, thermo-spray, direct liquid introduction and the particle beam (Chapman, 1993). The moving belt and the direct liquid introduction methods rely on evaporation of analyte in the ion-source vacuum chamber, which is less likely to produce pyrolysis than evaporation at atmospheric pressure. Thermospray and particle beam interfaces create droplets in vacuum from which solvent can evaporate, leaving the analyte in the vapour phase.

Liquid chromatography has not been used extensively for the analysis of coal or petroleum-derived materials. The reasons are twofold: (1) the HPLC methods have not been worked up to apply to whole samples but only to the PAC fractions of relatively low mass and (2) the high cost of mass spectrometers able to accept the input from such columns. The general principles and instrumentation of LC-MS (Niessen and Tinke, 1995) and applications to the detection of sulphur and nitrogen compounds in coal liquids have been reviewed by Neal (1995) and Herod (1998).

Moving belt interfaces have been used to examine pyrolysis and hydropyrolysis tars. Aliphatics including the biomarker pentacyclic triterpanes and aromatics from alkyl benzenes to alkyl dibenzopyrenes were detected, up to molecular masses of about m/z 550 (Herod et al., 1987) with high molecular mass alkanes and

cycloalkanes up to m/z 900 (C_{64}) as well as aromatic homologous series (up to 40 members) to similar high masses (Herod et al., 1988). Polar components of the aromatic fraction were not identified, but the evidence from electron impact and chemical ionisation pointed to the presence of nitrogen containing compounds. Similar data have been obtained using a particle beam interface to a magnetic sector mass spectrometer using similar samples (Herod et al., 1993a). The LC separation of the aromatic fraction was by compound type such as alkyl benzenes and alkyl benzopyrenes. Metalloporphyrins extracted from coals have been examined by Bonnett et al. (1991) using a moving belt interface, reverse phase chromatography and FAB ionisation, giving mass spectra up to m/z 600. A reverse phase liquid chromatographic separation of nitrogen-containing polynuclear aromatics from a solvent refined coal liquid was used to generate fractions for off-line mass spectrometry (Borra et al., 1987). Particle beam spectra of a hydropyrolysis tar have been shown with components to m/z 400 (Herod et al., 1993a).

LC-mass spectra are more complex than GC-mass spectra but LC-MS has not been used to examine the largest molecular mass components of coal liquids such as pyridine-insolubles. Further work is needed to extend the range of molecular masses and types eluted from HPLC columns, probably by using more polar solvents, such as pyridine and NMP, than have been used hitherto. The moving-belt interface is no longer available but thermospray methods may be able to overcome the problems of introducing into a mass spectrometer samples dissolved in relatively involatile solvents such as NMP. SEC has been used off-line to produce fractions of pitch for examination by MALDI-MS (Islas et al., 2003c; Morgan et al., 2009). Mass spectra showed envelopes of ion intensity over ranges of mass for fractions of relatively narrow polydispersity (see Section 8.7).

8.6.2 Thin layer or planar chromatography (TLC)

The technique is useful for fractionating samples before mass-spectrometric or other analyses. Its main advantage stems from the ability to recover and examine all fractions, including the heaviest, without significant loss of sample. The technique is non-destructive, and many samples can be run together (on the same plate) with standards to monitor the separation. Direct interfacing with mass spectrometry is possible but can be a disadvantage. In off-line operation, different mass spectrometric methods can be used to analyse different parts of one sample development if required. Reviews have covered the combination of planar chromatography with mass spectrometry (Somsen et al., 1995) and the application to coal derived materials (Herod, 1994), as well as nitrogen and sulphur compounds (Herod, 1998).

Pitch was fractionated on silica gel plates with development in solvent series from polar to non-polar (Parker et al., 1993; Herod and Kandiyoti, 1995a,b; Herod et al., 1996a; Domin et al., 1998). The fractions were examined directly by probe mass spectrometry showing PACs, neutral and basic nitrogen compounds with molecular mass increasing as mobility on the plate decreased. Subsequently, fractions were analysed by MALDI-MS or PDMS. Observed increases in molecular mass with mobility in more polar solvents were found to correlate with decreasing elution times

(larger molecular size) in SEC with NMP as eluent. The TLC separation took place largely on the basis of molecular size (Li et al., 2004). This work has involved the fractionation of coal tar pitch and a petroleum distillation residue (Petrox from Concepcion, Chile) using pentane, toluene, acetonitrile and pyridine. Fractions were collected from each migration zone and examined by SEC. For both samples, the elution time of the retained material in SEC shifted to earlier times (larger molecules) with decreasing mobility in TLC. Meanwhile, the proportion of excluded material increased with decreasing mobility in TLC. The fractions were not examined by MS methods, but both SEC and TLC indicated that the molecular size of the mobile material increased with decreasing mobility. We believe this may be the first indication of such an agreement between the two methods when applied to coal and petroleum liquids, with potential for examination by mass spectrometric techniques.

In more recent studies, TLC played a major role in the development and optimisation of a MALDI/LD-MS method for the analysis of polydisperse hydrocarbon mixtures (i.e., from coal-, biomass- or petroleum-derived liquids/tars) (Morgan 2008; Morgan et al., 2008a, 2010a; George et al., 2013). The LD-MS/TLC method development work is described in Section 8.6.8.

8.6.3 Field ionisation

FIMS and pyrolysis FIMS have been used to analyse coal and coal liquids (Schulten 1982; Malhotra et al., 1993; Cagniant et al., 1992). FIMS can detect those molecules, which are volatile in vacuum, or which form during pyrolysis in vacuum. High resolution FIMS may allow determination of atomic compositions of peaks, but the complexity of mass spectra observed for asphaltenes and pre-asphaltenes tends to limit the unambiguous use of high resolution. The problem is that the number of components with the same nominal mass (integer mass) increases as the number of atoms increases and as the mass number increases; mass resolution quickly becomes unable to deal with the complexity of molecular ions. The relative intensity of odd-mass peaks to even-mass peaks in spectra of asphaltenes tends to be greater than in spectra of aromatics or oil fractions, indicating that the molecular complexity has increased by the introduction of heteroatoms, further reducing the ability of high resolution mass measurement to give unambiguous results. The upper mass limit of the technique, defined by the requirement of volatility under the operating conditions, appears to be about m/z 1200, but that need not correspond to the largest mass present in any sample. Mass spectra of aromatics extended to m/z 700 (Herod et al., 1993a).

8.6.4 Field desorption

FD mass spectrometry should be able to ionize molecules which are thermally labile or involatile in FIMS, because ionisation is from the solid phase rather than the vapour phase, with no significant fragmentation. Mass ranges observed using this technique appear to exceed the range observed for FIMS (Herod et al., 1993a; Herod, 2005). The difference between the FIMS spectrum and the FD spectrum of the same asphaltene fraction suggests the two techniques may be detecting different materials found within

the samples. The maximum intensities appear at different masses with more intensity by FD above m/z 500. This difference may result from decreasing thermal volatility of the PAC with increasing molecular mass, a situation that should not affect FD-MS.

FD-MS of an asphaltene fraction from Maya crude gave ions up to m/z 800 (Douda et al., 2004). However, the proportion of the asphaltene ionised was not apparent. This exemplifies the problem with the FD method applied to mixtures of unknown mass range. The upper mass limit of the sample is not apparent and may not be reached by the FD method at all. Experimental details of a Maya asphaltene examined by SEC indicate the presence of material excluded from the column porosity that might be of relatively high mass, as in the pyridine insoluble fraction of pitch. In any case, the sample almost certainly contained material of larger masses than those indicated by FD-MS (Millan et al., 2005b; Morgan et al., 2005a).

8.6.5 Fast atom bombardment

Fast atom bombardment mass spectrometry (FAB-MS) relies on ionisation from the liquid phase, in the vacuum of the ion source. Pyrolysis tars from the Argonne set of coals (Vorres, 1990) gave FAB spectra up to m/z 1200 (Winans, 1991). FAB spectra of pentane insoluble material from coal liquefaction extracts showed ions up to about m/z 4000 (Herod et al., 1993d; Herod, 2005). Spectra of asphaltene and pre-asphaltene (benzene-insoluble) fractions of a hydropyrolysis tar were found to be similar, suggesting the technique may not have ionised the entire sample. Fractions collected from SEC of a hydropyrolysis tar asphaltene fraction also reached m/z 2000 (Herod et al., 1993a). The tar had been prepared in a hot-rod reactor. The calibration of the FAB source using CsI salt indicated that m/z values up to about 5000 were detected, but such high-mass ions were not observed from coal-derived liquids, where the upper mass limit was around m/z 3000–4000 (Herod et al., 1993d). The method does ionise quite large biomolecules, however, and the reasons for the lack of high-mass ions from coal liquids may be associated with the liquid matrix and the addition of additives such as acids to the matrix.

8.6.6 ^{252}Cf Plasma desorption-mass spectrometry (PDMS)

PDMS produces ions from solid samples. Many requirements of this technique are similar to those of MALDI-MS. In particular, a sufficiently large ion extraction voltage is required to accelerate ions through the time-of-flight analyser and allow detection of slow (large) as well as fast (small) ions from an unfractionated sample or one of relatively wide polydispersity. PDMS has been used to analyse heavy distillation residues from direct coal liquefaction processes (Larsen et al., 1994). The number of average molecular masses derived from PD were compared with those from SEC. Mass ranges extended to about 2000 u for the PD results using oils, asphaltenes, and preasphaltenes. A comparison of this method with MALDI-MS showed that although PDMS showed similar trends as MALDI, the maximum ion accelerating voltage of the plasma instrument was insufficient to allow detection of high-mass ions (Domin et al., 1998; Johnson et al., 1999).

An alternative view has been expressed favouring PDMS over MALDI-MS on the basis that VPO methods overestimate molecular masses because the sample in solution must consist of aggregates at the solution concentrations necessary for the method to work (Strausz et al., 2002). Therefore, if the MALDI-MS results were comparable with VPO results, they too must be an overestimate. However, work outlined above indicates that aggregation does not become important in NMP solutions at the concentrations used (see Section 8.5). MALDI can ionise and desorb aggregates when high laser fluence is applied to small molecules.

8.6.7 Laser desorption-mass spectrometry (LD-MS) and Matrix-Assisted Laser Desorption/Ionisation Mass Spectrometry (MALDI-MS)

Lasers and mass spectrometry have been combined to study fossil fuel–derived materials for more than 40 years. In early work, rapid laser pyrolysis of coal was observed in the mass spectrometer vacuum (Joy et al., 1970). The spatial variation of the elemental composition of coal macerals in UK and US coals was studied by Lyons et al. (1987, 1990). The laser ablation of coals, coal derived materials and PACs was examined by Greenwood et al. (1990). One salient feature of LD of UV-adsorbing carbon-based materials is the formation of positive and negative ion carbon clusters at relatively low masses, from C_1 up to about C_{29} (Herod et al., 1993c; Jiao et al., 1993; Burroughs et al., 1993). Greenwood (1994) reviewed the relation between mass spectrometry, coal and carbon clusters. The cluster formation increases as the laser power increases and the molecular ion intensity of pure compounds decreases (Herod et al., 1994a). As the laser power increases, the carbon clusters form the fullerene carbon compounds, from C60 (m/z 720) to higher masses. The presence of fullerenes in the spectra of coal-derived materials indicates that the laser power is considerably higher than the minimum fluence necessary for desorption, since fullerenes are easily desorbed by laser energy (Herod et al., 1994a). Fullerenes are much more readily formed from coal-derived materials than from graphite (Greenwood, 1994).

A number of LDI applications have avoided fullerene formation. Winans et al. (1991) examined vacuum pyrolysis tars from the Argonne series coals by LDI as well as by FAB and by DCI. Molecular mass ranges were only to about m/z 800 although the FAB spectrum was limited by the mass range of the instrument. LD-MS of high-temperature coal tar and supercritical-water extracts of coal gave major intensity peaks in the range m/z 200–400, with low-intensity ions up to m/z 15,000 (Wang and Takarada, 2003). LD work on coal tars and pitch from high-temperature coke ovens extended the range of material observed up to m/z 12,000 (Herod et al., 1993b, 1999) and subsequently to m/z 200,000 by MALDI (John et al., 1993, Parker et al., 1993; Islas et al., 2003a), possibly including cluster ions. Molecular mass distributions in coal-derived tars and liquefaction extracts have similarly been shown by LDI to extend up to m/z 12,000 (John et al., 1991; Parker et al., 1993; Herod et al., 1993b) and by MALDI to m/z 20,000–30,000 (John et al., 1993; Parker et al., 1993; Islas et al., 2003a).

Coal samples directly exposed to MALDI-MS showed signal that extended to the limit of the same instrument, m/z 270,000 (John et al., 1993; Parker et al., 1993; Islas

et al., 2003a). In these studies, the mass spectra showed a peak of intensity that was not instrument dependent, in the approximate mass range m/z 1000–5000 (John et al., 1991, 1993; Parker et al., 1993; Herod et al., 1993b; Islas et al., 2003a). Similarly, MALDI-MS spectra were obtained from a series of kerogens mixed as fine powders with matrix by Li et al. (1994b). In pyrolysis tars from maceral concentrates of a UK coal, this peak of intensity shifted significantly to higher masses in going from a coal vitrinite, to a coal liptinite and an inertinite (John et al., 1994). Similar work using the Argonne coals that range from lignite to semi-anthracite showed a range of intense peaks in the mass range m/z 1000–5000, extending at lower intensities up to m/z 270,000 (Herod et al., 1994b). The reproducibility of the ions of relatively low intensity at the upper mass range was not investigated, but the MALDI method did not appear to generate ions corresponding to clusters of molecules when used in samples of wide molecular mass range, using the mass spectrometer then available.

Pyrolysis tars and liquefaction extracts of the Argonne coals showed intense ions over the same mass range, m/z 1000–5000 which was sample dependent (Herod et al., 1994c). As expected, liquefaction extracts extended to rather larger molecular masses. Liquefaction extracts required lower laser fluences to desorb compared to pyrolysis tars. Oxidation and decarboxylated products from Pocahontas coal were examined by LD MS and the mass range of products exceeded m/z 1200 (Stock and Obeng, 1997). Some of the problems associated with LD-MS and MALDI-MS of coal extracts have been discussed (Hunt and Winans, 1995). These were the lack of high-mass components in the mass spectra, the need to identify an effective matrix and the difficulty of detecting high-mass ions in the presence of low mass ions generated from a sample of wide polydispersity. The problems of mass discrimination against the high-mass components of mixtures with high polydispersity (>1.1) have been discussed by several other groups (Lloyd et al., 1995; Montaudo et al, 1994; Shimada et al., 2001). It is relatively easy to detect the smallest molecular ions of a complex mixture but more difficult to observe the highest mass ions at the same time, either quantitatively or qualitatively. ‘Recipes’ for the successful ionisation of various polymers by methods of combining sample and matrix have been given by several researchers (Danis and Karr, 1993; Garozzo et al., 1995; Montaudo et al., 1995).

Comparisons of MALDI-mass determinations with results from SEC determinations have been made (Lehrle and Sarson 1995; Sheng et al., 1994). Calculations on the MALDI mass spectrum of pitch pyridine-insolubles to evaluate an upper mass limit for the spectrum suggested that m/z 95,000 could be the limit of that particular spectrum (Lazaro et al., 1999a). A comparison of a LD spectrum with a MALDI mass spectrum using MBTA as matrix, of the pyridine-insoluble fraction of coal tar pitch, extended to about m/z 9000 (Herod 2005; Millan et al., 2005a); the peak of intensity shifted to slightly higher mass in the MALDI spectrum compared with the LD spectrum.

Evidence of the underestimation of high-mass components of coal-liquids by MALDI-MS has come from the study of polymer standards of low polydispersity, where the relatively high-mass molecular ions were less intense than expected when compared with the low mass molecular ions on a molar ratio basis (Lloyd et al., 1995; Domin et al., 1997b). Fractionation of coal-derived samples to reduce the polydispersity of the fractions is seen as the way to overcome the mass

discrimination caused by too wide polydispersities. Peak masses from MALDI-MS, LD-MS and masses equivalent to elution times in SEC calculated from the PS calibration for three series of narrow time-fractions (collected from SEC) for a coal tar pitch were found to be in quantitative agreement up to m/z 3000 (Islas et al., 2003c). Similar results were obtained in a subsequent study where narrow time-fractions were recovered from the outlet of a SEC system from a pyridine-insoluble fraction of coal tar pitch and a petroleum asphaltene, examined by LD-MS, as discussed in Section 8.2.2. (Morgan et al., 2009). The complementary nature of LD and MALDI has been shown in a study of dichloromethane-solubles from soots produced from fuel rich flames (Herod et al., 2004).

Petroleum distillation residues have been examined by MALDI-MS and LD-MS and shown to have mass range distributions extending up to about m/z 6000 depending on the origin of the residue or asphaltene fraction (Suelves et al., 2001a, 2003). Peak intensity masses were generally below m/z 1000 and in reasonable agreement with estimates from SEC. Recent work has extended the mass range for these samples to m/z 40,000 with relatively low intensity ion strengths above m/z 10,000 but showing a peak of maximum intensity around m/z 2000 (Millan et al., 2005b). Others have shown LD-MS spectra for asphaltenes with a peak of intensity between m/z 1000 and 2000 and the upper limits of the spectra extending to m/z 10,000 (Tanaka et al., 2004; Acevedo et al., 2005). These different works are in broad agreement in terms of both the peak of intensity and the upper mass limits. They also agree in that the laser power required to ionise and volatilise the larger components is well above that required to ionise the smaller mass components of the asphaltenes.

Early work with fractions of an Athabasca bitumen showed that many of the fractions had a peak of maximum intensity below m/z 1000 that were lost in the matrix peaks, but that the fraction containing the largest molecular masses had a peak of maximum intensity around m/z 2800 (Domin et al., 1999). In the whole bitumen sample and the two fractions with the largest molecular masses, the upper mass limits of the spectra exceeded m/z 20,000. The measured masses were in reasonable agreement with VPO and SEC data and the ^{252}Cf plasma spectra followed similar trends but gave lower masses.

Reducing sample polydispersity to avoid cluster ion formation: A potential advance in developing a more robust method for estimating molecular mass distributions and average mass values was tested during an LD-MS study of creosote oil (CO) and anthracene oil (AO-1) (Morgan et al., 2008a). These were samples recovered from distillation of coke oven tars. CO has a nominal boiling point range of 200 – 300°C and the AO-1 sample 250 – 370°C. These boiling ranges limit the range of molecular mass in each sample, although they were commercial products rather than laboratory distillation samples.

LD-MS spectra recorded from analysis of the whole anthracene oil are presented in Fig. 8.17, showing the variability of results depending on the instrumental parameters used. At high laser power (>30%) higher mass components appear resulting from the formation of cluster ions. As explained in Section 8.4.1, in order to reduce the variability of the spectra and obtain more reliable results, the sample was subsequently fractionated by TLC followed by LD-MS analysis direct from the silica surface of the TLC plate (Morgan et al., 2008a).

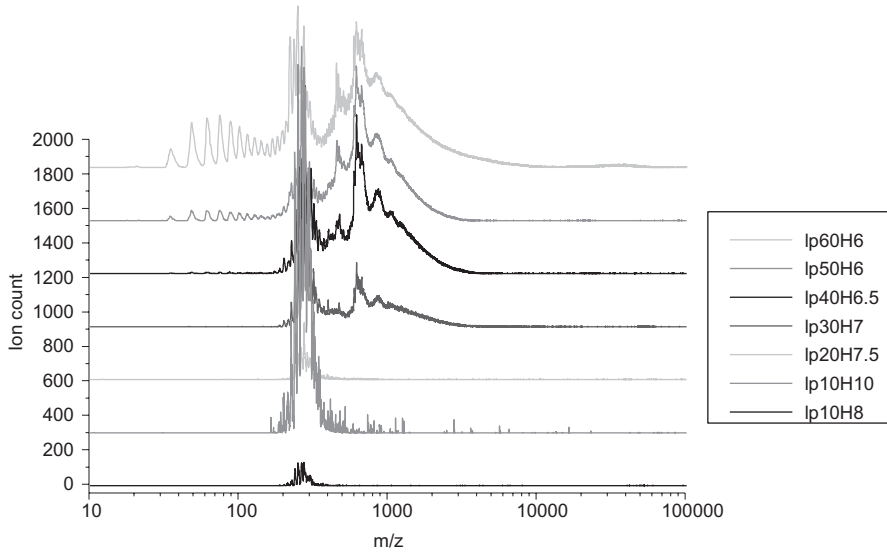

Figure 8.17 Effect of increasing laser power on LD-MS spectra of the neat AO-1. High-mass accelerator (H) voltage was reduced to keep the ion count below 100 units per shot. Linear mode, 600 ns delayed ion extraction time, laser power (percent of max)/H (kV) from bottom to top: 10/8, 10/10, 20/7.5, 30/7, 40/6.5, 50/6 and 60/6%/kV. Each mass spectrum is the sum of 10 scans.
Source: Reprinted with permission from Morgan, T.J., George, A., Álvarez, P., Millan, M., Herod, A.A., Kandiyoti, R., 2008a. Energy Fuels 22(5), 3275–3292. Copyright 2008 American Chemical Society.

Fig. 8.18 presents LD-MS spectra comparing the anthracene oil (AO-1) TLC fractions 1, 4 and 5, where mobility of samples on the plate increased from 1 (the origin) to 5 (the most mobile). Two points emerge when comparing the mass ranges observed from the TLC fractions (Fig. 8.18) with those from the whole sample (Fig. 8.17): (1) Analysing the whole sample gave ions ranging to m/z ~400 at low laser power and to ~3000 m/z as the laser power increased; (2) TLC fractions revealed ions to at least m/z 5000, and the mass distributions were largely independent of laser power (Morgan et al., 2008a). The range of masses observed in analysis of the whole sample was probably underestimated due to mass discrimination, which is common for polydisperse samples and leads to suppression of high-mass ions (Morgan et al., 2008a, 2010b; Herod 2010; Herod et al., 2012). When the high-mass material was isolated from the rest of the anthracene oil sample (TLC fraction 1), ions ranging to >5000 m/z could easily be detected by LD-MS (Fig. 8.18) (Morgan et al., 2008a) with no significant low mass signal. This high-mass fraction probably results from the commercial distillation producing the oil, with no sharp boiling point cut-off.

Analysis of the whole CO sample by LD-MS using low laser power gave ions ranging up to m/z ~300, and as the laser power was ramped the spectra drifted up to ~1200, whereas its TLC separated fractions showed ions to m/z ~1000. The difference between the higher-mass estimates is relatively small and due to either

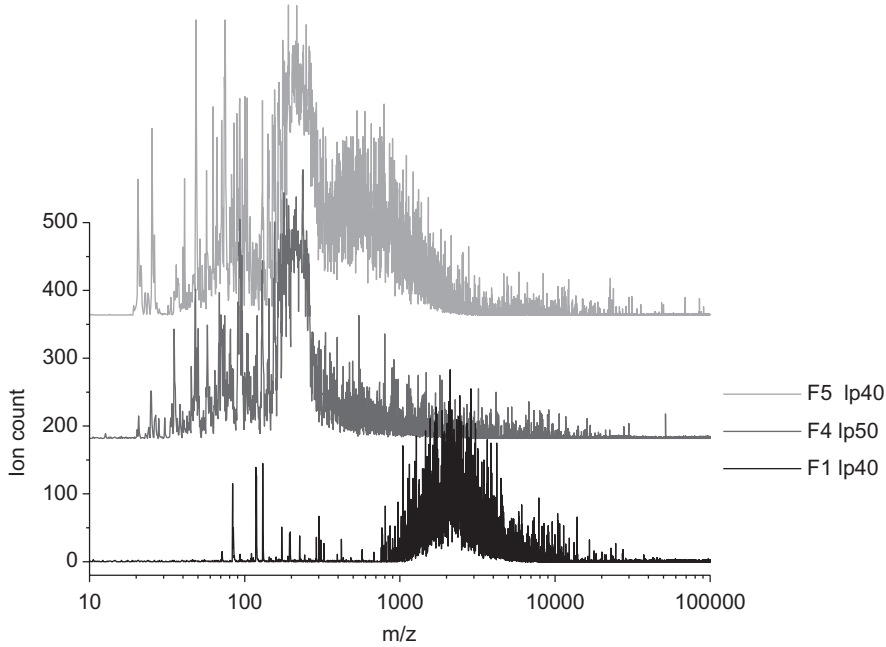

Figure 8.18 LD-MS spectra comparing the anthracene oil (AO-1) thin layer chromatography fractions 1, 4 and 5. Linear mode, no DIE, HMA 10 kV, and laser power 40 − 50% of max. Each mass spectrum is the sum of 10 scans.
Source: Reprinted with permission from Morgan, T.J., George, A., Álvarez, P., Millan, M., Herod, A.A., Kandiyoti, R., 2008a. Energy Fuels 22(5), 3275–3292. Copyright 2008 American Chemical Society.

(1) better ionisation of the higher mass components during analysis of the whole sample due to lighter components acting as matrix or (2) multimer ions being generated during analysis of the whole sample (Morgan et al., 2008a). The sample clearly contained molecular species with masses to at least m/z 1000.

With careful balancing of sample loading on the target, laser power, total ion current and delayed ion extraction, it was possible to observe high-mass materials without generating multimer (artifact) ions. The key to suppressing multimer and cluster ion formation, however, appears to be the low-target loading and consequent low, gas-phase sample concentrations following the laser pulse. Meanwhile, simply diluting the sample solution before application to the standard LD-MS target, as a way of reducing sample loading on the target, did not prove useful (Morgan et al., 2008a). This caused mass discrimination for the CO and AO-1 samples leading to underestimation of their mass distributions. Using TLC to prepare targets appears to be the best way (to date) to suppress multimer and cluster ion formation and reveal the high-mass materials unambiguously (Morgan 2008; Morgan et al., 2008a, 2010b; Herod et al., 2012; Morgan and Kandiyoti, 2014).

During this study a saturated solution in chloroform of a mixture of pyrene (approx. mass 202 u), benzo(a)pyrene (252 u), coronene (300 u) and rubrene (532 u) was also examined by LD-MS. Fig. 8.19 presents LD-MS spectra for the saturated

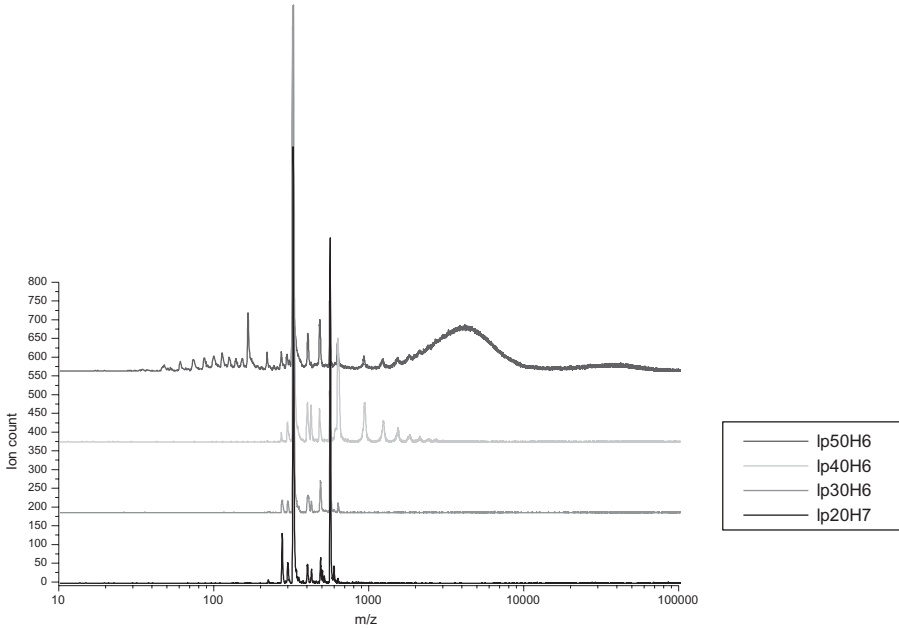

Figure 8.19 Effect of increasing laser power on the LD-MS spectra of the PAH mixture (saturated solution ~3% wt/vol.); where the HMA (high-mass accelerator) voltage was reduced to keep the ion count below 100 units per shot. Linear mode, 600 ns DIE, laser power (percent of maximum) and HMA voltage (kV) from bottom to top (LP/HMA): 20/7, 30/6, 40/6 and 50/6 %/kV. Each mass spectrum is the sum of 10 scans. Sample masses (approx): 202, 252, 300 and 533 u.
Source: Reprinted with permission from Morgan, T.J., George, A., Álvarez, P., Millan, M., Herod, A.A., Kandiyoti, R., 2008a. Energy Fuels 22(5), 3275–3292. Copyright 2008 American Chemical Society.

solution, as a function of increasing laser power, obtained with reduced HMA voltages, in order to avoid overloading the linear mode detector. At LP 50% and HMA 6.0 kV, cluster ions were clearly observed between m/z 3500 and 35,000 (Fig. 8.19). The detector was far from overloaded and was in what were previously thought to be safe operating conditions suggested by Bruker (i.e., fewer than 100 ion counts per laser shot). This shows that it is possible to observe cluster ions of significant intensity in relation to the molecular ions without overloading the detector system.

The mass distribution determinations from LD-MS were consistent with SEC analysis of the CO and AO samples (Morgan et al., 2008a). SEC chromatograms obtained from the whole CO and AO samples are presented in Fig. 8.20 and the TLC fractions from CO in Fig. 8.21; equivalent data for AO TLC fractions is not shown. The mass estimates derived from LD-MS and SEC for the CO and AO samples are listed in Table 8.2, showing good agreement considering the two techniques work in entirely independent ways (Herod et al., 2012; Morgan and Kandiyoti, 2014).

Comparison of the SEC chromatogram from the whole AO and CO (Fig. 8.20) with their TLC fractions (Fig. 8.21) shows how only analysing the whole sample

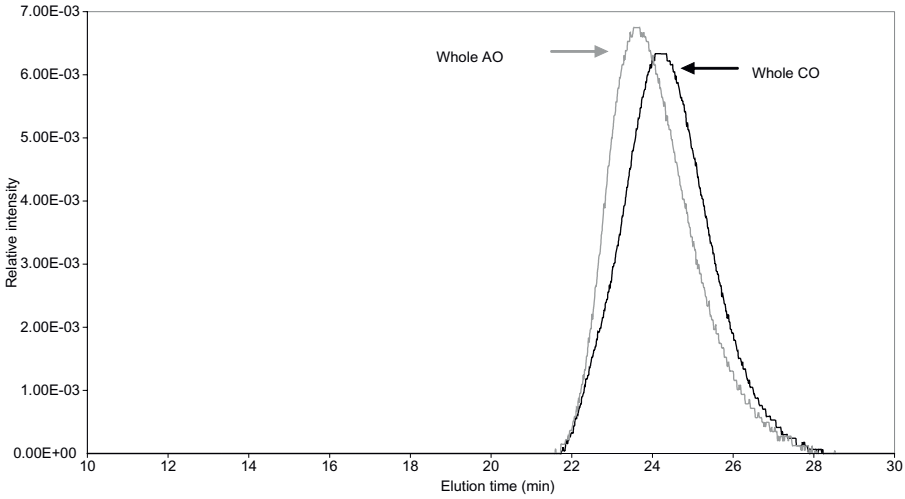

Figure 8.20 Area-normalized SEC chromatograms of the original whole creosote oil and anthracene oil. Detection was by UV-absorption at 300 nm; Mixed A column using NMP as eluent.
Source: Reprinted with permission from Morgan, T.J., George, A., Álvarez, P., Millan, M., Herod, A.A., Kandiyoti, R., 2008a. Energy Fuels 22(5), 3275–3292. Copyright 2008 American Chemical Society.

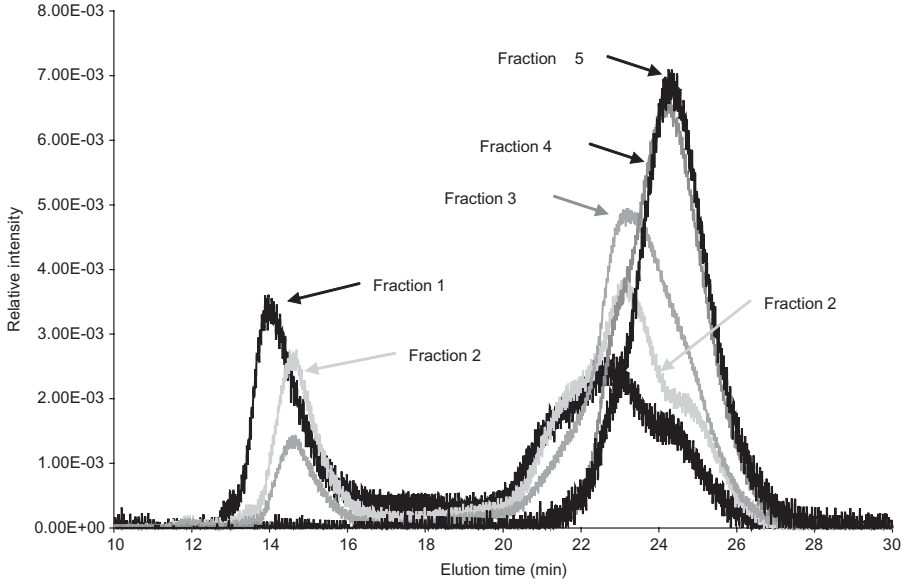

Figure 8.21 Area-normalized SEC chromatograms of creosote oil fractions separated by thin layer chromatography. Detection by UV-absorbance at 300 nm. Mixed A column with NMP as eluent.
Source: Reprinted with permission from Morgan, T.J., George, A., Álvarez, P., Millan, M., Herod, A.A., Kandiyoti, R., 2008a. Energy Fuels 22(5), 3275–3292. Copyright 2008 American Chemical Society.

Table 8.2 SEC-(300 nm) and LD-MS-based mass estimates for the creosote and anthracene oils and their TLC fractions

			Anthracene oil						Creosote oil					
		Unit	**Whole**	**F1**	**F2**	**F3**	**F4**	**F5**	**Whole**	**F1**	**F2**	**F3**	**F4**	**F5**
SEC[a]	Peak Max	u	200	1500	550	400	200	200	100	350	300	270	100	100
	Upper limit	u	700	5000	5000	1900	700	700	700	5000	5000	2700	700	700
LD-MS[b]	Peak Max	m/z	250–280	2,200	n/a	n/a	200	200	250–280	500	n/a	n/a	150	160
	Upper limit	m/z	900–2800	8,000	n/a	n/a	500	1600	450–1100	1000	n/a	n/a	400	500
	Tail	m/z	1500–8000	>10k	n/a	n/a	10k	10 k	1000–1200	2500	n/a	n/a	3000	2000

Source: Reprinted with permission from Morgan, T.J., George, A., Álvarez, P., Millan, M., Herod, A.A., Kandiyoti, R., 2008a. Energy Fuels 22(5), 3275–3292. Copyright 2008 American Chemical Society.

Tail for LD-MS refers to noisy signal that tails off to high mass; it is unclear if this is real signal or artefact.n/a means it was not possible to obtained satisfactory LD-MS spectra, either because the sample could not be ionised or it fragmented and/or due to low abundance.

[a]Upper limit for SEC refers to the forward edge of the retained peak; the time used is taken as +30 s from where the signal clearly deviates from the baseline. Excluded material which elutes before 18 min is not accounted for, therefore the mass values are underestimated.

[b]Upper limit for LD-MS refers to where there is clear ion intensity, assuming there are no multimer ions.

leads to limited information being obtained, even for these light distillate samples (Morgan et al., 2008a). The presence of high molecular mass aromatic molecules in light samples such as creosote and anthracene oils requires some explanation, even though the proportion of high-mass material in the CO and AO samples was rather small. These two samples are distillate cuts that should not have contained nonvolatile high-mass species and it is likely that these high-mass molecules represent carryover/entrainment of liquids and solids during distillation in an industrial process. Sample ageing after recovery may also have played a role (George et al., 2013).

Further confirmation of the presence of high molecular mass molecules in the AO-1 sample vacuum residues were produced by exposing the AO sample in the LD-MS vacuum chamber and acquiring spectra after various lengths of time up to 28 h. A clear trend was observed between the length of time the sample was exposed to the high-vacuum system of the mass spectrometer (~2×10^{-7} mbar) and the mass distribution of the sample. Material at low masses was lost with increased time under vacuum, with enhanced signal at high mass (Morgan et al., 2008a). The observed trend was confirmed by recovering the residue from the LD-MS target with subsequent characterization by SEC and UV-F spectroscopy (not shown). A small red-shift was observed by UV-F and larger masses by SEC for the vacuum residues compared to the original oils. This agreement between two independent techniques singles out the combination of SEC and LD-MS as a robust and reliable method (Herod et al., 2012; George et al., 2013; Morgan and Kandiyoti, 2014). Zubkova's (2011) review of fractionation methods for coal liquids has also suggested that combining TLC with LD-MS and SEC-based determinations appears as the most effective method currently available for estimating mass distributions. Zhang et al. (2015) characterized large PACs (LPAC) in solid petroleum pitch and coal tar pitch by high resolution MALDI-MS. The petroleum pitch was more complex than the coal tar pitch, having a wider distribution in carbon number and double bond equivalents. The petroleum pitch contained roughly equal amounts of odd and even carbon number LPAC while the coal tar pitch had more even carbon number LPAC than odd. The structures in the coal tar pitch were mainly highly condensed aromatic cores with little or no aliphatic side chains. For the petroleum pitch, the main structures were LPAC with short aliphatic side chains. The petroleum pitch contained molecules with masses to at least 2000 m/z and the coal tar pitch to at least 1700 m/z.

Claims made in the past that would limit the masses of heavy petroleum and coal derived fractions to below 1000 u appear unrealistic. Findings showing such low ceilings are limited by the capabilities of the techniques that have been used; structures and upper mass limits of the high mass components of heavy fuel liquids remain to be investigated.

8.6.8 Molecular mass methods using FT-ICR-MS for high mass materials

ESI was first used with FT-ICR-MS to give singly charged ions for petroleum-derived fractions: heavy crude oils by positive ion ESI (Qian et al., 2001a; Hughey et al., 2002b) and negative ion ESI (Hughey et al., 2002a), acids in a heavy crude by negative ion ESI (Qian, 2001b), naphthenic acids by negative ion ESI (Barrow et al., 2003), and Smackover oils (Hughey et al., 2004). These studies produced a wealth of information on components of different atomic compositions but of the same nominal molecular masses, with

information not available from other sources. Maximum masses detected were of the order of m/z 1200 and about 5000 separate ion peaks were detected (Qian et al., 2001a,b).

A series of five papers over the last few years provides an insight into the current state of analysing petroleum materials, both volatile fractions and residues (McKenna et al., 2010a,b; 2013a,b; Podgorski et al., 2013). A recent review by Cho et al. (2015) of developments in FT-ICR-MS instrumentation, ionisation methods, and data interpretation methods for 'Petroleomics' (Rodgers and Marshall, 2007) is aimed at newcomers to FT-ICR-MS. Routine mass resolving powers of 300,000 and more, allow measurement of mass (m/z) to sub-parts per million accuracy. Such accuracy allows calculation of atomic compositions of all molecules, but computerized assessment of such complex data is required.

It could be (and was) assumed that this very powerful mass spectrometric method would do away with the need to fractionate samples before mass spectrometry. This is not the case, partly because the various ionisation methods available for FT-ICR-MS ionize different molecular types. Fractionation methods are needed and two papers (Gaspar et al., 2012; Cho et al., 2012) show that analyses of separated fractions of crudes resulted in many more identified series of compounds than were detected by FT-ICR-MS of the unfractionated sample.

Most published work using FT-ICR-MS has been with petroleum materials or naphthenic acids, an environmental consequence of tar sands activities, liable to cause plant corrosion. Lobodin et al. (2013) investigated the use of a stronger base than ammonium hydroxide in –ve ion ESI by substituting tetramethyl ammonium hydroxide and detected an increase in the number of peaks in several samples. Cho et al. (2013) investigated the speciation of nitrogen compounds in heavy crude oils by APPI of SARA fractions. Griffiths et al. (2014) and Corilo et al. (2013) investigated oil spills; Smit et al. (2015) detected the trace polar components of diesel fuel; Nyadong et al. (2014) applied LD directly to Athabasca bitumen heavy gas oil distillates deposited onto a glass slide.

Although not much work has been done on coal-derived liquids by ESI, the acetone-soluble fraction of a coal tar pitch has been examined. The sample contained mainly PACs as indicated by GC-MS, with minor concentrations of azaarenes (Herod et al., 2005). Further work using reversed phase LC-MS of acetonitrile-soluble fractions of coal tar pitch, a coal digest, and a low temperature coal tar, have shown that the maximum mass detected by positive ion ESI was less than m/z 600 and included the ion m/z 414 which was tentatively identified as the protonated molecule methyl aza ovalene (Herod et al., 2005).

Other examples of coal extracts analysed by FT-ICR-MS include: Kong et al. (2015) extracted Buliangou subbituminous coal with three solvents; Li et al. (2014, 2015b) extracted Zhaotong lignite using hot ethanol; You et al. (2015) oxidized a subbituminous coal with aqueous sodium hypochlorite and extracted with diethyl ether and ethyl acetate; Zheng et al. (2015) hydrothermally extracted three brown coals; and Wu et al. (2003, 2004, 2005) examined pyridine extracts of coals, a coal liquefaction residue and its hydro-processed product. Applications of FT-ICR-MS to biomass oils are few, but Yan et al. (2015) examined biomass oils from sweet sorghum stalk by methanolysis and ethanolysis at 300°C for 30 min. He et al. (2015) demonstrated the collection and detection of levoglucosan from biomass combustion.

Without the combination of fractionation and FT-ICR-MS, it will be difficult to decide if the upper limit of mass of an asphaltene has been reached by the ionisation methods in use.

8.7 LD-mass spectrometry of successively eluting SEC fractions of a coal tar pitch and a petroleum asphaltene

The study presented in Section 8.2.3 gave convincing evidence that SEC with NMP eluent provides accurate molecular mass estimates for coal derived liquids and pitches for material eluting in the retained region (second peak, ~15–25 min, Mixed-A). However, at shorter elution times (i.e., <15 min, excluded region) the PS-PMMA calibration predicted extremely large molecular masses. For example, when pitch samples were examined by SEC, the PS-PMMA calibration indicated that material eluting in the excluded region corresponded to mass values exceeding 100,000 u. It was necessary to determine the molecular mass range of this 'excluded material' more accurately, by taking advantage of recent improvements in our understanding of the LD-MS method, discussed in Section 8.6.8 (Morgan et al., 2008a; Herod et al., 2012; Morgan and Kandiyoti, 2014).

In the follow-up study the pyridine-insoluble fraction of a coal tar pitch (PPI-N) and an asphaltene fraction from Maya crude oil were examined, dissolved in NMP (Morgan et al., 2009). Initially two sub-samples were collected from the outlet of an analytical SEC Mixed-D column for each material (2 min elution time fractions

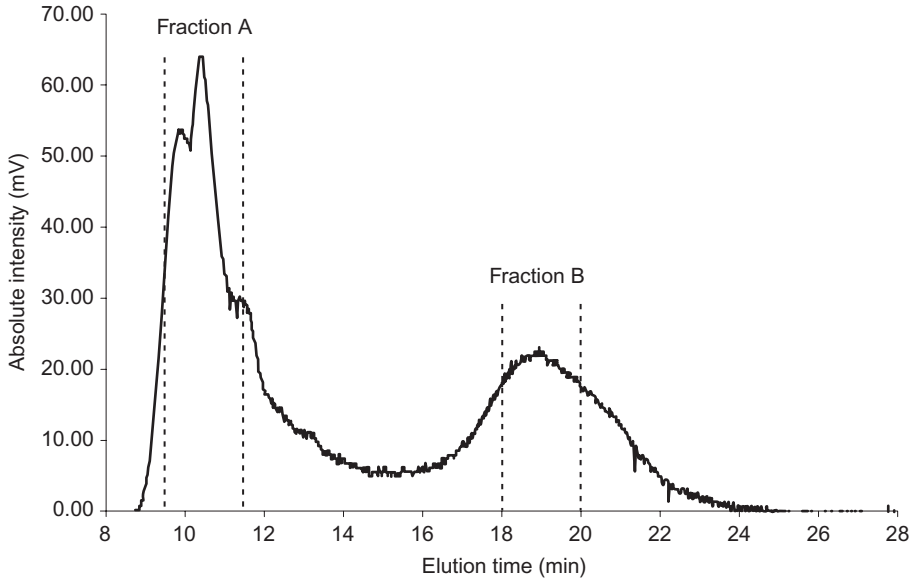

Figure 8.22 SEC chromatogram of the whole PPI-N used to produce the SEC elution-fractions A and B. NMP was used as eluent with a heated (80°C) Mixed-D column and detection by UV-A at 300 nm.
Source: Reprinted with permission from Morgan, T.J., George, A., Alvarez, P., Herod, A.A., Millan, M., Kandiyoti, R., 2009. Energy Fuels 23(12), 6003–6014. Copyright 2009 American Chemical Society.

from the excluded and retained regions; see Fig. 8.22) and examined by LD-MS. The elution-fractions were also reinjected into the SEC system to check for any changes in elution time compared to when the fractions were initially collected (Fig. 8.23); both fractions re-appeared at their collection times. The suggestion that these apparently large mass materials may be formed of aggregates of smaller molecules (Mullins et al., 2008) has been discounted in Section 8.5. There was no disaggregation of material in the excluded region (Fraction A) when the fraction was reinjected into the eluent stream (Morgan et al., 2009). The two elution-fractions were next analysed using LD-MS.

Fig. 8.24 presents LD-mass spectra of SEC elution-fractions A (excluded region) and B (retained region) from the PPI-N sample, with labels indicating the areas of the spectrum used for the mass estimates displayed in Table 8.3. The two spectra were recorded under identical conditions (Morgan et al., 2009). The spectrum for fraction B in Fig. 8.24 showed a clear shift in the peak maximum intensity to lower mass compared to fraction A. To compare the SEC based mass estimates (Table 8.3) with those obtained by LD-MS, the PS-PMMA calibration was extrapolated to cover the region where fraction A had eluted. Normally this would *not* be done, as it is known that in the excluded region (8–15 min), the PS calibration no longer correlates well with the mass of coal-derived materials.

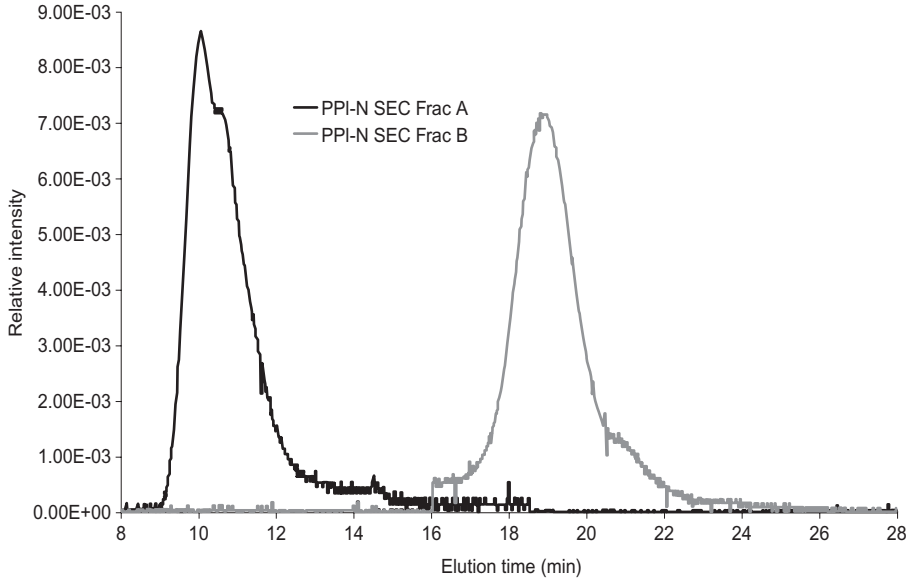

Figure 8.23 Area normalized SEC chromatogram of the PPI-N SEC elution-fractions A and B. NMP was used as eluent with a heated (80°C) Mixed-D column and detection by UV-A at 300 nm.

Source: Reprinted with permission from Morgan, T.J., George, A., Alvarez, P., Herod, A.A., Millan, M., Kandiyoti, R., 2009. Energy Fuels 23(12), 6003–6014. Copyright 2009 American Chemical Society.

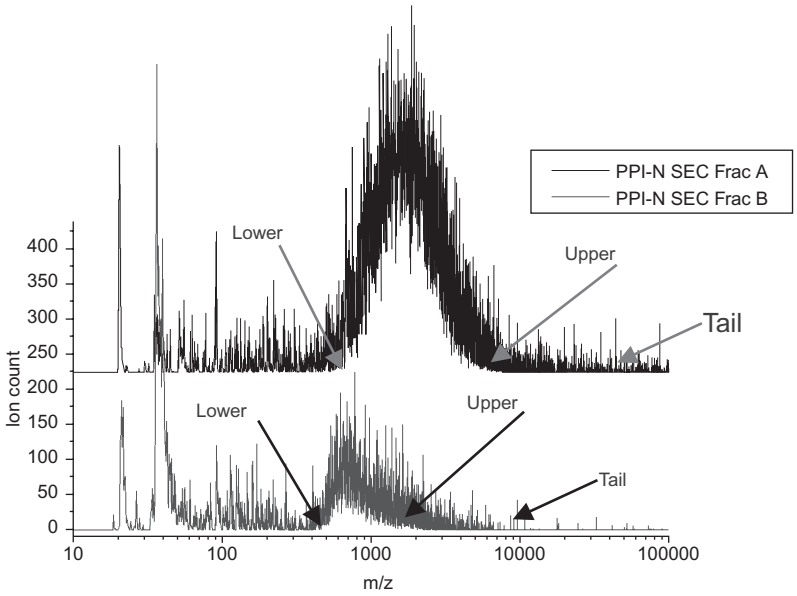

Figure 8.24 LD-mass spectra of the PPI-N SEC elution-fractions A (Black, top) and B (Grey, bottom).
Source: Reprinted with permission from Morgan, T.J., George, A., Alvarez, P., Herod, A.A., Millan, M., Kandiyoti, R., 2009. Energy Fuels 23(12), 6003–6014. Copyright 2009 American Chemical Society.

Table 8.3 Mass estimates from SEC and LD-MS for SEC elution-fractions A and B from the PPI-N sample

Sample	SEC[a]			LD-MS[b]			
	Peak max. int.	Lower limit	Upper limit	Peak max. int.	Lower limit	Upper limit	Tail
	Mass/u			m/z			
Fraction A	305,000[c]	32,600[c]	484,000[c]	1750	500	7100	>40 k
Fraction B	630	160	1660	650	450	2100	~6600

Source: Reprinted with permission from Morgan, T.J., George, A., Alvarez, P., Herod, A.A., Millan, M., Kandiyoti, R., 2009. Energy Fuels 23(12), 6003–6014. Copyright 2009 American Chemical Society.
[a]For the SEC mass estimate the method used is described in Morgan et al. (2009).
[b]For the LD-MS mass estimate the method is described in Morgan et al. (2008a) and the positions where the Tail, Upper and Lower Limit were taken from data shown in Fig. 8.24.
[c]The mass estimates for samples eluting earlier than 15 min are thought to be overestimated and would not normally be accounted for (Karaca et al., 2004; Morgan et al., 2008a, 2009), in this case they are shown to highlight the problem.

Table 8.4 Mass estimates from SEC and LD-MS for SEC elution-fractions (F1–F10) from the PPI-N sample

Sample	SEC[a]			LD-MS[b]			
	Peak Max. Int.	Lower Limit	Upper Limit	Peak Max. Int.	Lower limit	Upper limit	Tail
	Mass/u			m/z			
Fraction 1	305,000	32,600	484,000	1800	700	6500	>10k
Fraction 2	152,000	10,200	305,000	2100	750	6000	>10k
Fraction 3	192,000	10,200	356,000	1800	700	5000	>8000
Fraction 4	178,000	10,200	356,000	1500–1600	700	4600	~7500
Fraction 5	103,500	10,200	329,000	1400	600	4000	~7000
Fraction 6	1100	430	4750	1300–1500	600	3300	~6500
Fraction 7	900	350	3200	1000–1100	500	2500	~5500
Fraction 8	630	160	2200	750–900	500	2500	~6000
Fraction 9	450	100	1000	600	450	2000	~5000
Fraction 10	300	100	770	400–1000	300	2100	~4500

Source: Reprinted with permission from Morgan, T.J., George, A., Alvarez, P., Herod, A.A., Millan, M., Kandiyoti, R., 2009. Energy Fuels 23(12), 6003–6014. Copyright 2009 American Chemical Society.
[a]The SEC mass estimates are based on the method outlined in Morgan et al. (2009).
[b]The LD-MS mass estimates are based on the method described above (cf. Fig. 8.24). For some of the fractions the peak maximum intensity was unclear; in these cases a range is given.

The mass estimates by SEC in Table 8.3 for material eluting earlier than about 15 min (fraction A) are very high and almost certainly over-estimate actual values (Morgan et al., 2009). However, peak maxima and upper limit values for fraction B, obtained from SEC and LD-MS were within ~20% of each other. The LD-MS data clearly showed larger peak maximum intensity mass and average mass values for fraction A (excluded region) compared to fraction B (retained region in Fig. 8.24). There still remained significant differences between masses predicted by SEC (using the PS-PMMA calibration) and those obtained by LD-MS. To improve the mass resolution, narrower elution-time fractions were studied, in order to identify the molecular mass levels at which these differences become measurable.

Ten successive SEC elution-fractions were produced from the PPI-N sample, each fraction covering ~70 s of elution time (five fractions from the excluded region and five from the retained region) covering the 11-min elution time of the sample. A similar set of SEC elution-fractions were also produced from a Maya crude oil asphaltene (not shown) (Morgan et al., 2009). Table 8.4 compares the mass estimates from LD-MS and SEC, for the PPI-N SEC elution-fractions. To examine the relationship between the SEC elution times of the fractions and their mass ranges from LD-MS, peak maximum intensity values were plotted against one another (Fig. 8.25). A nearly linear relationship was observed between the elution times and the m/z peak maxima of elution-fractions from the retained region. The fractions recovered from samples

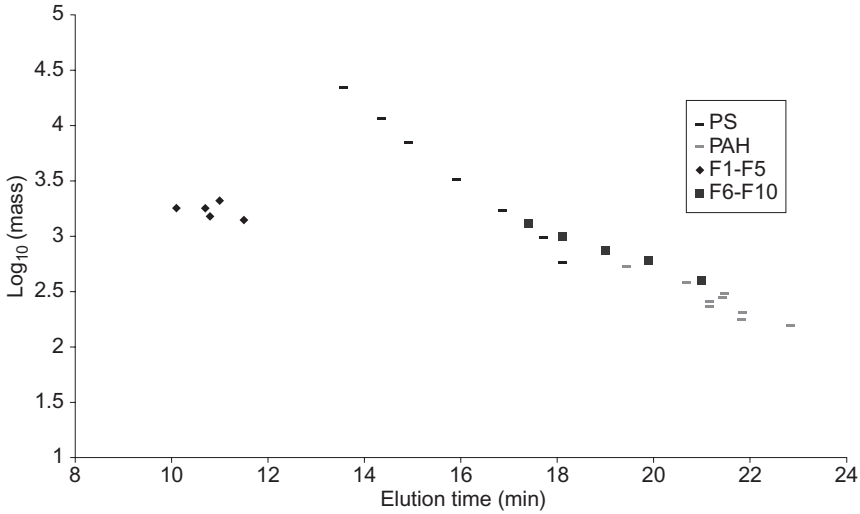

Figure 8.25 Plot of elution time (peak max.) from SEC versus log10 (m/z) of the peak max obtained from LD-MS analysis, for the PPI-N SEC elution-fractions, alongside PS and PAH standards. Mixed-D column was used with NMP as eluent.
Source: Reprinted with permission from Morgan, T.J., George, A., Alvarez, P., Herod, A.A., Millan, M., Kandiyoti, R., 2009. Energy Fuels 23(12), 6003–6014. Copyright 2009 American Chemical Society.

eluting in the excluded part of the chromatogram showed a less clear trend with large discontinuity between the two groups of data points, reflecting the bi-modal distributions of the SEC chromatograms.

Fractions F6–F10 fell close to the PS and PAH calibration results (Fig. 8.25). These data confirm earlier calibrations showing good agreement between SEC and LD-MS results up to a little over 3000 u in the retained region; showing that using PS and PAH standards to calibrate this region of the SEC chromatogram provides a good approximation for coal- and petroleum-derived materials.

The results for fractions F1 to F5 present further evidence of the unusual behaviour of the material eluting in the excluded region. Similar results have been obtained previously (Lazaro et al., 1999b; Islas, 2001; Islas et al., 2003c). In earlier work, these observations were attributed to the failure of LD to ablate the full range of larger mass species. The possible significance of the separation of excluded and retained peaks as likely pointing to a change of molecular conformation was not realised. Other materials observed in our previous work to show similarly early elution times compared to their masses were spherical samples: fullerenes, soots and silica particles (see Section 8.4, Fig. 8.5) (Karaca et al., 2004). These findings suggest that the material eluting as the excluded peak might be adopting quasi-spherical or cage-like conformations, which show up at earlier elution times than their molecular masses would lead us to expect. Alternatively, it is possible that these results represent an upper limit of LD-MS, when used for these types of samples – but there is no obvious reason why

this should be so. A suitable matrix may help increase the upper mass limit of material that can be observed in its entirety.

In separate work, Strausz et al. (2008, 2009) considered the mechanism of excitation of aromatic materials by photons in LD-MS work, to yield either fluorescence or ionisation. The conclusion was that the fluorescence intensity would decrease as molecular mass increased and the ionisation of large molecules would become less efficient with increasing molecular mass.

The PS and PAH calibrations provide a reasonable estimate of mass for material eluting in the retained region of SEC chromatograms. Fractions from the coal-derived sample (PPI-N) matched the SEC PS and PAC calibrations more closely than the petroleum-derived sample. At elution times shorter than 15 min for the Mixed-A column there was significant deviation from the PS calibration for both the coal tar pitch and the petroleum-derived samples. In all cases, material eluting early under the excluded peak was observed to be of significantly higher average masses compared to material eluting at longer times, in the 'retained' region. The data appears conclusive. No evidence was found to show that the early eluting material was composed of aggregates of smaller molecules.

When comparing mass estimates by LD-MS of SEC elution-fractions, similar molecular mass ranges were found for fractions collected at similar elution times, of material from the coal tar pitch and petroleum asphaltene. This suggests that the two samples studied show a similar relationship between size and mass. It provides a degree of confirmation for the suitability of SEC as a technique for estimating molecular masses of complex hydrocarbon mixtures. LD-MS results for the petroleum-derived materials were less coherent compared to those for the coal-derived sample. The differences appear related to the lower aromaticity of the petroleum-derived samples than coal-derived ones. The lower aromaticity of petroleum-derived samples may make it more difficult to observe the higher molecular mass compounds by LD-MS as discussed further in Section 8.8 (Morgan et al., 2010a,b; Herod et al., 2012).

8.8 NMR methods and recent developments

NMR methods for solid and liquid phase studies of coal, coal liquids and polymers have been described (Botto and Sanada 1993; Bovey and Mirau, 1996) for ^{13}C and ^{1}H. Periodic reviews of the techniques and applications of solid state NMR have been given in Analytical Chemistry (Dybowski and Bruch, 1996; Dybowski, 1998; Dybowski and Bai, 2000; Dybowski et al., 2002).

Solid state ^{13}C work on coals and coal tar pitch has been aimed at making the technique quantitative in terms of detecting carbon atoms. Snape et al. (1989a) came to the conclusion that the single pulse excitation method was likely to give the closest approach to quantitative analysis. The relation between carbon aromaticities and hydrogen/carbon ratios in a series of coals has been observed as a linear function using the single pulse excitation method (Maroto-Valer et al., 1998). Aromaticity is defined here as the percentage of total carbon that is aromatic: the relative integrated areas of the spectrum as $100 \times (C_{aromatic}/C_{aromatic} + C_{aliphatic})$.

More recent work aiming to define the molecular mass range of coal liquids has used the coal tar pitch sample as a standard to investigate the different analytical methods we have developed. Snape et al. (1989b) had earlier recognized that most coal tar pitches contain a significant proportion of chloroform-insolubles that could not be analysed by solution NMR techniques. Solid state methods were applied instead to the insoluble fraction. The aim of the investigation was to compare the concentrations of bridgehead carbons in the whole pitch and the toluene-insoluble fraction (comprising 44% of the whole). Using a combination of solution and solid state methods, the concentration of bridgehead carbons was found to increase from the toluene-solubles, to the whole pitch, to the toluene-insolubles (33:42:46% of total carbon respectively), as expected if the aromatic ring systems were becoming larger with increasing molecular mass. Bridgehead carbons are defined as those at the interface between adjoining aromatic groups; they carry no hydrogen atoms and only join other aromatic carbons in conjugated aromatic systems. The molecular weight (Mn) of the pyridine-soluble part of the toluene-insolubles (20% by weight, equivalent to 8.8% of the pitch sample) determined by VPO was 880 u, suggesting that the pyridine-insoluble part of the fraction had molecular weights considerably in excess of this value. This was earlier than the work with SEC and NMP solvent described above (see Section 8.2.2, Fig. 8.4) where the molecular mass up to 3000 u, as indicated by both PS standards and MALDI-MS, was related to elution times.

Andrésen et al. (1998) have examined toluene-insoluble fractions of coal tar pitch samples before and after heat treatment at temperatures much lower than the temperature of formation of the coal tar (>1000°C in a coke oven); the pitch was distilled from the coal tar at 350°C and heat treated at temperatures from 250°C to 380°C. The determination of bridgehead carbons revealed that the number of these carbons in the initial pitch remained constant with the heat treatment, even though the proportion of toluene-insoluble material increased with treatment. Molecular masses were considered to be very low, with number averages less than 500 u. Subsequent work on heat treatment of pitches (Menéndez et al., 2001, 2002) showed that in SEC using NMP as eluent, molecular mass increased significantly with increasing temperature of treatment or with air-blowing. Air-blowing polymerisation did not increase the oxygen content of the sample, indicating that the mode of reaction was by formation of water and the joining of aromatic systems through covalent C-C bonds as in diphenyl.

Initial work with solid state ^{13}C NMR appeared to indicate that the largest molecules of the coal-derived materials (pyridine-solubles and pyridine-insolubles from TLC (Herod et al., 1999) and NMP-solubles from column chromatography (Islas et al., 2002b) contained increasing quantities of carbonyl and aliphatic carbon with increasing molecular size. However, this was caused by a polymerisation or reaction of NMP with the coal-liquid fraction. Subsequent work (Millan et al., 2005c) showed that if NMP was not used in the fractionation, then no significant carbonyl signal was observed and the heavier, larger molecular fractions showed slightly increased aromaticity. A separate study of solution and solid state ^{13}C NMR of a coal digest and

hydrocracked products showed that the common solvents used in NMR were insufficient to allow detection of the largest molecules as defined by the quaternary carbon content (Begon et al., 2003).

The situation was improved using NMP as solvent but the aliphatic carbon signal of the solvent obscured the aliphatic carbon region of the samples. An additional problem arose when attempting to record the ^{13}C NMR spectra of pyridine-soluble and pyridine-insoluble fractions of pitch. These fractions are insoluble in the solvents often used for solution state NMR, such as chloroform as noted by Snape et al. (1989b), but are soluble in NMP. The normal parameters used for solution state NMR were applied to these fractions and no significant aromatic signal was detected. It appears that the instrumental parameters must be tuned to suit the aromatic carbon environments of the larger molecular mass fractions if adequate spectra are to be obtained, again indicating that these materials may have unusual structures. Another problem is that the heavy fractions of pitch (acetone-insoluble but pyridine-soluble and pyridine-insoluble) are insufficiently soluble in NMP for the normal procedures to be applied. Solution concentrations of 20–30% by weight are often cited for NMR measurements in solution, to give an adequate signal in a short analysis time of several minutes for ^{1}H NMR or a few hours for ^{13}C NMR.

Further experiments suggested that at concentrations much above a few percentages by weight, the sample was not in solution and no signal could be obtained in the normal few minutes of scanning for such a diluted solution. Solutions of these materials in NMP at these low concentrations appeared to be very black, hiding the material that was potentially soluble but remained insoluble because of an insufficient volume of solvent. To summarize the results, the acetone-soluble fraction gave a spectrum in solution that was very similar to that of the whole sample; the low-mass molecules would be soluble in most of the solvents commonly used in NMR, including NMP. The pyridine-soluble fraction in solution in NMP gave a weak spectrum in which the aromatic signal was detectable but without significant detail, while no aromatic signal was detected in the spectrum of the pyridine-insoluble fraction in solution in NMP. In the work described above on SEC and UV-fluorescence, the solution strengths involved were much less than a few percent by weight. A suitable test of the NMR method should be the determination of the proportion of carbon existing as bridgehead carbon, since this measure should increase with increasing molecular mass and complexity, as with the cases cited earlier.

An alternative approach to the investigation of structure in coal tar pitch has involved solution in carbon disulphide with the identification of carbon atoms in aromatic rings attached to two or three others in condensed ring systems (Diaz and Blanco, 2003). This approach enables the calculation of bridgehead carbon atoms as a proportion of the total carbon for the sample in CS_2. However, it seems likely that not all of the coal tar pitch would be soluble in this solvent.

From the above discussion, it becomes apparent that the new approach to molecular weight determination of coal- and petroleum-derived liquids will have an impact on the interpretation of NMR results. The solution state work on the relatively

insoluble fractions of coal liquids has not been satisfactory because of the limitations of the solvents able to dissolve the fractions. The work to date has defined the mode of operation in solid state scans – single pulse excitation with long relaxation times between scans as well as the parameter to measure the bridgehead carbon content. In addition, the atomic compositions of the heavy fractions are needed to allow for oxygen and nitrogen functions. While this measurement is routine on the micro scale for volatile molecules, some difficulty was encountered in obtaining reliable measurements for the pyridine insolubles of pitch. The problem arises from the mode of combustion in chromatographic methods for elemental analysis. A plug of oxygen arrives at the furnace just after injection of the sample in a tin capsule and the sample is intended to combust completely before the oxygen plug is swept through the combustion zone. In fact, the pyridine-insolubles of pitch do not combust completely under these conditions, probably because the pitch material forms a char rather than volatilising in the furnace. Therefore the oxygen plug is not seen by most of the sample which fails to burn completely, giving low carbon contents even though there is no significant inorganic content to the sample.

A fresh NMR study was undertaken to try and resolve the problems described above, associated with the analysis of complex hydrocarbon mixtures such as those found in coal tar pitch, petroleum asphaltene and tar sands (Morgan, 2008). A particular emphasis was placed on how to optimize the NMR method to make it possible to obtain reliable structural information on the heaviest, most insoluble portions of coal tar pitch, i.e., the pyridine soluble and insoluble fractions.

Solid-state NMR seems a useful analytical route for tackling heavy coal- and petroleum-derived fractions, as it avoids the need for a solvent. However, it is often found that the resolution of signal is not sufficient for identifying detailed structural differences between samples (Botto et al., 1987; Andrésen et al., 1998; Morgan, 2008; Morgan et al., 2008b). Instrument artifacts known as ‘spinning side bands’ often overlap with signal from the reference material or aliphatic groups, introducing errors that are significant when it is intended to use the NMR data quantitatively (Morgan, 2008; Morgan et al., 2008b), although recently a method was developed that overcomes the problems due to spinning side bands (Alemany et al., 2015). We focus on solution-state NMR methods suitable for obtaining quantitative structural information on aromatic carbon and hydrogen content of complex hydrocarbon mixtures as well as on the proportions of the different types of aromatic and aliphatic groups. Alemany et al. (2015) provide an account of recent developments in solid state NMR methods for quantitative determinations of structural features in petroleum asphaltenes.

The NMR pulse sequences of choice for the analysis of complex hydrocarbon mixtures are standard proton-NMR conditions (^{1}H), ^{13}C inverse gated (IG) (Dickinson, 1980), distortionless enhancement by polarisation transfer (DEPT), and quaternary only spectroscopy (QUAT) (Bendall and Pegg, 1983; Netzel, 1987). Although the latter two methods are not quantitative, they can provide useful additional structural information and confirmation of chemical shift classifications (Dickinson, 1980; Bendall and Pegg, 1983; Netzel, 1987; Morgan et al., 2008b, 2010a). By combining information from these pulse sequences, the following empirical parameters may be

determined (Bendall and Pegg, 1983; Netzel, 1987; Strom et al., 1994; Guillen et al., 1998; Diaz and Blanco, 2003; Morgan et al., 2008b, 2010a):

1. Proportion of aromatic hydrogen (H_{ar})
2. Proportion of aliphatic hydrogen (H_{ali}), further subdivided into:
   a. methine hydrogen (CH)
   b. methene hydrogen (CH_2)
   c. hydrogen in methyl groups (CH_3)
3. Proportion of aromatic carbon (C_{ar})
4. Proportion of aliphatic carbon (C_{ali}), further subdivided into:
   a. quaternary aliphatic carbon ($C_{ali\text{-}Q}$)
   b. tertiary aliphatic carbon (CH)
   c. secondary aliphatic carbon (CH_2)
   d. primary aliphatic carbon (CH_3).

These structural features can be readily quantified for light oils from coal or petroleum, as demonstrated in the late 1970s (Bartle et al., 1979; Dickinson, 1980; Bendall and Pegg, 1983). Here, particular attention has been paid to finding an analytical approach that can make use of these solution state NMR methods for the analysis of heavy coal tar pitch and petroleum (crude) fractions (Snape and Ladner, 1978; Bartle et al., 1979; Gillet et al., 1981; Wilson et al., 1982; Cookson and Smith, 1984; Qian et al., 1985; Rongbao et al., 1988; Kershaw and Black, 1993; Strom et al., 1994; Guillen et al., 1998; Herod et al., 1999; Diaz and Blanco, 2003; Morgan et al., 2008b, 2010a). In practice, these methods are not straightforward to use because working with these types of materials requires considerable experience, time and expense.

Proton-detected heteronuclear multidimensional NMR spectroscopy methods (HSQC, HMQC) are some of the mostly widely used in analytical chemistry. These pulse sequences, or those built upon them (DEPT), are increasingly being used for the analysis of lignin, oils/tars from biomass, coal and petroleum and asphaltenes. A comprehensive discussion of HSQC and HMQC pulse sequences can be found elsewhere (Mandal and Majumdar, 2004). These methods are extremely useful for studying CH, CH_2, CH_3 chemical environments in large molecules and complex mixtures from biomass, coal and petroleum (Kapur and Berger, 2005; Morgan et al., 2008b, 2010a; Rios et al., 2014; Alemany et al., 2015). However, HSQC and related NMR methods are not quantitative and can only provide information on carbon atoms attached to protons, which limits their usefulness for examining polycyclic aromatic compounds.

Many attempts have been made to gain more detailed NMR structural information on coal and petroleum samples, such as aromaticity, size of aromatic fused ring configurations, and degree of alkyl substitution (Dickinson, 1980; Qian et al., 1985; Rongbao et al., 1988; Diaz and Blanco, 2003). The mathematical relationships enabling calculation of average structural parameters (ASPs) have gone through phases of evolution: first proposed by Bartle et al. (1979) the approach has evolved through the work of Dickinson (1980) and Rongbao et al. (1988). To calculate ASPs requires data from ultimate analysis, the appropriate NMR spectra, and estimates of average molecular masses (Mn) (Morgan et al., 2008b, 2010a,b). Within this framework, two distinct approaches will be summarised: (1) where only material containing carbon

and hydrogen are considered (Dickinson, 1980; Rongbao et al., 1988), and (2) where the role of heteroatoms is also incorporated (Bartle et al., 1979; Kershaw and Black, 1993). The choice of which ASP approach to use depends on the samples (among others, their heteroatom content) and the information ultimately expected from the calculations.

A comparison of the two approaches for the maltene and asphaltene fractions of a heavy Mexican Maya crude oil, which has a relatively high heteroatom content, indicated that the information given by the two approaches were broadly similar (Morgan et al., 2010a). Information derived regarding alkyl chain lengths, protonated aromatic carbons, peri-condensed carbon and peripheral carbons of aromatic clusters, were found to be similar (Morgan et al., 2010a). The main benefit of including heteroatoms is that a parameter termed 'number of aromatic rings and rings containing ring joining methylene groups (Ra + RJM)' can be determined (Bartle et al., 1979). This includes certain heteroatoms and ring joining CH_2 groups as well as aromatic carbon atoms. The resulting total ring size can be significantly greater than the total number of aromatic and naphthenic rings found when considering only carbon and hydrogen (Alvarez et al., 2009a; Morgan et al., 2010a). Larger differences were found between the two approaches when the comparison was extended to a set of solubility fractions from a bitumen tar (tar-sand) (Alvarez et al., 2009b; Herod et al., 2012; Morgan and Kandiyoti, 2014). This appears to be due to the higher heteroatom contents of these samples. As expected, more information could be inferred when heteroatom contents were included in the calculations. However, uncertainties introduced through the requirement of the additional experimental data tend to partly diminish the advantages of the approach.

For coal derived materials, heteroatom contents are generally found to be relatively low (< 5 wt%/wt) and using the simpler approach is often sufficient (Dickinson, 1980; Rongbao et al., 1988; Morgan et al., 2008b). For petroleum derived asphaltenes, such as the Maya sample, combined heteroatom contents of up to about 7 (wt %) are possible. For samples with high heteroatom contents, such as bitumen tar asphaltenes (9 wt%), the second approach tends to be more realistic. ASP calculations allow the following parameters to be calculated (Dickinson, 1980; Rongbao et al., 1988; Morgan et al., 2008b, 2010a):

- Fraction of quaternary aromatic carbon ($C_{ar\text{-}Q}$)
- Fraction of protonated aromatic carbon ($C_{ar\text{-}US}$)
- Fraction of peri-condensed aromatic carbon ($C_{ar\text{-}PC}$)
- Fraction of cata-condensed (bridgehead) aromatic carbon (C_{Cata})
- Fraction of quaternary aromatic carbon substituted by alkyl groups ($C_{ar\text{-}S}$)
- Fraction of aromatic carbons substituted by aromatic groups ($C_{ar\text{-}AS}$)
- Average number of aromatic rings per average molecule (R_A)
- Average number of naphthenic rings per average molecule (R_N)

Clearly, information derived from ASP methods only provide averaged bulk parameters. Nevertheless, useful information can be determined such as the average size of fused aromatic ring systems and extents of substitution, among others (Dickinson, 1980; Rongbao et al., 1988; Guillen et al., 1998; Diaz and Blanco, 2003;

Morgan et al., 2008b, 2010a). Fractionation of the 'whole' sample helps in inferring more detailed structural information. This type of quantitative structural information has proved virtually impossible to gain by any technique other than by the use of NMR (Herod et al., 2007; Morgan et al., 2008b, 2010a; Morgan and Kandiyoti, 2014).

In general, most attempts to study the heavier fractions of coal- and petroleum-derived materials prove to be problematic, in particular when quantitative data are required (Snape and Ladner, 1978; Wilson et al., 1982; Gillet et al., 1981; Cookson and Smith, 1984; Strom et al., 1994; Herod et al., 1999; Diaz and Blanco, 2003; Islas et al., 2003b). This appears due to the use of solvents of insufficient strength to dissolve the whole sample, the inadequate choice of experimental conditions, or a combination of the two. Many of the earlier ASP investigations have only been able to gain useful information regarding lighter fractions, equivalent to acetone and chloroform soluble fractions of heavy coal derived samples. In studies examining petroleum asphaltenes, the sample is completely soluble in chloroform and is usually examined as a single bulk sample, i.e., without fractionation into narrower fractions. As already signalled, this approach severely limits the amount of information that can be obtained from these analyses (Morgan et al., 2010a).

Heavy coal tar pitch fractions that are insoluble in common NMR solvents may be dissolved by the use of (undeuterated) NMP as the NMR solvent. NMP is able to dissolve these samples in the high concentrations needed for NMR ($>$ 10% weight per volume) (Morgan et al., 2008b; Herod et al., 2012; Morgan and Kandiyoti, 2014). This approach tends to obscure important bands of the aliphatic part of the spectrum, through signal from the NMP itself. Thus, analysis in NMP solution provides information on only the aromatic part of the spectrum. A second analysis of the same sample is then required, by dissolving the sample in (undeuterated) quinoline. This allows quantitative data to be obtained from the aliphatic part of the spectrum. Using undeuterated solvents is useful for keeping the cost of the analyses within bounds. Coaxial NMR tubes may be used, so a second, more common, deuterated solvent could be used for locking the spectrometer as well as holding the quantitative reference material. Details of the method may be found elsewhere (Morgan et al., 2008b, 2010a).

For petroleum-derived materials, solubility is not an issue, since they mostly tend to be completely soluble in common NMR solvents such as chloroform or tetrachloroethane. The latter is the preferred solvent (Morgan et al., 2010a). However, a key factor in obtaining accurate ASP information with enough resolution to observe differences between solubility fractions, from coal- or petroleum-derived materials, turns out to be the accuracy of the number average molecular mass (Mn) used in the calculation (Morgan et al., 2008b, 2010a; Herod et al., 2012; Morgan and Kandiyoti, 2014). In recent work, the use of TLC fractionations combined with LD-MS analysis (Morgan et al., 2008a, 2010b), as described in Sections 8.3.1 and 8.6.8, has made it possible to obtain more robust Mn estimates, which in turn has led to more reliable structural information being calculated from NMR data (Morgan et al., 2008b, 2010a; Herod et al., 2012; Morgan and Kandiyoti, 2014).

It is also possible to use the information gained from ASP calculations, to arrive at a minimum number average molecular mass of a sample that is consistent with the NMR and ultimate analysis data. This can then be compared with mass estimates

derived from LD-MS and SEC (Morgan et al., 2008b, 2010a). This was possible because for a certain parameter a negative value was found, which was clearly incorrect (Morgan, 2008; Morgan et al., 2008b). On investigation it was found that the most likely reason for this error was the underestimated Mn-values used in the calculation. By assuming a zero value for this parameter (Morgan, 2008; Morgan et al., 2008b, Herod et al., 2012), it was possible to calculate the corresponding minimum average molecular mass for the sample.

As observed in relation to other analytical techniques discussed previously, fractionation of complex samples such as oils, asphaltenes or pitches significantly increases the amount of information that can be obtained from NMR studies. Where solubility becomes problematic during the examination of heavier fractions of such samples, the use of coaxial NMR tubes can greatly improve the quality of the NMR spectra. However, NMR by itself cannot reveal detailed quantitative information individually on the four quarternary aromatic carbon types. It appears that the accuracy of the Mn estimate is paramount in determining these structural features with greater certainty (Morgan et al., 2008b, 2010a,b; Herod et al., 2012; Morgan and Kandiyoti, 2014).

8.8.1 Application of ASP calculations to coal tar pitch and petroleum asphaltenes

The developments in average molecular mass determinations (from SEC and LD-MS) and structural methods (NMR and UV-F) described in this chapter have been used to characterize a number of coal-, petroleum- and bitumen-derived samples through ASP calculations (Morgan, 2008; Morgan et al., 2010a; Herod et al., 2012; Morgan and Kandiyoti, 2014). A brief summary of the conclusions from these studies are provided for solubility fractions of a coal tar pitch and a petroleum asphaltene.

Coal tar pitch: The pitch was fractionated into three sub-fractions: (1) the acetone solubles, (2) insoluble in acetone but soluble in pyridine and (3) insoluble in both acetone and pyridine. The samples were analysed by SEC, LD-MS, NMR, UV-F and elemental analysis to obtain the data required for ASP calculations. The solubility fractions were further sub-divided by TLC to aid the estimation of average mass values used in the ASP calculations (see Section 8.6.8). A detailed account of the methods and results is given in Morgan (2008), Morgan et al. (2008b), Herod et al. (2012), Morgan and Kandiyoti (2014).

Table 8.5 summarises the molecular mass estimates and structural features determined from the ASP analysis of the coal tar pitch solubility fractions. The results showed significant structural differences between the samples, with a trend of increased aromatisation, cata- and peri-condensed carbon content and size of conjugated aromatic ring systems with decreasing solubility (from acetone-soluble to pyridine-insoluble). The average molecular mass (M_n) increased from m/z ~ 300 for the acetone soluble fraction to m/z >2500 for the pyridine insoluble fraction.

Maya heavy crude oil: Analogous data have been reported for the maltene (heptane soluble) and asphaltene fractions of Maya crude as well as for the NMP soluble and insoluble fraction of the asphaltene (Table 8.6). The ASP calculations

Table 8.5 Mass values for pitch solubility fractions derived from LD-MS spectra along with the wavelength of maximum fluorescence (UV-F peak max.) and the average number of fused aromatic rings (ASP calculations)

	LD-MS				UV-F	NMR (ASP)
Pitch fraction	**Low mass limit**	**Most intense mass**	**Upper mass limit**	**M_n**	**Peak max**	**Number fused Ar-rings**
	m/z	**m/z**	**m/z**	**m/z**	**nm**	**Rings**
Acetone soluble	200	350	2500	300	390	3–5
Acetone insoluble – pyridine soluble	300	1200	>4000	1600	440	7–9
Pyridine insoluble	500	1800	>10,000	>2500	480	>30

Source: NMR data from (Morgan, T.J., George, A., Davis, D.B., Herod, A.A., Kandiyoti, R., 2008b. Energy Fuels 22(3), 1824–1835); LD-MS, Mn and UV-F values from (Morgan, T.J., 2008. Molecular mass and structural characterization of heavy hydrocarbon materials. PhD Thesis, Imperial College, London; Herod, A.A., Bartle, K.D., Morgan, T.J., Kandiyoti, R., 2012. Chem. Rev. 112, 3892–3923; Morgan, T.J., Kandiyoti, R., 2014. Chem. Rev. 114(3), 1547–1607).

Table 8.6 Mass values for Maya maltene and asphaltene solubility fractions derived from LD-MS spectra along with the wavelength of maximum fluorescence (UV-F peak max.) and the average number of fused aromatic rings (ASP calculations)

	LD-MS				UV-F	NMR (ASP)
Maya Fraction	**Low mass limit**	**Most intense mass**	**Upper mass limit**	**M_n**	**Peak Max**	**Number fused Ar-rings**
	m/z	**m/z**	**m/z**	**m/z**	**nm**	**Rings**
Maltene (MM)	200	*550*	>5000	500–900	390	2–5
Asphltene (MA)	250	*1800*	>7000	1100–1500	405	8–10
NMP Soluble Asph. (MNS)	200	*1100*	>7000	900–1100	405	5–6
NMP Insoluble Asph. (MNI)	300	*1900*	>10,000	1500–1700	490	>10

Source: NMR data from (Morgan, T.J., George, A., Alvarez-Rodriguez, P., Millan, M., Herod, A.A., Kandiyoti, R., 2010a. J. Chromatogr. A 1217(24), 3804–3818); LD-MS, Mn and UV-F values from (Morgan, T.J., Alvarez-Rodriguez, P., George, A., Herod, A.A., Kandiyoti, R., 2010b. Energy Fuels 24(7), 3977–3989; Herod, A.A., Bartle, K.D., Morgan, T.J., Kandiyoti, R., 2012. Chem. Rev. 112, 3892–3923).

showed that the NMP insoluble fraction (MNI) contained, on average, one large PAH system (>10 rings) surrounded by alkyl chains (average chain length (n) 4.5, aromaticity 54%); termed a continental structure. NMP is a good solvent for aromatic materials but a poor solvent for predominantly aliphatic material. The position of the alkyl chains around the aromatic core appears to have rendered these materials insoluble in NMP.

By contrast, the NMP soluble fraction (MNS) was found to be less aromatic (aromaticity: 50%) but on average contained two PAH groups (5–6 rings in each) connected via aliphatic bridges. This material is thus characterized by small aromatic cores connected by long alkyl-chains (archipelago structure); the solvent appears to access the aromatic cores relatively easily to solvate these molecules. These findings on the sizes of PAH groups correlated well with the positions of the peak maxima in their UV-fluorescence spectra. SEC results from the Maya fraction are discussed in Section 8.2.3; a thorough account of the average mass determinations are given by Morgan et al. (2010b) and for the NMR and ASP results, Morgan et al. (2010a).

This combination of analytical approaches made it possible to determine two distinct structural types present in the Maya asphaltene, the NMP-soluble portion having mainly archipelago structures, and the NMP-insoluble fraction containing mainly continental ones; the maltene had mainly 'island' structures (Morgan et al., 2010a). As with the pitch fractions discussed above, the values show a trend of increasing mass as solubility and/or mobility during TLC decrease (Morgan et al., 2010b). Examples of the application of this ASP approach have been reported for a number of heavy coal, petroleum, and bitumen (tar sands) samples (Herod et al., 2012; Morgan and Kandiyoti, 2014).

8.9 Summary and conclusions – structural features of the largest molecules

The evidence presented in this chapter indicates that there are molecules far larger than 1000 u in coal and petroleum liquids and liquids produced from biomass materials by pyrolysis or simple solvent extraction. The largest molecules found to be excluded from the porosity of SEC columns have molecular shapes that are probably three dimensional and different from the shapes of smaller molecules. These materials have different relations between molecular mass and molecular shape or elution time in SEC as shown by their molecular masses determined by LD-MS of excluded material. Fractionation using solvents of different polarities produces materials with different size ranges as detected by SEC, with the smallest size molecules in the least polar solvents. MALDI and LD mass spectrometric data have shown agreement with mass ranges indicated by SEC by use of the PS calibration curve. Realistic mass distributions were detected with MALDI and LD mass spectrometry, the peaks observed in either method showing broad agreement.

The formation of cluster ions in MALDI-MS and LD-MS occurs when ion intensities of small molecules become too intense, after which additional high-mass cluster ions form at relatively low intensities as shown in Fig. 8.19 for a mixture of PACs and

by Tanaka et al. (2004) from a pure compound. The laser power needed to ionize the largest molecules of a complex mixture is in excess of that for the smallest molecules of the mixture. In such cases, the small molecules can act as matrix for the largest molecules even in the presence of a MALDI-matrix, since the samples themselves are black and aromatic and absorb at the laser wavelength, normally 337 nm. Several methods have been used to give structural information about the larger molecular masses discussed above and their findings are summarised in the following.

UV-fluorescence spectroscopy (UV-F) has been reviewed (Lakowicz, 1986; Rendall, 1987; Oldham et al., 2000) and examples of its use given (Wolfbeis, 1993). Fluorescence spectra of complex aromatic mixtures have been discussed by Apicella et al. (2004) and Herod et al. (2012) and shown in Figs. 8.10 and 8.26. UV-F cannot be used to identify particular structural features or precise sizes of polycyclic aromatics within complex mixtures because of the multiplicity of possible types of structural changes contributing to shifts in the position and shape of the spectra. The synchronous spectrum is of more use for complex mixtures such as samples of coal-, petroleum-, and biomass-derived liquids since a single response is expected for each type of aromatic system, corresponding to excitation by the shortest wavelength for that system and emission by the longest wavelength for the system.

The fluorescence of large complex molecules is much weaker than that of small aromatic systems because of the greater ability of such molecules to lose the energy gained by absorbance of photons, by pathways other than through fluorescence such as degradation to vibrational energy and heat. The effect has been described in detail by Li et al. (1994c) and gives rise to low quantum yields from molecules in which one or more large PAC groups are embedded. Further evidence of decreasing quantum yield with increasing size of conjugated aromatic ring systems (determined by NMR) comes from the study of coal tar pitch, petroleum asphaltene and tar sand solubility fractions (Herod et al., 2012; Morgan and Kandiyoti, 2014).

Strausz et al. (2002, 2008, 2009) reported that fluorescence of asphaltene fractions was most intense for the low-molecular-mass materials and least for the high-mass material. The mechanism of excitation of aromatic materials by photons in LD-MS work, to either fluorescence or ionisation, indicated that the fluorescence intensity would decrease as molecular mass increased, so the ionisation of large molecules would become less efficient with increasing molecular mass. The feeble fluorescence from molecules above mass 1000 u and total lack of fluorescence from molecules of mass above 3000 u despite their strong UV absorbance has been confirmed by many studies (Li et al., 1994c; Herod et al., 1995a, 2012; Morgan et al., 2005a; Ascanius et al. 2004; Morgan and Kandiyoti, 2014).

UV-fluorescence spectroscopy can be used in two distinct ways: (1) using a static solution at high dilution to avoid self-adsorption effects, and (2) using a flow cell with solution flowing from the SEC column in real time with excitation and emission wavelengths set for the duration of the SEC run (Herod et al., 1996b; Morgan et al., 2005a). In static mode, the synchronous spectra of complex mixtures most closely resemble the spectrum of the smallest molecular mass, most abundant and least polar sample fraction. Synchronous spectra of heavier fractions such as pyridine-solubles and pyridine-insolubles tend to shift to longer wavelengths and show much weaker

fluorescence intensity than the smaller, less polar molecules (Morgan et al., 2005a; Karaca et al., 2009; Herod et al., 2012; Morgan and Kandiyoti, 2014). The same trend has also been observed for UF fractions from coal tar pitch (George et al., 2010), synthetic pitches made from the thermal treatment of anthracene oils (Álvarez et al., 2008; Morgan and Kandiyoti, 2014), solubility and TLC fractions from petroleum asphaltenes (Morgan et al., 2010a,b) and tar sands (Alvarez et al., 2009a,b; Herod et al., 2012; Morgan and Kandiyoti, 2014), and TLC fractions of tars from the cogasification of biomass and coal (George et al., 2013).

Fig. 8.10 shows examples of synchronous UV-F of coal tar pitch UF fractions with height normalization, since otherwise the spectra for the heavier fractions would be indistinguishable from the baseline of the spectrum of the lightest fraction, due to their low quantum yields. The shift of synchronous fluorescence to longer wavelengths and the reduction of intensity with increasing numbers of conjugated aromatic rings is shown in Fig. 8.26.

When used in the flow cell mode, the object was to compare the signal from UV-absorbance with the fluorescence signal. For the lightest fractions, UV-A and UV-F chromatograms are similar but chromatograms of heavier fractions show that the excluded material and some of the earliest parts of the retained peaks of SEC give no fluorescence because of the low fluorescence quantum yields. This lack

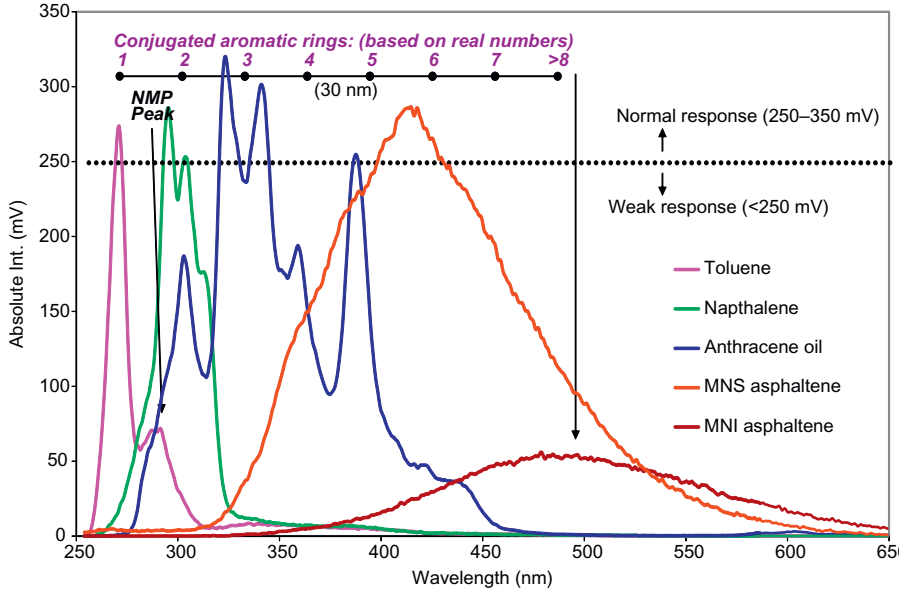

Figure 8.26 Synchronous UV-F spectra of standards and mixtures showing: (1) shift of intensity maximum and (2) the reduction of fluorescence intensity as the number of conjugated aromatic rings increases.
Source: Reprinted with permission from Herod, A.A., Bartle, K.D., Morgan, T.J., Kandiyoti, R., 2012. Chem. Rev. 112, 3892–3923. Copyright 2012 American Chemical Society.

of fluorescence is a sign that the molecular structures are very complex and the vibrational excitation induced by absorbing photons can be lost by methods other than fluorescence. An example of UV-F and UV-A detection in SEC is shown in Fig. 8.13; other examples have been shown previously (Herod et al., 1996b; Morgan et al., 2005a) and similar effects have been observed in petroleum asphaltenes and tar sands (Morgan et al., 2005a; Millan et al., 2005b; Alvarez et al., 2009b; Herod et al., 2012; Morgan and Kandiyoti, 2014). Apicella et al. (2004) have drawn attention to heavy atom quenching of synchronous fluorescence spectra where chlorine in solvents could promote the loss of fluorescence in soluble material from soots. Gargiulo et al. (2015) compared synchronous UV-F spectra of a coal tar pitch and a synthetic naphthalene pitch in solution in NMP; the naphthalene pitch had considerably more fluorescence in the longer wavelength region than found in coal tar pitch and this was attributed to the formation of naphthylene structures that were not present in the coal tar pitch.

Paul-Dauphin et al. (2007) indicated that SEC using a mixed solvent (NMP:chloroform) allowed the analysis of vacuum residues and in addition, the UV-F spectra of a vacuum residue 'C' showed more intensity in the long wavelength range from 400–600 nm in chloroform. Fig. 8.6 shows a comparison of synchronous fluorescence spectra in NMP and chloroform. The difference between the spectra indicates the presence of relatively large aromatic systems that are insoluble in NMP alone, probably because they are shielded by an array of aliphatic pendant groups. Rogel et al. (2015a,b) found shifts of fluorescence maximum wavelength and intensity in maltenes and fractions of heptane-asphaltenes of vacuum residues of crudes. Similar shifts in UV-F spectra in the soluble portions of heat exchanger deposits taken from a refinery have been reported (Chew et al., 2015).

Infrared spectroscopy has been reviewed and tables of IR frequencies are available (McKelvy et al., 1996, 1998; Gillie et al., 2000; Socrates, 2001). Spectra have been obtained for series of fractions from column chromatography (pitch, a coal digest, a low temperature tar) and fractions from solvent solubility (pitch) (Islas, 2001). The spectra provide evidence for large, flat aromatic plates and probably three-dimensional structures in the largest molecules.

Fossen et al. (2011) separated asphaltenes from crude oils into two fractions; the FTIR absorbance spectra for the two asphaltene fractions and the whole asphaltene were very similar. The spectra were interpreted to show small differences in aliphatic, aromatic and heteroatom structures, reflecting the higher molecular weight of the first fractions – the least soluble part of the asphaltene. Infrared spectra of petroleum asphaltenes obtained by Li et al. (2015a) gave a very different picture compared with coal liquids spectra. The relatively intense peak at about 3000 cm^{-1} reflects the methyl group vibrations as with coal liquid spectra, but is more prominent in petroleum work, reflecting the more aliphatic character of petroleum asphaltenes compared with those from coal liquids (Hurt et al., 2013). Rogel et al. (2015a) obtained infrared spectra by transmission measurements using a diamond anvil cell to compress the sample. The signals at 1600 cm^{-1} (aromatic ring stretch), 1700 cm^{-1} (C = O carboxylic acid stretch), and 2900 cm^{-1} (C – H aliphatic stretch) were used as an indication of the aromaticity and carboxylic acid content. The 1600 cm^{-1}/2900 cm^{-1} ratio (aromatic/

aliphatic signal ratio) was plotted as a function of the hydrogen content. The application of FTIR to deposits recovered from refinery plant has been described in detail (Chew et al. 2015; Tay and Kazarian 2009) where detailed analysis of both organic and inorganic components of deposits is possible. Using FTIR in macro- and micro-ATR with diamond or Ge crystals and limited fields of view to avoid critical angles of incidence, it was possible to image deposits from refinery heat exchangers.

VPO is a method based on the colligative property of the elevation of boiling point by reduction of the vapour pressure of a solvent by addition of an involatile solute (Atkins, 1986). Although not much used in our work, literature reports support the relatively high number average mass values (Mn) for coal liquids and petroleum residues (Acevedo et al., 1997; Domin et al., 1999; Torregrosa-Rodriguez et al, 2000; Ancheyta et al., 2002, 2003) giving values up to several thousand molecular mass units for resins and asphaltenes. Because the solute must be present at relatively high concentration, the possibility that aggregation of solute in solution takes place cannot easily be avoided (Strausz et al., 2002). Wiehe (2008) determined molecular weight changes of a residue by thermal treatment using VPO in solution in o-dichlorobenzene at 130°C; number average molecular weights (u) ranged from 920 (saturates), 613 (aromatics), 986 (resins) to 2980 (asphaltenes) before reaction. Wiehe (2008) considered that this data together with elemental compositions of the fractions showed that the whole material was a continuum of molecular size and that thermal treatment merely shifted components into different categories by reaction – either loss of fragments as volatiles or by condensation towards coke formation. The VPO measurements using good solvents indicated number average molecular weights for asphaltenes of several thousand mass units, corresponding to toluene-insoluble material. Wiehe stated that if average asphaltene molecular weights were around 800–1000 mass units, they would evaporate from the treatments already applied in refinery practice. Acevedo et al. (2010) used VPO to estimate the molecular weight of an asphaltene fraction where aggregation was considered negligible; when using toluene or o-dichlorobenzene, Mn was around 1000 g $mole^{-1}$ at temperatures from 80°C to 120°C. Yarranton et al. (2013) measured asphaltene number average molecular weights in toluene solution at 50°C. For pentane- and heptane-asphaltenes the value of Mn (g mol^{-1}) extrapolated to zero concentration was about 750 for lighter asphaltene fractions and around 2000 for the heavy asphaltene fractions; asphaltene association was evident as concentrations increased.

Asphaltene structures – island or archipelago? The aromatic systems of asphaltene molecules have long been a subject of debate. The situation up to 2007 has been summarised by Mullins et al. (2007) where it was considered proven that asphaltene molecules consist of an 'island or continental' aromatic system with pendant aliphatic and cyclo aliphatic groups arranged around the aromatic island or continent. The alternative structure, based on an 'archipelago' structure – more than one aromatic group in an asphaltene molecule – was ruled out by most investigators of asphaltene structure (Acevedo et al., 2005, 2010). However, several reports of archipelago structures have emerged.

The work outlined above using NMR methods (Morgan et al., 2010a) indicated the presence of continental (island) like structures as the dominant structural types in the

MNI fraction of a heptane asphaltene that was rich in aliphatic groups (aromatic carbon <50%), see Section 8.8.1. In the MNS fraction there was the more aromatic material (>50%) with mostly archipelago like structures (Morgan et al., 2008b, 2010a). LD-MS analysis of TLC fractions from the NMP soluble and insoluble fractions of a petroleum asphaltene (Maya crude) showed that some TLC fractions would undergo excessive fragmentation even when using low laser power, while other TLC fractions could be exposed to much higher laser power and generate few to no fragment ions (Morgan et al., 2010b). The excessive fragmentation was more common for TLC fractions from the NMP soluble fraction of the asphaltene. NMR revealed this sample mostly contained 'archipelago' structures while the NMP insoluble sample had mostly 'continental' structures with a large polyaromatic core surrounded by alkyl side chains (Morgan et al., 2010a). Similar results were found for the solubility and TLC fractions of a tar sand (Alvarez et al., 2009a,b; Morgan and Kandiyoti, 2014).

Others who have ventured into this area include the following. Sabbah et al. (2010, 2011, 2012) using a two-step laser ablation and ionisation technique with asphaltenes and model compounds and comparing ionisation behaviours, concluded that the lack of fragmentation of the asphaltenes on ionisation indicated that they were mainly 'island'-type aromatic systems, whereas model compounds based on assumed 'archipelago' structures showed significant fragmentation. Kim et al. (2014) examined naphtha derived pitches by MALDI-MS. Fragmentation occurred at relatively low laser power for one pitch, while a second pitch could be exposed to higher laser power without fragmenting. NMR revealed that the pitch which fragmented at low laser power contained CH_2 bridges between aromatic cores while the pitch that did not fragment had biphenyl-like single C-C bond links between aromatic cores. Archipelago structures have also been identified by NMR in studies of Ecuadorian (Alemany, et al., 2015) and Brazilian (Silva Oliveira et al., 2014) asphaltenes.

Alshareef et al. (2011) thermally cracked a series of model compounds with molecular weights from 534 to 763 g mol^{-1} in the liquid phase at 365–420°C, to simulate catagenesis of the large components in petroleum. NMR analysis showed that pyrene compounds reacted by addition through the attached alkyl groups, to form bridged archipelago products. Badu et al. (2012) calculated ^{13}C solid state NMR spectra of model asphaltenes to assess how valuable such studies of asphaltenes might be in guiding the development of representative three-dimensional models of asphaltenes.

Podgorski et al. (2013) showed the presence of archipelago structures using FT-ICR-MS in a heavy distillate cut of oil, fractionated according to the number of aromatic rings by an HPLC method. Tang et al. (2015) studied six petroleum asphaltene samples of different geographical origins; eight randomly selected molecular ions were subjected to MS-MS but the absence of facile losses of large aromatic structures supported the island (continental) structural model rather than the archipelago model. Schuler et al. (2015) used atomic force microscopy (AFM) and scanning tunnelling microscopy (STM) to visualize asphaltene molecules from coal liquids and petroleums; most of the molecules were island structures with some archipelago structures. Chacón-Patiño et al. (2015) looked at the compositional changes of asphaltenes after hydroconversion and thermal cracking and concluded that both island and archipelago structures were present in the initial asphaltene sample.

In summary, the existence of archipelago structures in asphaltenes is established beyond doubt, but the actual structures themselves are still unknown. In several of the investigations cited earlier, it was assumed that a simple aliphatic bridge would crack under pyrolysis or collisional activation, or through the ionisation energy applied, with release of small aromatic molecules into the products. That such products were not detected has implications for the more complex structures liable to exist in archipelago structural molecules. It is generally agreed that the bulk of the low-molecular-mass (<800 u) asphaltene molecules correspond to island (small continental) structures. There is also evidence of high-mass molecules (>1000 u) with 'continental' structures in the NMP insoluble fraction of asphaltenes. Given the complexity of asphaltene structures and the exceptionally large number of molecular types liable to be present, details of structures are not likely to be easily achieved.

The work on SEC and different mass spectrometric methods has shown that the largest molecules from coal liquids, petroleum asphaltenes and biomass tars are predominantly aromatic and apparently suffer a change of structure and/or conformation as molecular mass increases beyond masses of about 6000 u. The structural change is thought to be one tending to three-dimensional conformations or folding in solution, such that the relation between molecular size and mass observed for small molecules (<6000 u) no longer applies to larger molecules. In support of this, the IR spectra of larger molecular mass fractions fail to show the benzenoid substitution patterns from 600 to 900 cm^{-1}. The solution state ^{13}C NMR spectra of the large aromatic systems have proved difficult to obtain without retuning the instrumental parameters and allowing for solutions of low concentration, indicating that the largest molecules are structurally different from the smaller molecules.

The variety of analytical methods described in Chapter 7, Analytical techniques for low mass materials: method development, and Chapter 8, Analytical techniques for high mass materials: method development, all have their own drawbacks that we have attempted to highlight. It is important to understand these drawbacks in assessing the experimental results. Equally, it is desirable that the analytical methods are extended and developed to characterise the large molecular materials that evidently exist in coal-derived liquids, petroleum residues and biomass tars described in this work, designed around the need to isolate the large molecular mass fractions of these samples, to improve the chances of understanding the changes in structure and size indicated by the SEC and MALDI-MS results. In particular, it is necessary to avoid fractionation methods liable to lose the largest molecules to the fractionation medium.

The various pyrolytic and liquefaction treatments described in Chapter 3, Pyrolysis of solid fuels: experimental design and applications; Chapter 4, High-pressure reactor design: pyrolysis, hydropyrolysis and gasification; Chapter 5, Liquefaction: thermal breakdown in the liquid phase; Chapter 6, Elements of thermal breakdown: heating rate effects and retrogressive reactions; produce different proportions of the large-molecular mass material, are excluded in SEC and present problems for further processing into useful products such as transport fuels. Although these large molecules can be hydrocracked to smaller molecules, as shown for the pitch pyridine insoluble fraction, the catalysts used for this purpose are those regularly used in the petroleum cracking processes. More effective catalysts, tailored to cracking these materials are

clearly needed. In petroleum-derived asphaltenes, these large molecular mass materials present problems during further processing. The heavier crudes becoming available as lighter crudes are depleted tend to have higher levels of asphaltenes than previously. In both coal liquids and petroleum asphaltenes, the largest molecules tend to form char rather than crack to small molecules, if treated by ordinary thermal methods.

References

Abaecheril, A., Nguyen, T., Lora, J., Lepifre, S., Gosselink, R., Arx, U., 2009. Italian Meeting on Lignocellulosic Chemistry, September, Varenna (Lecco), Italy.

Acevedo, S., Escobar, G., Ranaudo, M.A., Pinate, J., Amorin, A., Diaz, M., et al., 1997. Energy Fuels 11, 774.

Acevedo, S., Gutierrez, L.B., Negrin, G., Pereira, J.C., Mendez, B., Delolme, F., et al., 2005. Energy Fuels 19, 1548–1560.

Acevedo, S., Guzman, K., Ocanto, O., 2010. Energy Fuels 24 (3), 1809–1812.

Adegoroye, A., Paterson, N., Morgan, T.J., Herod, A.A., Dugwell, D.R., Kandiyoti, R., 2004. Fuel 83, 1949–1960.

Aguiar, J.I.S., Mansur, C.R.E., 2015. Fuel 140, 462–469.

Alemany, L.B., Verma, M., Billups, W.E., Wellington, S.L., Shammai, M., 2015. Energy Fuels 29 (10), 6317–6329.

Alfi, M., Barrufet, M.A., Moreira, R.G., Da Silva, P.F., Mullins, O.C., 2015. Fuel 154, 152–160.

Al-Muhareb, E.M., Karaca, F., Morgan, T.J., Herod, A.A., Bull, I.D., Kandiyoti, R., 2006. Energy Fuels 20, 1165–1174.

Al-Muhareb, E.M., Morgan, T.J., Herod, A.A., Kandiyoti, R., 2007. Petrol. Sci. Technol 25, 81–91.

Alshareef, A.H., Scherer, A., Tan, X., Azyat, K., Stryker, J.M., Tykwinski, R.R., et al., 2011. Energy Fuels 25 (5), 2130–2136.

Álvarez, P., Granda, M., Sutil, J., Menendez, R., Fernández, J.J., Viña, J.A., et al., 2008. Energy Fuels 22 (6), 4077–4086.

Alvarez, P., Morgan, T.J., George, A., Vendetti, S., Berrueco, C., Millan, M., et al., 2009a. NMR characterization of an Athabasca bitumen. Chemistry of Petroleum and Emerging Technologies, Division of Petroleum Chemistry, ACS National Meeting, August. Washington, DC.

Alvarez, P., Berrueco, C., Venditti, S., George, A., Morgan, T.J., Millan, M., et al., 2009b. Syncrude characterization. In: Preprints ACS Fuel Division, vol. 54(1), ACS National Meeting, Salt Lake City, Utah, March. American Chemical Society: Washington, DC, p. 33.

Ancheyta, J., Centeno, G., Trejo, F., Marroquin, G., Garcia, J.A., Tenorio, E., et al., 2002. Energy Fuels 16, 1121–1127.

Ancheyta, J., Centeno, G., Trejo, F., Marroquin, G., 2003. Energy Fuels 17, 1233.

Andrésen, J.M., Luengo, C.A., Moinelo, S.R., Garcia, R., Snape, C.E., 1998. Energy Fuels 12, 524–530.

Anisimov, M.A., Ganeeva Yu, M., Gorodetskii, E.E., Deshabo, V.A., Kosov, V.I., Kuryakov, V.N., et al., 2014. Energy Fuels 28 (10), 6200–6209.

Anwarul Hasan, M.D., Fulem, M., Bazyleva, A., Shaw, J.M., 2009. Energy Fuels 23, 5012.

Apicella, B., Ciajolo, A., Suelves, I., Morgan, T.J., Herod, A.A., Kandiyoti, R., 2002. Comb. Sci. Technol. 174 (11–12), 345–359.

Apicella, B., Ciajolo, A., Barbella, R., Tregrossi, A., Morgan, T.J., Herod, A.A., et al., 2003a. Energy Fuels 17, 565–570.

Apicella, B., Barbella, R., Ciajolo, A., Tregrossi, A., 2003b. Chemosphere 51, 1063–1069.
Apicella, B., Ciajolo, A., Tregrossi, A., 2004. Anal. Chem. 76, 2138–2143.
Ascanius, B.E., Merino-Garcia, D., Andersen, S.I., 2004. Energy Fuels 18, 1827–1831.
Asikkala, J., Tamminen, T., Argyropoulos, D.S., 2012. J. Agri. Food Chem. 60 (36), 8968–8973.
Atkins, P.W., 1986. Physical Chemistry, third ed. Oxford University Press, UK.
Aust, N., 2003. J. Biochem. Biophys,. Methods 56, 323–334.
Avid, B., Purevsen, B., Paterson, N., Zhuo, Y., Peralta, D., Herod, A.A., et al., 2004. Fuel 83, 1105–1111.
Badre, S., Goncalves, C.C., Norinaga, K., Gustavson, G., Mullins, O.C., 2006. Fuel 85, 1–11.
Badu, S., Pimienta, I.S.O., Orendt, A.M., Pugmire, R.J., Facelli, J.C., 2012. Energy Fuels 26 (4), 2161–2167.
Barrera, D.M., Ortiz, D.P., Yarranton, H.W., 2013. Energy Fuels 27 (5), 2474–2487.
Barrow, M.P., McDonnell, L.A., Feng, X., Walker, J., Derrick, P.J., 2003. Anal. Chem. 75, 860.
Barth, H.G., Boyes, B.E., Jackson, C., 1996. Anal. Chem. 68, 445R.
Barth, H.G., Boyes, B.E., Jackson, C., 1998. Anal. Chem. 70, 251R.
Bartle, K.D., 1989.. In: Kershaw, J.R. (Ed.), Spectroscopic Analysis of Coal Liquids. Elsevier, Amsterdam, pp. 13–40.
Bartle, K.D., Ladner, W.R., Martin, T.G., Snape, C.E., Williams, D.F., 1979. Fuel 58, 413.
Bartle, K.D., Taylor, N., Mulligan, M.J., Mills, D.G., Gibson, C., 1983. Fuel 62, 1181–1185.
Bartle, K.D., Mulligan, M.J., Taylor, N., Martin, T.G., Snape, C.E., 1984. Fuel 63, 1556–1560.
Bartle, K.D., Mills, D.G., Mulligan, M.J., Amaechina, I.O., Taylor, N., 1986. Anal. Chem. 58, 2403–2408.
Baumberger, S., Abaecherli, A., Fasching, M., Gellerstedt, G., Gosselink, R., Hortling, B., et al., 2007. Holzforschung 61, 459.
Begon, V., Islas, C.A., Lazaro, M.-J., Suelves, I., Herod, A.A., Dugwell, D.R., et al., 2000. Eur. J. Mass Spectrom. 6, 39–48.
Begon, V., Suelves, I., Li, W., Lazaro, M.-J., Herod, A.A., Kandiyoti, R., 2002. Fuel 81, 185–202.
Begon, V., Suelves, I., Islas, C.A., Millan, M., Dubau, C., Lazaro, M.-J., et al., 2003. Energy Fuels 17, 1616–1629.
Bendall, M.R., Pegg, D.T., 1983. J. Magn. Reson. 53, 272.
Bermejo, J., Menendez, R., Fernandez, A.L., Granda, M., Suelves, I., Herod, A.A., et al., 2001a. Fuel 80, 2155–2162.
Bermejo, J., Fernandez, A.L., Granda, M., Suelves, I., Herod, A.A., Kandiyoti, R., et al., 2001b. J. Chromatogr. A 919, 255–266.
Berrueco, C., Venditti, S., Morgan, T.J., Álvarez, P., Millan, M., Herod, A.A., et al., 2008. Energy Fuels 22 (5), 3265–3274.
Berrueco, C., Venditti, S., Alvarez, P., Morgan, T.J., Herod, A.A., Millan, M., et al., 2009. Energy Fuels 23 (6), 3008–3015.
Blevins, L.G., Yang, N.Y.C., Mulholland, G.W., Davis, R.W., Steel, E.B., 2002. Am. Chem. Soc. Fuel Chem. Div. Preprints 47 (2), 740–741.
Bodman, S.D., McWhinnie, W.R., Begon, V., Suelves, I., Lazaro, M.-J., Morgan, T.J., et al., 2002. Fuel 81, 449–459.
Bodman, S.D., McWhinnie, W.R., Begon, V., Millan, M., Suelves, I., Lazaro, M.-J., et al., 2003. Fuel 82, 2309–2321.
Boenigk, W., Haenel, M.W., Zander, M., 1990. Fuel 69, 1226–1232.
Bonnett, R., Burke, P.J., Dewey, C.R., Fairbrother, A.E., Major, H.J., 1991. Fuel 70, 1227–1229.
Borra, C., Wiesler, D., Novotny, M., 1987. Anal. Chem. 59, 339–343.
Botto, R.E., Sanada, Y., 1993. Magnetic Resonance of Carbonaceous Solids. Adv. Chem Series 229, American Chem. Soc., Washington DC, USA.

Botto, R.E., Wilson, R., Winans, R.E., 1987. Energy Fuels 1, 173.
Bovey, F.A., Mirau, P.E., 1996. NMR of Polymers. Academic Press, San Diego, USA.
Burlingame, A.L., Boyd, R.K., Gaskell, S.J., 1996. Anal. Chem. 68, 599R.
Burroughs, J.A., Cadre, B.M., Hanley, L., 1993. Amer. Chem. Soc. Div. Fuel Chem 38 (1), 318–323.
Cagniant, D., Gruber, R., Lacordaire-Wilhelm, C., Schulten, H.-R., 1992. Energy Fuels 6, 694–701.
Chacón-Patiño, M.L., Blanco-Tirado, C., Orregon, J.A., Gómez-Escudero, A., Combariza, M.Y., 2015. Energy Fuels 29, 6330–6341.
Chapman, J.R., 1993. Practical Organic Mass Spectrometry, second ed. Wiley, London.
Chen, C., Iino, M., 2001. Fuel 80, 929–936.
Chew, J., Joshi, H.M., Kazarian, S.G., Millan-Agorio, M., Tay, F.H., Venditti, S., 2015. Chapter 4 Deposit characterisation and measurements Crude Oil Fouling. Elsevier. 95–178
Cho, Y., Na, J.-G., Nho, N.-S., Kim, S.H., Kim, S., 2012. Energy Fuels 26 (5), 2558–2565.
Cho, Y., Ahmed, A., Kim, S., 2013. Anal. Chem. 85, 9758–9763.
Cho, Y., Witt, M., Mi Jin, J., Hwan Kim, Y., Nho, N.-S., Kim, S., 2014. Energy Fuels 28 (11), 6699–6706.
Cho, Y., Ahmed, A., Islam, A., Kim, S., 2015. Mass Spectrom. Rev. 34, 248–263.
Choi, K., Mochida, I., 2002. Amer. Chem. Soc. Fuel Chem. Div. 47 (2), 776–777.
Collot, A.-G., 1999. PhD Thesis. University of London.
Cookson, D., Smith, B.J., 1984. Magn. Reson. 57, 355.
Corilo, Y.E., Podgorski, D.C., McKenna, A.M., Lemkau, K.L., Reddy, C.M., Marshall, A.G., et al., 2013. Anal. Chem. 85, 9064–9069.
Crittenden, B.D., Hewitt, G.F., Millan-Agorio, M., Rostani, K., Venditti, S., Yang, M., 2015. Chapter 3 Experimental Generation of Fouling Deposits Crude Oil Fouling. Elsevier. 51–94.
Cunico, R.L., Sheu, E.Y., Mullins, O.C., 2004. Petroleum Sci. Technol. 22 (7&8), 787–798.
Danis, P.O., Karr, D.E., 1993. Organic Mass Spectrom 28, 923–925.
Davison, R.R., Glover, C.J., Burr, B.L., Bullin, J.A., 1995. Chapter 8 Size exclusion chromatography of asphalts. In: Chi-san, W. (Ed.), Handbook of Size Exclusion Chromatography. Marcel Dekker Inc, NY, pp. 211–247.
Deelchand, J.-P., Naqvi, Z., Dubau, C., Shearman, J., Lazaro, M.-J., Herod, A.A., et al., 1999. J. Chromatogr. A. 830, 397–414.
de Wild, P.J., Huijgen, W.J.J., Heeres, H.J., 2012. J. Anal. Appl. Pyrol. 93, 95–103.
Diaz, C., Blanco, C.G., 2003. Energy Fuels 17, 907.
Dickinson, E.M., 1980. Fuel 59, 290.
Domin, M., Moreea, R., Lazaro, M.-J., Herod, A.A., Kandiyoti, R., 1997a. Rapid Commun. Mass Spectrom. 11, 638–645.
Domin, M., Moreea, R., Lazaro, M.-J., Herod, A.A., Kandiyoti, R., 1997b. Rapid Commun. Mass Spectrom. 11, 1845–1852.
Domin, M., Li, S., Lazaro, M.J., Herod, A.A., Larsen, J.W., Kandiyoti, R., 1998. Energy Fuels 12, 485–492.
Domin, M., Herod, A.A., Kandiyoti, R., Larsen, J.W., Lazaro, M.-J., Li, S., et al., 1999. Energy Fuels 13, 552–557.
Dong, S., Wu, L., Paterson, N., Herod, A.A., Dugwell, D.R., Kandiyoti, R., 2007. Energy Fuels 21, 1062–1070.
Douda, J., Llanos, Ma. E., Alvarez, R., Navarette Bolanos, J., 2004. Energy Fuels 18, 736–742.
Duong, A., Chattopadhyaya, G., Kwok, W.Y., Smith, K.J., 1997. Fuel 76, 821.
Durand, E., Clemancey, M., Lancelin, J.-M., Verstraete, J., Espinat, D., Quoineaud, A.-A., 2010. Energy Fuels 24 (2), 1051–1062.

Dutta Majumdar, R., Gerken, M., Hazendonk, P., 2015. Energy Fuels 29 (5), 2790–2800.
Dybowski, C., 1998. Anal. Chem. 70, 1R.
Dybowski, C., Bai, S., 2000. Anal. Chem. 72, 1R.
Dybowski, C., Bruch, M.D., 1996. Anal. Chem. 68, 161R.
Dybowski, C., Bai, S., Bramer, S.V., 2002. Anal. Chem. 74, 2713.
Fossen, M., Kallevik, H., Knudsen, K.D., Sjöblom, J., 2011. Energy Fuels 25 (8), 3552–3567.
Fulem, M., Becerra, M., Anwarul Hasan, M.D., Zhao, B., Shaw, J.M., 2008. Fluid Phase Equilibria 272, 32.
Gargiulo, V., Apicella, B., Alfè, M., Russo, C., Stanzione, F., Tregrossi, A., et al., 2015. Energy Fuels 29, 5714–5722.
Garozzo, D., Impallomeni, G., Spina, E., Sturiale, L., Zanetti, F., 1995. Rapid Commun. Mass Spectrom. 9, 937–941.
Gaspar, A., Zellermann, E., Lababidi, S., Reece, J., Schrader, W., 2012. Energy Fuels 26 (6), 3481–3487.
George, A., Morgan, T.J., Alvarez, P., Millan, M., Herod, A.A., Kandiyoti, R., 2010. Fuel 89 (10), 2953–2970.
George, A., Tran, K., Morgan, T.J., Benke, P.I., Berrueco, C., Lorente, L., et al., 2011. Green Chem. 13, 3375.
George, A., Lorente, E., Berrueco, C., Álvarez, P., Millan, M., Ungeheuer, J., et al., 2013. Energy Fuels 27 (7), 3786–3801.
Gibbins, J.R., Kimber, G.M., Gaines, A.F., Kandiyoti, R., 1991. Fuel 70, 380–385.
Gidh, A.V., Decker, S.R., Vinzant, T.B., Himmel, M.E., Williford, C., 2006. J. Chromatogr. A 1114 (1), 102–110.
Gillet, S., Rubini, P., Delpuecg, J.J., Escalier, J.C., Valentin, P., 1981. Fuel 60, 221.
Gillie, J.K., Hochlowsk, J., Arbuckle-Keil, G.A., 2000. Anal. Chem. 72, 71R.
Greenwood, R.E., 1994. Organic Mass Spectrom. 29, 61–77.
Greenwood, P.F., Strachan, M.G., Willett, G.D., Wilson, M.A., 1990. Org. Mass Spectrom. 25, 353–362.
Griffiths, M.T., Da Campo, R., O'Connor, P.B., Barrow, M.P., 2014. Anal. Chem. 86, 527–534.
Groenzin, H., Mullins, O.C., 2000. Energy Fuels 14, 677–684.
Guerra, A., Gaspar, A.R., Contreras, S., Lucia, L.A., Crestini, C., Argyropoulos, D.S., 2007. Phytochemistry 68 (20), 2570–2583.
Guillen, M., Blanco, J., Canga, J., Blanco, C., 1991. Energy Fuels 5, 188.
Guillen, M., Diaz, C., Blanco, J., 1998. Fuel Process. Technol. 58, 1.
Haberhauer, G., Bednar, W., Gerzabek, M.H., Rosenberg, E., 1999. MALDI-TOF-MS analysis of humic substances - a new approach to obtain additional structural information?. In: Ghabbour, E.A., Davies, G. (Eds.), Understanding Humic Substances: Advanced Methods, Properties and Applications. Royal Society of Chemistry, London, pp. 121–128. special publication no.247, (1999).
Haberhauer, G., Bednar, W., Gerzabek, M.H., Rosenberg, E., 2000. Application of MALDI-TOF-MS to the characterization of fulvic acids. In: Ghabbour, E.A., Davies, G. (Eds.), Humic Substances, Versatile Components of Plants, Soils and Water. Royal Society of Chemistry, London, pp. 143–152. special publication no. 259, (2000).
Hamilton, R., Hamilton, S., 1987. Thin layer chromatography ACOL. John Wiley, London, UK.
Hamming, M.C., Foster, N.G., 1972. Interpretation of Mass Spectra of Organic Compounds. Academic Press, NY.
He, S., Li, L., Duan, H., Naqwi, A., Hogan Jr., C.J., 2015. Aerosol analysis via electrostatic precipitation-electrospray ionization mass spectrometry. Anal. Chem. 87, 6752–6760.

Hedges, J.I., Eglinton, G., Hatcher, P., Kirchman, D.L., Arnosti, C., Derenne, S., et al., 2000. Org. Geochem. 31, 945.
Herod, A.A., 1994. J. Planar Chromatogr. 7, 180–196.
Herod, A.A., 1998. Azaarenes and thiaarenes. In: Neilson, A.H. (Ed.), Chapter 7 in *PAHs and related compounds* part 3. Springer-Verlag, Berlin, pp. 271–323.
Herod, A.A., 2005. Mass spectrometry of coal liquids; Chapter 8 Determination of organic compounds by methods using mass spectrometry. In: Nibbering, N.M.M. (Ed.), The Encyclopedia of Mass Spectrometry vol 4 Fundamentals of and Applications to organic (and organometallic) compounds. Elsevier, Oxford, UK, pp. 790–803.
Herod, A.A., 2010. Rapid Commun. Mass Spectrom. 24, 2507.
Herod, A.A., 2012. Chapter 33 'Hydrocarbon Processing: MALDI-MS of polydisperse hydrocarbon samples'. In: Lee, M.S. (Ed.), Mass Spectrometry Handbook. John Wiley & Sons, Hoboken, NJ, pp. 725–747. 2012.
Herod, A.A., Kandiyoti, R., 1995a. Characterisation of large molecular mass materials in coal tar pitch fractions separated by planar chromatography. In: Pajares, J.A., Tascon, J.M.D. (Eds.), Coal Science vol. I, 8th ICCS, Oviedo, Spain 10–15 September1995. Elsevier, Amsterdam, pp. 949–952.
Herod, A.A., Kandiyoti, R., 1995b. J. Chromatogr. A 708, 143–160.
Herod, A.A., Kandiyoti, R., 1995c. Fuel 74, 784–786.
Herod, A.A., Kandiyoti, R., 1996. J. Planar Chromatogr. 9, 16–24.
Herod, A.A., Kandiyoti, R., 2000. Unpublished work, October.
Herod, A.A., Lazaro, M.J., 2000. Thin layer (planar) chromatography In: Wilson, I. Adlard, E.R. Poole, C.F. Cook, M. (Eds.), Encyclopedia of separation science, vol. III. Academic Press, pp. 3690–3701.
Herod, A.A., Ladner, W.R., Stokes, B.J., Berry, A.J., Games, D.E., Hohn, M., 1987. Fuel 66, 935–946.
Herod, A.A., Ladner, W.R., Stokes, B.J., Major, H.J., Fairbrother, A., 1988. The Analyst 113, 797–804.
Herod, A.A., Stokes, B.J., Schulten, H.-R., 1993a. Fuel 72, 31–43.
Herod, A.A., Kandiyoti, R., Parker, J.E., Johnson, C.A.F., John, P., Smith, G.P., et al., 1993b. J. Chem. Soc. Chem. Comm 9, 767–769.
Herod, A.A., Kandiyoti, R., Parker, J.E., Johnson, C.A.F., John, P., Smith, G.P., et al., 1993c. Rapid Commun. Mass Spectrom. 7, 360–362.
Herod, A.A., Stokes, B.J., Tye, R.E., Kandiyoti, R., Gaines, A., Li, C.-Z., 1993d. Fuel 72, 1317–1325.
Herod, A.A., Stokes, B.J., Hancock, P., Kandiyoti, R., Parker, J.E., Johnson, C.A.F., et al., 1994a. J. Chem. Soc. Perkin 2, 499–506.
Herod, A.A., Li, C.-Z., Parker, J.E., John, P., Johnson, C.A.F., Smith, G.P., et al., 1994b. Rapid Commun. Mass Spectrom. 8, 808–814.
Herod, A.A., Li, C.-Z., Xu, B., Parker, J.E., Johnson, C.A.F., John, P., et al., 1994c. Rapid Commun. Mass Spectrom. 8, 815–822.
Herod, A.A., Johnson, B.R., Bartle, K.D., Carter, D.M., Cocksedge, M.J., Domin, M., et al., 1995a. Rapid Commun. Mass Spectrom. 9, 1446.
Herod, A.A., Johnson, B.R., Bartle, K.D., Kandiyoti, R., 1995b. Large molecules in coal, where do they hide? In: Parajes, J.A., Tascón, J.M.D. (Eds.), Coal Science vol. I, Paper to 8th ICCS, Oviedo, Spain, September 10–15, 1995. Elsevier, Amsterdam, pp. 315–318.
Herod, A.J., Gibb, T.C., Herod, A.A., Zhang, S.F., Xu, B., Kandiyoti, R., 1995d. Fuel 1995c 75, 437.
Herod, A.A., Zhang, S.-F., Carter, D.M., Domin, M., Cocksedge, M.J., Parker, J.E., et al., 1996a. Rapid Commun. Mass Spectrom. 10, 171–177.

Herod, A.A., Zhang, S.-F., Johnson, B.R., Bartle, K.D., Kandiyoti, R., 1996b. Energy Fuels 10, 743–750.
Herod, A.J., Gibb, T.C., Herod, A.A., Shearman, J., Dubau, C., Zhang, S.-F., et al., 1996c. J. Planar Chromatogr 9, 361–367.
Herod, A.A., Lazaro, M.-J., Rahman, M., Domin, M., Cocksedge, M.J., Kandiyoti, R., 1997. Rapid Commun. Mass Spectrom. 11, 1627–1634.
Herod, A.A., Shearman, J., Lazaro, M.-J., Johnson, B.R., Bartle, K.D., Kandiyoti, R., 1998. Energy Fuels 12, 174–182.
Herod, A.A., Islas, C.A., Lazaro, M.-J., Dubau, C., Carter, J.F., Kandiyoti, R., 1999. Rapid Commun. Mass Spectrom. 13, 201–210.
Herod, A.A., Lazaro, M.-J., Domin, M., Islas, C.A., Kandiyoti, R., 2000a. Fuel 79, 323–337.
Herod, A.A., Lazaro, M.-J., Suelves, I., Dubau, C., Richaud, R., Shearman, J., et al., 2000b. Energy Fuels 14, 1009–1020.
Herod, A.A., Zhuo, Y., Kandiyoti, R., 2003. J. Biochem. Biophys. Methods 56, 335–361.
Herod, A.A., Apicella, B., Ciajolo, A., Millan, M., Galmes, C., Kandiyoti, R., 2004. Rapid Commun. Mass Spectrom. 18, 331–338.
Herod, A.A., Millan, M., Morgan, T.J., Li, W., Feng, X., Kandiyoti, R., 2005. Eur. J. Mass Spectrom. 11, 429–442.
Herod, A.A., Bartle, K.D., Kandiyoti, R., 2007. Energy Fuels 21, 2176.
Herod, A.A., Bartle, K.D., Morgan, T.J., Kandiyoti, R., 2012. Chem. Rev. 112, 3892–3923.
Hessler, J.P., Seifert, S., Winans, R.E., 2002. Amer. Chem. Soc. Fuel Chem. Div. 47 (2), 736–737. Preprints.
Hillenkamp, F., Keras, M., Beavis, R.C., Chait, B.T., 1991. Anal. Chem. 63 (24), 1193A.
Homma, T., Tazaki, M., 1995. Size exclusion chromatography of natural and synthetic rubbers, Chapter 7 In: Chi-san, W. (Ed.), Handbook of size exclusion chromatography, vol. 69. Marcel Dekker, New York, pp. 185–210. Chromato-graphic Science Series.
Hourani, N., Muller, H., Adam, F.M., Panda, S.K., Witt, M., Al-Hajji, A.A., et al., 2015. Energy Fuels 29 (5), 2962–2970.
Hughey, C.A., Rodgers, R.P., Marshall, A.G., Qian, K.N., Robbins, W.K., 2002a. Org. Geochem. 33, 743.
Hughey, C.A., Rodgers, R.P., Marshall, A.G., 2002b. Anal. Chem. 74, 4145.
Hughey, C.A., Rodgers, R.P., Marshall, A.G., Walters, C.C., Qian, K.N., Mankiewicz, P., 2004. Org. Geochem. 35, 863.
Huisman, I.H., Prádanos, P., Hernández, A., 2000. J. Membr. Sci. 179, 79.
Hunt, J.E., Winans, R.E., 1995. Am. Chem. Soc. Div. Fuel Chem. 40 (3), 449–452.
Hurt, M.R., Borton, D.J., Choi, H.J., Kenttämaa, H.I., 2013. Energy Fuels 27, 3653–3658.
Islas, C.A., 2001. PhD Thesis, University of London.
Islas, C.A., Suelves, I., Carter, J.F., Herod, A.A., Kandiyoti, R., 2000. Rapid Commun. Mass Spectrom. 14, 1766–1782.
Islas, C.A., Suelves, I., Carter, J.F., Herod, A.A., Kandiyoti, R., 2001a. Pyrolysis-GC-MS of pitch fractions from preparative size exclusion chromatography In: Gelpi, E. (Ed.), Advances in mass spectrometry, vol. 15. Wiley, Chichester, pp. 923–924.
Islas, C.A., Suelves, I., Herod, A.A., Kandiyoti, R., 2001b. MALDI-TOF mass spectra of pitch fractions with narrow polydispersity for the calibration of SEC. ICCS-Paper 215, Proc. 11th Intl. Conf. Coal Sci., September 30–October 5, San Francisco, CA.
Islas, C.A., Suelves, I., Morgan, T.J., Herod, A.A., Kandiyoti, R., 2001c. Size exclusion chromatography with 1-methyl-2-pyrrolidinone as eluent: a structure independent method for molecular mass determination. ICCS-Paper 217, Proc. 11th Intl. Conf. Coal Sci., September 30–October 5, San Francisco, CA.

Islas, C.A., Suelves, I., Carter, X.E., Herod, A.A., Kandiyoti, R., 2001d. Rapid Commun. Mass Spectrom. 15, 845–856.
Islas, C.A., Suelves, I., Carter, J.F., Herod, A.A., Kandiyoti, R., 2001e. An investigation of Baltic amber and its solvent extracts by various mass spectrometric methods In: Gelpi, E. (Ed.), Advances in mass spectrometry, vol. 15. Wiley, Chichester, pp. 415–417.
Islas, C.A., Suelves, I., Carter, J.F., Herod, A.A., Kandiyoti, R., 2002a. Rapid Commun. Mass Spectrom. 16, 481–495.
Islas, C.A., Suelves, I., Carter, J.F., Li, W., Morgan, T.J., Herod, A.A., et al., 2002b. Rapid Commun. Mass Spectrom. 16, 774–784.
Islas, C.A., Suelves, I., Carter, I.E., Apicella, B., Herod, A.A., Kandiyoti, R., 2002c. Paper to Mediterranean Combustion Symposium, Egypt.
Islas, C.A., Suelves, I., Carter, I.E., Apicella, B., Herod, A.A., Kandiyoti, R., 2003a. Comb. Sci. Technol. 175, 775–791.
Islas, C.A., Suelves, I., Li, W., Morgan, T.J., Herod, A.A., Kandiyoti, R., 2003b. Fuel 82, 1813–1823.
Islas, C.A., Suelves, I., Millan, M., Apicella, B., Herod, A.A., Kandiyoti, R., 2003c. J. Sep. Sci. 26, 1422–1428.
Jarne, C., Cebolla, V., Membrado, L., Le Mapihan, K., Giusti, P., 2011. Energy Fuels 25 (10), 4586–4594.
Jiao, C.Q., Phelps, D.K., Lee, S., Huang, Y., Freiser, B.S., 1993. Rapid Commun. Mass Spectrom. 7, 404–408.
John, P., Johnson, C.A.F., Parker, J.E., Smith, G.P., Herod, A.A., Gaines, A.F., et al., 1991. Rapid Commun. Mass Spectrom. 5, 364–367.
John, P., Johnson, C.A.F., Parker, J.E., Smith, G.P., Herod, A.A., Li, C.-Z., et al., 1993. Rapid Commun. Mass Spectrom. 7, 795–799.
John, P., Johnson, C.A.F., Parker, J.E., Smith, G.P., Herod, A.A., Li, C.-Z., et al., 1994. Fuel 73, 1606–1616.
Johnson, B.R., Bartle, K.D., Herod, A.A., Kandiyoti, R., 1997. J. Chromatogr. A 758, 65–74.
Johnson, B.R., Bartle, K.D., Cocksedge, M., Herod, A.A., Kandiyoti, R., 1998. Fuel 77, 933–945.
Johnson, B.R., Bartle, K.D., Ross, A.B., Herod, A.A., Kandiyoti, R., Larsen, J.W., 1999. Fuel 78, 1659–1664.
Joy, W.K., Ladner, W.R., Pritchard, E., 1970. Fuel 49, 26–38.
Kapur, G.S., Berger, S., 2005. Energy Fuels 19, 508.
Karaca, F., Islas, C.A., Millan, M., Behrouzi, M., Morgan, T.J., Herod, A.A., et al., 2004. Energy Fuels 18, 778–788.
Karaca, F., Behrouzi, M., Morgan, T.J., Herod, A.A., Kandiyoti, R., 2005a. Energy Fuels 19, 164–169.
Karaca, F., Behrouzi, M., Morgan, T.J., Herod, A.A., Kandiyoti, R., 2005b. Fuel 84, 1805–1811.
Karaca, F., Morgan, T.J., George, A., Bull, I.D., Herod, A.A., Millan, M., et al., 2009. Rapid Commun. Mass Spectrom. 23 (13), 2087–2098.
Kershaw, J.R., Black, K.J.T., 1993. Energy Fuels 7, 420.
Kim, S.H., Fletcher, R.A., Zachariah, M.R., 2005. Environ. Sci. Technol. 39, 4021–4026.
Kim, B.-J., Eom, Y., Kato, O., Miyawaki, J., Kim, B.C., Mochida, I., et al., 2014. Carbon 77, 747–755.
Kong, J., Wei, X.-Y., Yan, H.-L., Li, Z.-K., Zhao, M.-X., Li, Y., et al., 2015. Fuel 159, 385–391.
Kostanski, L.K., Keller, D.M., Hamielec, A.E., 2004. J. Biochem. Biophys. Meth. 58 (2), 159–186.

Lafleur, A.L., Nakagawa, Y., 1989. Fuel 68, 741–752.
Lai, W.-C., Smith, K.J., 2001. Fuel 80, 1121.
Lakowicz, J.R., 1986. Principles of Fluorescence Spectroscopy. Plenum Press, New York.
Larsen, J.W., Wei, Y.-C., 1988. Energy Fuels 2, 344–350.
Larsen, J.W., Lapucha, A.R., Wernett, P.C., Anderson, W.R., 1994. Energy Fuels 8, 258–265.
Lazaro, M.-J., Herod, A.A., Cocksedge, M.J., Domin, M., Kandiyoti, R., 1997. Fuel 76, 1225–1233.
Lazaro, M.J., Herod, A.A., Domin, M., Zhuo, Y., Islas, C.A., Kandiyoti, R., 1999a. Rapid Commun. Mass Spectrom. 13, 1401–1412.
Lazaro, M.J., Islas, C.A., Herod, A.A., Kandiyoti, R., 1999b. Energy Fuels 13, 1212.
Lazaro, M.J., Domin, M., Herod, A.A., Kandiyoti, R., 1999c. J. Chromatogr. A 840, 107–115.
Lazaro, M.-J., Herod, A.A., Kandiyoti, R., 1999d. Fuel 78, 795–801.
Lazaro, M.-J., Moliner, R., Suelves, I., Herod, A.A., Kandiyoti, R., 2001. Fuel 80, 179–194.
Leenheer, J.A., Rostad, C.E., Gates, P.M., Furlong, E.T., Ferrer, I., 2001. Anal. Chem. 3, 1461–1471.
Lehrle, R.S., Sarson, D.S., 1995. Rapid Commun. Mass Spectrom. 9, 91–92.
Leonardo, J., Hurtado, A., Chodakowski, M., Long, B., Shaw, J.M., 2011. Energy Fuels 25 (11), 5100–5112.
Li, C.-Z., Bartle, K.D., Kandiyoti, R., 1993a. Fuel 72, 3–11.
Li, C.-Z., Bartle, K.D., Kandiyoti, R., 1993b. Fuel 72, 1459–1468.
Li, C.-Z., Madrali, E.S., Wu, F., Xu, B., Cai, H.-Y., Güell, A.J., et al., 1994a. Fuel 73, 851–865.
Li, C.-Z., Herod, A.A., John, P., Johnson, C.A.F., Parker, J.E., Smith, G.P., et al., 1994b. Rapid Commun. Mass Spectrom. 8, 823–828.
Li, C.-Z., Wu, F., Cai, H.-Y., Kandiyoti, R., 1994c. Energy Fuels 8, 1039–1048.
Li, C.-Z., Wu, F., Xu, B., Kandiyoti, R., 1995. Fuel 74, 37–45.
Li, W., Morgan, T.J., Suelves, I., Carter, J.F., Herod, A.A., Rahman, M., et al., 2002. Characterisation and liquefaction of Type 1 kerogens of different maturities. Unpublished work.
Li, W., Morgan, T.J., Herod, A.A., Kandiyoti, R., 2004. J. Chromatogr. A 1024, 227–243.
Li, Z.K., Zong, Z.M., Yan, H.L., Wang, Y.G., Ni, H.X., Wei, X.Y., 2014. Fuel Process Technol. 128, 297–302.
Li, K., Vasiliu, M., McAlpin, C.R., Yang, Y., Dixon, D.A., Voorhees, K.J., et al., 2015a. Fuel 157, 16–20.
Li, Z.-K., Zong, Z.-M., Yan, H.-L., Wei, Z.-H., Li, Y., Wei, X.-Y., 2015b. Fuel 141, 268–274.
Lloyd, P.M., Suddaby, K.G., Varney, J.E., Scrivener, E., Derrick, P.J., Haddleton, D.M., 1995. Eur. Mass Spectrom. 1, 293–300.
Lobodin, V.V., Juyal, P., McKenna, A.M., Rodgers, R.P., Marshall, A.G., 2013. Anal. Chem. 85, 7803–7808.
Loegel, T.N., Danielson, N.D., Borton, D.J., Hurt, M.R., Kenttämaa, H.I., 2012. Energy Fuels 26 (5), 2850–2857.
Lyons, P.C., Hercules, D.M., Morelli, J.J., Sellers, G.A., Mattern, D., Thompson-Rizer, C.L., et al., 1987. Int. J. Coal Geol. 7, 185–194.
Lyons, P.C., Morelli, J.J., Hercules, D.M., Lineman, D., Thompson-Rizer, C.L., Dulong, F.T., 1990. Fuel 69, 771–775.
Madrali, E.S., Wu, F., Rahman, M., Kinghorn, R.R.F., Herod, A.A., Kandiyoti, R., 1994. Fuel 73, 1829–1835.
Malawer, E.G., 1995. Chapter 1, Introduction to size exclusion chromatography. In: Chi-san, W. (Ed.), Handbook of Size Exclusion Chromatography. Marcel Dekker Inc., NY, pp. 1–24.
Malhotra, R., McMillen, D.F., Watson, E.L., Huestis, D.L., 1993. Energy Fuels 7, 1079–1087.

Mandal, P.K., Majumdar, A., 2004. Concepts in Magnetic Res. A. 20A (1), 1.
Maroto-Valer, M.M., Andrésen, J.M., Snape, C.E., 1998. Fuel 77, 783–785.
Marques, J., Merdrignac, I., Baudot, A., Barre, L., Guillaume, D., Espinat, D., et al., 2008. Oil Gas Sci. Technol.Rev. IFP 63, 139.
Marshall, A.D., Munro, P.A., Tragardh, G., 1993. Desalination 91, 65.
Masuda, K., Okuma, O., Knaji, M., Matsumara, T., 1996. Fuel 75, 1065–1070.
Mathis, M., Mohr, M., Kaegi, R., 2005. Environ. Sci. Technol. 39, 1887–1892.
McKelvy, M.L., Britt, T.R., Davies, B.L., Gillie, J.K., Lentz, L.A., Leugers, A., et al., 1996. Anal. Chem. 68, 93R.
McKelvy, M.L., Britt, T.R., Davies, B.L., Gillie, J.K., Graves, F.B., Lentz, L.A., 1998. Anal. Chem. 70, 119R.
McKenna, A.M., Purcell, J.M., Rodgers, R.P., Marshall, A.G., 2010a. Energy Fuels 24 (5), 2929–2938.
McKenna, A.M., Blakney, G.T., Xian, F., Glaser, P.B., Rodgers, R.P., Marshall, A.G., 2010b. Energy Fuels 24 (5), 2939–2946.
McKenna, A.M., Donald, L.J., Fitzsimmons, J.E., Juyal, P., Spicer, V., Standing, K.G., et al., 2013a. Energy Fuels 27 (3), 1246–1256.
McKenna, A.M., Marshall, A.G., Rodgers, R.P., 2013b. Energy Fuels 27 (3), 1257–1267.
McLafferty, F.W., Turecek, F., 1993. Interpretation of mass spectra, fourth ed. University Science Books, Mill Valley, CA.
Meehan, E., 1995. Chapter 2 Semirigid polymer gels for size exclusion chromatography. In: Chi-san, W. (Ed.), Handbook of size exclusion chromatography. Marcel Dekker Inc, NY, pp. 25–46.
Menéndez, R., Blanco, C., Santamaria, R., Bermejo, J., Suelves, I., Herod, A.A., et al., 2001. Energy Fuels 15, 214–223.
Menéndez, R., Blanco, C., Santamaría, R., Domínguez, A., Blanco, C.G., Suelves, I., et al., 2002. Energy Fuels 16, 1540–1549.
Merdrignac, I., Truchy, C., Robert, E., Guibard, I., Kressmann, S., 2004. Petrol. Sci. Technol. 22 (7–8), 1003–1022.
Messenböck, R.C., 1998. PhD Thesis. University of London.
Millan, M., 2005. PhD Thesis. University of London.
Millan, M., Morgan, T.J., Behrouzi, M., Karaca, F., Galmes, C., Herod, A.A., et al., 2005a. Rapid Commun. Mass Spectrom. 19, 1867–1873.
Millan, M., Behrouzi, M., Karaca, F., Morgan, T.J., Herod, A.A., Kandiyoti, R., 2005b. Catal. Today 109, 154–161.
Millan, M., Behrouzi, M., Karaca, F., Morgan, T.J., Herod, A.A., Kandiyoti, R., 2005c. Solid state ^{13}C NMR of fractions of coal liquids. Unpublished work.
Millipore web-site, 2015. Ultra filtration membrane information. <http://www.emdmillipore.com/US/en/product/Ultrafiltration-Discs,MM_NF-C3258#documentation>.
Mills, I., Cvitas, T., Homann, K., Kallay, N., Kuchitsu, K., 1993. Quantities, Units and Symbols in Physical Chemistry, second ed. Blackwell, Oxford, UK.
Mitchell, D.L., Speight, J.G., 1973. Fuel 52, 149–152.
Montaudo, G., Montaudo, M.S., Puglisi, C., Samperi, F., 1994. Rapid Commun. Mass Spectrom. 8, 1011–1015.
Montaudo, G., Montaudo, M.S., Puglisi, C., Samperi, F., 1995. Rapid Commun. Mass Spectrom. 9, 453–460.
Monte, M.B.M., Coelho, R.R., Middea, A., 2004. Petrol. Sci. Technol. 22 (7), 991–1001.
Morgan, T.J., 2008. Molecular mass and structural characterization of heavy hydrocarbon materials. PhD Thesis, Imperial College, London.

Morgan, T.J., Kandiyoti, R., 2014. Chem. Rev. 114 (3), 1547–1607.
Morgan, T.J., Millan, M., Behrouzi, M., Herod, A.A., Kandiyoti, R., 2005a. Energy Fuels 19, 164–169.
Morgan, T.J., Morden, W.E., Al-Muhareb, E., Herod, A.A., Kandiyoti, R., 2005b. Energy Fuels 2006 (20), 734–737.
Morgan, T.J., Herod, A.A., Brain, S., Chambers, F., Kandiyoti, R., 2005c. J. Chromatogr. A. 1095, 81–88.
Morgan, T.J., George, A., Álvarez, P., Millan, M., Herod, A.A., Kandiyoti, R., 2008a. Energy Fuels 22 (5), 3275–3292.
Morgan, T.J., George, A., Davis, D.B., Herod, A.A., Kandiyoti, R., 2008b. Energy Fuels 22 (3), 1824–1835.
Morgan, T.J., George, A., Alvarez, P., Herod, A.A., Millan, M., Kandiyoti, R., 2009. Energy Fuels 23 (12), 6003–6014.
Morgan, T.J., George, A., Alvarez-Rodriguez, P., Millan, M., Herod, A.A., Kandiyoti, R., 2010a. J. Chromatogr. A 1217 (24), 3804–3818.
Morgan, T.J., Alvarez-Rodriguez, P., George, A., Herod, A.A., Kandiyoti, R., 2010b. Energy Fuels 24 (7), 3977–3989.
Morgan, T.J., George, A., 2011. Unpublished work.
Morgan, T.J., George, A., Boulamanti, A.K., Álvarez, P., Adanouj, I., Dean, C., et al., 2015. Energy Fuels. 29 (3), 1669–1685.
Mori, S., 1983. Anal. Chem. 55, 2414.
Morimoto, M., Sato, T., Araki, S., Tanaka, R., Yamamoto, H., Sato, S., et al., 2015a. Energy Fuels 29 (5), 2808–2812.
Morimoto, M., Imamura, H., Shibuta, S., Morita, T., Nishikawa, K., Yamamoto, H., et al., 2015b. Energy Fuels 29 (9), 5737–5743.
Mozaffari, S., Tchoukov, P., Atias, J., Czarnecki, J., Nazemifard, N., 2015. Energy Fuels 29 (9), 5595–5599.
Mullins, O.C., Sheu, E.Y., Hammami, A., Marshall, A.G., 2007. Asphaltenes, Heavy Oils and Petroleomics. Springer, NY.
Mullins, O.C., Martínez-Haya, B., Marshall, A.G., 2008. Energy Fuels. 22 (3), 1765.
Mullins, O.C., Sabbah, H., Eyssautier, J., Pomerantz, A.E., Barré, L., Andrews, A.B., et al., 2012. Energy Fuels 26 (7), 3986–4003.
Neal, A.C., 1995. HPLC and column liquid chromatography, Chapter 12. In: Adlard, E.R. (Ed.), Chromatography in the petroleum industry. Elsevier, Amsterdam.
Netzel, D.A., 1987. Anal. Chem. 59, 1775.
Niessen, W.M.A., Tinke, A.P., 1995. J. Chromatogr. A 703, 37.
Nishioka, M., Larsen, J.W., 1990. Energy Fuels 4, 100–106.
Nyadong, L., Mapolelo, M.M., Hendrickson, C.L., Rodgers, R.P., Marshall, A.G., 2014. Anal. Chem. 86, 11151–11158.
Oldham, P.B., McCarroll, M.E., McGown, L.B., Warner, I.M., 2000. Anal. Chem. 72, 197R.
Ovalles, C., Rogel, E., Moir, M.E., Morazan, H., 2015. Fuel 146, 20–27.
Pacey, P.D., Glasier, G.F., 2002. Am. Chem. Soc. Fuel Chem. Div. Preprints 47 (2), 742–743.
Painter, P., Veytsman, B., Youtcheff, J., 2015. Energy Fuels 29 (4), 2120–2133.
Parker, J.E., Johnson, C.A.F., John, P., Smith, G.P., Herod, A.A., Stokes, B.J., et al., 1993. Fuel 72, 1381–1391.
Paul-Dauphin, S., Karaca, F., Morgan, T.J., Millan-Agorio, M., Herod, A.A., Kandiyoti, R., 2007. Energy Fuels 21 (6), 3484–3489.
Piccolo, A., Conte, P., Cozzolino, A., 2000. Differences in high performance size exclusion chromatography between humic substances and macromolecular polymers. In: Ghabbour,

E.A., Davies, G. (Eds.), Humic Substances—versatile components of plants, soil and water. Royal Soc Chemistry, Cambridge, UK, pp. 111–124.
Pindoria, R.V., Megaritis, A., Chatzakis, I.N., Vasanthakumar, L.S., Lazaro, M.J., Herod, A.A., et al., 1997a. Fuel 76, 101–113.
Pindoria, R.V., Lim, J.-Y., Hawkes, J.E., Lazaro, M.-J., Herod, A.A., Kandiyoti, R., 1997b. Fuel 76, 1013–1024.
Pindoria, R.V., Megaritis, A., Herod, A.A., Kandiyoti, R., 1998. Fuel 77, 1715–1726.
Pindoria, R.V., Chatzakis, I.N., Lim, J.-Y., Herod, A.A., Dugwell, D.R., Kandiyoti, R., 1999. Fuel 78, 55–63.
Pipatmanomai, S., Islas, C.A., Suelves, I., Herod, A.A., Kandiyoti, R., 2001. J. Anal. Appl. Pyrol. 58, 299–313.
Pipatmanomai, S., Herod, A.A., Morgan, T.J., Paterson, N., Dugwell, D.R., Kandiyoti, R., 2004. Energy Fuels 18, 68–76.
Podgorski, D.C., Corilo, Y.E., Nyadong, L., Lobodin, V.V., Bythell, B.J., Robbins, W.K., et al., 2013. Energy Fuels 27 (3), 1268–1276.
Poirier, N., Derenne, S., Rouzaud, J.-N., Largeau, C., Balesdent, J., Maquet, J., 2000. Org. Geochem. 31, 813.
Pokorna, L., Gajdosova, D., Havel, J., 1999. Characterisation of humic acids by capillary zone electrophoresis and matrix assisted laser desorption/ionisation time of flight mass spectrometry. In: Ghabbour, E.A., Davies, G. (Eds.), Understanding humic substances: advanced methods, properties and applications. Royal Society of Chemistry, London, pp. 107–119. special publication no.247.
Polman, J.K., Quigley, D.R., 1991. Energy Fuels 5, 352–353.
Purevsuren, B., Herod, A.A., Kandiyoti, R., Morgan, T.J., Avid, B., Gerelmaa, T.Ya, 2004a. Fuel 83, 799–805.
Purevsuren, B., Herod, A.A., Kandiyoti, R., Morgan, T.J., Avid, B., Davaajav, Ya, 2004b. Eur. J. Mass Spectrom. 10, 101–108.
Purón, H., Luis Pinilla, J., Berrueco, C., Montoya de la Fuente, J.A., Millán, M., 2013. Energy Fuels 27, 3952–3960.
Qian, S.A., Zhang, P.Z., Li, B.L., 1985. Fuel 64, 1085.
Qian, K.N., Rodgers, R.P., Hendrickson, C.L., Emmett, M.E., Marshall, A.G., 2001a. Energy Fuels 15, 492.
Qian, K.N., Robbins, W.K., Hughey, C.A., Cooper, H.J., Rodgers, R.P., Marshall, A.G., 2001b. Energy Fuels 15, 1505.
Rahman, M., Herod, A.A., Kandiyoti, R., 2000. Fuel 79, 201–205.
Ralph, J.P., Catcheside, D.E.A., 1996. J. Chromatogr. A 724, 97–105.
Reemstma, T., These, A., 2003. Anal. Chem. 75, 1500.
Rendall, D., 1987. Fluorescence and Phosphorescence Spectroscopy. J Wiley & Sons, Chichester, UK.
Richaud, R., Lachas, H., Collot, A.-G., Mannerings, A.G., Herod, A.A., Kandiyoti, R., 1998. Fuel 77, 359–368.
Richaud, R., Lazaro, M.-J., Lachas, H., Miller, B.B., Herod, A.A., Dugwell, D.R., et al., 2000a. Rapid Commun. Mass Spectrom. 14, 317–328.
Richaud, R., Lachas, H., Lazaro, M.-J., Clarke, L.J., Jarvis, K.E., Herod, A.A., et al., 2000b. Fuel 79, 57–67.
Ringena, O., Lebioda, S., Lehnen, R., Saake, B., 2006. J. Chromatogr. A 1102, 154.
Rios, S.M., Barquin, M., Nudelman, N.S., 2014. J. Phys. Org. Chem. 27, 352.
Rippe, B., Haraldsson, B., 1999. Physiol. Rev. 74, 163.
Robinson, N., Evershed, R.P., Higgs, W.J., Jerman, K., Eglinton, G., 1987. The Analyst 112, 637–644.

Rodgers, R.P., Marshall, A.G., 2007. Chapter 3, Petroleomics: advanced characterization of petroleum-derived materials by Fourier Transform Ion Cyclotron Resonance Mass Spectrometry (FT-ICR MS). In: Mullins, O.C., Sheu, E.Y., Hammami, A., Marshall, A.G. (Eds.), Asphaltenes, Heavy Oils and Petroleomics. New York: Springer, pp. 63–93.
Rodríguez, J., Requena, T., Fontecha, J., Goudédranche, H., Juárez, M., 1999. J. Agric. Food Chem. 47, 558.
Rogel, E., Roye, M., Vien, J., Miao, T., 2015a. Energy Fuels 29 (4), 2143.
Rogel, E., Miao, T., Vien, J., Roye, M., 2015b. Fuel 147, 155–160.
Rogel, E., Ovalles, C., Vien, J., Moir, M., 2015c. Energy Fuels 29, 6363–6369.
Rongbao, L., Zengmin, S., Bailing, L., 1988. Fuel 67, 565.
Sabbah, H., Morrow, A.L., Pomerantz, A.E., Mullins, O.C., Tan, X., Gray, M.R., et al., 2010. Energy Fuels 24 (6), 3589–3594.
Sabbah, H., Morrow, A.L., Pomerantz, A.E., Zare, R.N., 2011. Energy Fuels 25 (4), 1597–1604.
Sabbah, H., Pomerantz, A.E., Wagner, M., Müllen, K., Zare, R.N., 2012. Energy Fuels 26 (6), 3521–3526.
Sathitsuksanoh, N., Holtman, K.M., Yelle, D.J., Morgan, T., Stavila, V., Pelton, J., et al., 2014. Green Chem. 16, 1236–1247.
Sato, S., Takanohashi, T., Tanaka, R., 2005. Energy Fuels 19, 1991–1994.
Schuler, B., Meyer, G., Peña, D., Mullins, O.C., Gross, L., 2015. J. Am. Chem. Soc. 137, 9870–9876.
Schulten, H.-R., 1982. Fuel 61, 670–676.
Sheng, L.-S., Covey, J.E., Shew, S.L., Winger, B.E., Campana, J.E., 1994. Rapid Commun. Mass Spectrom. 8, 498–500.
Sherma, I., 1996. Anal. Chem. 68, 1R.
Sherma, I., 1998. Anal. Chem. 70, 7R.
Sherma, I., 2000. Anal. Chem. 72, 9R.
Shimada, K., Lusenkova, M.A., Sato, K., Saito, T., Matsuyama, S., Nakahara, H., et al., 2001. Rapid Commun. Mass Spectrom 15, 277–282.
Shui, Hl, Norinaga, K., Iino, M., 2002. Energy Fuels 16, 69.
Silva Oliveira, E.M., Neto, A.C., Lacerda Junior, V., Castro, E.V.R., Menezes, S.M.C., 2014. Fuel 117, 146.
Sim, A., Cho, Y., Kim, D., Witt, M., Birdwell, J.E., Kim, B.J., et al., 2015. Fuel 140, 717–723.
Sirota, E.B., 2005. Energy Fuels 19, 1290–1296.
Skhonde, M.P., Herod, A.A., van der Walt, T.J., Tsatsi, W.L., Mokoena, K., 2006. Int. J. Miner. Process 81, 51–57.
Smit, E., Rüger, C.P., Sklorz, M., De Goede, S., Zimmermann, R., Rohwer, E.R., 2015. Energy Fuels 29 (9), 5554–5562.
Smith, D.F., McKenna, A.M., Corilo, Y.E., Rodgers, R.P., Marshall, A.G., Heeren, R.M.A., 2014. Energy Fuels 28 (10), 6284–6288.
Smith, K.J., 1998. Upgrading heavy oil by ultrafiltration using ceramic membrane. Patent US5785860 A.
Snape, C., Ladner, W.R., 1978. Fuel 57, 685.
Snape, C.E., Axelson, D.E., Botto, R.E., Delpuech, J.J., Tekely, P., Gerstein, B.C., et al., 1989a. Fuel 68, 547–560.
Snape, C.E., Kenwright, A.M., Bermejo, J., Fernandez, J., Moinelo, S.R., 1989b. Fuel 68, 1605–1608.
Socrates, G., 2001. Infra red and Raman Characteristic Group Frequencies: Tables and Charts, third ed. Wiley.

Somsen, G.W., Morden, W., Wilson, I.D., 1995. J. Chromatogr. A 703, 613.
Soorghali, F., Zolghadr, A., Ayatollahi, S., 2015. Energy Fuels 29 (9), 5487–5494.
Stenson, A.C., Landing, W.M., Marshall, A.G., Cooper, W.T., 2002. Anal. Chem. 74, 4397–4409.
Stock, L.M., Obeng, M., 1997. Energy Fuels 11, 987–997.
Strausz, O.P., Peng, P., Murgich, J., 2002. Energy Fuels 16, 809–822.
Strausz, O.P., Safarik, I., Lown, E.M., Morales-Izquierdo, A., 2008. Energy Fuels 22, 1156.
Strausz, O.P., Safarik, I., Lown, E.M., 2009. Energy Fuels 23, 1555.
Strausz, O.P., Lown, E.M., Morales-Izquierdo, A., Kazmi, N., Montgomery, D.S., Payzant, J.D., et al., 2011. Energy Fuels 25 (10), 4552–4579.
Strlic, M., Kolar, J., 2003. J. Biochem. Biophys. Methods 56, 265–279.
Strom, D.A., Edwards, J.C., Decanio, S.J., Sheu, E.Y., 1994. Energy Fuels 8, 561.
Suelves, I., Herod, A.A., Kandiyoti, R., 2000. Abstr. Pap. Am. Chem. Soc. 219 p88-GEOC.
Suelves, I., Islas, C.A., Herod, A.A., Kandiyoti, R., 2001a. Energy Fuels 15, 429–437.
Suelves, I., Lazaro, M.-J., Begon, V., Morgan, T.J., Herod, A.A., Dugwell, D.R., et al., 2001b. Energy Fuels 15, 1153–1165.
Suelves, I., Islas, C.A., Millan, M., Galmes, C., Carter, I.E., Herod, A.A., et al., 2003. Fuel 82, 1–14.
Takanohashi, T., Iino, M., Nakumara, K., 1994. Energy Fuels 8, 395.
Tanaka, R., Sato, S., Takanohashi, T., Hunt, J.E., Winans, R.E., 2004. Energy Fuels 18, 1405–1413.
Tang, W., Hurt, M.R., Sheng, H., Riedeman, J.S., Borton, D.J., Slater, P., et al., 2015. Energy Fuels 29 (3), 1309–1314.
Tay, F.H., Kazarian, S.G., 2009. Energy Fuels 23, 4059–4067.
Tei, A., Herod, A.A., Dugwell, D.R., Kandiyoti, R., Vitolo, S., Tartarelli, R., 1997. Hydrocracking of biomass-derived tars. Project Report.
These, A., Reemstma, T., 2003. Anal. Chem. 75, 6276–6281.
These, A., Winkler, M., Thomas, C., Reemstma, T., 2004. Rapid Commun. Mass Spectrom. 18, 1777–1786.
Thiyagarajan, P., Cody, G.D., 1997. Am. Chem. Soc. Div. Fuel Chem. 42 (1), 253–257.
Torregrosa-Rodriguez, P., Martinez-Escandell, M., Rodriguez-Reinoso, F., Marsh, H., de Salazar, C.G., Palazon, E.R., 2000. Carbon 38, 535.
Touchstone, J.C., 1992. Practice of Thin Layer Chromatography, third ed. John Wiley & Sons, New York.
Tsang Mui Ching, M.-J., Pomerantz, A.E., Andrews, A.B., Dryden, P., Schroeder, R., Mullins, O.C., et al., 2010. Energy Fuels 24 (9), 5028–5037.
VanderHayden, Y., Popovici, S.T., Schoenmakers, P.J., 2002. J. Chromatogr. A 957, 127–137.
Vasanthakumar, L.S., Hewitt, G.F., Lazaro, M.-J., Herod, A.A., Dugwell, D.R., Kandiyoti, R., et al., (Eds.), 1998. Fluidised bed gasification and pyrolysis of biomass. Final Report, EU Contract No CI1*-CT93-0343(DG12HSMU). January.
Vorres, K.S., 1990. Energy Fuels 4, 420.
Wang, I., Takarada, T., 2003. Fuel Proc. Technol 81, 247–258.
Wiehe, I.A., 2008. Process Chemistry of Petroleum Macromolecules. CRC Press, Taylor & Francis Group, Boca Raton.
Wilson, M., Collin, P., Pugmire, R., Grant, D., 1982. Fuel 61, 959.
Winans, R.E., 1991. J. Anal. Appl. Pyrol. 20, 1–13.
Winans, R.E., McBeth, R.L., Hunt, J.E., Melnikov, P.E., 1991. *Proc. 1991 Int. Conf. Coal Sci.*, 16–20 September, Newcastle upon Tyne, UK, p. 44.

Wolfbeis, O.S. (Ed.), 1993. Fluorescence Spectroscopy, New Methods and Applications. Springer Verlag, Berlin.
Wong, K.K.Y., de Jong, E., 1996. J. Chromatogr. A 737, 193–203.
Wu, Chi-san (Ed.), 1995. Handbook of Size Exclusion Chromatography, Chromatographic Science Series, vol. 69. Marcel Dekker, New York.
Wu, Z., Rodgers, R.P., Marshall, A.G., 2005. Fuel 84, 1790–1797.
Wu, Z.G., Jernstrom, S., Hughey, C.A., Rodgers, R.P., Marshall, A.G., 2003. Energy Fuels 17,946 (2003).
Wu, Z.G., Rodgers, R.P., Marshall, A.G., 2004. Anal. Chem. 76, 2511.
Yan, H.-L., Zong, Z.-M., Li, Z.-K., Wei, X.-Y., 2015. Fuel 160, 596–604.
Yarranton, H.W., Ortiz, D.P., Barrera, D.M., Baydak, E.N., Barré, L., Frot, D., et al., 2013. Energy Fuels 27 (9), 5083–5106.
Yau, W.W., Kirkland, J.J., Bly, D.D., 1979. Modern Size Exclusion Liquid Chromatography. John Wiley & Sons Inc, NY.
Yevlampieva, N.P., Biryulin, Yu.F., Melenevskaja, E.Yu, Zgonnik, V.N., Rjumtsev, E.I., 2002. Colloids Surf. A 209, 167–171.
You, C.-Y., Fan, X., Zheng, A.-L., Wei, X.-Y., Zhao, Y.-P., Cao, J.-P., et al., 2015. Fuel 155, 122–127.
Zhang, S.-F., Xu, B., Herod, A.A., Kandiyoti, R., 1996a. Energy Fuels 10, 733–742.
Zhang, S.-F., Xu, B., Moore, S., Herod, A.A., Kandiyoti, R., 1996b. Fuel 75, 597–605.
Zhang, S.-F., Xu, B., Herod, A.A., Kimber, G.M., Dugwell, D.R., Kandiyoti, R., 1996c. Fuel 75, 1557–1567.
Zhang, S.-F., Herod, A.A., Kandiyoti, R., 1997a. Fuel 76, 39–49.
Zhang, S.-F., Shearman, J., Domin, M., Lazaro, M.-J., Herod, A.A., Kandiyoti, R., 1997b. Fuel 76, 207–217.
Zhang, L., Zhao, S., Xu, Z., Chung, K.H., Zhao, C., Zhang, N., et al., 2014a. Energy Fuels 28 (10), 6179–6187.
Zhang, Y., Zhang, L., Xu, Z., Zhang, N., Chung, K.H., Zhao, S., et al., 2014b. Energy Fuels 28 (12), 7448–7456.
Zhang, W., Andersson, J.T., Rader, H.J., Mullen, K., 2015. Carbon 95, 672.
Zhao, B., Shaw, J.M., 2007. Energy Fuels 21, 2795.
Zheng, Q., Morimoto, M., Sato, H., Takanohashi, T., 2015. Fuel 159, 751–758.
Zhuo, Y., Herod, A.A., Kandiyoti, R., 2003. The thermochemical reactions of middle rank coals Chapter 3. In: Ikan, R. (Ed.), Natural and laboratory-simulated thermal geochemical processes. Kluwer Academic Publishers, Dordrecht, pp. 53–151.
Ziechmann, W., Hubner, M., Jonassen, K.E.N., Batsberg, W., Nielsen, T., Hahner, S., et al., 2000. Humic substances and humification. In: Ghabbour, E.A., Davies, G. (Eds.), Humic substances, versatile components of plants, soils and water. Royal Society of Chemistry, London, pp. 9–20. special publication no. 259.
Zubkova, V., 2011. Anal. Bioanal. Chem. 399 (9), 3193–3209.

In closing: the current state and new perspectives

9

Chapter Outline

This chapter summarises key elements of the work presented in earlier chapters. Progress in experimental method development for investigating thermal breakdown in lignocellulosic biomass and coals has been reviewed. Advances made in the analytical characterization of high-mass heavy hydrocarbon liquids have been summarised. The chapter concludes with a short discussion on future perspectives for the utilisation of lignocellulosic biomass and coal as energy vectors.

9.1 The thermochemical reactions of solid fuels

Many of the products formed in the course of thermal breakdown are themselves reactive. Interactions between pyrolyzing solids and primary products tend to alter product distributions. In addition to the usual reaction parameters such as temperature, pressure and residence time, product distributions from thermochemical reactions may be altered by changes in reactor and sample configurations, heating rates, and the proximity and the design of the quench zone. Determining the thermal response of solid fuels in a manner that is free of spurious variables thus requires minimising contact between reactants and products as well as the rapid quenching of primary reaction products.

The conceptual tools needed for the design of thermochemical reactors thus differ significantly from those used in conventional chemical reaction engineering. The key challenge is to design experiments that allow discriminating between the thermal response of the fuel and effects arising from the configuration of the sample and that of the reactor. The underlying aim is the usual requirement for experimental results to be independent of the method of measurement. Experience suggests, however, that in the pyrolysis laboratory, this strict requirement is adhered to, as strictly as possible.

Pyrolyzing biomass and pyrolyzing coals: At the level of laboratory-scale research, thermochemical reaction work on biomass and coals is generally conducted with relatively little reference to the many common aspects and shared challenges. In fact, differences between experimental approaches devised for investigating thermal reactions

Solid Fuels and Heavy Hydrocarbon Liquids. DOI: http://dx.doi.org/10.1016/B978-0-08-100784-6.00009-6

of biomass and coals are often marginal. The preceding chapters bear testimony to the similarities of approach that naturally develop, when work on biomass and coals are considered under the same heading. We have already cited the sensitivity of product distributions of many coals and biomass materials to increasing heating rates, as well as the incipient plastic behaviour of many samples, when heated at high heating rates. These observations contain important pointers at the parallel, if not similar, sequences of pyrolytic events taking place during thermal breakdown. They provide a suitable starting point for developing a unified approach for the analysis of the thermochemical reactions of solid fuels as a whole.

Designing pyrolysis and gasification reactors: The wire-mesh reactor configuration described in Chapters 3, Pyrolysis of solid fuels: experimental design and applications, and Chapter 4, High-pressure reactor design: pyrolysis, hydropyrolysis and gasification, combines several design elements that enable determining sample behaviour during pyrolysis and gasification in a manner that is relatively free of reactor-related effects. Small amounts of sample particles are finely dispersed within a wire-mesh sample holder, which acts as a resistance heater. The design of the reactor developed at Imperial College features a support plate, placed under the sample-holder, which serves to guide a stream of carrier gas through the mesh and the reacting sample particles. The rapid removal of volatiles away from the reaction zone enables the recovery of products for further characterization in a state relatively uncontaminated by secondary reactions. The atmospheric pressure wire-mesh reactor described in Chapter 3, Pyrolysis of solid fuels: experimental design and applications, has been adopted as a standard design by numerous laboratories in Australia, China and Japan.

The configuration of wire-mesh reactors allows modification for operating over wide ranges of temperatures, pressures, and gas compositions. Chapter 4, High-pressure reactor design: pyrolysis, hydropyrolysis and gasification, describes pyrolysis and gasification experiments carried out at temperatures up to 2000°C and pressures up to 160 bars. The same chapter describes a version of the high-pressure reactor fitted with a steam-injection facility for steam-gasification experiments. Another modification of the reactor has enabled exposing sample particles to successive blasts of different gases, with millisecond-level resolution between the injection stages. This reconfiguration of the high-pressure wire-mesh reactor was used to simulate reactions during coal injection into blast-furnaces.

Nevertheless, wire-mesh reactors present several disadvantages. The requirement for uniform heating and the sparse distribution of sample particles restricts the sample size to 5–6 mg, which tends to limit the amounts of reaction products recovered during a single experiment. Similarly, it is not possible to provide uniform heating within larger particles at high heating-rates and the design is constrained to the use of sample particle diameters no greater than 106–152 μm.

Comparing results from different types of pyrolysis reactors (see Chapter 3: Pyrolysis of solid fuels: experimental design and applications and Chapter 4: High-pressure reactor design: pyrolysis, hydropyrolysis and gasification) has proved helpful in pin-pointing the strengths and weaknesses of each particular design. Wire-mesh reactors were found to require far longer holding times at low temperatures for pyrolysis reactions to reach completion. This appears due to poor radiative heat

transfer to particles in the lower temperature range (400–500°C). With temperatures increasing above 600°C, the fluidised-bed configuration allows the loss of tar product through cracking reactions, mostly in the reactor freeboard. Tar loss was also observed in fixed-bed reactors, due to solids-volatiles contact leading to secondary char formation. Entrained flow reactors were found to require longer residence times (i.e., longer reactors) to reduce scatter in sample weight-loss measurements. These reactors allow thermal degradation of tar vapours due to exposure to high temperatures, as tar vapours are carried along the length of the reactor. Entrained flow reactors are not generally preferred for assessing tar release and tar quality during pyrolysis and hydropyrolysis experiments.

Some space has also been devoted to the uses and misuses of thermogravimetric (TG) balances. These instruments offer a tempting combination of built-in simultaneous temperature and weight measurements. However, volatiles-solids interactions in TG balances do not allow determining pyrolytic weight loss in a manner that is independent of the method of measurement. The inherent errors are naturally amplified when data are differentiated for calculating reaction rate constants and energies of activation.

Synergistic effects between biomass components during pyrolysis: When small particles of woody biomass are pyrolysed at high heating-rates, char yields do not exceed 1–2% (see Chapter 3: Pyrolysis of solid fuels: experimental design and applications). The lignin content of such samples is usually around 25%. However, significantly larger char yields were observed when chemically isolated Kraft lignin samples were pyrolysed under similar conditions, compared to the pyrolysis of lignins naturally embedded in plant-derived material. The apparent 'lignin char deficit' during the pyrolysis of naturally occurring biomass has been confirmed by surveying a wide range of lignin pyrolysis experiments reported in the literature, which drew on a variety of original plant materials and lignin isolation methods.

Naturally occurring lignins are known to be intermeshed with other plant constituents within the composite matrices of lignocellulosic biomass. The 'deficit' is consistent with chemical reactions between plant lignin and the reactive, highly oxygenated molecular fragments generated by the prior thermal breakdown of the more labile biomass components: cellulose and hemicelluloses.

The 'lignin char deficit' observed during these pyrolysis experiments reflects the extent of synergistic effects between distinct plant components during the pyrolysis of naturally occurring lignocellulosic biomass.

Designing liquefaction reactors: Most bench-scale liquefaction research on coal and biomass is carried out in small, closed reactors operating in 'batch' mode. Such reactors are relatively easy to construct and operate. The basic difficulty with this experimental design, however, concerns the fate of products that are sequentially released into the liquid phase. Depending on the type of experiment intended, reaction times may last anywhere from 5–10 to 120 min, or even longer. Thus, liquefaction products remain exposed to reaction conditions during the entire length of the experiment, against a background of rising product concentrations, in an environment that would support secondary reactions.

The mix of reaction products recovered from batch reactors contains, therefore, primary extraction products, scrambled with products of whatever sequence of

secondary reactions has taken place during the experiment. The procedure does not allow characterising reaction pathways or working out reaction kinetics during the liquefaction process. The nature of the problem is similar for coal and biomass liquefaction.

However, it is possible to determine sample mass loss and assess products sequentially released from reacting solids, by continuously removing products from the reaction zone. The design and construction of the 'flowing-solvent reactor', described in Chapter 5, Liquefaction: thermal breakdown in the liquid phase, was undertaken in response to this need. The design is based on heating a fixed-bed of sample at a fixed rate to a pre-selected temperature, while continuously sweeping the sample bed with a stream of solvent. The products are continuously removed from the reaction zone and rapidly quenched. This reactor configuration allows discriminating between product fractions exiting the reactor, as a function of temperature during heatup, and as a function of time at the peak temperature.

The kinetic model outlined in the same chapter was set-up to distinguish between the initial dissolution of the more soluble parts of the sample, from product release following extensive covalent-bond cleavage reactions at higher temperatures. The energies of activation calculated for the (first) extraction stage were low, giving values similar to diffusion related processes. The second stage, reflecting the results of bond-scission reactions, gave activation energies close to covalent bond dissociation energies. Surveying recent literature on hydrothermal biomass processing suggests that moving on from the use of batch reactors might assist in developing a more detailed understanding of underlying processes.

Elements of thermal breakdown: Chapter 6, Elements of thermal breakdown: heating rate effects and retrogressive reactions, presented electron spin resonance (ESR) spectroscopy data on pyrolysing coals. These experiments allowed differentiating between the onset of covalent bond scission from the initial stages of extensive sample depolymerisation. The temperature gap observed between these two stages suggests that several bonds must break before large molecular fragments can detach from the coal matrix.

Also taking account of pyrolysis and liquefaction experiments performed in parallel, the work allowed addressing several fundamental questions about thermal breakdown in middle-rank coals: When does thermal breakdown begin? What are the similarities between initial reaction pathways in pyrolysis and liquefaction? When do these reaction pathways begin to diverge? The investigation provided clues regarding the reasons why changes in heating rates tend to affect product distributions and also influence the plastic behaviour of coals. It also helped explain the interplay between eventual product distributions and the way retrogressive reactions work. Moreover, we have observed that the boundary between softening and non-softening coals is not a rigid one. Using this framework, several questions thrown up by research on modern coke making could be addressed.

Thermal breakdown in lignocellulosic biomass: It is possible to identify analogous trends in coal and in biomass pyrolysis. Identifying links between sensitivity to heating rates and the (infrequently) observed tendency of woody biomass to soften and melt at high heating rates, appears as a significant starting point for exploring the

mechanics of thermal breakdown in biomass. These effects may be understood with greater clarity, furthermore, when studied in the context of the thermal reactions of other highly oxygenated materials that display plastic behaviour during pyrolysis at high heating rates (e.g., lignites, Kraft lignin). The body of related experience developed within the sphere of coal pyrolysis research looms large as a resource that has yet to be fully exploited. However, the examination of thermal breakdown in lignocellulosic biomass must also take account of the fiercely hydrogen-scavenging environment resulting from the higher oxygen contents (~40%) of these materials.

9.2 Characterising heavy hydrocarbon liquids

Materials amenable to analysis by gas chromatography: In Chapter 7, Analytical techniques for low mass materials: method development, we reviewed the analysis of materials amenable to analysis by gas chromatography (GC) in one and two dimensions, often in tandem with mass spectroscopic techniques (GC-MS, probe-MS). The work focused on analysing materials produced during the thermal reactions of biomass and coal, as well as on petroleum-derived heavy fractions. The upper limit of molecular mass for this type of analysis is normally confined to about 220 u for oxygenated aromatics, 300–350 u for polyaromatic materials, and about 500–550 u for aliphatics. Chapter 7, Analytical techniques for low mass materials: method development, also described how these limits may be extended by the use of supercritical fluid chromatography and liquid chromatography. Methods for the detection of aliphatic materials in coal and petroleum products were assessed, including size exclusion chromatography (SEC), fractionation, urea adduction, and silver ion adduction using thin layer chromatography and laser desorption mass spectrometry. Laser desorption of aliphatics is only possible following derivatisation.

Characterising materials too involatile to pass through a gas-chromatography column: Biomass- and coal-derived oils, tars, and extracts as well as many petroleum-derived heavy fractions contain significant proportions of high-mass material, which are not amenable to analysis by GC-MS, liquid chromatography or probe-MS techniques. Above the molecular mass levels just discussed, it is no longer relevant to talk about ‘analysis’. The characterization methods outlined in Chapter 8, Analytical techniques for high mass materials: method development, are usually initiated by fractionating the sample, broadly, in terms of molecular mass, using one of several separation methods. The molecular mass distributions of these fractions may then be characterised by MALDI (matrix assisted laser desorption/ionisation) mass spectroscopy and SEC. Quantitative agreement has been found between SEC and MALDI-MS up to masses just above 3000 u.

Mixed eluents for SEC: While coal-derived heavy fractions may be completely dissolved in NMP, petroleum-derived heavy fractions are not completely soluble in this solvent. It was also observed that pure chloroform, while an excellent solvent for most petroleum-derived materials, does not completely dissolve the more aromatic coal-derived fractions. It turns out, however, that NMP-chloroform mixtures are capable

of dissolving completely both coal and petroleum-derived heavy fractions, at the low concentrations required in SEC.

SEC column calibration work was carried out with an NMP-to-chloroform volume ratio of 6:1. The mixed solvents allowed elution of the fractions of petroleum asphaltenes that were insoluble in NMP alone. Significantly, mixing $CHCl_3$ with NMP was observed to reduce the structure dependence of elution times of many standard sample polymers compared to using NMP alone. Thus reviewing solvent properties has been instrumental in broadening the scope of SEC, as a method capable of characterising a wider range of samples than was hitherto thought likely.

Method development in LD-MS mass spectrometry: Earlier work had shown it was possible to form artefacts such as cluster ions, which could distort LD-MS measurements, even without overloading the detector system. Method development work was undertaken to improve estimates of mass ranges for complex hydrocarbon mixtures.

Experiments were carried out using a cocktail of four PAH compounds with molecular masses ranging from 202 to 532 u. Combinations of high laser power and high-mass accelerator voltage were found to be among the conditions likely to generate artefacts such as cluster ions. However, with careful balancing of sample concentration, laser power, total ion current and delayed ion extraction, higher-mass materials could be observed without generating high-mass cluster ion artefacts. Keeping low target concentrations helped in reducing gas phase sample concentrations formed by the laser pulse, which helped suppress cluster-ion formation.

These findings were tested by examining a creosote oil and an anthracene oil. The samples were fractionated by planar chromatography before analysis by LD-MS, directly from the chromatographic plates. The method was useful in separating the more abundant small molecules from the less abundant large molecules and permitted the generation of their mass spectra independently. Introducing the sample on the chromatographic plate also helped reduce the concentration of sample by thinly spreading over the PC-plate. The technique was shown to suppress cluster ion formation and greatly improved the reproducibility of the spectra. Results showed the presence of molecular ions in the m/z 1000–2000 range for the anthracene oil sample and m/z 600–1500 for the creosote oil sample, with the high-mass end tailing off towards m/z ~5000. The creosote oil contained significantly less of this high-mass material than the anthracene oil sample, and in both cases, high-mass material was only present in low concentrations. Ion mass range estimates were in close agreement with molecular mass ranges from SEC, and findings were consistent with changes observed in the UV-fluorescence spectra of the samples. The method was found to be directly applicable to the characterization of heavier coal- and petroleum-derived fractions (see Chapter 8: Analytical techniques for high mass materials: method development).

Correlation of molecular structure with molecular mass: To reduce errors and improve the quality of NMR spectra, high-resolution solution state ^{1}H and ^{13}C-NMR methods were optimised and calibrated. The modifications included the use of coaxial NMR tubes to isolate the lock solvent from the actual sample solution. The improved resolution of the spectra made it possible to calculate average structural parameters for all fractions of the samples analysed.

One set of method development work was performed using the maltene and asphaltene fractions of Maya (Mexico) crude oil. The asphaltenes were further subfractioned into NMP-soluble ('MNS') and NMP-insoluble ('MNI') fractions (see Chapter 8: Analytical techniques for high mass materials: method development). The samples were examined by quantitative liquid-state ^{1}H and ^{13}C-NMR spectroscopy and the data combined with molecular-mass estimates in order to calculate average structural parameters (ASP) for each of the fractions.

For the maltene sample, the calculated number of aromatic rings per average molecule was 2–5 and for the asphaltene, 8–10. The NMP soluble fraction of the asphaltene (MNS) showed about five aromatic rings per average molecule while a value of 11–38 rings was arrived at for the NMP insoluble fraction of the asphaltene sample. The MNS fraction turned out to be more aliphatic than the MNI fraction. On average, the MNS sample appeared to contain a greater number of smaller aromatic cores, linked by means of biphenyl-like aromatic-aromatic single bonds, aliphatic/naphthenic bridges, and shorter aliphatic side chains. If the aromatic groups are in external positions (or accessible to the solvent by other means), this would account for the solubility of these species in NMP. Meanwhile, results for the MNI sample strongly suggested fewer, larger aromatic cores per average molecule, surrounded by long alkyl side chains and naphthenic structures. Alkyl substituents would appear to form a barrier between the aromatic core and the solvent.

Application of the method to a coal tar pitch: The average molecular mass for the acetone-soluble fraction of the pitch, arrived at by the planar-chromatography–assisted LD-MS method was found to be about 550 u. On this basis, an average molecule was calculated to contain approximately four aromatic rings (RA) and three naphthenic rings (RN).

An M_n value of 1600 u was determined for the PPS (pitch pyridine soluble) fraction; the average molecule was found to contain about 21 aromatic rings (RA), along with an average of two naphthenic rings per molecule. For the PPI (pitch pyridine insoluble) sample, the M_n arrived at was about 6000 u. The average molecule was found to contain about 100 aromatic rings (RA) and an average of about seven naphthenic rings per molecule (RN). The structural parameter calculations have been presented in Chapter 8, Analytical techniques for high mass materials: method development.

ASP calculations for such complex samples need to be treated as broad indications of underlying trends. They provide qualitative information regarding changes in structure that are difficult to determine in any other way. Nonetheless, data acquired by these diverse methods have conveyed an internally consistent picture of the suite of samples examined.

In closing: Taken together, these methods are able to detect and partially characterize molecules far larger than the ranges of materials amenable to analysis by conventional chromatographic and mass spectrometric techniques. However, many problems, common to the characterization of coal-derived liquids, petroleum residues, kerogens, and humic substances remain to be studied.

In the past, the presence of high-mass material has often been attributed to the formation of aggregates. The expedient has not proved productive for the petroleum industry. It has not resolved any of the problems associated with demonstrably heavy

petroleum fractions and residues. Moreover, no one has been able to demonstrate how these 'aggregated' materials could be disaggregated. The work outlined above clearly shows that many of these high-mass materials are not aggregates but large molecules. In a world of rapidly depleting natural resources, getting some use out of these heavier fractions will require the careful evaluation of their structures and molecular weights. This is only a necessary first step in developing catalysts and catalytic processes appropriate to upgrading these materials.

9.3 Energy demand – energy supplies: the big questions

In the energy world, nothing remains quite the same for very long. When oil prices rise, the world of energy experts usually turns to visions of manufacturing synthetic fuels from coals and biomass. Champions of 'green' energy come forward with suggestions for exploiting opportunities afforded by prevailing high energy prices. Vast investments are planned, before the cyclical nature of the markets brings everyone down to earth yet again. Like so many of its predecessors, the last great leap towards biofuels has lost momentum in the latest crash of fossil fuel prices (2014–16) but not before enormous sums had been disbursed as subsidies.

However, some things do not change rapidly. Solar and wind energy still require direct subsidies. Might some of the money that was used for energy production, instead be used for research and development aimed at reducing costs? It is also important to consider that growing energy crops deplete the soil. Sugar beet and sugar cane as well as oily plants, such as sunflower and cotton, have deleterious effects on soil quality. In the world of capital intensive agriculture, the more usual response to soil depletion is to use fertilizers. In the rest of the world, soil depletion accelerates, if past practice in Brazil is anything to go by. Yet, fertilizer grade phosphate rock is also a finite resource, with reserves estimated to be good for another ~400–500 years at current rates of consumption (Bungay, 1985).

The second major obstacle to extensive energy crop cultivation is the competition with food production. Examples from two projects suggest that between 2500 and 3300 hectares of arable land are required to produce sufficient crops for an energy output of 10 MWe by combustion or gasification. These data are based on the experience of the SIGAME Project in Bahia State in North-Eastern Brazil (Worldenergy, 2005) and calculations for the ARBRE-Eggborough (Renewonline, 2002) gasification plant in North Yorkshire (UK). This amount of land may alternatively feed approximately 7500 people plus about 850 head of cattle (D. Kandiyoti, 2004).

Clearly, 10 MWe is a rather small amount of power. We would need 2.5–3.3 million hectares of arable land to cultivate enough energy crops to produce, say, 10 GWe of electric power. The total UK electric power requirement is a little more than 70 GWe, so 10 GWe is still a relatively small amount of energy. Meanwhile, 2.5–3.3 million hectares represent all the arable land of Angola or Zimbabwe or Mozambique or 60% of all the arable land of Zambia or of Uganda, or 20% of all arable land in agriculturally fabulously rich South Africa.

Other estimates would more than double the output of energy crops per unit of arable land (Morgan, 2015). Clearly, agricultural productivity may differ widely with regional and local conditions. Doubling or halving the intensity of energy production would not, however, be sufficient to alter the thrust of the present argument. Devoting agricultural land to energy farms on a large scale would compete with food production and cannot be allowed to make more than a marginal contribution to base load power production on a global scale.

However, not all is lost on the biomass front. Biomass utilisation is perceived as CO_2 neutral and there are obvious advantages in generating power from forestry, farming and municipal wastes. As already explained, we would need to develop a new generation of small and efficient gasifiers, to reduce transport costs for these low-density feedstocks. We would need gate fees to make up for the fundamentally inefficient process, compared to fossil fuel utilisation. This is not unrealistic. Anywhere in the industrialised world, disposing of a ton of waste costs about US $80–$90. Finally, we need long-term (~15–25 year) supply contracts. Experience suggests that the gate fee becomes vulnerable as soon as waste-to-power projects show a profit. This is not a universal quick fix. The reuse of waste may actually reduce global resource utilisation by a few percent. It would make a dent.

At present, we live in a world powered and fuelled with coal, gas, oil, and alas, nuclear energy. Received wisdom would have us believe we must recover the CO_2 generated by fossil fuel utilisation and store it somewhere and that we must burn hydrogen instead of these ‘dirty’ fuels and make up the balance with renewables. Nuclear energy has become politically undesirable and with decommissioning costs finally in the frame (why were they not calculated earlier?), it turns out to be commercially less attractive than it had seemed earlier. Thinking ahead for once, we might usefully compare the decommissioning costs of nuclear power stations with the potential costs of carbon dioxide capture and storage. A little perversely, perhaps, nuclear energy turns out to be the far cheaper alternative.

However, there have been unexpected developments in recent years (2013–15). As the glut of ‘fracked’ natural gas caused prices to collapse in the United States, cheap US coal has found its way to Europe. In Germany, two of the more modern and efficient gas-fired power stations have been mothballed in response to cheap power generation from coal (Kandiyoti, 2015). Clearly, renewable energies are being allowed to operate outside the cost-price nexus. This is not the place to review the costs of renewable energies. However, it seems worth pointing out that research and development budgets for renewable energies (potentially useful for reducing costs) are being dwarfed by budgets spent on subsidising renewable energy generation.

The foregoing must be read as a plea for doing our homework in respect of energy and environmental matters a little more carefully.

References

Bungay, H., 1985. Energy, the Biomass Options. Wiley Interscience, New York, 1985.
IEA 2005. Energy Statistics of OECD Countries 2002–2003. OECD/IEA, Paris.

Kandiyoti, D., 2004. School of Oriental & African Studies. London, unpublished field notes.
Kandiyoti, R., 2015. Powering Europe: Russia, Ukraine, and the Energy Squeeze. Palgrave Macmillan Palgrave Pivot, New York, NY.
Morgan T.J., 2015. Personal communication.
Renewonline 2002. <http://eeru.open.ac.uk/natta/renewonline/rol38/6.html>.
Worldenergy, 2005. <http://www.worldenergy.org/wec-geis/publications/reports/rural/case_studies/annII_brazil.asp>.

Index

Note: Page numbers followed by '*f*' and '*t*' refer to figures and tables, respectively.

T